ORGANIC TRANSFORMATIONS USING TRANSITION METALS AND PHOTOREDOX CATALYSTS

Klaudia Michaliszyn

UNIVERSITAT ROVIRA i VIRGILI

ICIQ Institute of Chemical Research of Catalonia

Organic Transformations using Transition Metals and Photoredox Catalysts

---

Klaudia Michaliszyn

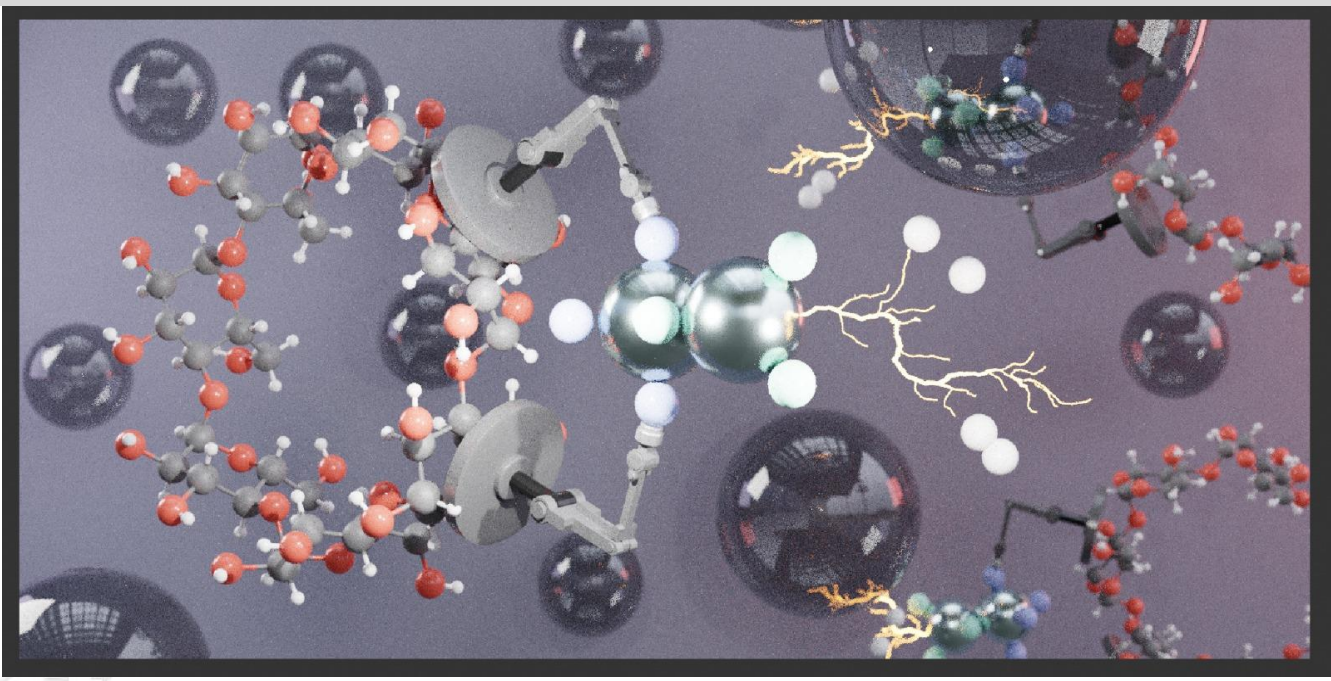

DOCTORAL THESIS
2022

UNIVERSITAT ROVIRA I VIRGILI
ORGANIC TRANSFORMATIONS USING TRANSITION METALS AND PHOTOREDOX CATALYSTS
Klaudia Michaliszyn

UNIVERSITAT ROVIRA I VIRGILI
ORGANIC TRANSFORMATIONS USING TRANSITION METALS AND PHOTOREDOX CATALYSTS
Klaudia Michaliszyn

UNIVERSITAT ROVIRA I VIRGILI
ORGANIC TRANSFORMATIONS USING TRANSITION METALS AND PHOTOREDOX CATALYSTS
Klaudia Michaliszyn

PhD Thesis

Organic Transformations using Transition Metals and Photoredox Catalysts

Klaudia Dominika Michaliszyn

Supervised by Prof. Julio Lloret-Fillol

Tarragona

January 2022

UNIVERSITAT ROVIRA i VIRGILI

ICIQ Institute of Chemical Research of Catalonia

UNIVERSITAT ROVIRA I VIRGILI
ORGANIC TRANSFORMATIONS USING TRANSITION METALS AND PHOTOREDOX CATALYSTS
Klaudia Michaliszyn

Prof. Dr. Julio Lloret Fillol, Group Leader of the Institut Català d'Investigació Química (ICIQ) and Research Professor of Institució Catalana de Recerca i Estudis Avançants (ICREA).

DECLARES that the present study entitled **"Organic Transformations using Transition Metals and Photoredox Catalysts"**, presented by Klaudia Dominika Michaliszyn to receive the PhD degree in Chemistry, has been carried out under his supervision, in the Institut Català d'Investigació Química (ICIQ).

Tarragona, 13th January 2022

PhD Thesis Supervisor

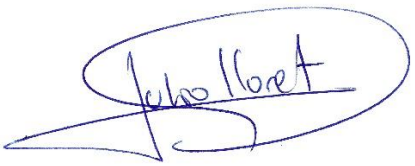

Prof. Dr. Julio Lloret-Fillol

UNIVERSITAT ROVIRA I VIRGILI
ORGANIC TRANSFORMATIONS USING TRANSITION METALS AND PHOTOREDOX CATALYSTS
Klaudia Michaliszyn

Acknowledgments

First of all I wanted to thank Julio for giving me this great opportunity to join his group and learn new skills. Thank you very much.

My grandma used to say "Ściskaj życie jak cytrynkę" and finally in the last years I understood what she meant by these words. In this process of understanding this saying participated my three Musketeers – Juan, Edvin and Kostek. Thank you for showing me the best of the scientific life and supporting me all these years. I don't know where I would be without you.

Moje kochane dziewczynki! Inezka, Kalina, Marlencia, Paulusia, Karcia, Mariolcia, Marlenka, zawsze miałam w Was wsparcie, wierzyłyście we mnie kiedy mi tej wiary brakowało, więc z całego serca Wam dziękuję za to i że nauczyłyście mnie wytrwałości. Z całą pewnością będę to pamiętała do końca życia!

I'm very grateful for people I had chance to work in the lab. Katia, Fede, Felix, Alicia, Sergi, Geyla, Jordi, Noufal, thank you for teaching me new techniques and sharing your knowledge with me. Special thanks to Carla for helping me in the lab and with my thesis. Miguel… (Or shall I rather call you my urgencias? Haha) toy to farta y tengo fame will stay with me forever, thanks for teaching me patience and standing me everyday in the lab. Together with Alberto you were there for me in good in bad asi que gracias/grazie for everything.

Na koniec chciałabym też podziękować moim rodzicom, za to że ułatwili mi ścieżkę mojej kariery zawodowej i dzięki nim mogłam dotrzeć do momentu, w którym się znajduję. Moim słodkim siostrom, Karolinie i Oliwii też chcę podziękować, bo były zawsze moją ostoją i mimo tego, że nigdy nie zrozumiały tego co robię (nie szkodzi, kiedyś Wam wytłumaczę) to wierzyły, że mogę wszystko. Tak więc dzięki max i dzięki też za głupkowanie i nasze imprezki, gdyby nie to wszystko to pewnie bym nie wytrzymała.

UNIVERSITAT ROVIRA I VIRGILI
ORGANIC TRANSFORMATIONS USING TRANSITION METALS AND PHOTOREDOX CATALYSTS
Klaudia Michaliszyn

Financial Support

The present doctoral thesis has been made possible thanks to funding received from the ERC project (648304 — GREENLIGHT_REDCAT).

European Research Council
Established by the European Commission

UNIVERSITAT ROVIRA I VIRGILI
ORGANIC TRANSFORMATIONS USING TRANSITION METALS AND PHOTOREDOX CATALYSTS
Klaudia Michaliszyn

List of publications

- Klaudia Michaliszyn, Ekaterina S. Smirnova, Alberto Bucci, Vlad Martin-Diaconescu and Julio Lloret-Fillol. "Well-defined Nickel P_3C Complexes as Hydrogenation Catalysts of *N*-Heteroarenes Under Mild Conditions" (submitted not accepted yet)

UNIVERSITAT ROVIRA I VIRGILI
ORGANIC TRANSFORMATIONS USING TRANSITION METALS AND PHOTOREDOX CATALYSTS
Klaudia Michaliszyn

Table of contents

Chapter III

Chapter IV

Chapter V

Chapter VI

Summary

The increasing global energy demand creates the need for the transition into greener and more sustainable methods to produce fuel and high-energy organic molecules, which are still challenging solutions. Nature offers high functional machinery – natural photosynthesis - to store sunlight energy into chemical bonds to sustain life and its only byproduct is molecular oxygen. Therefore, mimicking the natural system by the application of artificial photosynthetic (AP) schemes could be one of the green alternatives to produce solar fuels and solar organic molecules from CO_2, water and sunlight as a driving force. The chemical processes involved in AP include water splitting and CO_2 reduction. To make these photosynthetic processes more efficient, they should rely on robust and inexpensive photocatalytic materials. Consequently, new designed modular catalytic systems are required to understand the factors to control the catalytic activity and selectivity in sustainable manner.

This thesis discloses the fundamental understanding of the chemical processes occurring in AP schemes together with their application to produce fuel and fine organic molecules. Therefore, we describe the synthesis and characterization of new family of molecular cobalt catalysts based on aminopyridyne ligands for photocatalytic water reduction (WR) and light-driven organic transformations. The modularity and versatility of the ligand allowed us to change its electronic and structural features resulting in tuning the first coordination sphere of the metal complex. These modifications led us to desired ligand structures, efficient in hydrogen evolution reaction (HER) and organic transformations.

The high modularity of these systems allows to modify also the secondary coordination sphere of metal center. In this regard, the cobalt system with π–π stacking blocks was encapsulated into γ-cyclodextrins cavity to enhance the aggregations and solubility in aqueous solvents. We demonstrate the encapsulation in fluorescence studies and in the enhanced reactivity towards H_2 production in aqueous solvents.

Furthermore, the development of light-independent selective hydrogenation based on nickel P_3^C systems is also described as a method for hydrogen utilization. To remark is the unprecedented selectivity towards N-heterocycles with very good functional group tolerance. Detailed reactivity was studied based on NMR, isotopic labelling and DFT calculations point the heterolytic activation of the dihydrogen molecule after forming adduct trans to the metalated carbon.

This thesis opens new ways for novel sustainable generation and use of hydrogen.

List of Abbreviations

In this doctoral thesis, the abbreviations and acronyms most commonly used in organic chemistry are based on the recommendations of the ACS "Guidelines for authors" which can be found at https://pubs.acs.org/userimages/ContentEditor/1218717864819/joceah_abbreviations.pdf

General Abbreviations

[ ] Concentration
Å Angstrom
aq. Aqueous
bpy 2,2′-bipyridyl
cat catalyst
CV cyclic voltammetry
δ chemical shift
DFT Density functional theory
$E_{1/2}$ electrochemical potential
eq equivalent
eV electronvolt
HOMO Highest Occupied Molecular Orbital
K Kelvin
kcal kilocalorie
KIE Kinetic isotope effect
LUMO Lowest Unoccupied Molecular Orbital
max Maximum
min minute (s); minimum
mM milimolar (milimoles per liter)
PET Photoinduced Electron Transfer
PC Photocatalyst
RT Room Temperature
s second (s)

S0 Single Ground State

S1 Single Excited State

SET Single Electron Transfer

SM Starting Material

SPS Solvent Purification System

t time

T Temperature

T1 Triplet Excited State

TOF Time-Of-Flight; turnover frequency

TON Turnover Number

Characterization Techniques

Anal Combustion Elemental Analysis

AIS Automatic Identification System

Bp Boiling Point

CI Chemical Ionization

EI Electron Impact

EPR Electron Paramagnetic Resonance

ESR Electron Spin Resonance

ESI Electrospray Ionization

FAB Fast Atom Bombardment

FID Flame Ionization Detector

GC Gas Chromatography

HRMS High-Resolution Mass Spectrometry

MALDI Matrix-Assisted Laser Desorption Ionization

MS Mass Spectrometry

m/z mass-to-charge ratio

TLC Thin-Layer Chromatography

NMR

Nuclear Magnetic Resonance

δ Chemical shift in parts per million downfield from tetramethylsilane

J Coupling Constant (in NMR spectrometry)

ppm part(s) per million

br Broad

s Singlet

d Doublet

dd Doublet of doublets

ddd Double doublet of doublets

ddt Double doublet of triplets

t Triplet

td Triplet of doublets

tdd Triplet doublet of doublets

q Quartet

m Multiplet

Organic Abbreviations

Ar Aryl

Boc tert-butoxycarbonyl

Bpin Bis(pinacolato)diboron

DABCO 1,4-diazabicyclo[2.2.2]octanedansyl 5-(dimethylamino)- 1-naphthalenesulfonyl

DCM Dichloromethane

DIPEA Diisopropyl ethyl amine

DMAP 4-(N,N-dimethylamino)pyridine

DMF Dimethylformamide

DMSO Dimethyl Sulfoxide

Et_2O Diethylether

Et_3N Triethylamine

EtOAc Ethyl acetate

EtOH Ethanol

Me Methyl

MeCN Acetonitrile

MeOH Methanol

NHC N-heterocyclic Carbene

OTf Triflate

Ph Phenyl

Py Pyridine

TBABr Tetrabutylammonium Bromide

TBS *tert*-butyldimethylsilyl

THF Tetrahydrofuran

Structures and Abbreviations of the Catalysts

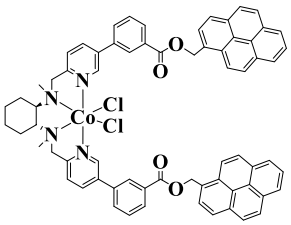

$[Co(^{PyB}mcp)Cl_2]$

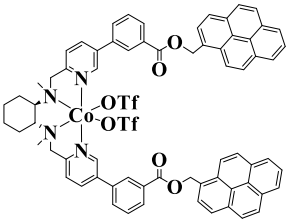

$[Co(^{PyB}mcp)(OTf)_2]$

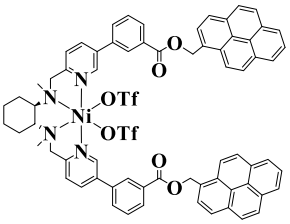

$[Ni(^{PyB}mcp)(OTf)_2]$

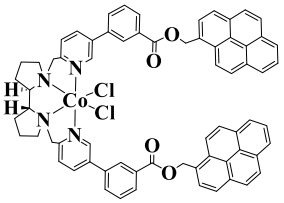

$[Co(^{PyB}pdp)Cl_2]$

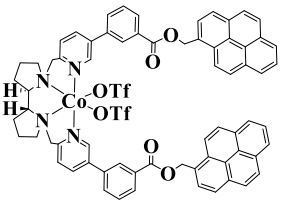

$[Co(^{PyB}pdp)(OTf)_2]$

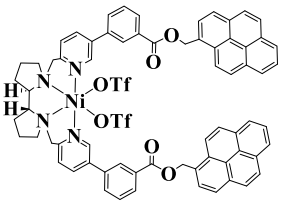

$[Ni(^{PyB}pdp)(OTf)_2]$

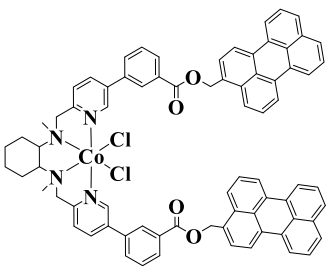

$[Co(^{PerB}mcp)Cl_2]$

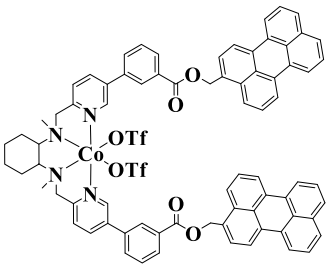

$[Co(^{PerB}mcp)(OTf)_2]$

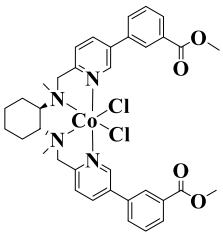

$[Co(^{CO2MeB}mcp)Cl_2]$

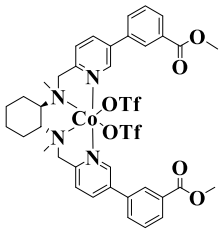

$[Co(^{CO2MeB}mcp)(OTf)_2]$

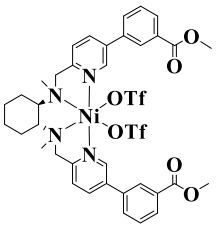

$[Ni(^{CO2MeB}mcp)(OTf)_2]$

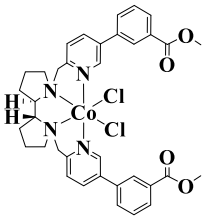

$[Co(^{CO2MeB}pdp)Cl_2]$

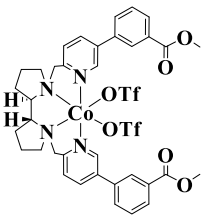

$[Co(^{CO2MeBpdp})(OTf)_2)]$

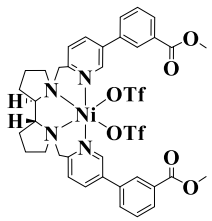

$[Ni(^{CO2MeB}pdp)(OTf)_2]$

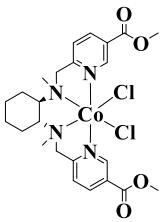

$[Co(^{CO2Me}mcp)Cl_2]$

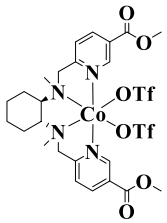

$[Co(^{CO2Me}mcp)(OTf)_2]$

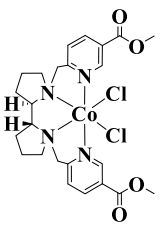

$[Co(^{CO2Me}pdp)Cl_2]$

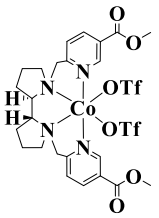

$[Co(^{CO2Me}pdp)(OTf)_2]$

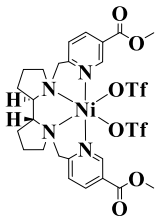

$[Ni(^{CO2Me}pdp)(OTf)_2]$

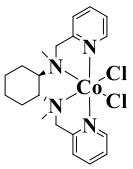

$[Co(mcp)Cl_2]$

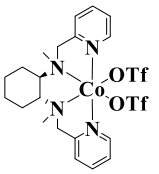

$[Co(mcp)(OTf)_2]$

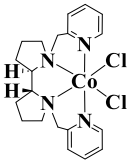

$Co(pdp)Cl_2$

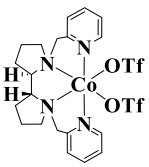

$Co(pdp)(OTf)_2$

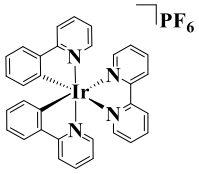

$[Ir(ppy)_2bpy]PF_6$ (PSIr)

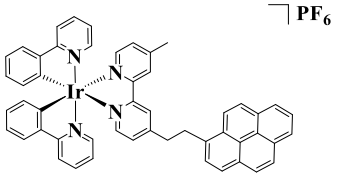

PSIrpyrene

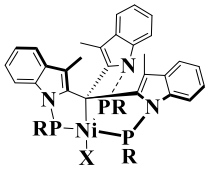

NiTIM(PPh$_2$)$_3$Br R = Ph$_2$, X = Br

NiTIM[P($^{p\text{-}Me}$**C$_6$H$_4$)$_2$]$_3$Br** R = ($^{p\text{-}Me}$**C$_6$H$_4$)$_2$

NiTIM[P($^{p\text{-}F}$**C$_6$H$_4$)$_2$]$_3$Br** R = ($^{p\text{-}F}$**C$_6$H$_4$)$_2$

NiTIM(PPh$_2$)$_3$NTf$_2$ R = Ph$_2$, X = NTf2

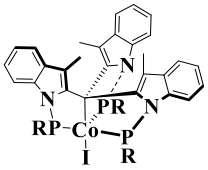

CoTIM(PPh$_2$)$_3$I R = Ph$_2$

CoTIM[P($^{p\text{-}Me}$**C$_6$H$_4$)$_2$]$_3$I** R = ($^{p\text{-}Me}$**C$_6$H$_4$)$_2$

CoTIM[P($^{p\text{-}F}$**C$_6$H$_4$)$_2$]$_3$I** R = ($^{p\text{-}F}$**C$_6$H$_4$)$_2$

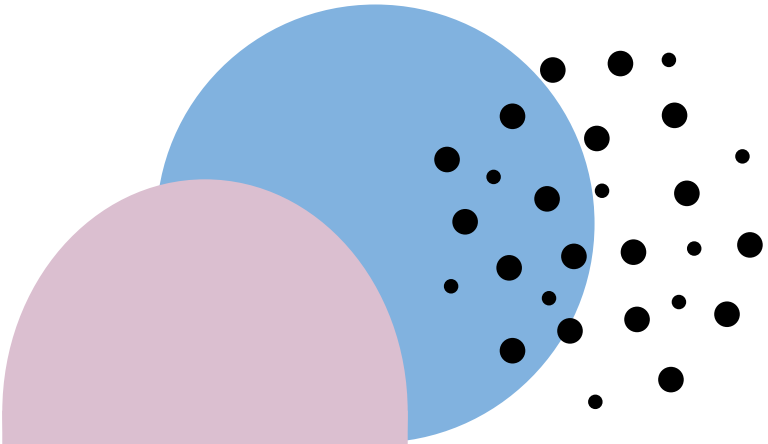

Chapter I

General Introduction

UNIVERSITAT ROVIRA I VIRGILI
ORGANIC TRANSFORMATIONS USING TRANSITION METALS AND PHOTOREDOX CATALYSTS
Klaudia Michaliszyn

UNIVERSITAT ROVIRA I VIRGILI
ORGANIC TRANSFORMATIONS USING TRANSITION METALS AND PHOTOREDOX CATALYSTS
Klaudia Michaliszyn

I.1 Global energy crisis

The reduction of the global energy demand and climate change is central in the massive and global transition to sustainable and renewable energy that the world is facing. However, world's energy demand increases to meet requirements of growing population. The world energy demand is expected to increase the energy consumption of about 48% from 2015 to 2040, where 80% of total final energy consumption is sustained by fossil fuels (See Figure I.1). In this context, the most challenging problem to overcome is the high consumption of fossil fuels that leads to the ecosystem damage by emission of the greenhouse gases into the atmosphere, hence global warming and the exhaustion of non-renewable resources.[1]

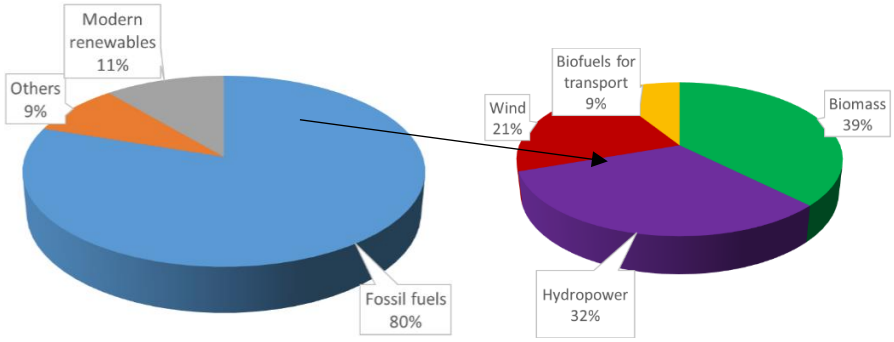

Figure I. 1 *Estimated Renewable Share of Total Final Energy Consumption, 2019.*

The increase of the CO_2 concentration in the atmosphere is behind the raise of global surface temperature during the last century (0.74 ± 0.18 ºC), that provoke the new extreme climate patterns, the rise of the sea level, the expansion of deserts and the retreat of glaciers.[2] The increasing energy demand will aggravate the problem in future, therefore carbon-based energy fuels need to be replaced for more sustainable sources of energy.

Therefore, to substitute the fossil fuels, it is required to find non-polluting, carbon-neutral, sustainable and renewable energy sources, economic comparable to these currently in use. In this regard, sunlight as the most abundant Earth´s energy source is an optimum energy source because of its availability, high density and it is cost-free. Indeed, solar energy due to the

accessibility in almost all planet regions exceeds other renewable energy sources. Human total energy consumption will be no less than 30 terawatts per year by 2050, but it can be covered by Earth's insolation since it over 120 000 terawatts of power per year.[3-5]

Undoubtedly, sunlight is very appealing energy source to fulfill the world energy needs. Nevertheless, the day/night cycles hinder the permanent energy supply and to overcome this problem a convenient energy storage system is required.[6] The application of the artificial photosynthesis mechanism to store the solar energy into chemical bonds is eligible, because of the easy transport and high energy storage densities of the chemical fuels, therefore it can be one of the possible methods applied for this purpose.

Hydrogen (H_2) has the highest specific enthalpy (140 MJ/Kg) among all chemical fuels, which makes it promising chemical energy carrier. Furthermore, its application represents one of the most promising approaches regarding sustainability and energy security due to the environmentally benign features of the oxidation of hydrogen (by combustion or in a fuel cell) that yields water as its only byproduct. Hydrogen fuel has the potential to meet the needs of world energy demand and avoid undesirable greenhouse gas emissions. Additionally, both water and sunlight are world abundant and inexhaustible, hence solar-driven hydrogen synthesis can be achieved on a large scale.

I.2 Conversion of solar energy into chemical energy in nature: Natural Photosynthesis

Natural photosynthesis is a complex system that converts light energy into chemical energy. This chemical energy is stored into the organic molecules of biomass, which is composed of mainly carbohydrates by reducing CO_2, using water as source of protons and electrons, and solar energy as a driving force. Photosynthesis is a complex natural machinery, which consists of light driven process (Kok cycle) and light independent process (Calvin cycle) that occurs in plants, algae and cyanobacteria (Scheme I.1).

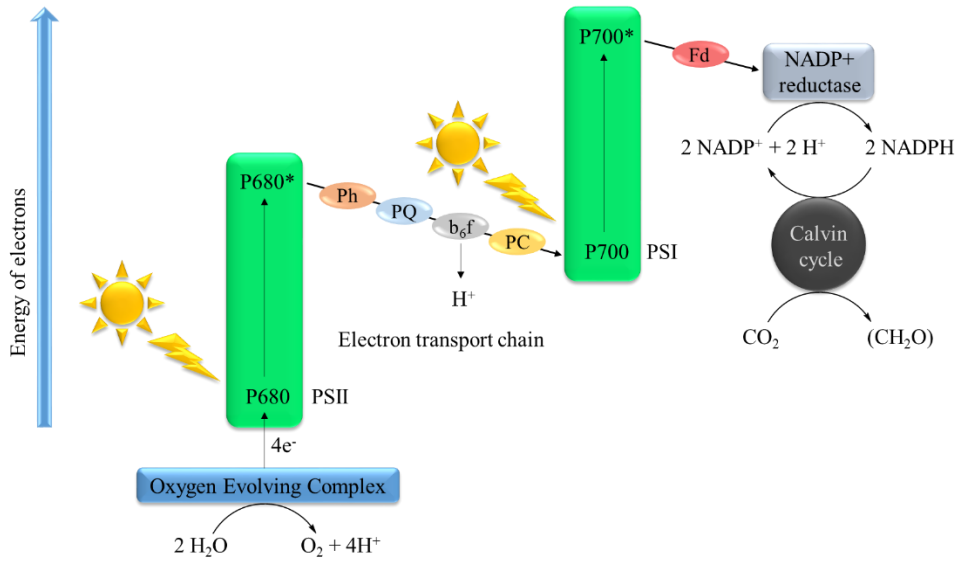

Scheme I. 1 *Energy diagram for electron transfer of light-driven process of natural photosynthesis (Z-scheme) and light independent process (Calvin cycle). Ph = Pheophytin, PQ = Plastoquinone, PC = Plastocyanin, b6f = Cytochrome b_6f complex, Fd = ferredoxin, P680 and P700 = light-harvesting complexes containing reaction centers, located in PSII and PSI respectively.*

Light driven reactions of photosynthesis are performed by three major protein complexes embedded in the thylakoid membrane of chloroplasts: Photosystem II (PSII), Cytochrome b_6f complex (b_6f) and Photosystem I (PSI).[7, 8] The energy transfer of light-driven processes of natural photosynthesis can be illustrated with the ¨Z-scheme¨ that gives the sequence of electron flow (oxidation and reduction) with an energy perspective.

PSII is the first of major proteins involved in the light-driven reactions. The role of this enzyme is to capture the photon from the sunlight energy by chlorophylls present in the light harvesting complexes of PSII. The energy of the photon is transported to chlorophyll P680, which leads to its excited form P680*, and this promotes the water oxidation by the Oxygen Evolving Complex (OEC) to dioxygen, releasing 4 electrons and 4 protons ($2\ H_2O \rightarrow O_2 + 4H^+ + 4e^-$). Protons obtained from water oxidation facilitate the proton gradient generation that triggers ATP synthesis.[9] The electrons generated in the oxidation of water are transferred from PSII to PSI by different redox mediators through electron transport chain. First, electrons are transferred from excited

chlorophyll P680* to pheophytin (Ph, the primary acceptor) and recovering chlorophyll P680 at the same time. Next, electrons from Ph reduce plastoquinone (PQ) to plastoquinol (PQH_2). The electron transfer from PQH_2 to plastocyanin is catalyzed by cytochrome b6f complex to plastocyanin (PC) and linking two major light-dependent proteins, PSII and PSI. In the PSI, the energy of the photon is transferred to chlorophyll P700, which gets excited to form P700*. An electron is then transferred through ferrodoxin (Fd) to NADP+ reductase, where the reduction of NADP+ to NADPH occurs. The sunlight energy stored in the chemical bonds of energy rich molecules, ATP and NADPH is used to reduce CO_2 to carbohydrates in the light-independent reactions of Calvin cycle. Therefore, natural synthesis stands as an excellent example of highly efficient catalytic solar-energy-converting method for synthesis of energy rich molecules as a high energy storage system.

I.3 Towards artificial photosynthesis

Inspired by the function of natural photosynthesis and its discovery path to reveal the secret of this extraordinary machinery, various attempts to mimic this process artificially were taken.[6, 10-12] Development of sustainable and environmental benign organic methodologies based on the application of artificial photosynthetic schemes to produce solar fuels and fine chemicals is still challenging.[13] Water oxidation and CO_2 reduction processes demand multiple electronic and protonic stages and they are still consider bottlenecks for the development of efficient artificial photosynthesis. Great effort is required to understand and overcome the challenges related to:

- Light harvesting;
- Charge separation;
- Light-driven water oxidation to O_2 (Eq. I.1) – source of electrons;
- Reduction of water to H_2 (Eq. I.2);
- CO_2 reduction either to CO, formic acid or methanol (Eq. I.3-5) – using electrons produced in water oxidation process.[14]

The study of photosynthesis is very difficult due to many reactions with similar thermodynamic reduction potentials (Eq. I.3-5) and charge transfer transformations involved in the CO_2 reduction, that impede the selectivity of this process.[15] Moreover, high oxidation states at the metal center for water oxidation (Eq. I.4) are needed due to endergonicity of the process. Facilitation of the access to high oxidation states at the metal center may lead to oxidizing damage side reactions.

Water Oxidation half reaction: an energetic ¨uphill¨ reaction

$2H_2O \xrightarrow{h\nu} O_2 + 4H^+ + 2e^-$	$E^o = 1.23$ V $\Delta G^o = 4.92$ eV (113 kcal·mol^{-1})	**(Eq. I.1)**

Proton and selected CO_2 reduction half reactions

$4H^+ + 2e^- \longrightarrow 2H_2$	$E^o = 0.0$ V	**(Eq. I.2)**
$CO_2 + 2H^+ + 2e^- \longrightarrow CO + H_2O$	$E^o = -0.53$ V	**(Eq. I.3)**
$CO_2 + 2H^+ + 2e^- \longrightarrow HCO_2H$	$E^o = -0.61$ V	**(Eq. I.4)**
$CO_2 + 6H^+ + 6e^- \longrightarrow CH_3OH + H_2O$	$E^o = -0.38$ V	**(Eq. I.5)**

In this regard, the development of efficient catalytic system with good catalytic activity together with selectivity that is based on abundant, non-toxic and inexpensive materials for an artificial photosynthesis is required.[16, 17] Therefore, the main scientific challenge is to construct a photocatalytic system able to capture photons, converting them in a redox difference and use it to produce endergonic chemical transformation that then store it in chemical bonds of energy rich molecules (density fuels) such as hydrogen and either CO, methanol, formic acid or methane obtained from H^+ and CO_2 while at the same time producing oxygen from water. These energy storage molecules are used as a simple alternative to the dark process of the photosynthetic cycle. Water oxidation, water and CO_2 reduction are very complex processes, to understand and improve them, it is required to study them separately to achieve better results. In this view, the highly efficient light-driven hydrogen evolution from proton to molecular hydrogen is still under development.

Complexity of catalytic systems used for light-driven proton reduction to molecular hydrogen is still challenging and to make this process highly efficient, new molecular complexes or light-harvesting systems to promote this transformation by photoinduced electron transfer events are required.

I.4 Hydrogen evolution in nature: Hydrogenases

Hydrogen evolution reaction (HER) and its consumption occur in nature with high efficiency mechanism. These processes are catalyzed reversibly by family of natural hydrogenase metalloenzymes. Hydrogenases are divided in three classes, based on the catalytically active metal center of the organometallic structure: [NiFe]-hydrogenases, [FeFe]-hydrogenases, and [Fe]-hydrogenases (Figure I.2).

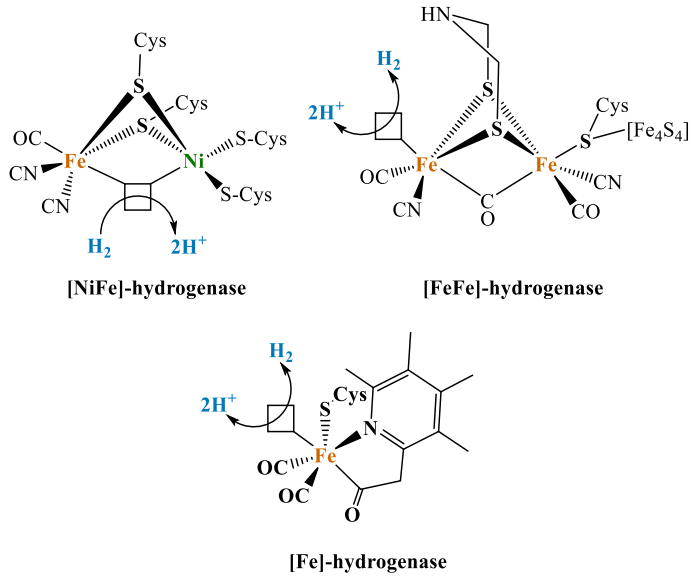

Figure I. 2 *Structures of natural hydrogenase metalloenzymes.*

[NiFe]-hydrogenases consist of two subunits, contain a nickel-iron active metal center, three iron-sulfur clusters and a magnesium ion (in case of [NiFeSe] an iron ion). [FeFe]-hydrogenases contain one or two subunits of iron-sulfur cluster, iron-iron active metal center connected through thiolate of a cysteine unit. [Fe]-hydrogenases are composed of unique iron-guanylylpyridinol cofactor.[18] The X-ray structures of all the above mentioned hydrogenases

show in their octahedral structure at least one iron in the active completed with CO, CN or thiolates.[19-23] However, one of the most important structural features of hydrogenases is a pendant amine, which is located near to metal, but not close enough to form a strong bond with metal center. The role of this base in the second coordination sphere act as a proton relay, which approaches protons to the metal center[24] and facilitates the heterolytic cleavage of H_2 and the transfer of the resulting proton to a proton-conduction channel leading to the exterior of the enzyme. DFT calculations show that pendant amine in hydrogenases leads to an energetic enhancement in the protonation of the metal.[25]

The role of hydrogenases in hydrogen evolution is not very well understood, however these enzymes use low-potential electrons and protons to produce H_2, that is one of the most promising clean and renewable fuels (if produced from carbon-neutral energy sources).[26]

$$\mathbf{H_2 \rightleftharpoons H^+ + H^- \rightleftharpoons 2H^+ + 2e^-}$$

The function of hydrogenases is to uptake and produce H_2. [NiFe]-hydrogenases show higher activity in H_2 oxidation, while [Fe]- and [FeFe]-hydrogenases in hydrogen evolution and their activity is very high, able to produce up to 10^4 molecules of H_2 per second. However, [NiFe]-hydrogenases have higher affinity for hydrogen and lower sensitivy to oxygen and carbon monoxide.[18, 23]

The application of hydrogenases in hydrogen production as an energy source to solve the world´s energy demand has been growing over the past few years. Many bio-inspired synthetic models of hydrogenases were developed to understand the role of the active site of natural metalloenzymes and to improve the evolution process of efficient and stable catalysts for H_2 production.[27]

I.5 Molecular complexes for light-driven H_2 evolution

The development of highly efficient catalysts for hydrogen production that to form H_2 requires the reduction of two protons by two electrons could have a remarkable impact on the feasibility of future energy production systems.

Hydrogenases and platinum metal can catalyze hydrogen evolution reaction in an efficient manner. The heterogenase metalloenzymes demonstrate that to catalyze this reaction, expensive precious metals are not needed because these enzymes use situated in their active sites either iron or iron in combination with nickel. X-ray crystallography of hydrogenases active sites provided information required for the development of similar but simpler structural active sites to develop effective and robust synthetic catalysts and probing its mechanistic features. More molecular photo-catalysts for hydrogen evolution reaction based on first row transition metal complexes will be discussed in following sections.[28]

I.5.1 Catalysts based on Cobalt

Although cobalt has no biological relevance for the catalytic water splitting into hydrogen, it has emerged as a major metal in the HER.[29, 30] Cobalt-based catalysts were found to be active in light-driven hydrogen production decades ago. However, the cobaloxime catalysts (**Cat.I.1-8**) in effect of detailed electrocatalytic studies found their application in photocatalytic studies in the mid-2000s.[31-35] Since then many homogeneous[29] and heterogeneous[36] photocatalytic systems based on cobaloxime catalysts such as multicomponent or supramolecular photosensitizer-catalyst assemblies were reported, showing activity in both organic and organic-aqueos solutions[37, 38].[39-56] The drawback of the system containing cobaloxime catalysts is its low stability in the reduced state and in water due to the hydrolysis of ligand, which limits their efficiency and applicability. Stability of these complexes could be slightly improved by using imine/oxime systems to avoid hydrolysis of ligand because of presence of the carbon bridge.

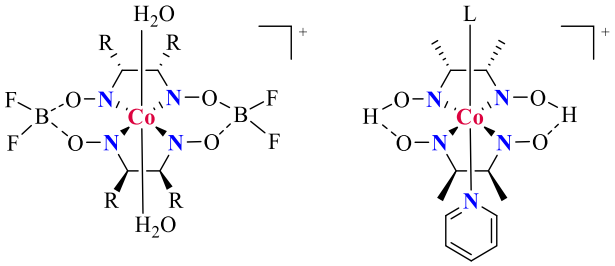

Cat.I.1 R = Me
Cat.I.2 R = Ph
Cat.I.3 L = Cl
Cat.I.4 L = py

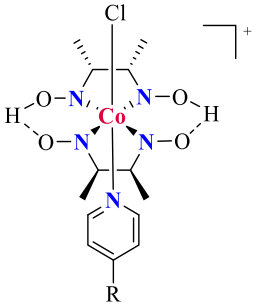

Cat.I.5 $R = NMe_2$
Cat.I.6 $R = CONH^tBu$
Cat.I.7 $R = CO_2Me$
Cat.I.8 $R = PO_3H_2$

Figure I. 3 *Cobaloxime catalysts for H_2 evolution.*

Inspired by $[Co(bpy)_3]^{2+}$ based system from the work of Sutin and co-workers in 1980, the development of more efficient and applicable catalysts for photocatalytic hydrogen evolution based on aminopyridine and polypyridyl ligands has been started. Cobalt(II)-polypyridyl and -aminopyridine catalysts started new chapter for cobalt-based catalysts used in hydrogen evolution (**Cat.I.9-16**).[57-62] The polypyridyl and aminopyridine based complexes revealed higher stability under both reductive and aqueous conditions than the parent $[Co(bpy)_3]^{2+}$ or cobaloximes. These ligands allow direct modification of structural and electronic properties of the complexes, therefore tuning their catalytic activity.[63] These properties have generated growing interest in designing new electro- and photocatalytic systems based on cobalt(II)-polypyridil and –aminopyridine complexes.

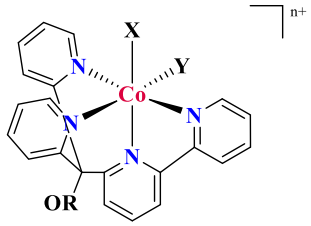

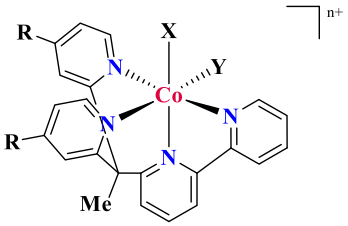

Cat.I.9 R = H, X = Br, no Y, n = 1
Cat.I.10 R = H, X = Y = CH_3CN, n = 2
Cat.I.11 R = Me, X = Y = CH_3CN, n = 2
Cat.I.12 R = H, X = CH3CN, Y = OTf, n = 1
Cat.I.13 R = CF_3, X = Y = CH_3CN, n = 2

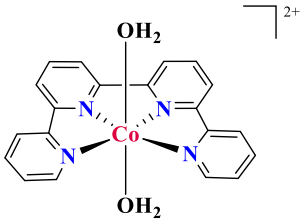

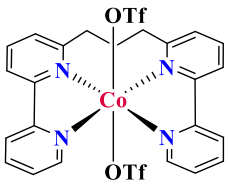

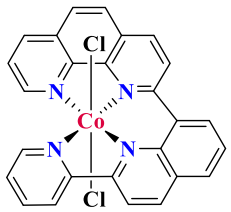

Cat.I.14 **Cat.I.15** **Cat.I.16**

Figure I. 4 *Tetradentate bipyridine-based ligands and their corresponding cobalt(II) complexes.*

In 2010, Chang and co-workers reported the first tetradentate cobalt(II)-polypyridyl electrocatalyst stable in the reduced state for hydrogen evolution. This was the starting point of effort that had been devoted to design of polypyrydil ligands and according complexes in photocatalytic hydrogen evolution.[64] In this regard, electronically modified complexes **Cat.I.12** and **Cat.I.13** by replacing OMe with Me in **Cat.I.12** and bearing substituted by CF_3 pyridine in **Cat.I.13**[65] could modulate the onset potential in proton reduction by modulation of the redox potential of $Co^{II/I}$ couple. Electrocatalytic experiments revealed that introduction of electron withdrawing group CF_3 decreases the electrocatalytic current, therefore the activity of Co^{I} species.[66]

The activity of bis-aqua catalyst (**Cat.I.14**) for hydrogen evolution was reported in 2012 by Lau and co-workers. This cobalt-based catalyst, in combination with iridium photoredox catalyst $[Ir(ppy)_2(bpy)]^+$ or $[Ir(dFCF_3ppy)_2(dtbbpy)]^+$, sacrificial electron donor TEOA and p-cyanoanilinium tetrafluoroborate as proton source showed to be active under

optimized conditions in acetonitrile/water(95:5) mixture with TON of 58.[67] Moreover, after addition of extra photosensitizer catalysis could be reinitiated. Bis-aqua cobalt complex (**Cat.I.14**) was reevaluated by Long, Chang, Castellano and co-workers. The catalytic system combined of cobalt catalyst in combination with $[Ru(bpy)_3]^{2+}$, ascorbic acid as electron donor at pH 5.5, performed in fully aqueous media reached the TON of 200. The catalytic activity of this catalyst is ranked among the less active polypyridyl catalysts comparing with performance of other cobalt-based complexes under the same conditions (150 – 1850 TON for catalysts **Cat.I.9-15** and **Cat.I.17-22**).[65] Long, Chang, Castellano and co-workers demonstrated for the first time photocatalytic activity under fully aqueous conditions of family of complexes in the presence of $[Ru(bpy)_3]^{2+}$ with ascorbate buffer at pH 7 (**Cat.I.17-19**), which were previously described as electrocatalysts.[66, 68] In these studies, **Cat.I.17** showed the highest activity under photocatalytic conditions (8 h of visible light radiation λ = 452 nm), producing double amount of H_2 than its analog **Cat.I.19.**[65, 66, 68, 69]

The same group of scientists expanded the family of cobalt-based complexes by structural changes of **Cat.I.17-19** (removing one pyridine moiety) to obtain **Cat.I.20-22**. This modification allow the direct comparison of tetra- and pentadentate cobalt catalysts.[65]

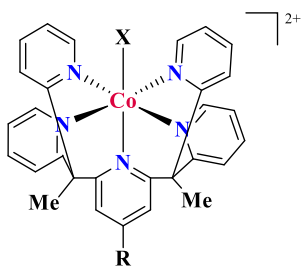

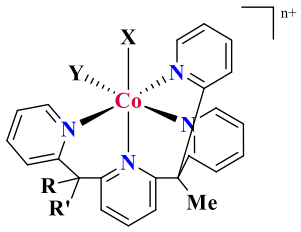

Cat.I.17 R = CF_3, X = H_2O or CH_3CN
Cat.I.18 R = H, X = H_2O or CH_3CN
Cat.I.19 R = NMe_2, X = H_2O or CH_3CN

Cat.I.20 R = R' = H, X = CH_3CN, Y = OTf, n = 1
Cat.I.21 R = Me, R' = H, X = CH_3CN, Y = OTf, n = 1
Cat.I.22 R = R' = Me, X = CH_3CN, no Y, n = 2

Figure I. 5 *Cobalt polypyridyl catalysts for H_2 evolution.*

Complexes based on tetradentate ligands revealed better activity in light-driven HER with 1550 TON (**Cat.I.20**) comparing with 330 TON of pentadentate

Cat.I.18. These results are relevant only for tested catalytic systems (**Cat.I.17-22)**, because there is no straightforward tendency in other related systems.[70, 71] However, catalytic systems based on tetradentate ligands fare better compared to some pentadentate systems. During catalysis, some pentadentate catalysts, structurally related to abovementioned complexes face decoordination of one pyridine units influencing catalytic activity.[72, 73]

New pentadentate cobalt complex containing bipyridine in the ligand backbone have been reported by Alberto and co-workers.[71] **Cat.I.23** (Figure I.6) has Bpy_2py coordination sphere and it revealed to be active in hydrogen evolution reaction with TON of 1380 in aqueous solution. **Cat.I.24** and **Cat.I.25** are another complexes based on bpy_2py ligands reported by Chang, Long, Castellano and coworkers.[69] It was demonstrated by electrocatalytic studies that **Cat.I.25** bearing electron-withdrawing CF_3 showed lower activity (1630 TON) than **Cat.I.24 (**1390 TON**)** in photocatalytic water reduction. Complexes based on bipyridine have been proposed to undertake ligand-centered redox processes.[63, 74]

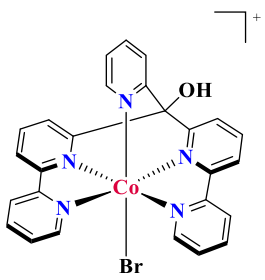

Cat.I.23

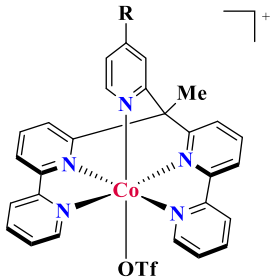

Cat.I.24 R = H
Cat.I.25 R = CF_3

Figure I. 6 *Cobalt bipyridine catalysts for H_2 evolution.*

Inspired by the good performance of cobalt polypyridine based catalysts, aminopyridine pentadenate complexes (**Cat.I.26-28,** Figure I.7) were developed by Webster, Zaho and co-workers. $[Co(DPA\text{-}Bpy)(OH_2)]^{3+}$ (**Cat.I.26**) was evaluated in light-driven H_2 evolution in purely aqueous solution and it displayed to be active (2100 TON).[75] The same authors reported another pentadentate complex (**Cat.I.27**), obtained by structural modification

of **Cat.I.26** by replacing two pyridine moieties by isoquinolines moieties.[76] The structural and electronic modification improved the photocatalytic efficiency by over 2 fold (5400 TON). In 2015, inspired by great performance of **Cat.I.26** and **Cat.I.27**, new cobalt complex was designed by modification of **Cat.I.26**, by replacing the bipyridine moiety to obtain **Cat.I.28** ([Co(DPA-Dmphen)(OH_2)]$^{2+}$ complex (Dmphen = 9-methyl-1,10- phenanthrolin-2-yl)methyl]bis-(pyridin-2-ylmethyl)amine)).[77] The photocatalytic performance of **Cat.I.28** was examined in combination with photosensitizer [Ir(ppy)$_2$(bpy)](PF_6) and Et_3N as sacrificial electron donor revealing low activity under applied conditions (210 TON).

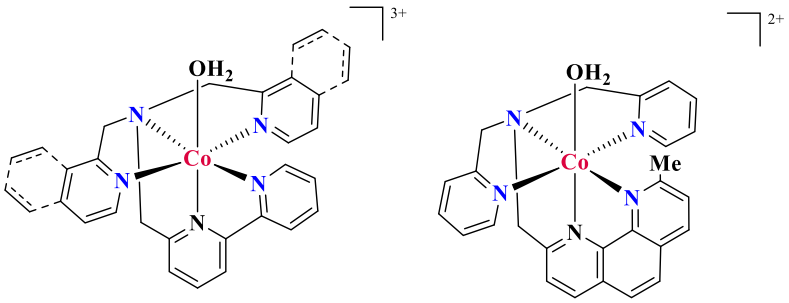

Cat.I.26 R = H
Cat.I.27 R = benzene

Cat.I.28

Figure I. 7 *Cobalt aminopyridine catalysts for H_2 evolution.*

I.5.2 Mechanism of Hydrogen Evolution Reaction in Cobalt-based systems

Light-driven hydrogen evolution reaction catalyzed by cobalt-based systems may be performed through homolytic or heterolytic pathway (Figure I.8).

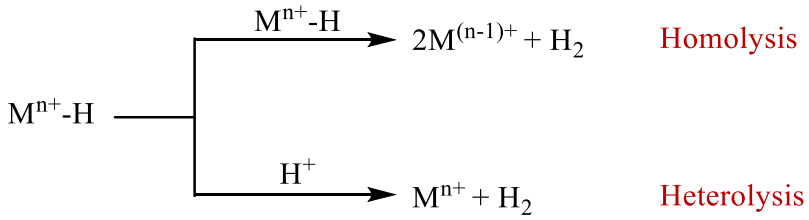

Figure I. 8 *Proposed homolytic and heterolytic HER pathways.*

The key intermediate to evolve H_2 of both mechanisms is the generation of cobalt hydride species (Co^{III}-H) through the oxidative protonation of Co^{I} intermediate.[29, 78-85]

In the homolytic pathway, two metal hydride complexes ($2M^{n+}$-H) evolve H_2 through the hemolytic cleavage of two Co^{n+}-H (Figure I.9). During the reaction time, either before the protonation (Figure I.9 homolytic 1) or after formation of the Co^{III}-H species (Figure I.9 homolytic 2), a single electron reduces each metal center.[31, 35, 86] In case of heterolytic pathway, the metal hydride intermediate Co^{n+}-H undergoes a protonation and evolves hydrogen.

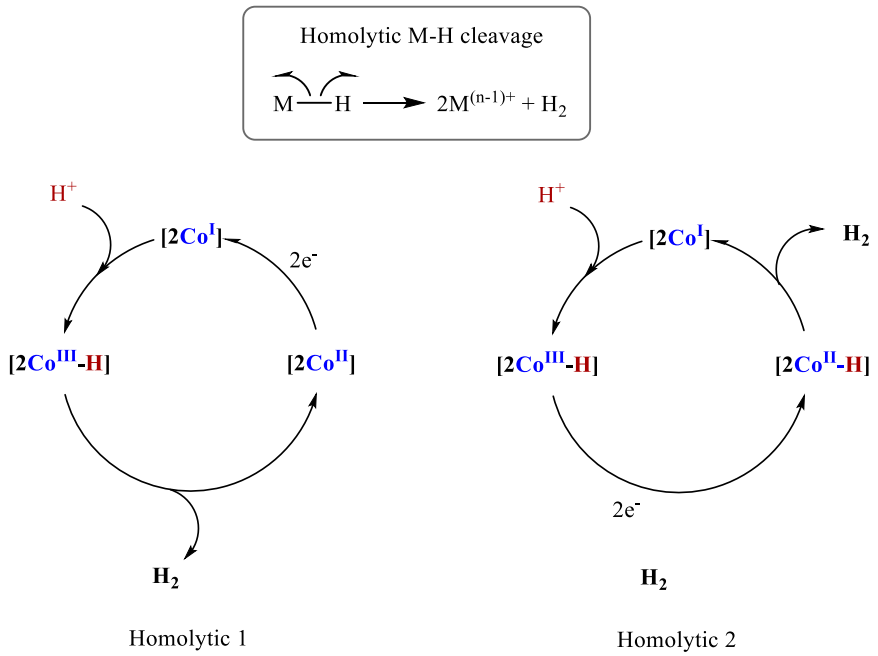

Figure I. 9 *Homolytic mechanism for H_2 evolution catalyzed by molecular cobalt complexes. The electrons can be provided by a photoredox catalyst.*

While the reaction occurs, two electrons are transported to the metal center either consecutively (Figure I.10 heterolytic 1), or alternating between two protonation steps (Figure I.10 heterolytic 2). A well-defined differences of these two mechanisms haven't been established, however DFT supported studies on cobaloxime systems revealed the preference for heterolytic mechanism involving a Co^{II}-H species as an intermediate to evolve

hydrogen.[87-89] Electrons involved in the photocatalytic system can be provided by a photoredox catalysts in combination with sacrificial electron donor.

The extensive mechanistic studies, due to the complexity of these systems impede understanding and solving some of the mechanistic details. Main difficulty is to detect the intermediates as Co^{n+}-H species which are the key to understand the mechanism in depth.[90-94] Both mechanistic pathways can coexists,[78, 79] however switching from a heterolytic to a homolytic pathway[33, 95] in a controllable manner is unprecedented.

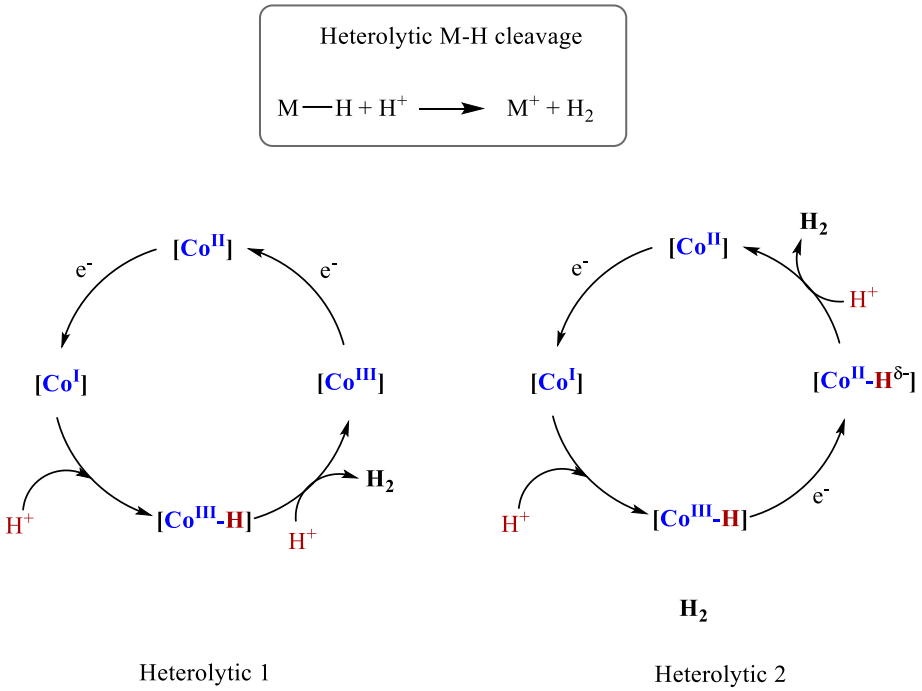

Figure I. 10 *Heterolytic mechanism for H_2 evolution catalyzed by molecular cobalt complexes. The electrons can be provided by a photoredox catalyst.*

Electrocatalytic and photocatalytic HER mechanistic and kinetic studies have been performed with Co-polypyridyl catalysts.[37, 65, 92, 96-99] Heterolytic pathway is proposed as the mechanism for this reaction, engaging Co^{II}-H species, although coexistence of hemolytic pathway is not discarded. However, these systems in comparison to cobaloximes catalysts have been investigated in lesser extent.[35, 79, 86, 94, 100, 101]

I.5.3 Catalysts based on Nickel

Nickel is considered as another great non-noble metal for the design of molecular complexes,[102, 103] due to its easy accessible oxidation states: Ni^0, Ni^I, Ni^{II}, Ni^{III} and Ni^{IV}. Usually in the HER Ni^{II} is reduced to Ni^I, which also involves the geometrical distortion of tetradentate planar coordination of Ni^{II} to a tetrahedral Ni^I.[104-106] Therefore, the redox and coordination properties help to design the ligand scaffolds able to coordinate Ni^{II} and give the complexes certain functions to develop water reduction catalysts. Moreover, nickel has been found to be an active metal center in natural enzymes such as [Ni-Fe]-hydrogenases for reversible conversion of proton and hydrogen,[107, 108] and [Ni-Fe]-dehydrogenases for reversible conversion of CO_2 and CO.[109, 110] These catalytic activities inspired scientists to mimic the natural enzymes by developing molecular catalysts based on nickel. Although intense studies were devoted in the HER[35, 111-118], the activities provided by these model catalysts are negligible compared to those of the natural systems. Moreover, the specific reviews on nickel-based molecular catalysts for energy conversion and storage are not reported as well as structure-activity relationship in the context of light-driven hydrogen production. In the latter case, only Co^{II} polypyridine complexes based on ligands bearing electron-withdrawing and electron-donating groups have been studied.[66, 69, 119, 120] The electrocatalytic studies on these complexes performed by Orio and co-workers[121] revealed that it is still unclear how the modification of ligand affects the reactivity of the catalysts.[122] However, recent reports on cobalt based catalysts suggests that a key element to control and understand the photocatalytic reaction is the position of substituent on the ligand rather than their chemical nature.

The difficulties to mimic the natural [Ni-Fe]-hydrogenase in hydrogen evolution come from the model complexes of this metalloenzyme that have been reported to function only in pure organic solvents, thus any of them use water as proton source.[123] Some [Ni-Fe] biomimetic systems for photochemical hydrogen evolution were reported by Rauchfuss and co-

workers[124] (Cat.I.29-30), and Ogo and co-workers[125] (Cat.I.31) that are shown in the Figure I.11.

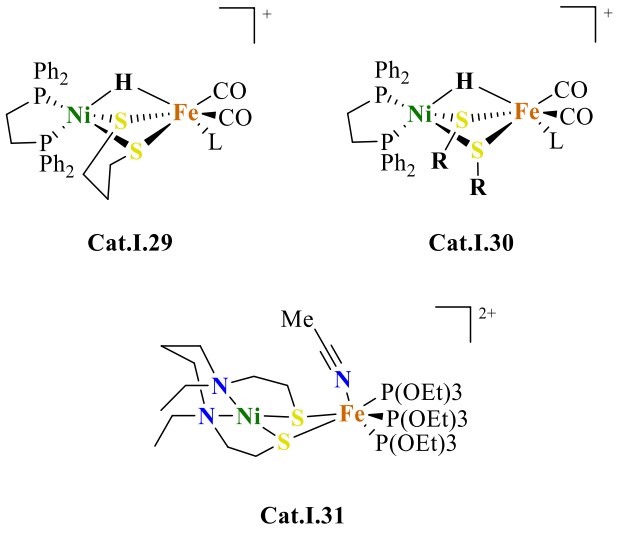

Figure I. 11 *Model [Ni-Fe] systems.*

The conception of pendant amine situated in proximity to vacant coordination site or hydride ligand present in natural enzymes has been used by Dubois and co-workers in the development of nickel-based molecular electrocatalysts with diphosphine ligands containing two pendant amines for the production of hydrogen (Figure I.12).[126]

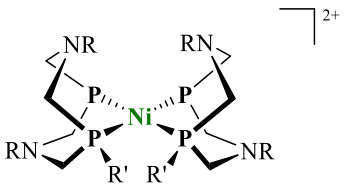

Cat.I.32 R = R' = Ph
Cat.I.33 R = Bz, R' = Ph

Figure I. 12 *Ni-based catalysts for H_2 evolution containing amine pendant arms.*

The pendant amine could play significant role in the catalyst to achieve high activity. Numerous studied report the influence of catalyst structure indicating the influence of the nature of these basic sites.[24, 104, 127-137] Catalytic performance of **Cat.I.32** and **Cat.I.33** showed their activity in hydrogen production with turnover rates of 350 s^{-1} (overpotential 300 mV and 5 s^{-1}

(overpotential 200 mV), respectively.[138, 139] In order to extent their application, Artero and co-workers grafted the DuBois' nickel complex on a carbon nanotube electrode for hydrogen evolution and obtained high stability and activity (more than 100.000 TON).[140] Holland, Eisenberg and co-workers employed described by DuBois catalyst with eosin Y or $[Ru(bpy)_3]^{2+}$ as a photoredox catalyst and ascorbate as a sacrificial electron donor for light-driven hydrogen production from water giving over 2700 TON in this performance.[141]

Nickel thiolate complexes were developed to mimic [NiFe] hydrogenase active site.[123, 142-144] Holland, Eisenberg and co-workers described first nickel(II) complex containing pyridine-2-thiolate ligands $[Ni(pyS)_3]^-$ (pyS = pyridine-2-thiolate) (**Cat.I.34**) with catalytic properties for photocatalytic proton reduction. $[Ni(pyS)_3]^-$ was found to have excellen activity in a homogenous system in combination with fluorescein as an organic photosensitizer and trimethylamine as an electron donor in basic aqueous mixture (1:1 EtOH:H_2O). The rate of hydrogen production achieved turnover number of 5500 moles H_2 per mole of catalyst.[145]

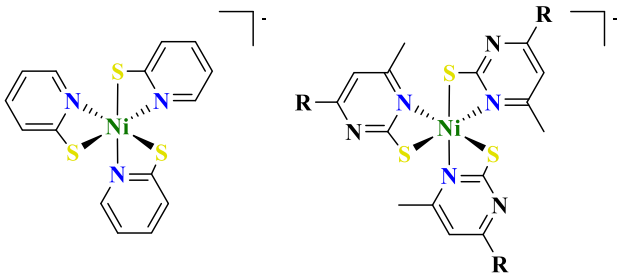

Figure I. 13 *Ni thiolate catalysts for H_2 evolution.*

More revealing was the examination for photo- and electrocatalytic H_2 evolution by pyridyl-and pyrimidylthiolate Ni^{II} catalysts (Figure I.13 **Cat.I.35** and **Cat.I.36**).[146, 147] Mechanistic studies revealed that formation of hydrogen at the nickel ion occurs involving protonation of the pyridine, which transfer

the H^+ to Ni-H intermediate to form H_2. The mechanism of nickel thiolate based catalysts mimics the mechanism of hydrogenases.[127, 143, 148, 149]

Examples of nitrogen based nickel catalysts are quite scarce, however their quite limited scope in hydrogen production is reported in the literature (Figure I.14). First, reported by Fisher and Eisenberg was homogeneous Ni^{II} catalyst for electrocatalytic proton reduction.[150] These studies inspired Collin and Sauvage to develop another macrocyclic nickel complexes $[Ni(cyclam)]^{2+}$ (**Cat.I.37** and **Cat.I.38**) and $[Ni_2(biscyclam)_2]^{4+}$ (**Cat.I.39**), which activities were compared at the same fixed potential (-1.25 V vs. SCE).[151] Under applied conditions $[Ni_2(biscyclam)_2]^{4+}$ (**Cat.I.39**) proved to be the most active (TON up to 100) probably due to the two nickel centers in proximity with Ni-H species as an active intermediate.

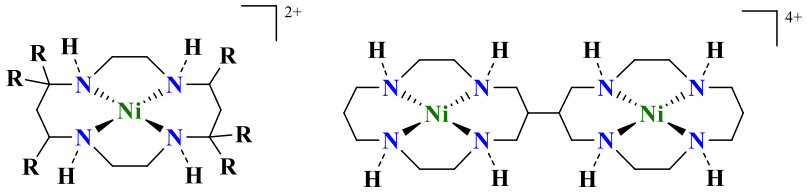

Cat.I.37 R = H
Cat.I.38 R = Me

Cat.I.39

Figure I. 14 *Cyclam-based nickel (II) complexes for water reduction.*

Nickel complexes began to receive more attention and the growing interest led to development of (poly)pyridine based catalysts. Reported by Sun and co-workers molecular nickel catalyst **Cat.I.40** containing internal bases and **Cat.I.41** were found to be very active catalysts under photocatalytic conditions with fluorescein as a photosensitizer and Et_3N as sacrificial donor obtaining turnover numbers of 3230 and 2160, respectively.[38, 152]

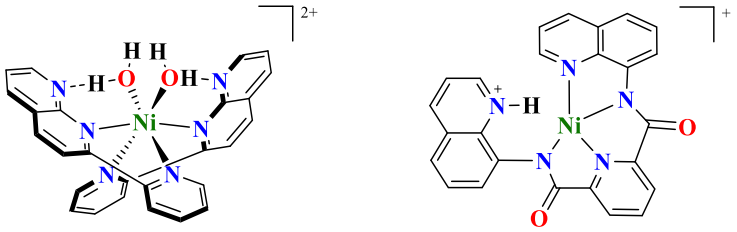

Cat.I.40 **Cat.I.41**

Figure I. 15 *Polypyridine nickel based complexes for photocatalytic proton reduction.*

The photo- and electrocatalytic studies of more nickel complexes based on macrocyclic ligands were carried out by Robert, Lau and co-workers.[153] The series of tetradentate macrocyclic ligands N_3X (X = NH, PPh or S) are shown in Figure I.16 (**Cat.I.42-47**). Catalyst Cat.I.43 bearing phosphorus atom showed the highest photocatalytic efficiency with turnover number of 5000 moles H_2 per mole of catalyst. Under photocatalytic conditions, nickel (0) nanoparticles are formed, which are the real catalytic species for the hydrogen production. However, this event was not observed under electrocatalytic conditions.

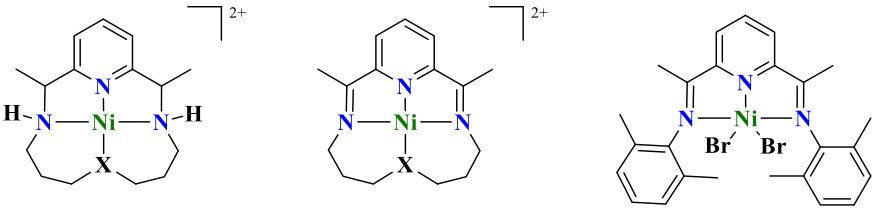

Cat.I.42 X = NH
Cat.I.43 X = PPh
Cat.I.44 X = S

Cat.I.45 X = NH
Cat.I.46 X = PPh
Cat.I.47 X = S

Cat.I.48

Figure I. 16 *Macrocyclic nickel catalysts for H_2 evolution.*

The use of nickel diamine complexes as efficient and stable catalysts for water reduction have become of great interest because they provide the reduction of protons at low overpotentials. Remarkable example of tridentate redox active pincer nickel catalyst (**Cat.I.48**) was reported by Batista, Crabtree and co-workers to reduce protons at a low overpotential (140 mV) with a rate 105 s^{-1} in aqueous acidic solutions.[154] Related structurally to Cat.I.48 pincer ligands were used to support nickel catalysts due to their high impact on stability on

transition metal complexes.[155] The phosphine bearing pincer ligands were examined in electrocatalytic water reduction with excellent results at low overpotentials.[156]

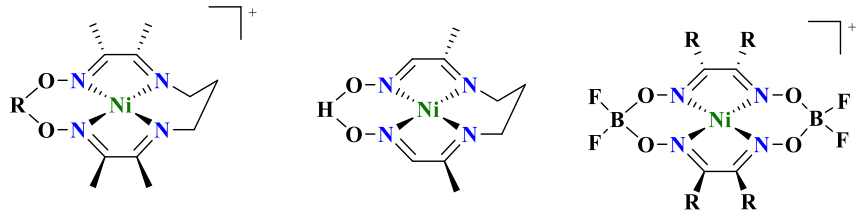

Cat.I.49 R = H
Cat.I.50 R = BF_2

Cat.I.51

Cat.I.52 R = CH_3
Cat.I.53 R = CH_3

Figure I. 17 *Selected Ni^{II} catalysts for water reduction.*

Family of nickel diamine-glyoxime catalysts (Cat.I.49-53) have showed to be effective and stable electrocatalysts activities for hydrogen evolution from acidic nonaqueous solutions with slightly lower overvoltage and much better stabilities towards hydrolysis compared to reported cobaloxime complexes.[157-159]

I.6 Photophysical properties of polycyclic aromatic hydrocarbons

Pyrene and perylene can serve as photosensitizers, and π-stacking units for supramolecular assembling like in the photosynthetic machinery. In particular they are polycyclic aromatic hydrocarbons (PAH) that contain 4 and 5 carbon fused rings (Figure I.18) that generally have low vapor pressure and unfortunately are globally distributed in atmospheric, terrestrial and aquatic systems. Solubility of PAH decreases with the increase of molecular weight or ring structure[160] (solubility of pyrene in water 0.135 mg/L and perylene – 0.0004 mg/L at 25 ^{o}C). The solubility of PAHs is enhanced while incorporated into micelles and host-guest interactions with hydrophilic molecules. Pyrene, perylene and their derivative have been widely used as fluorescence probes as well as models of drugs with low solubility in water.[161-164] Pyrene and perylene own their high stability, high quantum yield and lifetime to polycyclic aromatic structure.

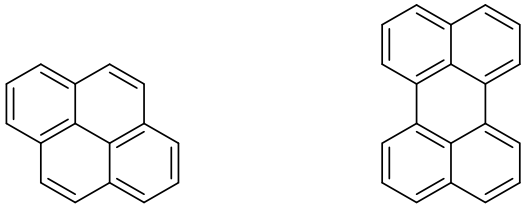

pyrene **perylene**

Figure I. 18 *Structures of pyrene and perylene*

Polycyclic aromatic hydrocarbons (PAHs) bring significant interest because of their unique photophysical and electronic properties, which make them attractive as candidates as chromophores and functional materials in organic electronics.[165-168] The most studied PAH is pyrene, which exhibits blue fluorescence together with high quantum yield ($\Phi = 0.32$)[169],high thermal and photochemical stability, and ability to form self-aggregates by π–π stacking interactions resulting in interesting emissive properties.[170-174] Therefore, pyrene and its derivatives are frequently applied in the development of new fluorescent sensors.[169, 175-182]

I.6.1 Photophysical properties of pyrene

The emission of pyrene monomer occurs between 370 and 420 nm, excimer fluorescence showing as a broad structureless band occurs around 480 nm and the distinction of the monomer and excimer fluorescence bands is straightforward. Stevens and Huttos introduced the term excimer and described it as an excited dimer associated in an electronic excited state and dissociated in the ground state.[183] To form a pyrene excimer, an electronically excited pyrene requires the encounter of a second pyrene in a ground electronic state. Accordingly, when the light is absorbed two pyrene units must be far apart to localize the excitation on only one of them. Consequently, excimer emission indicates the encounter of two pyrenes.[184, 185]

Pyrene became one of the most utilized indicators as a molecular probe of microenvironments due to the ability of the excimer formation, combined with long-lived excited states, high quantum yield, high fluorescence and the sensitivity of the excitation spectra to environmental changes.[186]

The combination of these unique properties of pyrene, has raised the interest to study its photophysical properties and made it become one of the most studied organic molecules. As a chromophore, pyrene is utilized as a probe to measure properties of surfactant micelles, phospholipid vesicles and various aggregates. The investigation of supramolecular design and probing the structural properties of macromolecular system also engage the tendency of pyrene to form excimers.[175] The fluorescence of pyrene and its derivatives excimer has been also applied in sensing the environmental changes as temperature, pressure and pH[187-189] as it affects the fluorescence intensity. It can be also employed in detection of guest molecules such as gases (O_2 or NH_3), metals, organic molecules as well as other analytes.[175, 190-195]

Aromatic hydrocarbons are known to be electron shuttles and it was reported in 1867 that their direct reduction by alkali metals generates strong one-electron donors that have become standard reagents in organic synthesis. Reported by Konig and co-workers one electron reduction of aromatic hydrocarbons, generating their arene radical anions under visible-light photoexcitation and in absence of additional reducing metal.[196] $Ru(bpy)_3^{2+}$ under visible-light irradiation acts as a sensitizer in the presence of polycyclic aromatic hydrocarbons (as catalytic units) and initiate an energy transfer between triplet-excited $^3[Ru(bpy)_3^{2+}]^*$ and the aromatic acceptors.[197]

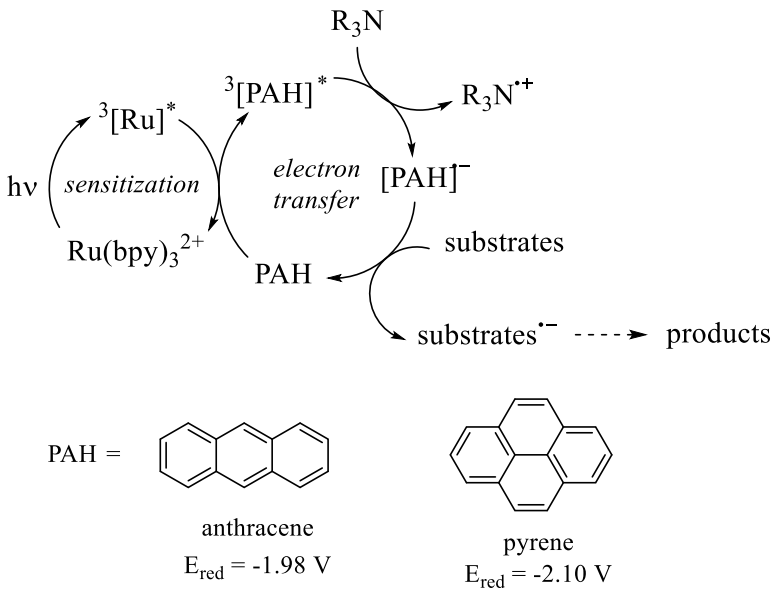

Scheme I. 2 *Visible light sensitization initiated electron transfer for the photocatalytic generation of arene radical anions (redox potentials are vs. SCE).*

The arenes' triplet states $^3[PAH]^*$ undergoes one electron reduction by sacrificial electron donor (tertiary amines) to provide strongly reducing ground state arene radical anions $[PAH]^{\cdot-}$ (Scheme I.2). Particularly important in this electron transfer steps is the adjusting between the triplet energy donor $Ru(bpy)_3^{2+}$ and the aromatic acceptors, together with the higher rate of energy transfer between the excited ruthenium photosensitizer and the arenes in comparison with the competing photoelectron transfer between the $^3[Ru]^*$ and the sacrificial electron donor. This new approach called "sensitization-initiated electron transfer" (SenI-ET) imitate the role of inspired by nature artificial photosynthetic systems[198, 199], while the outstanding redox potentials of arene radical anions ($[PAH]^{\cdot-}$ ~ 2V) may be employed in reductive organic photocatalytic transformations.[196]

I.6.2 Photophysical properties of perylene

Perylene is a molecule that exhibits blue fluorescence, very high quantum yield ($\Phi = 0.94$) and prone to form stacked assemblies. Consequently, perylene and its derivatives have been used as pigments, colorants, photoreceptors and found an application in fluorescent labels[200], or bulk materials like organic

semiconductors[201] due to their characteristic combination of thermal- and photo-stability together with redox and optical properties.[202-208] The application of perylene and derivatives as homogeneous photocatalysts requires novel designs due to their poor solubility in organic solvents.[209, 210] Icli and co-workers reported modification of perylene diimides (PDI) which improve solubility in organic solvents.[211, 212] However, the emission studies have shown that perylene and derivatives can be quenched in the presence of amines which make them suitable for photoredox catalysis.[213-215] Recently, perylene based photocatalysts became of great interest due to their lower cost than metal based reducing catalysts, their wide availability and properties that in some cases can perform better than their inorganic and organometalic counterparts.[216-220]

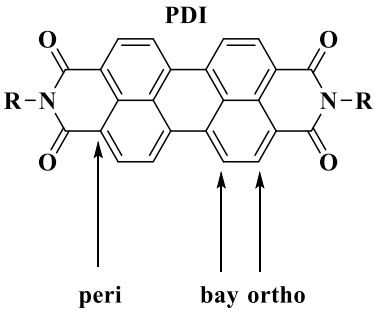

Figure I. 19 *Structure of PDI and possible positions of substituents.*

The modification of PDI are generally performed on bay and ortho positions (Figure I.19) to obtain PDI derivatives (PDIs). Optical and electronic properties of PDI have found an application in studies of Hayes and co-workers on fluorescent switches[221], of Gao et al. on sensors[222], light harvesting materials[223] and solar cells.[224] The large π–π electronic conjugate structure together with rigid plane of PDI molecule develop ability to π–π stacking interactions, high electron affinity, long lifetime of excited state, capacity of absorbing visible light and high fluorescence quantum yield.[225-227] These properties allow perylene based materials to be applied in fluorescence spectroscopy.[228-232]

The unique features of organic dyes such as their large π-conjugated scaffold delocalization system and high spectrum efficiency have been applied

in materials for photochemical hydrogen evolution. Supramolecular monomers exhibit hydrophobicity and are difficult to dissolve in water limiting their applications. Even if soluble in organic solvents, they present some disadvantages. Professor Bai and coworkers reported, that with the assistance of the emulsifier micelles, these π-conjugated molecules can self-assemble to form well-defined structures driven by interactions of π-π stacking and other noncovalent interactions to achieve a great improvement in physicochemical properties to be used in photocatalytic hydrogen evolution (Figure I.20).[233]

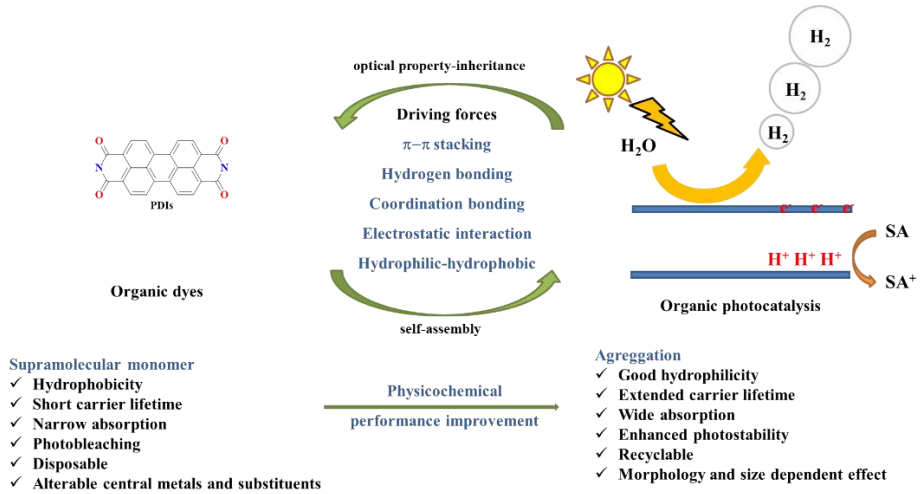

Figure I. 20 *Self-assembly strategies and further application of supramolecular nanostructures in hydrogen production.*

I.6.3 Supramolecular interactions of PAH with cyclodextrins

The aggregations of molecules containing organic dyes can be achieved by creating inclusion complexes with cyclodextrins. Cyclodextrines are well known cyclic oligomers of glucose units. CDs have hydrophilic exterior and inner hydrophobic cavity, this allows the recognition and interaction with guest molecules of certain size and shape to form inclusion complexes.[234] The most typical CD that contain 6, 7 and 8 glucopyranose units are called α-CD, β-CD and γ-CD. Dimensions of their cavities are known and as a rule of thumb, α-CD hosts substituted benzene molecules, β-CD naphthalene molecules and γ-CD anthracene ones, thus the only suitable size for organic dyes is γ-CD.

Host-guest complexes between pyrene and β- and γ-cyclodextrin were described by J. Mohanty, D.D Malkhede, revealing that fluorescence behavior of pyrene containing compound in presence of CD is significantly modulated (fluorescence is higher due to protected pyrene by CD from quenchers). Moreover, higher cavity size of γ-CD leads to dimerization of two pyrene units and showing excimer emission. However, at the lower concentration of γ-CD intermolecular excimer is formed (>1.2mM) and mixture of intra- and intermolecular excimer at higher concentrations (41.2 mM).[235]

Perylene and its derivatives tend to form complexes with cyclodextrins by π–π stacking interactions. Encapsulation of a guest PDI inside of the cavity of γ-CD was reported by Mitsui and co-authors, revealing that gradual addition of the host molecule to an aqueous solution of DMP-PDI enhance the fluorescent intensity, therefore DMP-PDI- γ-CD complex was created. It is important to mention that while the study was carried out with α-CD, the fluorescence intensity was not enhanced, indicating that cavity size of α-CD is not efficient to form inclusion complex.[236] Perylene excimer was not observed in the γ-CD, probably due to the size of the cavity.

The purpose of the supramolecular catalysis is to control the selectivity and rate of noncovalent interactions in chemical reactions that reach or even go beyond the imitation of natural enzymatic system.[237-242] In the last decades, several macrocyclic molecules have been developed as supramolecular catalysts to act as a host and control chemical reactions such as cyclodextrins, cucurbit[n]urils, organometallic cages etc.[243] One of the macrocyclic hosts, cyclodextrine is a good candidate due to its controllable molecular size to form aggregations containing PAH with high binding affinity in aqueous solutions. On the other hand, CD can preserve its physical and chemical properties during the reaction process as a supramolecular catalyst depending on the reaction conditions.[244]

I.7 Catalytic systems for light-driven reduction of molecules

Over last years, visible light as a driving force to perform chemical reactions has received significant attention in organic chemistry[245, 246] and photoredox catalysis has become a powerful tool to transform organic molecules.[247-251] Certain metal complexes, semiconductors and organic dyes are able to involve the single-electron transfer with organic molecules under photoexcitation. The ability of organic substrates to generate radicals with the use of light as a driving force, extends the photochemical reactivity beyond the substrate reduction (by single electron transfer) to another synthetically useful organic transformations, such as reductive additions[252, 253], cycloaddition reactions[254], cross-coupling[255], C-H functionalization.[256, 257] Ketones have been efficiently reduced by single electron transfer to corresponding alcohols using TiO_2[258-262], CdS[263, 264], Au nanoparticles[265, 266] and organic polypyridinic systems.[267, 268]

Light-driven transformations are based on the absorption of photons by a molecule, where occurs a reorganization of electrons. Consequently, the molecule is in the excited state becoming more reactive that in the ground state.

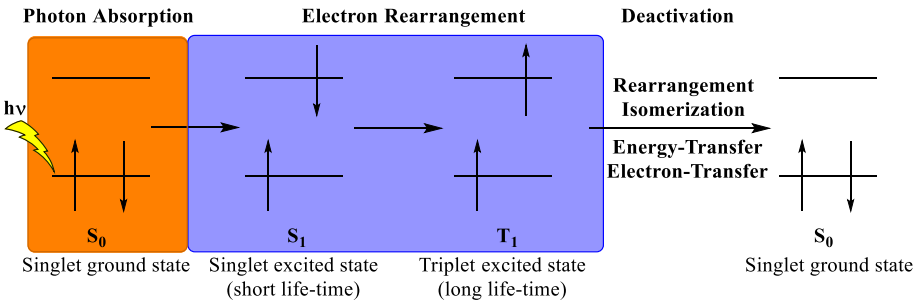

Figure I. 21 *Pathway of electrons of the irradiated molecule in HOMO.*

Excited state deactivation takes place by unimolecular processes which correspond to classical photochemical transformations such as rearrangements, isomerizations or by interaction with other species (biomolecular processes) (**Figure I.21**). In the latter case, the excited state is deactivated by energy-transfer[269] or by electron-transfer process.

The complex reactivity of excited states is possible to control to be used in chemical transformation. However, it is limited to direct reactivity of substrates with light and to several intrinsic properties. The use of a photocatalysts (PC) - molecules triggered by the absorption of photons, which engage in catalytic cycles - decouple the light absorption and leads to direct reaction between excited states and light. The energy of the excited state is delivered by energy-transfer mechanism or photoinduced electron-transfer process that occurs in bimolecular processes. Moreover, the interaction of excited PC with organic substrate leads to generation of several intermediates. The advantage of it, is the wide range of powerful synthetic transformations can be developed involving electron-transfer, atom-transfer and energy-transfer processes.[270] Success of photocatalysis stands most probably behind versatility if this strategy to promote and design new photochemical reactions.[271-273]

Direct substrate reduction by single electron transfer by the photoredox catalyst is limited by the redox potential of the chromophore and very often the high energy light (quite short wavelengths of ultraviolet (UV)) is needed.[270] Another drawback of the direct application is the formation of by-products as dimers.[263, 264] In this context, the ketyl radical intermediates are formed in the photoredox reductive coupling of aldehydes and ketones.[274]

Modification of photoredox catalysts by tuning the redox potential of the chromophore system is one of possible strategies to overcome this disadvantage. Nevertheless, it is not straightforward considering the control of selectivity. Another possible solution is to introduce functionalized molecules (organometallic complexes, biocatalytic systems) as electron mediators or hydride donors between the reactants and photosensitizers or semiconductors. The functionalized molecules may act as co-catalysts, triggered by photoinduced electron-transfer to perform catalytic reactions. This solution comes with intrinsic advantages:

- Facilitation of the charge separation process,
- Reduction of energy barrier of reactants by multistep electron-transfer,

- Controlled selectivity of the (bio)catalysts through their active sites,
- Rational design of the reactions through given activity of the catalyst.

In past years, the cooperation of photoredox catalysis with other types of catalysis (transition-metal-, bio-, electrocatalysis) for organic transformations has been explored.[275] These systems reveals the best properties of both, a light-dependent and light-independent cycle for the organic transformations.

I.7.1 Photocatalytic reduction of ketones and aldehydes to alcohols

The combination of photoredox system with synthetic catalysts have been widely used in photocatalytic water reduction reactions. The molecular catalyst plays the role of the redox enzyme without the need to use an electron mediator and natural cofactor. The general scheme of the photocatalysis is simplified due to easier modulation of the activity by changed structural and electronic features of the molecular catalysts (Scheme I.3).

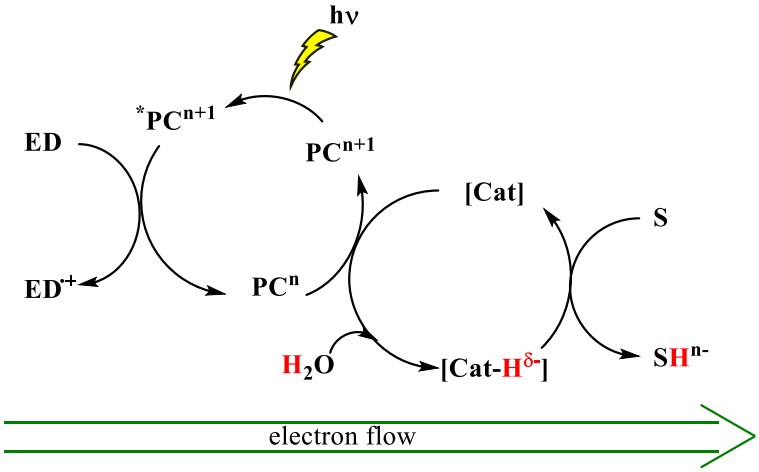

ED (Sacrificial electron donor):
Et_3N, H_2O, Ascorbic Acid, HCO_2H
PC (Photoredox catalyst)
Cat (Molecular catalyst)
S (Substrate)

Scheme I. 3 *General scheme of photocatalytic reductions using molecular catalyst.*

Moreover, these modifications can improve the efficiency and lifetime of whole catalytic system. These two merged systems bring the chance to investigate new reactivities and selectivity by modifying the nature of the light-dependent cycle.

First reported photoreduction of ketones and aldehydes to alcohols triggered by visible light was performed employing based on semiconductor suitable as a photoredox catalyst CdS in combination with metal complexes of iridium[276] and ruthenium[277] (Scheme I.4). CdS nanoparticles harvested the visible-light energy ($\lambda > 400$ nm) to activate the homogeneous metal complex (Ir or Ru) by photoexcited electron and then they reduced the substrate. Lactic acid was used as reducing agent. This catalytic system despite its limited scope, reduced aromatic and aliphatic carbonyls with very good selectivity.

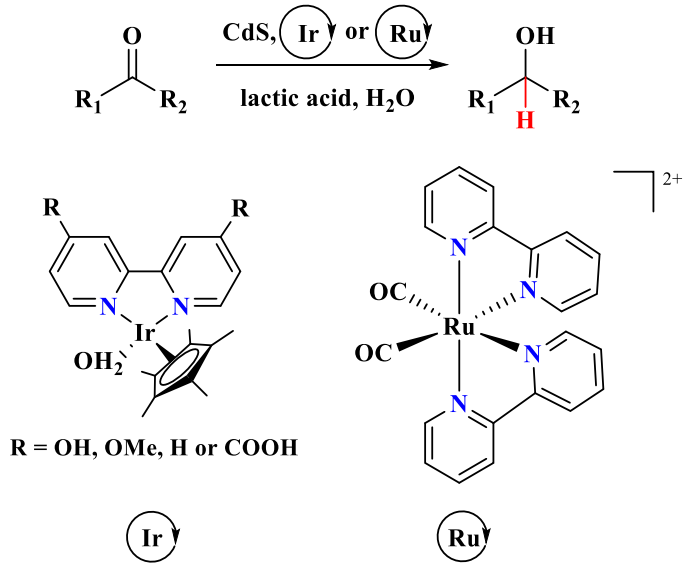

Scheme I. 4 *Photoreduction of ketones and aldehydes catalyzed by combined system of CdS photoredox catalyst and Ir or Ru metal complexes.*

The chemoselective photoreduction of aldehydes to alcohols in presence of ketones reported by König and co-workers was achieved by combination of two catalytic cycles.[278] The combined system consists of proflavine (PF) as a photocatalyst with [Cp*Rh^{III}(bpy)Cl]Cl as a mediator and triethanolamine (TEOH) as a sacrificial electron donor. Mechanistic studies showed that the photoreduction process occurs through the reaction of photoreduced PF with

rhodium catalysts that leads to formation of active intermediate for organic substrates reduction – metal hydride complex Rh^{III}-H (Scheme I.5).

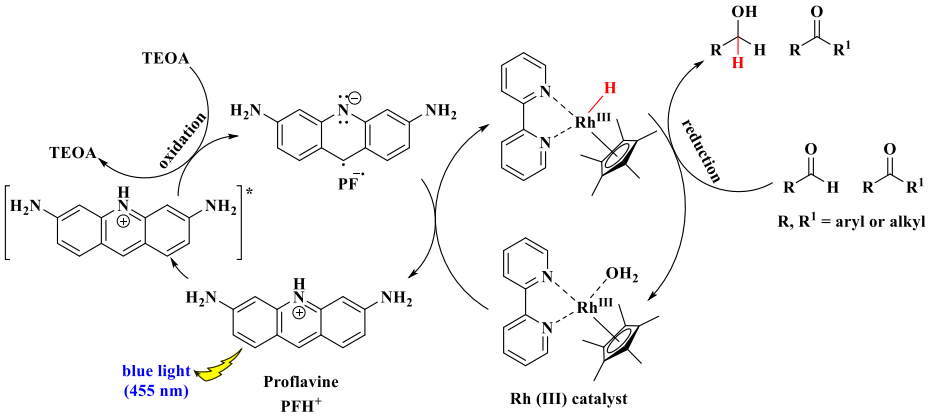

Scheme I. 5 *Schematic phototcatalytic cycle for the reduction of carbonyls involving PF as a photocatalysts and [Cp*Rh^{III}(bpy)Cl]Cl as a mediator.*

The formation of Rh^{III}-H is very slow, which makes the kinetically possible to distinguish aldehydes from ketones (Scheme I.6). In case of the absence of the aldehyde in the catalytic system, the reduction of ketones was not efficient due to the steric effects of rhodium catalyst which is sufficiently crowded to create selectivity even between similar substrates.

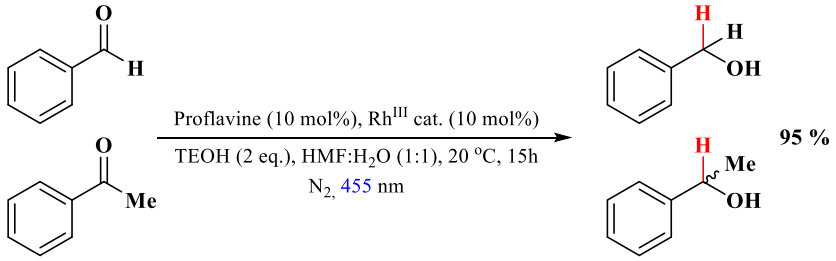

Scheme I. 6 *Chemoselective photoreduction of benzaldehyde in the presence of acetophenone.*

I.8 Catalytic methods for hydrogen storage

The hydrogen storage on large scale plays very important role in a hydrogen economy. Since hydrogen is the lightest molecule and has very low density (at room temperature and atmospheric pressure, 1 kg of hydrogen occupies 11 m^3)[279], its storage is challenging. To make storage of hydrogen economically viable, its density must be increased. Some methods to store hydrogen with increased density already exist, however they require input of energy in form

of heat and in some cases hydrogen-binding materials. One of the used methods is storage of gaseous hydrogen in salt caverns on industrial scale, but unfortunately this approach cannot be applied in all regions because of the varying geological conditions. Consequently, another storage methods are needed. Several of these storage technologies applications such as liquid hydrogen, methanol, ammonia were found to be efficient in terms of storage density, cost of storage, and safety. The cost of the high-density storage technologies are connected with high electricity and heat demand for storage and the hydrogen release processes, respectively.[280]

To overcome the drawbacks of the high-density methods, the appealing approach is to use the catalytic methods for storing hydrogen in chemical bonds. Liquid organic hydrogen carriers (LOHCs) have high-energy density and enable easy energy storage under ambient conditions without any leakages. They are used by industry and also by private consumers in efficient and safe manner.[281] Catalytic hydrogenation of N-heterocycles is applicable to the field of liquid organic hydrogen storage materials and commercial fuel cells. The dehydrogenation of N-heteroatoms require lower energy inputs than another organic materials.[282]

Recently, an elegant iridium-catalyzed hydrogenation of N-heterocyclic compounds was reported by Eisenstein, Crabtree and co-workers (Scheme I.7).[283]

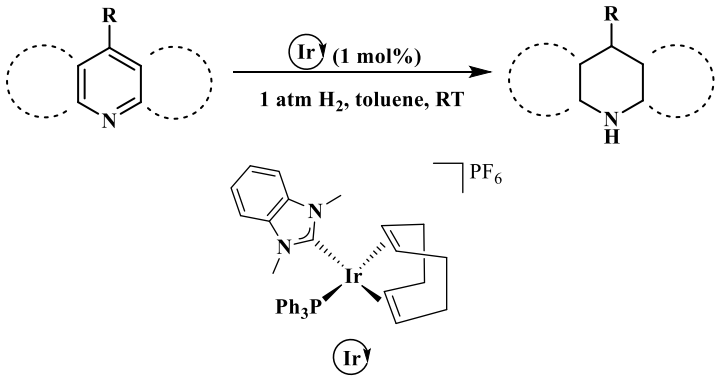

Scheme I. 7 *Hydrogenation of quinolines with iridium catalyst.*

It was achieved by using $[Ir(cod)(NHC)PPh_3]PF_6$ as a catalyst, molecular hydrogen as reducing agent and PPH_3 as an additive. Mechanistic studies showed that Ir metal complex activates H_2 and leads to formation of dihydrogen dihydride complex, which is the key species to reduce N-heteroarenes by proton transfer followed by hydride transfer. The used method applies mild conditions for the hydrogenation of N-heteroarenes and encourages to find milder conditions than existing and new catalyst design.

I.9 References of the chapter

1. Kannan, N. and D. Vakeesan, *Solar energy for future world: - A review.* Renewable and Sustainable Energy Reviews, 2016. **62**: p. 1092-1105.
2. Eisenberg, R. and D.G. Nocera, *Preface: Overview of the Forum on Solar and Renewable Energy.* Inorganic Chemistry, 2005. **44**(20): p. 6799-6801.
3. Rongé, J., et al., *Monolithic cells for solar fuels.* --, 2014. **43**(23): p. 7963-7981.
4. Lewis, N.S., et al., 2005.
5. Hisatomi, T., J. Kubota, and K. Domen, *Recent advances in semiconductors for photocatalytic and photoelectrochemical water splitting.* --, 2014. **43**(22): p. 7520-7535.
6. Lewis, N.S. and D.G. Nocera, *Powering the planet: Chemical challenges in solar energy utilization.* Proceedings of the National Academy of Sciences, 2006. **103**(43): p. 15729-15735.
7. Barber, J., *Towards a full understanding of water splitting in photosynthesis.* International Journal of Photoenergy, 2004. **6**(2): p. 43-51.
8. Ferreira, K.N., et al., *Architecture of the Photosynthetic Oxygen-Evolving Center.* Science, 2004. **303**(5665): p. 1831-1838.
9. Biesiadka, J., et al., *Crystal structure of cyanobacterial photosystem II at 3.2 Å resolution: a closer look at the Mn-cluster.* Phys. Chem. Chem. Phys., 2004. **6**(20): p. 4733-4736.
10. Lewis, N.S., *Research opportunities to advance solar energy utilization.* Science, 2016. **351**(6271).
11. Nocera, D.G., *The Artificial Leaf.* Accounts of Chemical Research, 2012. **45**(5): p. 767-776.
12. Blankenship, R.E., et al., *Comparing Photosynthetic and Photovoltaic Efficiencies and Recognizing the Potential for Improvement.* Science, 2011. **332**(6031): p. 805-809.

13. Razeghifard, R., 2013.
14. Berardi, S., et al., *Molecular artificial photosynthesis.* --, 2014. **43**(22): p. 7501-7519.
15. Qiao, J., et al., *A review of catalysts for the electroreduction of carbon dioxide to produce low-carbon fuels.* --, 2014. **43**(2): p. 631-675.
16. Jessop, P.G., T. Ikariya, and R. Noyori, *Homogeneous Hydrogenation of Carbon Dioxide.* Chemical Reviews, 2002. **95**(2): p. 259-272.
17. Lee, K.J., et al., *Electrochemical and spectroscopic methods for evaluating molecular electrocatalysts.* Nature Reviews Chemistry, 2017. **1**(5).
18. Lubitz, W. and H. Ogata, *Hydrogenases, Structure and Function.* 2013: p. 562-567.
19. Peters, J.W., *X-ray Crystal Structure of the Fe-Only Hydrogenase (CpI) from Clostridium pasteurianum to 1.8 Angstrom Resolution.* Science, 1998. **282**(5395): p. 1853-1858.
20. Volbeda, A., et al., *Crystal structure of the nickel–iron hydrogenase from Desulfovibrio gigas.* Nature, 1995. **373**(6515): p. 580-587.
21. Dance, I., *Structural variability of the active site of Fe-only hydrogenase and its hydrogenated forms.* Chemical Communications, 1999(17): p. 1655-1656.
22. Montet, Y., et al., *Gas access to the active site of Ni-Fe hydrogenases probed by X-ray crystallography and molecular dynamics.* Nature Structural Biology, 1997. **4**(7): p. 523-526.
23. Volbeda, A., et al., *Structure of the [NiFe] Hydrogenase Active Site: Evidence for Biologically Uncommon Fe Ligands.* Journal of the American Chemical Society, 1996. **118**(51): p. 12989-12996.
24. Appel, A.M., et al., *Frontiers, Opportunities, and Challenges in Biochemical and Chemical Catalysis of CO2 Fixation.* Chemical Reviews, 2013. **113**(8): p. 6621-6658.

25. Wang, Y., et al., *Pendant amine bases speed up proton transfers to metals by splitting the barriers.* Chemical Communications, 2012. **48**(37): p. 4450.
26. Lenz, O., *Hydrogen comes alive.* Nature Energy, 2020. **5**(6): p. 426-427.
27. Sit, P.H.L., et al., *Oxygen tolerance of an in silico-designed bioinspired hydrogen-evolving catalyst in water.* Proceedings of the National Academy of Sciences, 2013. **110**(6): p. 2017-2022.
28. Jacobsen, G.M., et al., *Hydrogen production using cobalt-based molecular catalysts containing a proton relay in the second coordination sphere.* Energy & Environmental Science, 2008. **1**(1): p. 167.
29. Artero, V., M. Chavarot-Kerlidou, and M. Fontecave, *Splitting Water with Cobalt.* Angewandte Chemie International Edition, 2011. **50**(32): p. 7238-7266.
30. Losse, S., J.G. Vos, and S. Rau, *Catalytic hydrogen production at cobalt centres.* Coordination Chemistry Reviews, 2010. **254**(21-22): p. 2492-2504.
31. Razavet, M., V. Artero, and M. Fontecave, *Proton Electroreduction Catalyzed by Cobaloximes: Functional Models for Hydrogenases.* Inorganic Chemistry, 2005. **44**(13): p. 4786-4795.
32. Hu, X., et al., *Electrocatalytic hydrogen evolution by cobalt difluoroboryl-diglyoximate complexes.* Chemical Communications, 2005(37): p. 4723.
33. Baffert, C., V. Artero, and M. Fontecave, *Cobaloximes as Functional Models for Hydrogenases. 2. Proton Electroreduction Catalyzed by Difluoroborylbis(dimethylglyoximato)cobalt(II) Complexes in Organic Media.* Inorganic Chemistry, 2007. **46**(5): p. 1817-1824.
34. Hu, X., B.S. Brunschwig, and J.C. Peters, *Electrocatalytic Hydrogen Evolution at Low Overpotentials by Cobalt Macrocyclic Glyoxime and*

Tetraimine Complexes. Journal of the American Chemical Society, 2007. **129**(29): p. 8988-8998.

35. Dempsey, J.L., et al., *Hydrogen Evolution Catalyzed by Cobaloximes.* Accounts of Chemical Research, 2009. **42**(12): p. 1995-2004.
36. Krawicz, A., et al., *Photofunctional Construct That Interfaces Molecular Cobalt-Based Catalysts for H2 Production to a Visible-Light-Absorbing Semiconductor.* Journal of the American Chemical Society, 2013. **135**(32): p. 11861-11868.
37. Liu, J., et al., *Electrocatalytic Hydrogen Evolution by Cobalt Complexes with a Redox Non-Innocent Polypyridine Ligand.* Inorganic Chemistry, 2021. **60**(23): p. 17976-17985.
38. Majee, K., et al., *Proton reduction by a nickel complex with an internal quinoline moiety for proton relay.* Physical Chemistry Chemical Physics, 2016. **18**(31): p. 21640-21650.
39. Du, P., K. Knowles, and R. Eisenberg, *A Homogeneous System for the Photogeneration of Hydrogen from Water Based on a Platinum(II) Terpyridyl Acetylide Chromophore and a Molecular Cobalt Catalyst.* Journal of the American Chemical Society, 2008. **130**(38): p. 12576-12577.
40. Du, P., et al., *Visible Light-Driven Hydrogen Production from Aqueous Protons Catalyzed by Molecular Cobaloxime Catalysts.* Inorganic Chemistry, 2009. **48**(11): p. 4952-4962.
41. Lazarides, T., et al., *Making Hydrogen from Water Using a Homogeneous System Without Noble Metals.* Journal of the American Chemical Society, 2009. **131**(26): p. 9192-9194.
42. McCormick, T.M., et al., *Reductive Side of Water Splitting in Artificial Photosynthesis: New Homogeneous Photosystems of Great Activity and Mechanistic Insight.* Journal of the American Chemical Society, 2010. **132**(44): p. 15480-15483.

43. Probst, B., et al., *An Efficient Homogeneous Intermolecular Rhenium-Based Photocatalytic System for the Production of H2.* Inorganic Chemistry, 2009. **48**(5): p. 1836-1843.
44. Probst, B., et al., *A Highly Stable Rhenium−Cobalt System for Photocatalytic H2 Production: Unraveling the Performance-Limiting Steps.* Inorganic Chemistry, 2010. **49**(14): p. 6453-6460.
45. Li, X., et al., *Noncovalent Assembly of a Metalloporphyrin and an Iron Hydrogenase Active-Site Model: Photo-Induced Electron Transfer and Hydrogen Generation.* The Journal of Physical Chemistry B, 2008. **112**(27): p. 8198-8202.
46. Wang, X., et al., *Homogeneous Photocatalytic Hydrogen Production Using π-Conjugated Platinum(II) Arylacetylide Sensitizers.* Inorganic Chemistry, 2011. **50**(3): p. 705-707.
47. Khnayzer, R.S., et al., *Robust Cuprous Phenanthroline Sensitizer for Solar Hydrogen Photocatalysis.* Journal of the American Chemical Society, 2013. **135**(38): p. 14068-14070.
48. Fihri, A., et al., *Cobaloxime-Based Photocatalytic Devices for Hydrogen Production.* Angewandte Chemie International Edition, 2008. **47**(3): p. 564-567.
49. Fihri, A., et al., *Efficient H2-producing photocatalytic systems based on cyclometalated iridium- and tricarbonylrhenium-diimine photosensitizers and cobaloxime catalysts.* DALTON TRANSACTIONS, 2008(41): p. 5567.
50. Li, Y., et al., *Oxidative dimerization of N-protected and free indole derivatives toward 3,3'-biindoles via Pd-catalyzed direct C–H transformations.* Chemical Communications, 2010. **46**(25): p. 4553.
51. Cropek, D.M., et al., *A novel ruthenium(ii)–cobaloxime supramolecular complex for photocatalytic H2 evolution: synthesis, characterisation and mechanistic studies.* DALTON TRANSACTIONS, 2012. **41**(42): p. 13060.

52. Veldkamp, B.S., et al., *Photoinitiated multi-step charge separation and ultrafast charge transfer induced dissociation in a pyridyl-linked photosensitizer–cobaloxime assembly.* Energy & Environmental Science, 2013. **6**(6): p. 1917.

53. Bartelmess, J., W.W. Weare, and R.D. Sommer, *Synthesis, characterization and structural investigation of novel meso-pyridyl BODIPY–cobaloxime complexes.* DALTON TRANSACTIONS, 2013. **42**(41): p. 14883.

54. Peuntinger, K., et al., *Photoinduced Charge Transfer in Porphyrin–Cobaloxime and Corrole–Cobaloxime Hybrids.* The Journal of Physical Chemistry C, 2013. **117**(4): p. 1647-1655.

55. Natali, M., et al., *Photocatalytic Hydrogen Evolution with a Self-Assembling Reductant-Sensitizer-Catalyst System.* Chemistry - A European Journal, 2013. **19**(28): p. 9261-9271.

56. Manton, J.C., et al., *Porphyrin–cobaloxime complexes for hydrogen production, a photo- and electrochemical study, coupled with quantum chemical calculations.* DALTON TRANSACTIONS, 2014. **43**(9): p. 3576.

57. Krishnan, C.V. and N. Sutin, *Homogeneous catalysis of the photoreduction of water by visible light. 2. Mediation by a tris(2,2'-bipyridine)ruthenium(II)-cobalt(II) bipyridine system.* Journal of the American Chemical Society, 2002. **103**(8): p. 2141-2142.

58. Krishnan, C.V., et al., *Homogeneous Catalysis of the Photoreduction of Water by Visible Light. 3. Mediation by Polypyridine Complexes of Ruthenium(II) and Cobalt(II).* Israel Journal of Chemistry, 1982. **22**(2): p. 98-106.

59. Creutz, C., H.A. Schwarz, and N. Sutin, *Free radical route to formation of the metal hydride complex hydridoaquobis(2,2'-bipyridine)cobalt(III).* Journal of the American Chemical Society, 2002. **106**(10): p. 3036-3037.

60. Krishnan, C.V., et al., *Homogeneous catalysis of the photoreduction of water. 6. Mediation by polypyridine complexes of ruthenium(II) and cobalt(II) in alkaline media.* Journal of the American Chemical Society, 2002. **107**(7): p. 2005-2015.

61. Schwarz, H.A., C. Creutz, and N. Sutin, *Homogeneous catalysis of the photoreduction of water by visible light. 4. Cobalt(I) polypyridine complexes. Redox and substitutional kinetics and thermodynamics in the aqueous 2,2'-bipyridine and 4,4'-dimethyl-2,2'-bipyridine series studied by the pulse-radiolysis technique.* Inorganic Chemistry, 2002. **24**(3): p. 433-439.

62. Creutz, C. and N. Sutin, *Photogeneration and reactions of cobalt(I) complexes.* Coordination Chemistry Reviews, 1985. **64**: p. 321-341.

63. Queyriaux, N., et al., *Recent developments in hydrogen evolving molecular cobalt(II)–polypyridyl catalysts.* Coordination Chemistry Reviews, 2015. **304-305**: p. 3-19.

64. Bigi, J.P., et al., *Electrocatalytic reduction of protons to hydrogen by a water-compatible cobalt polypyridyl platform.* --, 2010. **46**(6): p. 958-960.

65. Khnayzer, R.S., et al., *Towards a comprehensive understanding of visible-light photogeneration of hydrogen from water using cobalt(ii) polypyridyl catalysts.* Energy Environ. Sci., 2014. **7**(4): p. 1477-1488.

66. Sun, Y., et al., *Photocatalytic generation of hydrogen from water using a cobalt pentapyridine complex in combination with molecular and semiconductor nanowire photosensitizers.* --, 2013. **4**(1): p. 118-124.

67. Leung, C.-F., et al., *A cobalt(ii) quaterpyridine complex as a visible light-driven catalyst for both water oxidation and reduction.* Energy & Environmental Science, 2012. **5**(7): p. 7903.

68. Sun, Y., et al., *Molecular Cobalt Pentapyridine Catalysts for Generating Hydrogen from Water.* Journal of the American Chemical Society, 2011. **133**(24): p. 9212-9215.

69. Nippe, M., et al., *Catalytic proton reduction with transition metal complexes of the redox-active ligand bpy2PYMe.* Chemical Science, 2013. **4**(10): p. 3934.
70. Guttentag, M., et al., *A highly stable polypyridyl-based cobalt catalyst for homo- and heterogeneous photocatalytic water reduction.* Dalton Trans., 2013. **42**(2): p. 334-337.
71. Bachmann, C., et al., *3d Element Complexes of Pentadentate Bipyridine-Pyridine-Based Ligand Scaffolds: Structures and Photocatalytic Activities.* Inorganic Chemistry, 2013. **52**(10): p. 6055-6061.
72. Xie, J., et al., *An unexpected role of the monodentate ligand in photocatalytic hydrogen production of the pentadentate ligand-based cobalt complexes.* Chemical Communications, 2014. **50**(49): p. 6520.
73. Lewandowska-Andralojc, A., et al., *Mechanistic Studies of Hydrogen Evolution in Aqueous Solution Catalyzed by a Tertpyridine–Amine Cobalt Complex.* Inorganic Chemistry, 2015. **54**(9): p. 4310-4321.
74. Tong, L., R. Zong, and R.P. Thummel, *Visible Light-Driven Hydrogen Evolution from Water Catalyzed by A Molecular Cobalt Complex.* Journal of the American Chemical Society, 2014. **136**(13): p. 4881-4884.
75. Singh, W.M., et al., *Electrocatalytic and Photocatalytic Hydrogen Production in Aqueous Solution by a Molecular Cobalt Complex.* Angewandte Chemie International Edition, 2012. **51**(24): p. 5941-5944.
76. Vennampalli, M., et al., *Electronic Effects on a Mononuclear Co Complex with a Pentadentate Ligand for Catalytic H2 Evolution.* Inorganic Chemistry, 2014. **53**(19): p. 10094-10100.
77. Song, X., et al., *Hydrogen photogeneration catalyzed by a cobalt complex of a pentadentate aminopyridine-based ligand.* NEW JOURNAL OF CHEMISTRY, 2015. **39**(3): p. 1734-1741.

78. Guo, X., et al., *Homolytic versus Heterolytic Hydrogen Evolution Reaction Steered by a Steric Effect.* Angewandte Chemie International Edition, 2020. **59**(23): p. 8941-8946.
79. Marinescu, S.C., J.R. Winkler, and H.B. Gray, *Molecular mechanisms of cobalt-catalyzed hydrogen evolution.* Proceedings of the National Academy of Sciences, 2012. **109**(38): p. 15127-15131.
80. Valdez, C.N., et al., *Catalytic hydrogen evolution from a covalently linked dicobaloxime.* Proceedings of the National Academy of Sciences, 2012. **109**(39): p. 15589-15593.
81. Lee, C.H., D.K. Dogutan, and D.G. Nocera, *Hydrogen Generation by Hangman Metalloporphyrins.* Journal of the American Chemical Society, 2011. **133**(23): p. 8775-8777.
82. Wang, P., et al., *Electronic and Steric Tuning of Catalytic H2 Evolution by Cobalt Complexes with Pentadentate Polypyridyl-Amine Ligands.* Journal of the American Chemical Society, 2018. **140**(29): p. 9219-9229.
83. Elgrishi, N., D.A. Kurtz, and J.L. Dempsey, *Reaction Parameters Influencing Cobalt Hydride Formation Kinetics: Implications for Benchmarking H2-Evolution Catalysts.* Journal of the American Chemical Society, 2016. **139**(1): p. 239-244.
84. Rose, M.J., H.B. Gray, and J.R. Winkler, *Hydrogen Generation Catalyzed by Fluorinated Diglyoxime–Iron Complexes at Low Overpotentials.* Journal of the American Chemical Society, 2012. **134**(20): p. 8310-8313.
85. Han, Y., et al., *Singly versus Doubly Reduced Nickel Porphyrins for Proton Reduction: Experimental and Theoretical Evidence for a Homolytic Hydrogen-Evolution Reaction.* Angewandte Chemie International Edition, 2016. **55**(18): p. 5457-5462.
86. Dempsey, J.L., J.R. Winkler, and H.B. Gray, *Kinetics of Electron Transfer Reactions of H2-Evolving Cobalt Diglyoxime Catalysts.*

Journal of the American Chemical Society, 2009. **132**(3): p. 1060-1065.

87. Muckerman, J.T. and E. Fujita, *Theoretical studies of the mechanism of catalytic hydrogen production by a cobaloxime.* Chemical Communications, 2011. **47**(46): p. 12456.
88. Solis, B.H. and S. Hammes-Schiffer, *Theoretical Analysis of Mechanistic Pathways for Hydrogen Evolution Catalyzed by Cobaloximes.* Inorganic Chemistry, 2011. **50**(21): p. 11252-11262.
89. Solis, B.H., Y. Yu, and S. Hammes-Schiffer, *Effects of Ligand Modification and Protonation on Metal Oxime Hydrogen Evolution Electrocatalysts.* Inorganic Chemistry, 2013. **52**(12): p. 6994-6999.
90. Bhattacharjee, A., et al., *Combined Experimental–Theoretical Characterization of the Hydrido-Cobaloxime [HCo(dmgH)2(PnBu3)]*. Inorganic Chemistry, 2012. **51**(13): p. 7087-7093.
91. Lacy, D.C., G.M. Roberts, and J.C. Peters, *The Cobalt Hydride that Never Was: Revisiting Schrauzer's "Hydridocobaloxime".* Journal of the American Chemical Society, 2015. **137**(14): p. 4860-4864.
92. Singh, W.M., et al., *Voltammetric and spectroscopic characterization of early intermediates in the Co(ii)–polypyridyl-catalyzed reduction of water*. Chemical Communications, 2013. **49**(77): p. 8638.
93. Estes, D.P., D.C. Grills, and J.R. Norton, *The Reaction of Cobaloximes with Hydrogen: Products and Thermodynamics.* Journal of the American Chemical Society, 2014. **136**(50): p. 17362-17365.
94. Dempsey, J.L., J.R. Winkler, and H.B. Gray, *Mechanism of H2 Evolution from a Photogenerated Hydridocobaloxime.* Journal of the American Chemical Society, 2010. **132**(47): p. 16774-16776.
95. Costentin, C., H. Dridi, and J.-M. Savéant, *Molecular Catalysis of H2 Evolution: Diagnosing Heterolytic versus Homolytic Pathways.* Journal of the American Chemical Society, 2014. **136**(39): p. 13727-13734.

96. Shan, B., et al., *Mechanistic Details for Cobalt Catalyzed Photochemical Hydrogen Production in Aqueous Solution: Efficiencies of the Photochemical and Non-Photochemical Steps.* Inorganic Chemistry, 2013. **52**(9): p. 4853-4859.

97. Rodenberg, A., et al., *Mechanism of Photocatalytic Hydrogen Generation by a Polypyridyl-Based Cobalt Catalyst in Aqueous Solution.* Inorganic Chemistry, 2014. **54**(2): p. 646-657.

98. Varma, S., et al., *Efficient photocatalytic hydrogen production in water using a cobalt(iii) tetraaza-macrocyclic catalyst: electrochemical generation of the low-valent Co(i) species and its reactivity toward proton reduction.* Physical Chemistry Chemical Physics, 2013. **15**(40): p. 17544.

99. Natali, M., et al., *Photoinduced hydrogen evolution with new tetradentate cobalt(ii) complexes based on the TPMA ligand.* DALTON TRANSACTIONS, 2016. **45**(37): p. 14764-14773.

100. Kahnt, A., et al., *Kinetic Studies of the Reduction of [Co(dmgH)2(py)(Cl)] Revisited: Mechanisms, Products, and Implications.* The Journal of Physical Chemistry A, 2014. **118**(25): p. 4382-4391.

101. Smolentsev, G., et al., *Microsecond X-ray Absorption Spectroscopy Identification of CoIIntermediates in Cobaloxime-Catalyzed Hydrogen Evolution.* Chemistry - A European Journal, 2015. **21**(43): p. 15158-15162.

102. Keim, W., *Nickel: An Element with Wide Application in Industrial Homogeneous Catalysis.* Angewandte Chemie International Edition in English, 1990. **29**(3): p. 235-244.

103. Rosen, B.M., et al., *Nickel-Catalyzed Cross-Couplings Involving Carbon−Oxygen Bonds.* Chemical Reviews, 2010. **111**(3): p. 1346-1416.

104. Wiese, S., et al., *[Ni(PMe2NPh2)2](BF4)2 as an Electrocatalyst for H2 Production.* ACS Catalysis, 2012. **2**(5): p. 720-727.

105. Gan, L., et al., *A Nickel Phosphine Complex as a Fast and Efficient Hydrogen Production Catalyst.* Journal of the American Chemical Society, 2015. **137**(3): p. 1109-1115.
106. Thoi, V.S., et al., *Visible-Light Photoredox Catalysis: Selective Reduction of Carbon Dioxide to Carbon Monoxide by a Nickel N-Heterocyclic Carbene–Isoquinoline Complex.* Journal of the American Chemical Society, 2013. **135**(38): p. 14413-14424.
107. Shafaat, H.S., et al., *[NiFe] hydrogenases: A common active site for hydrogen metabolism under diverse conditions.* Biochimica et Biophysica Acta (BBA) - Bioenergetics, 2013. **1827**(8-9): p. 986-1002.
108. Greene, B.L., et al., *Proton Inventory and Dynamics in the Nia-S to Nia-C Transition of a [NiFe] Hydrogenase.* Biochemistry, 2016. **55**(12): p. 1813-1825.
109. Jeoung, J.-H. and H. Dobbek, *Carbon Dioxide Activation at the Ni,Fe-Cluster of Anaerobic Carbon Monoxide Dehydrogenase.* Science, 2007. **318**(5855): p. 1461-1464.
110. Fesseler, J., J.-H. Jeoung, and H. Dobbek, *How the [NiFe4S4] Cluster of CO Dehydrogenase Activates CO2and NCO−.* Angewandte Chemie International Edition, 2015. **54**(29): p. 8560-8564.
111. Wang, M., et al., *Light-driven hydrogen production catalysed by transition metal complexes in homogeneous systems.* DALTON TRANSACTIONS, 2009(33): p. 6458.
112. Mondal, B. and A. Dey, *Development of air-stable hydrogen evolution catalysts.* Chemical Communications, 2017. **53**(55): p. 7707-7715.
113. Zee, D.Z., et al., *Metal–Polypyridyl Catalysts for Electro- and Photochemical Reduction of Water to Hydrogen.* Accounts of Chemical Research, 2015. **48**(7): p. 2027-2036.
114. Wang, M., L. Chen, and L. Sun, *Recent progress in electrochemical hydrogen production with earth-abundant metal complexes as catalysts.* Energy & Environmental Science, 2012. **5**(5): p. 6763.

115. Thoi, V.S., et al., *Complexes of earth-abundant metals for catalytic electrochemical hydrogen generation under aqueous conditions.* --, 2013. **42**(6): p. 2388-2400.
116. Coutard, N., N. Kaeffer, and V. Artero, *Molecular engineered nanomaterials for catalytic hydrogen evolution and oxidation.* Chemical Communications, 2016. **52**(95): p. 13728-13748.
117. Willkomm, J., et al., *Dye-sensitised semiconductors modified with molecular catalysts for light-driven H2 production.* Chemical Society Reviews, 2016. **45**(1): p. 9-23.
118. DuBois, D.L. and R.M. Bullock, *Molecular Electrocatalysts for the Oxidation of Hydrogen and the Production of Hydrogen – The Role of Pendant Amines as Proton Relays.* European Journal of Inorganic Chemistry, 2011. **2011**(7): p. 1017-1027.
119. Lucarini, F., et al., *Rationalizing Photo-Triggered Hydrogen Evolution Using Polypyridine Cobalt Complexes: Substituent Effects on Hexadentate Chelating Ligands.* ChemSusChem, 2021. **14**(8): p. 1874-1885.
120. Schnidrig, S., et al., *Structure-Activity and Stability Relationships for Cobalt Polypyridyl-Based Hydrogen-Evolving Catalysts in Water.* ChemSusChem, 2017. **10**(22): p. 4570-4580.
121. Papadakis, M., et al., *Ligand-based electronic effects on the electrocatalytic hydrogen production by thiosemicarbazone nickel complexes.* DALTON TRANSACTIONS, 2020. **49**(16): p. 5064-5073.
122. Ladomenou, K., et al., *Nickel Complexes and Carbon Dots for Efficient Light-Driven Hydrogen Production.* European Journal of Inorganic Chemistry, 2021. **2021**(30): p. 3097-3103.
123. Tard, C. and C.J. Pickett, *Structural and Functional Analogues of the Active Sites of the [Fe]-, [NiFe]-, and [FeFe]-Hydrogenases.* Chemical Reviews, 2009. **109**(6): p. 2245-2274.

124. Barton, B.E., et al., *Nickel−Iron Dithiolato Hydrides Relevant to the [NiFe]-Hydrogenase Active Site.* Journal of the American Chemical Society, 2009. **131**(20): p. 6942-6943.

125. Ogo, S., et al., *A Functional [NiFe]Hydrogenase Mimic That Catalyzes Electron and Hydride Transfer from H*

2. Science, 2013. **339**(6120): p. 682-684.

126. Rakowski Dubois, M. and D.L. Dubois, *Development of Molecular Electrocatalysts for CO2 Reduction and H2 Production/Oxidation.* Accounts of Chemical Research, 2009. **42**(12): p. 1974-1982.

127. Rakowski DuBois, M. and D.L. DuBois, *The roles of the first and second coordination spheres in the design of molecular catalysts for H2production and oxidation.* --, 2009. **38**(1): p. 62-72.

128. Wiedner, E.S., et al., *Comparison of Cobalt and Nickel Complexes with Sterically Demanding Cyclic Diphosphine Ligands: Electrocatalytic H2 Production by [Co(PtBu2NPh2)(CH3CN)3](BF4)2.* Organometallics, 2010. **29**(21): p. 5390-5401.

129. Appel, A.M., et al., *[Ni(PPh2NBn2)2(CH3CN)]2+ as an Electrocatalyst for H2 Production: Dependence on Acid Strength and Isomer Distribution.* ACS Catalysis, 2011. **1**(7): p. 777-785.

130. Kilgore, U.J., et al., *Studies of a Series of [Ni(PR2NPh2)2(CH3CN)]2+ Complexes as Electrocatalysts for H2 Production: Substituent Variation at the Phosphorus Atom of the P2N2 Ligand.* Inorganic Chemistry, 2011. **50**(21): p. 10908-10918.

131. Fernandez, L.E., S. Horvath, and S. Hammes-Schiffer, *Theoretical Analysis of the Sequential Proton-Coupled Electron Transfer Mechanisms for H2 Oxidation and Production Pathways Catalyzed by Nickel Molecular Electrocatalysts.* The Journal of Physical Chemistry C, 2012. **116**(4): p. 3171-3180.

132. Dutta, A., et al., *Minimal Proton Channel Enables H2 Oxidation and Production with a Water-Soluble Nickel-Based Catalyst.* Journal of the American Chemical Society, 2013. **135**(49): p. 18490-18496.

133. Hoffert, W.A., et al., *Production of H2 at fast rates using a nickel electrocatalyst in water–acetonitrile solutions.* Chemical Communications, 2013. **49**(71): p. 7767.

134. Horvath, S., et al., *pH-Dependent Reduction Potentials and Proton-Coupled Electron Transfer Mechanisms in Hydrogen-Producing Nickel Molecular Electrocatalysts.* Inorganic Chemistry, 2013. **52**(7): p. 3643-3652.

135. Wiese, S., et al., *Hydrogen Production Using Nickel Electrocatalysts with Pendant Amines: Ligand Effects on Rates and Overpotentials.* ACS Catalysis, 2013. **3**(11): p. 2527-2535.

136. DuBois, D.L., *Development of Molecular Electrocatalysts for Energy Storage.* Inorganic Chemistry, 2014. **53**(8): p. 3935-3960.

137. Song, L.-C., et al., *Synthesis, Structural Characterization, and Catalytic H2 Production of Ferrocenyl (Fc) Group Containing Complexes [Ni(PFc2NAr2)2](BF4)2 (Ar = Ph, p-BrC6H4).* Organometallics, 2014. **33**(19): p. 5246-5253.

138. Wilson, A.D., et al., *Hydrogen Oxidation and Production Using Nickel-Based Molecular Catalysts with Positioned Proton Relays.* Journal of the American Chemical Society, 2005. **128**(1): p. 358-366.

139. Wilson, A.D., et al., *Nature of hydrogen interactions with Ni(II) complexes containing cyclic phosphine ligands with pendant nitrogen bases.* Proceedings of the National Academy of Sciences, 2007. **104**(17): p. 6951-6956.

140. Le Goff, A., et al., *From Hydrogenases to Noble Metal–Free Catalytic Nanomaterials for H_2 Production and Uptake.* Science, 2009. **326**(5958): p. 1384-1387.

141. McLaughlin, M.P., et al., *A stable molecular nickel catalyst for the homogeneous photogeneration of hydrogen in aqueous solution.* Chemical Communications, 2011. **47**(28): p. 7989.

142. Bouwman, E. and J. Reedijk, *Structural and functional models related to the nickel hydrogenases.* Coordination Chemistry Reviews, 2005. **249**(15-16): p. 1555-1581.

143. Fontecilla-Camps, J.C., et al., *Structure/Function Relationships of [NiFe]- and [FeFe]-Hydrogenases.* Chemical Reviews, 2007. **107**(10): p. 4273-4303.

144. Carroll, M.E., et al., *Active-Site Models for the Nickel–Iron Hydrogenases: Effects of Ligands on Reactivity and Catalytic Properties.* Inorganic Chemistry, 2011. **50**(19): p. 9554-9563.

145. Han, Z., et al., *A Nickel Thiolate Catalyst for the Long-Lived Photocatalytic Production of Hydrogen in a Noble-Metal-Free System.* Angewandte Chemie International Edition, 2012. **51**(7): p. 1667-1670.

146. Han, Z., et al., *Nickel Pyridinethiolate Complexes as Catalysts for the Light-Driven Production of Hydrogen from Aqueous Solutions in Noble-Metal-Free Systems.* Journal of the American Chemical Society, 2013. **135**(39): p. 14659-14669.

147. Rao, H., et al., *Highly efficient photocatalytic hydrogen evolution from nickel quinolinethiolate complexes under visible light irradiation.* Journal of Power Sources, 2016. **324**: p. 253-260.

148. Ezzaher, S., et al., *Influence of a Pendant Amine in the Second Coordination Sphere on Proton Transfer at a Dissymmetrically Disubstituted Diiron System Related to the [2Fe]H Subsite of [FeFe]H2ase.* Inorganic Chemistry, 2008. **48**(1): p. 2-4.

149. Helm, M.L., et al., *A Synthetic Nickel Electrocatalyst with a Turnover Frequency Above 100,000 s −1 for H_2 Production.* Science, 2011. **333**(6044): p. 863-866.

150. Fisher, B.J. and R. Eisenberg, *Electrocatalytic reduction of carbon dioxide by using macrocycles of nickel and cobalt.* Journal of the American Chemical Society, 2002. **102**(24): p. 7361-7363.

151. Collin, J.P., A. Jouaiti, and J.P. Sauvage, *Electrocatalytic properties of (tetraazacyclotetradecane)nickel(2+) and Ni2(biscyclam)4+ with respect to carbon dioxide and water reduction.* Inorganic Chemistry, 2002. **27**(11): p. 1986-1990.

152. Yang, Y., et al., *Nickel Complex with Internal Bases as Efficient Molecular Catalyst for Photochemical H2Production.* ChemSusChem, 2014. **7**(10): p. 2889-2897.

153. Chen, L., et al., *Dual Homogeneous and Heterogeneous Pathways in Photo- and Electrocatalytic Hydrogen Evolution with Nickel(II) Catalysts Bearing Tetradentate Macrocyclic Ligands.* ACS Catalysis, 2014. **5**(1): p. 356-364.

154. Luca, O.R., et al., *A tridentate Ni pincer for aqueous electrocatalytic hydrogen production.* NEW JOURNAL OF CHEMISTRY, 2012. **36**(5): p. 1149.

155. Morales-Morales, D., C.M. Jensen, and ScienceDirect (Servicio en línea), *The chemistry of pincer compounds*2007, Amsterdam ; Oxford: Elsevier. 1 online resource (xiii, 450 p.).

156. Luca, O.R., et al., *Organometallic Ni Pincer Complexes for the Electrocatalytic Production of Hydrogen.* Inorganic Chemistry, 2012. **51**(16): p. 8704-8709.

157. Jacques, P.A., et al., *Cobalt and nickel diimine-dioxime complexes as molecular electrocatalysts for hydrogen evolution with low overvoltages.* Proceedings of the National Academy of Sciences, 2009. **106**(49): p. 20627-20632.

158. Pantani, O., et al., *Electroactivity of cobalt and nickel glyoximes with regard to the electro-reduction of protons into molecular hydrogen in acidic media*. Electrochemistry Communications, 2007. **9**(1): p. 54-58.

159. Cherdo, S., et al., *A nickel dimethyl glyoximato complex to form nickel based nanoparticles for electrocatalytic H2 production.* --, 2014. **50**(88): p. 13514-13516.

160. *A quantitative assessment of the sources and fate of petroleum compounds in the marine environment.* Philosophical Transactions of the Royal Society of London. B, Biological Sciences, 1997. **297**(1087): p. 193-218.

161. Sasatsu, M., H. Onishi, and Y. Machida, *Preparation and biodisposition of methoxypolyethylene glycol amine–poly(dl-lactic acid) copolymer nanoparticles loaded with pyrene-ended poly(dl-lactic acid).* International Journal of Pharmaceutics, 2008. **358**(1-2): p. 271-277.

162. Tan, J., et al., *Micellization and sustained drug release behavior of EC-g-PPEGMA amphiphilic copolymers.* Carbohydrate Polymers, 2010. **81**(2): p. 213-218.

163. Goddard, E.D., et al., *Fluorescence probes for critical micelle concentration determination.* Langmuir, 2002. **1**(3): p. 352-355.

164. Bains, G., A.B. Patel, and V. Narayanaswami, *Pyrene: A Probe to Study Protein Conformation and Conformational Changes.* Molecules, 2011. **16**(9): p. 7909-7935.

165. Anthony, J.E., *Functionalized Acenes and Heteroacenes for Organic Electronics.* Chemical Reviews, 2006. **106**(12): p. 5028-5048.

166. Wu, J., W. Pisula, and K. Müllen, *Graphenes as Potential Material for Electronics.* Chemical Reviews, 2007. **107**(3): p. 718-747.

167. Sun, Z., et al., *Low band gap polycyclic hydrocarbons: from closed-shell near infrared dyes and semiconductors to open-shell radicals.* Chemical Society Reviews, 2012. **41**(23): p. 7857.

168. Ye, Q. and C. Chi, *Recent Highlights and Perspectives on Acene Based Molecules and Materials.* Chemistry of Materials, 2014. **26**(14): p. 4046-4056.

169. Vanga, M., R.A. Lalancette, and F. Jäkle, *Controlling the Optoelectronic Properties of Pyrene by Regioselective Lewis Base-Directed Electrophilic Aromatic Borylation.* Chemistry – A European Journal, 2019. **25**(43): p. 10133-10140.

170. Nussbaumer, A.L., et al., *Amplification of Chirality by Supramolecular Polymerization of Pyrene Oligomers.* Angewandte Chemie, 2011. **123**(24): p. 5604-5608.

171. Osaki, H., et al., *A Macrocyclic Fluorophore Dimer with Flexible Linkers: Bright Excimer Emission with a Long Fluorescence Lifetime.* Angewandte Chemie International Edition, 2016. **55**(25): p. 7131-7135.

172. Taki, M., et al., *Color-tunable fluorescent nanoparticles encapsulating trialkylsilyl-substituted pyrene liquids.* Journal of Materials Chemistry C, 2017. **5**(8): p. 2142-2148.

173. Vyborna, Y., et al., *Morphological diversity of supramolecular polymers of DNA-containing oligopyrenes – formation of chiroptically active nanosheets.* Chemical Communications, 2017. **53**(89): p. 12128-12131.

174. El Idrissi, M., et al., *Template-free hierarchical self-assembly of a pyrene derivative into supramolecular nanorods.* Chemical Communications, 2017. **53**(12): p. 1973-1976.

175. Figueira-Duarte, T.M. and K. Müllen, *Pyrene-Based Materials for Organic Electronics.* Chemical Reviews, 2011. **111**(11): p. 7260-7314.

176. Østergaard, M.E. and P.J. Hrdlicka, *Pyrene-functionalized oligonucleotides and locked nucleic acids (LNAs): Tools for fundamental research, diagnostics, and nanotechnology.* Chemical Society Reviews, 2011. **40**(12): p. 5771.

177. Liu, S.-Y., et al., *Pyrene and Diketopyrrolopyrrole-Based Oligomers Synthesized via Direct Arylation for OSC Applications.* ACS applied materials & interfaces, 2014. **6**(9): p. 6765-6775.

178. Yemam, H.A., et al., *Boron-rich benzene and pyrene derivatives for the detection of thermal neutrons.* Scientific Reports, 2015. **5**(1).

179. Feng, X., et al., *Functionalization of Pyrene To Prepare Luminescent Materials-Typical Examples of Synthetic Methodology.* Chemistry - A European Journal, 2016. **22**(34): p. 11898-11916.

180. Gong, Y., et al., *Progress of pyrene-based organic semiconductor in organic field effect transistors.* Science China Chemistry, 2016. **59**(12): p. 1623-1631.

181. Shellaiah, M., et al., *Novel pyrene containing monomeric and dimeric supramolecular AIEE active nano-probes utilized in selective "off–on" trivalent metal and highly acidic pH sensing with live cell applications.* Journal of Materials Chemistry C, 2016. **4**(10): p. 2056-2071.

182. Abeywickrama, C.S., et al., *Bright red-emitting pyrene derivatives with a large Stokes shift for nucleus staining.* Chemical Communications, 2017. **53**(43): p. 5886-5889.

183. Stevens, B. and E. Hutton, *Radiative Life-time of the Pyrene Dimer and the Possible Role of Excited Dimers in Energy Transfer Processes.* Nature, 1960. **186**(4730): p. 1045-1046.

184. Winnik, F.M., *Photophysics of preassociated pyrenes in aqueous polymer solutions and in other organized media.* Chemical Reviews, 2002. **93**(2): p. 587-614.

185. Howarth, A.J., M.B. Majewski, and M.O. Wolf, *Photophysical properties and applications of coordination complexes incorporating pyrene.* Coordination Chemistry Reviews, 2015. **282-283**: p. 139-149.

186. Kalyanasundaram, K. and J.K. Thomas, *Environmental effects on vibronic band intensities in pyrene monomer fluorescence and their application in studies of micellar systems.* Journal of the American Chemical Society, 2002. **99**(7): p. 2039-2044.

187. *'Excimer' fluorescence V. Influence of solvent viscosity and temperature.* Proceedings of the Royal Society of London. Series A. Mathematical and Physical Sciences, 1997. **280**(1381): p. 289-297.

188. Templer, R.H., et al., *Sensing isothermal changes in the lateral pressure in model membranes using di-pyrenyl phosphatidylcholine.* Faraday Discussions, 1999. **111**: p. 41-53.

189. Hodak, J.H., A. Henglein, and G.V. Hartland, *Photophysics of Nanometer Sized Metal Particles: Electron−Phonon Coupling and Coherent Excitation of Breathing Vibrational Modes.* The Journal of Physical Chemistry B, 2000. **104**(43): p. 9954-9965.

190. Fujiwara, Y. and Y. Amao, *Optical oxygen sensor based on controlling the excimer formation of pyrene-1-butylic acid chemisorption layer onto nano-porous anodic oxidized aluminium plate by myristic acid.* Sensors and Actuators B: Chemical, 2003. **89**(1-2): p. 58-61.

191. Ikeda, H., et al., *Fluorescent Cyclodextrins for Molecule Sensing: Fluorescent Properties, NMR Characterization, and Inclusion Phenomena of N-Dansylleucine-Modified Cyclodextrins.* Journal of the American Chemical Society, 1996. **118**(45): p. 10980-10988.

192. Ueno, A., I. Suzuki, and T. Osa, *Host-guest sensory systems for detecting organic compounds by pyrene excimer fluorescence.* Analytical Chemistry, 2002. **62**(22): p. 2461-2466.

193. Valeur, B., *Design principles of fluorescent molecular sensors for cation recognition.* Coordination Chemistry Reviews, 2000. **205**(1): p. 3-40.

194. Suzuki, Y., et al., *New Fluorimetric Alkali and Alkaline Earth Metal Cation Sensors Based on Noncyclic Crown Ethers by Means of Intramolecular Excimer Formation of Pyrene.* The Journal of Physical Chemistry B, 1998. **102**(40): p. 7910-7917.

195. Monahan, C., *Fluorescence sensing due to allosteric switching of pyrene functionalized cis-cyclohexane-1,3-dicarboxylate.* Chemical Communications, 1998(3): p. 431-432.

196. Ghosh, I., R.S. Shaikh, and B. König, *Sensitization-Initiated Electron Transfer for Photoredox Catalysis.* Angewandte Chemie International Edition, 2017. **56**(29): p. 8544-8549.

197. Wrighton, M. and J. Markham, *Quenching of the luminescent state of tris(2,2'-bipyridine)ruthenium(II) by electronic energy transfer.* The Journal of Physical Chemistry, 2002. **77**(26): p. 3042-3044.

198. Barber, J., *Photosynthetic energy conversion: natural and artificial.* --, 2009. **38**(1): p. 185-196.

199. McConnell, I., G. Li, and G.W. Brudvig, *Energy Conversion in Natural and Artificial Photosynthesis.* Chemistry & Biology, 2010. **17**(5): p. 434-447.

200. Lavis, L.D. and R.T. Raines, *Bright Ideas for Chemical Biology.* ACS Chemical Biology, 2008. **3**(3): p. 142-155.

201. Schwoerer, M. and H.C. Wolf, *Organic molecular solids*. Physics textbook2007, Weinheim: Wiley-VCH. XI, 427 p.

202. Sun, H., et al., *Imide-Functionalized Polymer Semiconductors.* Chemistry – A European Journal, 2018. **25**(1): p. 87-105.

203. Nowak-Król, A., et al., *Naphthalene and perylene diimides – better alternatives to fullerenes for organic electronics?* Chemical Communications, 2018. **54**(98): p. 13763-13772.

204. Arzoumanian, E., et al., *Transparent Organosilica Photocatalysts Activated by Visible Light: Photophysical and Oxidative Properties at the Gas–Solid Interface.* ACS applied materials & interfaces, 2013. **6**(1): p. 275-288.

205. Mathew, S. and H. Imahori, *Tunable, strongly-donating perylene photosensitizers for dye-sensitized solar cells.* Journal of Materials Chemistry, 2011. **21**(20): p. 7166.

206. Wu, Y., et al., *Exceptional Intersystem Crossing in Di(perylene bisimide)s: A Structural Platform toward Photosensitizers for Singlet Oxygen Generation.* The Journal of Physical Chemistry Letters, 2010. **1**(17): p. 2499-2502.

207. Würthner, F., *Perylene bisimide dyes as versatile building blocks for functional supramolecular architectures.* --, 2004(14): p. 1564-1579.

208. Ferrere, S. and B.A. Gregg, *New perylenes for dye sensitization of TiO2.* NEW JOURNAL OF CHEMISTRY, 2002. **26**(9): p. 1155-1160.

209. Céspedes-Guirao, F.J., et al., *A water-soluble perylene dye functionalised with a 17β-estradiol: a new fluorescent tool for steroid hormones.* Chemical Communications, 2011. **47**(29): p. 8307.

210. Céspedes-Guirao, F.J., et al., *Synthesis and Photophysics of Silicon Phthalocyanine-Perylenebisimide Triads Connected through Rigid and Flexible Bridges.* Chemistry - A European Journal, 2011. **17**(33): p. 9153-9163.

211. Bodapati, J.B. and H. Icil, *Highly soluble perylene diimide and oligomeric diimide dyes combining perylene and hexa(ethylene glycol) units: Synthesis, characterization, optical and electrochemical properties.* Dyes and Pigments, 2008. **79**(3): p. 224-235.

212. Türkmen, G., S. Erten-Ela, and S. Icli, *Highly soluble perylene dyes: Synthesis, photophysical and electrochemical characterizations.* Dyes and Pigments, 2009. **83**(3): p. 297-303.

213. Sriramulu, D., et al., *Molecular Organization Induced Anisotropic Properties of Perylene – Silica Hybrid Nanoparticles.* Scientific Reports, 2017. **7**(1).

214. Wahab, M.A., H. Hussain, and C. He, *Photoactive Perylenediimide-Bridged Silsesquioxane Functionalized Periodic Mesoporous Organosilica Thin Films (PMO-SBA15): Synthesis, Self-Assembly, and Photoluminescent and Enhanced Mechanical Properties.* Langmuir, 2009. **25**(8): p. 4743-4750.

215. Carrillo, A.I., et al., *Perylene-Grafted Silicas: Mechanistic Study and Applications in Heterogeneous Photoredox Catalysis.* Chemistry – A European Journal, 2019. **25**(65): p. 14928-14934.

216. Miranda, M.A. and H. Garcia, *2,4,6-Triphenylpyrylium Tetrafluoroborate as an Electron-Transfer Photosensitizer.* Chemical Reviews, 2002. **94**(4): p. 1063-1089.

217. Fagnoni, M., et al., *Photocatalysis for the Formation of the C−C Bond.* Chemical Reviews, 2007. **107**(6): p. 2725-2756.

218. Ravelli, D. and M. Fagnoni, *Dyes as Visible Light Photoredox Organocatalysts.* --, 2012. **4**(2): p. 169-171.

219. Marin, M.L., et al., *Organic Photocatalysts for the Oxidation of Pollutants and Model Compounds.* Chemical Reviews, 2011. **112**(3): p. 1710-1750.

220. Fukuzumi, S. and K. Ohkubo, *Selective photocatalytic reactions with organic photocatalysts.* --, 2013. **4**(2): p. 561-574.

221. Hayes, R.T., M.R. Wasielewski, and D. Gosztola, *Ultrafast Photoswitched Charge Transmission through the Bridge Molecule in a Donor−Bridge−Acceptor System.* Journal of the American Chemical Society, 2000. **122**(23): p. 5563-5567.

222. García-Espinoza, J.D., P. Mijaylova-Nacheva, and M. Avilés-Flores, *Electrochemical carbamazepine degradation: Effect of the generated active chlorine, transformation pathways and toxicity.* Chemosphere, 2018. **192**: p. 142-151.

223. Langhals, H. and S. Saulich, *Bichromophoric Perylene Derivatives: Energy Transfer from Non-Fluorescent Chromophores.* Chemistry - A European Journal, 2002. **8**(24): p. 5630-5643.

224. Duan, Y., et al., *Pronounced Effects of a Triazine Core on Photovoltaic Performance-Efficient Organic Solar Cells Enabled by a PDI Trimer-Based Small Molecular Acceptor.* Advanced Materials, 2017. **29**(7): p. 1605115.

225. Kalinin, S., et al., *A new and versatile fluorescence standard for quantum yield determination.* Physical Chemistry Chemical Physics, 2001. **3**(2): p. 172-174.

226. Langhals, H., J. Karolin, and L.B.Å. Johansson, *Spectroscopic properties of new and convenient standards for measuring fluorescence quantum yields.* Journal of the Chemical Society, Faraday Transactions, 1998. **94**(19): p. 2919-2922.

227. Würthner, F., et al., *Synthesis and Optical and Electrochemical Properties of Core-Fluorinated Perylene Bisimides.* Organic Letters, 2006. **8**(17): p. 3765-3768.

228. Feng, X., et al., *A Turn-on Fluorescent Sensor for Pyrophosphate Based on the Disassembly of Cu2+-Mediated Perylene Diimide Aggregates.* ACS applied materials & interfaces, 2012. **4**(2): p. 614-618.

229. Lin, J., et al., *A Highly Selective and Turn-on Fluorescent Probe for Fe3+Ion Based on Perylene Tetracarboxylic Diimide.* Chinese Journal of Chemistry, 2014. **32**(11): p. 1116-1120.

230. Zhang, L., et al., *An efficient approach for rapid detection of polymyxins B based on the optically active supramolecular aggregates of water-soluble perylene diimide.* Sensors and Actuators B: Chemical, 2020. **321**: p. 128594.

231. Zhang, Y., et al., *Fluorescent and photoconductive nanoribbons as a dual-mode sensor for selective discrimination of alkyl amines versus aromatic amines.* Chemical Communications, 2015. **51**(81): p. 15004-15007.

232. Weil, T., et al., *The Rylene Colorant Family-Tailored Nanoemitters for Photonics Research and Applications.* Angewandte Chemie International Edition, 2010. **49**(48): p. 9068-9093.

233. Zhong, Y., et al., *Self-assembled supramolecular nanostructure photosensitizers for photocatalytic hydrogen evolution.* APL Materials, 2020. **8**(12): p. 120706.

234. Smolková-Keulemansová, E. *Cyclodextrins and their inclusion complexes : by J. Szejtli, Akadémiai Kiadó, Budapest, 1982, 296 pp*. 1982.

235. Kalyani, V.S., D.D. Malkhede, and J. Mohanty, *Cyclodextrin-assisted modulation of the photophysical properties and acidity constant of pyrene-armed calix[4]arene.* Physical Chemistry Chemical Physics, 2017. **19**(32): p. 21382-21389.

236. Mitsui, M., et al., *Single-Molecule Fluorescence Spectroscopy of Perylene Diimide Dyes in a γ-Cyclodextrin Film: Manifestation of Photoinduced H-Atom Transfer via Higher Triplet (n, π*) Excited States.* The Journal of Physical Chemistry A, 2017. **121**(8): p. 1577-1586.

237. Breslow, R. and L.E. Overman, *"Artificial enzyme" combining a metal catalytic group and a hydrophobic binding cavity.* Journal of the American Chemical Society, 2002. **92**(4): p. 1075-1077.

238. Tabushi, I., *Cyclodextrin catalysis as a model for enzyme action.* Accounts of Chemical Research, 2002. **15**(3): p. 66-72.

239. Kang, J. and J. Rebek, *Acceleration of a Diels–Alder reaction by a self-assembled molecular capsule.* Nature, 1997. **385**(6611): p. 50-52.

240. Sokolov, A.N., et al., *Supramolecular Catalysis in the Organic Solid State through Dry Grinding.* Angewandte Chemie, 2010. **122**(25): p. 4369-4373.

241. Dydio, P. and J.N.H. Reek, *Supramolecular control of selectivity in transition-metal catalysis through substrate preorganization.* --, 2014. **5**(6): p. 2135-2145.

242. Raynal, M., et al., *Supramolecular catalysis. Part 2: artificial enzyme mimics.* --, 2014. **43**(5): p. 1734-1787.

243. Tang, X., et al., *Efficient Fenton Degradation of Perylene Diimide Dye Promoted by a Catalytic Amount of Cucurbit[8]uril.* Langmuir, 2020. **36**(21): p. 5954-5959.

244. Connors, K.A., *The Stability of Cyclodextrin Complexes in Solution.* Chemical Reviews, 1997. **97**(5): p. 1325-1358.

245. Yoon, T.P., M.A. Ischay, and J. Du, *Visible light photocatalysis as a greener approach to photochemical synthesis.* Nature Chemistry, 2010. **2**(7): p. 527-532.

246. Zeitler, K., *Photoredox Catalysis with Visible Light.* Angewandte Chemie International Edition, 2009. **48**(52): p. 9785-9789.

247. Prier, C.K., D.A. Rankic, and D.W.C. MacMillan, *Visible Light Photoredox Catalysis with Transition Metal Complexes: Applications in Organic Synthesis.* Chemical Reviews, 2013. **113**(7): p. 5322-5363.

248. Rueping, M., et al., *Photoredox Catalysis as an Efficient Tool for the Aerobic Oxidation of Amines and Alcohols: Bioinspired Demethylations and Condensations.* ACS Catalysis, 2012. **2**(12): p. 2810-2815.

249. Narayanam, J.M.R. and C.R.J. Stephenson, *Visible light photoredox catalysis: applications in organic synthesis.* --, 2011. **40**(1): p. 102-113.

250. Narayanam, J.M.R., J.W. Tucker, and C.R.J. Stephenson, *Electron-Transfer Photoredox Catalysis: Development of a Tin-Free Reductive Dehalogenation Reaction.* Journal of the American Chemical Society, 2009. **131**(25): p. 8756-8757.

251. Pitre, S.P., C.D. McTiernan, and J.C. Scaiano, *Understanding the Kinetics and Spectroscopy of Photoredox Catalysis and Transition-Metal-Free Alternatives.* Accounts of Chemical Research, 2016. **49**(6): p. 1320-1330.

252. Turro, N.J., et al., *Molecular photochemistry. L. Molecular photochemistry of alkanones in solution. .alpha.-Cleavage, hydrogen abstraction, cycloaddition, and sensitization reactions.* Accounts of Chemical Research, 2002. **5**(3): p. 92-101.

253. Darling, T.R., et al., *Photochemistry of .alpha.-cycloalkoxyacetophenones. Type II and vibronic pathways for radiationless triplet decay.* Journal of the American Chemical Society, 2002. **96**(2): p. 434-439.

254. Kärkäs, M.D., J.A. Porco, and C.R.J. Stephenson, *Photochemical Approaches to Complex Chemotypes: Applications in Natural Product Synthesis.* Chemical Reviews, 2016. **116**(17): p. 9683-9747.

255. Ryu, D., et al., *Single-Electron Transmetalation: Synthesis of 1,1-Diaryl-2,2,2-trifluoroethanes by Photoredox/Nickel Dual Catalytic*

Cross-Coupling. Chemistry - A European Journal, 2016. **22**(1): p. 120-123.

256. Chen, Y. and G. Feng, *Visible light mediated sp3 C–H bond functionalization of N-aryl-1,2,3,4-tetrahydroisoquinolines via Ugi-type three-component reaction.* Organic & Biomolecular Chemistry, 2015. **13**(14): p. 4260-4265.
257. Jin, J. and D.W.C. MacMillan, *Alcohols as alkylating agents in heteroarene C–H functionalization.* Nature, 2015. **525**(7567): p. 87-90.
258. Molinari, R., C. Lavorato, and P. Argurio, *Photocatalytic reduction of acetophenone in membrane reactors under UV and visible light using TiO2 and Pd/TiO2 catalysts.* Chemical Engineering Journal, 2015. **274**: p. 307-316.
259. Kohtani, S., et al., *Kinetic study on photocatalytic hydrogenation of acetophenone derivatives on titanium dioxide.* Catalysis Science & Technology, 2014. **4**(4): p. 1084.
260. Miyabe, H. and S. Kohtani, *Photocatalytic single electron transfer reactions on TiO2 semiconductor.* Science China Chemistry, 2019. **62**(11): p. 1439-1449.
261. Kohtani, S., et al., *Dye-sensitized photo-hydrogenation of aromatic ketones on titanium dioxide under visible light irradiation.* Catalysis Communications, 2014. **43**: p. 61-65.
262. Kohtani, S., et al., *Photohydrogenation of Acetophenone Using Coumarin Dye-Sensitized Titanium Dioxide under Visible Light Irradiation.* Catalysts, 2015. **5**(3): p. 1417-1424.
263. Shiragami, T., C. Pac, and S. Yanagida, *Nonmetallised CdS-catalysed photoreduction of aromatic ketones to alcohols and/or pinacols.* Journal of the Chemical Society, Chemical Communications, 1989(13): p. 831.
264. Shiragami, T., C. Pac, and S. Yanagida, *Visible-light-induced two-electron-transfer photoreductions on cadmium sulfide: effects of*

morphology. The Journal of Physical Chemistry, 2002. **94**(2): p. 504-506.

265. Ke, X., et al., *Tuning the reduction power of supported gold nanoparticle photocatalysts for selective reductions by manipulating the wavelength of visible light irradiation.* Chemical Communications, 2012. **48**(29): p. 3509.
266. Ke, X., et al., *Selective reductions using visible light photocatalysts of supported gold nanoparticles.* Green Chem., 2013. **15**(1): p. 236-244.
267. Matsuoka, S., et al., *Visible-light-induced photocatalysis of poly(pyridine-2,5-diyl). Photoreduction of water, carbonyl compounds and alkenes with triethylamine.* Journal of the Chemical Society, Perkin Transactions 2, 1992(4): p. 679.
268. Matsuoka, S., et al., *Efficient visible-light-driven photocatalysis. Poly(pyridine-2,5-diyl)-catalysed hydrogen photoevolution and photoreduction of carbonyl compounds.* Journal of the Chemical Society, Chemical Communications, 1991(8): p. 580.
269. Müller, C., A. Bauer, and T. Bach, *Light-Driven Enantioselective Organocatalysis.* Angewandte Chemie International Edition, 2009. **48**(36): p. 6640-6642.
270. Skubi, K.L., T.R. Blum, and T.P. Yoon, *Dual Catalysis Strategies in Photochemical Synthesis.* Chemical Reviews, 2016. **116**(17): p. 10035-10074.
271. Burstall, F.H., *34. Optical activity dependent on co-ordinated bivalent ruthenium.* Journal of the Chemical Society (Resumed), 1936: p. 173.
272. Balzani, V., et al., *Bimolecular electron transfer reactions of the excited states of transition metal complexes.* ChemInform, 1978. **9**: p. 1-64.
273. Kalyanasundaram, K., *Photophysics, photochemistry and solar energy conversion with tris(bipyridyl)ruthenium(II) and its analogues.* Coordination Chemistry Reviews, 1982. **46**: p. 159-244.

274. Nakajima, M., et al., *Photoredox-Catalyzed Reductive Coupling of Aldehydes, Ketones, and Imines with Visible Light.* Angewandte Chemie International Edition, 2015. **54**(30): p. 8828-8832.

275. Lang, X., J. Zhao, and X. Chen, *Cooperative photoredox catalysis.* Chemical Society Reviews, 2016. **45**(11): p. 3026-3038.

276. Li, J., et al., *A visible-light-driven transfer hydrogenation on CdS nanoparticles combined with iridium complexes.* Chemical Communications, 2011. **47**(25): p. 7080.

277. Liu, X., et al., *Efficient visible-light-induced hydrogenation over composites of CdS and ruthenium carbonyl complexes.* Journal of Catalysis, 2013. **304**: p. 1-6.

278. Ghosh, T., T. Slanina, and B. König, *Visible light photocatalytic reduction of aldehydes by Rh(iii)–H: a detailed mechanistic study.* Chemical Science, 2015. **6**(3): p. 2027-2034.

279. Schlapbach, L. and A. Züttel, *Hydrogen-storage materials for mobile applications.* Nature, 2001. **414**(6861): p. 353-358.

280. Andersson, J. and S. Grönkvist, *Large-scale storage of hydrogen.* International Journal of Hydrogen Energy, 2019. **44**(23): p. 11901-11919.

281. Teichmann, D., et al., *A future energy supply based on Liquid Organic Hydrogen Carriers (LOHC).* Energy & Environmental Science, 2011. **4**(8): p. 2767.

282. Makowski, P., et al., *Organic materials for hydrogen storage applications: from physisorption on organic solids to chemisorption in organic molecules.* Energy & Environmental Science, 2009. **2**(5): p. 480.

283. Dobereiner, G.E., et al., *Iridium-Catalyzed Hydrogenation of N-Heterocyclic Compounds under Mild Conditions by an Outer-Sphere Pathway.* Journal of the American Chemical Society, 2011. **133**(19): p. 7547-7562.

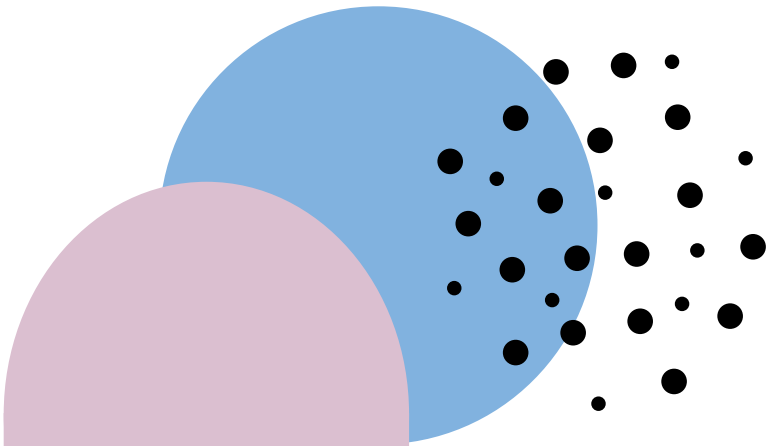

Chapter II

Objectives

UNIVERSITAT ROVIRA I VIRGILI
ORGANIC TRANSFORMATIONS USING TRANSITION METALS AND PHOTOREDOX CATALYSTS
Klaudia Michaliszyn

II.1 Thesis Objectives

The development of efficient molecular photocatalytic systems for water reduction to molecular hydrogen and production of high-value organic molecules is the main aim of this thesis. The use of homogeneous coordination metal complexes for hydrogen production have expanded but the structural factors to control the reactivity and selectivity are not well understood. The light-driven reduction of organic molecules performed under mild conditions is limited and mostly catalyzed by noble metals. Therefore, synergistic merging of a photocatalyst and well-defined coordination metal complex enable the efficient photocatalytic synthesis of fuels together with their storage and reduction of organic molecules. In this regard, rational design and architecture of water-soluble catalyst based on earth-abundant elements is important to control these transformations.

Chemical hydrogen storage are predominant technologies to store and release hydrogen from the storage material through a chemical reaction. Chemical compounds containing hydrogen as methanol, ammonia and methyl cyclohexane can also be considered a kind of hydrogen storage. In this regard, using chemical compounds as a storage material for hydrogen has clear advantage comparing with gaseous hydrogen, which requires leak-proof, preferably seamless piping and vessels. Various types of hydrogen storages have been developed, however they demand high temperature and energy. Moreover, the dehydrogenation process in many cases release highly environmentally unfavorable products. Consequently, new robust catalysts able to store hydrogen in chemical compounds are required as well as effective processes to implement the compounds successfully as practical hydrogen storage materials.

The first part of this thesis (**Chapter III**) focus on the design and development of new aminopyridine ligand scaffold based on three main parts: π-stacking unit (Polycyclic aromatic hydrocarbons -PAH), spacer and catalyst. The synthesis and characterization of Co^{II} and Ni^{II} catalysts with the new ligand and each scaffold part will aid towards understanding of key aspects on the

catalysis. To achieve this aim we will synthetize catalysts with two different backbones: *N,N′*-dimethyl-1,2-cyclohexanediamine and 2,2′-bipyrrolidine. The second coordination of these systems will be modified by introducing γ-cyclodextrin as a transition source from organic media into aqueous media and we will try to aim the supramolecular structure with γ-cyclodextrins and nanomaterials to obtain well-defined cavity. The catalytic activity of these systems will be evaluated in hydrogen production and organic transformations.

In **Chapter IV**, the study focuses on understanding the supramolecular interaction of our systems. First, we will study and discuss parts of ligands and catalysts by spectroscopic methods, which will be followed by spectroscopic studies of π-stacking interactions of Co^{II} and Ni^{II} complexes with γ-cyclodextrins and carbon-based nanomaterials.

Finally, the aim of **Chapter V** is development of new class of catalysts based on earth-abundant metals for molecular hydrogen activation as a method of hydrogen storage. The $HTIM(PPh_2)_3$ ligand and its derivatives will be used for synthesis of Co^{II} and Ni^{II} complexes. The synthetized catalysts will be characterized and optimization of the reaction conditions for the hydrogenation of quinoline will be performed. The catalytic activity of these new complexes will be studied towards N-heteroarenes.

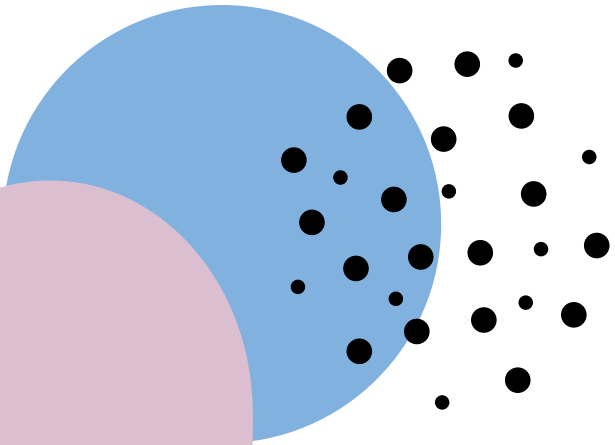

Chapter III

Synthesis and characterization of cobalt and nickel complexes based on modular aminopyridine ligands with π-stacking units for application in photoredox catalysis

UNIVERSITAT ROVIRA I VIRGILI
ORGANIC TRANSFORMATIONS USING TRANSITION METALS AND PHOTOREDOX CATALYSTS
Klaudia Michaliszyn

III.1 State-of-the-art

Catalysts developed for the reduction of H_2O and CO_2 in the context of artificial photosynthesis (AP) have the potential to provide greener light-driven methodologies for sustainable synthetic methods.[284-292] In this regard, the synthesis of fine chemicals has less scaling and economic restriction than the production of energy carriers. Therefore, the use of catalytic systems derived for AP to perform selective organic transformations is highly appealing. Remarkable examples of catalytic systems based on semiconductors[117, 293, 294], enzymes[143, 295-299] and more recently, homogeneous catalysts[300, 301] have been shown to be active for specific transformations. However, due to the complexity of these catalytic systems, both optimization and mechanistic studies are still challenging.[302]

Indeed, the combination of photoredox catalysts with well-defined molecular complexes is a powerful approach to better understand light driven synthesis of fuels but also the reduction of organic molecules. The introduction of a photoredox catalytic cycle potentially enables the use of water and an electron donor as reductive equivalents, while organometallic or coordination complexes can serve as selective hydrogenation catalysts.[303, 304]

Notable efforts have been focused on developing hydrogenation catalysts based on earth-abundant elements. Catalysts based on earth-abundant elements can reduce organic substrates for the synthesis of fine chemicals such as drugs or pesticides by using light as the energy source and water as a source of protons. A remarkable example was reported by König and co-workers for the selective visible light photoreduction of aldehydes to alcohols in the presence of ketones (See Scheme III.1a). [278] In this context, first row transition metal systems mostly based on cobalt with different kinds of ligands as glyoxime, diimine-glyoxime, and aminopyridine ligands, were shown to be efficient catalysts for the reduction of water to hydrogen.[305-307] Mechanistic investigations on these systems suggest that molecular [Co–H] species are key intermediates in H_2 formation and the reduction of organic functionalities.[308] Nevertheless, outstanding example was reported by our group for light-driven

catalytic reduction of aldehydes and aromatic ketones in aqueous media by well-defined catalyst based earth abundant metal – cobalt and copper photocatalyst (Scheme III.1b).

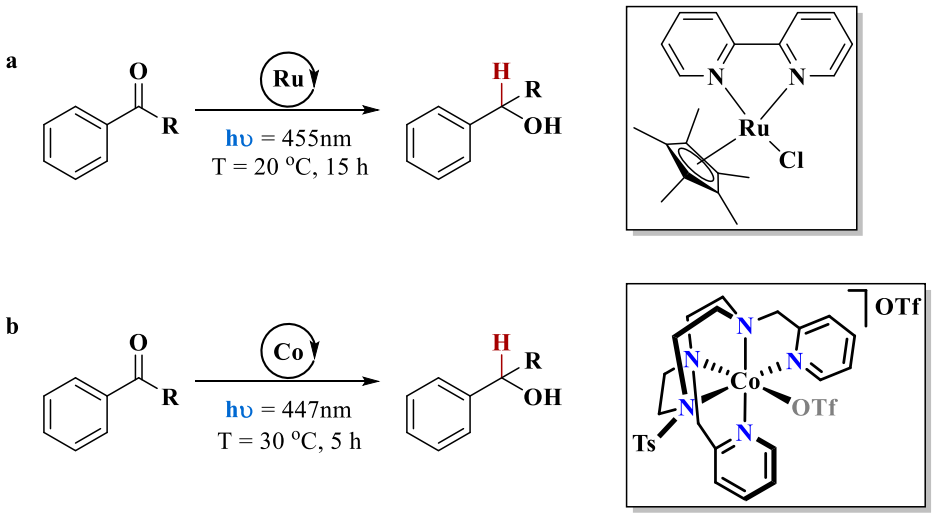

Scheme III. 1 *Light-driven reduction of ketones in presence of alcohol with [Cp*Rh(III)(bpy)Cl]Cl as a photosensitizer (a) and photoreduction of aldehydes and ketones in aqueous media by Co(OTf)(Py$_2$Tstacn)](OTf) and Cu(bathocuproine)(Xantphos)](PF$_6$).*

On the other hand, fluorescent dye molecules[309] found an application in the photoredox catalysis due to their characteristic combination of photostability, optical and redox properties which can perfectly fulfill the requirements of dye-based catalysts. Outstanding precedent of applying these systems in catalysis was reported by König and co-workers for reduction of aryl halides using perylene diimide as a catalyst (Scheme III.2).[310]

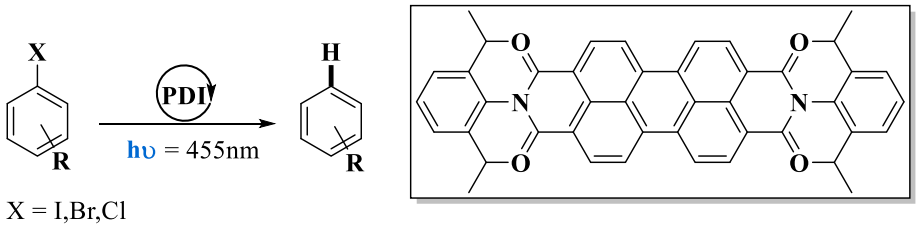

Scheme III. 2 *Reduction of aryl halides using reduced by visible light photoinduced electron transfer perylene bisimide.*

In certain cases, the solubility of cobalt precursors in aqueous media can be an issue and having strategies to solubilize them could be beneficial. In this regard,

introducing polar groups in the catalysts could help its solubilization. Another less explored alternative is based on the derivatization of catalysts with functionalities that interact well with a water-soluble receptor such as cyclodextrin. The amphiphilic property of cyclodextrin make it ideal to be used as solubilizer agent. Indeed, their ability to enhance molecule solubility has been showed when acting as carriers by keeping hydrophobic molecules in solution.[311, 312] Among the different hydrophobic molecules that have been probed to interact well with cyclodextrin cavities are the pyrenes and perylenes.[313-317] Both are excellent photocatalysts, which were found to form host-guest interactions with molecules containing hydrophobic cavity enabling organic dyes to aggregate inside.[318] Complexes formed with macrocyclic family of cucurbiturils or cyclodextrins with encapsulated hydrophobic molecules containing pyrene or perylene increase their water-solubility.[315, 319, 320] On the other hand, catalytic centers flanked by hydrophobic molecules that can engage π-stacking interactions can allow the formation of dynamic cavities with effect in catalytic activity and selectivity. Moreover, the tendency of pyrene and perylene to form π-stacking interactions was described by J. Mata and co-workers representing a copper catalyst with pyrene ¨tail¨ anchored by strong aromatic π-π-stacking on reduced graphene oxide surface. This operation effectively combined homogeneous and heterogeneous systems toward hydrocarbon functionalization enhance catalytic activity when it is supported.[321]

In this context, we designed new tetradentate ligands by connecting three main synthons: a polyaromatic moiety responsible for π–π stacking, a spacer to control the distance between the catalytic center and the surface of the nanomaterial, the third fragment is an aminopyridine moiety used as a modular coordinating moiety of the metal ion (Scheme III.3). The corresponding cobalt and nickel complexes were synthetized to study the catalytic reduction of water and ketones, using in both cases light as a source of energy and water as a source of protons, and to compare their photocatalytic activity. These complexes were

also used to explore the effect of π–π stacking with surface as C_{60}, nanotubes and graphene oxide to tune the reactivity and selectivity.

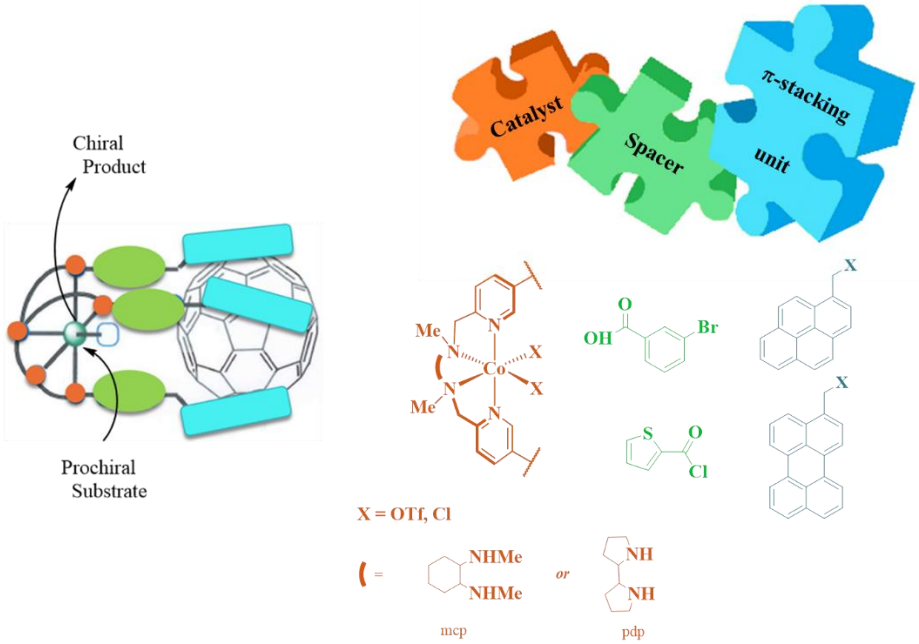

Scheme III. 3 *Proposed design for a new family of complexes containing π-stacking unit, spacer and catalyst. The π-stacking unit (in blue) can interact with other hydrophobic systems such as cyclodextrine cavities or fullerene surface, as depicted in the example.*

The cyclodextrins were applied to increase solubility of catalysts in water and to study the potential modification of the catalytic reactivity. In addition, the employed aminopyridine fragments are chiral, and therefore, although is it a challenging topic in the context of photocatalytic reduction of ketones in aqueous solution, these systems allow to explore enantioselective transformations.

Objectives:

- To develop a robust methodology to synthetize aminopyridine ligands that contain a π-stacking polyaromatic unit such as pyrene or perylene;
- To obtain cobalt and nickel metal complexes with new designed anchoring ligands;

- To explore the influence of ligand's fragments in H_2 evolution;
- To study the effect of π–π stacking of carbon-based nanomaterials and γ-CD and its influence in light-driven catalysis;

III.2 Results and Discussion

III.2.1 Synthesis and Characterization of L_1, L_2 and L_9 Co and Ni complexes

Based on the above-mentioned precedents we developed a new synthetic protocol for the synthesis of (bis(pyren-1-ylmethyl)-3,3'-((((*1R,2R*)-cyclohexane-1,2-diyl)bis(methylazanediyl)) bis(methylene))bis(pyridine-6,3-diyl))dibenzoate (**^{PyB}mcp**), bis(pyren-1-ylmethyl)-3,3'-((([*2R,2'R*)-[2,2'-bipyrrolidine]-1,1'diyl)bis(methylene))bis(pyridine-6,3-diyl))dibenzoate (**^{PyB}pdp**) and bis(perylen-3-ylmethyl) 3,3'-(((((*1R,2R*)-cyclohexane-1,2-diyl)bis(methylazanediyl))bis(methylene))bis(pyridine-6,3-diyl))dibenzoate (**^{PerB}mcp**)) ligands (Scheme III.4). Although the methodology employed for the synthesis of the ligands follows similar synthetic pathways to known ligands, the discovery of the best synthetic strategy for the anchoring ligands was not trivial. Therefore, the studied synthetic routes will be discussed, including the ones that unfortunately failed. Though, the drawbacks found in these studies were key to find reliable synthetic pathways.

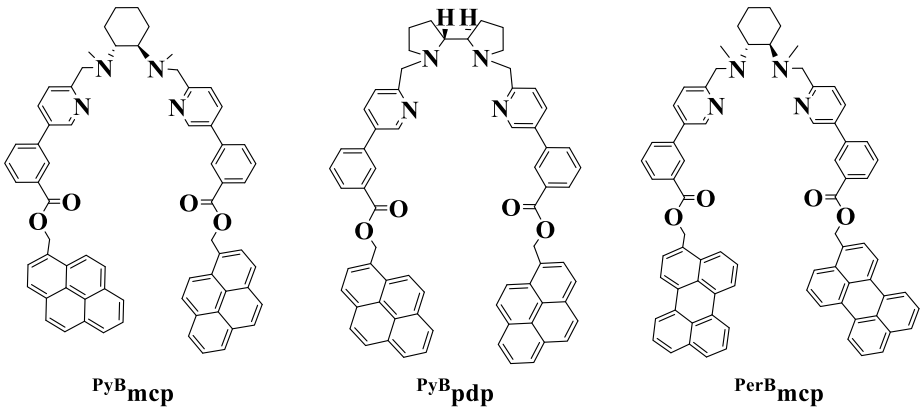

Scheme III. 4 *New tetradentate chiral ligands* ***^{PyB}mcp***, ***^{PyB}pdp*** *and* ***^{PerB}mcp***.

The first designed ligand (**^{PyT}mcp**) consisted of three main parts: pyrene moiety as a π–stacking unit, thiophene moiety as a spacer and *N,N′*-dimethyl-1,2-cyclohexanediamine with pyridines as a backbone (Scheme III.5).

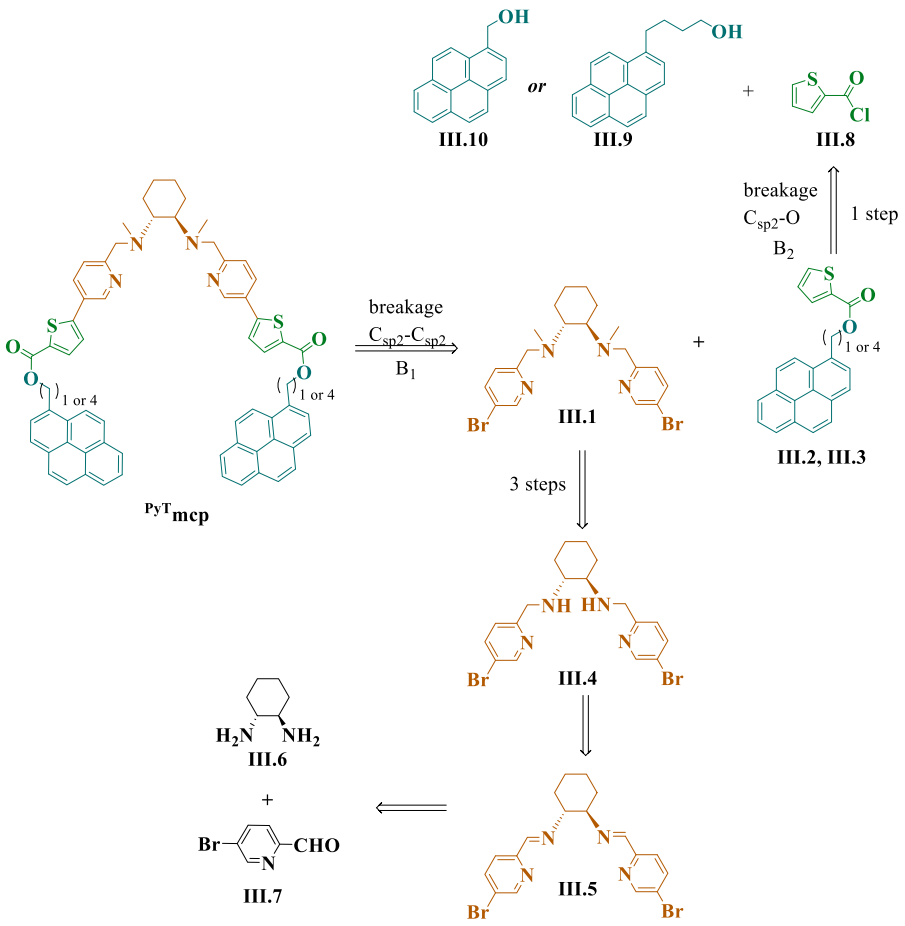

Scheme III. 5 *Retrosynthetic plan for the synthesis of ligand* ***^{PyT}mcp****.*

We chose the pyrene moiety as a small and readily accessible polycyclic aromatic hydrocarbon (PAH) to induce significant π-π or host-guest interactions. Pyrene has four fused rings, resulting in a flat aromatic system that shows interesting photophysical and spectroscopic properties[322]: strong absorption cross-section in the visible light region, excellent emission properties and a long-excited state lifetime.[323] Thiophene moiety was found to be good candidate for spacer unit, because it can easily be asymmetrically functionalized in the ortho positions. The sulfur atom in thiophenes is relatively

unreactive, however the carbon centers, the 2- and 5-positions, are highly liable to be attacked by electrophiles, which makes them good candidates for synthetic purposes.[324, 325] Finally, we selected the *N,N′*-dimethyl-1,2-cyclohexanediamine since this moiety can led us to C_2 symmetric ligands with a chiral backbone. Certainly, *N,N′*-dimethyl-1,2-cyclohexanediamine is a common skeleton for the development of privileged ligands for enantioselective catalytic transformations.[326-336]

We defined a retrosynthetic plan to synthesize the ligand (**^{PyT}mcp**) following 3 main criteria: minimizing the cost of chemical precursors, maintaining a low number of synthetic steps, and obtaining the product in good yield (Scheme III.6). First, we disconnected the ligand **^{PyT}mcp** at two different points, at the C_{sp2}-C_{sp2} connection between the pyridine and thiophene (**B_1**), and between the π-stacking end and the thiophene spacer (**B_2**). In that way, the *(1R,2R)-N1,N2*-bis((5-bromopyridin-2-yl)methyl)-*N1,N2*-dimethylcyclohexane-1,2-diamine (**III.I**) which is a known tetradentate ligand can be prepared by typical synthetic routes. For instance, the synthesis of bis 5-bromopyridine dimethylcyclohexane diamine (**III.I**) would be performed by dialkylation of cyclohexane diamine (**III.6**) by 5-bromopicolinaldehyde (**III.7**) to obtain **III.5** and followed by the sequence reduction (**III.4)** and methylation reactions. An alternative to obtain **III.1** would be the reaction of 5-bromo 2-chloromethyl pyridine with dimethylcyclohexane diamine, and both fragments, can be easily obtained by dialkylation from cheap commercially available compounds. The pyrene-thiophene unit (**III.2, III.3**) should be also easily obtained by the reaction between thiophene-2-carbonyl chloride (**III.8**) and pyrene alcohol derivatives (**III.9 and III.10**). Finally, the connection between units **III.1** and **III.2** or **III.3** could be made *via* cross-coupling reaction. For the synthesis of the π-stacking units **III.1** and **III.2** we selected two different commercially available alcohols, butyl thiophene-2-carboxylate (**III.9**) and pyren-1-ylmethyl (**III.10**), to play with the distance between the π-stacking unit and the metal center.

The first approach to synthetize **^{PyT}mcp** started from the substitution reaction of cheap commercially available 2,5-dibromopyridine (**III.11**)

(Bouveault aldehyde synthesis) yielding 5-bromopicolinaldehyde[337] (**III.7**) (30%) (Scheme III.6). We found that the reaction yield was very sensitive to the reaction conditions, most probably due to the low solubility of the starting materials and sensitivity of the final product. Next, the dialkylation of (*R,R*)-1,2-cyclohexanediamine (**III.6**) with the aforementioned aldehyde (**III.7**) gave the (*1R,2R*)-*N,N'*-bis(3-bromopyridine-2-ylmethylene)-1,2-cyclohexanediamine (**III.5**, 14%), which was then reduced to (*1R,2R*)-*N,N'*-bis(3-bromopyridine-2-ylmethyl)-1,2-cyclohexanediamine (**III.4**, 30%) with sodium borohydride ($NaBH_4$). The amine groups of (*1R,2R*)-*N,N'*-bis(3-bromopyridine-2-ylmethyl)-1,2-cyclohexanediamine were then methylated yielding (*1R,2R*)-*N,N'*-dimethyl-*N,N'*-bis(3-bromopyridine-2-ylmethyl)-1,2-cyclohexanediamine (**III.1**, 32%). The ^{1}H-NMR spectra of compounds **III.1** and **III.7** are showed in Figure III.1. The overall low yield of <1% together with the arduous purification led us to explore other alternatives.

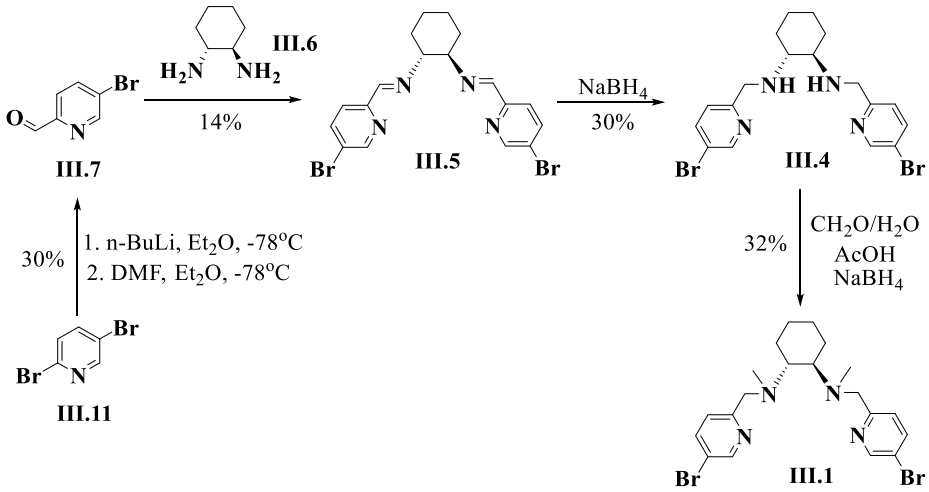

Scheme III. 6 *Synthetic route for ligands.*

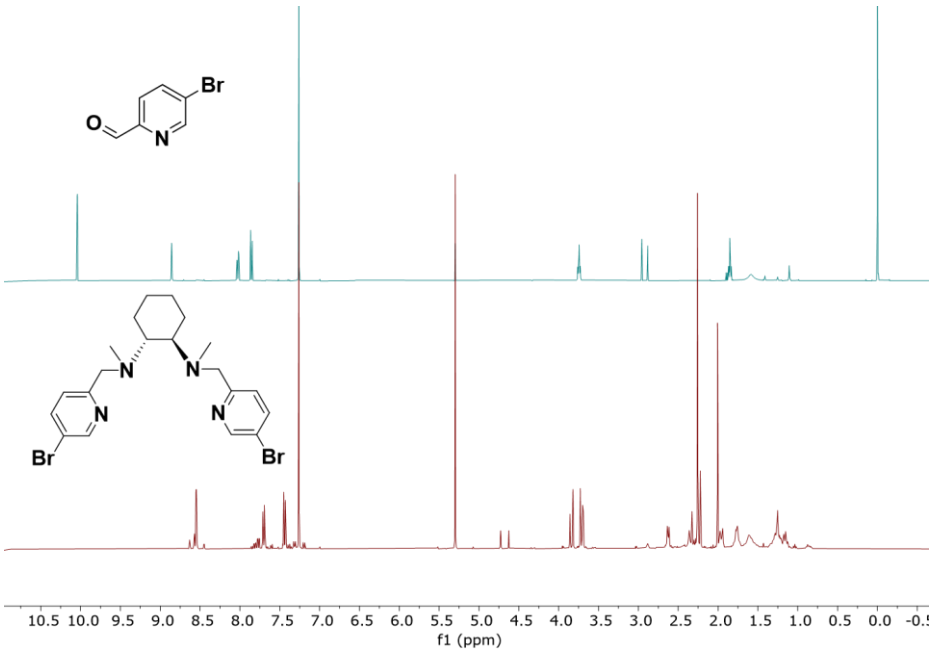

Figure III. 1 *^{1}H-NMR spectra of 5-bromopicolinaldehyde and (*1R,2R*)-N,N'-dimethyl-N,N'-bis(3-bromopyridine-2-ylmethyl)-1,2-cyclohexanediamine from first synthesis.*

We also explored the alkylation of the dimethylcyclohexane-1,2-diamine (**III.16**) as an alternative route to obtain the desired anchoring ligand **^{PyT}mcp**.

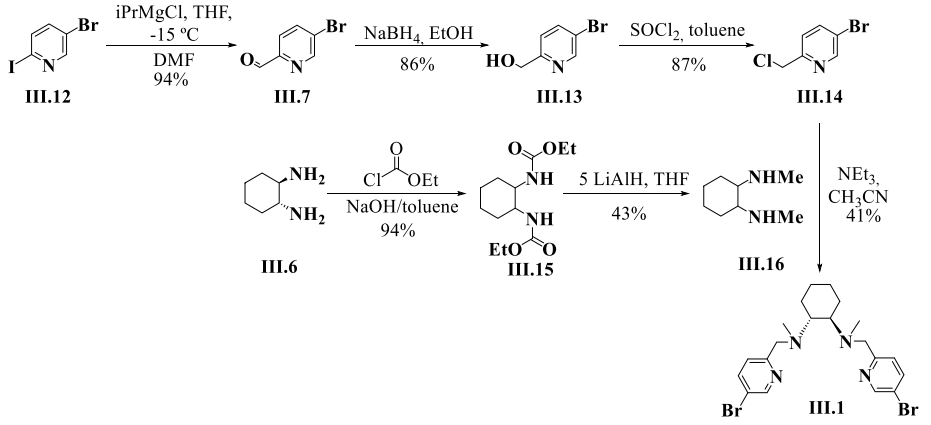

Scheme III. 7 *Improved pathway for the synthesis of ligands.*

In this case, the synthesis started from the commercially available 5-bromo-2-iodopyridine (**III.12**) giving 5-bromopicolinaldehyde (**III.7**, 94%[338]), followed by its reduction to the corresponding alcohol (5-bromopyridin-2-yl)methanol (**III.13**, 86%), which was chlorinated yielding the 5-bromo-2-

(chloromethyl)pyridine (**III.14**, 87%[339]). The *N1*,*N2*-dimethylcyclohexane-1,2-diamine (**III.16**) was synthetized in two steps from cyclohexane-1,2-diamine (**III.6**) and ethyl chloroformate resulting in diethyl cyclohexane-1,2-diyldicarbamate (**III.15**, 94%), which was reduced to the desired compound (**III.16**, 43%[340]). These two compounds were used in the reaction with triethylamine to give *N1*,*N2*-bis((5-bromopyridin-2-yl)methyl)-*N1*,*N2*-dimethylcyclohexane-1,2-diamine in a (**III.1**) 41% yield (Scheme III.7). The overall yield amounted to 12%.

Second fragment of ligand ^{PyT}**mcp** was synthetized by following a general esterification procedure of reaction between the alcohol pyrene - pyren-1-ylmethyl (**III.10**) or butyl thiophene-2-carboxylate (**III.9**) with the thiophene-2-carbonyl chloride (**III.8**) to obtain the desired products - pyren-1-ylmethyl thiophene-2-carboxylate (**III.3**) or 4-(pyren-1-yl)butyl thiophene-2-carboxylate (**III.2**) in 38% and 40% yield (Scheme III.8). The ligand fragments were characterized by NMR spectroscopy (Figure III.2).

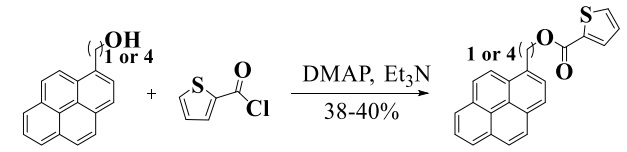

III.9 and III.10 **III.8** **III.2 and III.3**

Scheme III. 8 *Synthesis of pyrene-thiophene esters.*

The last step of the synthesis was supposed to connect first and second part of the ligand. First trial was carried out using reported procedure[341] by Knochel, consists on the selective lithiation in ortho position of thiophenes **III.2 or III.3** with n-BuLi, followed by transmetalation with zinc chloride providing thienyl-zinc reagent. Then the thienyl-zinc reagent should undergo Negishi cross-coupling with **III.1** in the presence of tetrakis(triphenylphosphine)palladium(0) [$Pd(PPh_3)_4$] (5 mol%) delivering the arylated product. However, all attempts failed.

More successful was the Kumada-Corriu cross-coupling catalyzed by palladium 1,10-bis(diphenylphosphino)ferrocene of the **III.3** magnesian.[342]

The **III.3** magnesian was obtained using lithium tributyl-magnesate (Bu_3MgLi, 1/3 equiv.) with TMEDA in THF at room temperature. However, after optimization of the conditions, we only obtained the desired product with the maximum yield of 15%, which was characterized by ^{1}H-NMR spectroscopy at room temperature (Figure III.3). The low yield of this procedure was most likely due to the lability of the ester group in **III.2** and **III.3**. Despite alternative attempts to deprotonate the thiophenes and cross-coupling them, the yields of desired products were low. These difficulties prompted us to shift our strategy replacing the thiophene for the substituted benzoic derivative.

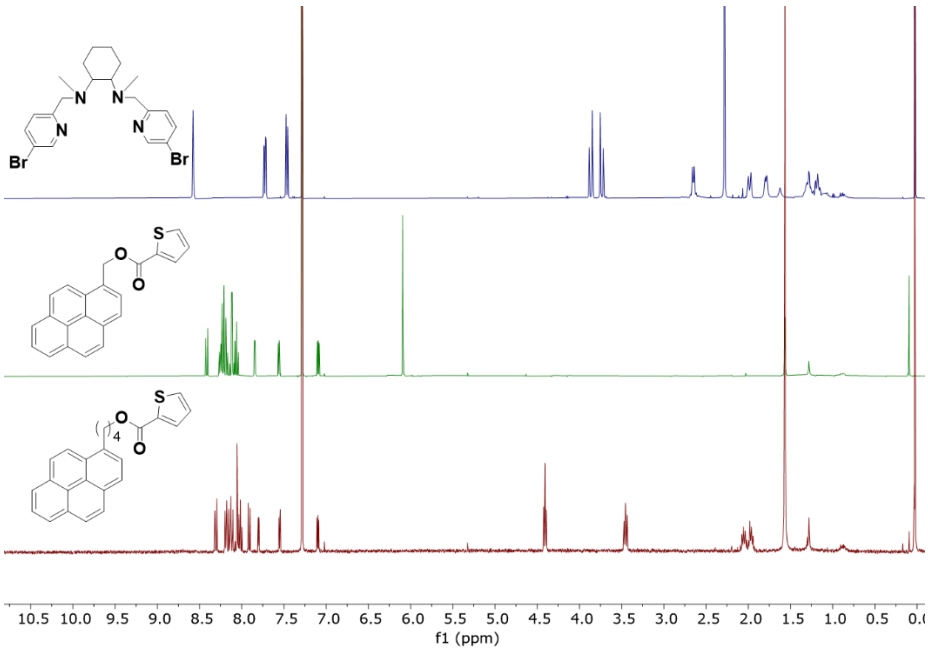

Figure III. 2 *^{1}H-NMR spectrum of the two main parts of the ligand.*

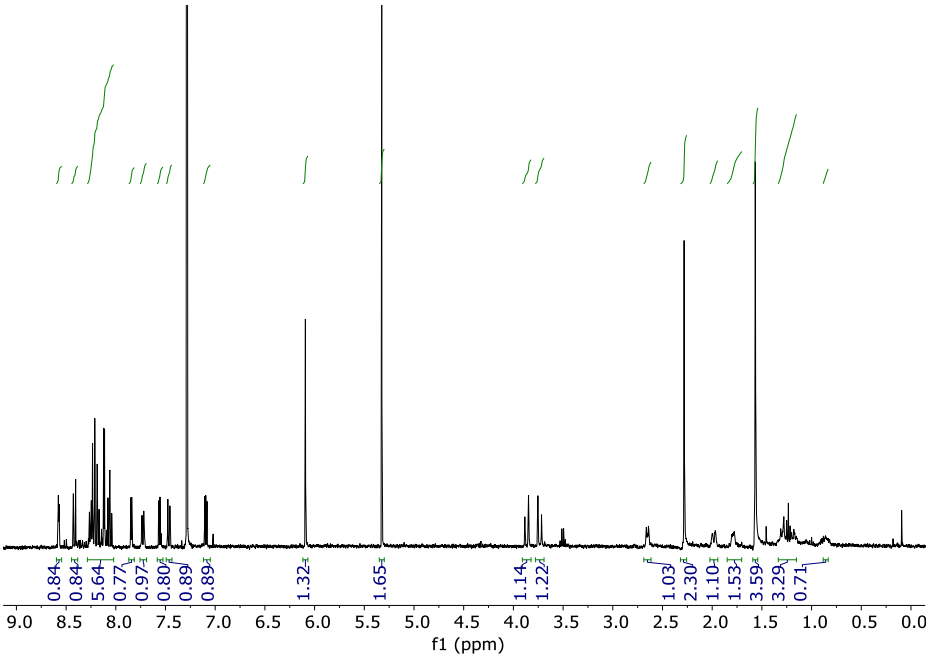

Figure III. 3 *^{1}H-NMR spectrum of the ligand* ^{PyT}***mcp***.

Finally, the successful synthetic pathway started from the condensation between the carboxylic acid (**III.20**) and alcohol containing polycyclic aromatic hydrocarbon (PAH) to get an ester (**III.22** or **III.26**). Then **III.22** or **III.26** was Suzuki-Miyaura cross-coupled with 2-(((tert-butyldimethylsilyl)oxy)methyl)-5-(4,4,5,5-tetramethyl-1,3,2-dioxaborolan-2-yl)pyridine (**III.21**) to get protected with TBS group 'arm' of a ligand (**III.23** or **III.27**). The protecting group TBS was removed, and the free hydroxyl group was treated with $SOCl_2$ to obtain the corresponding pyridyl chloride (**III.24**, **III.28**). The last step involved a direct dialkylation of *N,N′*-dimethyl-1,2-cyclohexanediamine (**III.16**) or 2,2′-bipyrrolidine (**III.25**) as backbones. Successful proceed gave ^{PyB}**mcp** (six steps, 73%)**,** ^{PyB}**pdp** (six steps, 74%) and ^{PerB}**mcp** (eight steps, 66%) in excellent total yields (Scheme III.9 and III.10). The ligands, their synthesis and their precursors were characterized by NMR, ESI-MS and elemental analysis (See section III.4.4).

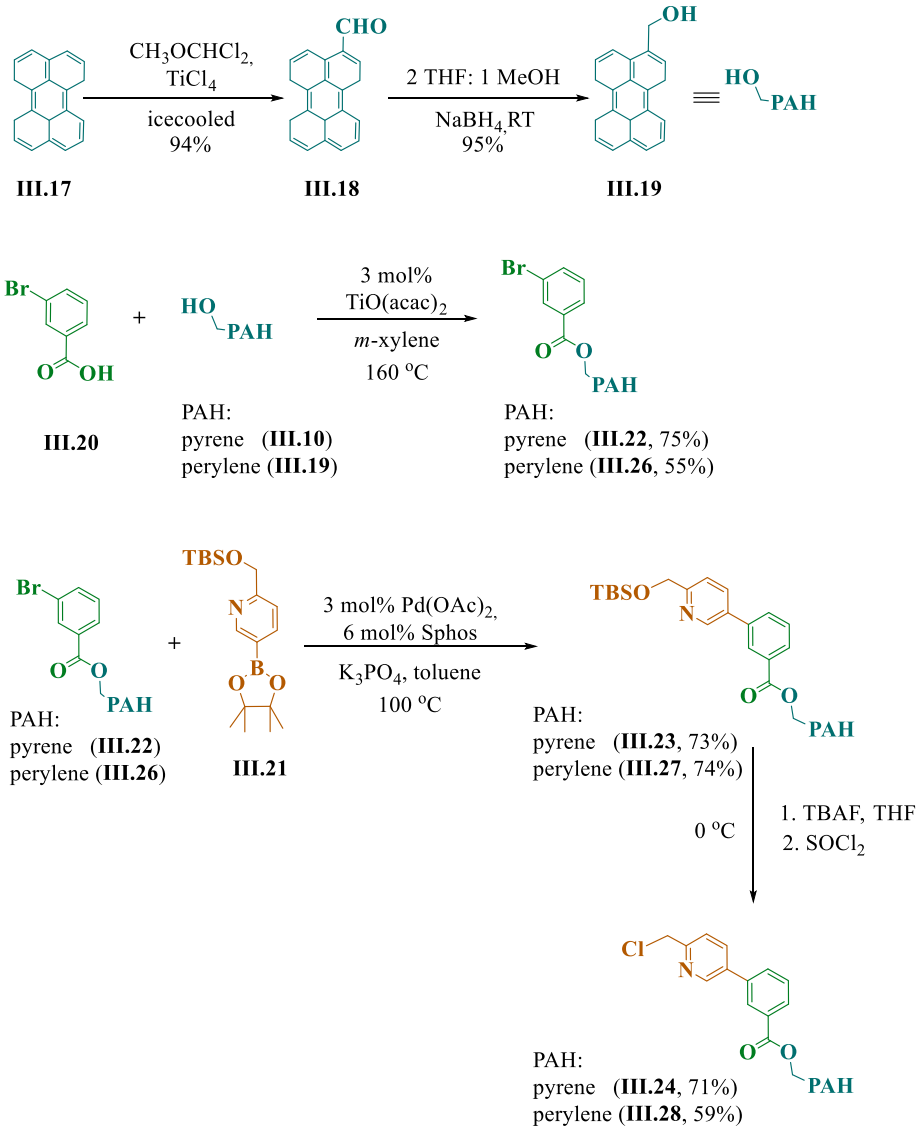

Scheme III. 9 *Synthesis of building block for the synthesis of ligands* ^{PyB}***mcp***, ^{PyB}***pdp*** *and* ^{PerB}***mcp***.

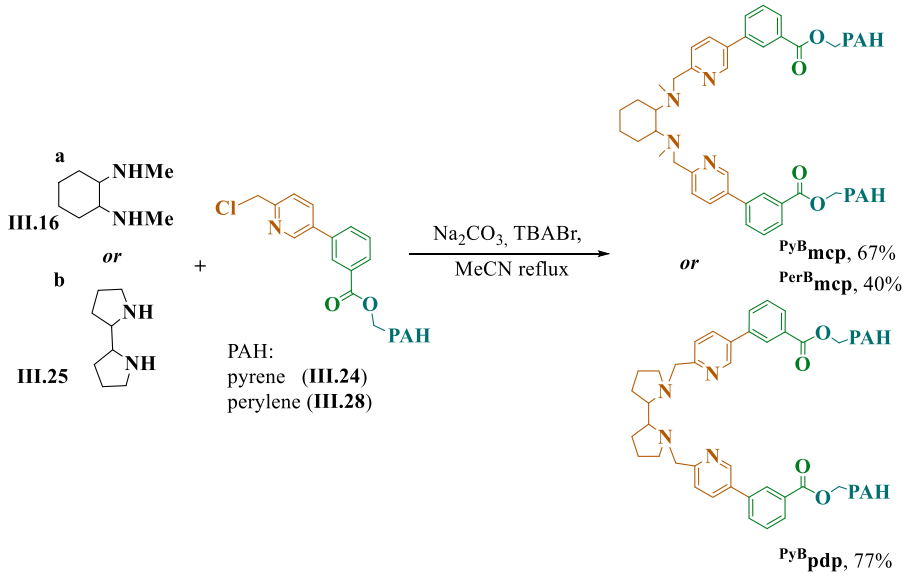

Scheme III. 10 *Synthesis of ligands* ^{PyB}***mcp***, ^{PyB}***pdp*** *and* ^{PerB}***mcp***.

Mcp type ligands are known to give rise to complexes that form two topological isomers: *cis-*α and *cis-*β. This happens during the coordination process and depends on specific metal salt employed.

We were interested in synthetizing isomers α, the C_2 symmetry, which simplifies the spectroscopy, have the advantage the produce less potential transition state during catalysis, also simplifying the study and understanding of the catalytic mechanisms and also because they revealed different catalytic activity (Scheme III.11).[343]

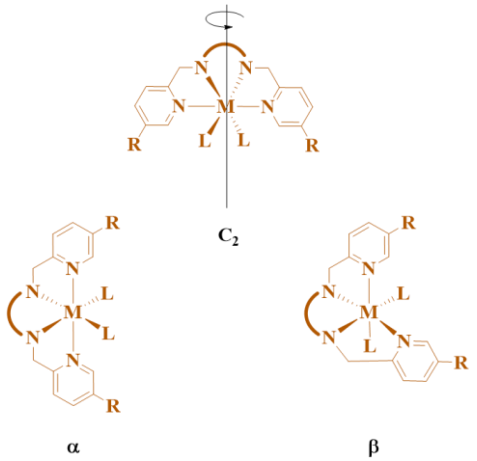

Scheme III. 11 *Two different topologies that can be adopted by tetradentate ligands such* ***mcp***.

However, direct reaction of **mcp** ligand with metal triflates generally yields the mixture of the two isomers. Despite the expected lability of 1st row metal complex in low oxidation states, like iron, cobalt and nickel, the interconversion between these two geometries is slow and does not occur even after heating for long time, because of the different configurations in the two topologies (*anti* in α isomer and *syn* in β isomer).[344]

Therefore, we selected a reaction method that produce a single isomer. The α isomers where obtained by the reaction of ligand with $CoCl_2$ salt. For di-chloride salts the preferred isomer is the α, since the chloride atoms have large enough *trans* effect to be preferentially located *trans* to the amines. Then a following halogen abstraction with AgOTf maintains the α isomer, while liberate the coordination site for more labile ligands to explore the reactivity.

Cobalt complexes (CoL_xCl_2) were obtained by reaction of the synthesized ligands with $CoCl_2$ (0.9 eq.). Then, the obtained complexes when treated with AgOTf (2.2 eq.) yielded complexes with the general structure $CoL_x(OTf)_2$ (x= ^{PyB}**mcp**, ^{PyB}**pdp**, ^{PerB}**mcp**).

To note is that for the ^{PyB}**pdp** ligand, the backbone is very rigid, which prevents the formation of other complex conformations. Therefore, in can be use directly $M(OTf)_2$ for the synthesis of the alfa isomer, but for consistency we always started with the MCl_2 in the case of the cobalt complexes. In the case of the nickel complexes we prepared them directly by reacting ^{PyB}**mcp** or ^{PyB}**pdp** with 0.9 equiv. of $Ni(OTf)_2*2CH_3CN$ (Scheme III.12).

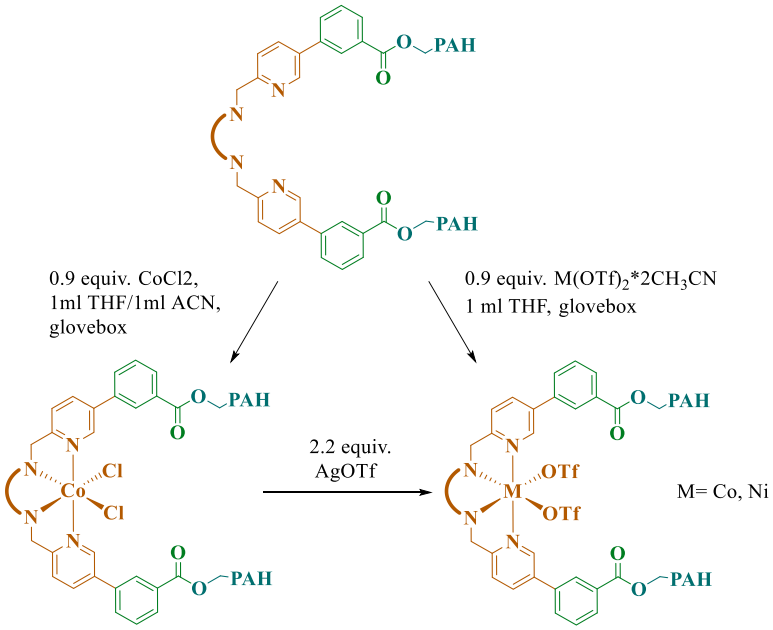

Scheme III. 12 *Synthesis of Co and Ni complexes of* ^{PyB}***mcp***, ^{PyB}***pdp*** *and* ^{PerB}***mcp***.

^{1}H-NMR spectroscopy at room temperature (Figure III.4, Figure III.5) revealed paramagnetic spectra expanding from -60 to 240 ppm. The broad window covered by the ^{1}H-NMR spectra is consistent with d^7 Co^{II} high-spin complexes. Synthetized nickel complexes also showed paramagnetic behavior, but in lower extent than in case of cobalt high-spin complexes most probably due to the location of the unpaired electrons in the eg orbitals of a pseudo-octahedral geometry.

In general, the paramagnetic spectra for these species exhibit spectral windows that expand from -20 to 250 ppm and are collected in Figure III.6. The most deshielded peaks belong to the α-protons of pyridines, since these are the hydrogens closest to the paramagnetic M^{II} center[345], because of Fermi contact interactions with the metal center.

Intense peaks found nearby the diamagnetic region are assigned to PAH moieties, indicating that these parts are placed far away from the metal center, hence the influence of the metal affect them in slight manner. All complexes exhibit features, which are united with the configuration of octahedral M^{II} paramagnetic family.

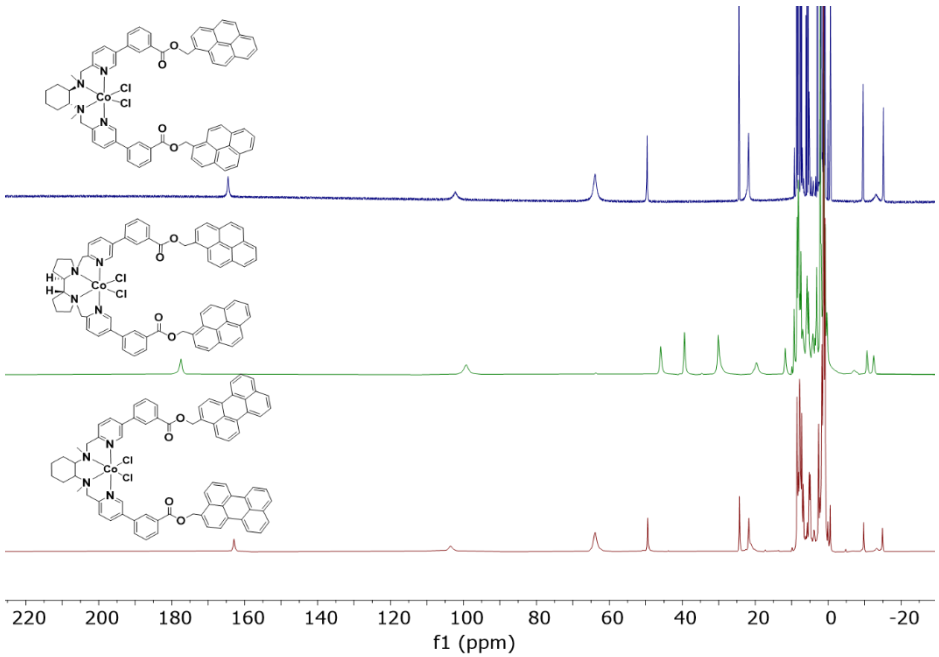

Figure III. 4 *^{1}H-NMR spectrum of* ***Co(^{PyB}mcp)Cl$_2$****,* ***Co(^{PyB}pdp)Cl$_2$*** *and* ***Co(^{PerB}mcp)Cl$_2$***

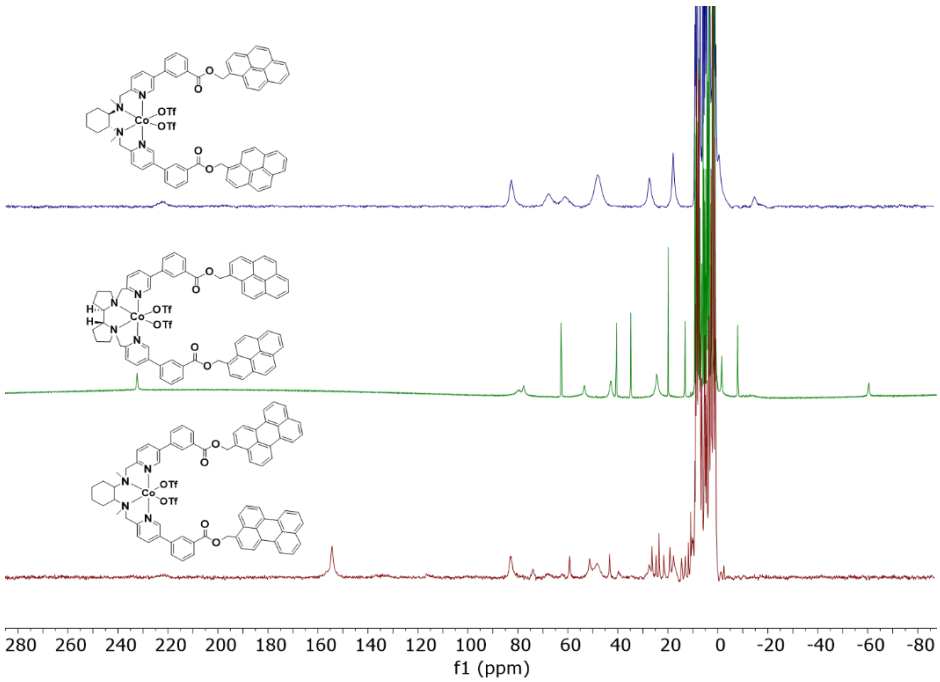

Figure III. *5 ^{1}H-NMR spectrum of* ***Co(^{PyB}mcp)(OTf)$_2$****,* ***Co(^{PyB}pdp)(OTf)$_2$*** *and* ***Co(^{PerB}mcp)(OTf)$_2$***

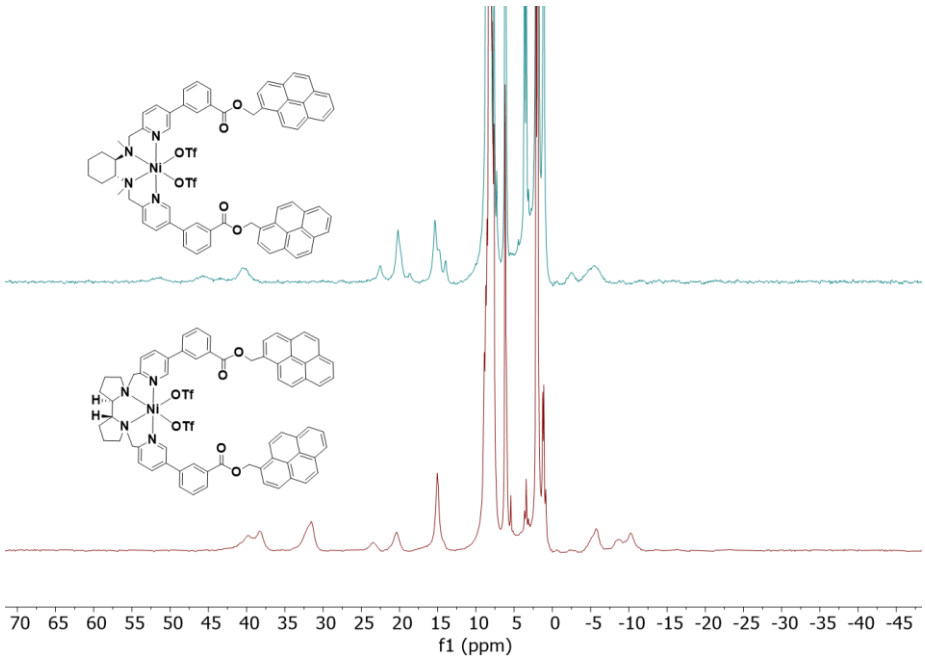

Figure III. 6 *^{1}H-NMR spectrum of* ***Ni(^{PyB}mcp)(OTf)$_2$*** *and* ***Ni(^{PyB}pdp) (OTf)$_2$.***

High resolution mass spectrometry using electrospray ionization (ESI) and matrix-assisted laser desorption/ionization (MALDI) agree with the characterization. Mono charged molecular peaks were observed for complexes Co(^{PyB}mcp)Cl$_2$ ([M-Cl]$^+$; 1086.3384 m/z), Co(^{PyB}pdp)(OTf)$_2$ ([M-OTf]$^+$; 1198.3015 m/z), Co(^{PerB}mcp)(OTf)$_2$ ([M-OTf]$^+$; 1300.3453 m/z) and the double charged molecular peak of dicationic complexes without the presence of chlorides nor triflates for Co(^{PyB}mcp)(OTf)$_2$ ([M-2OTf]$^{2+}$; 525.6828 m/z), Co(^{PyB}pdp)Cl$_2$ ([M-Cl]$^{2+}$; 524.6759 m/z), Ni(^{PyB}mcp)(OTf)$_2$ ([M-2OTf]$^{2+}$; 525.1835 m/z) and Ni(^{PyB}pdp)(OTf)$_2$ ([M-2OTf]$^{2+}$; 524.1769 m/z).

Unfortunately, any of the desired structures could be stablished by X-Ray diffraction analysis. Attempts performed to grow crystalline structures by slow diffusion yielded precipitates. However, after addition of an excess of CoCl$_2$ to **^{PyB}mcp**, recrystallization of the resulting compound by slow diffusion of a dichloromethane solution with ethyl ether formed small blue crystals of Co$_2$(^{PyB}mcp)Cl$_4$. This single-crystal analysis showed the formation of a distorted octahedral complex formed by the tetracoordinated ligand bonded to

the cobalt with two pyridines and two amines of the *N,N′*-dimethyl-1,2-cyclohexanediamine backbone. The coordination sphere of the cobalt complex was completed with two chlorides bridging a cobalt dichloride (Figure III.7)

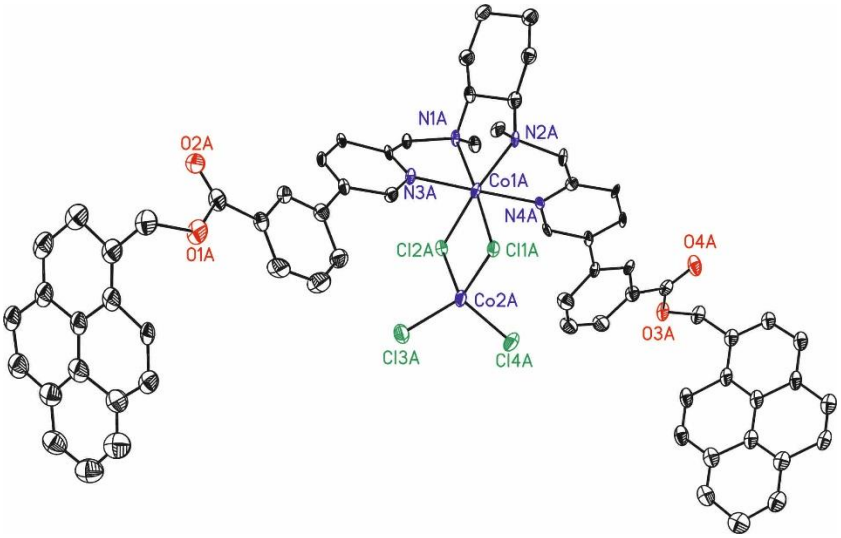

Figure III. 7 *ORTEP with ellipsoids of* ***$Co_2(^{PyB}mcp)Cl_4$*** *from the X-ray diffraction analysis. Hydrogen atoms have been omitted for clarity.*

Table III.1 Selected bond lengths (Å) and angles (°) of $Co_2(^{PyB}mcp)Cl_4$.

$Co_2(^{PyB}mcp)Cl_4$			
Co1A-N1A	2.13(2)	N1A-Co1A-N2A	83.1(8)
Co1A-N2A	2.14(2)	N1A-Co1A-N3A	78.2(8)
Co1A-N3A	2.15(2)	N2A-Co1A-N2A	101.5(7)
Co1A-N4A	2.157(19)	N1A-Co1A-N4A	100.3(7)
Co1A-Cl1A	2.509(8)	N2A-Co1A-N4A	78.4(7)
Co1A-Cl2A	2.489(8)	N3A-Co1A-N4A	178.5(9)
		N1A-Co1A-Cl1A	170.7(5)
		N2A-Co1A-Cl2A	170.6(5)

Selected bond distances (Å) and angles (°) are collected in Table III.1. The average Co-N bond lengths are between 2.0 and 2.2 Å, which is characteristic for high-spin Co^{II} complexes with S = 3/2. The bond lengths of Co-N for two pyridines are in the range of expected values ca. 2.16 as well as for the alkyl amines ca. 2.14.[65, 346]

III.2.2 Synthesis and Characterization of model ligands and their complexes

The model ligands and their complexes were synthetized with aim of understanding the influence of each part of the ligand and to value the difficulties involved in the synthesis of the desired ligands and complexes. All ligands and complexes were prepared following the analogous procedures which were used for the desired compounds (Scheme III.8 and Scheme III.9). Synthesis of model complexes started from the smallest molecules of **mcp** and **pdp**, together with their cobalt complexes by direct dialkylation of the commercially available backbone (*R*,*R*)-(−)-*N*,*N*′-Dimethyl-1,2-diaminocyclohexane (**mcp**) or (R,R)-2,2′-bipyrrolidine L-tartrate trihydrate (**pdp**) with 2.1 equivalents of 2-(chloromethyl)pyridine hydrochloride giving the product in 60% and 62% of yield, respectively.

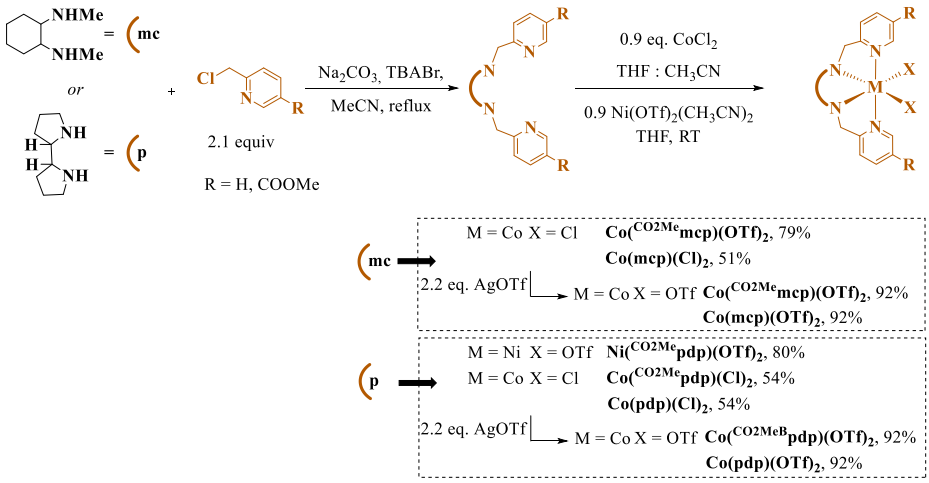

Scheme III. 13 *Synthesis of* ^{CO2Me}***mcp***, ^{CO2Me}***pdp***, ***mcp***, ***pdp*** *and their cobalt complexes.*

These ligands were then transformed into corresponding cobalt complexes in good yields (up to 92%). Next, ligands ^{CO2Me}**mcp** and ^{CO2Me}**pdp** were obtained by the same synthetic method as the one employed for **mcp** and **pdp**, but using 2.1 equivalents of methyl 6-(chloromethyl)nicotinate for alkylation as a β-substituted pyridine analog of 2-(chloromethyl)pyridine. In this case, the yields were 44% and 51% of product for ^{CO2Me}**mcp** and ^{CO2Me}**pdp**, respectively. Their chloride cobalt complexes were obtained by mixing the ligand with 0.9 equivalent of $CoCl_2$. Then, the obtained complexes were transformed to their bis-triflate analogs by halogen abstraction using 2.2 equivalent of AgOTf (Scheme III.13).

Ligands ^{CO2MeB}**mcp** and ^{CO2MeB}**pdp (B** –benzoic moiety) are the closest model to our designed ligands with π-staking units (Figure III.8).

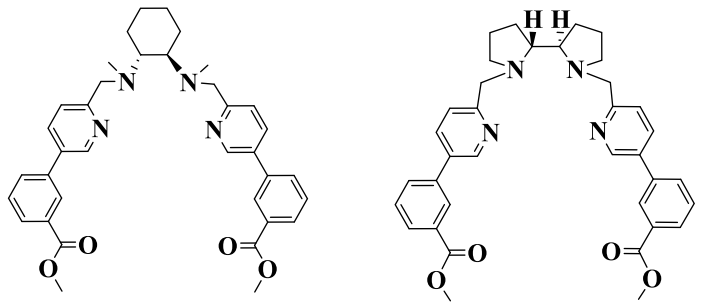

^{CO2MeB}**mcp** ^{CO2MeB}**pdp**

Figure III. 8 *New tetradentate chiral ligands* ^{CO2MeB}***mcp*** *and* ^{CO2MeB}***pdp***

First step to derivatize the arm of the ligand was the cross-coupling reaction between methyl 3-bromobenzoate and 2-(((tertbutyl-dimethylsilyl)oxy)methyl)-5-(4,4,5,5-tetramethyl-1,3,2-dioxaborolan-2-yl)pyridine providing methyl 3-(6-(((tert-butyldimethylsilyl)oxy)methyl)pyridin-3-yl)benzoate. Then, the deprotection reaction of this compound with TBAF followed by chlorination with $SOCl_2$ gave methyl 3-(6-(chloromethyl)pyridin-3-yl)benzoate. Having the new arm of ligand in hand, alkylation of the backbones was performed, delivering new ligands in 45% (^{CO2MeB}**mcp**) and 40% (^{CO2MeB}**pdp**), which went through a

reaction with cobalt and nickel salts to give new four-coordinated complexes (Scheme III.14).

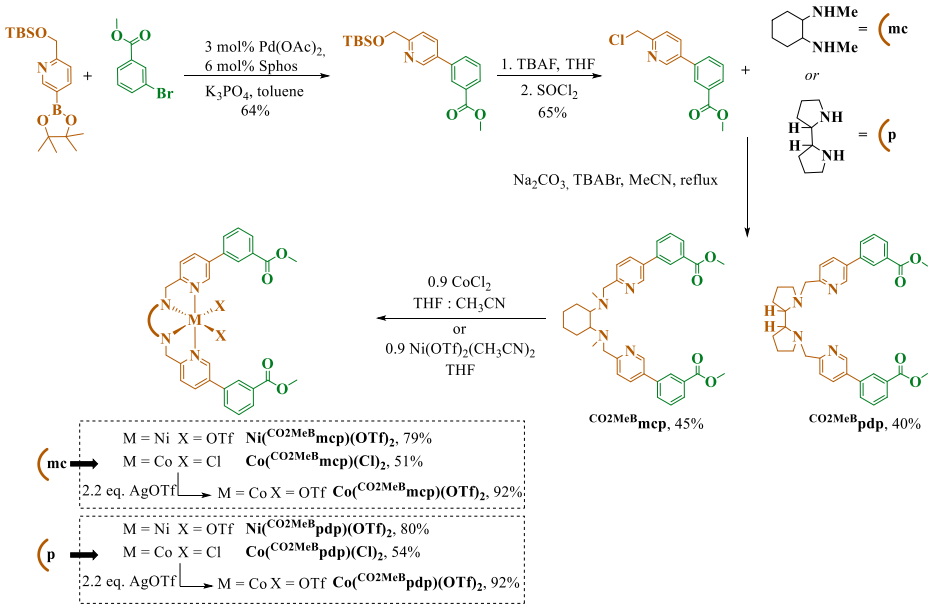

Scheme III. 14 *Synthesis of* ^{CO2Me}***mcp***, ^{CO2Me}***pdp*** *and their cobalt and nickel complexes.*

The ligands, their precursors and cobalt and nickel complexes were characterized by NMR, ESI-MS, X-Ray analysis and elemental analysis (See section III.4.6).

^{1}H-NMR spectra of cobalt chloride complexes at room temperature are collected in the Figure III.7, bis-triflate cobalt and nickel complexes in Figure III.8. Model complexes revealed to be paramagnetic species expanded in the region from -20 to 180 ppm. As aforementioned complexes, model cobalt complexes showed to be more paramagnetic than model nickel complexes.

The formation of model complexes was confirmed by high resolution mass spectrometry using electrospray ionization (ESI) (See section III.4.6).

All of model cobalt complexes structures could be stablished by X-Ray diffraction analysis. The recrystallization of compounds to grow the crystals was carried out by slow diffusion and small crystals were obtained in all cases. These single-crystal were analyzed and the analysis confirms the formation of distorted octahedral complexes formed by a tetracoordinated ligand bonded to

the cobalt by two pyridines, two amines of the *N*,*N*′-dimethyl-1,2-cyclohexanediamine or 2,2′-bipyrrolidine.

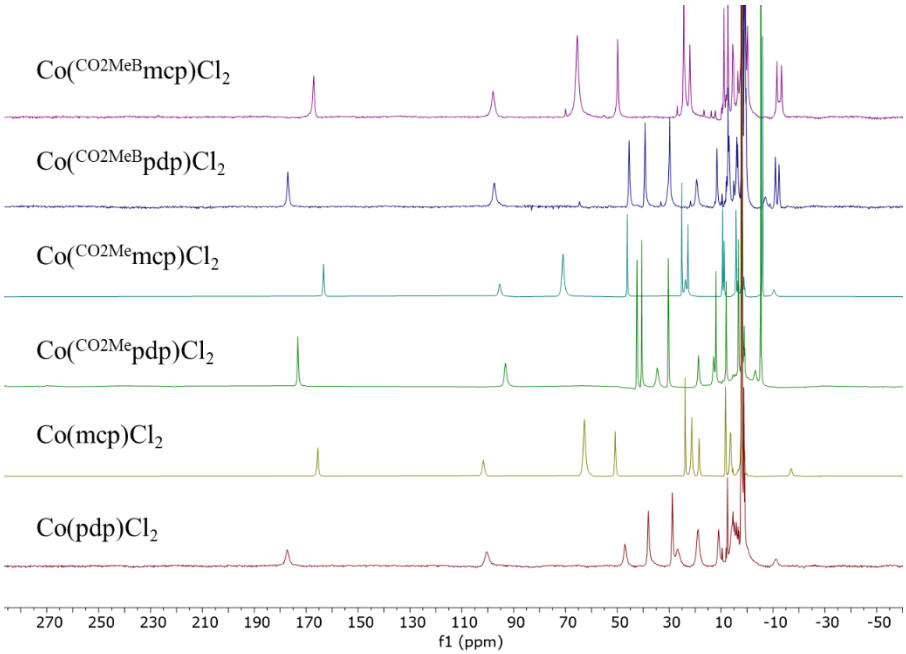

Figure III. 9 *^{1}H-NMR spectra of* ***Co(^{CO2MeB}mcp)Cl$_2$, Co(^{CO2MeB}pdp)Cl$_2$, Co(^{CO2Me}mcp)Cl$_2$, Co(^{CO2Me}pdp)Cl$_2$, Co(mcp)Cl$_2$*** *and* ***Co(pdp)Cl$_2$.***

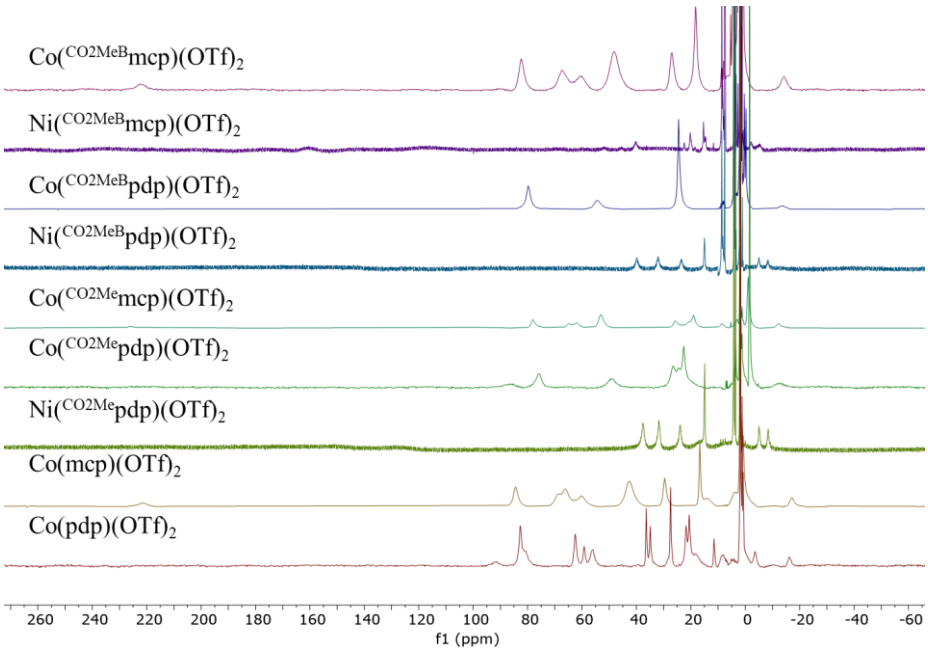

Figure III. 10 *^{1}H-NMR spectra of* ***Co(^{CO2MeB}mcp)(OTf)$_2$, Ni(^{CO2MeB}mcp)(OTf)$_2$, Co(^{CO2MeB}pdp)(OTf)$_2$, Ni(^{CO2MeB}pdp)(OTf)$_2$, Co(^{CO2Me}mcp)(OTf)$_2$, Co(^{CO2Me}pdp)(OTf)$_2$, Ni(^{COOMe}pdp)(OTf)$_2$, Co(mcp)(OTf)$_2$*** *and* ***Co(pdp)(OTf)$_2$.***

III.2.3 Photocatalytic hydrogen evolution from water

III.2.3.1 Influence of the counterion, metal and ligand

The photocatalytic reactions employing Co^{II} complexes were examined towards their catalytic activity. Catalysis was performed under irradiation with LED (450±20 nm) using photocatalyst and a sacrificial electron donor. Light-driven reduction of water was online-monitored by recording the increase in pressure of the headspace, the difference of pressure between the reaction mixture and reference reaction vial. The catalytic reactions were performed in a mixture of water and acetonitrile. In this system, the role of acetonitrile was to ensure the dissolution of the photocatalyst. After the reaction was finished (reached plateau), the amount of hydrogen obtained in the reaction was quantified by the analysis of an aliquot of gas at the headspace by gas chromatography (GC-TCD) (See section III.4.3) confirming the monitored traces with the pressure sensors.

The catalytic ability of complexes with chlorides or triflates as the counterions towards photocatalytic water reduction to H_2 was carried out by preparing the reaction mixture containing 50 μM of cobalt complex, 150 μM of [Ir(ppy)$_2$bpy] (**PC$_{Ir}$**, ppy: phenyl pyridine, bpy: bipyridine) photosensitizer and 200 μL of triethylamine (Et_3N) in water/acetonitrile solvent mixture (6:4 mL) at room temperature (25 ^oC) under nitrogen atmosphere which was irradiated in septum-capped vial.

The effect of the ligand parts was tested by studying the different complexes to understand their influence on the total catalytic activity in the photocatalytic water reduction. Principally, catalysts bearing chloride counterions were found to be active under applied conditions (Figure III.11). Interestingly, complexes possessing in their ligand the spacer unit alone (Co(^{PyB}mcp)Cl$_2$, Co(^{B}mcp)Cl$_2$) and the spacer-polyaromatic unit (Co(^{PyB}pdp)Cl$_2$ and Co(^{B}pdp)Cl$_2$) revealed higher catalytic activity than the simpler counterparts. The highest TONs ($n_{H2}/n_{complex}$) were achieved by Co(^{PyB}pdp)Cl$_2$ and Co(^{B}pdp)Cl$_2$ with a value of 264 (2.4 mL H_2) and 240 (2.2 mL H_2) along with TOF (TON/h) values of 158 and 143, respectively. Their analogs, Co(^{PyB}mcp)Cl$_2$ and Co(^{B}mcp)Cl$_2$, produced also substantially amount of hydrogen, 1.8 mL (192 TON) and 1.9 mL (201 TON) with TOF of 115 and 120 h^{-1}, respectively. The least active complexes were the Co(^{CO2Me}pdp)Cl$_2$ unveil to carry out the reduction of water with still high activity (174 TON), delivering 1.7 mL of H_2, and the Co(pdp)Cl$_2$ with much lower activity (96 TON, 1.0 mL H_2).

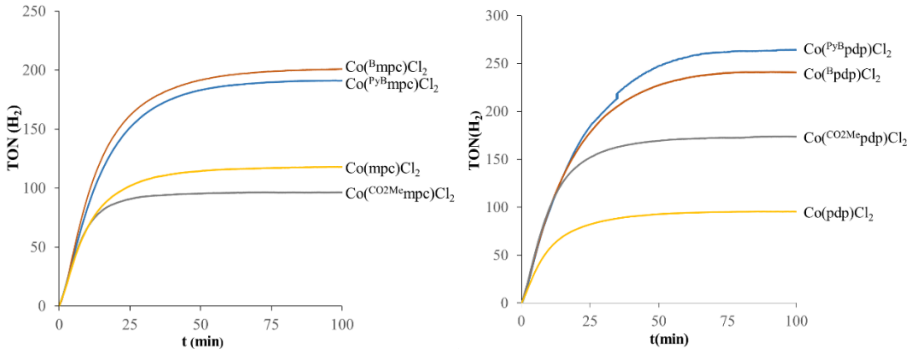

Figure III. 11 *Traces of photocatalytic hydrogen evolution (TON) by anchoring pyrene complexes with* ***mcp*** *(left) and* ***pdp*** *skeleton bearing chloride counterions with* ***PC$_{Ir}$*** *in solvent mixture $CH_3CN:H_2O:Et_3N$ (4:6:0.2) under irradiation with LED (450±20 nm), under nitrogen.*

Subsequently, complexes with triflate counterions were examined in hydrogen evolution light-driven reaction (Figure III.12). An interesting result was observed for complexes Co(^{B}mcp)(OTf)$_2$ and Co(^{B}pdp)(OTf)$_2$. These two cobalt complexes operate slightly better than their polyaromatic correlates, reaching in both cases similar activity (ca. 2.3 mL of H_2, and about TON 245 – 246 and TOF 146 h^{-1}). Next most active species were complexes with pyrene Co(^{PyB}mcp)(OTf)$_2$ and Co(^{PyB}pdp)(OTf)$_2$ reaching 1.8 mL (194 TON) and 2.2 mL (239 TON) of H_2. Complexes without benzoic group (spacer) but carrying carboxyl group were also examined, revealing lower activity towards hydrogen evolution for both - cyclohexanediamine (mcp) and bipyrrolidine (pdp) based complexes. Co(^{CO2Me}mcp)(OTf)$_2$ performed with the lower activity than previous complexes with triflate counterions, giving rise to 1.4 mL of H_2 with a TON and TOF values of 122 and 73 h^{-1} and its counterpart Co(^{CO2Me}pdp)(OTf)$_2$ gave of 1.8 mL of H_2 with a TON and TOF values 145 and 86 h^{-1}. Finally, simple complexes Co(mcp)(OTf)$_2$ and Co(pdp)(OTf)$_2$ disclosed the lowest activity.

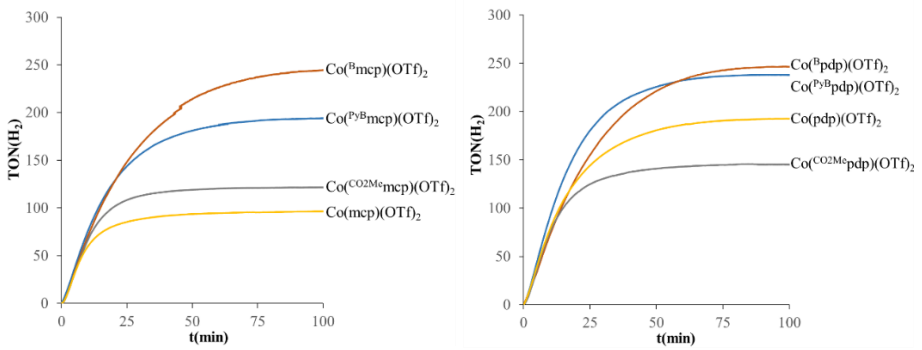

Figure III. 12 *Traces of photocatalytic hydrogen evolution (TON) by anchoring pyrene complexes with* ***mcp*** *(left) and* ***pdp*** *backbone bearing triflate counterions with* ***PC$_{Ir}$*** *in solvent mixture $CH_3CN:H_2O:Et_3N$ (4:6:0.2) under irradiation with LED (450±20 nm), under nitrogen.*

The light-driven hydrogen evolution activity was tested for complexes bearing perylene unit and compared the performance with their pyrene analogs (Figure III.13).

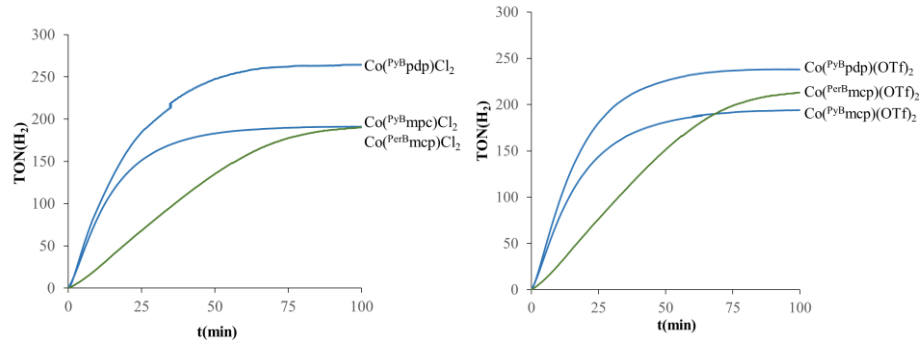

Figure III. 13 *Traces of photocatalytic hydrogen evolution to compare the catalytic ability of anchoring complexes bearing pyrene and perylene with chloride (left) and triflate counterions with* ***PC$_{Ir}$*** *in solvent mixture $CH_3CN:H_2O:Et_3N$ (4:6:0.2) under irradiation with LED (450±20 nm), under nitrogen.*

For the two synthesized cobalt complexes with the perylene unit, the effect on catalysis is different. In particular, the TOF was significantly lower in both cases when compared with the rest, but TON values were similar after 100 min of reaction. Co(^{PerB}mcp)Cl_2 produced 1.8 mL of H_2 (192 TON), reaching the similar amounts as produced by Co(^{PyB}mcp)Cl_2. While Co(^{PerB}mcp)$(OTf)_2$ showed to perform slightly better than its pyrene counterpart Co(^{PyB}mcp)$(OTf)_2$ with 216 TON and 2.4 mL of H_2.

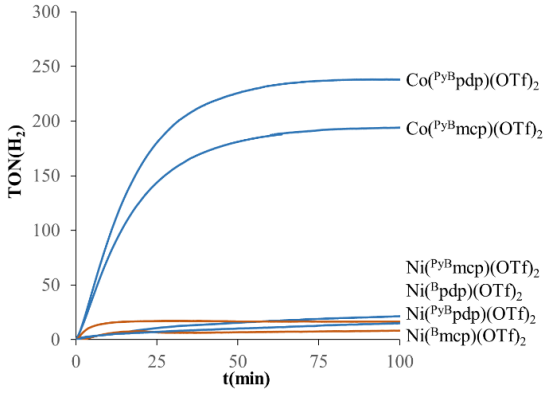

Figure III. 14 *Traces of photocatalytic hydrogen evolution (TON) by Co^{II} and Ni^{II} anchoring pyrene complexes with* ***mcp*** *(left) and* ***pdp*** *backbone bearing triflate counterions with* ***PC_{Ir}*** *in solvent mixture $CH_3CN:H_2O:Et_3N$ (4:6:0.2) under irradiation with LED (450±20 nm), under nitrogen.*

Photocatalytic water reduction activity was also tested for nickel complexes prepared with the ^{PyB}**mcp**, ^{PyB}**pdp**, ^{B}**mcp** and ^{B}**pdp** ligands under the same reaction conditions than the cobalt complexes. The results showed a general lower activity compared to their cobalt analogues. Ni(^{PyB}mcp)$(OTf)_2$ Ni(^{PyB}pdp)$(OTf)_2$ Ni(^{B}mcp)$(OTf)_2$ and Ni(^{B}pdp)$(OTf)_2$ reached TONs of 23,–16, 9 and 18, respectively (Figure III.14). We attributed this difference in reactivity because it's less favorable for the nickel complexes to form Ni-H structure at the pH (11.9) imposed by the Et_3N (2% v/v, pKb = 3.25). [302]

To prove that all components (catalyst, photosensitizer and electron source) are needed for the H_2 photochemical generation control experiment were performed. Additionally, reactions performed in dark did not produce any detectable amount of gas.

In summary, we report a new methodology for the synthesis of new aminopyridine ligands that contain a π-stacking polyaromatic unit such as pyrene or perylene. Cobalt complexes of new designed ligands showed to be highly active in water reduction using H_2O as the source of hydrides, an iridium photoredox catalyst, an amine (Et_3N) as the sacrificial electron donor and visible light as the driving force. Due to the easy decoordination of chlorides from the catalysts, it results in very similar activity to catalysts with triflate ion.

Moreover, our system shows that the combination with the bromobenzoic spacer (**B**) and polyaromatic moiety fragments enhances the catalysis and it forms very competitive to previously reported in literature catalysts.

III.2.3.2 Towards photochemical H_2 evolution in pure water using supramolecular interactions.

Water, from noncatalytic aspect is green, nontoxic and inexpensive solvent that meets the principles of green chemistry.[347] However, all synthetized cobalt complexes in this chapter present very low solubility in pure water, especially insoluble are those more active in H_2 evolution, the ones bearing the pyrene and perylene moiety. Thus, we propose to use supramolecular interactions to help solubilizing the catalysts in pure water. In particular, pyrene and perylene are known to strongly interact with γ-cyclodextrin, which thanks to their 24 alcohol groups is highly soluble in water (232 g/L or 179 mM).

First, the catalytic activity for hydrogen evolution was studied under the same reaction conditions previously employed for the Co(^{PyB}mcp)$(OTf)_2$ and Co(^{PyB}pdp)$(OTf)_2$ complexes (See section III.2.2.1), but with the addition of 50 μM of γ-cyclodextrin (γ-CD). Vials with reaction mixtures were stirred for 60 minutes before irradiation to ensure the interaction between pyrene unit and cyclodextrin cavity.

Both complexes were active in light-driven H_2 evolution without a significant change when compared with reactions without γ-CD. Since the quantity of produced H_2 was 1.8 mL and 2.5 mL with TON values of 198 and 274 along with TOF of 99 and 137 h^{-1} for Co(^{PyB}mcp)$(OTf)_2$ and Co(^{PyB}pdp)$(OTf)_2$ Second, the amount of γ-CD in water reduction was increased to 2 mM and to 12.5 mM (Figure III.15), but as in the previous case, the changes were insignificant with the resulting 1.8 and 2.5 mL of hydrogen for Co(^{PyB}mcp)$(OTf)_2$ and Co(^{PyB}pdp)$(OTf)_2$, respectively.

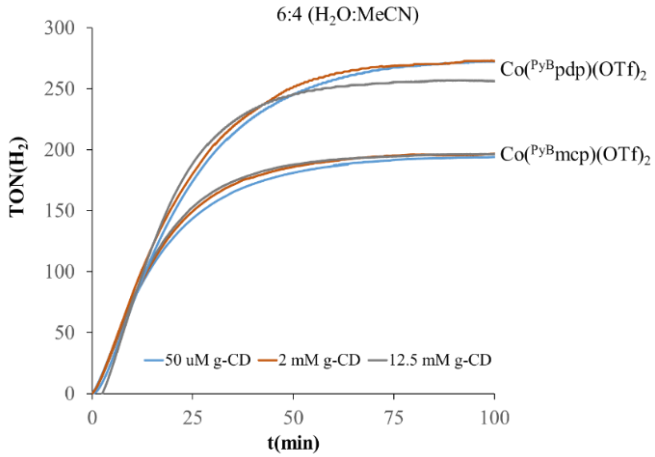

Figure III. 15 Traces of photocatalytic hydrogen evolution (TON) by cobalt model complexes with γ-CD with **PC_{Ir}** under irradiation with LED (450±20 nm), under nitrogen in solvent mixture $CH_3CN:H_2O:Et_3N$ (4:6:0.2).

Furthermore, the volume of water in the reaction mixture was increased from 6 mL to 7 mL and catalysis was set up both ways - with and without γ-CD. Both cases showed increase in the reaction time indicating possible interaction between pyrene unit and cyclodextrin ring. Set ups with cyclodextrin were slightly less active than without it, for $Co(^{PyB}mcp)(OTf)_2$ the TON was 162 with 2 mM of γ-CD (1.5 mL H_2) and 193 without (1.8 mL H_2). For $Co(^{PyB}pdp)(OTf)_2$ the TON was 199 with γ-CD (1.8 mL H_2) and 223 without the γ-CD (2.1 mL H_2) (Figure III.16). Surprisingly, higher concentration of γ-CD (12.5 mM) in the reaction mixture with cobalt complexes revealed to have slightly better activity than the catalysis containing 2 mM of γ-CD, producing 1.6 mL of H_2 with TON of 167 for $Co(^{PyB}mcp)(OTf)_2$ and 1.8 mL of H_2 with 202 TON for $Co(^{PyB}pdp)(OTf)_2$.

Then, we tested the effect of increasing the ratio of water from 7.5 and 8 mL. This change showed a lower general activity, but longer reaction time for both cobalt complexes. When tested water as the only solvent, hydrogen evolution was much lower (TON = 11) in comparison with previous results. We rationalize this fact due to the low solubility of photosensitizer in water, since yellow precipitates were apparent.

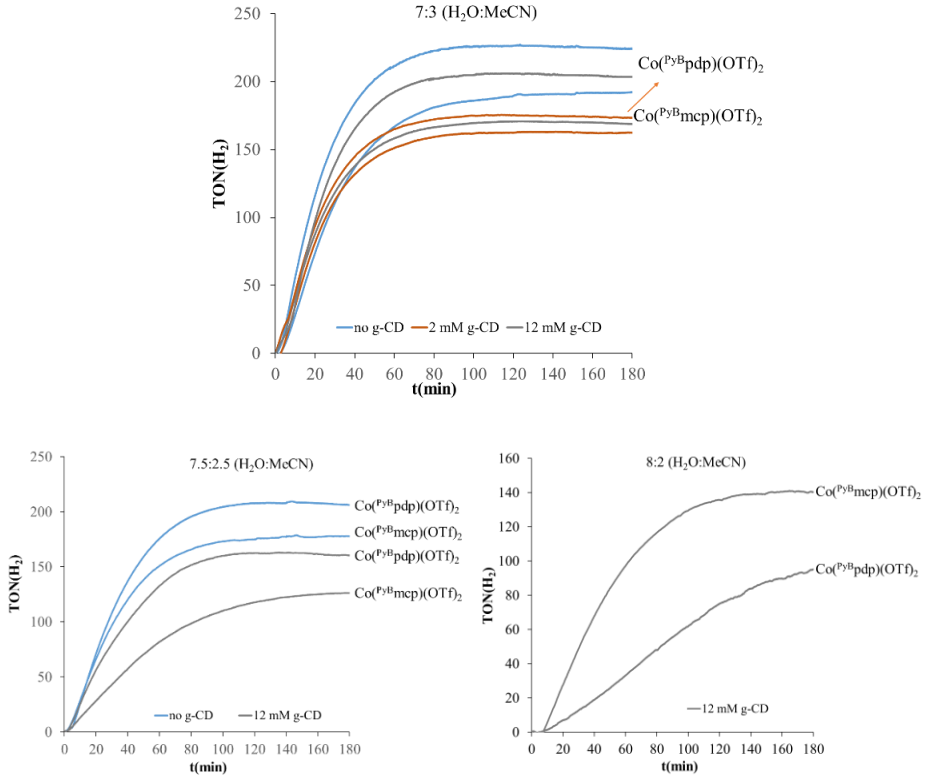

Figure III. 16 *Traces of photocatalytic hydrogen evolution (TON) by cobalt model complexes with γ-CD with* ***PC$_{Ir}$*** *under irradiation with LED (450±20 nm), under nitrogen in solvent mixture H_2O:CH_3CN:Et_3N (7:3:0.2) (top). H_2O:CH_3CN:Et_3N (7.5:2.5:0.2) (left) and in solvent mixture H_2O:CH_3CN:Et_3N (8:2:0.2) (right).*

Then, with the aim to have the same concentration of photoredox catalyst in solution to be able to compare the reactivity, we employed the same strategy to increase the solubility of the photosensitizer in water. In this regard, a new Ir-pyrene-photosensitizer (**PC$_{Irpyrene}$**) was synthetized (See section III.4.7) aiming for π-π stacking interaction with the γ-CD and perhaps the catalysts containing polyaromatic units *via* supramolecular interactions. The strategy was successful archiving the requited solubility, proceeding to the catalytic studies. Catalytic studies of H_2 production were carried out in a similar manner as before, preparing the reaction mixture containing 50 μM of cobalt complex, 150 μM of **PC$_{Irpyrene}$** photosensitizer, 12.5 mM of γ-CD and 200 μL of triethylamine (Et_3N) in water/acetonitrile solvent mixture (8:2, 8.5:1.5, 9:1,

9.5:0.5 and 10:0) at room temperature (25 ºC) under nitrogen atmosphere which was irradiated from 2 to 16 h.

The first result that is interesting to analyze is the general reduction of catalytic activity when using the new photoredox catalyst (TON < 100, Figure III.17).

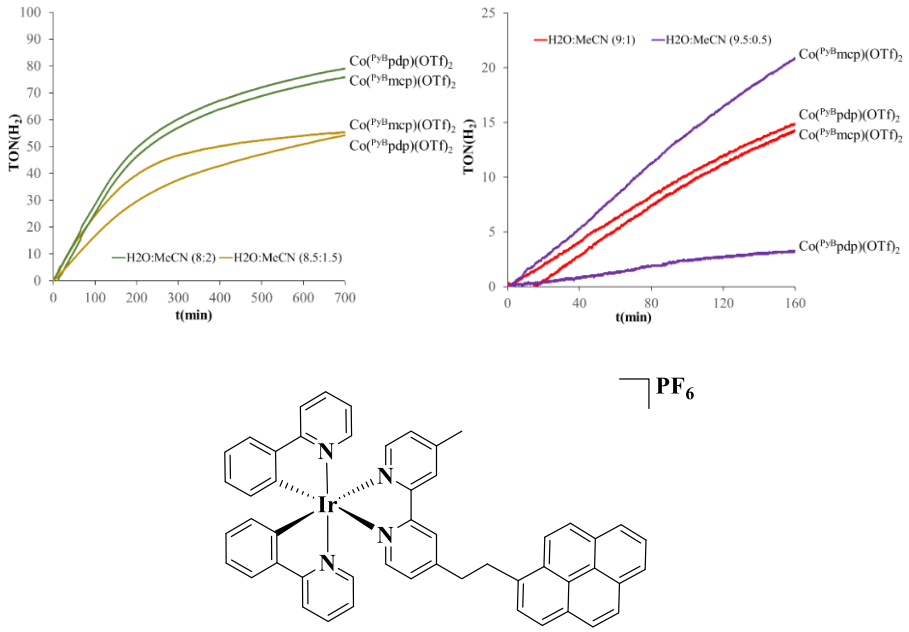

Figure III. 17 *Top) Traces of photocatalytic hydrogen evolution (TON) by cobalt model complexes with γ-CD (12.5 mM) with* ***PC****Irpyr* *under irradiation with LED (450±20 nm), under nitrogen in solvent mixture* H_2O:CH_3CN:Et_3N *(8:2:0.2 and 8.5:1.5:0.2) (left) and in solvent mixture* H_2O:CH_3CN:Et_3N *(9:1:0.2 and 9.5:0.5:0.2) (right). Bottom) Line drawing structure of* ***PC****Irpyr*.

This result is consistent with a model where the PC and cobalt catalyst does not share the same CD. We discarded that changes in redox potentials could decrease the catalytic activity since donating groups over the bpy (in this case weakly electron-donating alkyl chains) brings more reductive complex. However, at the moment we also cannot discard potential changes in the photochemistry. Nevertheless, at this point we favor the reasonable hypothesis that the highly solvated systems prevent from a close interaction between the PC and the cobalt catalyst preventing from the single electron transfer process (SET) between them.

Therefore, we replaced the iridium photocatalyst for a water soluble one, the [Cu(Batho-SO_3^-)(Xantphos)Na] (**PC_{Cu}**) designed and synthetized previously in our group.[348] Now, the catalysis in pure water yielded 83 TON for Co(^{PyB}mcp)$(OTf)_2$ and 39 for Co(^{PyB}pdp)$(OTf)_2$ (Figure III.18). Although the catalytic activity was low compared to systems with the organic phase, the result is significant, since the amount of H_2 obtained with PC_{Ir} or $PC_{Irpyrene}$ under the same conditions was in the detection limit < 2 TONs. More interestingly, the results all together indicate that the supramolecular interaction can be used to facilitate the catalytic activity in pure water.

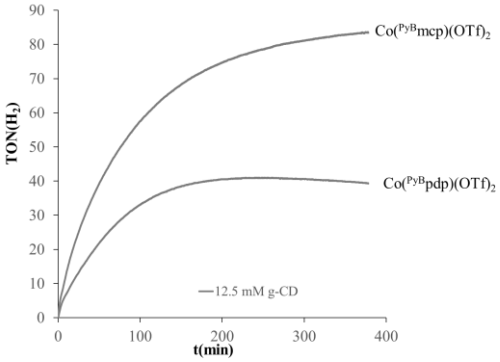

Figure III. 18 *Traces of photocatalytic hydrogen evolution (TON) by cobalt model complexes with γ-CD with* ***PC_{Cu}*** *under irradiation with LED (450±20 nm), under nitrogen in solvent mixture H_2O:Et_3N (10:0.2).*

III.2.4 Photocatalytic reduction of acetophenone and cross-coupling reaction

Encouraged by the excellent performance of cobalt complexes in hydrogen evolution, we executed further studies on catalysis. Taking advantage of polyaromatic moiety in the structure of the ligand, we used two different strategies to obtain a non-covalently attached to material catalyst. First, we further explored the interaction between the cyclodextrin (γ-CD) and the pyrene complexes in a similar manner than explained above. Second procedure involved the use for carbon nanomaterials[349] by anchoring the pyrene species on material's surface. We employed, fullerene (C_{60}), nanotubes (NT), functionalized nanotubes with COOH (NT-COOH) and nanofibers (NF) as a

nanomaterials for the anchoring of the catalyst. The catalysts prepared by sonication of metal complexes with carbon nanomaterials, then stirring for 24 h and washing them with DCM were used in catalysis.

Photocatalytic studies involve the reduction of acetophenone and cross-coupling reaction. These catalytic tests were carried out in collaboration with D. Pascual, J. Aragon and Dr. C. Casadevall, PhD students of our research group.

For the reduction of acetophenone to 1-phenylethanol catalyzed by Co(^{PyB}mcp)(OTf)$_2$ and Co(^{PyB}pdp)(OTf)$_2$ (See Scheme III.15) the reactions were carried out using acetophenone (10 mM), cobalt catalyst (3 mol% of Co(^{PyB}mcp)(OTf)$_2$ or Co(^{PyB}pdp)(OTf)$_2$) anchored to the material in a 1:10 or 1:33 ratio and with [Ir(^{NMe2}bpy)(ppy)$_2$]PF$_6$ (^{NMe2}**PC$_{Ir}$** 1.5 mol%) in a solvent mixture of MeCN:H_2O:Et_3N (0.4:0.6:0.02, total volume - 300 uL) at room temperature (25 ^{o}C) under nitrogen atmosphere. The mixtures were irradiated during 48 h with blue LEDs (See Table III.2). The two studied cobalt catalysts (Co(^{PyB}mcp)(OTf)$_2$ and Co(^{PyB}pdp)(OTf)$_2$) were active for ketone reduction in combination with ^{NMe2}PC$_{Ir}$ and blue light (entry 1 and 12, Table III.2).

Since the tested cobalt catalysts contain pyrene units, which can favor intermolecular interactions with carbon-based macromolecules or nanomaterials, we explored the possibility of anchoring them to create nano-sized fixed reaction cavities. First, we analyzed how the reactivity of the two complexes was affected in the presence of different commercially available materials in excess (10 and 33 times the mass of the cobalt catalyst) to see if the catalytic activity is preserved or modified and to which extend. It was found that, the two complexes are active for the reduction of ketones with the new photoredox catalyst ^{NMe2}PC$_{Ir}$ (Table III.2, entries **1** and **12**). This is important because it opens the possibility to do this study. Unfortunately, the enantioselectivity values (calculated as enantiomeric excess) were low. Nevertheless, to obtain asymmetric induction under photocatalytic conditions and in aqueous solution is a significant challenge.

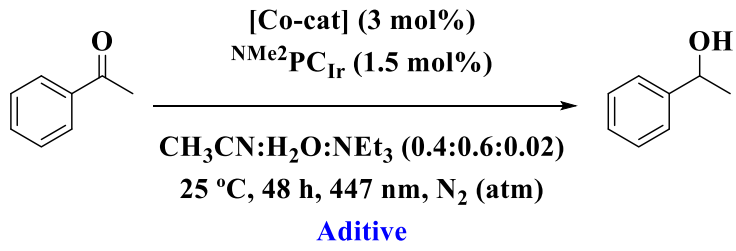

Scheme III. 15 Photocatalytic reduction of acetophenone

Table III.2 Conditions optimization for the photocatalytic reduction of acetophenone.

Entry	Catalyst	Additive	Ratio Additive / Co	Conv (%)	Yield (%)	ee (%)
1	**Co(^{PyB}mcp)(OTf)$_2$**	**none**	**-**	**99**	**82**	**-5**
2	Co(^{PyB}mcp)(OTf)$_2$	γ -CD	10	100	98	-3
3	Co(^{PyB}mcp)(OTf)$_2$	C60	10	68	56	-12
4	Co(^{PyB}mcp)(OTf)$_2$	NF	10	100	86	-12
5	Co(^{PyB}mcp)(OTf)$_2$	NT	10	61	47	-11
6	Co(^{PyB}mcp)(OTf)$_2$	NT-COOH	10	8	0	-
7	Co(^{PyB}mcp)(OTf)$_2$	γ -CD	33	100	81	-4
8	Co(^{PyB}mcp)(OTf)$_2$	C60	33	38	11	-11
9	Co(^{PyB}mcp)(OTf)$_2$	NF	33	100	93	-8
10	Co(^{PyB}mcp)(OTf)$_2$	NT	33	40	28	-9
11	Co(^{PyB}mcp)(OTf)$_2$	NT-COOH	33	10	0	-
12	**Co(^{PyB}pdp)(OTf)$_2$**	**none**	**-**	**100**	**75**	**-8**
13	Co(^{PyB}pdp)(OTf)$_2$	γ -CD	10	60	53	-5
14	Co(^{PyB}pdp)(OTf)$_2$	C60	10	93	77	-1
15	Co(^{PyB}pdp)(OTf)$_2$	NF	10	100	56	-15
16	Co(^{PyB}pdp)(OTf)$_2$	NT	10	41	24	-5
17	Co(^{PyB}pdp)(OTf)$_2$	NT-COOH	10	6	0	-
18	Co(^{PyB}pdp)(OTf)$_2$	γ -CD	33	76	89	-8
19	Co(^{PyB}pdp)(OTf)$_2$	C60	33	63	40	-1
20	Co(^{PyB}pdp)(OTf)$_2$	NF	33	100	88	-10
21	Co(^{PyB}pdp)(OTf)$_2$	NT	33	29	6	0
22	Co(^{PyB}pdp)(OTf)$_2$	NT-COOH	33	8	0	-

Although, a direct comparison between both cobalt catalysts apparently does not follow a tendency, some observations can be abstracted from the general results. In general terms NF and γ-CD maintain the catalytic activity, while in the presence of carbon nanotubes or C60 the catalytic

activitydecreases. This could be attributed to the quenching of the PC by the C60 or the CNT (See chapter IV). Alternatively, it could also be explained due to the light absorption of the material. The system shows a very good tolerance to γ-cyclodextrine (γ-CD), which was the only of these materials soluble in the aqueous reaction media, and in some conditions, it clearly improved the yield respect to the reaction without material (entries 2, 7 and 18). Fullerene (C_{60}) and carbon nanofibers (NF) have shown to be in general well tolerated, but this was not the case for carbon nanotubes (NT). Indeed, reactivity was fully inhibited when the introduced nanotubes were functionalized with COOH groups (NT-COOH). Since we expect from both the tested iridium and cobalt catalysts to present long stability under these conditions, we still cannot justify such a loss of reactivity (entries 6, 11, 17, 22).

To prove that catalyst and light are needed for the photochemical reduction of acetophenone, control experiments were performed. In the absence of light or PC, the starting material is fully recovered (Entries 1[a]-4b, Table III.3). Additionally, while the use of nanofibers (NF) in the absence of cobalt-catalyst, the dimerization of the ketones occurs via the know formation of ketyl radicals (Entry 5).[308]

Table III.3 Control experiments for the photocatalytic reduction of acetophenone.

Entry	Catalyst	Other components	Mat/cat	Conv (%)	Yield (%)	Dimer (%)
1[a]	$Co(^{PyB}mcp)(OTf)_2$	No PC	-	0	0	0
2[a]	$Co(^{PyB}pdp)(OTf)_2$	No PC	-	0	0	0
3[b]	$Co(^{PyB}mcp)(OTf)_2$	No light	-	0	0	0
4[b]	$Co(^{PyB}pdp)(OTf)_2$	No light	-	0	0	0
5	none	With NF	10	100	0	88

Other observation is that, the reaction with NT and C60 reveal decreased yield when adding higher concentration of heterogeneous material. Despite we still cannot explain neither generalize this result, some primary hypotheses may be related with the more challenging excitation of the PC in a dark heterogeneous environment, or to some effect of aggregation that encages the catalysts making it inactive. Further spectroscopic studies to gain deeper understanding about the

interaction between these catalysts and two of these materials (CD and C_{60}) have been described in following chapter IV.

Catalytic studies were also performed to test the catalytic activity of $MX(OTf)_2$ (M = Co, Ni; X = ^{PyB}mcp, ^{PyB}pdp) for the activation of C_{sp3}-Cl bonds. Our group developed a novel photoredox methodology for the reductive cross-coupling reaction between inert alkyl chlorides using styrene as a radical acceptor.[350] In the aforementioned work, a dual catalytic system formed by an iridium photocatalyst [Ir(^{NMe2}bpy)(ppy)$_2$]PF_6 and a N-based pentacoordinated nickel complex (Ni(OTf)(Py_2^{Ts}tacn), which can reach low-valent Ni species under blue LED irradiation. In this case, low-valent M intermediates can be photogenerated by $MX(OTf)_2$. The examination of the cross-coupling reaction was performed applying in the reaction the substrate - (3-chlorobutyl)-1-benzene (10 mM), cobalt or nickel catalyst (5 mol% of Co(^{PyB}mcp)$(OTf)_2$, Co(^{PyB}pdp)$(OTf)_2$, Ni(^{PyB}mcp)$(OTf)_2$ or Ni (^{PyB}pdp)$(OTf)_2$) and ^{NMe2}**PC$_{Ir}$** (2 mol%) of in solvent mixture of MeCN:EtOH (2:3) at 30 ^{o}C under nitrogen atmosphere which was irradiated during 24 h (Scheme III.16).

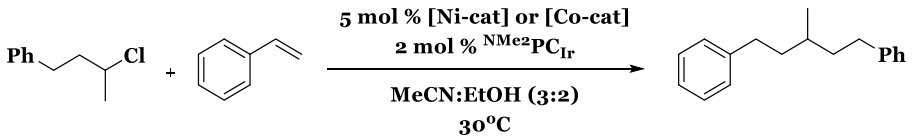

Scheme III. 16 *Photocatalytic cross-coupling reaction of (3-methylpentane-1,5-diyl)dibenzene.*

$NiX(OTf)_2$ catalysts presented moderate reactivity in comparison with the optimized system, obtaining 35% yield for the cross-coupling product instead of 82% yield. However, the cobalt catalyst analogue showed a diminished reactivity, yielding only 21%, as expected, considering the parallel reaction of H_2 formation in the presence of protic solvents, which was observed in previous sections.

III.3 Conclusion

We designed, synthetized and characterized a family of new ligands with *N*,*N*′-dimethyl-1,2-cyclohexanediamine and 2,2′-bipyrrolidine backbones and their corresponding cobalt and nickel complexes. Cobalt complexes were superior as catalysts in water reduction to hydrogen. While nickel complexes showed to have very low activity under the same conditions. We found that the activity of complexes was not dominated by the employed anions, chloride and triflate complexes showed similar catalytic activity. Introducing linker to the polyaromatic moiety into the ligand structure increased the photocatalytic reduction of water to hydrogen, most probably due to electronic effects.

Addition of γ-cyclodextrin into the catalytic solution for hydrogen evolution enhance solubility of catalyst in water due to the non-covalent interactions with PAH moiety, showing a catalytic enhancement not only in pure water, but also in solvent mixtures. However, when the same strategy was applied to the photosensitizer, although cyclodextrins enhanced the solubility of $\mathbf{PC_{Irpyrene}}$ in the aqueous solution, its catalytic activity was very low. In the other hand, the water soluble $\mathbf{PC_{Cu}}$ gave a good performance in pure water suggesting the need for closer contact between the catalyst and PS to trigger SET events.

Co(^{PyB}mcp)$(OTf)_2$ and Co(^{PyB}pdp)$(OTf)_2$ catalysts were active in the reduction of acetophenone while using $^{NMe2}\mathbf{PC_{Ir}}$ as a photosensitizer and Et_3N as a source of electrons, yielding the desired product. The systems are promising, and more studies are needed to increase the enantioselectivity, and to explore anchoring strategies with different nanomaterials.

Ni(^{PyB}mcp)$(OTf)_2$ and Ni(^{PyB}pdp)$(OTf)_2$ were found to be active for the cleavage of C_{sp3}-Cl bonds and its use in the cross-coupling reaction, with $^{NMe2}\mathbf{PC_{Ir}}$ photosensitizer obtaining the product with good yield while Co(^{PyB}mcp)$(OTf)_2$ and Co(^{PyB}pdp)$(OTf)_2$ were inactive in this reaction.

These studies shed light on all taken considerations for the development of effective first row transition metal catalysts for photocatalytic water reduction and various organic transformations.

III.4 Experimental Section

III.4.1 Material and Reagents

Reagents and solvents were used as received from the commercial supplier unless otherwise stated. Triethylamine was distilled over potassium hydroxide and stored under argon. For the synthesis of ligands and complexes, the solvents (Hexane, Et_2O, DCM, MeCN, DMF and toluene) were used from a SPS-400, Innovative Technology solvent purification system and stored under argon.

Anhydrous acetonitrile was purchased from Sigma-Aldrich® and water was purified with a Milli-Q Millipore Gradient AIS system. Water used for photoreactions were degassed by freeze-pump-thaw method (repeated 3 cycles) and stored under argon.

The synthesis of air-sensitive reagents as well as the preparation of visible light photocatalytic reactions were conducted inside a nitrogen-filled glove box (mBraun Unilab) with concentrations of O_2 and H_2O lower than 0.5 ppm and using Schlenk techniques under argon atmosphere.

III.4.2 Instrumentation

Nuclear magnetic resonance (NMR) spectra were recorded on a Bruker 300 MHz, 400 MHz or 500 MHz spectrometers at room temperature. All ^{1}H and ^{13}C NMR chemical shifts are reported in parts per million (ppm), relative to the residual solvent peak as the internal reference. Multiplicities are reported as follows: singlet (s), doublet (d), doublet of doublet (dd), triplet of doublets (td), triplet (t) and multiplet (m). Deuterated solvents ($CDCl_3$, CD_3CN) were stored with activated 4 Å molecular sieves, and they were degassed by freeze-pump-thaw method when it was required for photocatalytic reactions.

High resolution Mass Spectrometry (HRMS) data was collected on an HPLC-QqTOF (Maxis Impact, Bruker Daltonics), HPLC-TOF (MicroTOF Focus, Bruker Daltonics) or MALDI-TOF-MS (Autoflex, bruker Daltonics) mass spectrometer using 1 mM solution of the analyzed compound.

Parallel Pressure Trandsucer Hardware. The parallel pressure transducer device is composed of 8 differential pressure transducers (Honeywell-ASCX15DN, ± 15 psi) connected to a hardware data-acquisition system (based on an Atmega microcontroller) controlled by a home-developed software program. The differential pressure transducer Honeywell-ASCX15DN hands a 100 microseconds response with a signal-conditioned output (high-level span, 4.5 V), with a calibrated sensor that is temperature compensated (from 0 ºC to 70 ºC). The differential sensor has two sensing ports that can be used for differential pressure measurements. The pressure calibration devices were offset within ± 0.5 matm and the span adjusted *via* software with a high precision pressure transducer (PX409-030GUSB, 0.08 % of accuracy). Each of the 8 differential 4 pressure transducers (Honeywell-ASCX15DN, ±15 psi) produce a voltage output that can be directly transformed to a pressure difference between two measuring ports. The voltage output was digitalized with a resolution of 0.25 matm from 0 to 175 matm, and 1 matm from 176 to 1000 matm using an Atmega microcontroller with an independent voltage auto-calibration. The firmware for the Atmega microcontroller and the control software were developed in-house. The sensitivity for H_2 allows qualifying the gas formed even when low H_2 quantities are produced.

Gas chromatography identification and quantification of gases. Gases at the headspace were analyzed with an Agilent 7820A GC System equipped with columns Washed Molecular Sieve 5Å, 2m x 1/8'' OD, Mesh 60/80 SS and Porapak Q, 4m x 1/8'' OD, SS. Mesh: 80/100 SS and a Thermal Conductivity Detector. The quantification of obtained H_2 was measured through the interpolation of a previous calibration using different H_2/N_2 mixtures.

X-Ray crystallography. Crystal structure determinations were carried out using a MM-007HF diffractometer equipped with a Pilatus 200K hybrid pixel detector, a rotating anode for Mo $K\alpha$ radiation and Oxfrod Cryostream 700 plus low temperature device (T = – 183º C). Full-sphere data collection was used with ω scans. Programs used: Data collection and data reduction, CrysAlisPro 1.171.39.12b and absorption correction SADABS-2014/5.[351] Structure

Solution and Refinement: Crystal structure solution was achieved using the VLD procedure implemented in SIR2014.[352] Spherical model refinement was done using the program ShelXle.[353] All non-hydrogen atoms were refined including anisotropic displacement parameters.

Elemental analyses were performed using a CHNS-O EA-1108 elemental analyzer from Fisons.

III.4.3 Experimental Procedure

Gas evolution monitoring studies for the light-driven reduction of water. All catalytic reactions were conducted in a 20 mL septum-capped vial. Each reaction vial was connected to one of the ports of a differential pressure transducer sensor (Honeywell-ASCX15DN) and the other port to a reference reaction. Reference reactions (blanks), have all components of the reaction but the catalyst. The reaction and blanks are kept under the same experimental conditions to compensate the noise due to temperature-pressure fluctuations. In order to ensure a constant and stable irradiation, the LED sources were equipped with a water refrigeration system. This block is shaken by an Orbital Shaker (IKA® KS 260 Basic Package) which provides the agitation of the reaction vessels during the irradiation time. The aluminum block accommodates 25 vials. Each vial is placed in the block in which the reaction takes place under vigorous stirring using an orbital stirrer and irradiation with LED (450±20 nm at ca. 0.3 $W \cdot cm^2$) for 6h under N_2 atmosphere at 25 ºC, unless otherwise indicated. The reaction began when the LEDs were turned on. At this point, the hydrogen evolved from the reactions was monitored by recording the increase in pressure of the headspace. The pressure increase is the result of the difference in pressure between the reaction vial and blank. After the reaction reached a plateau, the amount of the gas formed was measured equilibrating the pressure between reaction and reference vials. Gas at the headspace of reaction vials and references in each of the reactions was quantified by the analysis of an aliquot of gas at the headspace (200 μL) by gas chromatography (GC-TCD).

III.4.4 Syntheses and Characterization of Ligands

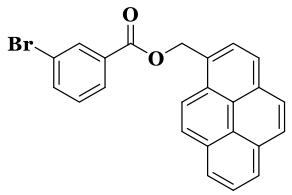

Pyren-1-ylmethyl 3-bromobenzoate. 100 mL Schlenk flask was charged with magnetic stirring bar, 1-pyrenemethanol (2.5 g, 10.76 mmol, 1.0 equiv.), 3-bromobenzoic acid (2.6 g, 12.91 mmol, 1.2 equiv.), $Ti(acac)_2$ (21.02 mg, 3 mmol%) and closed with a rubber septum. The flask was evacuated and filled with N_2. Anhydrous m- xylene (120 mL) was added and rubber septum was quickly exchanged with a reflux condenser and the reaction was heated at 160 ^oC during 18 h. After cooling to room temperature, the reaction was quenched with saturated, aqueous $NaHCO_3$ solution and then extracted with CH_2Cl_2 (3x30 mL). The combined organic layers were washed with NaCl (40 mL), dried ($MgSO_4$), filtered and evaporated to give a crude product that was purified by column chromatography on deactivated (Et_3N) silica gel eluting with 5% EtOAc/hexanes to give the product (3.53 g, 8.5 mmol, 76% yield) as a pale-yellow solid. ^1H NMR (400 MHz, $CDCl_3$) δ = 8.36 (d, *J* = 9.2 Hz, 1H), 8.26 – 8.17 (m, 5H), 8.16 – 8.01 (m, 4H), 7.99 (dt, *J* = 7.9, 1.3 Hz, 1H), 7.65 (ddd, *J* = 8.0, 2.1, 1.1 Hz, 1H), 7.31 – 7.23 (m, 1H), 6.08 (s, 2H) ppm; ^{13}C = NMR (101 MHz, $CDCl_3$) δ 165.4 (C), 138.3 (C), 136.2 (CH), 132.8 (CH), 132.2 (C), 132.1 (C), 131.4 (C), 130.8 (C), 130.1 (CH), 129.8 (C), 128.6 (C), 128.6 (CH), 128.5 (CH), 128.1 (CH), 128.1 (CH), 127.5 (CH), 126.3 (CH), 125.8 (CH), 125.7 (CH), 125.1 (C), 124.8 (CH), 123.0 (CH), 122.6 (C), 65.9 (CH_2) ppm; HRMS (ESI) *m/z* calculated for $C_{24}H_{15}BrNaO_2$ $[M+Na]^+$; 437.0148, found 437.0156; Elemental Analysis (%) calculated for $C_{24}H_{15}BrO_2$: %C 69.41 %H 3.64, found %C 69.31 %H 3.67.

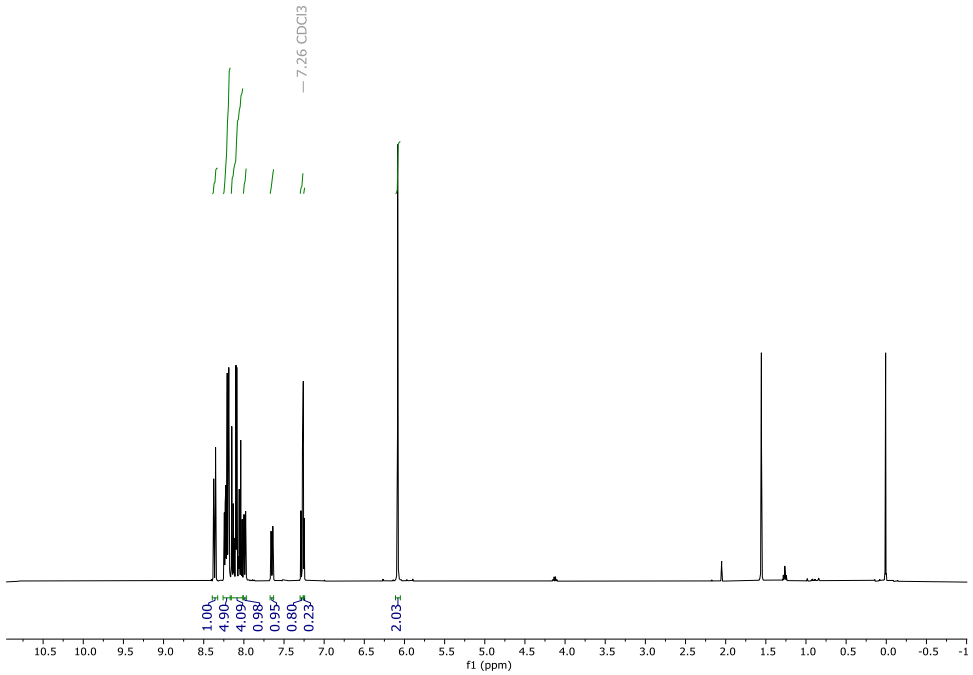
7.26 CDCl3
1.00
4.90
4.09
0.98
0.95
0.80
0.23
2.03
f1 (ppm)

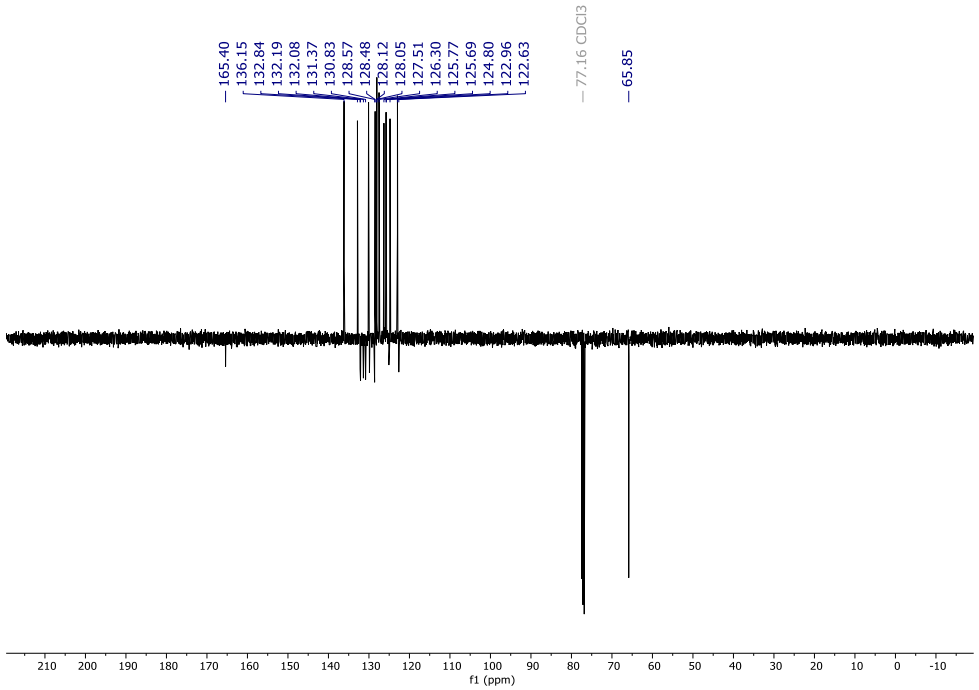
165.40
136.15
132.84
132.19
132.08
131.37
130.83
128.57
128.48
128.12
128.05
127.51
126.30
125.77
125.69
124.80
122.96
122.63
77.16 CDCl3
65.85
f1 (ppm)

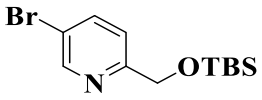

5-bromo-2-(((tert-butyldimethylsilyl)oxy)methyl)pyridine.[354] 2,5-Dibromopyridine (25 g, 105.5 mmol, 1.0 equiv) was suspended in PhMe (0.2 M) in a 1 L round bottomed flask. The suspension was cooled to -78 °C and nBuLi (79 mL, 1.2 equiv, 1.6 M in hexanes) was added dropwise over 10 min. The reaction was stirred for 2 h at -78 °C, at which time DMF (16 mL, 211 mmol, 2.0 equiv) was added dropwise and stirring continued an additional 1h. The dark solution was warmed to 0 °C and MeOH (105 mL) followed by $NaBH_4$ (4.0 g, 105.5 mmol, 1.0 equiv.) were added carefully. Stirring was continued for 1 h allowing the reaction to warm to room temperature. The reaction was quenched with H_2O (~100 mL). The resulting layers were separated and the aqueous layer was extracted with CH_2Cl_2 (3x100 mL). The combined organic layers were dried (Na_2SO_4), filtered and concentrated to give a crude oil. The crude was dissolved in CH_2Cl_2 (120 mL) in a 500 mL round bottomed flask. TBSCl (19.1 g, 1.2 equiv.), imidazole (10.8 g, 1.5 equiv.) and DMAP (1.3 g, 0.1 equiv.) were added in one portion and the reaction was stirred for 12 h at room temperature. The reaction was quenched with H_2O (100 mL) and the resulting layers were separated. The aqueous layer was extracted with CH_2Cl_2 (3x50 mL) and the combined organic layers were dried (Na_2SO_4), filtered and concentrated. Purification by flash chromatography on silica eluting with 5% EtOAc/hexanes afforded the title compound (23,1 g, 73 % yield) as a light yellow oil. ^{1}H NMR (400 MHz, $CDCl_3$) δ = 8.23 (dd, *J* = 2.6, 0.9 Hz, 1H), 7.48 – 7.41 (m, 1H), 7.35 (dd, *J* = 8.2, 0.7 Hz, 1H), 4.63 (d, *J* = 0.9 Hz, 2H), 0.85 (s, 9H), 0.03 (s, 6H) ppm; ^{13}C NMR (101 MHz, $CDCl_3$) δ = 148.1 (CH), 140.4 (C), 136.6 (CH), 136.1 (C), 127.6 (CH), 61.5 (CH_2), 25.8 (x3 CH_3), -5.4 (x2 CH_3) ppm.

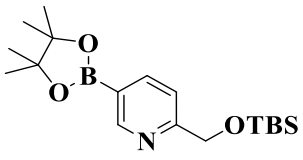

2-(((tert-butyldimethylsilyl)oxy)methyl)-5-(4,4,5,5-tetramethyl-1,3,2-dioxaborolan-2-yl)pyridine.[354] 5-Bromo-2-(((tert-butyldimethylsilyl)oxy)methyl)pyridine (20 g, 1.0 equiv) and triisopropyl borate (18.5 mL, 1.2 equiv.) were dissolved in THF (130 mL) in a 500 mL round bottomed flask. The solution was cooled to -78 °C and nBuLi (51 mL, 1.2 equiv, 1.6 M in hexanes) was added over 1 h via syringe pump. After the addition was complete, the reaction was stirred for an additional 2 h at -78 °C, at which time it was allowed to warm to 0 °C. The reaction was carefully quenched to pH=6 with 1 M KH_2PO_4. The layers were separated and the aqueous layer was extracted with CH_2Cl_2 (3x30 mL). The combined organic layers were dried (Na_2SO_4), filtered and concentrated to give a crude oil. The oil was dissolved in PhH (130 mL) in a 250 mL round bottomed flask, to which pinacol (9.5 g, 1.2 equiv.) was added. The flask was fitted with a dean-stark trap and the reaction was refluxed overnight. After cooling to room temperature, water (50 mL) was added and the layers were separated. The aqueous layer was extracted with EtOAc (3x30 mL) and the combined organic layers were dried (Na_2SO_4), filtered and concentrated. Purification by flash chromatography on silica eluting with 20% EtOAc/hexanes afforded the title compound (13.8 g, 60 % yield) as a yellow oil. ^{1}H NMR (400 MHz, $CDCl_3$) δ = 8.80 (dd, *J* = 1.8, 1.0 Hz, 1H), 8.04 (dd, *J* = 7.8, 1.8 Hz, 1H), 7.47 (dq, *J* = 7.8, 0.9 Hz, 1H), 4.82 (d, *J* = 0.8 Hz, 2H), 0.91 (s, 9H), 0.07 (s, 7H) ppm; ^{13}C NMR (101 MHz, $CDCl_3$) δ = 164.1 (C), 154.6 (CH), 143.1 (CH), 119.3 (CH), 84.1 (C), 66.3 (CH_2), 26.0 (x4 CH_3), 24.9 (x3 CH_3). 18.3 (x2 C) -5.4 (x2 CH_3) ppm;

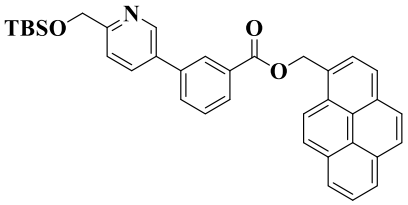

Pyren-1-ylmethyl 3-(6-(((tert-butyldimethylsilyl)oxy)methyl)pyridin-3-yl)benzoate. In a 250 mL Schlenk flask equipped with stirring bar were

dissolved $Pd(OAc)_2$ (3 mmol%), SPhos (6 mmol%), pyren-1-ylmethyl 3-bromobenzoate (3.2 g, 7.66 mmol, 1 equiv.) in 120 mL of toluene and K_3PO_4 (3.25 g, 15.32 mmol, 2 equiv.) in DI H_2O (4 mL). 2-(((tertbutyl-dimethylsilyl)oxy)methyl)-5-(4,4,5,5-tetramethyl-1,3,2-dioxaborolan-2-yl)pyridine (4.01 g, 11.48 mmol, 1.5 equiv.) was added and reaction was heated at 100 ºC during 18 h, cooled to room temperature and quenched with water (40 mL). The layers were separated and the aqueous layer was extracted with CH_2Cl_2 (3x 50 mL). The combined organic layers were dried ($MgSO_4$), filtered and evaporated to give a crude product that was purificated by column chromatography on deactivated (Et_3N) silica gel eluting with 20% EtOAc/hexanes to give the product (3.13 g, 5.6 mmol, 73% yield) as a white, shiny solid. ^{1}H NMR (400 MHz, $CDCl_3$) δ = 8.71 (dd, *J* = 2.4, 0.8 Hz, 1H), 8.41 (d, *J* = 9.3 Hz, 1H), 8.30 – 8.27 (m, 1H), 8.25 – 8.14 (m, 6H), 8.13 – 7.99 (m, 4H), 7.88 (dd, *J* = 8.1, 2.4 Hz, 1H), 7.74 (ddd, *J* = 7.7, 2.0, 1.2 Hz, 1H), 7.56 (dq, *J* = 8.2, 0.9 Hz, 1H), 7.50 (td, *J* = 7.8, 0.6 Hz, 1H), 6.13 (s, 2H), 4.87 (d, *J* = 0.8 Hz, 2H), 0.97 (s, 9H), 0.13 (s, 6H) ppm; ^{13}C NMR (101 MHz, $CDCl_3$) δ = 166.4 (C), 146.6 (CH), 134.33 (CH), 132.0 (x2 C), 131.7 (CH), 131.4 (C), 131.2 x2 (C), 130.9 (C), 129.9 (C), 129.4 (CH), 128.9 (x2 C), 128.5 (x2 CH), 128.1 (x2 CH), 127.5(CH), 126.29(CH), 125.8 (CH), 125.7 (CH), 125.1 (C), 124.8 (x2 CH), 123.1 (CH), 120.4 (CH), 65.74 (x2 CH_2), 26.07 (x3 CH_3), -6.16 (x2 CH_3) ppm; HRMS (ESI) *m/z* calculated for $C_{36}H_{36}NO_3Si$ $[M+H]^+$; 558.2459, found 558.2469; Elemental Analysis (%) calculated for $C_{36}H_{35}NO_3Si$: %C 77.52 %H 6.33 %N 2.51, found %C 77.34 %H 6.28 %N 2.60.

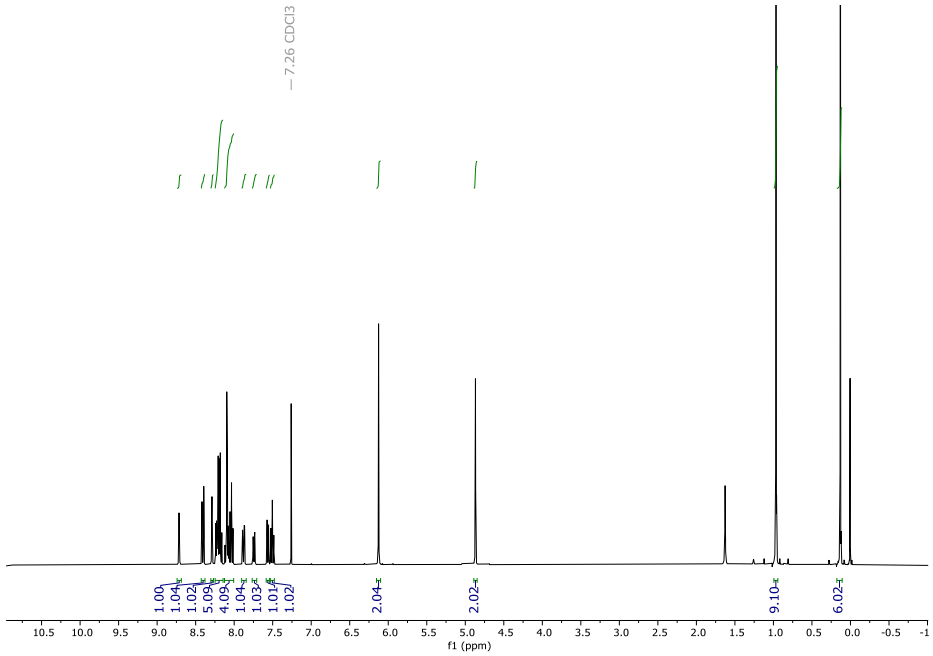
7.26 CDCl3
1.00
1.04
1.02
5.09
4.09
1.04
1.03
1.01
1.02
2.04
2.02
9.10
6.02
f1 (ppm)

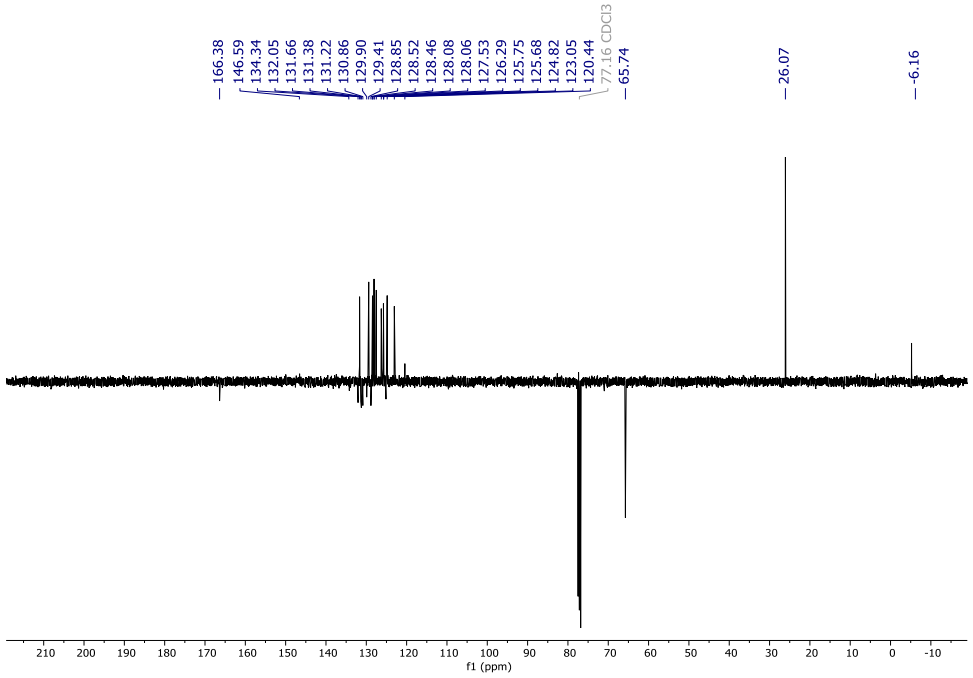
166.38
146.59
134.34
132.05
131.66
131.38
131.22
130.86
129.90
129.41
128.85
128.52
128.46
128.08
128.06
127.53
126.29
125.75
125.68
124.82
123.05
120.44
77.16 CDCl3
65.74
26.07
-6.16
f1 (ppm)

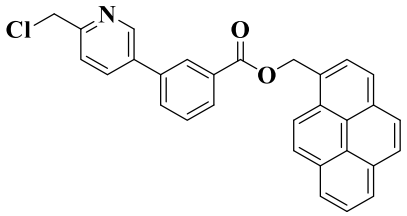

Pyren-1-ylmethyl 3-(6-(chloromethyl)pyridin-3-yl)benzoate. In a 100 mL round bottom flask pyren-1-ylmethyl 3-(6-(((tert-butyldimethylsilyl)oxy)methyl)pyridin-3-yl)benzoate (2.15 g, 3.85 mmol, 1 equiv.) was dissolved in 50 mL of THF, cooled to 0 ºC and TBAF (1M THF, 3.85 mL, 1 equiv.) was added dropwise. The reaction was stirred vigorously 30 min and quenched with NH_4Cl_{sat}. The layers were separated, and the aqueous layer was extracted with Et_2O (3x20 mL). The combined organic layers were dried ($MgSO_4$), filtered and evaporated to give a crude solid. The solid was dissolved in 60 mL of anhydrous CH_2Cl_2 and cooled to 0 ºC and $SOCl_2$ (0.9 mL, 12.32 mmol, 3.2 equiv.) was added dropwise. The reaction was stirred during 4 h and quenched to neutral pH with $NaHCO_3$. The layers were separated and the aqueous layer was extracted with CH_2Cl_2 (3x20 mL). The combined organic layers were dried ($MgSO_4$), filtered and evaporated to give a crude product that was purificated by column chromatography on deactivated (Et_3N) silica gel eluting with 55% EtOAc/hexanes to give the product (1.8 g, 86% yield) as a white solid. ^{1}H NMR (400 MHz, $CDCl_3$) δ = 8.78 (dd, *J* = 2.4, 0.8 Hz, 1H), 8.41 (d, *J* = 9.2 Hz, 1H), 8.28 (t, *J* = 1.6 Hz, 1H), 8.25 – 8.15 (m, 5H), 8.14 – 8.07 (m, 3H), 8.08 – 8.00 (m, 1H), 7.90 (dd, *J* = 8.1, 2.4 Hz, 1H), 7.74 (ddd, *J* = 7.7, 2.0, 1.2 Hz, 1H), 7.57 – 7.49 (m, 2H), 6.13 (s, 2H), 4.72 (s, 2H) ppm; ^{13}C NMR (101 MHz, $CDCl_3$) δ = 166.2 (C), 155.8 (C), 147.8 (CH), 137.6 (C), 135.4 (CH) , 134.9 (C), 131.8 (C), 131.5 (CH), 131.2 (C), 131.1 (C), 130.7 (C), 129.7 (C), 129.5 (CH) , 129.4 (CH), 128.7 (C), 128.4 (2x CH), 127.9 (CH), 127.8 (CH), 127.4 (CH), 126.3 (CH), 125.8 (CH), 125.5 (CH), 124.9 (C), 124.7 (CH), 124.6 (C), 122.9 (CH), 122.8 (CH), 65.8 (CH_2), 46.5 (CH_2) ppm; HRMS (ESI) *m/z* calculated for $C_{30}H_{21}ClNO_2$ $[M+H]^+$; 462.1255, found 462.1249;

Elemental Analysis (%) calculated for $C_{30}H_{20}ClNO_2$: %C 78.00 %H 4.36 %N 3.03, found %C 77.48 %H 4.48 %N 3.11.

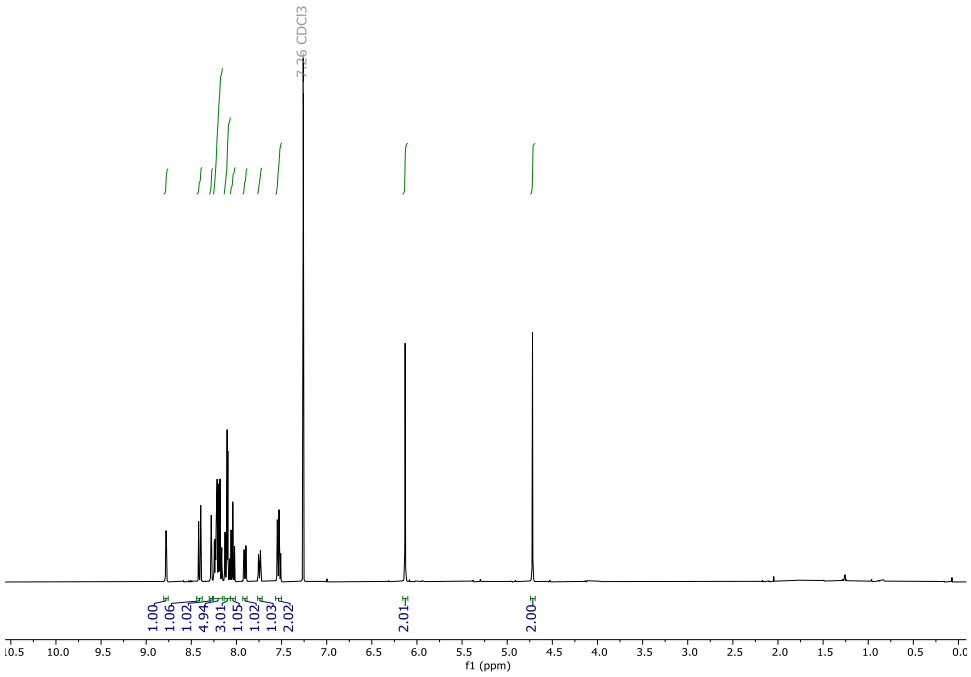

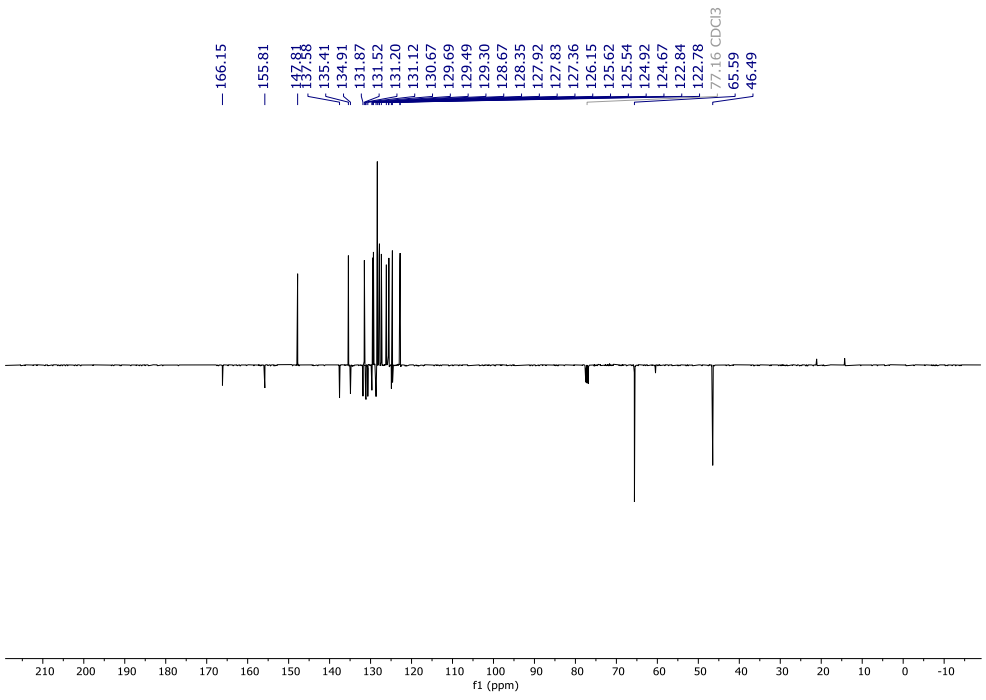

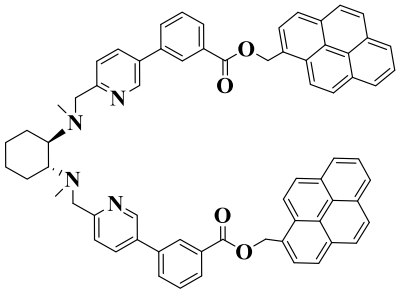

Bis(pyren-1-ylmethyl)3,3'-(((((1R,2R)-cyclohexane-1,2-diyl)bis(methylazanediyl)) bis(methylene))bis(pyridine-6,3-diyl))dibenzoate (^{PyB}mcp$_{(R,R)}$) and Bis(pyren-1-ylmethyl)3,3'-(((((1S,2S)-cyclohexane-1,2-diyl)bis(methylazanediyl)) bis(methylene))bis(pyridine-6,3-diyl))dibenzoate (^{PyB}mcp$_{(S,S)}$) Pyren-1-ylmethyl 3-(6-(chloromethyl)pyridin-3-yl)benzoate (1.45 g, 3.15 mmol, 2.1 equiv.), (*R*,*R*)-(−)-*N*,*N*′-Dimethyl-1,2-diaminocyclohexane (213 mg, 1.5 mmol, 1 equiv.), were dissolved in MeCN (40 mL). Na_2CO_3 (3 equiv.) and tetrabutylammonium bromide – TBABr (0.1 equiv.) were added directly as solids and the resulting mixture was heated at reflux under N_2 for 24 h. After cooling to the RT mixture was concentrated under reduced pressure. Resulting residue was dissolved in CH_2Cl_2 and washed with water to remove remaining TBABr. The layers were separated and the aqueous layer was extracted with CH_2Cl_2 (3x20 mL). The organic layer was dried ($MgSO_4$), filtered and evaporated to give a crude product that was purificated by column chromatography on deactivated (Et_3N) silica gel eluting with CH_2Cl_2 to give the product (1.02 g, 68% yield). ^{1}H NMR (400 MHz, $CDCl_3$) δ = 8.72 (d, *J* = 2.3 Hz, 2H), 8.35 – 8.24 (m, 4H), 8.15 – 8.06 (m, 10H), 8.04 (dt, *J* = 7.8, 1.4 Hz, 2H), 8.01 – 7.92 (m, 6H), 7.74 (dd, *J* = 8.1, 2.4 Hz, 2H), 7.66 (dt, *J* = 7.8, 1.5 Hz, 2H), 7.60 (d, *J* = 8.1 Hz, 2H), 7.41 (t, *J* = 7.8 Hz, 2H), 6.04 (s, 4H), 3.97 (d, *J* = 14.7 Hz, 2H), 3.84 (d, *J* = 14.7 Hz, 2H), 2.72 – 2.65 (m, 2H), 2.32 (s, 6H), 2.00 (d, *J* = 12.8 Hz, 2H), 1.77 (d, *J* = 8.6 Hz, 2H), 1.29 (td, *J* = 12.2, 11.4, 3.6 Hz, 2H), 1.17 (t, *J* = 10.3 Hz, 2H) ppm; ^{13}C NMR (101 MHz, $CDCl_3$) δ = 166.3 (C), 160.8 (C), 147.0 (CH), 138.3 (C), 134.9 (CH), 133.6(C), 131.8 (C), 131.5 (CH), 131.2 (C), 131.0 (C), 130.6 (C), 129.6 (C), 129.2 (CH), 129.0 (CH), 128.7 (C), 128.3 (CH), 128.2 (CH), 127.8

(CH), 127.7 (CH), 127.3 (CH), 126.01 (CH), 125.5 (CH), 125.5 (CH), 124.9 (C), 124.6 (CH), 124.6 (C), 122.8 (CH), 122.8 (CH), 65.5 (CH_2), 64.7 (CH), 60.2 (CH_2), 36.8 (CH_3), 26.0 (CH_2), 25.8 (CH_2) ppm; HRMS (ESI) *m/z* calculated for $C_{68}H_{57}N_4O_4$ $[M+H]^+$; 993.4374, found 993.4354. Elemental Analysis (%) calculated for $C_{68}H_{56}N_4O_4 + CH_2Cl_2$: %C 76.87 %H 5.42 %N 5.20, found %C 77.07 %H 5.89 %N 4.89.

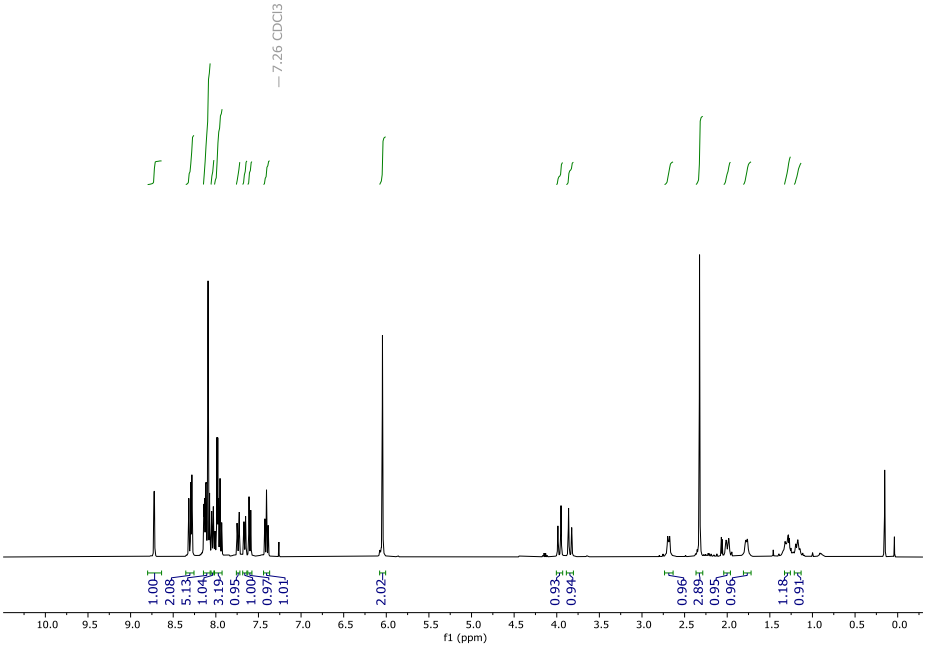

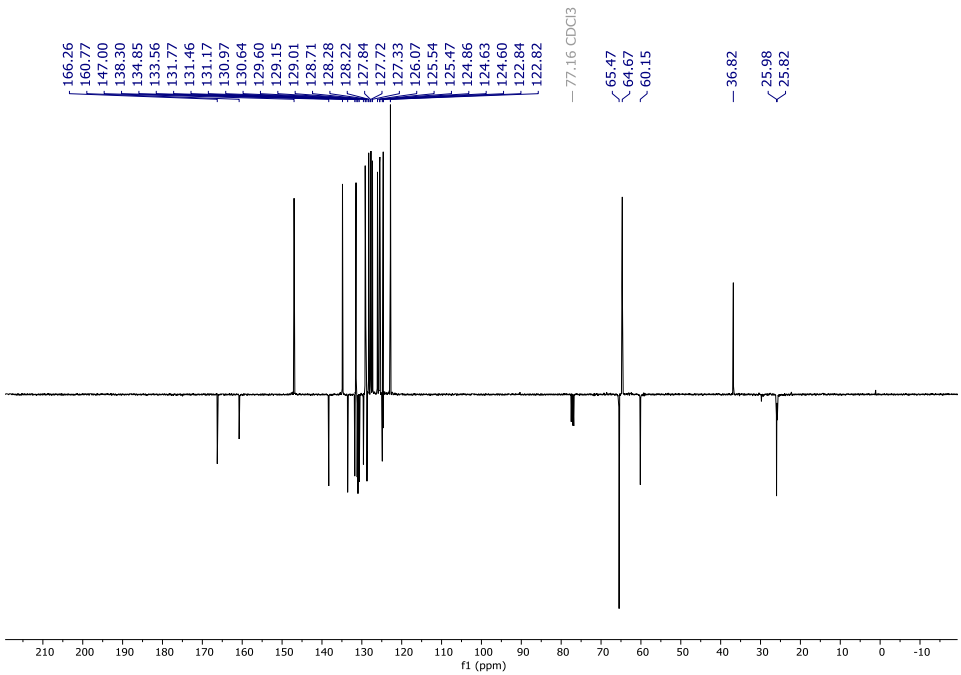

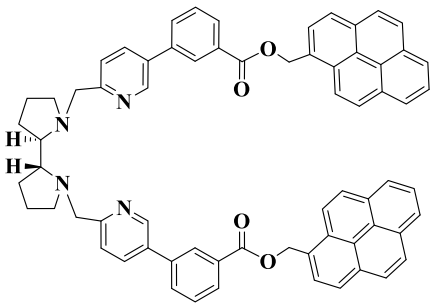

Bis(pyren-1-ylmethyl)3,3'-((((2R,2'R)-[2,2'-bipyrrolidine]-1,1'diyl) bis(methylene))bis(pyridine-6,3-diyl))dibenzoate (^{PyB}pdp$_{(R,R)}$) and Bis(pyren-1-ylmethyl)3,3'-((((2S,2'S)-[2,2'-bipyrrolidine]-1,1'diyl) bis(methylene))bis(pyridine-6,3-diyl))dibenzoate (^{PyB}pdp$_{(S,S)}$). Pyren-1-ylmethyl 3-(6-(chloromethyl)pyridin-3-yl)benzoate (0.4 g, 0.87 mmol, 2 equiv.), (R,R)/(S,S)-2,2′-bipyrrolidine L-tartrate trihydrate (149 mg, 0.43 mmol, 1 equiv.) were dissolved in MeCN (40 mL). Na_2CO_3 (3 equiv.) and tetrabutylammonium bromide – TBABr (0.1 equiv.) were added directly as solids and the resulting mixture was heated at reflux under N_2 for 24h. After cooling to the RT mixture was concentrated under reduced pressure. Resulting residue was dissolved in CH_2Cl_2 and washed with water to remove remaining

TBABr. The layers were separated and the aqueous layer was extracted with CH_2Cl_2 (3x20 mL). The organic layer was dried ($MgSO_4$), filtered and evaporated to give a crude product that was purificated by column chromatography on deactivated (Et_3N) silica gel eluting with CH_2Cl_2 to give the product (0.34 g, 76% yield). ^{1}H NMR (400 MHz, $CDCl_3$) δ = 8.72 (dd, *J* = 2.3, 0.8 Hz, 2H), 8.30 (d, *J* = 9.2 Hz, 2H), 8.25 (t, *J* = 1.8 Hz, 2H), 8.16 – 8.06 (m, 10H), 8.03 (dt, *J* = 7.8, 1.4 Hz, 2H), 8.02 – 7.93 (m, 6H), 7.71 (dd, *J* = 8.1, 2.4 Hz, 2H), 7.66 – 7.59 (m, 2H), 7.43 – 7.34 (m, 4H), 6.04 (s, 4H), 4.28 (d, *J* = 14.6 Hz, 2H), 3.58 (d, *J* = 14.6 Hz, 2H), 3.03 (dt, *J* = 9.2, 4.5 Hz, 2H), 2.83 (d, *J* = 7.9 Hz, 2H), 2.26 (q, *J* = 8.3 Hz, 2H), 1.86 (tt, *J* = 9.0, 4.8 Hz, 2H), 1.74 (tq, *J* = 8.0, 4.8, 3.3 Hz, 6H) ppm; ^{13}C NMR (101 MHz, $CDCl_3$) δ = 165.8 (x2 C), 160.0 (x2 C), 147.1 (x2 CH),, 138.2 (x2 C), 134.7 (x2 CH), 133.4 (x2 C), 131.7 (x2 C), 131.4 (x2 CH), 131.1 (x2 C), 130.9 (x2 C), 130.6 (x2 C), 129.6 (x2 C), 129.1 (x2 CH), 129.0 (x2 CH), 128.7 (x2 C), 128.3 (x2 CH), 128.2 (x2 CH), 127.8 (x2 CH), 127.7 (x2 CH), 127.3(x2 CH), 126.0 (x2 CH), 125.5 (x2 CH), 125.5 (x2 CH), 124.8 (x2 C), 124.6 (x2 CH), 124.6 (x2 C), 122.8 (x2 CH), 122.5 (x2 CH), 66.2 (x2 CH), 65.4 (x2 CH_2), 61.0 (x2 CH_2), 54.5 (x2 CH_2), 26.3 (x2 CH_2), 23.0 (x2 CH_2) ppm; HRMS (ESI) *m/z* calculated for $C_{68}H_{55}N_4O_4$ $[M+H]^+$; 991.4218, found 991.4172. Elemental Analysis (%) calculated for $C_{68}H_{54}N_4O_4$: %C 82.40 %H 5.49 %N 5.65, found %C 81.26 %H 5.56 %N 5.62

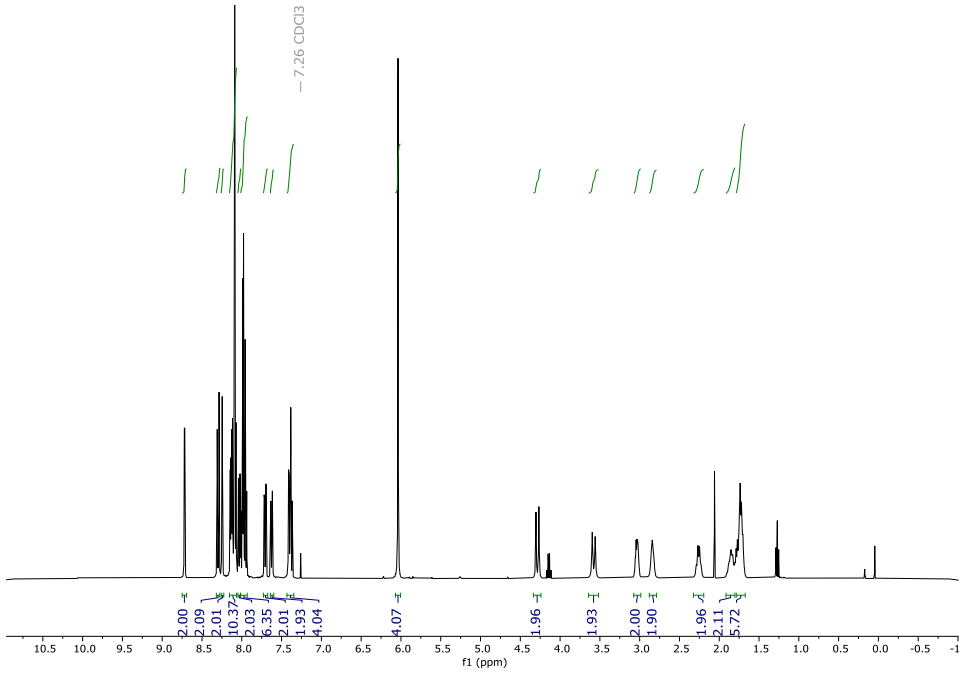
7.26 CDCl3
2.00
2.09
2.01
10.37
2.03
6.35
2.01
1.93
4.04
4.07
1.96
1.93
2.00
1.90
1.96
2.11
5.72
f1 (ppm)

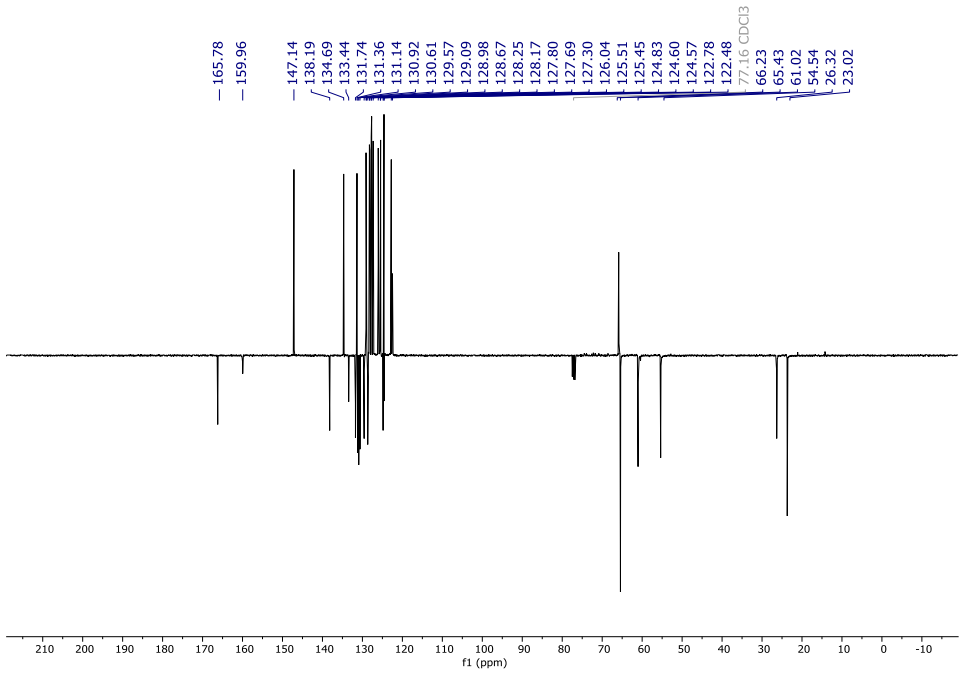
165.78
159.96
147.14
138.19
134.69
133.44
131.74
131.36
131.14
130.92
130.61
129.57
129.09
128.98
128.67
128.25
128.17
127.80
127.69
127.30
126.04
125.51
125.45
124.83
124.60
124.57
122.78
122.48
77.16 CDCl3
66.23
65.43
61.02
54.54
26.32
23.02
f1 (ppm)

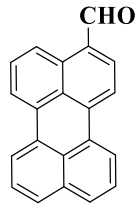

Perylene-3-carbaldehyde.[355] To a magnetically stirred ice cooled suspension of perylene (2.05 g, 8.12 mmol) in 1,2-dichlorobenzene (120 mL) 1,1-dichloromethyl methyl ether (955 uL, 10.56 mmol) and $TiCl_4$ (1.33 mL, 12.19 mmol) were subsequently added. The mixture was stirred for 1 h, then allowed to warm to room temperature and poured on ice (300 g) and concentrated HCl (45 mL). The organic layer was diluted with chloroform (300 mL), washed with 5% HCl (300 mL), water (3x100 mL), dried over Na_2SO_4 and evaporated. The residue was purified by column chromatography on silica gel in CHCl3 to give the desired compound. ^{1}H NMR (400 MHz, $CDCl_3$) δ = 10.27 (s, 1H), 9.11 (dd, *J* = 8.5, 1.0 Hz, 1H), 8.27 – 8.16 (m, 5H), 7.86 (d, *J* = 7.8 Hz, 1H), 7.78 (dd, *J* = 8.0, 1.0 Hz, 1H), 7.72 (dd, *J* = 8.1, 1.0 Hz, 1H), 7.64 (dd, *J* = 8.5, 7.6 Hz, 1H), 7.55 – 7.46 (m, 2H) ppm; ^{13}C NMR (101 MHz, $CDCl_3$) δ = 192.8 (CH), 137.7 (C), 137.2 (CH), 134.5 (C), 132.4 (C), 131.3 (C), 130.8 (C), 130.2 (CH), 130.0 (C), 129.9 (C), 129.4 (CH), 129.0 (C), 128.6 (CH), 128.2 (C), 127.1 (CH), 126.8 (CH), 124.7 (CH), 122.9 (CH), 121.6 (CH), 121.2 (CH), 119.5 (CH) ppm.

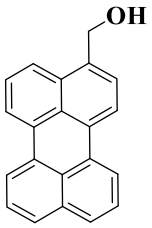

Perylen-3-ylmethanol.[355] To the solution of 3-formylperylene (500 mg, 1.79 mmol) in the mixture of THF (50 mL) and methanol (25 mL) sodium borohydride (70 mg, 1.85 mmol) was added. The mixture was stirred for 30 min, diluted with water (50 mL), and pH was adjusted to 1–2 with concd HCl. The intermediate alcohol was extracted with CHCl3 (300 mL), organic layer was washed with water (2x300 mL) and saturated solution of $NaHCO_3$ (300

mL), dried over Na_2SO_4, and evaporated. The residue was purified by column chromatography on silica gel in $CHCl_3$ to give the desired compound. ^{1}H NMR (400 MHz, $CDCl_3$) δ 8.28 – 8.14 (m, 4H), 7.96 (dd, *J* = 8.5, 1.0 Hz, 1H), 7.70 (dd, *J* = 8.3, 1.0 Hz, 2H), 7.60 – 7.52 (m, 2H), 7.49 (ddd, *J* = 8.2, 7.5, 0.9 Hz, 2H), 5.11 (d, *J* = 5.6 Hz, 2H) ppm; ^{13}C NMR (101 MHz, $CDCl_3$) δ 127.98 (CH), 126.9 (x2 CH), 126.7 (CH), 126.6 (CH) 126.1 (CH), 123.5 (CH), 120.4 (CH), 120.4 (CH), 120.4 (CH), 119.8 (CH), 63.82 (CH_2) ppm.

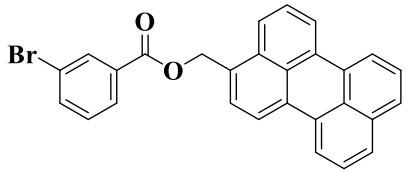

Perylen-3-ylmethyl 3-bromobenzoate. 250 mL Schlenk flask was charged with magnetic stirring bar, perylen-3-ylmethanol (2.0 g, 7.12 mmol, 1.0 equiv.), 3-bromobenzoic acid (1.43 g, 7.12 mmol, 1.0 equiv.), $Ti(acac)_2$ (56.11 mg, 3 mmol%) and closed with a rubber septum. The flask was evacuated and filled with N_2. Anhydrous toluene (100 mL) was added and rubber septum was quickly exchanged with a reflux condenser and the reaction was heated at 160 ^{o}C during 18 h. After cooling to room temperature, the reaction was quenched with saturated, aqueous $NaHCO_3$ solution and then extracted with CH_2Cl_2 (3x20 mL). The combined organic layers were washed with NaCl (20 mL), dried ($MgSO_4$), filtered and evaporated to give a crude product that was purified by column chromatography on deactivated (Et_3N) silica gel eluting with 5% EtOAc/hexanes to give the product (1.83 g, 3.9 mmol, 55% yield) as a yellow solid. ^{1}H NMR (400 MHz, $CDCl_3$) δ = 8.27 – 8.16 (m, 5H), 8.00 (dt, *J* = 7.8, 1.3 Hz, 1H), 7.91 (dd, *J* = 8.4, 0.9 Hz, 1H), 7.70 (d, *J* = 3.0 Hz, 3H), 7.62 (d, *J* = 7.7 Hz, 1H), 7.57 (d, *J* = 0.9 Hz, 1H), 7.49 (t, *J* = 7.8 Hz, 2H), 7.30 (t, *J* = 7.84 Hz, 1H), 5.75 (s, 2H) ppm; ^{13}C NMR (101 MHz, $CDCl_3$) δ = 165.4 (C), 136.2 (CH), 134.7 (C), 133.2 (C), 132.9 (CH), 132.6 (C), 132.2 (C), 132.1 (C), 131.2 (C), 130.9 (C), 130.7 (C), 130.1 (CH), 129.2 (C), 128.6 (CH), 128.5 (CH), 128.4 (CH), 128.3 (CH), 127.4 (CH), 126.8 (CH), 126.8 (CH), 123.4 (CH), 122.7 (C), 120.8(CH), 120.8 (CH), 120.6 (CH), 119.7 (CH), 65.77 (CH_2) ppm;

HRMS (ESI) *m/z* calculated for $C_{28}H_{17}BrNaO_2$ $[M+Na]^+$; 487.0304, found 487.0288.

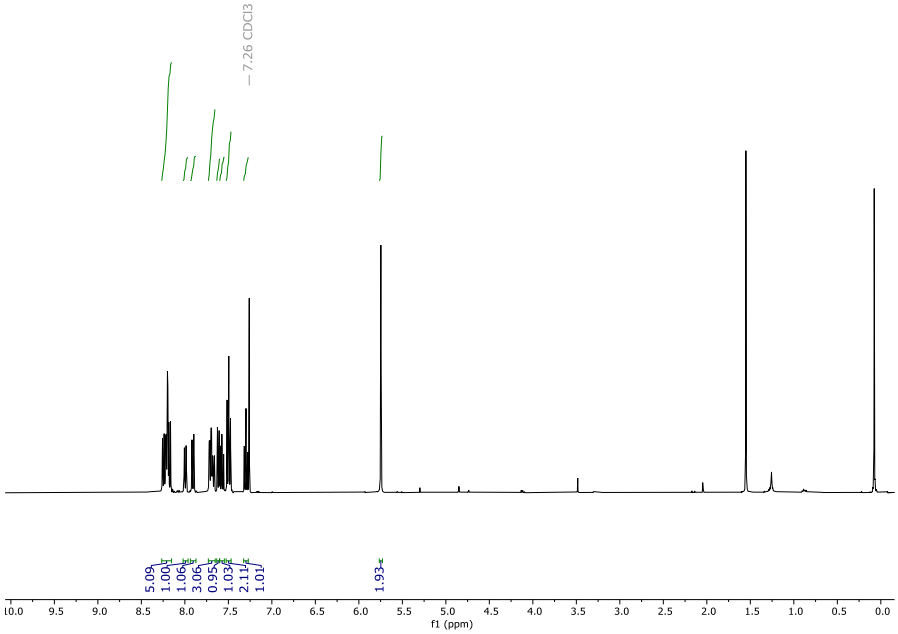

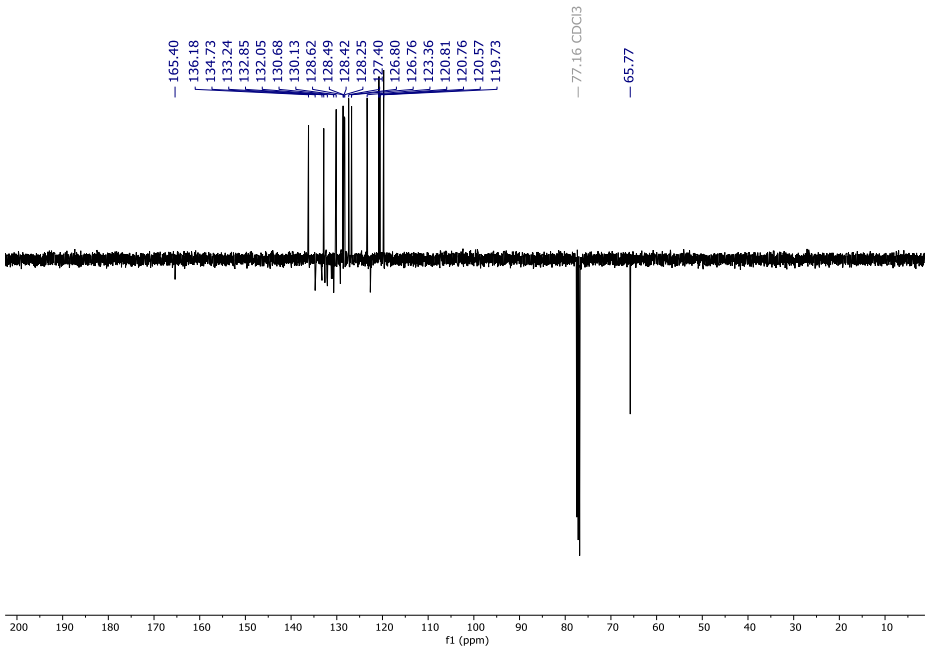

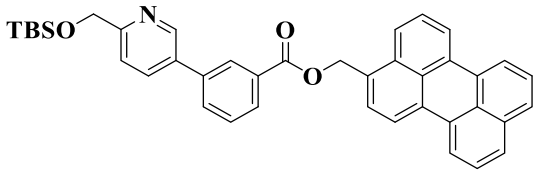

Perylen-3-ylmethyl 3-(6-(((tert-butyldimethylsilyl)oxy)methyl)pyridin-3-yl)benzoate. In a 250 mL Schlenk flask equipped with stirring bar were dissolved $Pd(OAc)_2$ (26 mg, 3 mol%), SPhos (97 mg, 6 mol%), perylen-3-ylmethyl 3-bromobenzoate (1.8 g, 3.9 mmol, 1 equiv.) in 100 mL of toluene and K_3PO_4 (1.6 g, 7.8 mmol, 2 equiv.) in DI H_2O (6 mL). 2-(((tertbutyl-dimethylsilyl)oxy)methyl)-5-(4,4,5,5-tetramethyl-1,3,2-dioxaborolan-2-yl)pyridine (2.0 g, 5.85 mmol, 1.5 equiv.) was added and reaction was heated at 100 ^oC during 24 h, cooled to room temperature and quenched with water (50 mL). The layers were separated and the aqueous layer was extracted with CH_2Cl_2 (3x100 mL). The combined organic layers were dried ($MgSO_4$), filtered and evaporated to give a crude product that was purificated by column chromatography on deactivated (Et_3N) silica gel eluting with 20% EtOAc/hexanes to give the product (1.77 g, 2.9 mmol, 74% yield) as a yellow solid. ^1H NMR (400 MHz, $CDCl_3$) δ = 8.73 (dd, *J* = 2.4, 0.8 Hz, 1H), 8.29 (s, 1H), 8.26 (dd, *J* = 7.7, 1.0 Hz, 1H), 8.24 – 8.18 (m, 3H), 8.09 (dt, *J* = 7.8, 1.4 Hz, 1H), 7.99 – 7.94 (m, 1H), 7.90 (dd, *J* = 8.1, 2.4 Hz, 1H), 7.78 – 7.74 (m, 1H), 7.71 (dd, *J* = 8.1, 2.8 Hz, 2H), 7.66 (d, *J* = 7.7 Hz, 1H), 7.61 – 7.55 (m, 2H), 7.54 – 7.47 (m, 3H), 5.80 (s, 2H), 4.88 (s, 2H), 0.97 (s, 9H), 0.14 (s, 6H) ppm; ^{13}C NMR (101 MHz, $CDCl_3$) δ = 166.4 (C), 161.0 (C), 147.2 (CH), 138.5 (C), 135.3 (CH), 134.7 (C), 134.0 (C), 133.3 (C), 132.5 (C), 132.0 (C), 131.7 (CH), 131.2 (C), 131.1 (C), 131.0 (C), 130.9 (C), 129.4 (CH), 129.3 (CH), 129.2 (C), 128.6 (C), 128.5 (CH), 128.5 (CH), 128.4 (CH), 128.2 (CH), 127.3 (CH), 126.8 (CH), 126.8 (CH), 123.4 (CH), 120.8 (CH), 120.7 (CH), 120.6 (CH), 120.2 (CH), 119.8 (CH), 66.1 (CH_2), 65.6 (CH_2), 26.1 (x3 CH_3), -5.20 (x2 CH_3) ppm; HRMS (ESI) *m/z* calculated for $C_{40}H_{38}NO_3Si$ $[M+H]^+$; 608.2615, found 608.2600.

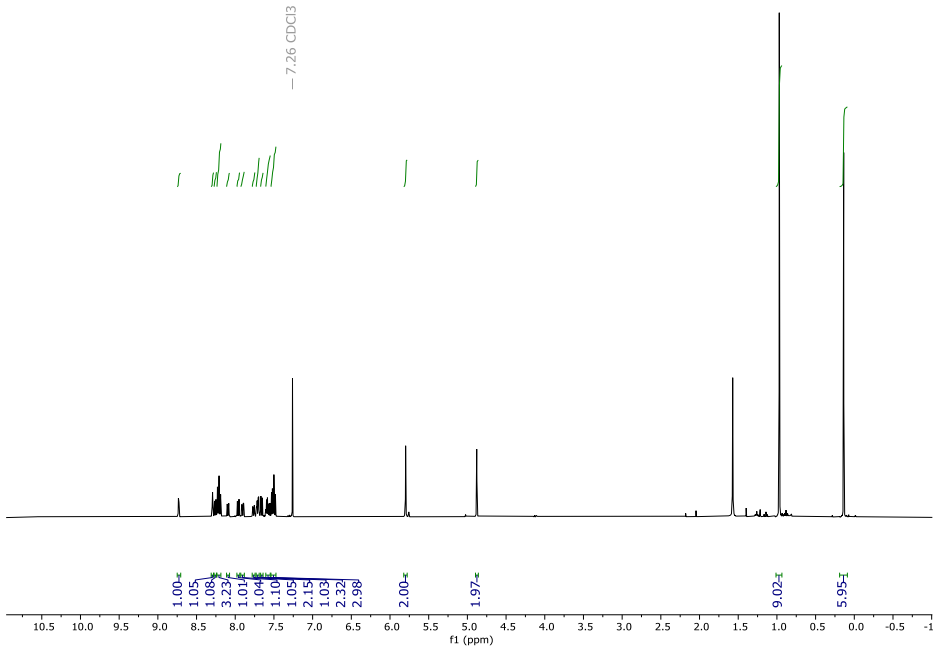
7.26 CDCl3
1.00
1.05
1.08
3.22
1.01
1.04
1.10
1.05
2.15
1.03
2.32
2.98
2.00
1.97
9.02
5.95
f1 (ppm)

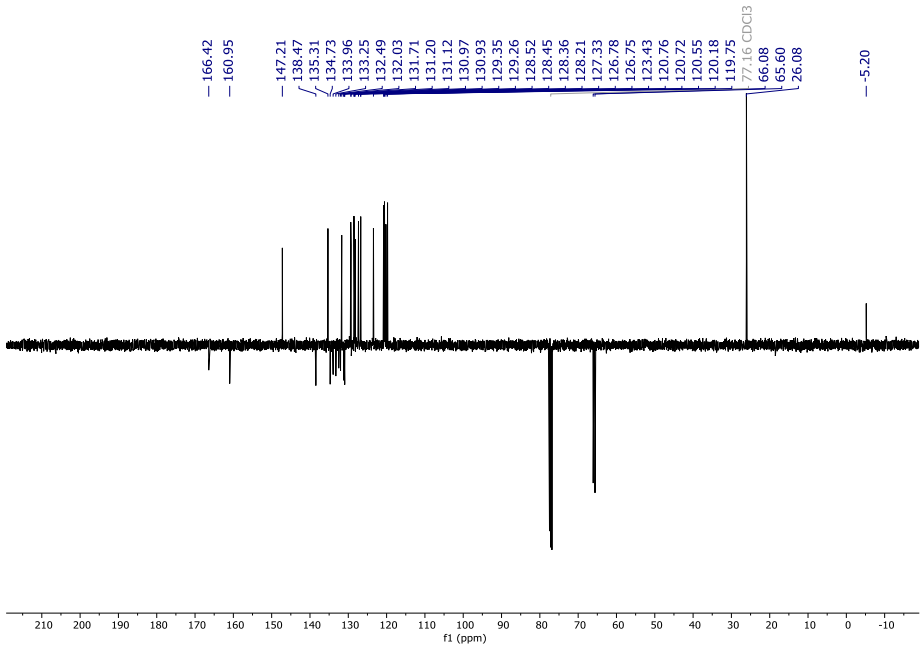
166.42
160.95
147.21
138.47
135.31
134.73
133.96
133.25
132.49
132.03
131.71
131.20
131.12
130.97
130.93
129.35
129.26
128.52
128.45
128.36
128.21
127.33
126.78
126.75
123.43
120.76
120.72
120.55
120.18
119.75
77.16 CDCl3
66.08
65.60
26.08
-5.20
f1 (ppm)

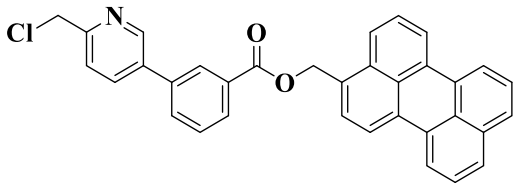

Perylen-3-ylmethyl 3-(6-(chloromethyl)pyridin-3-yl)benzoate. In a 250 mL round bottom flask perylen-3-ylmethyl 3-(6-(((tert-butyldimethylsilyl)oxy)methyl)pyridin-3-yl)benzoate (1.8 g, 2.9 mmol, 1 equiv.) was dissolved in 100 mL of THF, cooled to 0 ºC and TBAF (1M THF, 2.9 mL, 1 equiv.) was added dropwise. The reaction was stirred vigorously 30 min and quenched with NH_4Cl_{sat}. The layers were separated and the aqueous layer was extracted with Et_2O (3x20 mL). The combined organic layers were dried ($MgSO_4$), filtered and evaporated to give a crude solid. The solid was dissolved in 100 mL of anhydrous CH_2Cl_2 and cooled to 0 ºC and $SOCl_2$ (0.75 mL, 10.22 mmol, 3.5 equiv.) was added dropwise. The reaction was stirred during 4 h and quenched to neutral pH with $NaHCO_3$. The layers were separated and the aqueous layer was extracted with CH_2Cl_2 (3x100 mL). The combined organic layers were dried ($MgSO_4$), filtered and evaporated to give a crude product that was purificated by column chromatography on deactivated (Et_3N) silica gel eluting with 55% EtOAc/hexanes to give the product (0.88 g, 59% yield) as a yellow solid. ^{1}H NMR (400 MHz, $CDCl_3$) δ = 8.79 (dd, *J* = 2.4, 0.8 Hz, 1H), 8.31 – 8.26 (m, 1H), 8.23 (dd, *J* = 7.7, 1.0 Hz, 1H), 8.19 (ddd, *J* = 7.7, 2.5, 1.1 Hz, 2H), 8.16 (d, *J* = 7.8 Hz, 1H), 8.13 – 8.09 (m, 1H), 7.93 (dd, *J* = 8.4, 0.9 Hz, 1H), 7.89 (dd, *J* = 8.1, 2.4 Hz, 1H), 7.75 (ddd, *J* = 7.7, 2.0, 1.2 Hz, 1H), 7.72 – 7.67 (m, 2H), 7.63 (d, *J* = 7.7 Hz, 1H), 7.58 – 7.45 (m, 5H), 5.78 (s, 2H), 4.71 (s, 2H) ppm; ^{13}C NMR (101 MHz, $CDCl_3$) δ = 166.3 (C), 155.8 (C), 148.0 (CH), 137.6 (C), 135.7 (CH), 135.2 (C), 134.7 (C), 133.3 (C), 132.6 (C), 132.1 (C), 131.8 (CH), 131.3 (C), 131.2 (C), 131.0 (C), 130.9 (C), 129.7 (CH), 129.5 (CH), 129.2 (C), 128.6 (2x CH), 128.4 (CH), 128.3 (CH), 127.8 (C), 127.4 (CH), 126.8 (CH), 126.8 (CH), 123.4 (CH), 123.0 (CH), 120.8 (CH), 120.8 (CH), 120.6 (CH), 119.8 (CH), 65.7 (CH_2), 46.5 (CH_2). HRMS (ESI) *m/z* calculated for $C_{34}H_{22}ClNO_2$ $[M+H]^+$; 512.1412, found 512.1417.

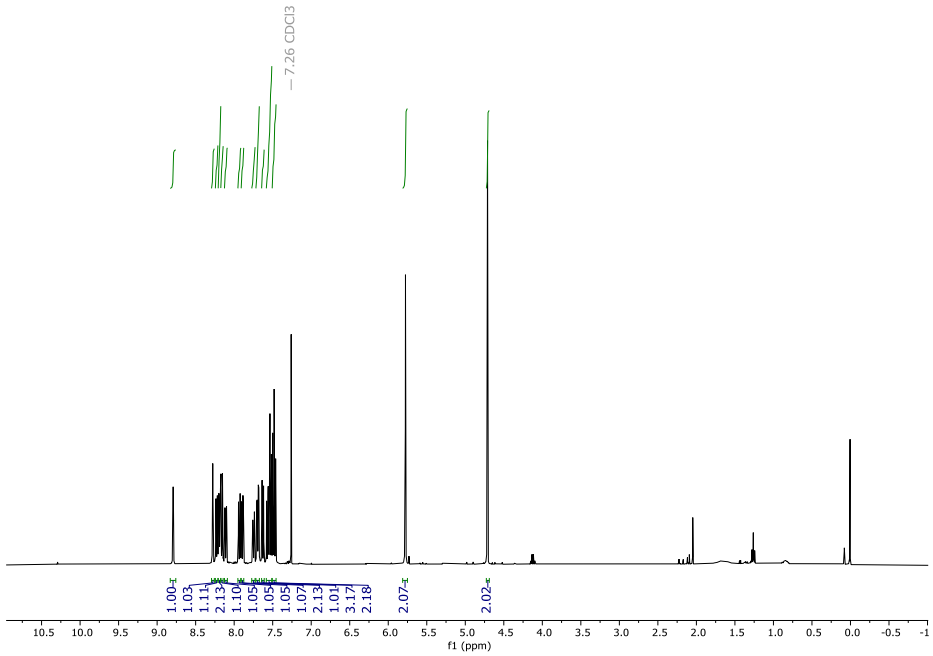
7.26 CDCl3
1.00
1.03
1.11
2.13
1.10
1.05
1.05
1.05
1.07
2.13
1.01
3.17
2.18
2.07
2.02
f1 (ppm)

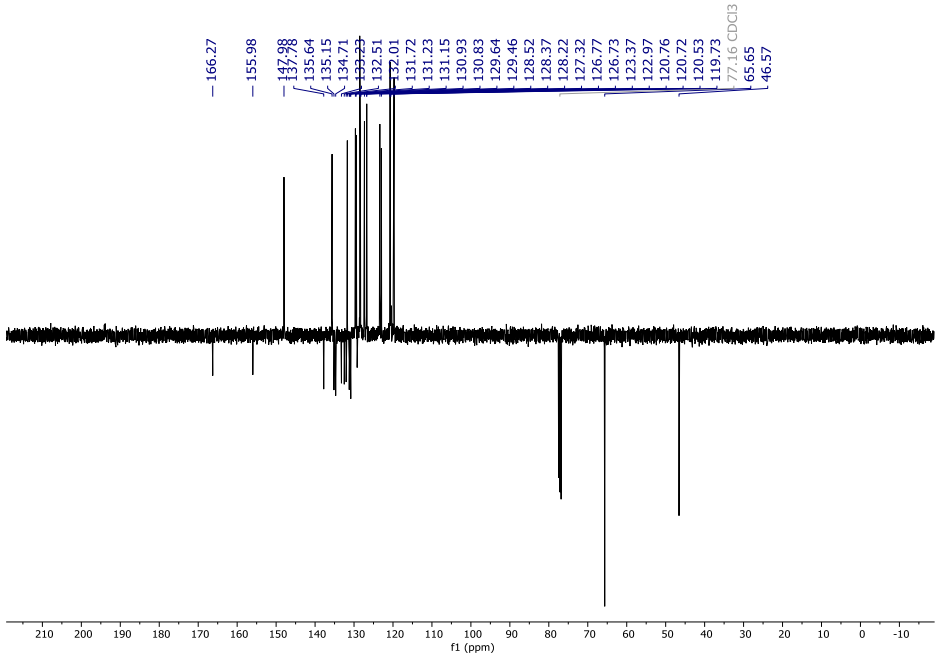
166.27
155.98
147.98
137.88
135.64
135.15
134.71
133.23
132.51
132.01
131.72
131.23
131.15
130.93
130.83
129.64
129.46
128.52
128.37
128.22
127.32
126.77
126.73
123.37
122.97
120.76
120.72
120.53
119.73
77.16 CDCl3
65.65
46.57
f1 (ppm)

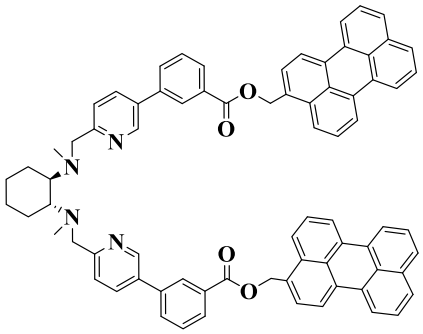

Bis(perylen-3-ylmethyl) 3,3'-(((((1R,2R)-cyclohexane-1,2-diyl)bis(methylazanediyl)) bis(methylene))bis(pyridine-6,3-diyl))dibenzoate (^{PerB}mcp). Perylen-3-ylmethyl 3-(6-(chloromethyl)pyridin-3-yl)benzoate (0.89 g, 1.73 mmol, 2.1 equiv.), (*R*,*R*)-(−)-*N*,*N*′-Dimethyl-1,2-diaminocyclohexane (117 mg, 0.82 mmol, 1 equiv.), were dissolved in MeCN (150 mL). Na_2CO_3 (6 equiv.) and tetrabutylammonium bromide – TBABr (0.1 equiv.) were added directly as solids and the resulting mixture was heated at reflux under N_2 for 24 h. After cooling to the RT mixture was concentrated under reduced pressure. Resulting residue was dissolved in CH_2Cl_2 and washed with water to remove remaining TBABr. The layers were separated and the aqueous layer was extracted with CH_2Cl_2 (3x100 mL). The organic layer was dried ($MgSO_4$), filtered and evaporated to give a crude product that was purificated by column chromatography on deactivated (Et_3N) silica gel eluting with CH_2Cl_2 to give the product (0.36 g, 40% yield). ^{1}H NMR (400 MHz, $CDCl_3$) δ = 8.71 (s, 1H), 8.25 (d, *J* = 1.8 Hz, 1H), 8.16 – 8.10 (m, 3H), 8.08 (d, *J* = 7.8 Hz, 1H), 8.05 (dt, *J* = 7.8, 1.4 Hz, 1H), 7.88 (dd, *J* = 8.3, 0.9 Hz, 1H), 7.76 (dd, *J* = 8.1, 2.4 Hz, 1H), 7.69 (dt, *J* = 7.6, 1.6 Hz, 1H), 7.67 – 7.65 (m, 1H), 7.65 – 7.59 (m, 2H), 7.56 (d, *J* = 7.7 Hz, 1H), 7.52 – 7.40 (m, 4H), 5.71 (s, 2H), 3.97 (d, *J* = 14.6 Hz, 1H), 3.83 (d, *J* = 14.7 Hz, 1H), 2.71 (s, 1H), 2.33 (s, 3H), 2.01 (d, *J* = 12.2 Hz, 1H), 1.78 (d, *J* = 8.6 Hz, 1H), 1.20 (d, *J* = 10.5 Hz, 1H), 0.85 (d, *J* = 3.4 Hz, 1H) ppm; ^{13}C NMR (101 MHz, $CDCl_3$) δ = 166.4 (2x C), 147.1 (2x CH), 138.4 (2x C), 135.0 (2x C), 134.7 (2x CH), 133.7 (2x C), 133.1 (2x C), 132.6 (2x C), 132.4 (2x C), 131.9 (2x C), 131.6 (2x CH) , 131.1 (2x C), 131.0 (2x C), 130.9 (2x C), 130.9 (2x C), 129.30 (2x CH), 129.2

(2x CH) , 129.1 (2x C), 128.5 (2x C), 128.4 (4x CH), 128.3 (2x CH), 128.1 (2x CH), 127.2 (2x CH), 126.7 (2x CH), 126.7 (2x CH), 123.4 (2x CH), 123.0 (2x CH), 120.7 (2x CH), 120.6 (2x CH), 120.5 (2x CH), 119.7 (2x CH), 65.5 (2x CH_2), 64.8 (2x CH), 60.1 (2x CH_2), 37.0 (2x CH_3), 29.9 (2x CH_2), 25.9 (2x CH_2) ppm. HRMS (ESI) *m/z* calculated for $C_{76}H_{60}N_4O_4$ $[M+H]^+$; 1093.4687, found 1093.4682.

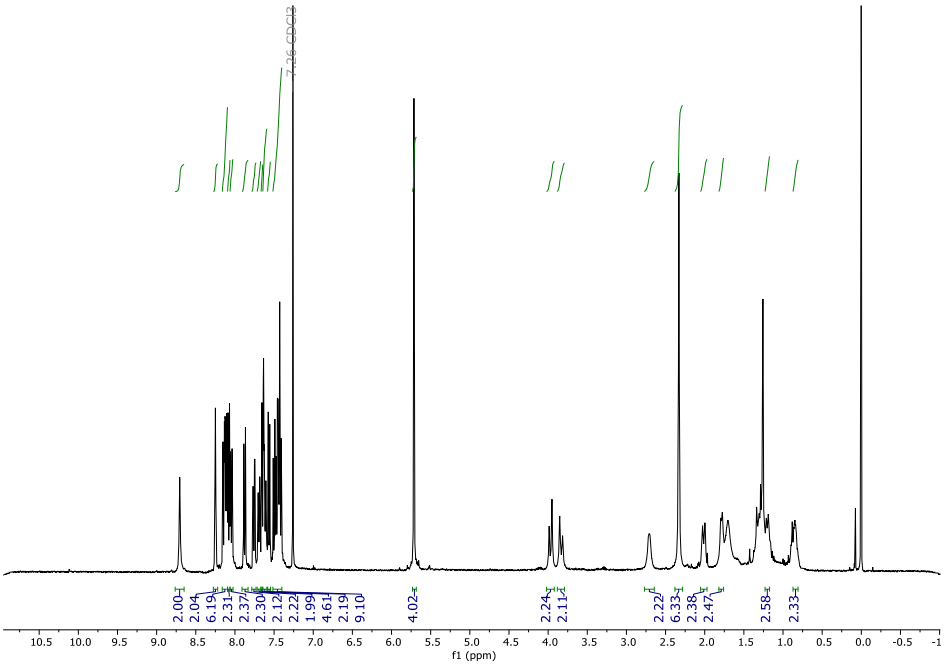

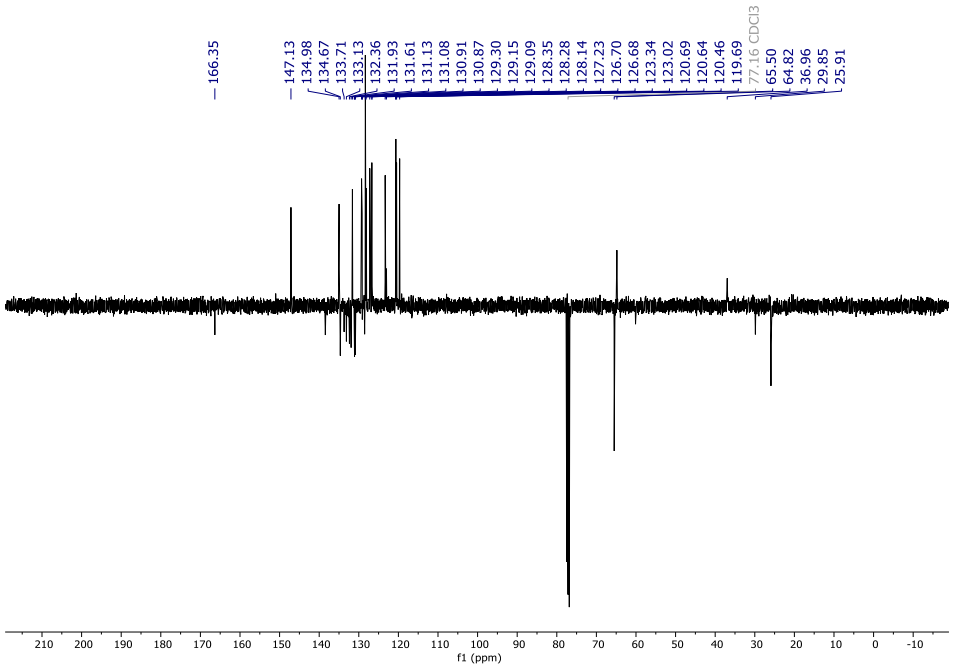

III.4.5 Syntheses and Characterization of Complexes

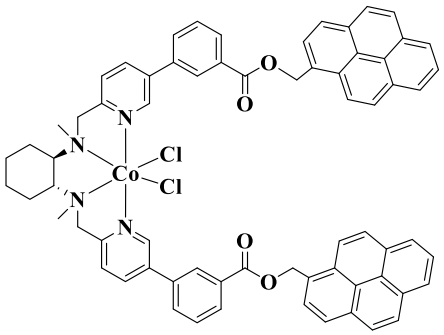

[Co(^PyB^mcp)Cl$_2$]. Inside a glovebox, a vial was charged with $CoCl_2$ (25 mg, 0.1953 mmol) and anhydrous THF (0.5 mL). Then a solution of ^{PyB}mcp (194 mg, 0.1953 mmol) in THF (0.5 mL) was added dropwise to the vigorously stirred suspension of cobalt salt in THF. The resulting mixture was stirred overnight which caused the formation of a purple precipitate, the resulting solid was filtered off, washed with CH_3CN (3x 2 mL) and dried under vacuum. This solid was dissolved in CH_2Cl_2 and the slow diffusion of diethyl ether into this solution produced desired clean product (47 mg, 22% yield). ^{1}H NMR (400 MHz, $CDCl_3$) δ = 164.52, 102.23, 63.91, 49.65, 24.44, 21.83, 9.25, 8.71, 8.69,

8.62, 8.35, 8.34, 8.32, 8.16, 8.06, 8.04, 8.00, 7.87, 7.85, 7.58, 7.47, 7.42, 6.04, 5.69, 5.68, 5.45, 5.43, 5.22, 2.97, 1.26, 1.20, 0.84, 0.81, 0.02, -0.64, -9.56, -13.37, -15.14 ppm; HRMS (MALDI) *m/z* calculated for $C_{68}H_{56}ClCoN_4O_4$ [M-Cl]$^+$; 1086.3322, found 1086.3384. Elemental Analysis (%) calculated for $[C_{68}H_{56}ClCoN_4O_4]$*CH_2Cl_2: %C 68.61 %H 4.84 %N 4.64, found %C 68.75 %H 5.18 %N 4.55.

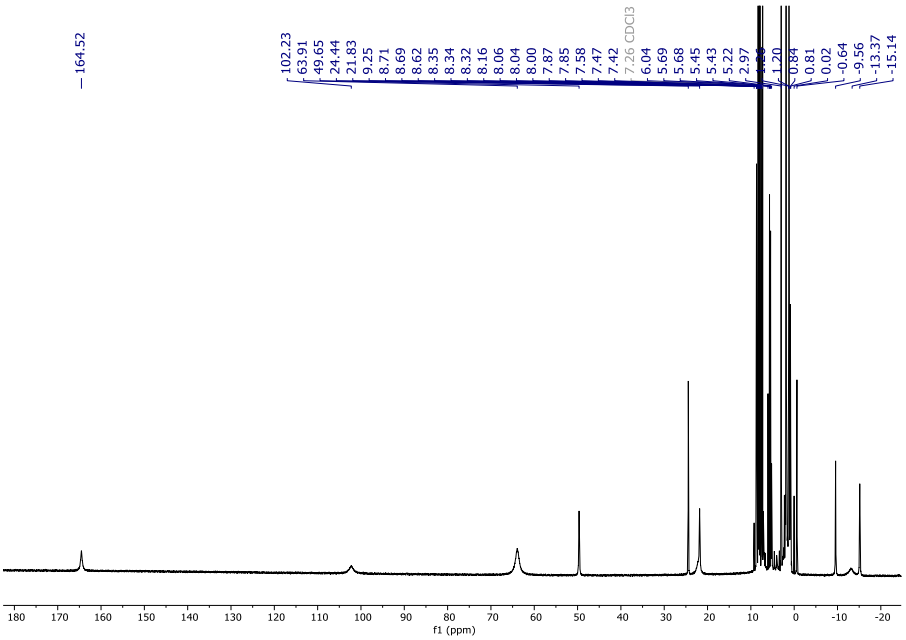

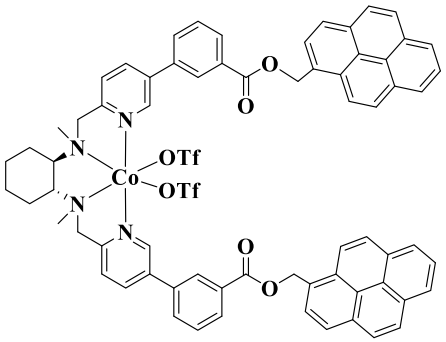

[Co(^PyB^mcp)(OTf)$_2$] In a glovebox, a solution of [Co(^PyB^mcp)Cl_2] (240 mg, 0.214 mmol), dissolved in anhydrous DCM (1 mL) and added dropwise to a vigorously stirred solution of AgOTf (121 mg, 0.471 mmol) in DCM (1 mL). After few minutes, the solution become cloudy and a purple precipitate appeared. The resulting mixture was stirred overnight, the solution was filtered

off and dried under vacuum giving desired product. This solid was dissolved in CH_3CN and the slow diffusion of diethyl ether into this solution produced desired clean product (249 mg, 86% yield). ^{1}H NMR (400 MHz, CD_3CN) δ = 177.45, 99.25, 45.91, 39.41, 30.12, 19.60, 11.75, 9.93, 9.33, 8.59, 8.19, 7.66, 7.47, 6.96, 5.77, 5.36, 4.18, 3.64, 3.17, 2.18, 1.21, 0.81, 0.31, -10.66, -12.49 ppm; HRMS (ESI) *m/z* calculated for $C_{68}H_{56}CoN_4O_4$ $[M\text{-}2OTf1]^{2+}$; 525.6811, found 525.6828. Elemental Analysis (%) calculated for $[C_{70}H_{56}CoF_6N_4O_{10}S_2]$*$CH_2Cl_2$: %C 59.42 %H 4.07 %N 3.90, found %C 58.66 %H 4.55 %N 4.03.

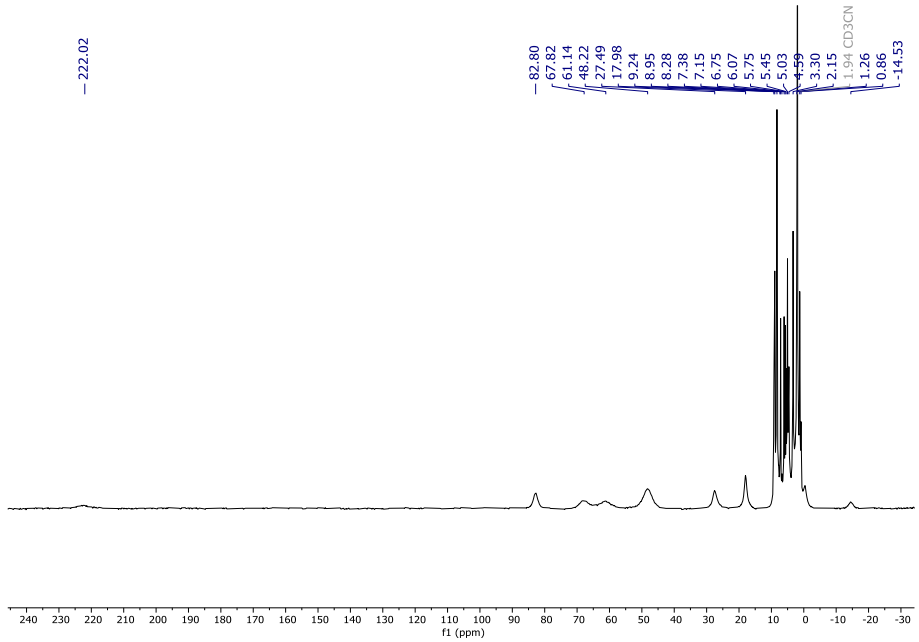

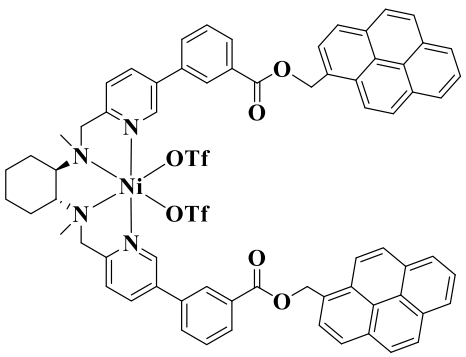

[Ni(^{PyB}**mcp)(OTf)$_2$].** In a glovebox, a solution of $Ni(OTf)_2$*$2CH_3CN$ (42 mg, 0.096 mmol), dissolved in anhydrous THF (1 mL) and added dropwise to a

vigorously stirred solution of ^{PyB}mcp (100 mg, 0.1mmol) in THF (1 mL). After few minutes, the solution become cloudy and a pale green precipitate appeared. The resulting mixture was stirred overnight, the solution was filtered off and the resulting solid dried under vacuum giving desired product. This solid was dissolved in CH_3CN and the slow diffusion of diethyl ether into this solution produced desired clean product (110 mg, 81% yield). ^{1}H NMR (400 MHz, CD_3CN) δ = 40.68, 22.58, 20.24, 15.38, 13.99, 8.30, 7.55, 7.29, 6.17, 3.65, 3.42, 2.14, 1.13, -2.50, -5.50 ppm. HRMS (ESI) *m/z* calculated for $C_{68}H_{56}NiN_4O_4$ $[M\text{-}2OTf1]^{2+}$; 525.1822, found 525.1835.

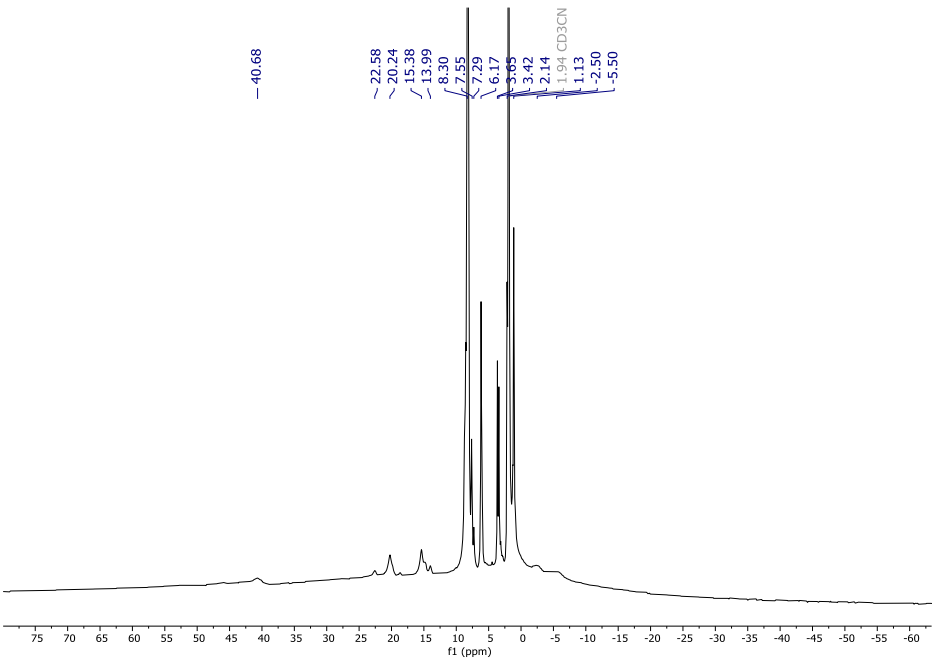

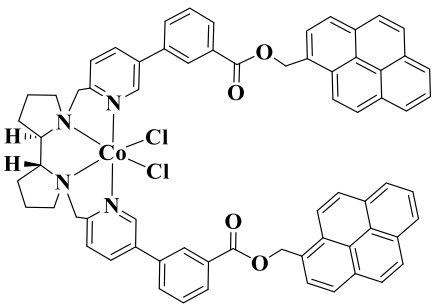

[Co(^{PyB}pdp)Cl_2]. Inside a glovebox, a vial was charged with $CoCl_2$ (18 mg, 0.1363 mmol) and anhydrous THF (0.5 mL). Then a solution of ^{PyB}pdp (150 mg, 0.1515 mmol) in THF (0.5 mL) was added dropwise to the vigorously stirred suspension of cobalt salt in THF. The resulting mixture was stirred overnight which caused the formation of a turquoise precipitate, the resulting solid was filtered off, washed with CH_3CN (3x 2 mL) and dried under vacuum. This solid was dissolved in CH_2Cl_2 and the slow diffusion of diethyl ether into this solution produced desired clean product (47 mg, 22% yield). ^{1}H NMR (400 MHz, CD_3CN) δ 177.45, 99.25, 45.91, 39.41, 30.12, 19.60, 11.75, 9.93, 9.33, 8.59, 8.19, 7.66, 7.47, 6.96, 5.77, 5.36, 4.18, 3.64, 3.17, 2.18, 1.21, 0.81, 0.31, -10.66, -12.49 ppm; HRMS (ESI) *m/z* calculated for $C_{68}H_{54}CoN_4O_4$ $[M\text{-}2Cl]^{2+}$; 524.6733, found 524.6759. Elemental Analysis (%) calculated for $[C_{69}H_{56}ClCoN_4O_4]$*CH_2Cl_2: %C 70.80 %H 4.82 %N 4.79, found %C 70.82 %H 4.94%N 4.83.

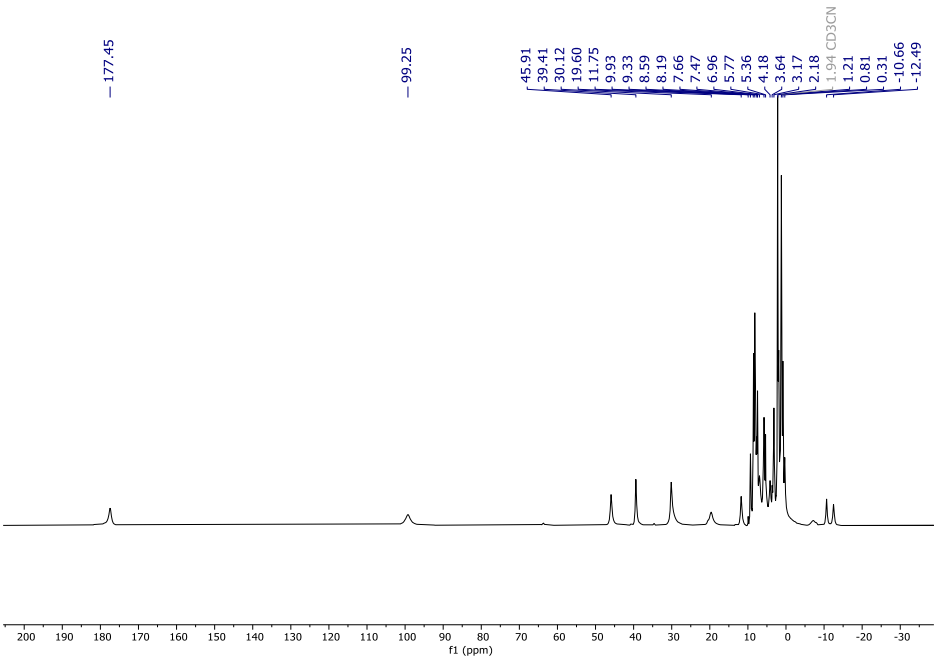

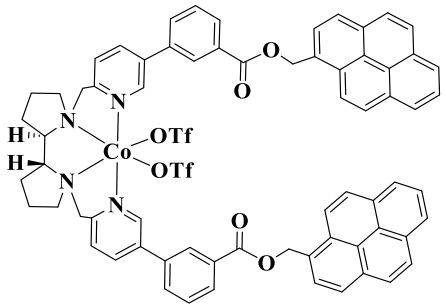

[Co(^{PyB}pdp)(OTf)$_2$]. In a glovebox, a solution of Co(OTf)$_2$·2CH$_3$CN (151 mg 0.344 mmol) in anhydrous THF (1 mL) was added dropwise to a vigorously stirred solution of ^{PyB}pdp (436 mg, 0.444 mmol) in THF (1 mL). After few minutes, the solution become cloudy and a pale pink precipitate appeared. The resulting mixture was stirred overnight, the solution was filtered off and the resulting solid dried under vacuum. This solid was dissolved in CH_2Cl_2 and the slow diffusion of diethyl ether into this solution produced desired clean product (0.3243g, 55% yield). ^{1}H NMR (400 MHz, CD_3CN) δ = 231.97, 79.68, 77.60, 62.54, 53.22, 42.78, 40.49, 34.74, 24.33, 19.79, 13.07, 9.17, 8.80, 8.63, 8.21, 8.04, 7.86, 7.61, 7.52, 7.16, 6.48, 6.02, 5.86, 5.53, 5.26, 5.09, 4.76, 4.27, 4.01, 3.89, 3.38, 2.84, 2.11, 1.49, 1.23, 1.11, 0.83, -1.55, -7.97 ppm; HRMS (MALDI) *m/z* calculated for $C_{69}H_{54}CoF_3N_4O_7S$ $[M\text{-}OTf]^+$; 1198.2997, found 1198.3015. Elemental Analysis (%) calculated for $C_{69}H_{54}CoF_3N_4O_7S$: %C 62.36 %H 4.04 %N 4.16, found %C 63.09 %H 4.40 %N 4.26.

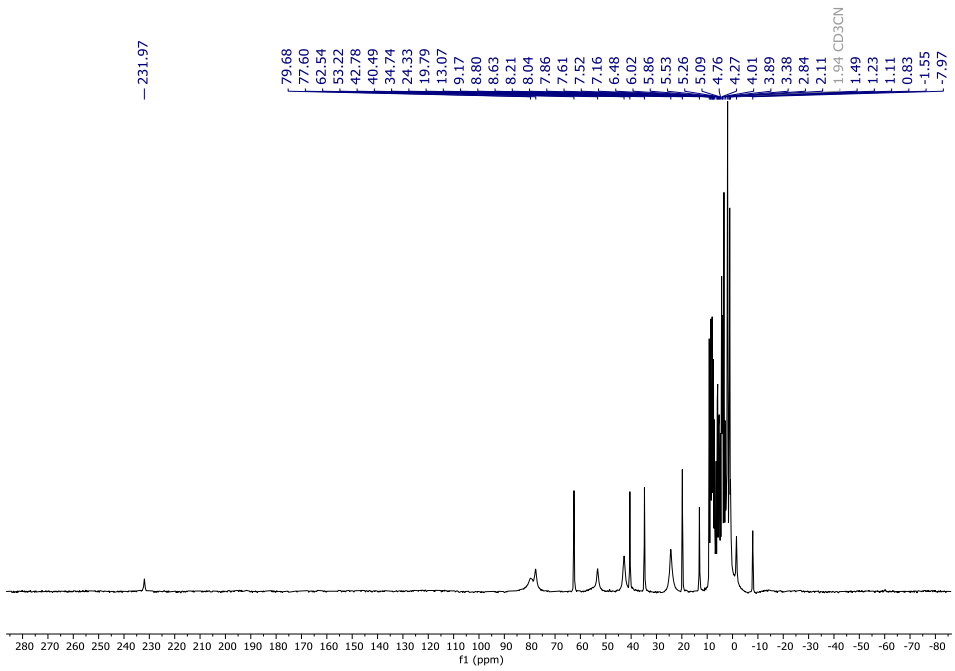

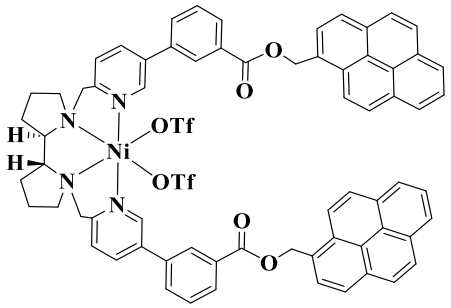

[Ni(^{PyB}pdp)(OTf)$_2$]. In a glovebox, a solution of Ni(OTf)$_2$*2CH$_3$CN (84 mg, 0.19 mmol), dissolved in anhydrous THF (1 mL) and added dropwise to a vigorously stirred solution of ^{PyB}pdp (210 mg, 0.21mmol) in THF (1 mL). After few minutes, the solution become cloudy and a pale green precipitate appeared. The resulting mixture was stirred overnight, the solution was filtered off and the resulting solid dried under vacuum giving desired product. This solid was dissolved in CH$_3$CN and the slow diffusion of diethyl ether into this solution produced desired clean product (225 mg, 79% yield). ^{1}H NMR (400 MHz, CD$_3$CN) δ = 39.73, 38.27, 31.55, 23.38, 20.39, 15.07, 8.28, 6.17, 5.45, 3.42, 1.12, -5.76, -10.25 ppm. HRMS (ESI) *m/z* calculated for $C_{68}H_{54}N_{4Ni}O_4$ [M-2OTf]$^{2+}$; 524.1744, found 524.1769.

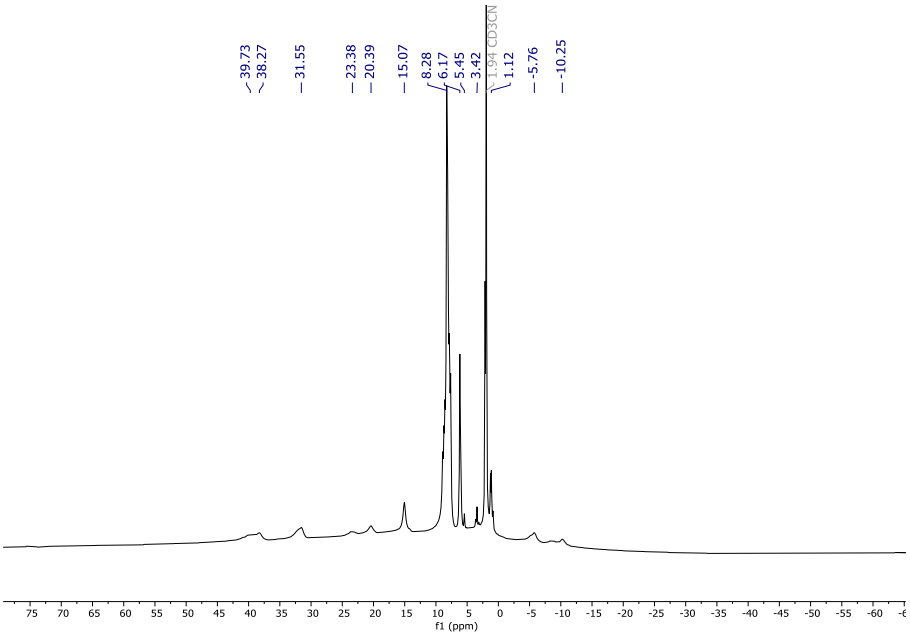

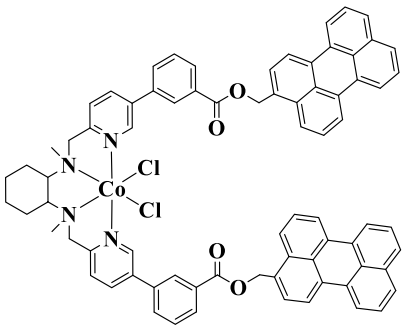

[(Co(^{PerB}mcp)Cl_2)]. Inside a glovebox, a vial was charged with $CoCl_2$ (11 mg, 0.085 mmol) and anhydrous THF (1 mL). Then a solution of ^{PerB}mcp (104 mg, 0.095 mmol) in THF (1 mL) was added dropwise to the vigorously stirred suspension of cobalt salt in THF, which caused the formation of a dark yellow precipitate after few minutes. The resulting mixture was stirred overnight, the resulting solid was filtered off, washed with CH_3CN (3 x 1 mL) and dried under vacuum. This solid was dissolved in CH_2Cl_2 and filtered through Celite. Finally, slow diffusion of diethyl ether into the clear solution produced a purple solid. The solution was siphoned off by cannula and the solid material that corresponds to the targeted complex was dried under vacuum (74 mg, 63%). ^{1}H NMR (400 MHz, $CDCl_3$) δ 163.60, 104.24, 64.61, 50.18, 25.03, 22.46, 10.56,

9.22, 9.09, 8.80, 8.54, 8.42, 8.16, 7.50, 6.46, 5.89, 5.65, 4.63, 4.43, 3.32, 3.02, 2.42, 1.94, 1.55, 0.76, 0.14, -9.05, -12.64, -14.20 ppm;

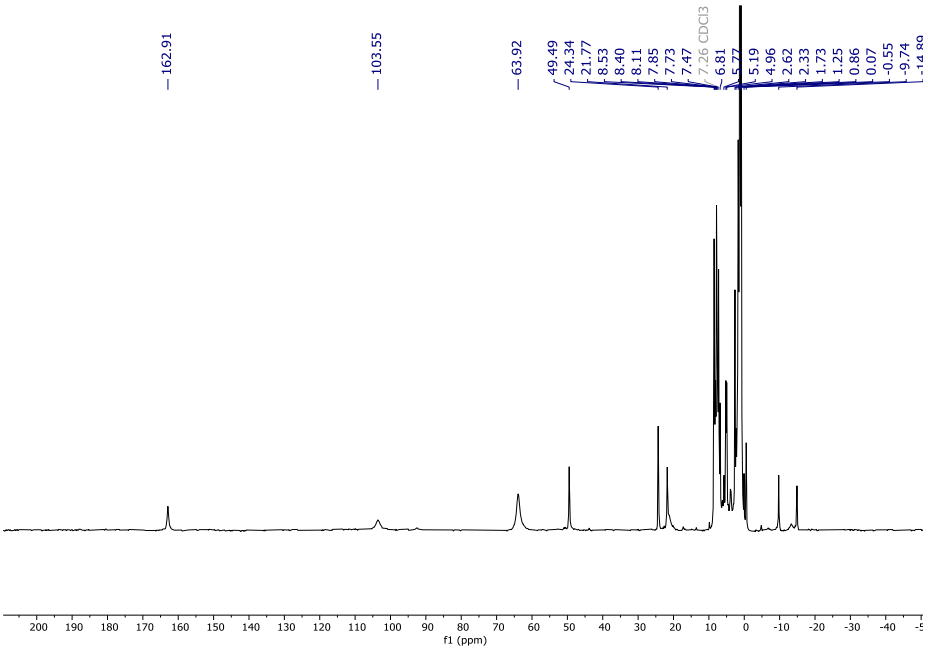

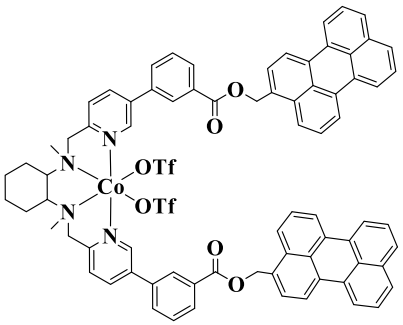

(Co(^PerB^mcp)(OTf)$_2$). In a glovebox, a solution of [Co(^PerB^mcp)Cl$_2$] (130 mg, 0.106 mmol), dissolved in anhydrous DCM (1 mL) was added dropwise to a vigorously stirred solution of AgOTf (60 mg, 0.234 mmol) in DCM (1 mL). After few minutes, the solution become cloudy and a purple precipitate appeared. The resulting mixture was stirred overnight, the solution was filtered off and dried under vacuum giving desired product. This solid was dissolved in CH_3CN and the slow diffusion of diethyl ether into this solution produced desired clean product (0.117mg, 76% yield). ^{1}H NMR (400 MHz, CD_3CN) δ = 154.41, 83.34, 74.08, 59.04, 51.08, 48.43, 43.42, 26.43, 23.61, 21.72, 17.81,

14.59, 13.11, 11.85, 10.93, 9.27, 8.87, 7.69, 6.60, 5.52, 5.26, 4.44, 3.64, 2.77, 1.27, 1.13, 0.86, -0.48, -2.29, -14.29 ppm; HRMS (ESI) *m/z* calculated for $C_{77}H_{60}CoF_3N_4O_7S$ $[M\text{-}OTf]^+$; 1300.3461, found 1300.3453.

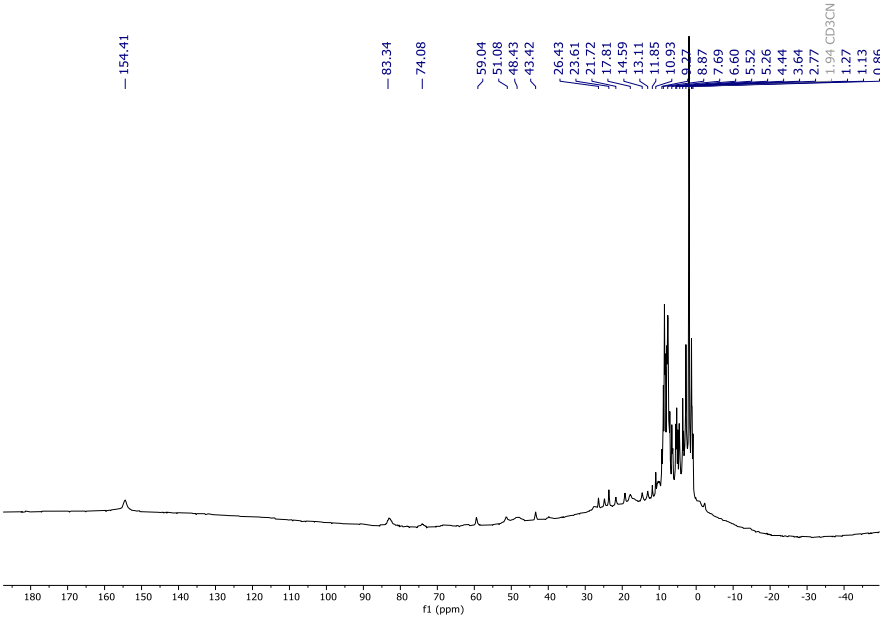

III.4.6 Syntheses and Characterization of Model Ligands and Their Complexes

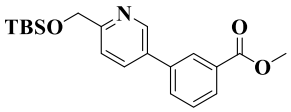

Methyl 3-(6-(((tert-butyldimethylsilyl)oxy)methyl)pyridin-3-yl)benzoate. In a 250 mL Schlenk flask equipped with stirring bar were dissolved $Pd(OAc)_2$ (3 mmol%), SPhos (6 mmol%), methyl 3-bromobenzoate (2.5 g, 11.6 mmol, 1 equiv.) in 100 mL of toluene and K_3PO_4 (4.92 g, 23.2 mmol, 2 equiv.) in DI H_2O (4 mL). 2-(((tertbutyl-dimethylsilyl)oxy)methyl)-5-(4,4,5,5-tetramethyl-1,3,2-dioxaborolan-2-yl)pyridine (4.67 g, 13.37 mmol, 1.2 equiv.) was added and reaction was heated at 100 ^oC during 18 h, cooled to room temperature and quenched with water (40 mL). The layers were separated and the aqueous layer was extracted with CH_2Cl_2 (3x 50 mL). The combined organic layers were dried ($MgSO_4$), filtered and evaporated to give a crude product that was purified by column chromatography on silica gel eluting with 20% EtOAc/hexanes to give

the product (2.74 g, 66 % yield) as a yellow oil. ^{1}H NMR (400 MHz, $CDCl_3$) δ 8.60 (dd, *J* = 2.4, 0.9 Hz, 1H), 8.10 (t, *J* = 1.8 Hz, 1H), 7.87 (dt, *J* = 7.8, 1.4 Hz, 1H), 7.75 (dd, *J* = 8.1, 2.4 Hz, 1H), 7.58 (ddd, *J* = 7.8, 2.0, 1.2 Hz, 1H), 7.45 (dd, *J* = 8.1, 1.0 Hz, 1H), 7.34 (t, *J* = 7.8 Hz, 1H), 4.76 (s, 2H), 3.77 (s, 3H), 0.85 (s, 9H), 0.02 (s, 6H) ppm; ^{13}C NMR (101 MHz, $CDCl_3$) δ 166.3 (C), 160.6 (C), 146.8 (CH), 137.9 (C), 134.7 (CH), 133.5 (C), 131.0 (CH), 130.8 (C), 128.9 (CH), 128.6 (CH), 127.9 (CH), 119.7 (CH), 65.8 (CH_2), 51.9 (CH_3), 25.7 (x3 CH_3), -5.55 (x2 CH_3) ppm;

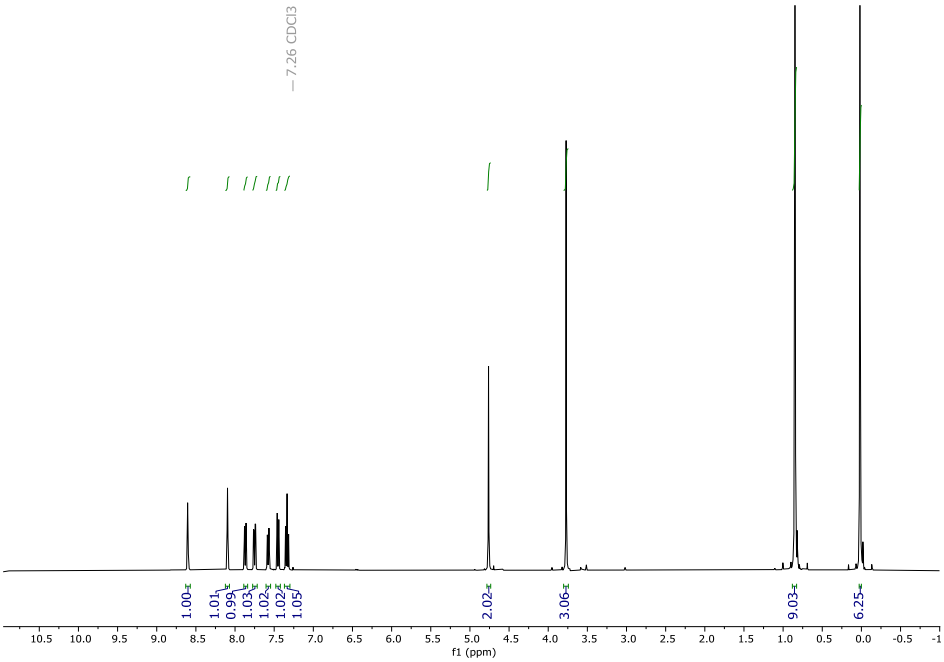

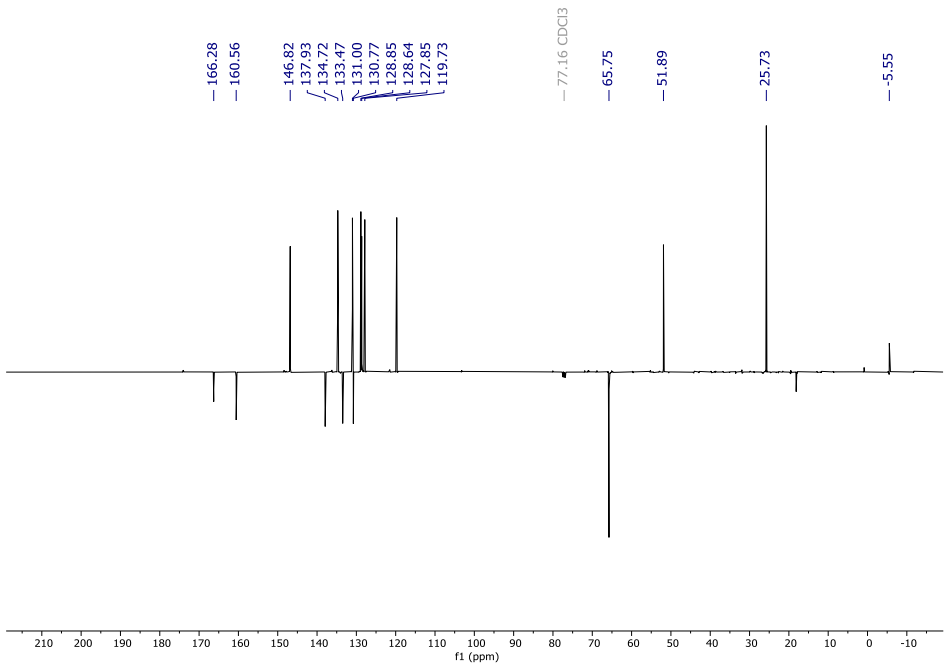

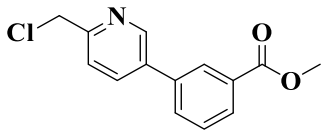

Methyl 3-(6-(chloromethyl)pyridin-3-yl)benzoate. In a 100 ml round bottom flask methyl 3-(6-(((tert-butyldimethylsilyl)oxy)methyl)pyridin-3-yl)benzoate (1.3 g, 3.5 mmol, 1 equiv.) was dissolved in 50 ml of THF, cooled to 0 ºC and TBAF (1M THF, 3.5 mL, 1 equiv.) was added dropwise. The reaction was stirred vigorously 30 min and quenched with NH_4Cl_{sat}. The layers were separated and the aqueous layer was extracted with Et_2O (3x20 mL). The combined organic layers were dried ($MgSO_4$), filtered and evaporated to give a crude solid. The solid was dissolved in 50 ml of anhydrous CH_2Cl_2 and cooled to 0 ºC and $SOCl_2$ (0.83 ml, 11.3 mmol, 3.2 equiv.) was added dropwise. The reaction was stirred during 4 h and quenched to neutral pH with $NaHCO_3$. The layers were separated and the aqueous layer was extracted with CH_2Cl_2 (3x20 mL). The combined organic layers were dried ($MgSO_4$), filtered and evaporated

to give a crude product that was purificated by column chromatography on deactivated (Et_3N) silica gel eluting with 55% EtOAc/hexanes to give the product (0.57 g, 62 % yield) as a white solid. ^1H NMR (400 MHz, $CDCl_3$) δ = 8.79 (dd, *J* = 2.4, 0.8 Hz, 1H), 8.22 (t, *J* = 1.8 Hz, 1H), 8.04 (dt, *J* = 7.8, 1.4 Hz, 1H), 7.90 (dd, *J* = 8.1, 2.4 Hz, 1H), 7.73 (ddd, *J* = 7.8, 2.0, 1.2 Hz, 1H), 7.56 – 7.48 (m, 2H), 4.70 (s, 2H), 3.92 (s, 3H) ppm; ^{13}C NMR (101 MHz, $CDCl_3$) δ = 166.7 (C), 156.9 (C), 147.9 (CH), 137.6 (C), 135.5 (CH), 135.1 (C), 132.0 (CH), 131.2 (C), 129.4 (CH), 129.3 (CH), 128.3 (CH), 122.9 (CH), 52.4 (CH_3), 46.5 (CH_2) ppm.

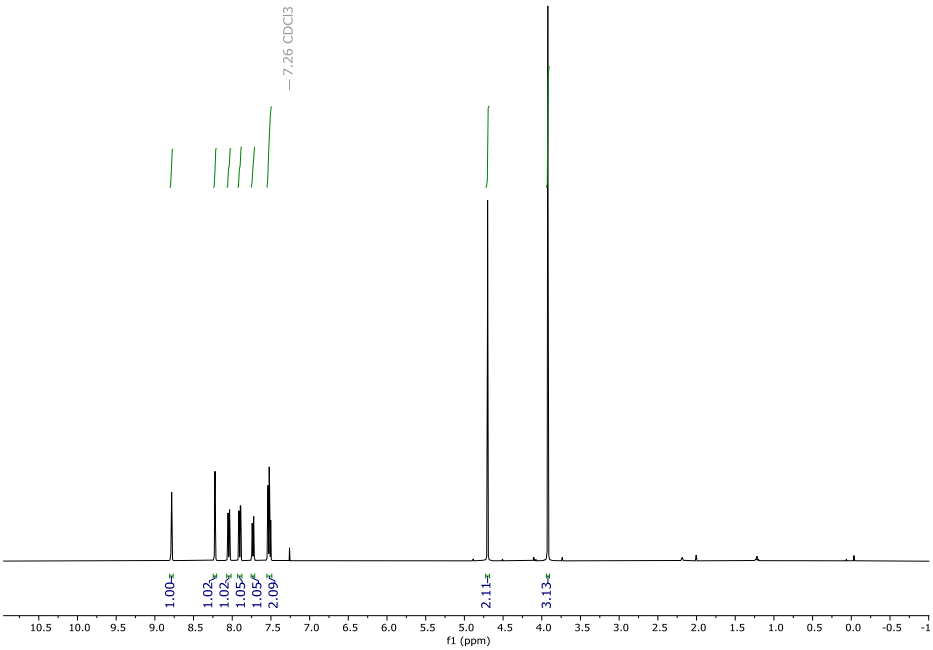

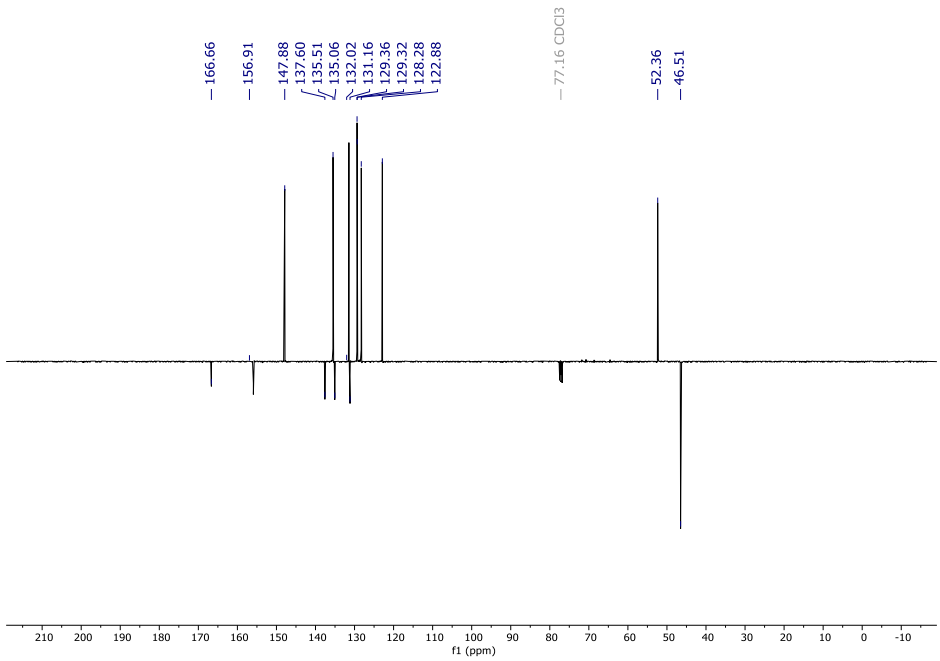

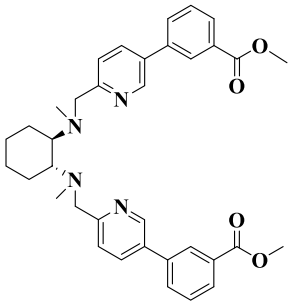

Dimethyl 3,3'-(((((1R,2R)-cyclohexane-1,2-diyl) bis(methylazanediyl)) bis(methylene))bis(pyridine-6,3-diyl))dibenzoate (^{CO2MeB}mcp). Methyl 3-(6-(chloromethyl) pyridin-3-yl)benzoate (0.6 g, 2.3 mmol, 2.1 equiv.), (*R*,*R*)-(−)-*N*,*N*′-Dimethyl-1,2-diaminocyclohexane (156 mg, 1.1 mmol, 1 equiv.), were dissolved in MeCN (100 mL). Na_2CO_3 (6 equiv.) and tetrabutylammonium bromide – TBABr (0.1 equiv.) were added directly as solids and the resulting mixture was heated at reflux under N_2 for 24 h. After cooling to the RT mixture was concentrated under reduced pressure. Resulting residue was dissolved in CH_2Cl_2 and washed with water to remove remaining TBABr. The layers were separated and the aqueous layer was extracted with CH_2Cl_2 (3x100 mL). The organic layer was dried ($MgSO_4$), filtered and evaporated to give a crude

product that was purified by column chromatography on deactivated (Et_3N) silica gel eluting with CH_2Cl_2 to give the product (0.29 g, 45 % yield). ^{1}H NMR (400 MHz, $CDCl_3$) δ 8.54 – 8.49 (m, 2H), 8.01 (t, *J* = 1.8 Hz, 2H), 7.80 (dt, *J* = 7.8, 1.4 Hz, 2H), 7.60 (dd, *J* = 8.1, 2.4 Hz, 2H), 7.51 (ddd, *J* = 7.8, 2.0, 1.2 Hz, 2H), 7.44 (d, *J* = 8.1 Hz, 2H), 7.28 (t, *J* = 7.8 Hz, 2H), 3.75 (d, *J* = 14.7 Hz, 2H), 3.69 (s, 8H), 3.63 (d, *J* = 14.7 Hz, 2H), 2.47 (d, *J* = 8.8 Hz, 2H), 2.11 (s, 6H), 1.82 – 1.74 (m, 2H), 1.61 – 1.47 (m, 2H), 1.09 (d, *J* = 10.6 Hz, 2H), 1.00 – 0.90 (m, 2H) ppm; ^{13}C NMR (101 MHz, $CDCl_3$) δ 166.9 (x2 C), 161.0 (x2 C), 147.1 (x2 CH), 138.4 (x2 C), 134.9 (x2 CH), 133.7 (x2 C), 131.4 (x2 CH), 131.0 (x2 C), 129.2 (x2 CH), 128.9 (x2 CH), 128.2 (x2 CH), 122.9 (x2 CH), 64.7 (x2 CH), 60.3 (x2 CH_2), 52.3 (x2 CH_3), 36.8 (x2 CH_2), 26.0 (x2 CH_2), 25.9 (x2 CH_2) ppm; HRMS (ESI) *m/z* calculated for $C_{36}H_{41}N_4O_4$ $[M+H]^+$; 593.3122, found 593.3139.

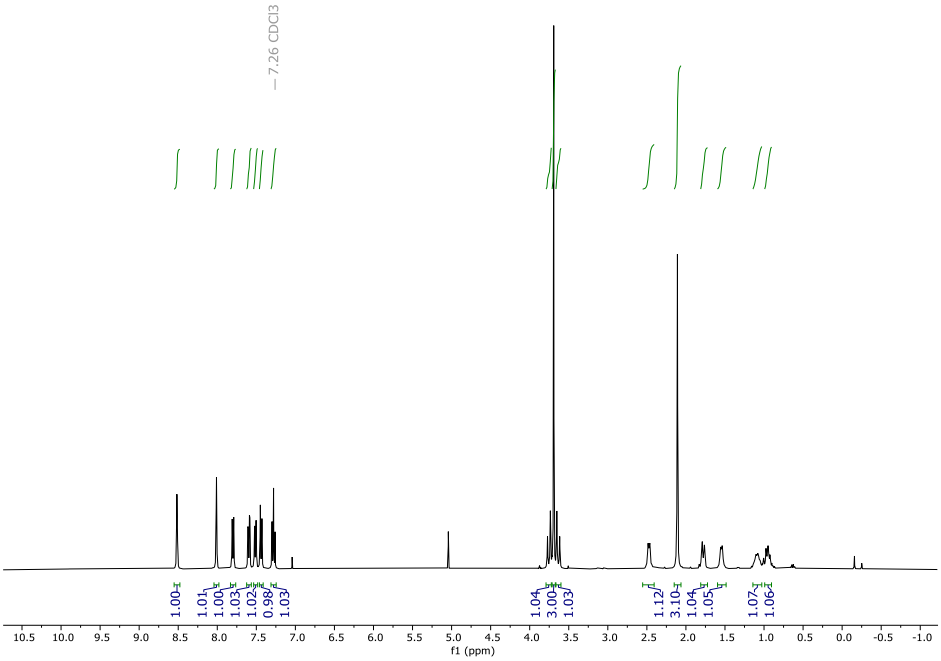

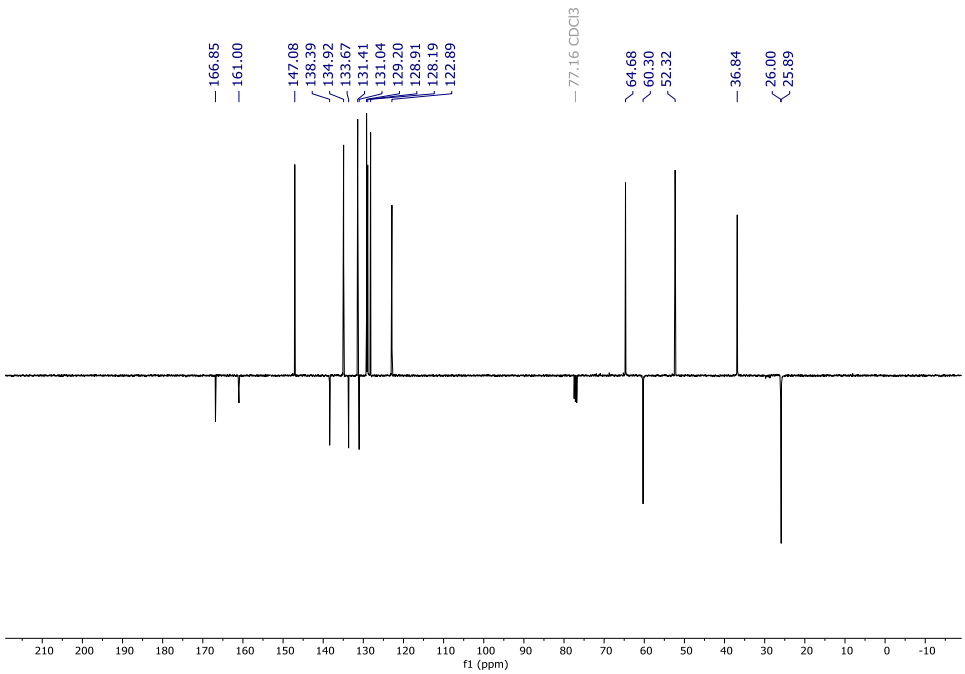

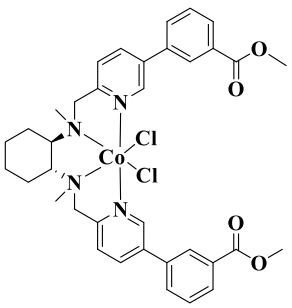

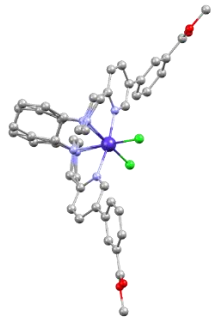

[(Co(^{CO2MeB}mcp)Cl_2)]. Inside a glovebox, a vial was charged with $CoCl_2$ (104 mg, 0.81 mmol) and anhydrous THF (1 mL). Then a solution of ^{CO2MeB}mcp (530 mg, 0.9 mmol) in THF (1 mL) was added dropwise to the vigorously stirred suspension of cobalt salt in THF, which caused the formation of a purple precipitate after few minutes. The resulting mixture was stirred overnight, the resulting solid was filtered off, washed with CH_3CN (3x 1 mL) and dried under vacuum. This solid was dissolved in CH_2Cl_2 and filtered through Celite. Finally, slow diffusion of diethyl ether into the clear solution produced a purple solid. The solution was siphoned off by cannula and the solid material that corresponds to the targeted complex was dried under vacuum (341 mg, 51%).

^{1}H NMR (400 MHz, CD_3CN) δ 167.08, 97.27, 65.45, 49.87, 24.40, 22.03, 8.91, 7.33, 5.52, 5.19, 3.57, 1.71, 0.77, -0.17, -11.50, -13.32 ppm; HRMS (ESI) *m/z* calculated for $C_{36}H_{40}ClCoN_4O_4$ $[M - CH_3 - Cl]^+$; 686.2065, found 686.2066.

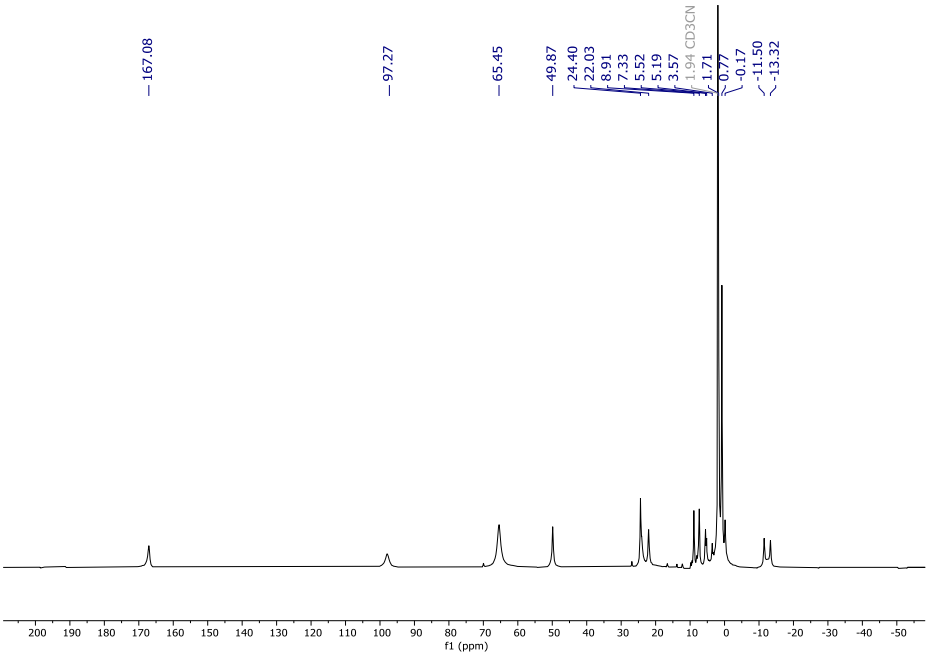

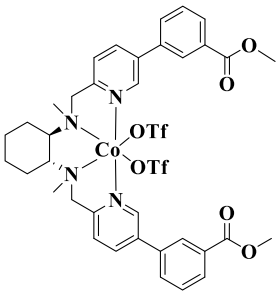

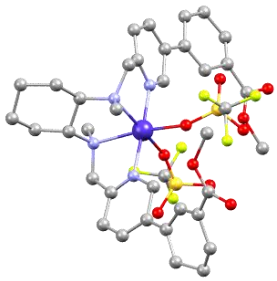

[(Co(^{CO2MeB}mcp)(OTf)$_2$)]. In a glovebox, a solution of Co(^{CO2MeB}mcp)Cl_2 (150 mg 0.2 mmol) in anhydrous DCM (1 mL) was added dropwise to a vigorously stirred solution of AgOTf (123 mg, 0.5 mmol, 2.5 eq.) in DCM (1 mL). After few minutes, the solution become orange cloudy and a purple precipitate appeared. The resulting mixture was stirred overnight, the solution was filtered through syringe filter to remove resultant AgCl. Solvent was collected and dried under vacuum to obtain desired solid. This solid was dissolved in CH_3CN and the slow diffusion of diethyl ether into this solution produced desired clean

product (190 mg, 92% yield). ^{1}H NMR (400 MHz, CD_3CN) δ 221.82, 83.28, 67.26, 59.39, 48.22, 28.43, 17.72, 6.22, -13.98 ppm; HRMS (ESI) *m/z* calculated for $C_{37}H_{40}CoF_3N_4O_7S$ [M – CH_3 – CF_3SO_3]$^+$; 800.1896, found 800.1901.

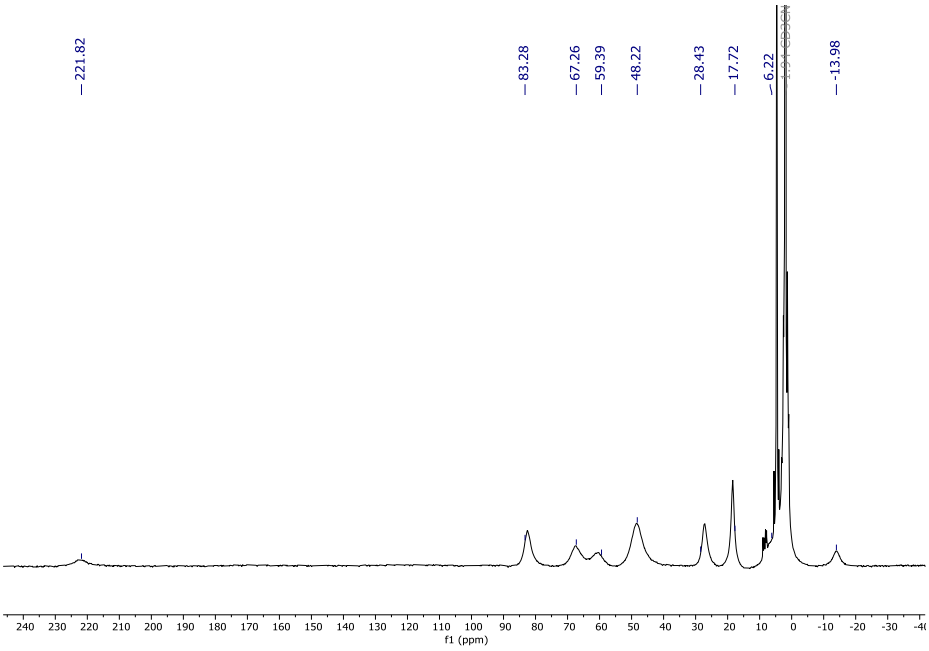

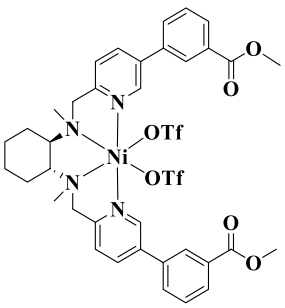

[Ni(^{CO2MeB}mcp)(OTf)$_2$]. In a glovebox, a solution of $Ni(OTf)_2$*$2CH_3CN$ (207 mg, 0.47 mmol), dissolved in anhydrous THF (2 mL) and added dropwise to a vigorously stirred solution of ^{CO2MeB}mcp (310 mg, 0.52 mmol) in THF (2 mL). After few minutes, the solution become cloudy and a pale green precipitate appeared. The resulting mixture was stirred overnight, the solution was filtered

off and the resulting solid dried under vacuum giving desired product. This solid was dissolved in CH_3CN and the slow diffusion of diethyl ether into this solution produced desired clean product (392 mg, 79% yield). ^1H NMR (500 MHz, CD_3CN) δ = 40.71, 22.53, 20.32, 15.43, 14.82, 8.70, 8.65, 8.57, 8.47, 7.63, 7.34, 3.98, 3.96, 3.88, 3.65, 2.74, 1.81, 1.28, 1.14, -2.20, -5.21 ppm; HRMS (ESI) *m/z* calculated for $C_{37}H_{40}F_3N_4NiO_7S$ $[M - CF_3SO_3]^+$; 799.1879, found 799.1918.

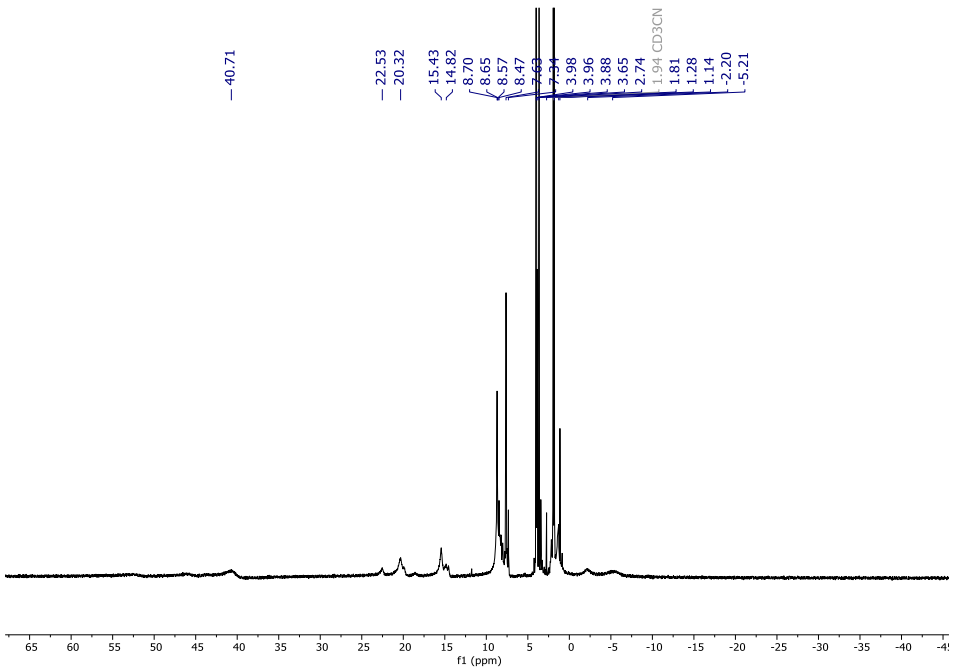

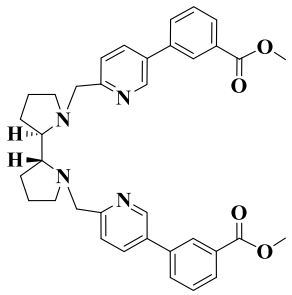

Dimethyl 3,3'-((((2R,2'R)-[2,2'-bipyrrolidine]-1,1'-diyl)bis(methylene))bis(pyridine-6,3-diyl))dibenzoate) (^{CO2MeB}pdp). Methyl 3-(6-(chloromethyl) pyridin-3-yl)benzoate (0.6 g, 2.3 mmol, 2.1 equiv.), (R,R)-

2,2′-bipyrrolidine L-tartrate trihydrate (149 mg, 0.43 mmol, 1 equiv.), were dissolved in MeCN (100 mL). Na_2CO_3 (6 equiv.) and tetrabutylammonium bromide – TBABr (0.1 equiv.) were added directly as solids and the resulting mixture was heated at reflux under N_2 for 24 h. After cooling to the RT mixture was concentrated under reduced pressure. Resulting residue was dissolved in CH_2Cl_2 and washed with water to remove remaining TBABr. The layers were separated and the aqueous layer was extracted with CH_2Cl_2 (3x100 mL). The organic layer was dried ($MgSO_4$), filtered and evaporated to give a crude product that was purified by column chromatography on deactivated (Et_3N) silica gel eluting with CH_2Cl_2 to give the product (0.36 g, 40% yield). ^{1}H NMR (400 MHz, $CDCl_3$) δ 8.75 (d, *J* = 2.3 Hz, 1H), 8.17 (d, *J* = 1.8 Hz, 1H), 8.00 (dt, *J* = 7.8, 1.4 Hz, 1H), 7.88 (dd, *J* = 8.1, 2.4 Hz, 1H), 7.75 – 7.65 (m, 2H), 7.49 (t, *J* = 7.8 Hz, 1H), 4.63 (d, *J* = 14.4 Hz, 1H), 4.42 (d, *J* = 14.5 Hz, 1H), 3.86 (s, 3H), 3.58 (s, 1H), 3.42 – 3.31 (m, 1H), 3.07 (s, 1H), 2.21 (q, *J* = 8.0, 7.0 Hz, 1H), 1.94 (dtt, *J* = 20.3, 13.2, 6.4 Hz, 2H), 1.78 – 1.63 (m, 1H) ppm; ^{13}C NMR (101 MHz, $CDCl_3$) δ 166.6 (x2 C), 147.4 (x2 CH), 137.4 (x4 C), 135.5 (x2 CH), 135.0 (x2 C), 131.4 (x2 CH), 131.01 (x2 C), 129.3 (x4 CH), 128.1 (x2 CH), 124.7 (x2 CH), 67.7 (x2 CH), 59.9 (x2 CH_2), 54.1 (x2 CH_2), 52.3 (x2 CH_3), 28.1 (x2 CH_2), 23.7 (x2 CH_2) ppm.

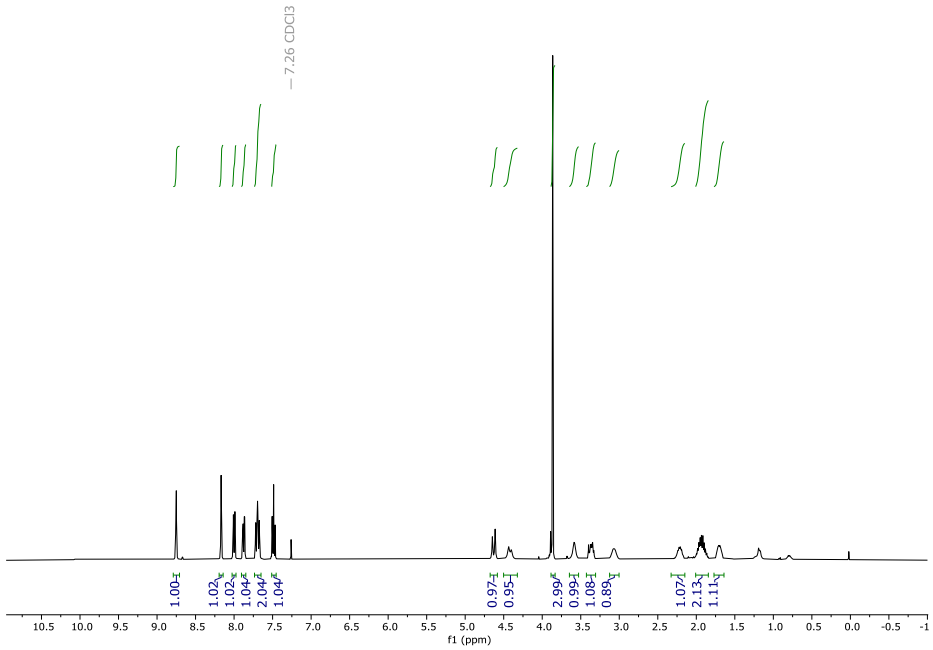
7.26 CDCl3
1.00
1.02
1.02
1.04
2.04
1.04
0.97
0.95
2.99
0.99
1.08
0.89
1.07
2.13
1.11
f1 (ppm)

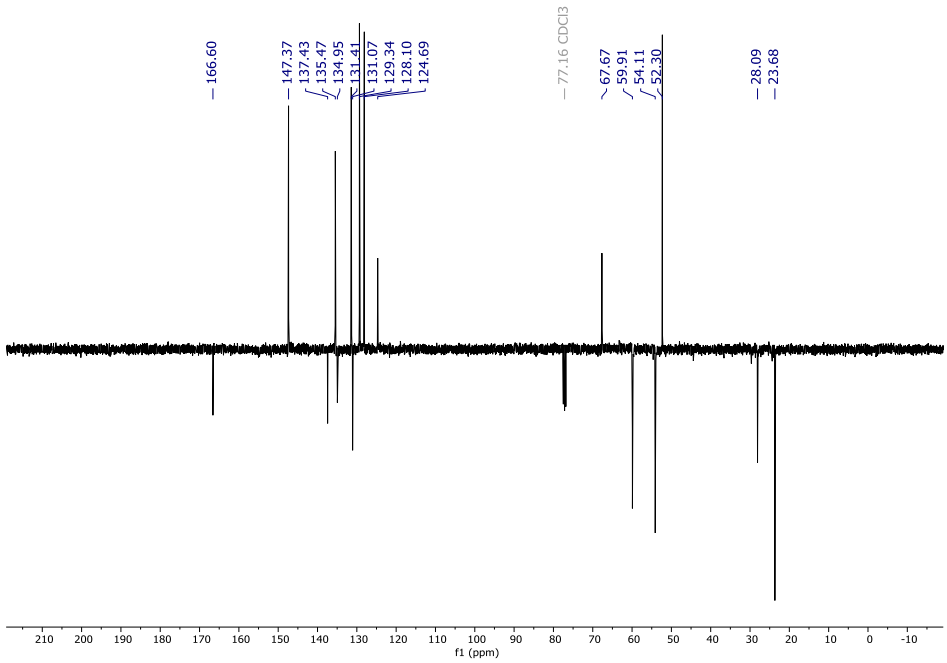
166.60
147.37
137.43
135.47
134.95
131.41
131.07
129.34
128.10
124.69
77.16 CDCl3
67.67
59.91
54.11
52.30
28.09
23.68
f1 (ppm)

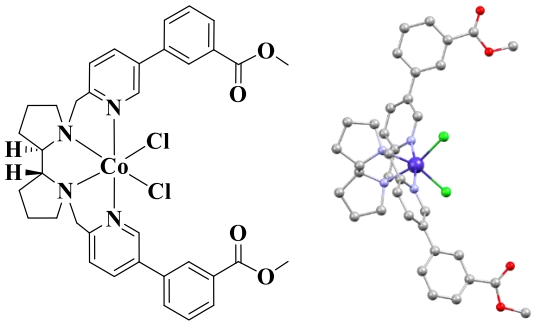

[(Co(^{CO2MeB}pdp)Cl_2)]. Inside a glovebox, a vial was charged with $CoCl_2$ (81 mg, 0.62 mmol) and anhydrous THF (1 mL). Then a solution of ^{CO2MeB}pdp (401 mg, 0.69 mmol) in THF (1 mL) was added dropwise to the vigorously stirred suspension of cobalt salt in THF, which caused the formation of a dark yellow precipitate after few minutes. The resulting mixture was stirred overnight, the resulting solid was filtered off, washed with CH_3CN (3x 1 mL) and dried under vacuum. This solid was dissolved in CH_2Cl_2 and filtered through Celite. Finally, slow diffusion of diethyl ether into the clear solution produced a purple solid. The solution was siphoned off by cannula and the solid material that corresponds to the targeted complex was dried under vacuum (201 mg, 54%). ^{1}H NMR (400 MHz, CD_3CN) δ 176.69, 96.77, 45.18, 38.59, 30.11, 19.67, 11.86, 7.56, 7.23, 5.43, 4.23, 3.91, 2.16, 1.16, 0.62, -6.80, -10.67, -12.07 ppm; HRMS (ESI) *m/z* calculated for $C_{36}H_{38}ClCoN_4O_4$ [M – – Cl]$^+$; 684.1908, found 684.1880.

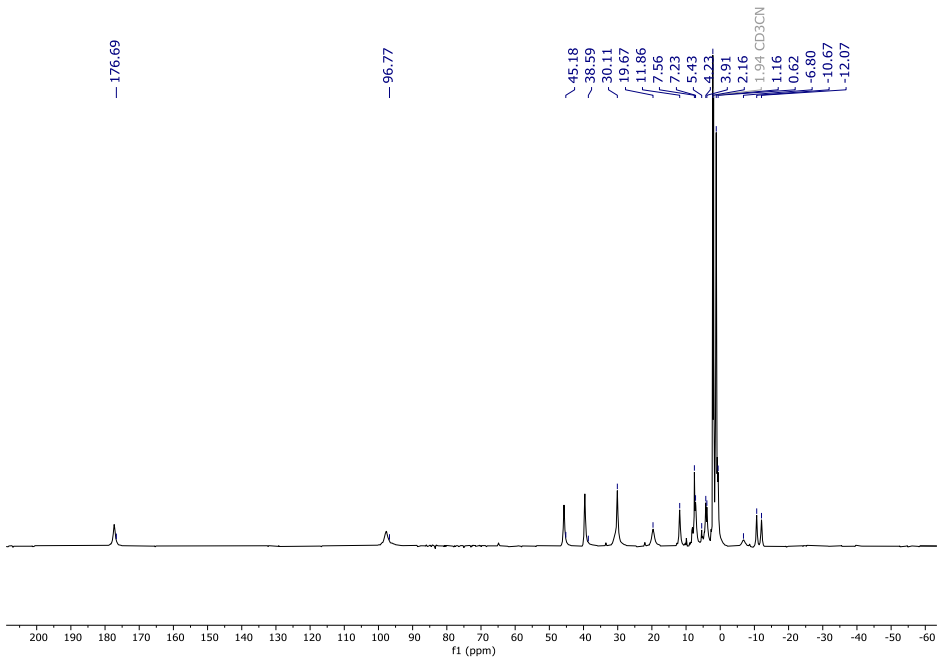

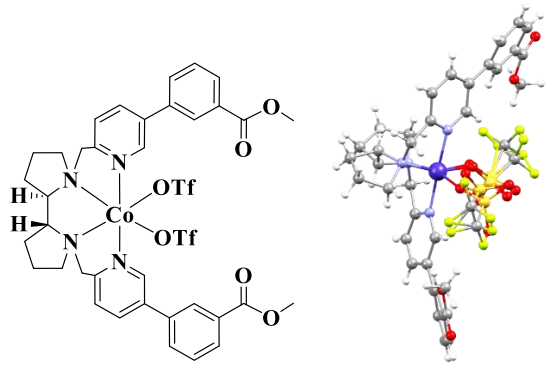

[(Co(CO2MeBpdp)(OTf)$_2$)]. In a glovebox, a solution of Co(CO2MeBpdp)Cl$_2$ (150 mg, 0.2 mmol) in anhydrous DCM (1 mL) was added dropwise to a vigorously stirred solution of AgOTf (129 mg, 0.5 mmol, 2.5 eq.) in DCM (1 mL). After few minutes, the solution become orange cloudy and a purple precipitate appeared. . The resulting mixture was stirred overnight, the solution was filtered through syringe filter to remove resultant AgCl. Solvent was collected and dried under vacuum to obtain desired solid. This solid was dissolved in CH_3CN and the slow diffusion of diethyl ether into this solution produced desired clean product (181 mg, 92% yield). ^{1}H NMR (400 MHz, CD_3CN) δ 80.20, 54.73, 24.87, 8.03, 4.52, 4.40, 2.21, 1.54, 1.13, 0.69, 0.09, -14.36 ppm; HRMS (ESI)

m/z calculated for $C_{37}H_{38}CoF_3N_4O_7S$ $[M - CF_3SO_3]^+$; 798.1740, found 798.1737.

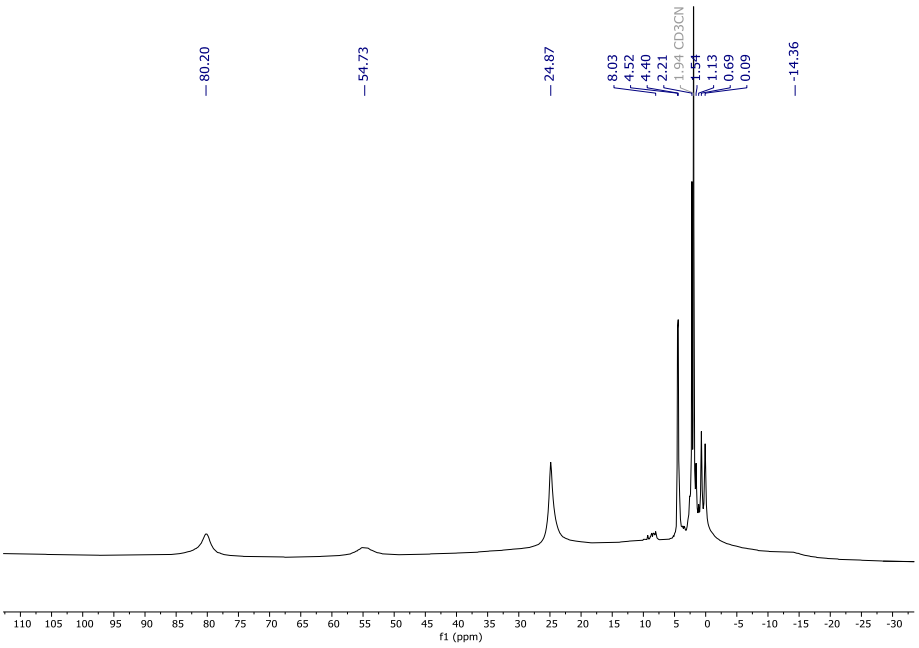

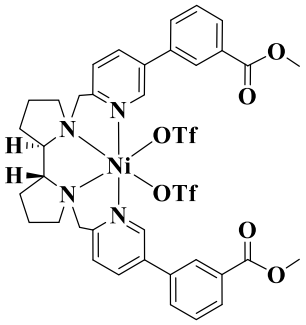

[Ni(^{CO2MeB}pdp)(OTf)$_2$]. In a glovebox, a solution of $Ni(OTf)_2$*$2CH_3CN$ (250 mg, 0.571 mmol), dissolved in anhydrous THF (2 mL) and added dropwise to a vigorously stirred solution of $L_{\mathbf{COOMeB\text{-}pdp}}$ (375 mg, 0.635 mmol) in THF (2 mL). After few minutes, the solution become cloudy and a pale green precipitate appeared. The resulting mixture was stirred overnight, the solution was filtered off and the resulting solid dried under vacuum giving desired product. This solid was dissolved in CH_3CN and the slow diffusion of diethyl ether into this solution produced desired clean product (480 mg, 80% yield). ^{1}H

NMR (500 MHz, CD_3CN) δ = 40.39, 32.43, 23.69, 15.09, 8.71, 8.37, 7.62, 3.97, 3.64, 2.16, 1.80, 1.27, -5.03, -8.36 ppm; HRMS (ESI) *m/z* calculated for $C_{37}H_{38}F_3N_4NiO_7S$ $[M - CF_3SO_3]^+$; 797.1761, found 797.1738.

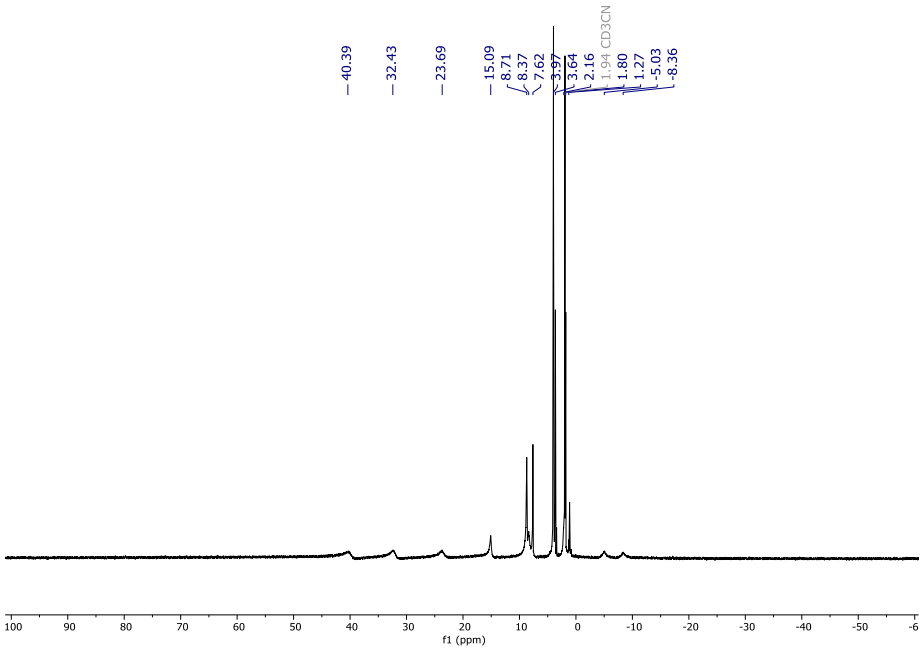

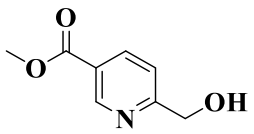

Methyl 6-(hydroxymethyl)nicotinate. A solution of dimethylpyridine-2,5-dicarboxylate (5 g, 25 mmol) and $CaCl_2$ (11.35 g, 100 mmol) in THF/CH_3OH (1:2, 160 mL) was cooled to 0°C, and $NaBH_4$ (1.45 g, 37 mmol) was added slowly. The reaction was maintained at 0°C and monitored by TLC. After consumption of the starting material, H_2O (100 mL) was added slowly. The product was extracted with $CHCl_3$(6×40 mL), and the combined organic layers were dried with anhydrous MgSO4. The solvent was evaporated under reduced pressure yielding an off white solid, which was purified by column chromatography. Elution with hexane/AcOEt (1:1) afforded methyl 6-(hydroxymethyl)nicotinate as a white solid (3.9 g, 90% yield). ^1H NMR (400 MHz, $CDCl_3$) δ = 9.17 (dd, *J* = 2.2, 0.9 Hz, 1H), 8.29 (dd, *J* = 8.2, 2.1 Hz, 1H),

7.36 (dq, *J* = 8.1, 0.8 Hz, 1H), 4.84 (s, 2H), 3.96 (s, 3H) ppm; ^{13}C NMR (101 MHz, $CDCl_3$) δ = 165.7 (C), 163.6 (C), 150.1 (CH), 138.3 (CH), 125.2 (C), 120.1 (CH), 63.9 (CH_2), 52.6 (CH_3) ppm.

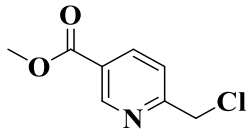

Methyl 6-(chloromethyl)nicotinate. Methyl 6-(hydroxymethyl)nicotinate (2 g, 12.2 mmol) was dissolved in CH_2Cl_2 (30 mL). $SOCl_2$ (2 mL, 28.17 mmol) was cautiously added dropwise, and the mixture was stirred overnight at room temperature. The solvent was removed by bubbling nitrogen into the crude reaction mixture (gaseous HCl is formed during this process and extreme caution must be taken) and a greenish solid was obtained. This product was suspended in Et_2O (3.5 mL) and stirred for 1 h to give a fine solid which was then filtered, washed with Et_2O(2×10 mL), and dried under vacuum. Methyl 6-(chloromethyl)nicotinate was obtained as a white solid (1.8 g, 81%). ^{1}H NMR (400 MHz, $CDCl_3$) δ = 9.24 (d, *J* = 1.7 Hz, 1H), 8.90 – 8.83 (m, 1H), 8.10 (d, *J* = 8.2 Hz, 1H), 5.19 (s, 2H), 4.05 (s, 3H) ppm; ^{13}C NMR (101 MHz, $CDCl_3$) δ = 162.4 (C), 156.7 (C), 144.5 (CH), 143.6 (CH), 128.0 (C), 126.1 (CH), 53.8 (CH_3), 41.4 (CH_2) ppm.

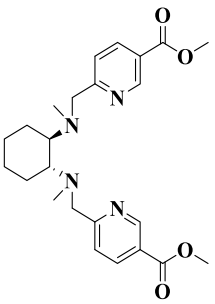

Dimethyl 6,6'-((((1R,2R)-cyclohexane-1,2-diyl)bis(methylazanediyl))bis(methylene))dinicotinate (^{CO2Me}mcp). Methyl 6-(chloromethyl)nicotinate (1 g, 5.4 mmol, 2.1 equiv.), (*R*,*R*)-(−)-*N*,*N*′-Dimethyl-1,2-diaminocyclohexane (380 mg, 2.7 mmol, 1 equiv.), were

dissolved in MeCN (150 mL). Na_2CO_3 (6 equiv.) and tetrabutylammonium bromide – TBABr (0.1 equiv.) were added directly as solids and the resulting mixture was heated at reflux under N_2 for 24 h. After cooling to the RT mixture was concentrated under reduced pressure. Resulting residue was dissolved in CH_2Cl_2 and washed with water to remove remaining TBABr. The layers were separated and the aqueous layer was extracted with CH_2Cl_2 (3x100 mL). The organic layer was dried ($MgSO_4$), filtered and evaporated to give a crude product that was purified by column chromatography on deactivated (Et_3N) silica gel eluting with CH_2Cl_2 to give the product (0.7 g, 44% yield). ^{1}H NMR (400 MHz, $CDCl_3$) δ 8.71 (q, *J* = 2.1 Hz, 2H), 7.80 (dq, *J* = 8.2, 2.0 Hz, 2H), 7.27 (dt, *J* = 8.3, 1.9 Hz, 2H), 3.63 – 3.53 (m, 8H), 3.45 (dd, *J* = 15.4, 2.6 Hz, 2H), 2.34 – 2.23 (m, 2H), 1.93 – 1.89 (m, 6H), 1.64 – 1.57 (m, 2H), 1.43 – 1.35 (m, 2H), 1.03 – 0.66 (m, 4H) ppm; ^{13}C NMR (101 MHz, $CDCl_3$) δ 165.9 (x2 C), 165.6 (x2 C), 149.8 (x2 CH), 137.0 (x2 CH), 123.9 (x2 C), 121.9 (x2 CH), 64.4 (x2 CH), 60.0 (x2 CH_2), 51.9 (x2 CH_3), 36.5 (x4 CH_2), 25.49 ppm; HRMS (ESI) *m/z* calculated for $C_{24}H_{33}N_4O_4$ $[M+H]^+$; 441.2496, found 441.2499.

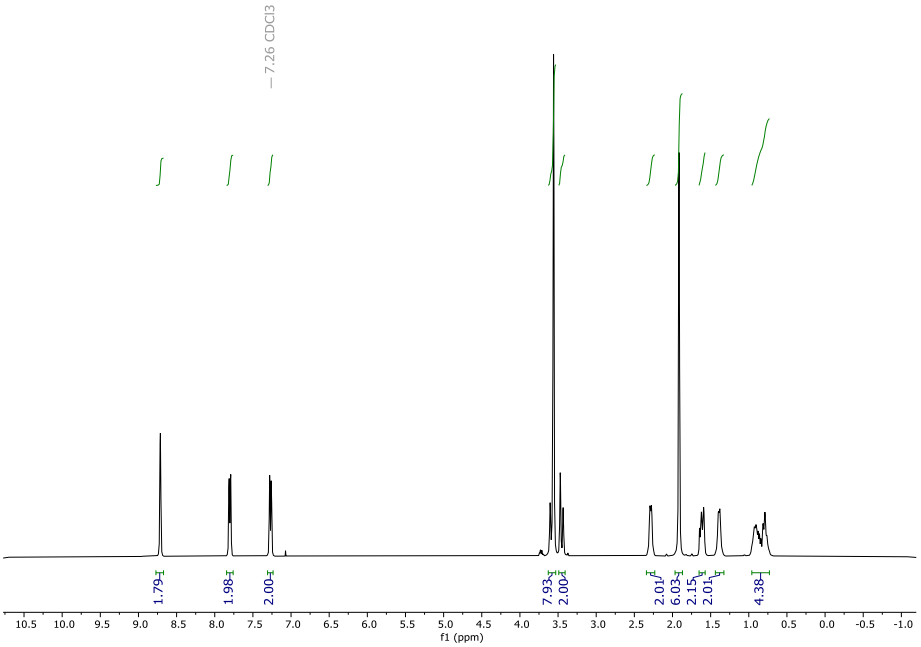

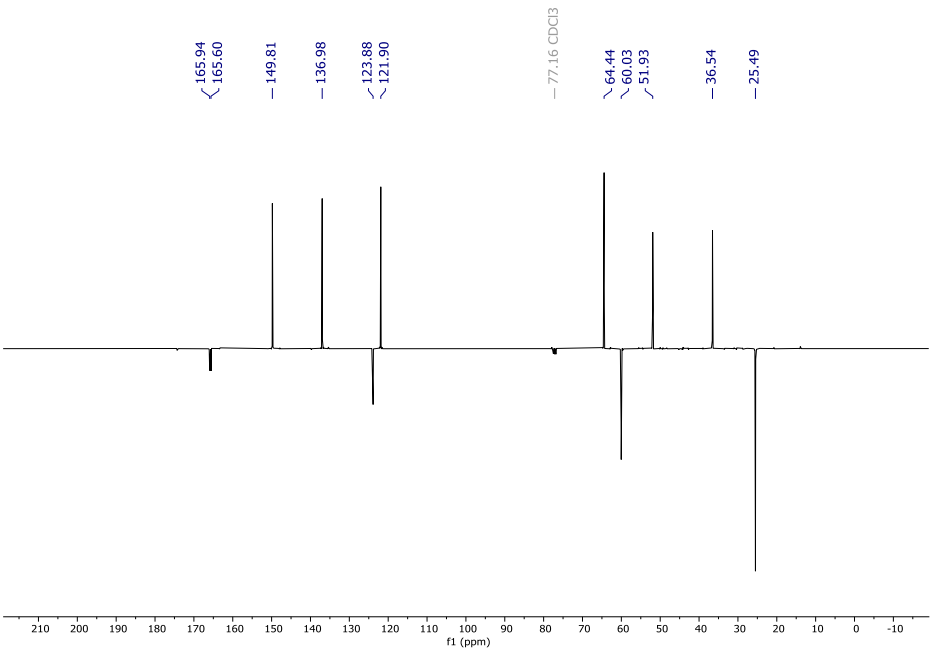

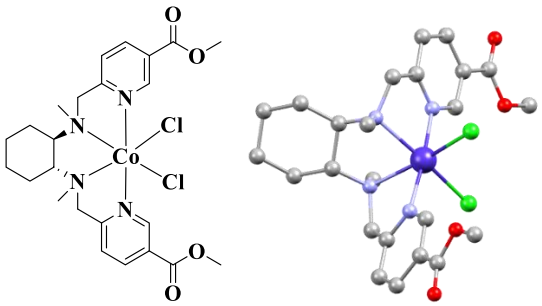

[(Co(^{CO2Me}mcp)Cl$_2$)]. Inside a glovebox, a vial was charged with $CoCl_2$ (117 mg, 0.9 mmol) and anhydrous THF (1 mL). Then a solution of ^{CO2Me}**mcp** (440 mg, 1.0 mmol) in THF (1 mL) was added dropwise to the vigorously stirred suspension of cobalt salt in THF, which caused the formation of a purple precipitate after few minutes. The resulting mixture was stirred overnight, the resulting solid was filtered off, washed with CH_3CN (3x 1 mL) and dried under vacuum. This solid was dissolved in CH_2Cl_2 and filtered through Celite. Finally, slow diffusion of diethyl ether into the clear solution produced a purple solid. The solution was siphoned off by cannula and the solid material that corresponds to the targeted complex was dried under vacuum (370 mg, 65%). ^{1}H NMR (400 MHz, CD_3CN) δ = 163.28, 95.34, 68.90, 46.20, 25.11, 23.74,

22.81, 9.44, 8.81, 4.24, 3.63, 2.16, 1.27, 1.12, -5.99, -11.06 ppm; HRMS (ESI) *m/z* calculated for $C_{24}H_{32}Cl_2CoN_4O_4$ [M]: 569.112707, found 569.112524.

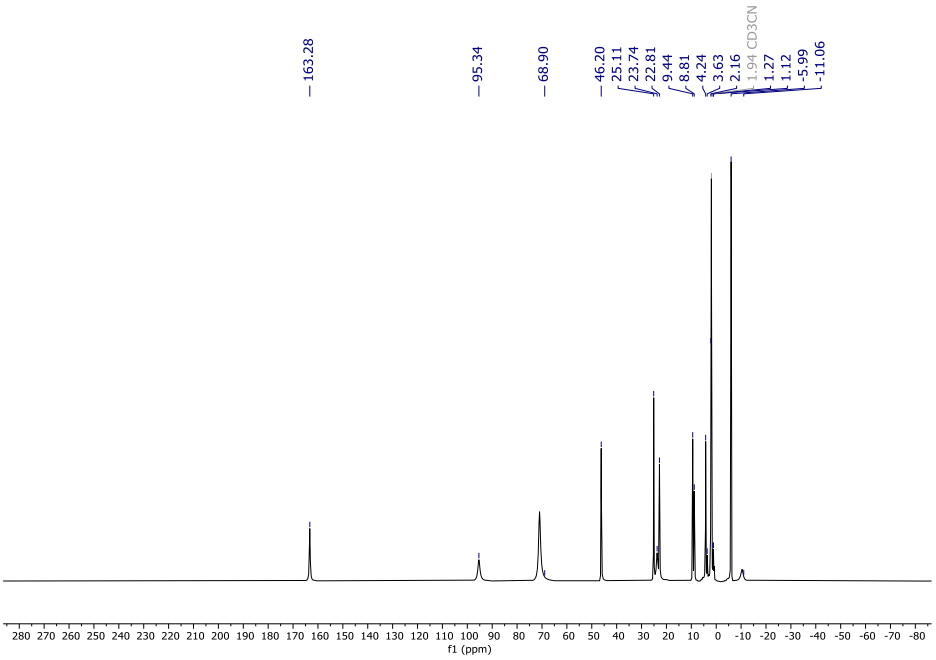

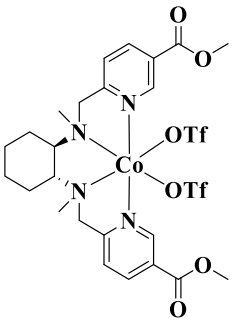

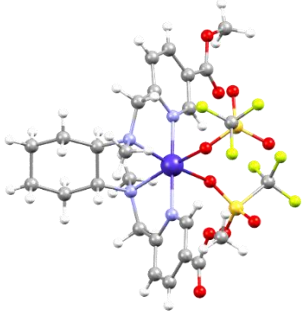

[(Co(^{CO2Me}mcp)(OTf)$_2$)]. In a glovebox, a solution of Co(^{CO2Me}mcp)Cl_2 (121 mg, 0.21 mmol) in anhydrous DCM (1 mL) was added dropwise to a vigorously stirred solution of AgOTf (114 mg, 0.45 mmol, 2.5 eq.) in DCM (1 mL). After few minutes, the solution become orange cloudy and a purple precipitate appeared. . The resulting mixture was stirred overnight, the solution was filtered through syringe filter to remove resultant AgCl. Solvent was collected and dried under vacuum to obtain desired solid. This solid was dissolved in CH_3CN and the slow diffusion of diethyl ether into this solution produced desired clean

product (117 mg, 69% yield). ^{1}H NMR (400 MHz, CD_3CN) δ 225.80, 96.85, 79.96, 64.39, 62.16, 55.39, 26.66, 19.15, 9.88, -0.93, -12.07 ppm; HRMS (ESI) *m/z* calculated for $C_{25}H_{32}CoF_3N_4O_7S$ [M - CF_3SO_3]$^+$: 648.1270, found 648.1299.

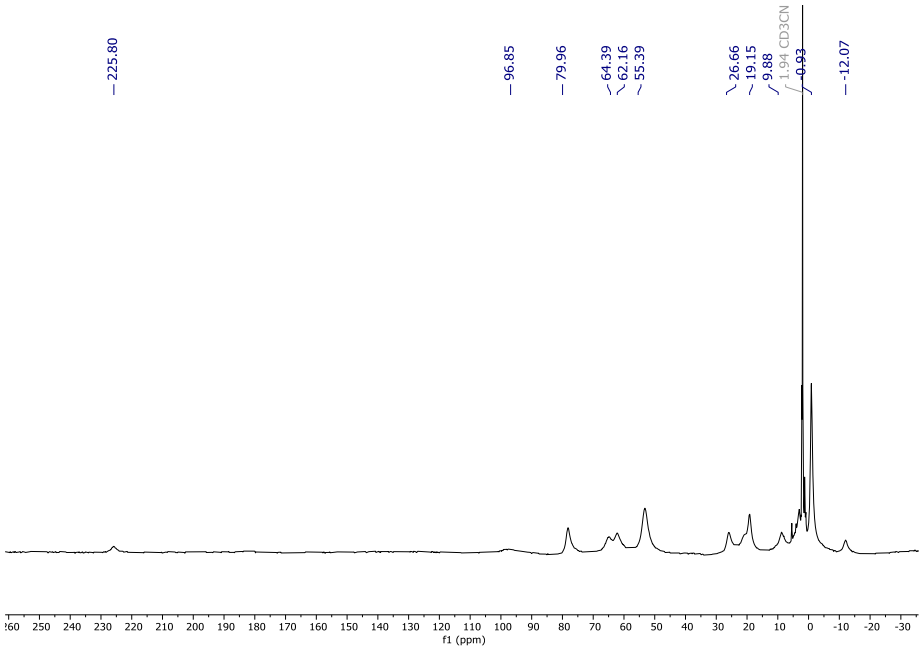

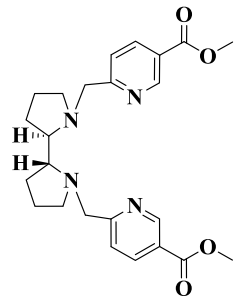

Dimethyl 6,6'-(((2R,2'R)-[2,2'-bipyrrolidine]-1,1'-diyl)bis(methylene))dinicotinate (^{CO2Me}pdp). Methyl 6-(chloromethyl)nicotinate (0.5 g, 3.0 mmol, 2.1 equiv.), (R,R)-2,2′-bipyrrolidine L-tartrate trihydrate (320 mg, 1.25 mmol, 1.0 equiv.), were dissolved in MeCN (100 mL). Na_2CO_3 (6 equiv.) and tetrabutylammonium bromide – TBABr (0.1 equiv.) were added directly as solids and the resulting mixture was heated at reflux under N_2 for 24 h. After cooling to the RT mixture was concentrated

under reduced pressure. Resulting residue was dissolved in CH_2Cl_2 and washed with water to remove remaining TBABr. The layers were separated and the aqueous layer was extracted with CH_2Cl_2 (3x100 mL). The organic layer was dried ($MgSO_4$), filtered and evaporated to give a crude product that was purified by column chromatography on deactivated (Et_3N) silica gel eluting with CH_2Cl_2 to give the product (0.21 g, 51% yield. ^{1}H NMR (400 MHz, $CDCl_3$) δ 9.02 (dd, *J* = 2.2, 0.9 Hz, 2H), 8.12 (dd, *J* = 8.2, 2.2 Hz, 2H), 7.43 (d, *J* = 8.2 Hz, 2H), 4.23 (d, *J* = 15.4 Hz, 2H), 3.88 (s, 6H), 3.57 (d, *J* = 15.3 Hz, 2H), 2.96 (ddd, *J* = 8.3, 5.2, 3.7 Hz, 2H), 2.76 (dd, *J* = 7.1, 4.2 Hz, 2H), 2.25 – 2.14 (m, 2H), 1.87 – 1.74 (m, 2H), 1.75 – 1.62 (m, 6H).; ^{13}C NMR (101 MHz, $CDCl_3$) δ 165.9 (C), 165.4 (C), 150.2 (CH), 137.4 (CH), 124.1 (C), 121.9 (CH), 66.18, 61.40, 55.48, 52.28, 26.52, 24.17 ppm; HRMS (ESI) *m/z* calculated for $C_{24}H_{31}N_4O_4$ $[M+H]^+$; 439.2340, found 439.2341.

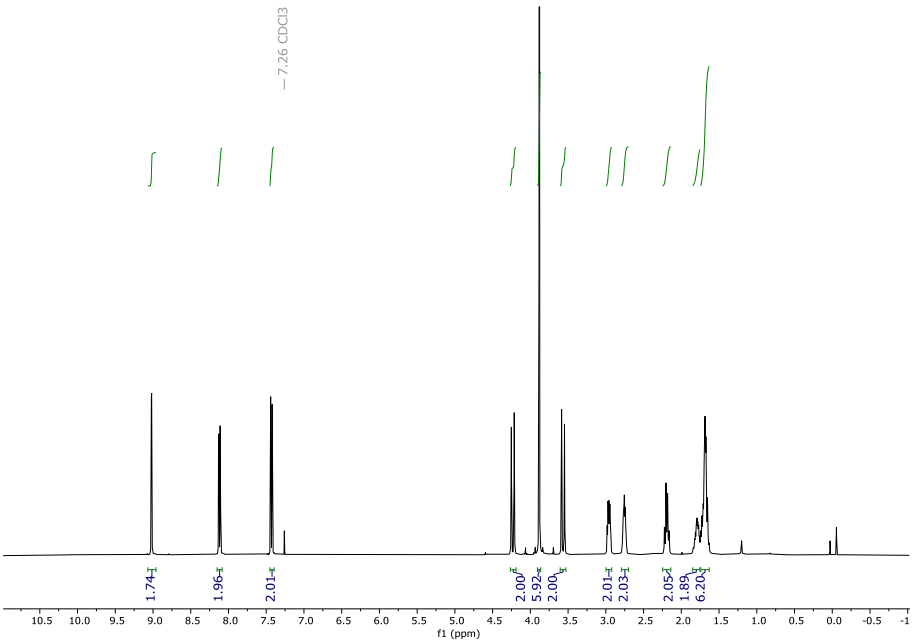

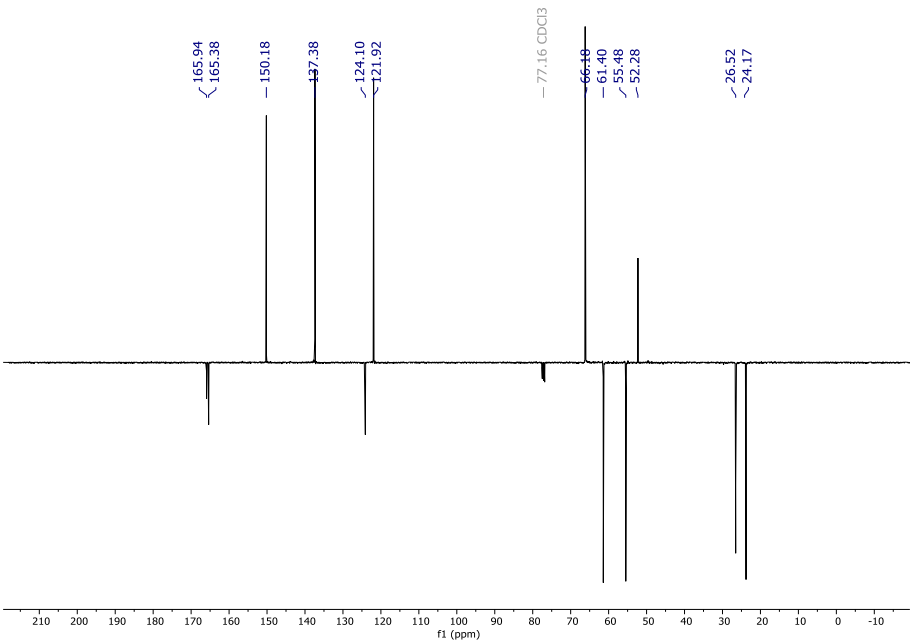

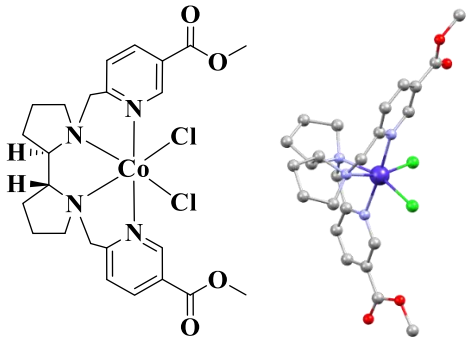

[(Co^{CO2Me}pdpCl$_2$)]. Inside a glovebox, a vial was charged with $CoCl_2$ (54 mg, 0.41 mmol) and anhydrous THF (1 mL). Then a solution of ^{CO2Me}pdp (204 mg, 0.46 mmol) in THF (1 mL) was added dropwise to the vigorously stirred suspension of cobalt salt in THF, which caused the formation of a purple precipitate after few minutes. The resulting mixture was stirred overnight, the resulting solid was filtered off, washed with CH_3CN (3x 1 mL) and dried under vacuum. This solid was dissolved in CH_2Cl_2 and filtered through Celite. Finally, slow diffusion of diethyl ether into the clear solution produced a purple solid. The solution was siphoned off by cannula and the solid material that corresponds to the targeted complex was dried under vacuum (127 mg, 69%).

^{1}H NMR (400 MHz, CD_3CN) δ 173.19, 93.16, 42.44, 40.65, 34.60, 30.34, 18.70, 12.86, 12.03, 8.05, 3.29, 2.17, 1.27, 0.86, -3.19, -5.33 ppm; HRMS (ESI) *m/z* calculated for $C_{24}H_{32}ClCoN_4O_4$ $[M - Cl]^+$: 532.1282, found 532.1281.

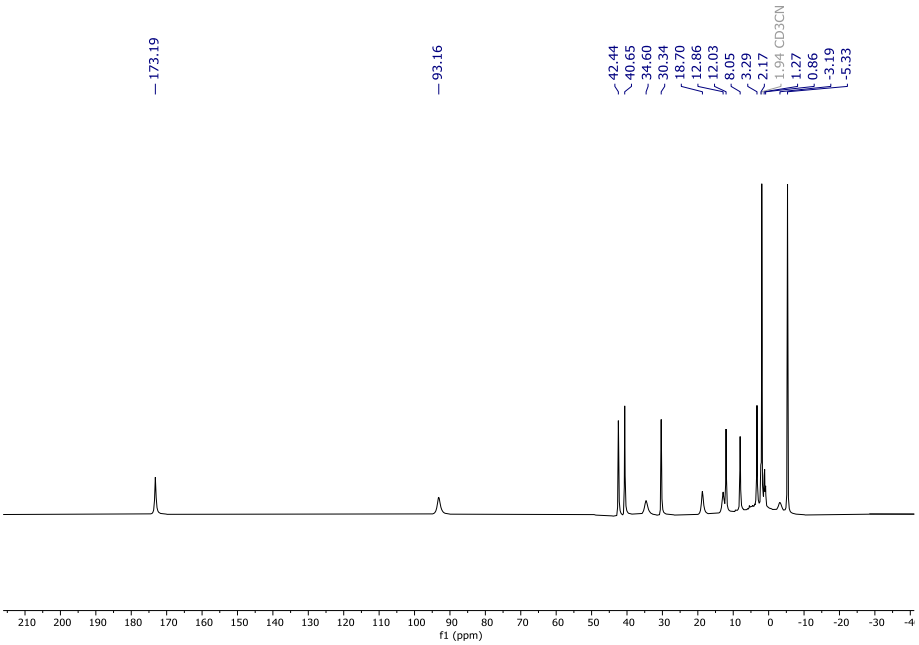

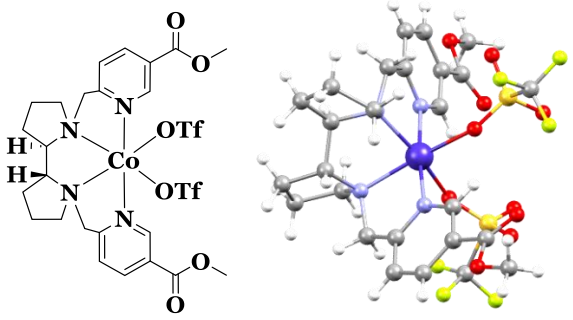

[Co(^{CO2Me}pdp)(OTf)$_2$]. In a glovebox, a solution of Co(^{CO2Me}pdp)Cl_2 (105 mg, 0.19 mmol) in anhydrous DCM (1 mL) was added dropwise to a vigorously stirred solution of AgOTf (119 mg, 0.46 mmol, 2.5 eq.) in DCM (1 mL). After few minutes, the solution become orange cloudy and a purple precipitate appeared. . The resulting mixture was stirred overnight, the solution was filtered through syringe filter to remove resultant AgCl. Solvent was collected and dried

under vacuum to obtain desired solid. This solid was dissolved in CH_3CN and the slow diffusion of diethyl ether into this solution produced desired clean product (111 mg, 75% yield). ^{1}H NMR (400 MHz, CD_3CN) δ 86.42, 76.08, 49.36, 26.64, 24.65, 22.73, 3.64, -1.47, -12.88 ppm; HRMS (ESI) *m/z* calculated $C_{25}H_{30}CoF_3N_4O_7S$ $[M\text{-}OTf]^+$; 646.1114, found 646.1229.

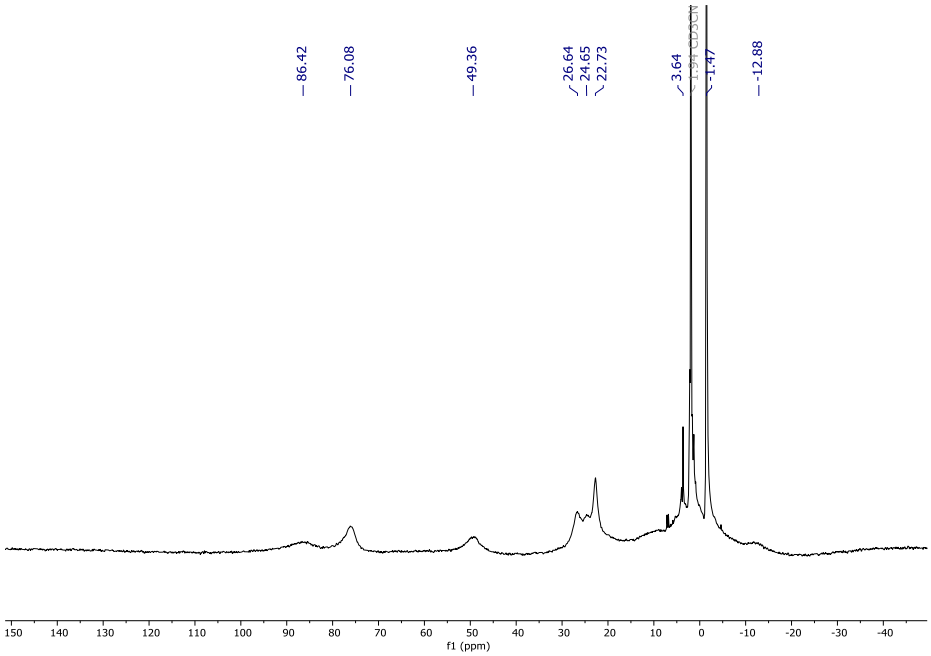

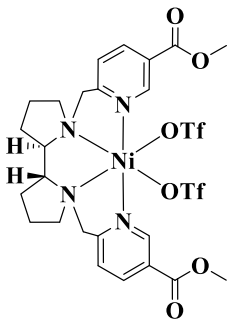

[Ni(^{CO2Me}pdp)(OTf)$_2$]. In a glovebox, a solution of $Ni(OTf)_2$*$2CH_3CN$ (150 mg, 0.342 mmol), dissolved in anhydrous THF (2 mL) and added dropwise to a vigorously stirred solution of ^{CO2Me}pdp (166 mg, 0.379 mmol) in THF (2 mL). After few minutes, the solution become cloudy and a pale green precipitate appeared. The resulting mixture was stirred overnight, the solution was filtered off and the resulting solid dried under vacuum giving desired product. This

solid was dissolved in CH_3CN and the slow diffusion of diethyl ether into this solution produced desired clean product (214 mg, 71% yield). ^1H NMR (500 MHz, CD_3CN) δ = 37.77, 31.99, 24.10, 15.00, 4.28, 3.64, -5.10, -8.39 ppm; HRMS (ESI) *m/z* calculated $C_{25}H_{30}F_3N_4NiO_7S$ $[M\text{-}OTf]^+$; 645.1135, found 645.1115.

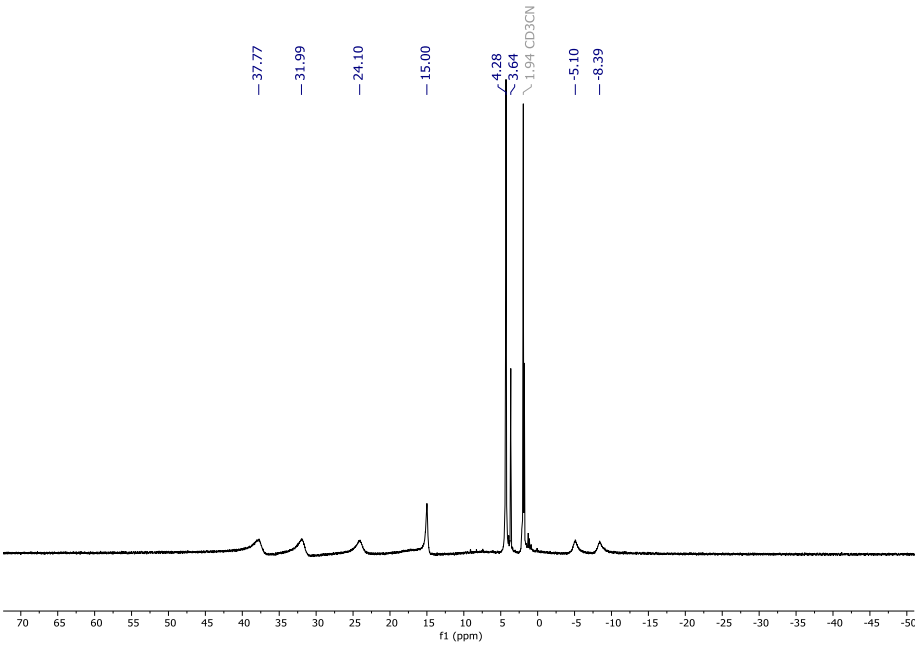

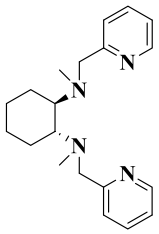

(1R,2R)-N1,N2-dimethyl-N1,N2-bis(pyridin-2-ylmethyl)cyclohexane-1,2-diamine (mcp). 2-(chloromethyl)pyridine hydrochloride (0.6 g, 3.7 mmol, 2.1 equiv.), (*R*,*R*)-(−)-*N*,*N*′-Dimethyl-1,2-diaminocyclohexane (228 mg, 1.6 mmol, 1 equiv.), were dissolved in MeCN (100 mL). Na_2CO_3 (6 equiv.) and tetrabutylammonium bromide – TBABr (0.1 equiv.) were added directly as solids and the resulting mixture was heated at reflux under N_2 for 24 h. After cooling to the RT mixture was concentrated under reduced pressure. Resulting

residue was dissolved in CH_2Cl_2 and washed with water to remove remaining TBABr. The layers were separated and the aqueous layer was extracted with CH_2Cl_2 (3x100 mL). The organic layer was dried ($MgSO_4$), filtered and evaporated to give a crude product that was purificated by column chromatography on deactivated (Et_3N) silica gel eluting with CH_2Cl_2 to give the product (0.31 g, 60% yield). ^{1}H NMR (400 MHz, $CDCl_3$) δ = 8.49 (dt, *J* = 4.9, 1.4 Hz, 2H), 7.59 – 7.55 (m, 4H), 7.11 (td, *J* = 5.0, 3.5 Hz, 2H), 3.92 (d, *J* = 14.6 Hz, 2H), 3.80 (d, *J* = 14.6 Hz, 2H), 2.73 – 2.60 (m, 2H), 2.28 (s, 6H), 1.98 (dt, *J* = 12.8, 2.6 Hz, 2H), 1.76 (dt, *J* = 9.1, 2.8 Hz, 2H), 1.34 – 1.23 (m, 2H), 1.15 (ddd, *J* = 11.7, 9.4, 2.5 Hz, 2H) ppm; ^{13}C NMR (101 MHz, $CDCl_3$) δ = 161.4 (x2 C), 148.8 (x2 CH), 136.4 (x2 CH), 123.0 (x2 CH), 121.7 (x2 CH), 64.7 (x2 CH), 60.6 (x2 CH_2), 36.8 (x2 CH_3), 25.9 (x4 CH_2) ppm.

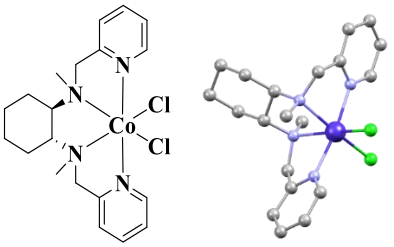

[Co(mcp)Cl_2]. Inside a glovebox, a vial was charged with $CoCl_2$ (210 mg, 1.61 mmol) and anhydrous THF (1 mL). Then a solution of mcp (582 mg, 1.794 mmol) in THF (2 mL) was added dropwise to the vigorously stirred suspension of cobalt salt in THF, which caused the formation of a purple precipitate after few minutes. The resulting mixture was stirred overnight, the resulting solid was filtered off, washed with CH_3CN (3x 2 mL) and dried under vacuum. This solid was dissolved in CH_2Cl_2 and filtered through Celite. Finally, slow diffusion of diethyl ether into the clear solution produced a purple solid. The solution was siphoned off by cannula and the solid material that corresponds to the targeted complex was dried under vacuum (529 mg, 1.165 mmol, 65%). ^{1}H NMR (400 MHz, CD_3CN) δ 165.52, 101.67, 62.71, 50.84, 24.52, 21.28, 18.48, 8.29, 6.50, 6.19, 2.16, 1.27, 0.86 ppm;.HRMS (ESI) *m/z* calculated for $C_{20}H_{28}ClCoN_4$ $[M\text{-}Cl]^+$; 418.1329, found 418.1328.

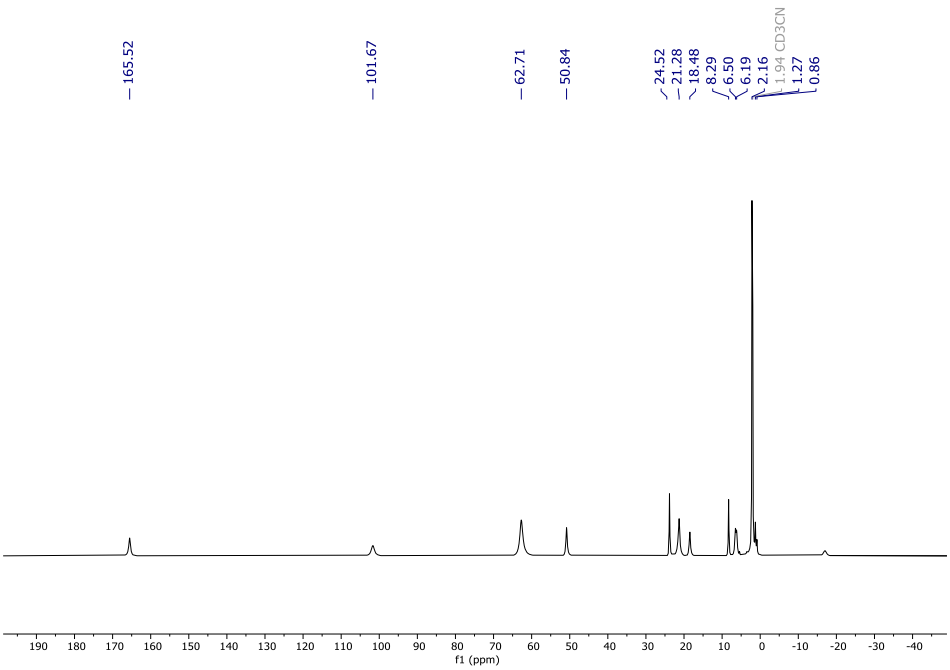

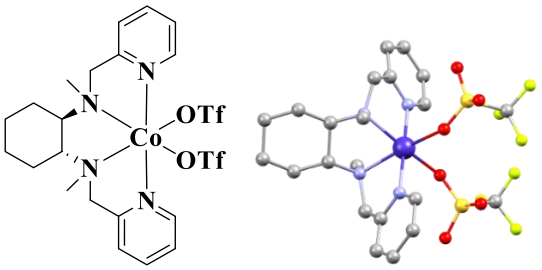

[Co(mcp)(OTf)$_2$]. In a glovebox, a solution of Co(mcp)Cl$_2$ (300 mg, 0.66 mmol) in anhydrous DCM (1 mL) was added dropwise to a vigorously stirred solution of AgOTf (356 mg, 1.39 mmol, 2.5 eq.) in DCM (1 mL). After few minutes, the solution become orange cloudy and a purple precipitate appeared. . The resulting mixture was stirred overnight, the solution was filtered through syringe filter to remove resultant AgCl. Solvent was collected and dried under vacuum to obtain desired solid. This solid was dissolved in CH_3CN and the slow diffusion of diethyl ether into this solution produced desired clean product (365 mg, 81% yield). ^{1}H NMR (400 MHz, CD_3CN) δ 221.30, 83.84, 68.77, 66.32, 59.01, 41.90, 29.71, 17.67, 13.57, 3.57, 1.27, 0.87, -17.74 ppm; HRMS (ESI) *m/z* calculated for $C_{21}H_{28}CoF_3N_4O_3S$ $[M\text{-}OTf]^+$; 532.1161, found 532.1169.

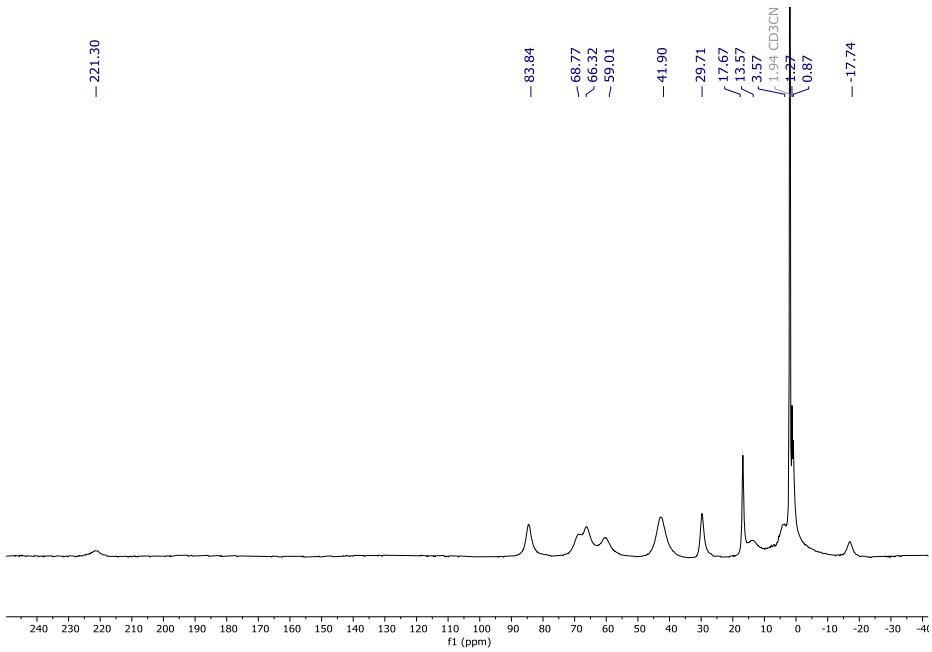

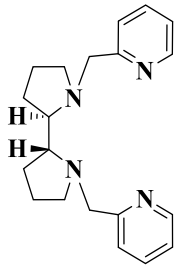

(2R,2'R)-1,1'-bis(pyridin-2-ylmethyl)-2,2'-bipyrrolidine (pdp). 2-(chloromethyl)pyridine hydrochloride (0.5 g, 3.0 mmol, 2.1 equiv.), (R,R)-2,2′-bipyrrolidine L-tartrate trihydrate (491 mg, 1.4 mmol, 1.0 equiv.), were dissolved in MeCN (100 mL). Na_2CO_3 (6 equiv.) and tetrabutylammonium bromide – TBABr (0.1 equiv.) were added directly as solids and the resulting mixture was heated at reflux under N_2 for 24 h. After cooling to the RT mixture was concentrated under reduced pressure. Resulting residue was dissolved in CH_2Cl_2 and washed with water to remove remaining TBABr. The layers were separated and the aqueous layer was extracted with CH_2Cl_2 (3x100 mL). The organic layer was dried ($MgSO_4$), filtered and evaporated to give a crude product that was purified by column chromatography on deactivated (Et_3N) silica gel eluting with CH_2Cl_2 to give the product (0.29 g, 62% yield. ^{1}H NMR

(400 MHz, $CDCl_3$) δ 8.50 (ddd, *J* = 4.9, 1.8, 0.9 Hz, 2H), 7.59 (td, *J* = 7.6, 1.8 Hz, 2H), 7.40 (dt, *J* = 7.9, 1.1 Hz, 2H), 7.10 (ddd, *J* = 7.6, 4.9, 1.2 Hz, 2H), 4.19 (d, *J* = 14.3 Hz, 2H), 3.50 (d, *J* = 14.3 Hz, 2H), 3.00 (dt, *J* = 9.5, 4.6 Hz, 2H), 2.84 – 2.75 (m, 2H), 2.29 – 2.18 (m, 2H), 1.88 – 1.74 (m, 4H), 1.74 – 1.65 (m, 4H) ppm; ^{13}C NMR (101 MHz, $CDCl_3$) δ 160.6 (x2 C), 149.0 (x2 CH), 136.4 (x2 CH), 122.8 (x2 CH), 121.8 (x2 CH), 65.6 (x2 CH), 61.3 (x2 CH_2), 55.5 (x2 CH_2), 26.1 (x2 CH_2), 23.2 (x2 CH_2) ppm; HRMS (ESI) *m/z* calculated for $C_{20}H_{27}N_4$ $[M+H]^+$; 323.2230, found 323.2229.

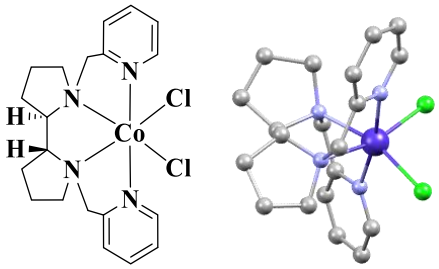

Co(pdp)Cl_2. Inside a glovebox, a vial was charged with $CoCl_2$ (106 mg, 0.815 mmol) and anhydrous THF (2 mL). Then a solution of pdp (292 mg, 0.906 mmol) in THF (2 mL) was added dropwise to the vigorously stirred suspension of cobalt salt in THF, which caused the formation of a purple precipitate after few minutes. The resulting mixture was stirred overnight, the resulting solid was filtered off, washed with CH_3CN (3x 2 mL) and dried under vacuum. This solid was dissolved in CH_2Cl_2 and filtered through Celite. Finally, slow diffusion of diethyl ether into the clear solution produced a purple solid. The solution was siphoned off by cannula and the solid material that corresponds to the targeted complex was dried under vacuum (201.4 mg, 0.445 mmol, 76%). ^1H NMR (400 MHz, CD_3CN) δ 177.02, 100.14, 46.81, 37.83, 29.59, 26.50, 18.68, 10.74, 7.31, 1.02, 0.61, -11.32 ppm; HRMS (ESI) *m/z* calculated for $C_{20}H_{26}ClCoN_4$ $[M-Cl]^+$; 416.1172, found 416.1179.

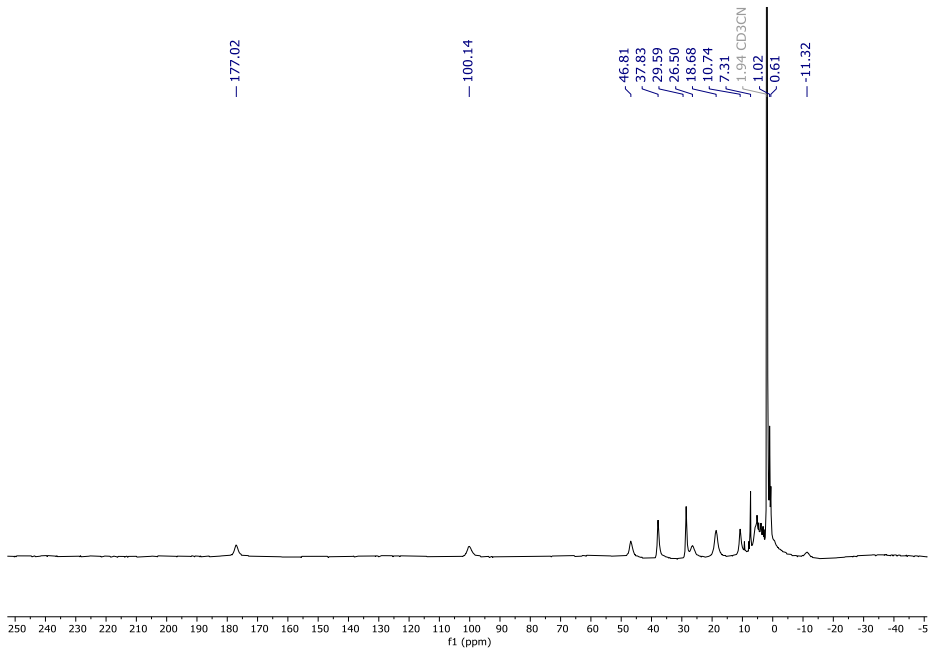

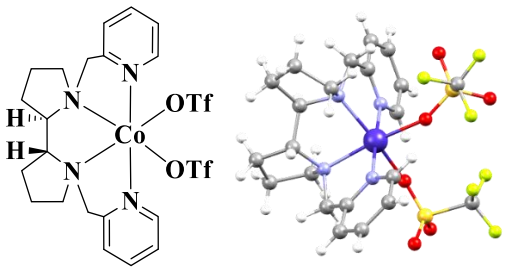

[Co(pdp)(OTf)$_2$]. Inside a glovebox, a vial was charged with $CoL_{pdp}Cl_2$ (72 mg, 0.283 mmol) and anhydrous DCM (1 mL). Then AgOTf was added as a solid (61 mg, 0.135 mmol) to the vigorously stirred solution of cobalt complex in DCM, which. The resulting mixture was stirred overnight, the resulting solid was filtered off by syringe filter to remove AgCl, and dried under vacuum. This solid was dissolved in CH_2Cl_2 and slow diffusion of diethyl ether into the clear solution produced a red solid. The solution was siphoned off by cannula and the solid material that corresponds to the targeted complex was dried under vacuum (137 mg, 0.202 mmol, 91 %). ^{1}H NMR (400 MHz, CD_3CN) δ 90.40, 82.77, 62.59, 59.31, 56.30, 37.92, 35.03, 26.19, 21.87, 20.70, 11.58, 8.92, 1.27, 0.86, -4.89, -16.07, -16.56 ppm.

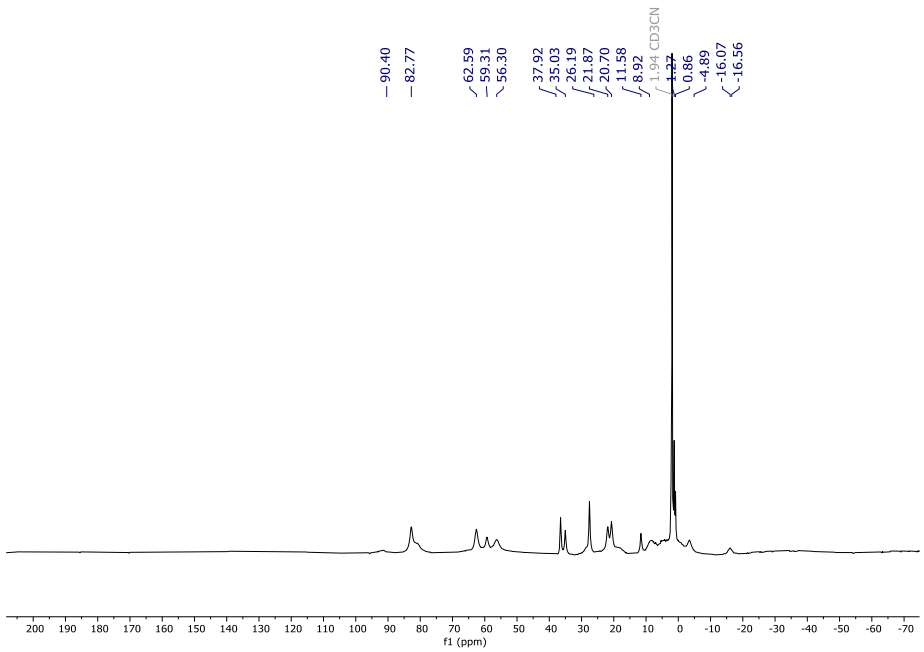

III.4.7 Syntheses of Photosensitizers

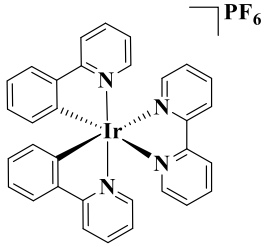

[Ir(ppy)$_2$bpy]PF$_6$ (PS$_{Ir}$). **PS$_{Ir}$** was synthesized following a reported procedure yielding 0,8 g of the corresponding iridium salt as a light-yellow solid (74% of yield). ^{1}H NMR (400 MHz, $CDCl_3$) δ = 8.68 (d, *J* = 8.2 Hz, 1H), 8.15 (td, *J* = 7.9, 1.6 Hz, 1H), 7.96 – 7.89 (m, 2H), 7.79 – 7.73 (m, 1H), 7.69 (d, *J* = 8.3 Hz, 1H), 7.51 (d, *J* = 5.2 Hz, 1H), 7.44 – 7.39 (m, 1H), 7.07 – 6.99 (m, 2H), 6.92 (td, *J* = 7.4, 1.3 Hz, 1H), 6.30 (d, *J* = 7.4 Hz, 1H) ppm.

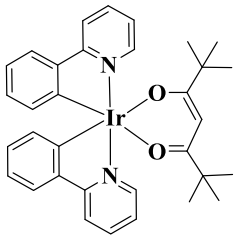

Ir-complex 1. TBAOH*30H_2O (2.45 g, 3.1 mmol, 6.1 eq.) was added to a 100 mL 2-neck flask containing 2,2,6,6-tetramethyl- 3,5-heptane-3,5-dione (0.56 mL, 2.70 mmol, 5.4 eq.) in CH_2Cl_2 (30 mL). The solution was degassed by bubbling argon for 15 min, followed by addition of Ir-dimer (0.54 g, 0.54 mmol, 1.0 eq.) and the mixture was again degassed by bubbling argon for 15 min. The mixture was refluxed overnight. The solvent was removed under reduced pressure and and the crude solid was supended in MeOH/H_2O (1:3, 80 mL). The mixture was filtered and the orange precipitate was washed with H_2O and with cold MeOH (washing solution became yellow). After washing one time with MeOH a fine, brighter (yellow) powder was obtained and dried on the high vacuum. Delivered 450mg (61%) of the title compound as a fine bright yellow powder. ^{1}H NMR (400 MHz, $CDCl_3$): δ = 8.39 (ddd, *J* = 5.7, 1.6, 0.8 Hz, 2H), 7.82 (dt, *J* = 8.3, 1.2 Hz, 2H), 7.68 (ddd, *J* = 8.1, 7.4, 1.6 Hz, 2H), 7.55 (dd, *J* = 7.7, 1.4 Hz, 2H), 7.05 (ddd, *J* = 7.3, 5.7, 1.4 Hz, 2H), 6.81 (td, *J* = 7.4, 1.2 Hz, 2H), 6.68 (td, *J* = 7.4, 1.4 Hz, 2H), 6.38 (dd, *J* = 7.7, 1.2 Hz, 2H), 5.47 (s, 1H), 0.89 (s, 18H) ppm.

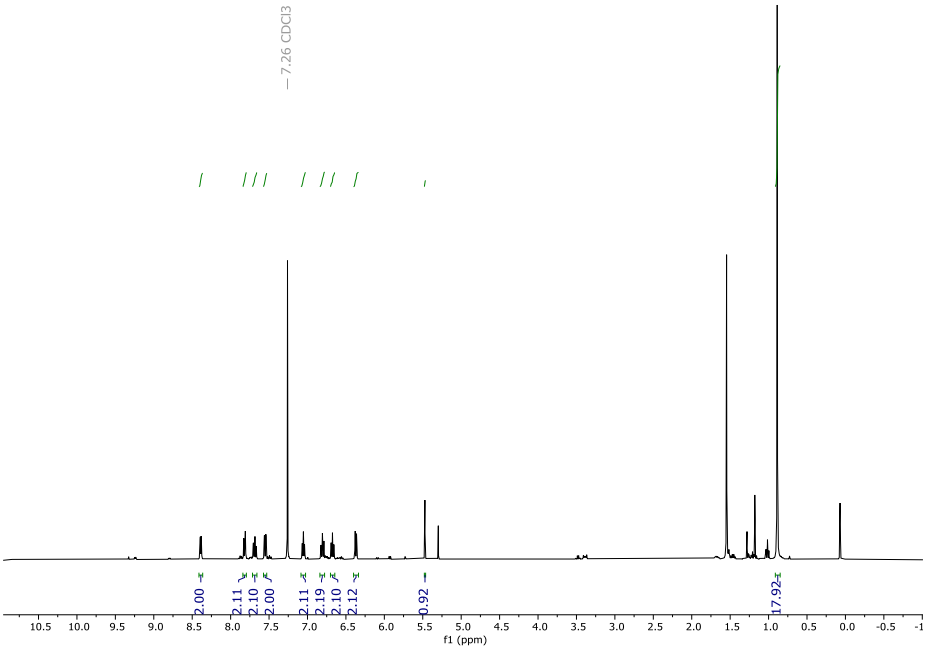

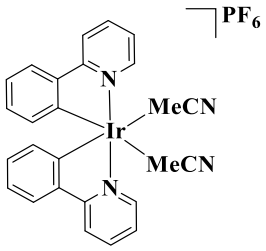

Ir-complex 2. In a 250 mL 2-neck-flask, Ir-complex 1 (0.24 g, 0.353 mmol) was dissolved in MeCN (50 mL) and degassed by bubbling argon for 10 min. BF_3*OEt_2 (1.5 mL, 11.8 mmol, 18.5 eq.) was added and the mixture was stirred at room temperature for 2 h. 100 mL of a sat. aq. KPF6 was added and the mixture was stirred for 1 h at ambient temperature. The volatiles were gently evaporated until a precipitate was formed. The mixture was left in the fridge for 2-3 h and the precipitate was filtered, washed with water, and dried on the filter. CH_2Cl_2 (2*20mL) was added (dissolving the yellow filter cake on the sintered glass filter) to remove the excess of KPF_6 (white solid remains on the filter). The yellow solution was collected and the solvent was removed under reduced pressure to obtain 405 mg (85%) of a bright yellow solid. ^{1}H NMR (400 MHz, CD_3CN) δ = 9.06 (ddd, *J* = 5.8, 1.5, 0.9 Hz, 2H), 8.10 – 7.98 (m, 4H), 7.66 –

7.62 (m, 2H), 7.43 (ddd, *J* = 7.1, 5.8, 1.9 Hz, 2H), 6.88 (ddd, *J* = 7.8, 7.3, 1.2 Hz, 2H), 6.72 (td, *J* = 7.5, 1.4 Hz, 2H), 6.03 (ddd, *J* = 7.7, 1.3, 0.5 Hz, 2H), 1.94 (s, 6H) ppm; ^{13}C NMR (101 MHz, CD_3CN) δ = 167.0 (2x C), 150.9 (2x CH), 144.6 (2x C), 143.7 (2x C), 138.9 (2x C), 131.1 (2x CH) , 129.6 (2x CH), 124.2 (2x CH), 123.5 (2x CH), 122.6 (2x CH), 119.7 (2x CH), 119.4 (2x C), 117.3 (2x CH_3) ppm; HRMS (ESI) *m/z* calculated for $C_{26}H_{22}N_4{}^{\wedge 191}Ir$ $[M\text{-}PF_6]^+$; 581.1445, found 581.1428.

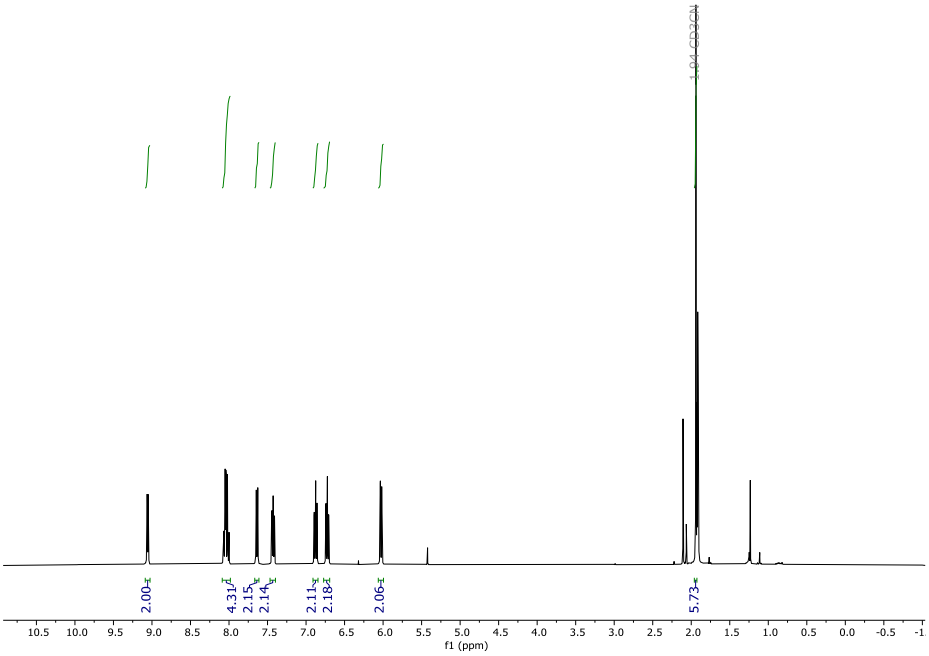

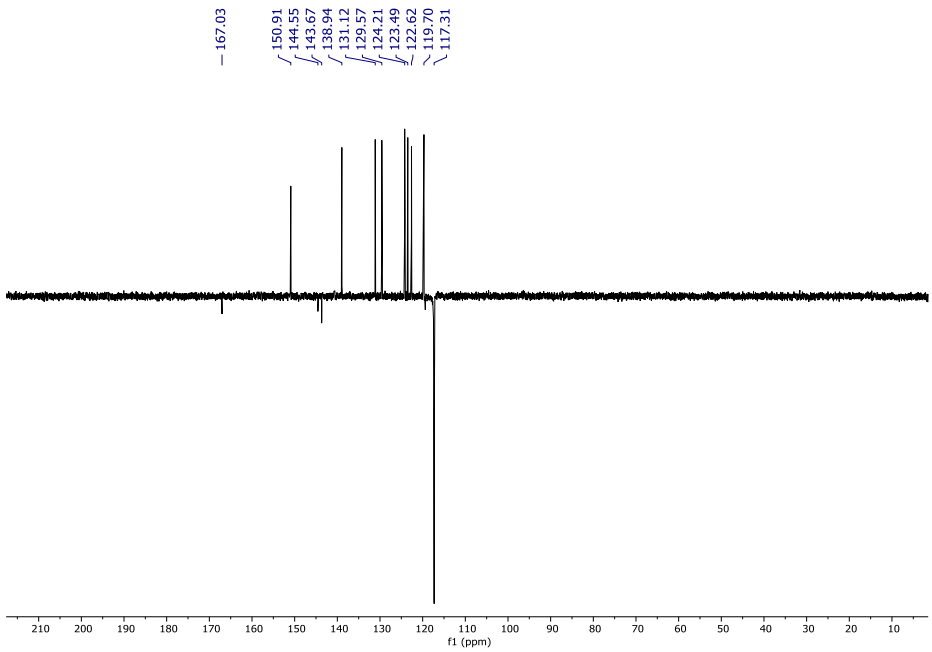

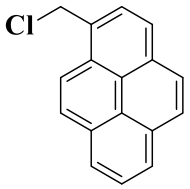

1-(chloromethyl)pyrene. To a suspension of pyrene-methanol (1.0 g, 4,27 mmol, 1.0 eq.) in toluene (30 mL) was added $SOCl_2$ (0,4 mL, 5,55 mmol, 1.3 eq.) at 0 ºC. The cooling bath was removed and the mixture was refluxed overnight. The reaction was quenched by careful addition of H_2O (20 mL) and the organic layer was separated and washed with H_2O (2*15 mL). The solvent was removed under reduced pressure to yield 0.91g (84%) of the title compound as an off-white solid. ^{1}H NMR (400 MHz, $CDCl_3$) δ = 8.38 (d, *J* = 9.2 Hz, 1H), 8.27 – 8.17 (m, 3H), 8.14 (d, *J* = 7.8 Hz, 1H), 8.11 – 8.00 (m, 4H), 5.33 (s, 2H) ppm; ^{13}C NMR (101 MHz, $CDCl_3$) δ = 132.2 (C), 131.3 (C), 130.9 (C), 130.5 (C), 129.3 (C), 128.6 (CH), 128.2 (CH), 127.8 (CH), 127.5 (CH), 126.4 (CH), 125.8 (2x CH), 125.2 (C), 124.9 (CH), 124.8 (C), 122.9 (CH), 44.9 (CH_2) ppm; HRMS (APCI) *m/z* calculated for $C_{17}H_{12}Cl$ $[M+H]^+$; 251.0618, found 251.0622.

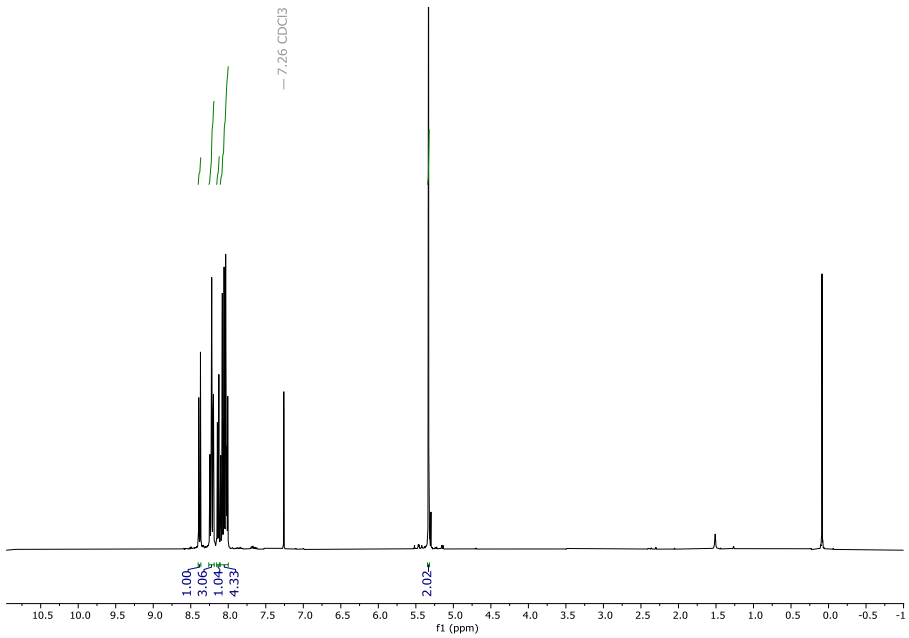
7.26 CDCl3
1.00
3.06
1.04
4.33
2.02
f1 (ppm)

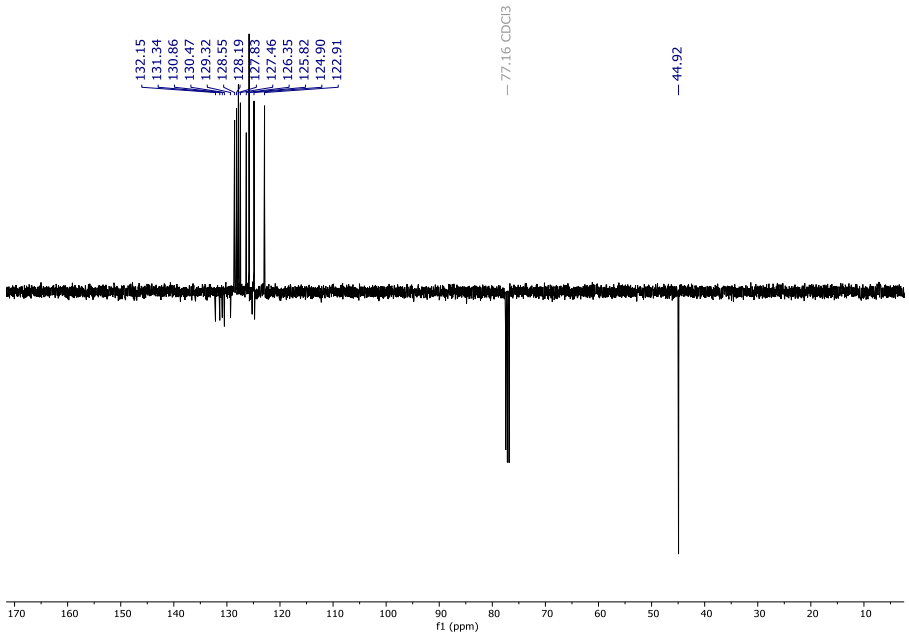
132.15
131.34
130.86
130.47
129.32
128.55
128.19
127.83
127.46
126.35
125.82
124.90
122.91
77.16 CDCl3
44.92
f1 (ppm)

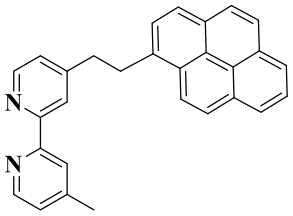
N
N

4-methyl-4'-(2-(pyren-1-yl)ethyl)-2,2'-bipyridine. 4,4'-Dimethyl- 2,2'-bipyridine (0.10 g, 0.54 mmol, 1.0 eq) was dissolved in anhydrous THF (8 ml) under an inert atmosphere. After cooling to -10 °C, LDA (1 M in hexane/THF; 0.49 ml, 0.48 mmol 0.9 eq.) was added dropwise via syringe. After stirring for an additional 45 min. at -10 C, a solution of 1- (chloromethyl)pyrene (0.11 g, 0.43 mmol, 0.8 eq.) in THF (4 ml) was added dropwise. The mixture was stirred at -10 °C for 30 min, and then allowed to reach ambient temperature overnight. H_2O (5 ml) was added dropwise and the solvent was removed under reduced pressure. The residue was dissolved in CH_2Cl_2 and washed with H_2O. The org. phase was dried over $MgSO_4$, filterered and the solvent was removed under reduced pressure. The residue was then triturated (sonicated 30s to 1 min.) with MeOH:H_2O (4:1, 5 ml) and the solution was removed by filtration (remaining solid collected). The resulting solid was collected and then triturated (sonicated) again with pure MeOH (5 ml) to yield 120mg (55%) of the title compound as a yellow solid. ^{1}H NMR (400 MHz, $CDCl_3$): δ = 8.56 (t, *J* = 5.0 Hz, 2H), 8.41 – 8.39 (m, 1H), 8.32 (d, *J* = 9.2 Hz, 1H), 8.25 – 8.24 (m, 1H), 8.21 – 8.09 (m, 4H), 8.04 – 8.04 (m, 2H), 8.01 (t, *J* = 7.6 Hz, 1H), 7.83 (d, *J* = 7.8 Hz, 1H), 7.17 – 7.15 (m, 1H), 7.13 – 7.10 (m, 1H), 3.73 (dd, *J* = 9.7, 6.7 Hz, 2H), 3.25 (dd, *J* = 9.6, 6.7 Hz, 2H), 2.45 (s, 3H) ppm; ^{13}C NMR (101 MHz, $CDCl_3$) δ 156.4 (C), 156.0 (C), 151.9 (C), 149.2 (CH), 149.0 (CH), 148.5 (C), 135.1 (C), 131.6 (C), 131.0 (C), 130.3 (C), 128.7 (C), 127.7 (CH), 127.6 (CH), 127.4 (CH), 127.0 (CH), 126.0 (CH), 125.3 (C), 125.2 (CH), 125.1 (C), 125.0 (2x CH), 124.9 (CH), 124.8 (CH), 124.2 (CH), 123.1 (CH), 122.3 (CH), 121.4 (CH), 37.7 (CH_2), 34.6 (CH_2), 21.4 (CH_3) ppm; HRMS (ESI) *m/z* calculated for $C_{29}H_{23}N_2$ $[M+H]^+$; 399.1856, found 399.1862.

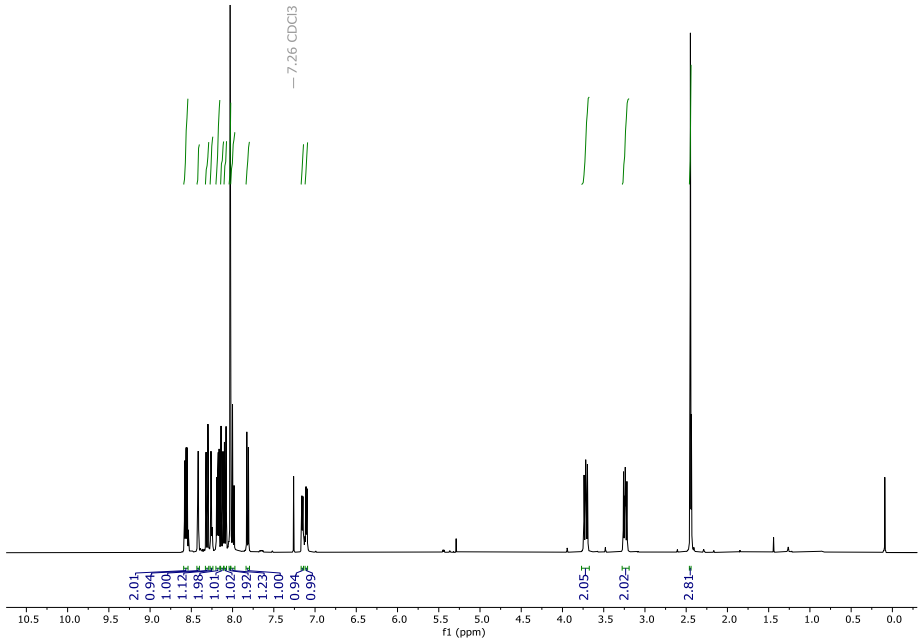
7.26 CDCl3
2.01
0.94
1.00
1.12
1.98
1.01
1.02
1.92
1.23
1.00
0.94
0.99
2.05
2.02
2.81
f1 (ppm)

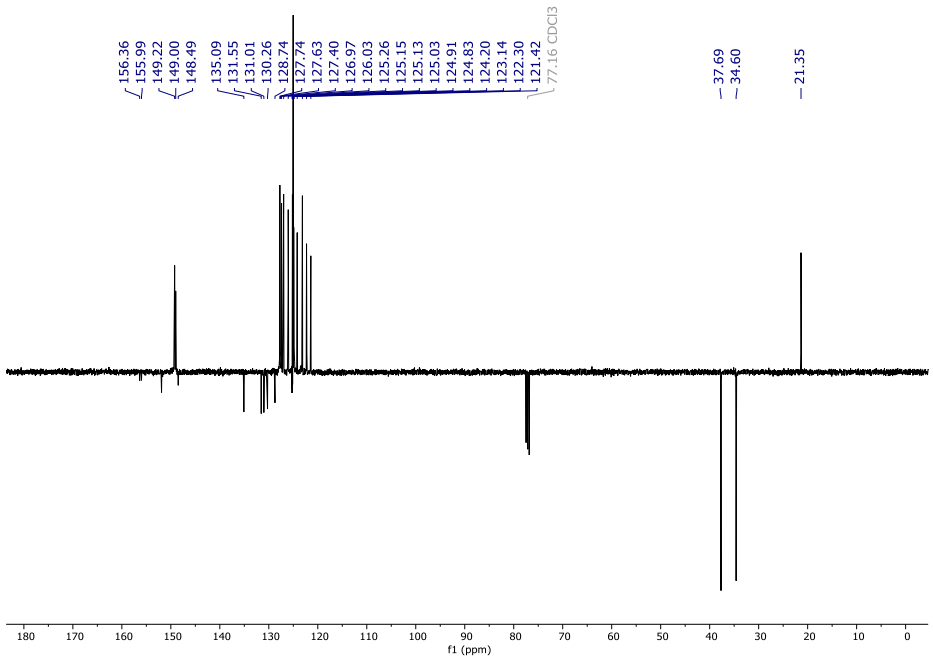
156.36
155.99
149.22
149.00
148.49
135.09
131.55
131.01
130.26
128.74
127.74
127.63
127.40
126.97
126.03
125.26
125.15
125.13
125.03
124.91
124.83
124.20
123.14
122.30
121.42
77.16 CDCl3
37.69
34.60
21.35
f1 (ppm)

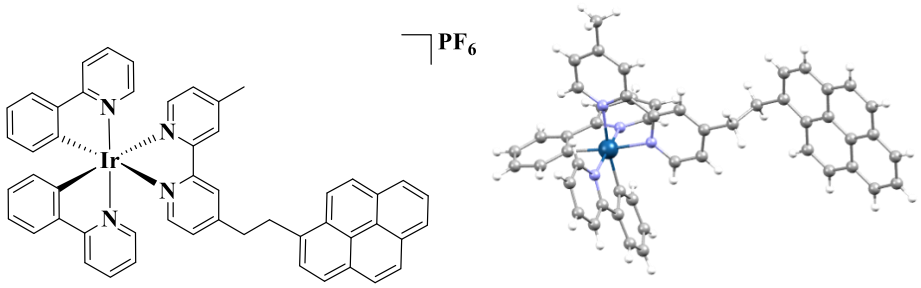

Ir-pyrene-photosensitizer ($PS_{Irpyrene}$). Ir-complex 2 (64mg, 0.088 mmol, 1.0 eq.) was dissolved in CH_2Cl_2/MeOH (9:1, 10 mL) and 4-methyl-4`[2-(pyren-1-yl)ethyl]-2,2`-bipyridine (53mg, 0.132 mmol, 1.5 eq.) was added and the mixture was heated to reflux for 18 h. The solvent was evaporated and the crude powder was dissolved in 10 mL of MeCN. A saturated aqeous KPF_6 (40 mL) solution was added and the mixture was stirred at room temperature for 1 h. The solvent was gently evaporated until a precipitate was formed. The mixture was left in the fridge for 2-3 h and the solid was filtered off via a sintered glass filter. The powder was then dissolved in CH_2Cl_2 (4 mL) and Et_2O (20 mL) was added to precipitate the complex. The mixture was left in the freezer for 1-2 h and filtered again through sintered glass. The powder was washed several times with Et_2O. The title compound was obtained a bright yellow powder (41 mg). ^{1}H NMR (400 MHz, CD_3CN): δ = 8.35 (d, *J* = 9.3 Hz, 1H), 8.30 – 8.24 (m, 2H), 8.16 – 8.04 (m, 8H), 7.99 (s, 1H), 7.87 (t, *J* = 8.0 Hz, 2H), 7.83 – 7.71 (m, 5H), 7.53 (dd, *J* = 10.9, 5.8 Hz, 2H), 7.27 (d, *J* = 5.6 Hz, 2H), 7.09 – 6.98 (m, 4H), 6.95 – 6.88 (m, 2H), 6.27 (dd, *J* = 7.5, 5.2 Hz, 2H), 3.83 – 3.76 (m, 2H), 3.38 (dt, *J* = 7.7, 4.5 Hz, 2H), 2.40 (s, 3H) ppm; ^{13}C NMR (101 MHz, CD_3CN) δ =168.5 (C), 168.4 (C), 156.3 (C), 156.2 (C), 155.6 (C), 152.7 (C), 151.6 (C), 151.5 (C) , 150.8 (C), 150.8 (CH), 150.7 (CH), 149.9 (CH), 149.7 (CH), 145.0 (C), 144.9 (C), 139.4 (C), 139.5 (2x CH), 135.5 (C), 132.5 (2x CH), 132.3 (C), 131.7 (C), 131.3 (2x CH), 131.1 (C), 130.7 (C), 129.8 (CH), 129.5 (CH), 128.8 (CH), 128.4 (2x CH), 127.9 (CH), 127.2 (CH), 126.2 (CH), 126.0 (2x CH), 125.8 (4x CH), 124.4 (2x CH), 124.3 (CH), 123.4 (2x CH), 120.8 (CH), 120.7 (CH), 37.7 (CH_2), 34.1 (CH_2), 21.3 (CH_3) ppm; HRMS (ESI) *m/z* calculated for $C_{51}H_{38}IrN_4$ $[M\text{-}PF_6]^+$; 899.2726, found 899.2698.

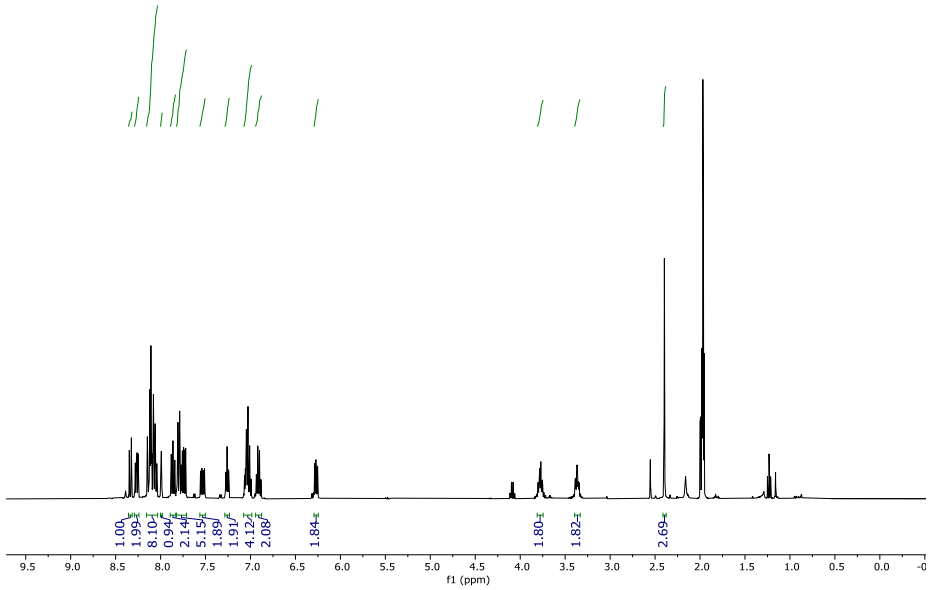
1.00
1.99
8.10
0.94
2.14
5.15
1.89
1.91
4.12
2.08
1.84
1.80
1.82
2.69
9.5 9.0 8.5 8.0 7.5 7.0 6.5 6.0 5.5 5.0 4.5 4.0 3.5 3.0 2.5 2.0 1.5 1.0 0.5 0.0
f1 (ppm)

III.5 References of the Chapter

284. Li, C.-J. and L. Chen, *Organic chemistry in water*. --, 2006. 35(1): p. 68-82.

285. Lindström, U.M. and F. Andersson, *Hydrophobically Directed Organic Synthesis.* Angewandte Chemie International Edition, 2006. 45(4): p. 548-551.

286. Pirrung, M.C., *Acceleration of Organic Reactions through Aqueous Solvent Effects.* Chemistry - A European Journal, 2006. 12(5): p. 1312-1317.

287. Li, C.-J., *Organic Reactions in Aqueous Media with a Focus on Carbon−Carbon Bond Formations: A Decade Update.* Chemical Reviews, 2005. 105(8): p. 3095-3166.

288. Joó, F., *Aqueous Biphasic Hydrogenations.* Accounts of Chemical Research, 2002. 35(9): p. 738-745.

289. Sinou, D., *Asymmetric Organometallic-Catalyzed Reactions in Aqueous Media.* Advanced Synthesis & Catalyis, 2002. 344(3-4): p. 221-237.

290. Dwars, T. and G. Oehme, *Complex-Catalyzed Hydrogenation Reactions in Aqueous Media.* Advanced Synthesis & Catalyis, 2002. 344(3-4): p. 239-260.

291. Lindström, U.M., *Stereoselective Organic Reactions in Water*. Chemical Reviews, 2002. 102(8): p. 2751-2772.

292. Kobayashi, S. and K. Manabe, *Development of Novel Lewis Acid Catalysts for Selective Organic Reactions in Aqueous Media.* Accounts of Chemical Research, 2002. 35(4): p. 209-217.

293. Morikawa, T., et al., *Molecular Catalysts Immobilized on Semiconductor Photosensitizers for Proton Reduction toward Visible-Light-Driven Overall Water Splitting.* ChemSusChem, 2019. 12(9): p. 1807-1824.

294. Chen, S., et al., *Semiconductor-based photocatalysts for photocatalytic and photoelectrochemical water splitting: will we stop with photocorrosion?* Journal of Materials Chemistry A, 2020. 8(5): p. 2286-2322.

295. Zhao, L., et al., *A host–guest approach to combining enzymatic and artificial catalysis for catalyzing biomimetic monooxygenation.* Nature Communications, 2020. 11(1).

296. Fontecilla-Camps, J.C., et al., *Structure–function relationships of anaerobic gas-processing metalloenzymes.* Nature, 2009. 460(7257): p. 814-822.

297. Lemon, B.J. and J.W. Peters, *Photochemistry at the Active Site of the Carbon Monoxide Inhibited Form of the Iron-Only Hydrogenase (CpI).* Journal of the American Chemical Society, 2000. 122(15): p. 3793-3794.

298. Call, A., et al., *Improved Electro- and Photocatalytic Water Reduction by Confined Cobalt Catalysts in Streptavidin.* ACS Catalysis, 2019. 9(7): p. 5837-5846.

299. Eckenhoff, W.T., et al., *Cobalt complexes as artificial hydrogenases for the reductive side of water splitting.* Biochimica et Biophysica Acta (BBA) - Bioenergetics, 2013. 1827(8-9): p. 958-973.

300. Du, P. and R. Eisenberg, *Catalysts made of earth-abundant elements (Co, Ni, Fe) for water splitting: Recent progress and future challenges.* Energy & Environmental Science, 2012. 5(3): p. 6012.

301. Cline, E.D., S.E. Adamson, and S. Bernhard, *Homogeneous Catalytic System for Photoinduced Hydrogen Production Utilizing Iridium and Rhodium Complexes.* Inorganic Chemistry, 2008. 47(22): p. 10378-10388.

302. Call, A., et al., *Photo- and Electrocatalytic H2Production by New First-Row Transition-Metal Complexes Based on an Aminopyridine Pentadentate Ligand.* Chemistry - A European Journal, 2014. 20(20): p. 6171-6183.

303. Pavlova, A. and E.J. Meijer, *Understanding the Role of Water in Aqueous Ruthenium-Catalyzed Transfer Hydrogenation of Ketones.* ChemPhysChem, 2012. 13(15): p. 3492-3496.

304. Wu, X., et al., *RhIII- and IrIII-Catalyzed Asymmetric Transfer Hydrogenation of Ketones in Water*. Chemistry - A European Journal, 2008. 14(7): p. 2209-2222.

305. Hawecker, J., J.M. Lehn, and R. Ziessel, *ChemInform Abstract: EFFICIENT HOMOGENEOUS PHOTOCHEMICAL HYDROGEN GENERATION AND WATER REDUCTION MEDIATED BY COBALOXIME OR MACROCYCLIC COBALT COMPLEXES.* Chemischer Informationsdienst, 1983. 14(40).

306. Call, A., et al., *Understanding light-driven H2 evolution through the electronic tuning of aminopyridine cobalt complexes.* Chemical Science, 2018. 9(9): p. 2609-2619.

307. Kaeffer, N., M. Chavarot-Kerlidou, and V. Artero, *Hydrogen Evolution Catalyzed by Cobalt Diimine–Dioxime Complexes.* Accounts of Chemical Research, 2015. 48(5): p. 1286-1295.

308. Call, A., et al., *Dual cobalt–copper light-driven catalytic reduction of aldehydes and aromatic ketones in aqueous media.* Chemical Science, 2017. 8(7): p. 4739-4749.

309. Gong, H.-X., et al., *Photoexcited perylene diimide radical anions for the reduction of aryl halides: a bay-substituent effect.* Organic Chemistry Frontiers, 2018. 5(15): p. 2296-2302.

310. Ghosh, I., et al., *Reduction of aryl halides by consecutive visible light-induced electron transfer processes.* Science, 2014. 346(6210): p. 725-728.

311. Szejtli, J., *Medicinal Applications of Cyclodextrins.* Medicinal Research Reviews, 1994. 14(3): p. 353-386.

312. Crini, G., *Review: A History of Cyclodextrins.* Chemical Reviews, 2014. 114(21): p. 10940-10975.

313. Takashima, Y., et al., *Emission properties of cyclodextrin dimers linked with perylene diimide—effect of cyclodextrin tumbling.* Polymer Journal, 2012. 44(3): p. 278-285.

314. Schuette, J. and I. Warner, *Structural considerations and fluorescence spectral definition of cyclodextrin/perylene complexes in the presence of 1-pentanol.* Talanta, 1994. 41(5): p. 647-649.

315. Dyck, A.S.M., U. Kisiel, and C. Bohne, *Dynamics for the Assembly of Pyrene−γ-Cyclodextrin Host−Guest Complexes.* The Journal of Physical Chemistry B, 2003. 107(42): p. 11652-11659.

316. Yorozu, T., M. Hoshino, and M. Imamura, *Fluorescence studies of pyrene inclusion complexes with .alpha.-, .beta.-, and .gamma.-cyclodextrins in aqueous solutions. Evidence for formation of pyrene dimer in .gamma.-cyclodextrin cavity.* The Journal of Physical Chemistry, 2002. 86(22): p. 4426-4429.

317. Zhang, Q., et al., *Cyclodextrin supramolecular inclusion-enhanced pyrene excimer switching for time-resolved fluorescence detection of biothiols in serum.* Biosensors and Bioelectronics, 2015. 68: p. 253-258.

318. Singh, G. and P.K. Singh, *Stimulus-Responsive Supramolecular Host–Guest Assembly of a Cationic Pyrene Derivative with Sulfated β-Cyclodextrin.* Langmuir, 2019. 35(45): p. 14628-14638.

319. Dai, N., et al., *Supramolecular Regulation of Catalytic Activity for an Amphiphilic Pyrene-Ruthenium Complex in Water.* Chemistry – A European Journal, 2021. 27(45): p. 11567-11573.

320. Liu, P., et al., *Competitive Host–Guest Interaction between β-Cyclodextrin Polymer and Pyrene-Labeled Probes for Fluorescence Analyses.* Analytical Chemistry, 2015. 87(5): p. 2665-2671.

321. Ballestin, P., et al., *Improving Catalyst Activity in Hydrocarbon Functionalization by Remote Pyrene–Graphene Stacking.* Chemistry – A European Journal, 2019. 25(40): p. 9534-9539.

322. Rasmussen, S.C., *The nomenclature of fused-ring arenes and heterocycles: a guide to an increasingly important dialect of organic chemistry.* ChemTexts, 2016. 2(4).

323. Ottonelli, M., et al., *Tuning the Photophysical Properties of Pyrene-Based Systems: A Theoretical Study.* The Journal of Physical Chemistry A, 2011. 116(1): p. 611-630.

324. Ji Ram, V., et al., *Five-Membered Heterocycles.* 2019: p. 149-478.

325. Katritzky, A.R., et al., *Reactivity of Five-Membered Rings with One Heteroatom.* 2010: p. 383-472.

326. Trost, B.M., et al., *On the Question of Asymmetric Induction with Acyclic Allylic Substrates. An Asymmetric Synthesis of (+)-Polyoxamic Acid.* Journal of the American Chemical Society, 1996. 118(27): p. 6520-6521.

327. Trost, B.M. and X. Ariza, *Catalytic Asymmetric Alkylation of Nucleophiles: Asymmetric Synthesis ofα-Alkylated Amino Acids.* Angewandte Chemie International Edition in English, 1997. 36(23): p. 2635-2637.

328. Trost, B.M., R. Radinov, and E.M. Grenzer, *Asymmetric Alkylation of β-Ketoesters.* Journal of the American Chemical Society, 1997. 119(33): p. 7879-7880.

329. Trost, B.M., E.J. McEachern, and F.D. Toste, *A Two-Component Catalyst System for Asymmetric Allylic Alkylations with Alcohol Pronucleophiles.* Journal of the American Chemical Society, 1998. 120(48): p. 12702-12703.

330. Trost, B.M. and G.M. Schroeder, *Palladium-Catalyzed Asymmetric Alkylation of Ketone Enolates.* Journal of the American Chemical Society, 1999. 121(28): p. 6759-6760.

331. Evans, P.A., J.E. Robinson, and J.D. Nelson, *Enantiospecific Synthesis of Allylamines via the Regioselective Rhodium-Catalyzed Allylic Amination Reaction [J. Am. Chem. Soc. 1999, 121, 6761−6762].*

Journal of the American Chemical Society, 1999. 121(51): p. 12214-12214.

332. Trost, B.M., et al., *Chiral Recognition for Control of Alkene Geometry in a Transition Metal Catalyzed Allylic Alkylation.* Journal of the American Chemical Society, 1999. 121(37): p. 8667-8668.

333. Trost, B.M., D.E. Patterson, and E.J. Hembre, *Dynamic Kinetic Asymmetric Transformations of Conduritol B Tetracarboxylates: An Asymmetric Synthesis of d-myo-Inositol 1,4,5-Trisphosphate.* Journal of the American Chemical Society, 1999. 121(46): p. 10834-10835.

334. Kim, Y.K., S.J. Lee, and K.H. Ahn, *New Hybrid Ligands with a trans-1,2-Diaminocyclohexane Backbone: Competing Chelation Modes in Palladium-Catalyzed Enantioselective Allylic Alkylation.* The Journal of Organic Chemistry, 2000. 65(23): p. 7807-7813.

335. Trost, B.M., et al., *Enantioselective Divergent Synthesis of C19-Oxo Eburnane Alkaloids via Palladium-Catalyzed Asymmetric Allylic Alkylation of an N-Alkyl-α,β-unsaturated Lactam.* Journal of the American Chemical Society, 2019. 141(12): p. 4811-4814.

336. Trost, B.M., et al., *Palladium-Catalyzed Decarboxylative Asymmetric Allylic Alkylation of Dihydroquinolinones.* Organic Letters, 2019. 21(6): p. 1784-1788.

337. Landa, A., et al., *Bis(oxazoline) Lewis Acid Catalyzed Aldol Reactions of PyridineN-Oxide Aldehydes—Synthesis of Optically Active 2-(1-Hydroxyalkyl)pyridine Derivatives: Development, Scope, and Total Synthesis of an Indolizine Alkaloid.* Chemistry - A European Journal, 2006. 12(13): p. 3472-3483.

338. Roberts, D.A., et al., *Post-assembly Modification of Tetrazine-Edged FeII4L6 Tetrahedra.* Journal of the American Chemical Society, 2015. 137(32): p. 10068-10071.

339. van den Heuvel, M., et al., *Synthesis of a Non-Heme Template for Attaching Four Peptides: An Approach to Artificial Iron(II)-*

Containing Peroxidases. The Journal of Organic Chemistry, 2003. 69(2): p. 250-262.

340. Stepanenko, V., et al., *Spiroborate esters in the borane-mediated asymmetric synthesis of pyridyl and related heterocyclic alcohols.* Tetrahedron: Asymmetry, 2007. 18(23): p. 2738-2745.
341. Knochel, P., et al., *Preparation of a New Spirobi[thieno[2,3-c]pyran] and Its Selective Mono- and Dimetalation: Application for the Preparation of Soluble Conjugated Oligothiophenes and Pyrene Derivatives.* Synthesis, 2015. 47(24): p. 3972-3982.
342. Bayh, O., et al., *Deprotonation of thiophenes using lithium magnesates.* Tetrahedron, 2005. 61(20): p. 4779-4784.
343. Codolà, Z., et al., *Design of Iron Coordination Complexes as Highly Active Homogenous Water Oxidation Catalysts by Deuteration of Oxidation-Sensitive Sites.* Journal of the American Chemical Society, 2018. 141(1): p. 323-333.
344. Costas, M. and J.L. Que, *Ligand Topology Tuning of Iron-Catalyzed Hydrocarbon Oxidations We thank the National Institutes of Health for financial support (GM33162 to L.Q.) and Fundacio La Caixa for a postdoctoral fellowship (M.C.).* Angewandte Chemie International Edition, 2002. 41(12): p. 2179.
345. Prat, I., et al., *Assessing the Impact of Electronic and Steric Tuning of the Ligand in the Spin State and Catalytic Oxidation Ability of the FeII(Pytacn) Family of Complexes.* Inorganic Chemistry, 2013. 52(16): p. 9229-9244.
346. Newkome, G.R., et al., *Multidentate ligands containing 2,2'-bipyridine and/or pyridine moieties: structural aspects of their octahedral and pentagonal-bipyramidal complexes.* Inorganic Chemistry, 2002. 23(16): p. 2400-2408.
347. Anastas, P. and N. Eghbali, *Green Chemistry: Principles and Practice.* --, 2010. 39(1): p. 301-312.

348. Casadevall Serrano, C., J. Lloret Fillol, and Universidad Rovira i Virgili. Departament de Química Física i Inorgànica, *Mechanistic Studies of Water Oxidation Catalyzed by Homogeneous Iron and Ruthenium Complexes and Light-driven Organic Reductions with a Dual Cobalt/Copper Catalytic System*. Tesis doctorals. 1 recurs en línia.

349. Sabater, S., J.A. Mata, and E. Peris, *Catalyst Enhancement and Recyclability by Immobilization of Metal Complexes onto Graphene Surface by Noncovalent Interactions.* ACS Catalysis, 2014. 4(6): p. 2038-2047.

350. Claros, M., et al., *Reductive Cyclization of Unactivated Alkyl Chlorides with Tethered Alkenes under Visible-Light Photoredox Catalysis.* Angewandte Chemie International Edition, 2019. 58(15): p. 4869-4874.

351. Sheldrick, G.M., *Crystal structure refinement withSHELXL*. Acta Crystallographica Section C Structural Chemistry, 2015. 71(1): p. 3-8.

352. Burla, M.C., et al., *Crystal structure determination and refinementviaSIR2014*. Journal of Applied Crystallography, 2015. 48(1): p. 306-309.

353. Hübschle, C.B., G.M. Sheldrick, and B. Dittrich, *ShelXle: a Qt graphical user interface forSHELXL*. Journal of Applied Crystallography, 2011. 44(6): p. 1281-1284.

354. Gormisky, P.E. and M.C. White, *Catalyst-Controlled Aliphatic C–H Oxidations with a Predictive Model for Site-Selectivity.* Journal of the American Chemical Society, 2013. 135(38): p. 14052-14055.

355. Skorobogatyi, M.V., et al., *5-Alkynyl-2′-deoxyuridines, containing bulky aryl groups: evaluation of structure–anti-HSV-1 activity relationship*. Tetrahedron, 2006. 62(6): p. 1279-1287.

UNIVERSITAT ROVIRA I VIRGILI
ORGANIC TRANSFORMATIONS USING TRANSITION METALS AND PHOTOREDOX CATALYSTS
Klaudia Michaliszyn

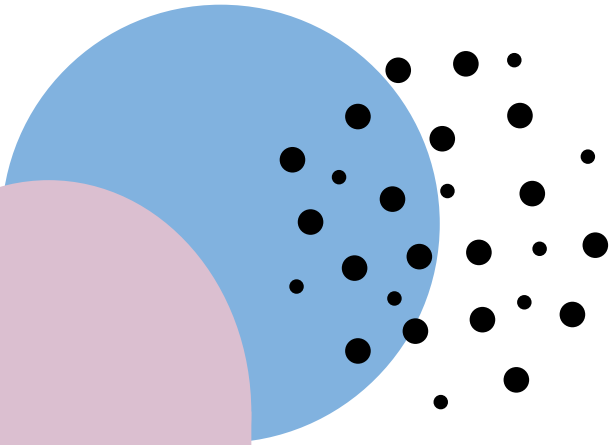

Chapter IV

Study of the supramolecular interactions of the cobalt and nickel pyrene-based catalysts with cyclodextrins and carbon-based nanomaterials through the photophysical properties.

UNIVERSITAT ROVIRA I VIRGILI
ORGANIC TRANSFORMATIONS USING TRANSITION METALS AND PHOTOREDOX CATALYSTS
Klaudia Michaliszyn

UNIVERSITAT ROVIRA I VIRGILI
ORGANIC TRANSFORMATIONS USING TRANSITION METALS AND PHOTOREDOX CATALYSTS
Klaudia Michaliszyn

IV.1 State-of-the-art

Supramolecular chemistry is the interdisciplinary study of chemistry concerning the chemical, physical, and biological features of non-covalent interactions of molecular assemblies like host-guest complexes and materials having a greater complexity than the individual molecules themselves. This field of chemistry explores the structures and functions of the assemblies by intermolecular interactions of two or more entities (molecules) in an organized manner.[356] This class of interactions include hydrogen bonding, dipole–dipole and ion–dipole interactions and hydrophobic interactions, such as van der Waals, π–π interactions, and dispersion interactions.[357] The most spectacular examples of supramolecular chemistry have been found in nature such as the enzyme-substrate complex, protein-protein interactions and the DNA structure (its packing and replication mechanisms).[358] A major objective in supramolecular chemistry is to mimic the nature with designed synthetic systems and to mediate in biological systems by creating functional architecture that cannot be found in nature.[359, 360] Among the different molecular receptors studied in supramolecular chemistry, cyclodextrins (CD) were found as exceptional due to their unique properties. CDs are applied[361] in artificial enzymes formation, sensors, drug formulations, cosmetics and food technology, among others. Therefore, cyclodextrins are ideal candidates to be studied as receptors for the catalysts developed in chapter III, and their effect on the catalyst's properties.

IV.1.1 Application of cyclodextrins related to catalysis

Cyclodextrins are cyclic oligomers composed from macrocyclic units of D(+)-glucopyranose units joined through α-1,4 glycoside bonds. They are designated by Greek letter to indicate the number of glucose units, thus the most common containing 6, 7 and 8 glucopyranose units are called α-CD, β-CD and γ-CD, respectively[362] (Scheme IV.1).[363] Structurally present a unique conical shape with two rims. Primary hydroxyl groups are placed on a narrower rim and secondary hydroxyl groups on the wider rim. Therefore, CDs have

hydrophilic exterior and inner hydrophobic cavity. This provides high solubility in polar solvents and the recognition and interaction with non-polar guest molecules of certain size and shape to form inclusion complexes.[234, 364-367] The combination of these two properties has been exploited in dissolving non-polar compounds in polar solvents.

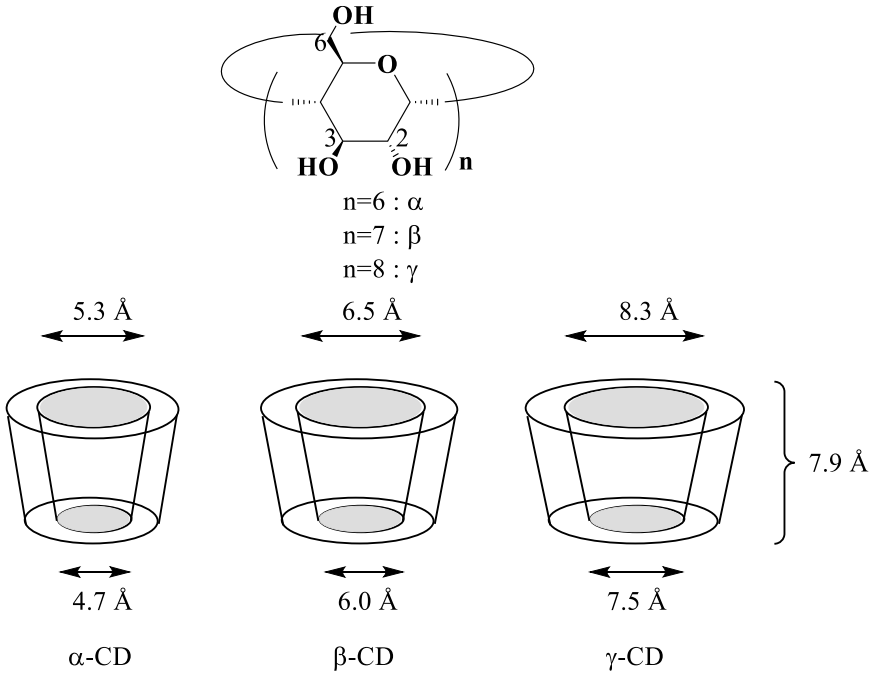

Scheme IV. 1 *Cyclodextrin structure.*

Fluorescence studies applying CDs has witnessed increasing interest in the effects of on photochemical reactions.[368-370] In 1980, it was described by Nicholas J. Turro, Michael Gratzel, and Andre M. Braudt that the radiation capacity of organic fluorophores hosted in CD-based inclusion complexes is enhanced due to their protection from external quenching agents by CDs. Contribution of cyclodextrins in the development of innovative homogeneous or heterogeneous catalytic processes can be tracked back to 1967, to Bender's studies in the hydrolysis of phenyl acetate in the presence of CD.[371] Ever since a broad reactivity mediated by native and modified CDs has been reported,

which can be divided in two types: (a) covalent, where the cyclodextrin and the substrate form intermediate by the covalent bondings, (b) non-covalent when the interactions between CD and reactants are non-covalent and the reaction occurs in the hydrophobic cavity of the CD.[372-376] Outstanding example of covalent interaction of cyclodextrin was described by R. J. M. Nolte and co-workers for the catalytic trans-selective epoxidation of *cis*-polybutadiene (Scheme IV.2).[377]

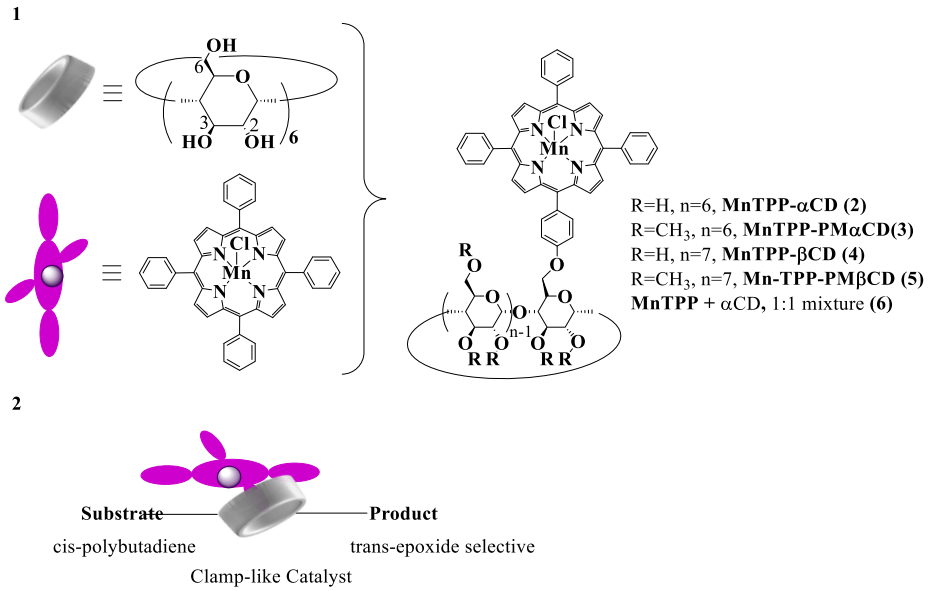

Scheme IV. 2 Schematic representations of structures of the catalysts, proposed catalytic epoxidation by the clamp-like catalyst MnTPP–α*CD following a distributive mechanism and the reaction.*

Recently published precedent by D. Tilley et al. for ammonia oxidation using cyclodextrins to immobilize the catalyst by non-covalent interactions on the surface of electrode (Scheme IV.3).

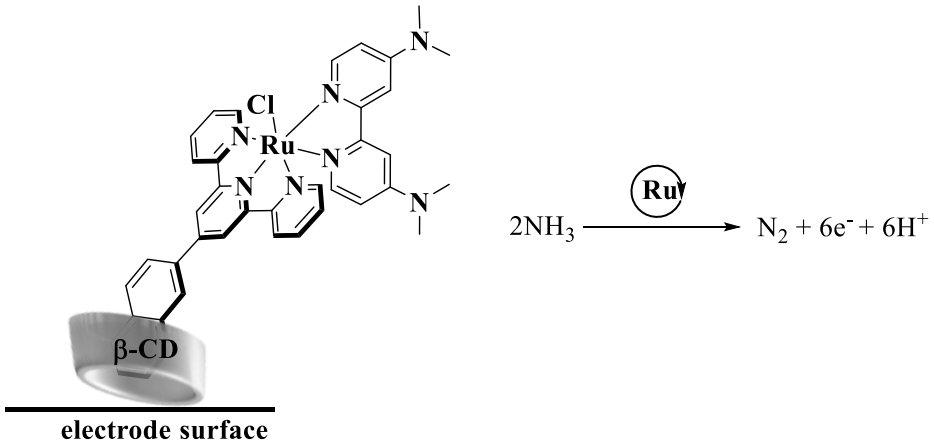

Scheme IV. 3 *Ammonia oxidation by immobilized catalyst onto electrode by β-CD.*

In addition, transition metal complexes with CDs have been used as water-soluble organometallic catalysts in several reactions[378, 379] i.a.: hydroformylation of terminal alkenes, hydrogenation of alkenes, Tsuji-Trost substitution reaction, and cyclic epoxidation. These properties encouraged us to study in detail the mechanism of non-covalent linking between the catalyst incorporated within the hydrophobic cavity of γ-CDs. The aim of this chapter is to get insights in the utilization of γ-CDs to form inclusion complexes with catalysts designed in chapter III by photophysical studies.

IV.1.2 Pyrene properties regarding their interaction with CDs

Pyrene is the smallest peri-fused polycyclic aromatic hydrocarbon (PAH) consisting of four benzene rings, extensively explored for its interesting electronic and structure properties.[175] Its planar geometry and rigid structure confer to pyrene a strong tendency to form π-stacking interactions, a feature which has been used to attach a variety of functional groups onto cyclodextrins and carbon-based nanomaterials such as graphite-like structures, carbon nanotubes or graphene.[380]

Apart from the characteristics discussed above, pyrene is a molecular aromatic hydrocarbon model that has found application in the study of biomolecules, sensing of metal ions and its distinctive spectral features have

been exploited to evaluate the structure and molecular organization and conformation of certain molecules.

Pyrene's high extinction coefficient is an advantage in conformational analysis because pyrene-labelled samples can be analyzed at very low concentrations.[381] Monomer and excimer fluorescence emission of pyrene can be distinguished and detected with highly sensitive spectroscopic methods (fluorescence spectroscopy) at low levels.[382] Pyrene molecules tend to self-associate and its strong propensity to form excimers it's the main pyrene's utility that have found wide use in sensing application. When two pyrene units are close to each other (<5 Å) an excimer emission is observed. The first observation of intermolecular excimers in pyrene solution was reported in 1954 by Förster and Kasper.[383, 384] Owing to its photophysical properties as the excimer formation, combined with long-lived excited states, strong absorption cross section, high fluorescence quantum yield,[385] unusual distinction of the fluorescence bands for monomer and excimer and the sensitivity of its excitation spectra to microenvironmental changes[186], pyrene became one of the most studied organic molecules.[323] Pyrene is frequently applied organic dye in the investigation and also employed as a probe to measure various properties of surfactant micelles, phospholipid vesicles and surfactant/polymers aggregates.[184, 386] As aforementioned, pyrene and its derivatives prone to easily form excimers or π-aggregates. This property was widely used for supramolecular design and exploring the structural properties of macromolecular systems. The tendency of forming excimers was employed in fluorescence studies to sense environmental parameters such as temperature, pressure of pH.[187] Changes observed in the excimer fluorescence intensity are the reflection of the changes in the environment. Pyrene was also used in examination of lipid membranes, in structural studies of proteins and DNA recognition[387][388-393] as well as in can be also used in the recognition of guest molecules as gases, metals, organic molecules and another various analytes.[190, 191, 394-398]

The encapsulation of molecules into macrocycle cavities to improve their solubility and electro-optical properties received much attention. Using CDs as macrocycles have been reported, and this method has been shown not only to increase the solubility but also to enhance chemical stability of encapsulated units.[399] Pyrene and its derivatives are known to interact with cyclodextrins as host molecules and to form with them inclusion complexes[234] in different manners, β-CD includes monomeric pyrene, while γ-CD includes dimeric pyrene[316, 400-402] (Scheme IV.4). It was reported by group of Ripmeester that for this structural arrangement that likely also exists in solution, pyrene would be remarkably well protected from the influence of external influences such as fluorescence quenchers when it is inside of the cavity of cyclodextrins.[403]

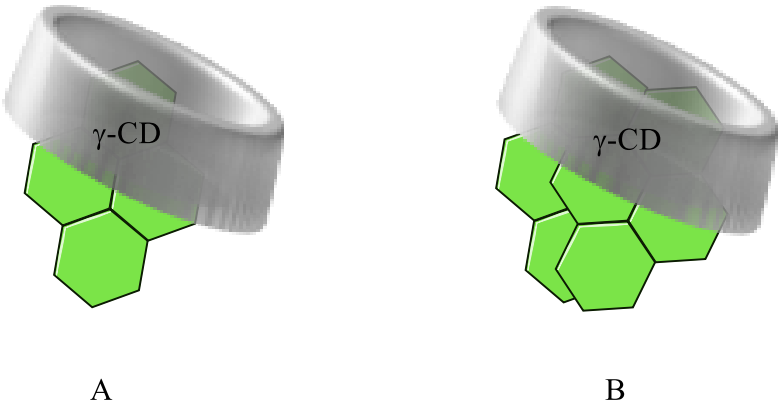

Scheme IV. 4 *Schematic representation of the interaction of pyrene monomer (A) and pyrene excimer (B) with γ-cyclodextrin.*

γ-cyclodextrin in host-guest inclusion complex with incorporated anchoring catalysts from chapter III would offer less polar and more protective environment, enhance the fluorescence of the guest molecule by reducing the interaction between the catalyst and quenching agents, while water molecules would be removed.[404] Remarkable example was reported by prof. Mohanty and co-workers[235] using β- and γ-cyclodextrins for the modulation of photophysical properties of and acidity constant of pyrene-armed calix[4]arene.

Molecular catalysts can be tuned to achieve excellent control over the steric and electronic properties, hence they become highly active and selective under mild conditions. This rational catalyst design is difficult to be achieve in heterogeneous materials. Therefore, immobilization of homogeneous catalysts offer the possibility of combining both the stability and recyclability of heterogeneous catalysts with the development facility of the homogeneous ones. Immobilization methods can be divided into three main categories:

- Covalent (chemical reactions e.g. adding functional anchoring group to the catalyst, electrochemical reactions e.g. electropolymerization)
- Non-covalent (electrostatic interactions, π–π stacking, coordination, insolubility immobilization)
- Periodic assembly (Metal Organic Frameworks, Porous Organic Polymers, hybrid materials)[405, 406]

This kind of system could be achieved by anchoring the catalyst with pyrene moieties from chapter III onto carbon-based nanomaterials by non-covalent interactions such as π–π stacking (Scheme IV.5). Studies reported by Chen and co-workers showed the affinity of pyrene to graphene, GO (graphene oxide) or rGO (reduced graphene oxide)[407, 408] and together with precedent reported by Prato et al.[409] about the interaction of carbon nanotubes with pyrene encouraged us to explore similar system.

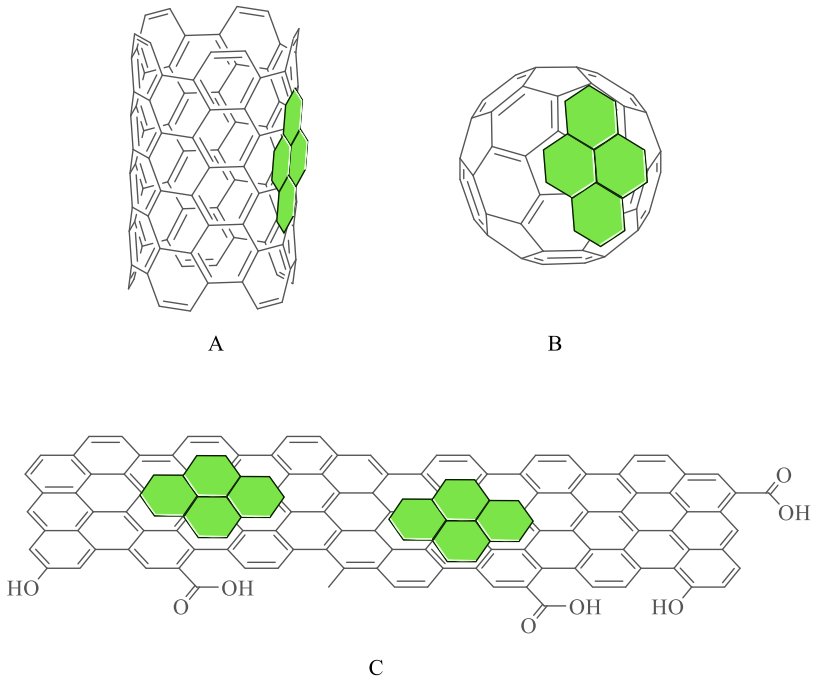

Scheme IV. *5 Pyrene anchored onto nantotube (A), buckyball C60 (B) and graphene oxide (C).*

Based on this, we performed nuclear magnetic resonance, ultraviolet and visible spectroscopic studies of the family of new tetradentate ligands and their cobalt and nickel complexes with various nanomaterials. Due to the photophysical properties of pyrene and its derivatives, the inclusion and anchoring interactions of complexes and nanomaterials allows studying the mechanism of the formation of supramolecular structures and comparing their stability.

Objectives:

- Characterization of certain parts of ligands that contain a □-stacking polyaromatic unit such as pyrene or perylene and ligands by spectroscopic methods;
- Characterization of corresponding Ni^{II} and Co^{II} metal complexes in different solvent systems;
- To explore the influence of π-stacking interactions between metal complexes with γ-cyclodextrins and carbon-based nanomaterials.

IV.2 Results and Discussion

III.2.1 Photophysical characterization of ^{PyB}mcp, ^{PyB}pdp and and their precursors

Before studying the photochemistry of the catalysts, we studied the prepared ligands and ligands' parts. In particular, the ligand parts selected are those containing the polyaromatic moiety – pyrene (Scheme IV.6). This study will serve as starting point to understand the more likely intricate behavior of the metal complexes.

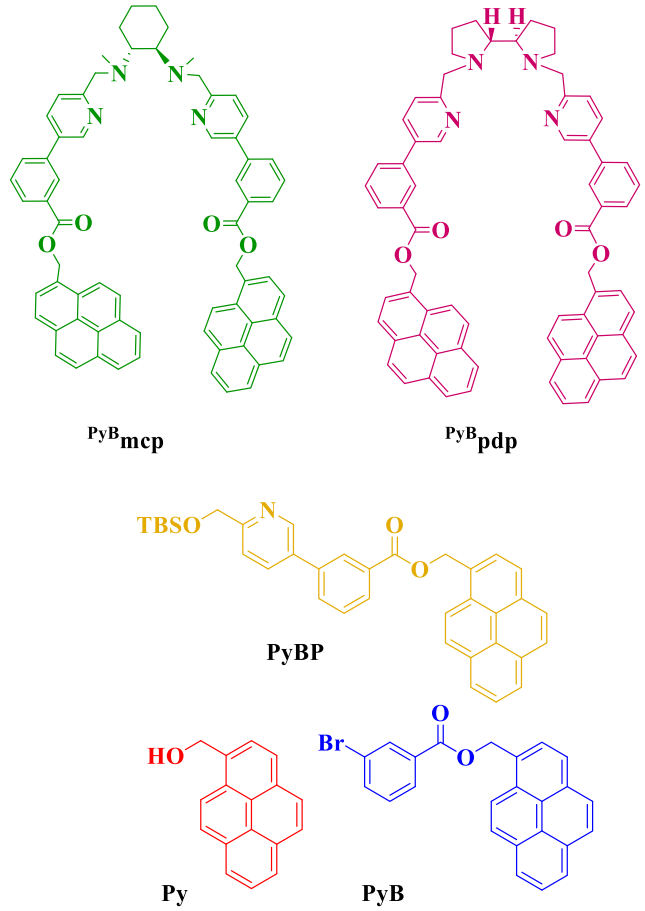

***Scheme IV. 6** Ligands ^{PyB}**mcp**, ^{PyB}**pdp** and their building blocks used in photophysical studies.*

First, we measured absorption spectra of molecules reported in Figure IV.1 (For a detailed description of the absorption and fluorescence spectroscopy studies see the experimental section.). As expected, all building blocks and

ligands showed the characteristic absorption spectrum of the pyrene monomer; three absorption peaks in the 310-350 nm range (Figure IV.1 top). The differences in absorption intensity could be due to the presence of additional absorption features of the 3-phenylpyridine and the rest of the ligand. The emission spectra of the fragments **Py**, **PyB** and **PyBP** revealed the characteristic pyrene monomer in the 360-400 nm range. However, under the same conditions **^{PyB}mcp** and **^{PyB}pdp** disclose an intense characteristic broad band at ca. 475 nm, which correspond to the excimer emission.

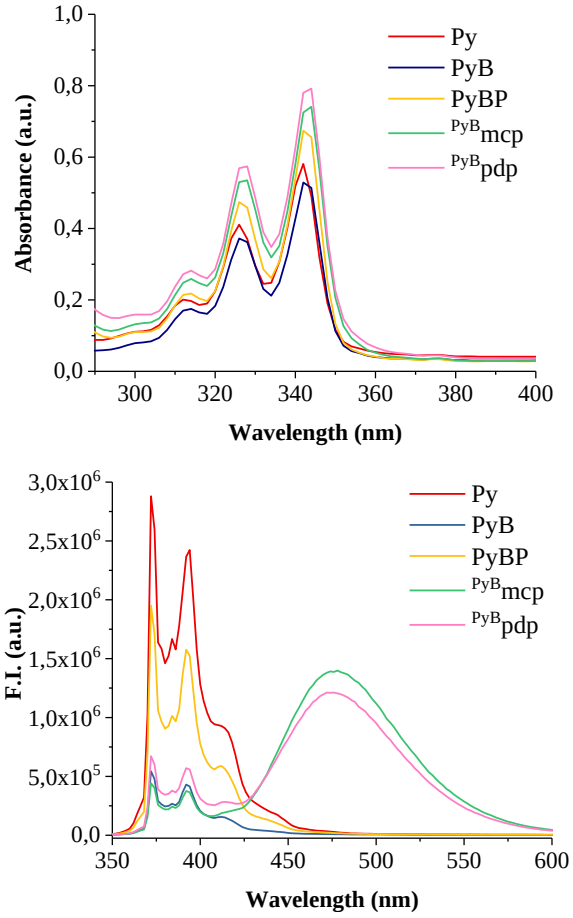

Figure IV. 1 *Absorption (top) and emission (bottom) spectra of ligands* ***^{PyB}mcp***, ***^{PyB}pdp*** *and their building blocks* ***Py***, ***PyB*** *and* ***PyBP*** *(20 μM) in acetonitrile.*

This feature is relevant because help us to understand the ligand conformation and aggregation in solution. Pyrene has a strong propensity to form aggregation *via* a π-stacking of two or more pyrene molecules in solution (Figure IV.1

bottom). See the introduction section IV.1.2 for the general characteristics of pyrenes π-stacking).

The fact that fragments did not present excimer emission it is expected for well solvated pyrene molecules. Therefore, we rationalized that acetonitrile efficiently prevent the aggregation independently of bearing an alcohol group (**Py**) or more apolar molecules like **PyB** or **PyBN**. However, for ^{PyB}**mcp** and ^{PyB}**pdp** ligands there is a strong excimer emission, although ligand polarity is expected to be more polar than the latter fragments, due to the diamine backbone. Therefore, since the ligands have two pyrene units per molecule, we suggested, at this point, that the interaction is intramolecular. On the other hand, ^{PyB}**mcp** and ^{PyB}**pdp** also presents some monomer emission which imply that besides the intramolecular interactions between two pyrene units of the ligand, they are in equilibrium with a conformation where the two pyrene units are solvated.

Additional information about ligands and their complexes could be obtain by measuring absorption spectra of different concentrations to get molar extinction coefficient (how strongly a substance absorbs light at the given wavelength per molar concentration).

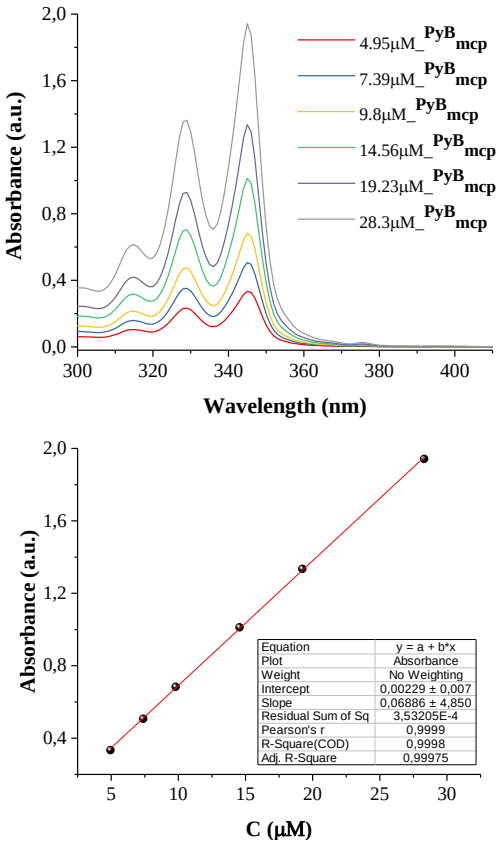

Figure IV. 2 *Absorption of* ^{PyB}*mcp at different concentrations and Beer's Law plot.*

The extinction coefficient is the absorbance divided by the concentration and light path length in centimeters, according to Beer's Law which states that the absorptive capacity of dissolved compound is directly proportional to its concentration ($A= \varepsilon*C*L \Rightarrow \varepsilon=A/(C*L)$). The units of extinction coefficients are usually $M^{-1}cm^{-1}$. Performed experiments demonstrate linear dependence of measured ligands at different concentrations, which allowed us to determined extinction coefficient at 345 nm in acetonitrile for ^{PyB}**mcp** the value was $\varepsilon = 6.89*10^4$ L $mol^{-1}cm^{-1}$ and for ^{PyB}**pdp,** $\varepsilon = 8.03*10^4$ L $mol^{-1}cm^{-1}$.

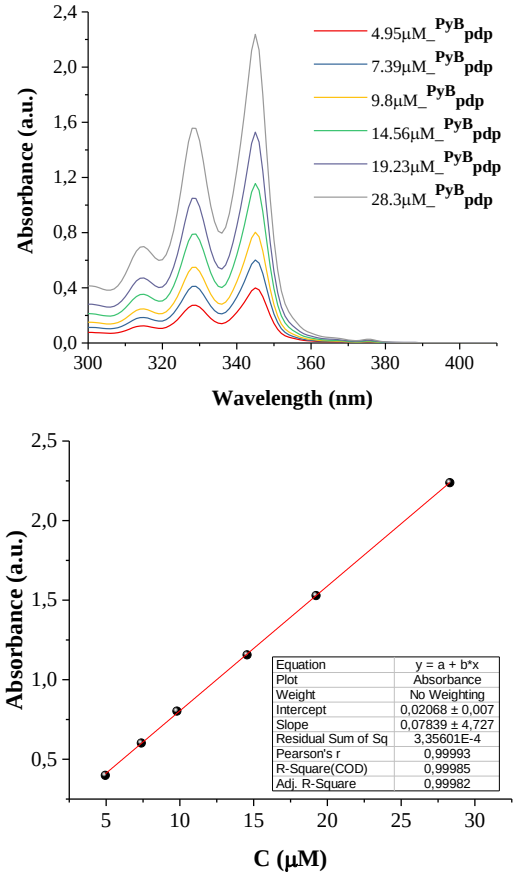

Figure IV. 3 *Absorption of* ^{PyB}*pdp at different concentrations and Beer's Law plot.*

The molar attenuation coefficient could be also determined from the extinction coefficient trend line. The value established from the slope for **^{PyB}mcp** had the same exact value as from the calculations i.e. $\varepsilon = 6.89*10^4$ L mol^{-1}cm^{-1} (Figure IV.2), but the value for **^{PyB}pdp** was determined as $\varepsilon = 7.95*10^4$ L mol^{-1}cm^{-1} (Figure IV.3).

III.2.2 Photophysical characterization of ^{PerB}mcp and its preursors

We also analyzed the perylene systems as in the previous section (Scheme IV.7).

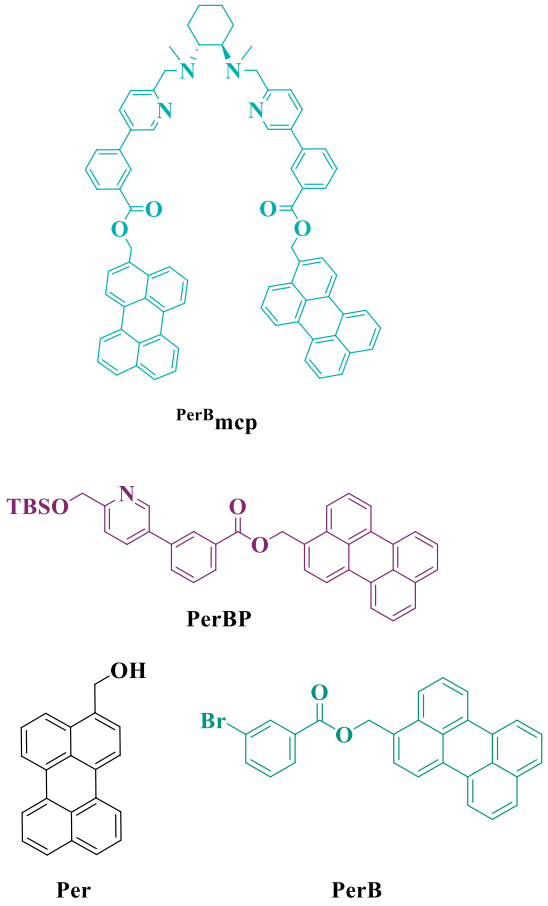

^{PerB}**mcp**

PerBP

Per **PerB**

Scheme IV. 7 *Ligand* ^{PerB}***mcp*** *and its building blocks used in photophysical studies.*

The absorbance of perylene analogs exhibit typical perylene monomer in the 350-460 nm range (See Figure IV.4 top), while the emission spectra of **Per**, **PerB**, **PerBP** and ^{PerB}**mcp** display mainly the perylene monomer in the 420-530 nm range (See Figure IV.4 bottom). This result encouraged us for a deeper insight into the perylene based system.

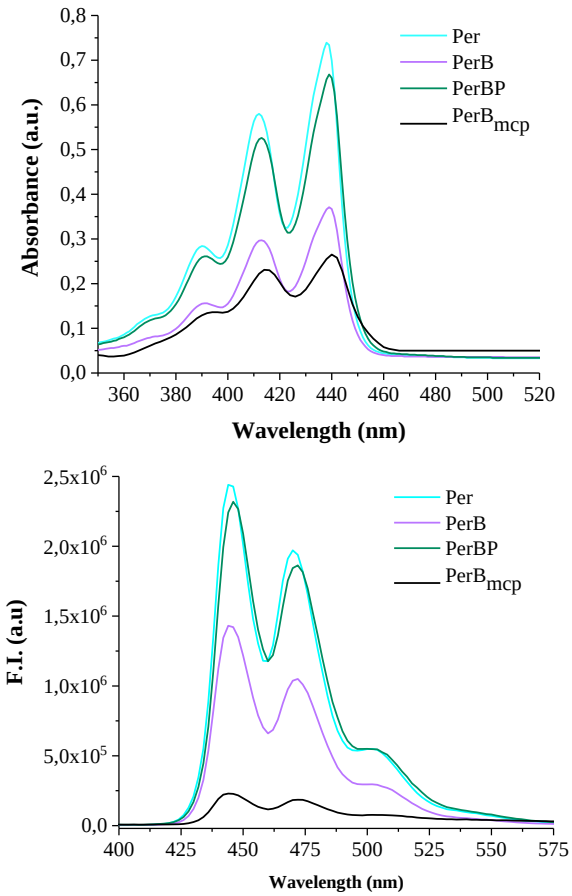

Figure IV. 4 *Absorption (top) and emission (bottom) spectra of ligand* ^{PerB}*mcp and its building blocks (20 μM) in acetonitrile.*

The shape emission spectrum of concentrated solutions of perylene appear as a broad band at 545 nm due to molecular aggregation Absorbance and fluorescence studies at different concentration could illustrate if the molecular aggregation takes place.

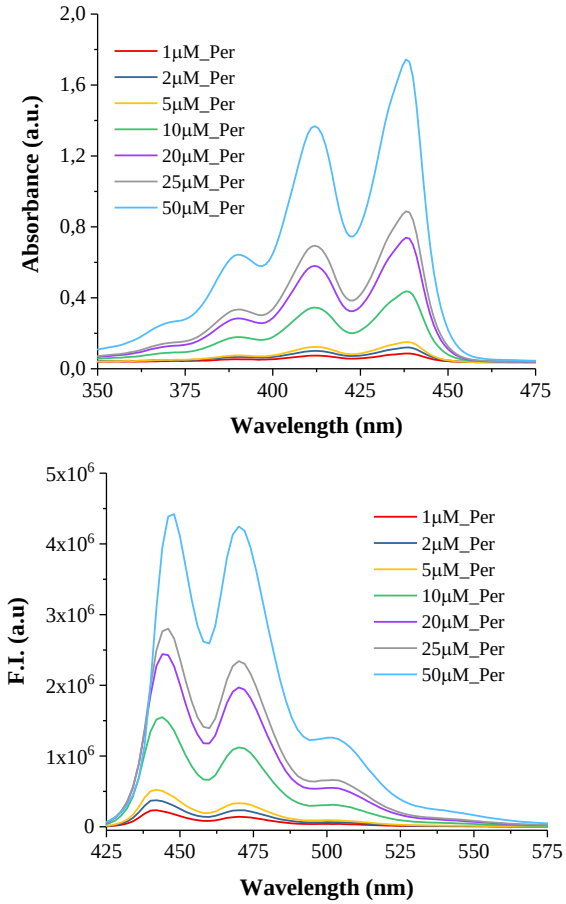

Figure IV. 5 *Absorption (top) and emission (bottom) spectra of* ***Per*** *at different concentrations in acetonitrile.*

Absorption and emission spectrum of **Per** were measured in the 1 to 50 μM range. In the Figure IV.5, the observed relative emission change between the peaks at ca. 440 and 470 nm indicated that the amount of aggregation is small.

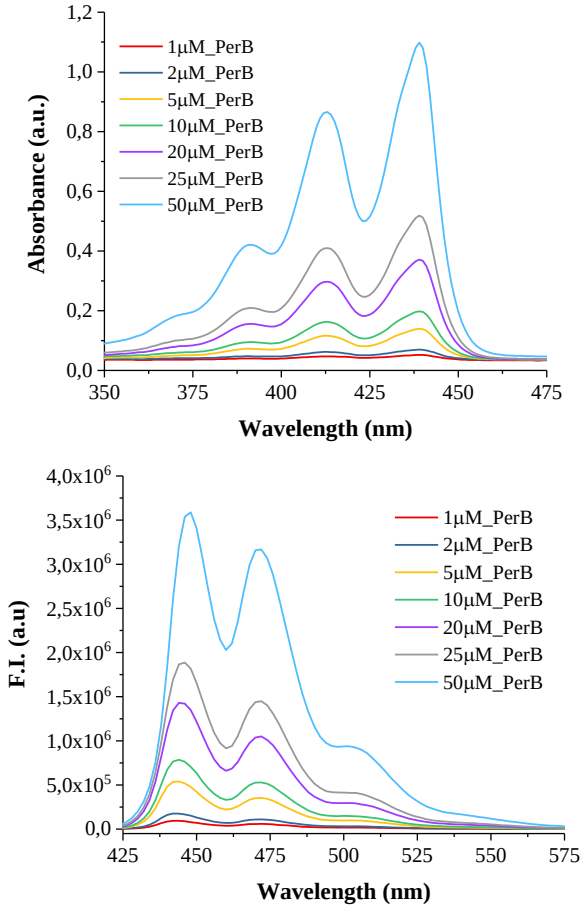

Figure IV. 6 *Absorption (top) and emission (bottom) spectra of* ***PerB*** *at different concentrations in acetonitrile.*

Equivalent results were obtained for **PerB** and **PerBP** (Figure IV.6 and IV.7). ^{PerB}mcp, which contains two perylene units showed the same behavior for the 1 - 50 µM concentration range. The calculated extinction coefficient at 416 nm was $\varepsilon = 1.5*10^4$ L $mol^{-1}cm^{-1}$ for ^{PerB}mcp, which is much lower than the coefficient for ligands with pyrene moiety. The value established from the slope was similar, i.e. $\varepsilon = 9.5*10^3$ L $mol^{-1}cm^{-1}$ (Figure IV.8).

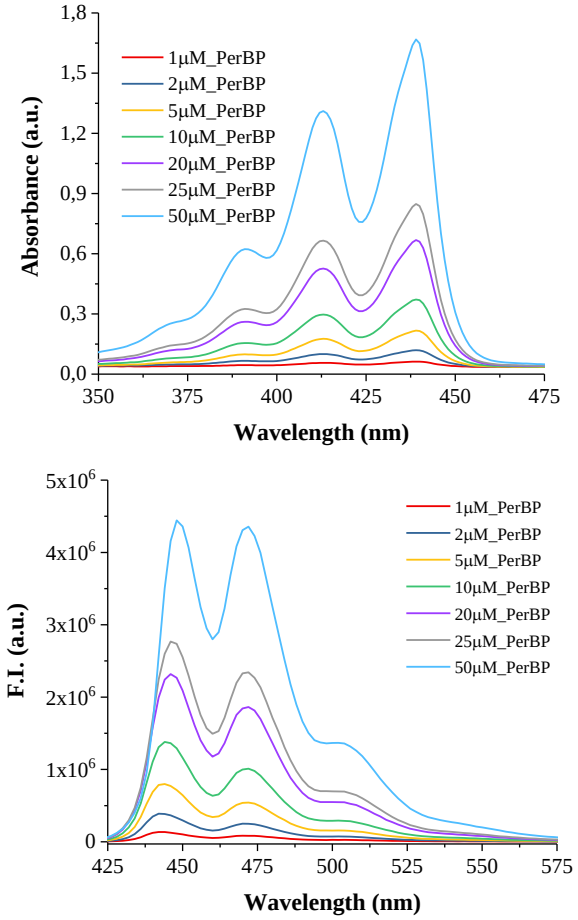

Figure IV. 7 *Absorption (top) and emission (bottom) spectra of* ***PerBP*** *at different concentrations in acetonitrile.*

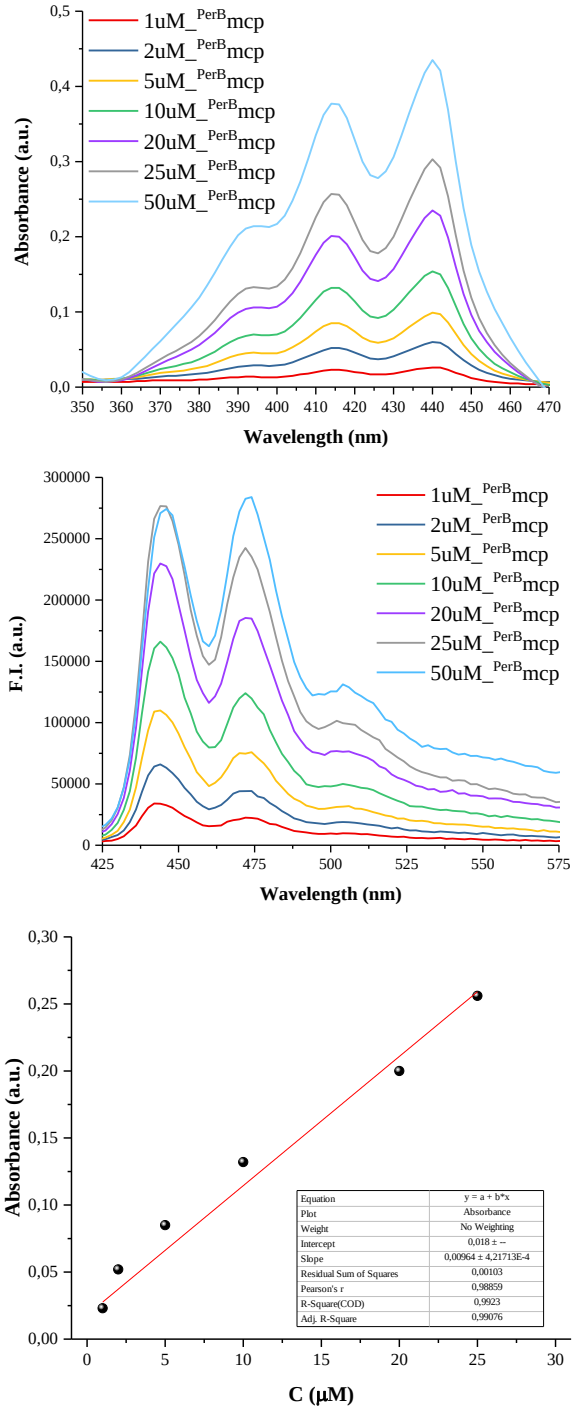

Figure IV. 8 *Absorption (top) and emission (middle) spectra of* ***^{PerB}mcp*** *at different concentrations in acetonitrile and Beer's Law plot.*

IV.2.2 Photophysical characterization of cobalt and nickel complexes

The absorption and emission spectrum of the cobalt and nickel ($Co(^{PyB}mcp)(OTf)_2$, $Co(^{PyB}pdp)(OTf)_2$, $Ni(^{PyB}mcp)(OTf)_2$ and $Ni(^{PyB}pdp)(OTf)_2$) complexes were also studied in different solvent mixtures. First, the excimer was not found for $Co(^{PyB}mcp)(OTf)_2$ and $Co(^{PyB}pdp)(OTf)_2$ in CH_3CN (Figure IV.9) nor in the solvent mixture used in the photocatalytic reactions (acetonitrile:water, 4:6 (Figure IV.10). But in practically pure water (20 μL of were used to prepare the stock solution of the complexes, Figure IV.11),[410] the fluorescence spectrum revealed the presence of pyrene excimers, being more prone for nickel complexes.

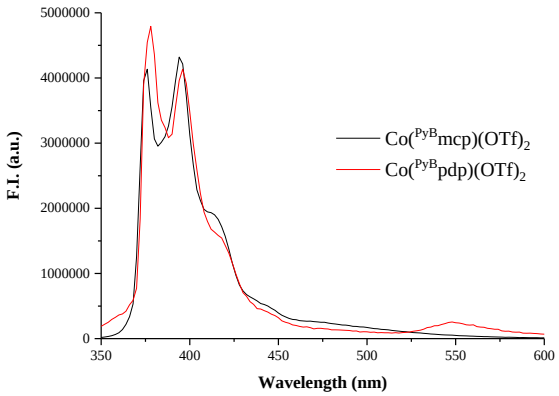

Figure IV. 9 *Emission spectra of $Co(^{PyB}mcp)(OTf)_2$ and $Co(^{PyB}pdp)(OTf)_2$ in acetonitrile.*

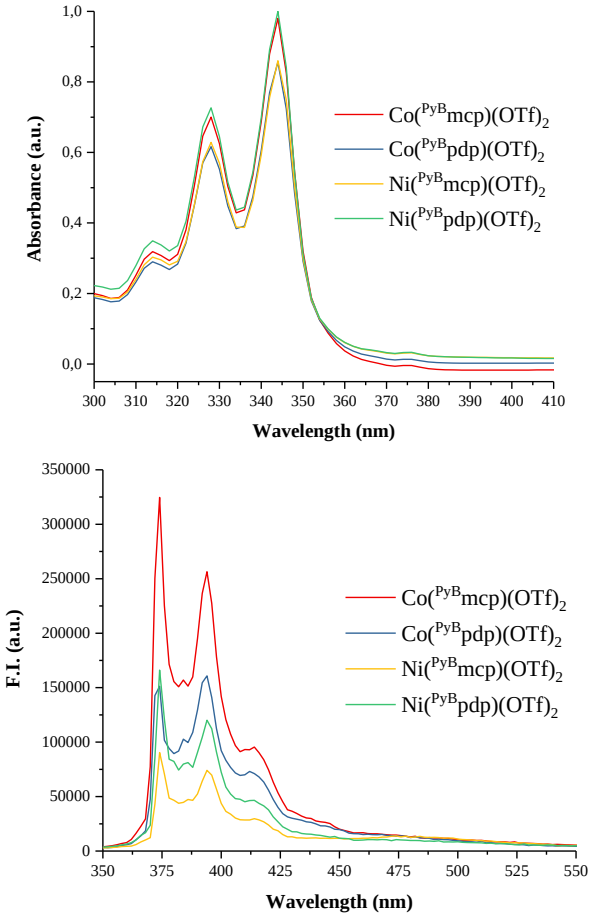

Figure IV. 10 *Absorption (top) and emission (bottom) spectra of 20 μM solutions of Co(^{PyB}mcp)(OTf)$_2$, Co(^{PyB}mcp)(OTf)$_2$, Ni(^{PyB}mcp)(OTf)$_2$ and Ni(^{PyB}mcp)(OTf)$_2$ in solvent mixture CH$_3$CN:H$_2$O (4:6).*

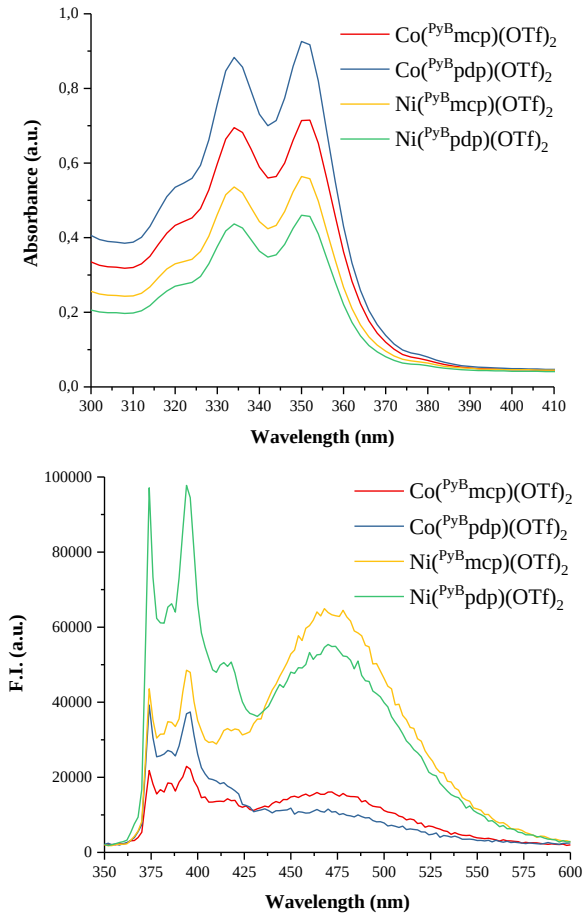

Figure IV. 11 *Absorption (top) and emission (bottom) spectra of 20 μM solutions of Co(PyBmcp)(OTf)2, Co(PyBmcp)(OTf)2, Ni(PyBmcp)(OTf)2 and Ni(PyBmcp)(OTf)2 in water.*

IV.2.3 Encapsulation of PAH

Cyclodextrins are known as good hosts for non-polar molecules with the ability to selectively interact with substances of certain geometry in their chiral nanocavities. The photophysical studies, engaging Co^{II} and Ni^{II} complexes and γ-cyclodextrin were investigated towards the encapsulation of the π-conjugated units. The experiments were carried out by preparing a mixture containing 20 μM of catalyst in water/acetonitrile mixture (6:4 mL) or in water at room temperature (25 ºC) under nitrogen atmosphere followed by titration with a solution of γ-cyclodextrine or vice-versa, 20 μM of γ-cyclodextrin and titration with the catalyst. The method of continuous variation (known as the Job plot)

was applied to calculate the host to guest stoichiometry between the Co^{II} and Ni^{II} catalysts with γ-cyclodextrins. Most supra-molecular systems usually form 1:1 host (H) to guest (G) complexes, but stoichiometry, the most common among them being 1:2 and 2:1 (HG_2 and H_2G) are also common.

IV.2.3.1 Encapsulation in mixture of water and acetonitrile

The titration of γ-cyclodextrin with $Co(^{PyB}mcp)(OTf)_2$ aliquots until a final concentration of 20 μM (Figure IV.12) gradually increased the absorbance. The emission spectra showed increasing intensity till $Co(^{PyB}mcp)(OTf)_2$ concentration reached 8 μM and subsequently decreasing. We could rationalize this behavior considering the creation of double (or multiple) inclusion complexes (1·M : 2·γ-CD) up to ca. 8 μM. The first titration steps, with low concentration of $Co(^{PyB}mcp)(OTf)_2$ compared with the excess of γ-CD, favors the complete inclusion of the pyrenes in the γ-CD, then enhancing the emission, due to the minimization of the expected metal quenching of the pyrene excited state. At higher concentrations than 8 μM of catalyst the mono inclusion increases (1·M : 1·γ-CD), and at 10 μM, the stoichiometry pyrene·γ-CD is 1 to 1. Then, the lower emission can by interpreted as the internal quenching by the metal (Figure IV.12). The absence of excimer suggests that the incorporation of the two pyrenes in one·γ-CD is not occurring.

Then the experiment was also carried out in reverse order, to a 20 μM of $Co(^{PyB}mcp)(OTf)_2$ solution aliquots of γ-cyclodextrin were added and measured by spectroscopy (Figure IV.13). The reverse experiment displayed only monotonic changes in absorption spectra. Gentle increase of fluorescence intensity was detected while solution of γ-CD was added. Guest molecule peaks intensities may be increased because of interaction with cyclodextrin, protectocting from external quenchers. Therefore, we conclude a 1:1 γ-CD:M as the main encapsulation stoichiometry since no excimer was detected in the emission spectrum.

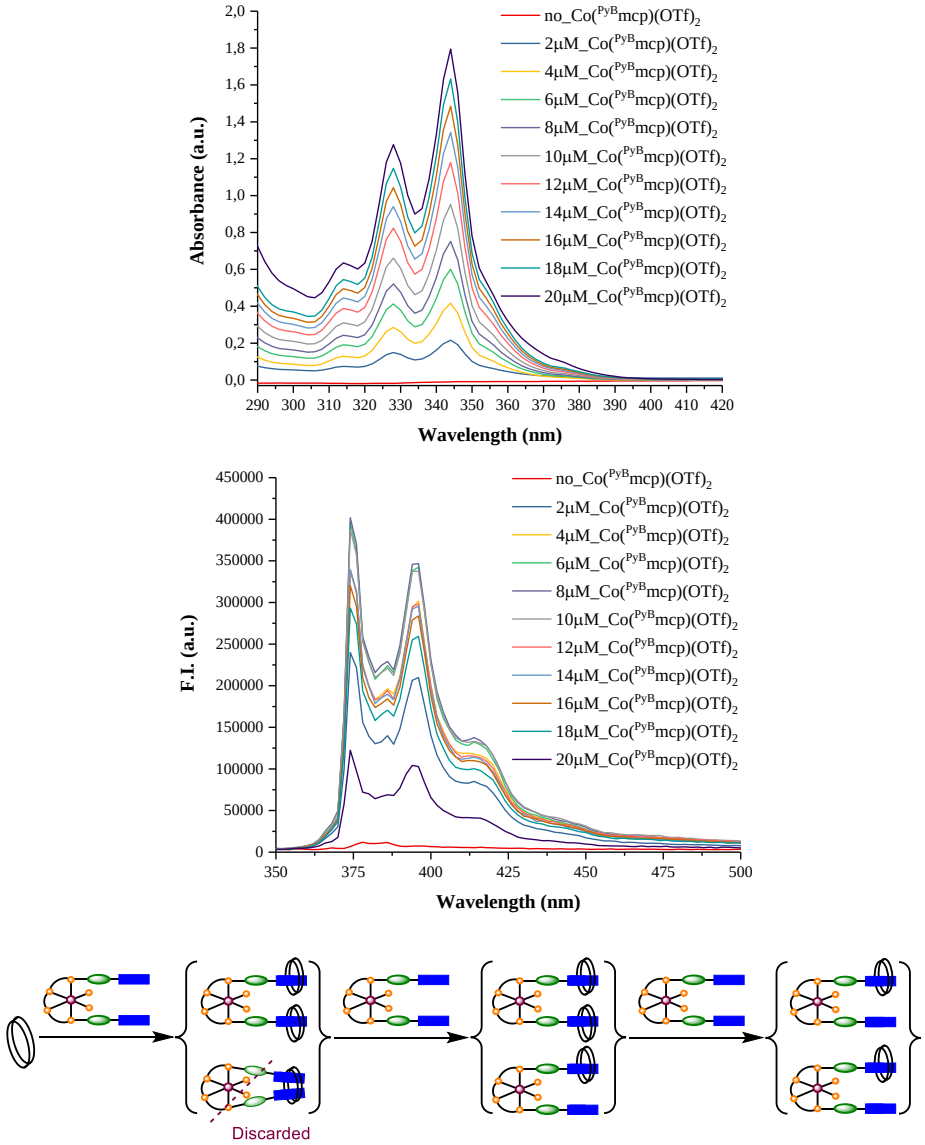

Figure IV. 12 *Titration of Co(PyBmcp)(OTf)2 into solution of γ-cyclodextrin measured by absorption (top) and emission (middle) spectra in water/acetonitrile (6:4 mL) mixture. (Bottom) Schematic model of the potential interactions between the pyrenes of the catalyst and the γ-CD cavity and the evolution during the titration process.*

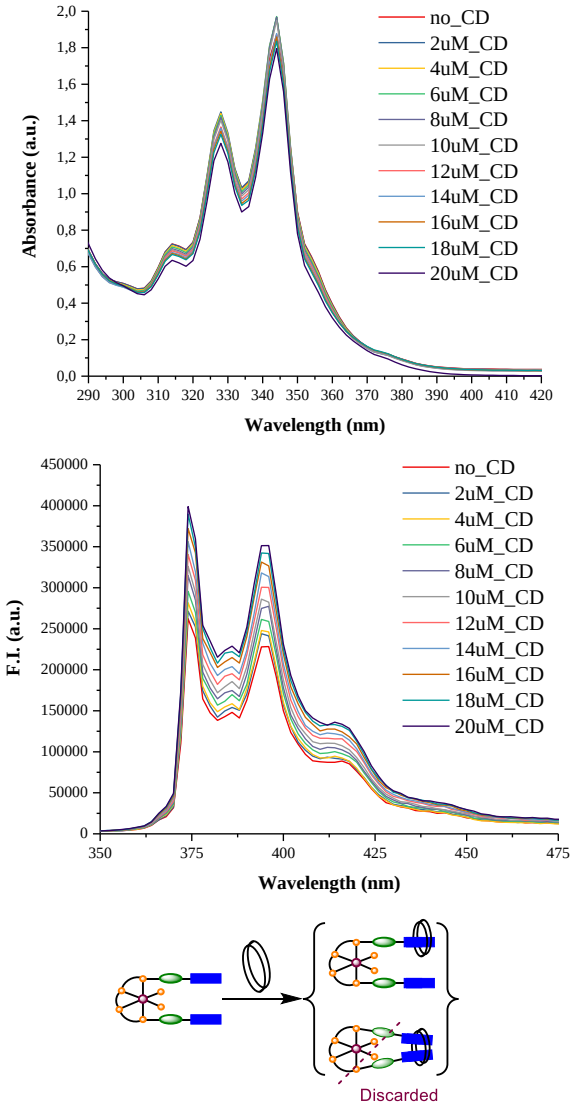

Figure IV. 13 *Titration of γ-cyclodextrin into solution of Co(^{PyB}mcp)(OTf)$_2$ measured by absorption (top) and emission (middle) spectra in water/acetonitrile (6:4 mL) mixture. (Bottom) Schematic model of the potential interactions between the pyrenes of the catalyst and the γ-CD cavity.*

Complexes, Co(^{PyB}pdp)$(OTf)_2$, Ni(^{PyB}mcp)$(OTf)_2$ and Ni(^{PyB}pdp)$(OTf)_2$ behave similar (Figures in the appendix of the chapter IV.4.4 Figure IVa.1 – IVa.6). To note is the appreciable larger increase in the emission intensity for the ^{PyB}pdp complexes than the ^{PyB}mcp in titration of M(^{PyB}mcp)$(OTf)_2$ (M = Co or Ni) with the γ-cyclodextrin, which could be an indication of a stronger association.

The Job plots of the absorption spectra obtained from the titration of metal complex (20 μM) with the γ-CD (20mM) are shown in Figure IV.14. Job plot interpretation should be proceeded ver carefully on account of the complex supermolecular interactions, like the one found here. [411] Nevertheless, the maximums in all the analyzed catalysts were near 0.5, which indicates mainly 1:1 model from the 0 to 0.5 molar ratio.

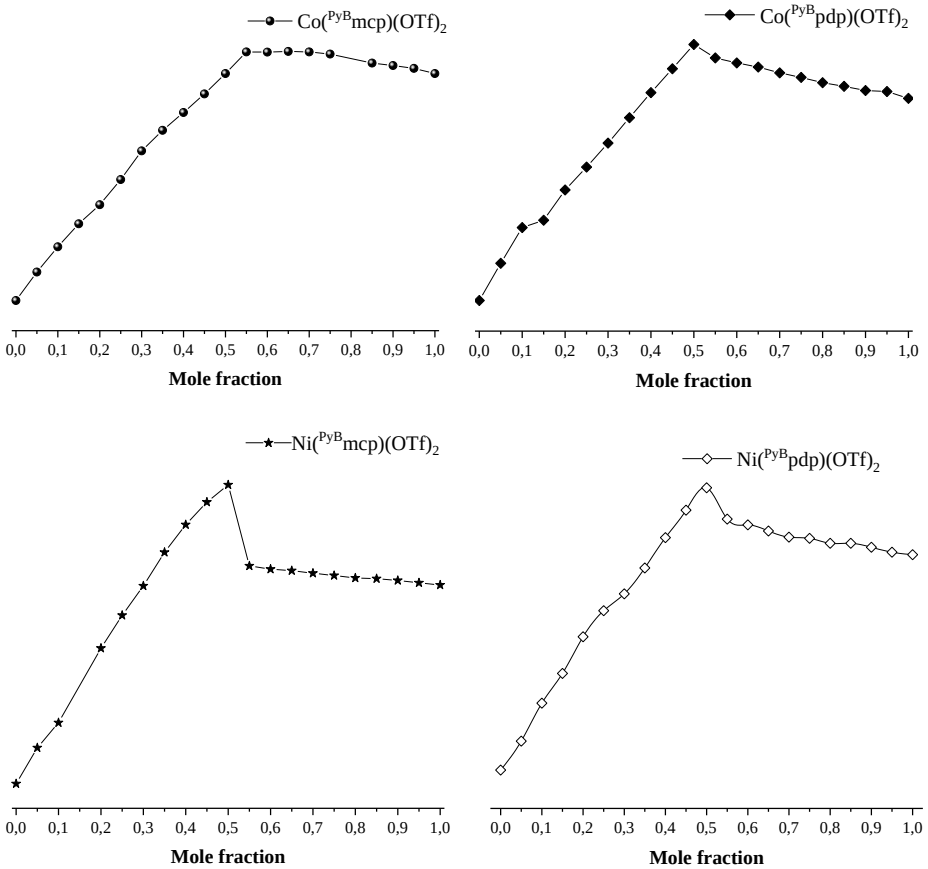

Figure IV. 14 *Job plots for Co(^{PyB}mcp)$(OTf)_2$, Co(^{PyB}mcp)$(OTf)_2$, Ni(^{PyB}mcp)$(OTf)_2$ and Ni(^{PyB}mcp)$(OTf)_2$ with γ-cyclodextrin for 10 titrations. Mole fraction of γ-cyclodextrin.*

We performed experiments at highest possible concentration on account of other pyrene and γ-cyclodextrin interaction ratios including multiple interactions between host and guest molecules, but also the potential coordination of the alcohol units of the γ-CD to the metal center. Therefore, the the metal complexes (20 μM) will be titrated from 1 to 20 mM of γ-CD.

The Co(^{PyB}mcp)$(OTf)_2$ (20 μM) titration with a concentrated solution of γ-cyclodextrin with increments of 1mM caused a small decrease of the peaks in absorbance spectra with a concomitant increasing of the baseline, suggesting an interactions between host and guest molecule (Figure IV.15). The encapsulation effect was clearer in the fluorescence spectra, indicated by the increase in the intensity. Interestingly there is a change in the shape of the spectra as well, a new peak appears at 380 nm.

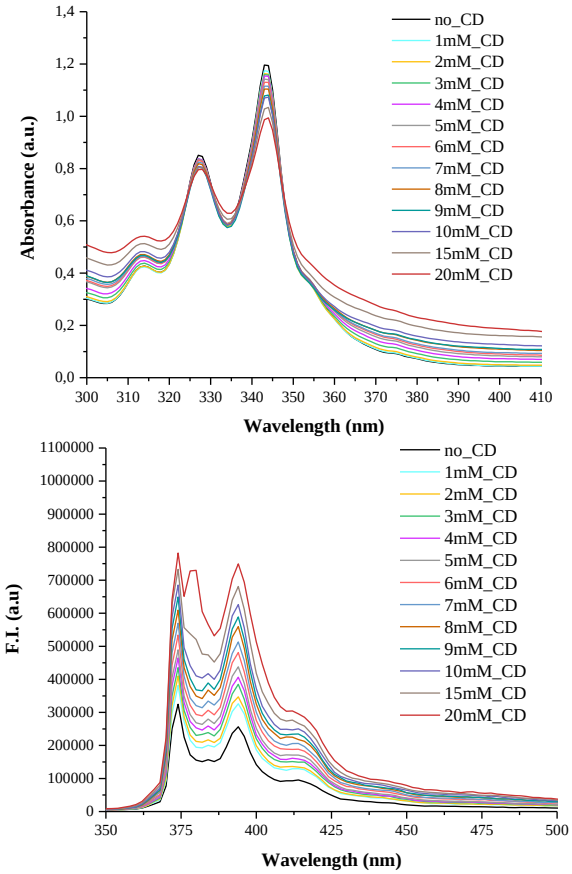

Figure IV. 15 *Titration of Co(^{PyB}mcp)(OTf)$_2$ (20 μM) with concentrated solution of γ-cyclodextrin measured by absorption (top) and emission (bottom) spectroscopy in water/acetonitrile (6:4 mL) mixture.*

When Co(^{PyB}pdp)(OTf)$_2$ was titrated under the same conditions, the absorption spectra revealed the same behavior, and fluorescence spectra became more intense with addition of host molecules, but this time spectra did not change its shape. This is once again, could be interpreted as the host acting as a quenching protector and a guest molecule (Figure IV.16).

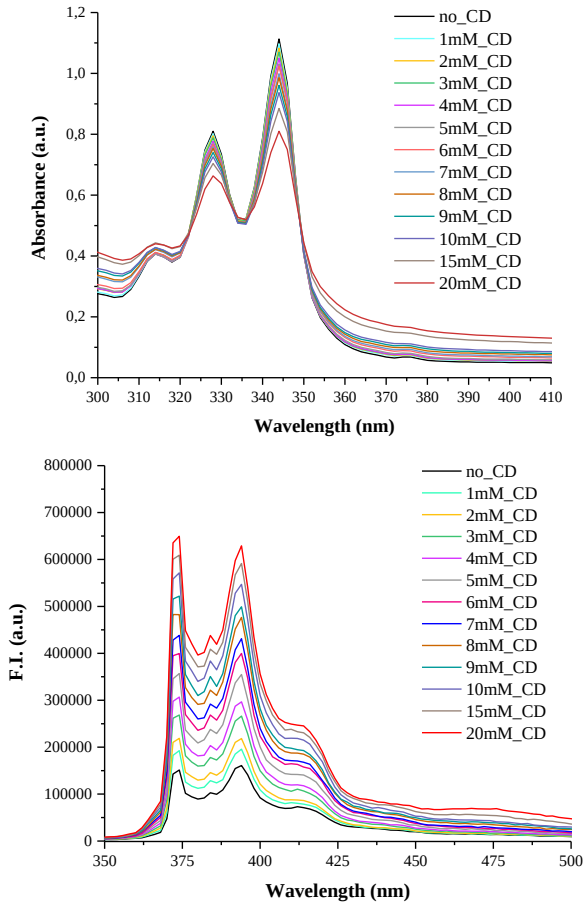

Figure IV. 16 *Titration of concentrated solution of γ-cyclodextrin into solution Co(^{PyB}pdp)(OTf)$_2$ measured by absorption (top) and emission (bottom) spectroscopy in water/acetonitrile (6:4 mL) mixture.*

Later, concentrated solution of γ-cyclodextrin was titrated into 20 μM solution of Ni(^{PyB}mcp)(OTf)$_2$. The obtained results also showed interaction between

molecules by slight drop in absorption intensity and growth in fluorescence as in previous cases (Figure IV.17).

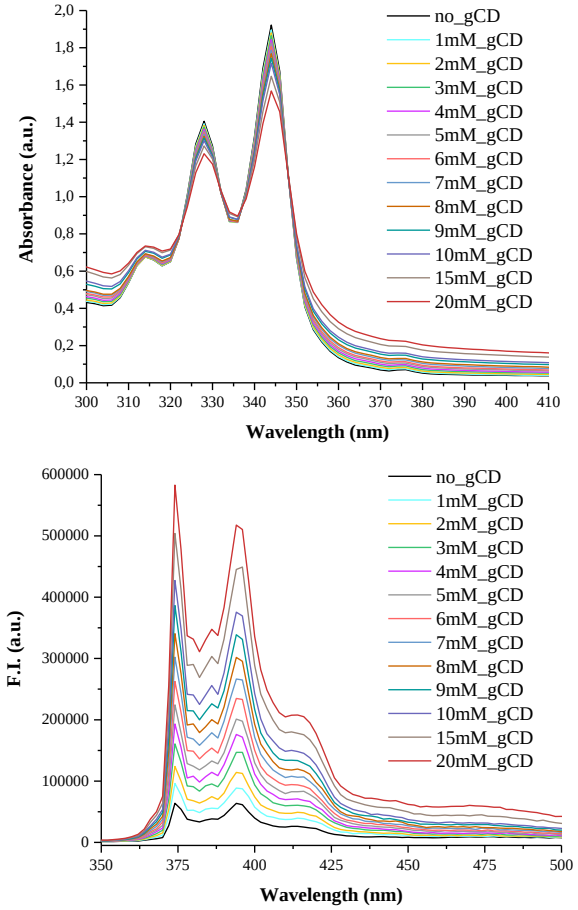

Figure IV. 17 *Titration of concentrated solution of γ-cyclodextrin into solution Ni(^{PyB}mcp)(OTf)$_2$ measured by absorption (top) and emission (bottom) spectroscopy in water/acetonitrile (6:4 mL) mixture.*

Our curiosity led us to perform the reverse experiment. To a solution of γ-cyclodextrin (20 mM), aliquots of Ni(^{PyB}mcp)(OTf)$_2$ were added (with increments of 2 μM) and absorption and emission spectra were measured (Figure IV.18). A progressive increase in absorbance intensity was observed because of increasing the catalyst's concentration (higher amount of pyrene unit). In the fluorescence spectrum another confirmation of pyrene encapsulation into γ-CD was the rise of the intensity of peaks in fluorescence

spectrum until the concentration of Ni(^{PyB}mcp)(OTf)$_2$ reached 8 μM, then reaching a plateau. Although it indicates a compensation of the emission due to potential dissociation as interpreted in the previous experiments, other interpretation should be also considered since the concentration of γ-CD is now 1000-fold higher. Titrations performed for complex Ni(^{PyB}pdp)(OTf)$_2$ (20 μM) with γ-cyclodextrin behaved in similar way to Ni(^{PyB}mcp)(OTf)$_2$ (Figures in the appendix of the chapter IV.4 Figure IVa.7 – IVa.8).

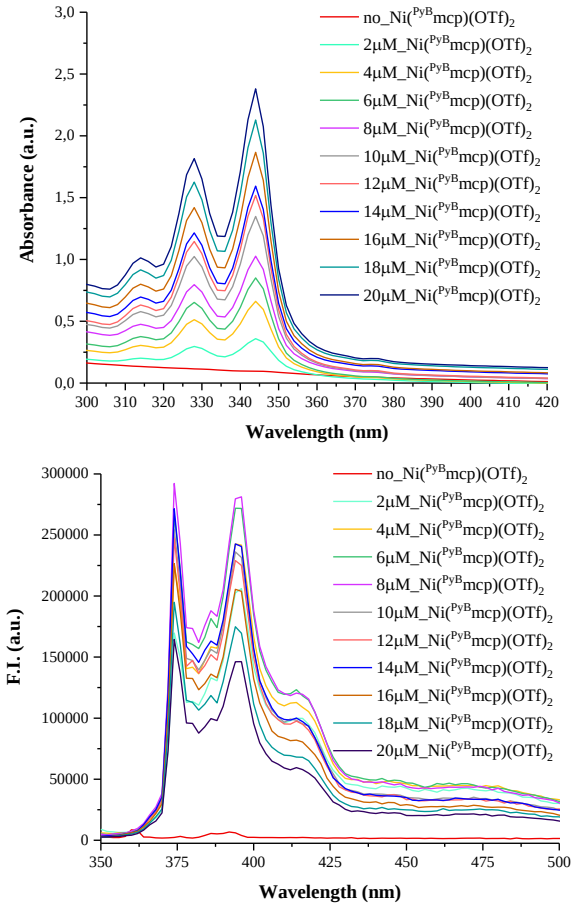

Figure IV. 18 *Titration of Ni(^{PyB}mcp)(OTf)$_2$ solution into concentrated solution of γ-cyclodextrin measured by absorption (top) and emission (bottom) spectroscopy in water/acetonitrile (6:4 mL) mixture.*

To get more information about the interaction between Co(^{PyB}mcp)(OTf)$_2$, Co(^{PyB}pdp)(OTf)$_2$, Ni(^{PyB}mcp)(OTf)$_2$, Ni(^{PyB}pdp)(OTf)$_2$ with γ-CD, ^{1}H NMR spectroscopy was used. All stock solutions of complexes were prepared in the

glovebox with degassed deuterated acetonitrile and solution of γ-CD was prepared in the crimped vial with deuterated water using Schlenk technique under nitrogen atmosphere.

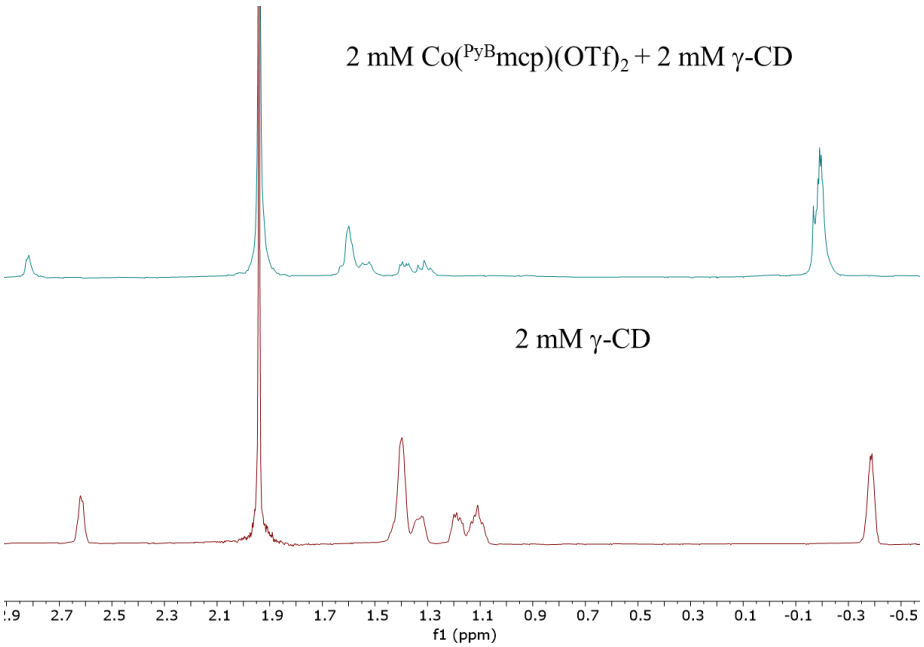

Figure IV. 19 *Diamagnetic ^{1}H NMR spectra of 2 mM of Co(^{PyB}mcp)(OTf)$_2$ and 2 mM of γ-CD (top) and 2 mM of γ-CD in deuterated water and deuterated acetonitrile mixture (1:1).*

Then, the NMR tubes were prepared under nitrogen atmosphere with the final concentration 2mM of catalyst and 2mM of γ-CD in acetonitrile water mixture (1:1). Diamagnetic ^{1}H NMR of Co(^{PyB}mcp)(OTf)$_2$ with γ-CD compared to ^{1}H NMR of only γ-CD, appeared to be deshielded because of the interactions between these two species (Figure IV.19). Paramagnetic ^{1}H NMR (Figure IV.20) disclosed small shifts of the peaks due to the π-stacking interactions supporting the formation of the host-guest complex.

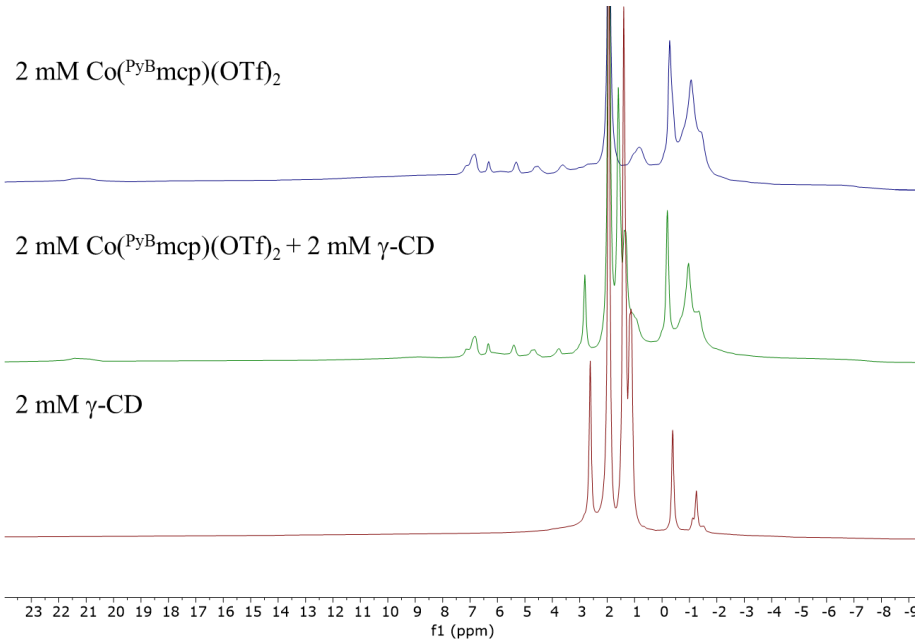

Figure IV. 20 *Paramagnetic ^{1}H NMR spectra of 2 mM of Co(^{PyB}mcp)(OTf)$_2$, 2 mM of Co(^{PyB}mcp)(OTf)$_2$ with 2 mM of γ-CD (top) and 2 mM of γ-CD in deuterated water and deuterated acetonitrile mixture (1:1).*

Changes in the chemical shifts in the diamagnetic NMR spectra of Co(^{PyB}pdp)(OTf)$_2$ in the presence of γ-CD were observed (IV.21). Upon the addition of host molecules to catalyst, its peaks got shifted and broader than with absence of catalyst. Analysis of the paramagnetic NMR also concerned the interaction of γ-CD with guest molecules (Figure IV.22). However, the peaks in the paramagnetic NMR are only slightly shifted to the downfield. This results, agree with the host-guest interactions between γ-cyclodextrins and Co(^{PyB}pdp)(OTf)$_2$ in water acetonitrile mixture (1:1).

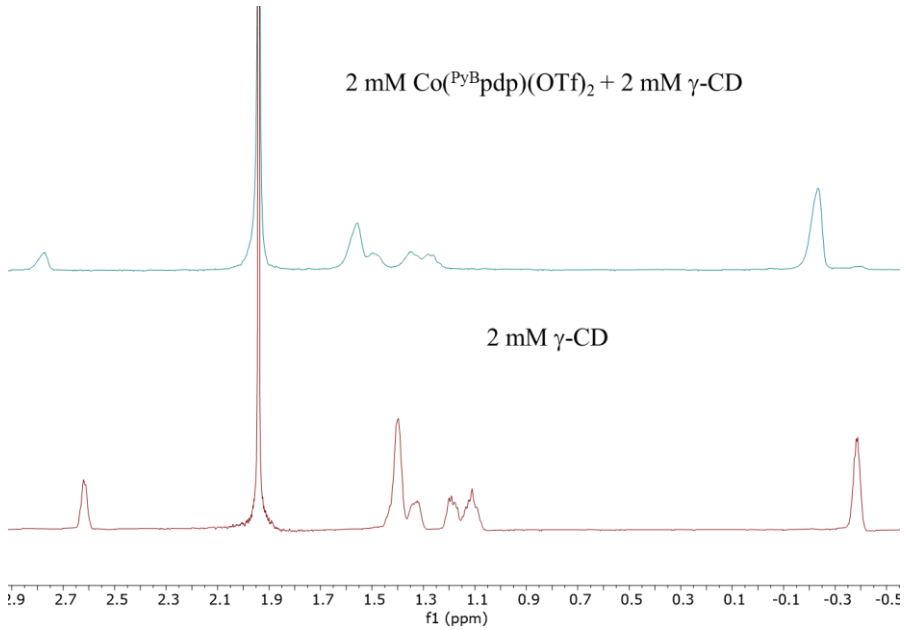

Figure IV. 21 *Diamagnetic ^{1}H NMR spectra of 2 mM of Co(^{PyB}pdp)(OTf)$_2$ and 2 mM of γ-CD (top) and 2 mM of γ-CD in deuterated water and deuterated acetonitrile mixture (1:1).*

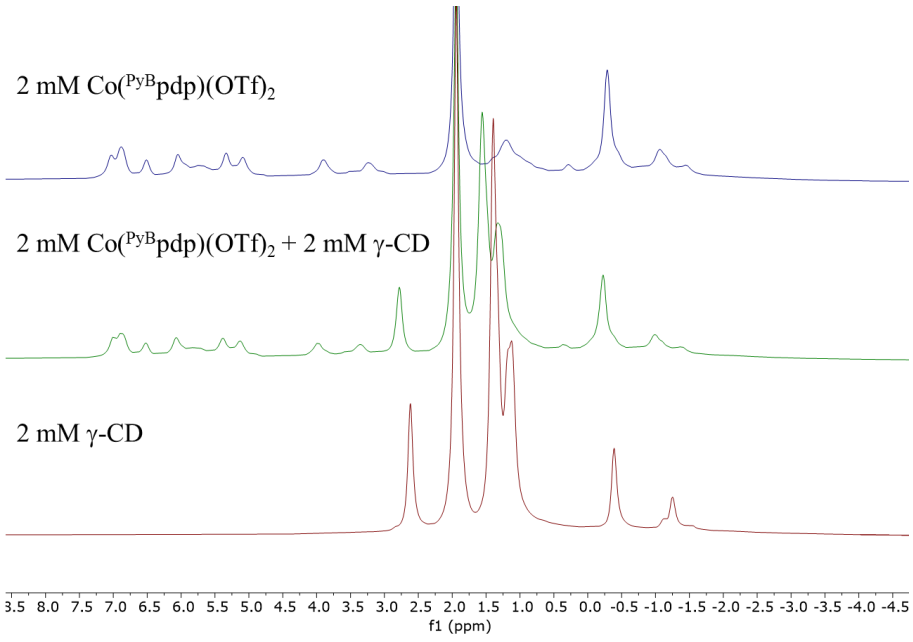

Figure IV. 22 *Paramagnetic ^{1}H NMR spectra of 2 mM of Co(^{PyB}pdp)(OTf)$_2$, Co(^{PyB}pdp)(OTf)$_2$ with 2 mM of γ-CD (top) and 2 mM of γ-CD in deuterated water and deuterated acetonitrile mixture (1:1).*

Nickel anchoring complexes containing pyrene were also analyzed by NMR spectroscopy. Peaks in diamagnetic region of γ-CD became sharper and shifted to downfield while in solution together with Ni(^{PyB}mcp)(OTf)$_2$ (Figure IV.23). This slight shift is a confirmation of encapsulation of pyrene inside the hydrophobic cavity of the host. Small shifts were also observed in paramagnetic spectra of analyzed complex (Figure IV.24). Peak at 2.7 ppm (γ-CD) is shifted slightly to higher ppms, however peaks coming from pyrene at 5.5 and 5.9 ppm are shifted upfield.

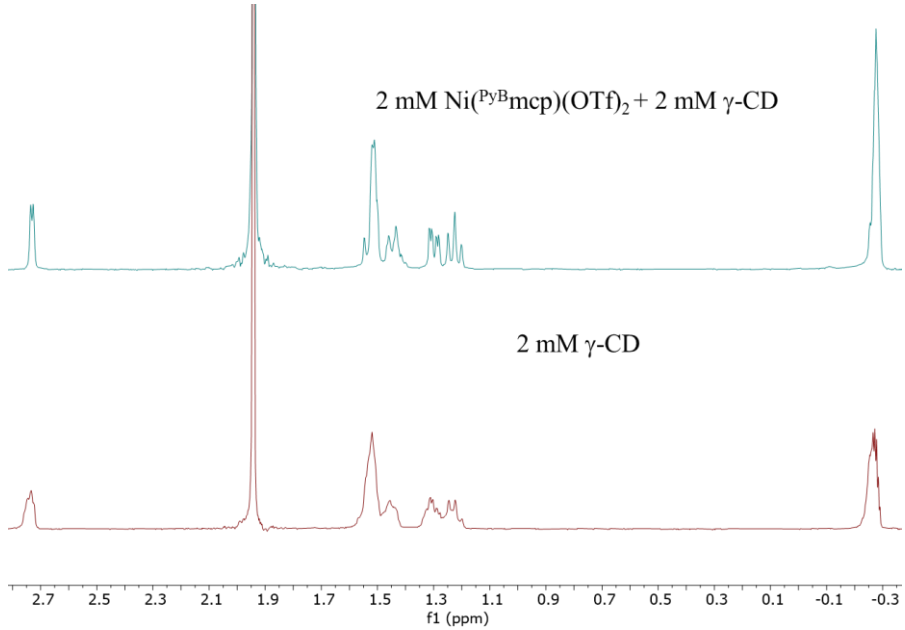

Figure IV. 23 *Diamagnetic ^{1}H NMR spectra of 2 mM of Ni(^{PyB}mcp)(OTf)$_2$ with 2 mM of γ-CD (top) and 2 mM of γ-CD in deuterated water and deuterated acetonitrile mixture (1:1).*

Similar response of system was observed in case of host-guest interaction between Ni(^{PyB}pdp)(OTf)$_2$ and γ-cyclodextrins. Upon addition of nickel catalyst into the solution of γ-cyclodextrins, the peaks in the diamagnetic spectra belonging to the macrocyclic ring of glucose subunits were sharper and also shifted downfield (Figure IV.25). Moreover the peaks in the paramagnetic spectra revealed the shift of the host-guest complex mixture to be deshielded, both peaks of cyclodextrins likewise Ni(^{PyB}pdp)(OTf)$_2$ (Figure IV.26. Obtained results in the NMR spectroscopy shows that the cobalt complexes induces

major downfield shift comparing to nickel complexes, which confirms that Co(^{PyB}mcp)$(OTf)_2$, Co(^{PyB}pdp)$(OTf)_2$ penetrate more deeply into the cavity of γ-CD and create stronger complexes than Ni(^{PyB}mcp)$(OTf)_2$ and Ni(^{PyB}pdp)$(OTf)_2$.

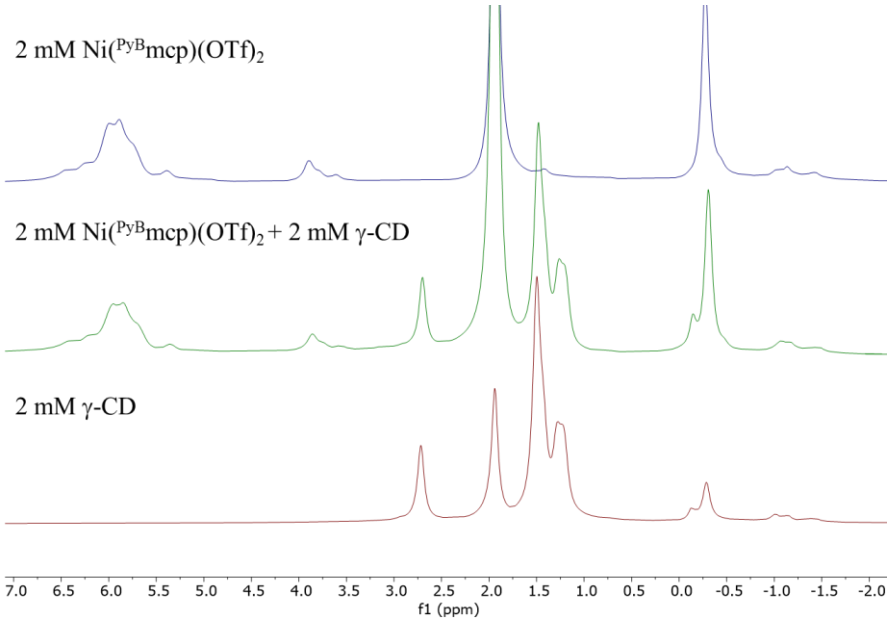

Figure IV. 24 *Paramagnetic ^{1}H NMR spectra of 2 mM of Ni(^{PyB}mcp)$(OTf)_2$, Ni(^{PyB}mcp)$(OTf)_2$ with 2 mM of γ-CD (top) and 2 mM of γ-CD in deuterated water and deuterated acetonitrile mixture (1:1).*

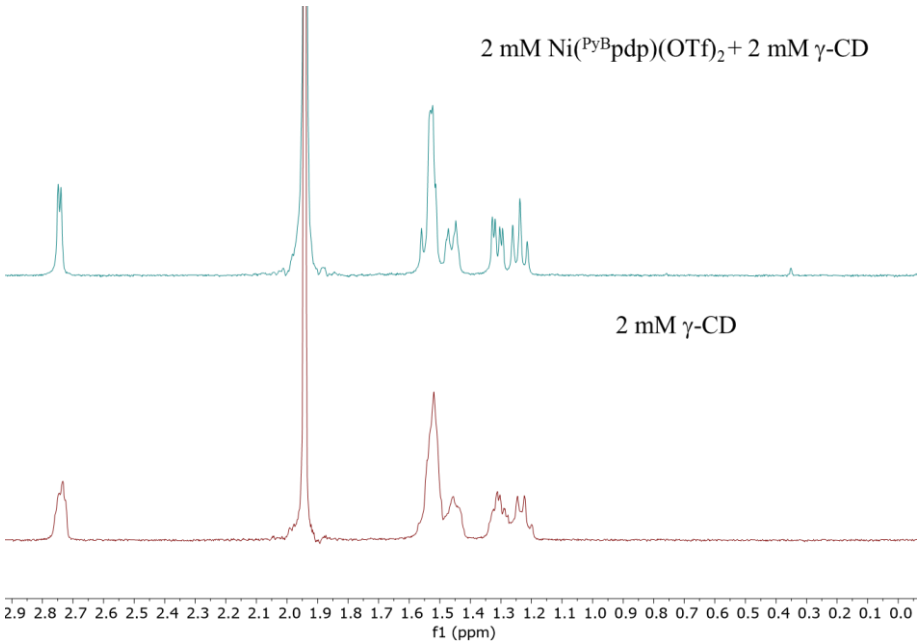

Figure IV. 25 *Diamagnetic ^{1}H NMR spectra of 2 mM of Ni(^{PyB}pdp)(OTf)$_2$ with 2 mM of γ-CD (top) and 2 mM of γ-CD in deuterated water and deuterated acetonitrile mixture (1:1).*

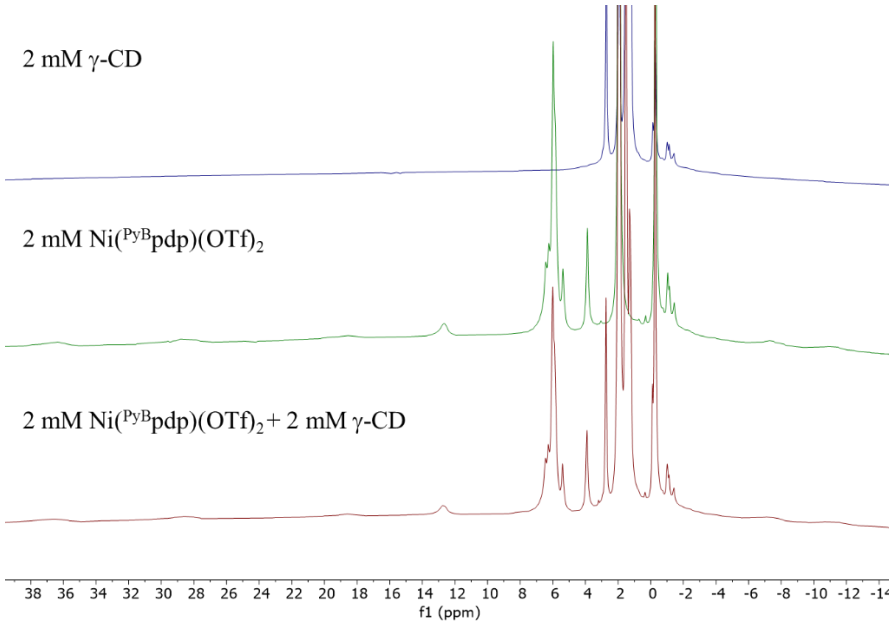

Figure IV. 26 *Paramagnetic ^{1}H NMR spectra of 2 mM of Ni(^{PyB}pdp)(OTf)$_2$, Ni(^{PyB}mcp)(OTf)$_2$ with 2 mM of γ-CD (top) and 2 mM of γ-CD in deuterated water and deuterated acetonitrile mixture (1:1).*

These data confirmed that under used conditions i.e. water/acetonitrile mixture (6:4) and (1:1) encapsulation of catalysts, precisely pyrene unit into γ-cyclodextrins occurs. Nonetheless, formation of pyrene excimer was not detected in applied system. As stated before, our goal was to arrange the chiral cavity of catalyst by anchoring it to nanomaterials or encapsulating into γ-cyclodextrins which involves forming stable excimers. Implementation of different conditions are required to form stable excimer inside the cavity, which will be applied and studied in detail in next sections.

IV.2.3.2 Encapsulation in water solution

We became interested in gaining a deeper understanding of the differences in encapsulation of PAH into cavity of γ-CD while using more polar solvent and if possible the excimer formation inside the γ-CD cavity.

For this purpose, the characterization was performed by the titration of complexes ($Co(^{PyB}mcp)(OTf)_2$ (Figure IV.27), $Co(^{PyB}pdp)(OTf)_2$, $Ni(^{PyB}mcp)(OTf)_2$, $Ni(^{PyB}pdp)(OTf)_2$ and $Co(^{PerB}mcp)(OTf)_2$) by absorption and emission spectroscopy in water (Appendix of the chapter Figure IVa.9 – IVa.12). In water the reinforcements of the non-covalent interactions between polyaromatic moieties because of the hydrophobic nature of π-interactions, revealed the excimer formation in a region 430 – 600 nm for pyrene based complexes and 490 – 700 nm for perylene based complex.[412] We observed new bands by titration of cobalt and nickel complexes with γ-cyclodextrins in water. These interesting results show that complexes with N,N′-dimethyl-1,2-cyclohexanediamine as a backbone are more prone to form excimers than complexes based on 2,2′-bipyrrolidine.

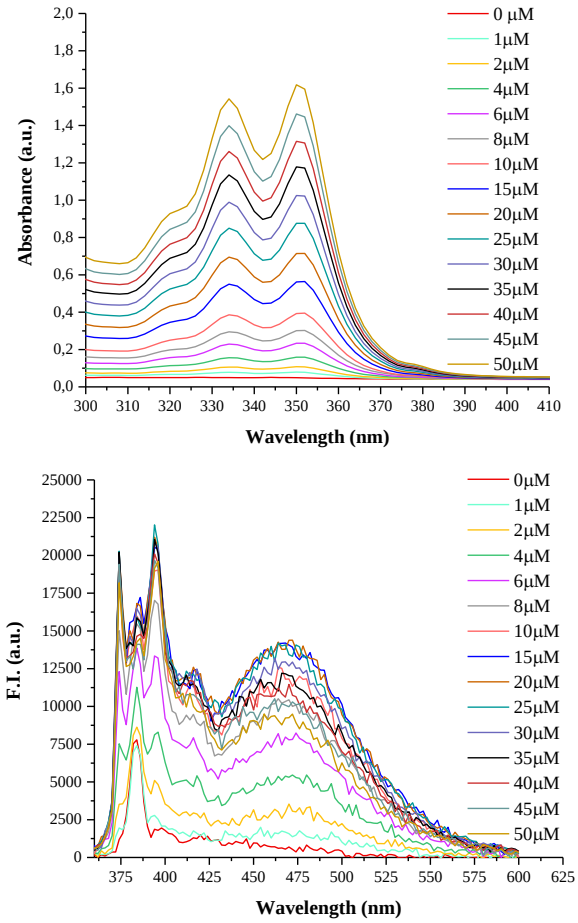

Figure IV. 27 *Absorption (top) and emission (bottom) spectra of Co(^{PyB}mcp)(OTf)$_2$ at different concentrations in water.*

The titration of Co(^{PyB}mcp)(OTf)$_2$ (20 µM) with γ-CD (2 µM increments) was performed in water (Figure IV.28) and revealed the formation of both, the monomer and excimer as it was observed before, but with some differences. The monomer species (360 – 420 nm) grown with the addition of γ-CD, while excimer is maintained, showing the same intensity of pyrene excimer (420 – 550 nm) (Figure IV.28 (bottom)). Therefore, the excimer is γ-CD independent and should occur externally. Encapsulation is mainly happening with a single pyrene unit, therefore increasing the monomer emission.

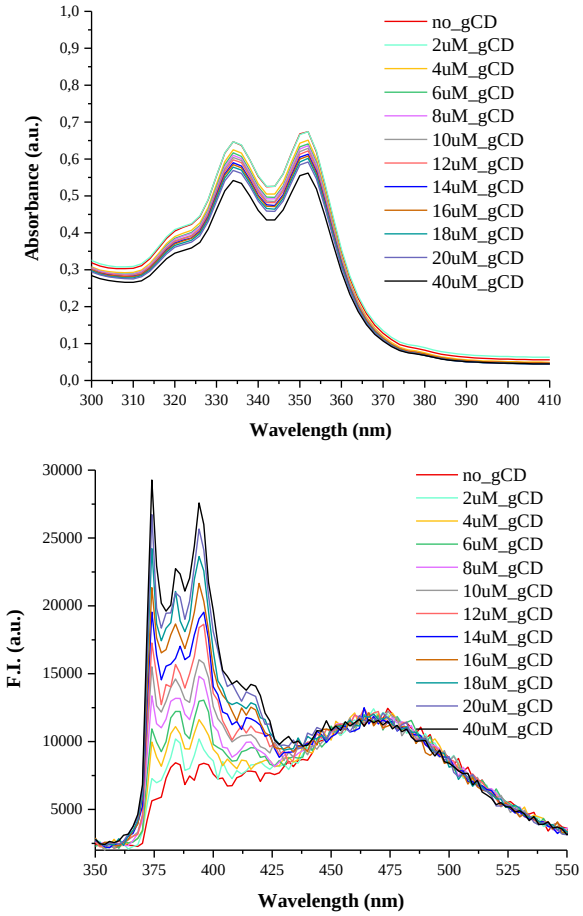

Figure IV. 28 *Titration of γ-cyclodextrin into solution of Co(^{PyB}pdp)(OTf)$_2$ measured by absorption (top) and emission (bottom) spectroscopy in water solution.*

To get further insights into the nature of the inclusion complexes and to understand if the excimer can be formed inside the γ-CD cavity, we titrated complexes with higher host concentrations (Co(^{PyB}mcp)(OTf)$_2$ - Figure IV.29 and Co(^{PyB}pdp)(OTf)$_2$, Ni(^{PyB}mcp)(OTf)$_2$, Ni(^{PyB}pdp)(OTf)$_2$ - Figures in appendix of the chapter - Figure IVa.13 – IVa.15). Interestingly, at higher γ-CD concentrations, Co(^{PyB}mcp)(OTf)$_2$ showed a fluorescence increase in both the monomer and excimer. . This results suggest that the encapsulation of the excimer could occur.

Co(^{PerB}mcp)(OTf)$_2$ under applied conditions showed increase in the fluorescence intensity in the region of perylene monomer (425 – 490 nm) and

insignificant changes in excimer region (500 – 650 nm) (Figure IV.30). This specifies that catalyst containing perylene moiety forms inclusion complex with perylene and cyclodextrine ring in ratio 1:1. However, additional experiments of titration solution of catalysts with higher concentrations of γ-CD were performed to comprehend forming of host – guest interactions.

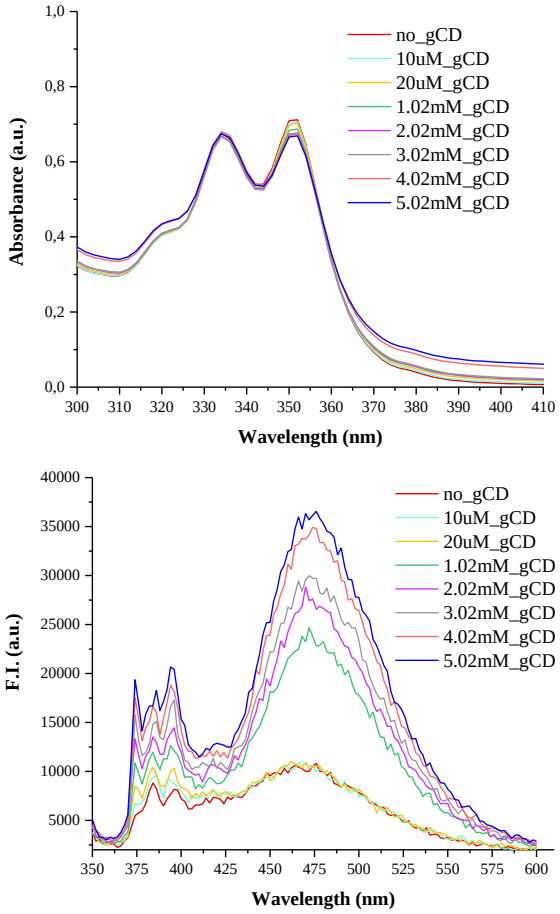

Figure IV. 29 *Absorption (top) and emission (bottom) spectra after addition of aliquots of γ-CD into 20 μM solution of* $Co(^{PyB}mcp)(OTf)_2$.

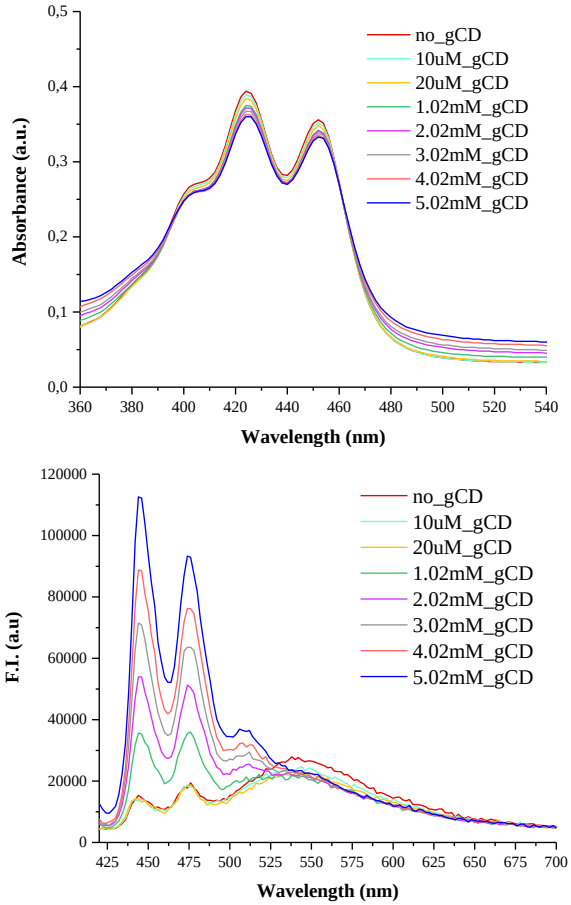

Figure IV. 30 *Absorption (top) and emission (bottom) spectra after addition of aliquots of γ-CD into 20 μM solution of Co(^{PerB}mcp)(OTf)$_2$*

At even higher solutions of the γ-CD for Co(^{PyB}mcp)(OTf)$_2$ the absorption spectrum revealed only insignificant changes after addition of host molecules in the peak at 335 nm probably due to the increased polarity of solvent,[410] however at the concentration higher than 5 mM of γ-CD, the excimer intensity in the fluorescence spectra stabilizes up to 20 mM (Figure IV.31). At the same time, monomer intensity significantly increased, indicating further formation of 1:1 inclusion complex. This could be interpreted as all formed excimers by the π–π stacking interactions of pyrene are included as guest in the γ-CD, and no more are formed by the extra addition of γ-CD. Therefore, the excimer should form before the interaction with the γ-CD.

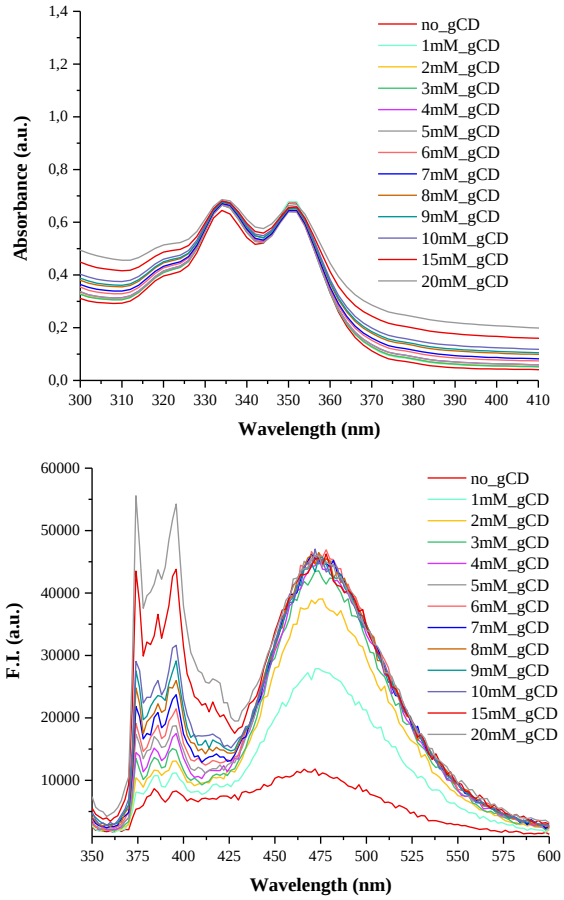

Figure IV. 31 *Titration of concentrated solution of γ-cyclodextrin into solution Co(^{PyB}mcp)(OTf)$_2$ measured by absorption (top) and emission (bottom) spectroscopy in water.*

For the titration of Co(^{PyB}pdp)(OTf)$_2$ solution, concentrated aliquots of γ-CD were added and solutions were measured by spectroscopic methods (Figure IV.32). This experiment also displayed only small changes in absorption spectra of the analyzed complex formation. Gentle increase of fluorescence intensity was detected while solution of γ-CD was added. However, after the concentration of cyclodextrins passed 10mM, intensity of monomer and excimer band in fluorescence spectra stayed unchanged. The propotion of monomer to excimer in cobalt complexes differentiate. In case of Co(^{PyB}mcp)(OTf)$_2$ intensity of excimer with reference to monomer is higher than in Co(^{PyB}pdp)(OTf)$_2$.

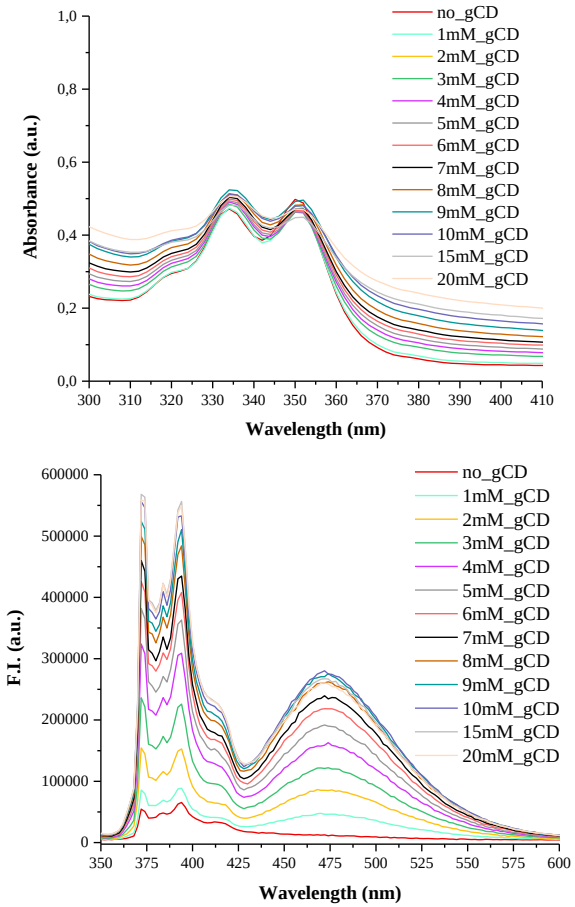

Figure IV. 32 *Titration of concentrated solution of γ-cyclodextrin into solution Co(^{PyB}pdp)(OTf)$_2$ measured by absorption (top) and emission (bottom) spectroscopy in water.*

The titration performed for Ni(^{PyB}mcp)(OTf)$_2$ showed small changes in absorbance spectrum due to the interaction with γ-cyclodextrins together with increase of polarity of the solvent (Figure IV.33). Formation of excimer inside the cavity was confirmed by emission spectra by sizable growth of intensity between 430 and 575 nm. Excimer band intensity with high concentration of host in the solution (15mM – 20mM) started decreasing. This interesting result, could be explained as a release of one of arm of the ligand from the cavity, excimer diminish due to the presence only of one pyrene arms of ligand inside the cavity of γ-CD.

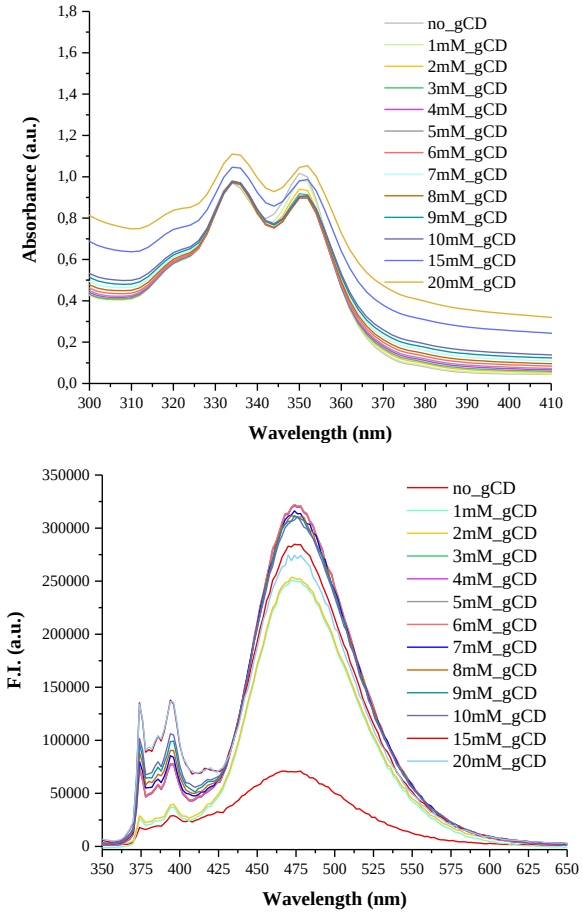

Figure IV. 33 *Titration of concentrated solution of γ-cyclodextrin into solution Ni(^{PyB}mcp)(OTf)$_2$ measured by absorption (top) and emission (bottom) spectroscopy in water.*

The 20 mM solution of Ni(^{PyB}pdp)(OTf)$_2$ prepared in the cuvette was titrated as mentioned above. Changes in absorbance spectra were very similar to the ones observed in Ni(^{PyB}mcp)(OTf)$_2$. The fluorescence intensity of monomer and excimer band increase with addition of host molecules and as also observed before, when the concentration of γ-CD extend 10mM, intensity of dimer in the excited state drops (Figure IV.34).

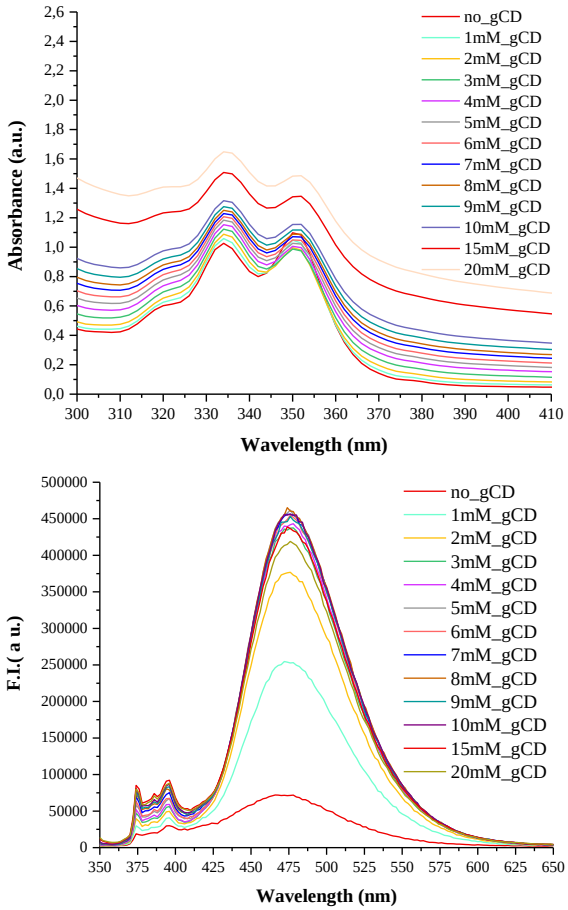

Figure IV. 34 *Titration of concentrated solution of γ-cyclodextrin into solution Ni(^{PyB}pdp)(OTf)$_2$ measured by absorption (top) and emission (bottom) spectroscopy in water.*

The last but not least performed experiment of complexes in water was titration of Co(^{PerB}mcp)(OTf)$_2$ measured by absorption and emission spectroscopy (See Figure IV.35). Absorption spectra did not differ from the previous ones, however, fluorescence analysis did not show any formation of excimer under applied conditions. This result confirms that only one unit of perylene forms inclusion complex with one unit of γ-cyclodextrins. Perylene is structurally close to pyrene and have high fluorescence quantum yield, but there are only a few reports for their excimer emissions in solutions.[413] This difference is most likely to emerge from the extremely short fluorescence lifetime of perylene. Thus, the excited perylene is too short-lived to encounter with another, mostly that of the ground state.[414] Another reason is that larger polycyclic aromatic

hydrocarbins than pyrene have been shown to form 1:2 complexes in aqueous solutions with γ-cyclodextrines but they are too small to accommodate two perylene units inside the cavity.[415]

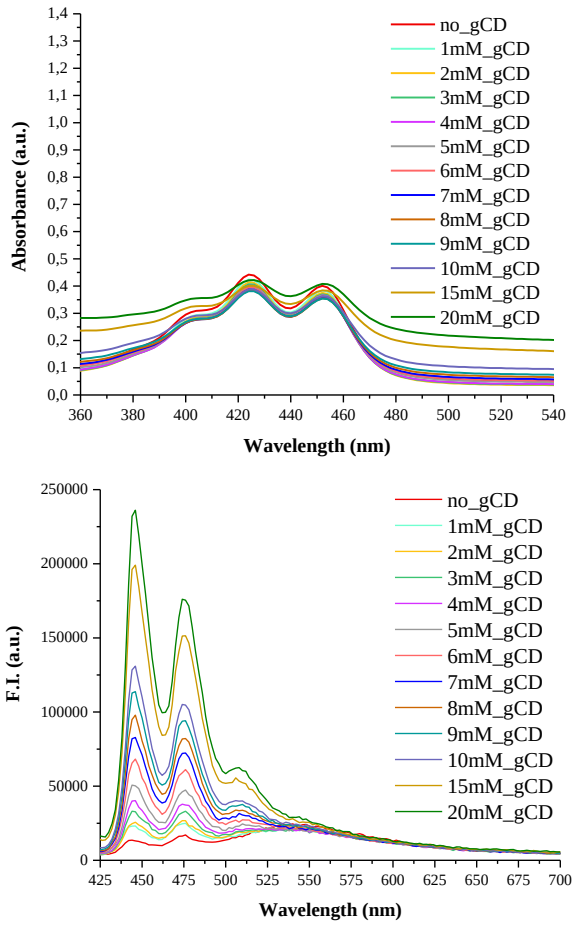

Figure IV. 35 *Titration of concentrated solution of γ-cyclodextrin into solution* $Co(^{PerB}mcp)(OTf)_2$ *measured by absorption (top) and emission (bottom) spectroscopy in water.*

In summary the dynamics of the γ-CD – pyrene is complex, and therefore, the formation of adducts although it is clear, a precise description of the interactions at this point is not possible, but could be propose several possible interactions (Scheme IV.8).

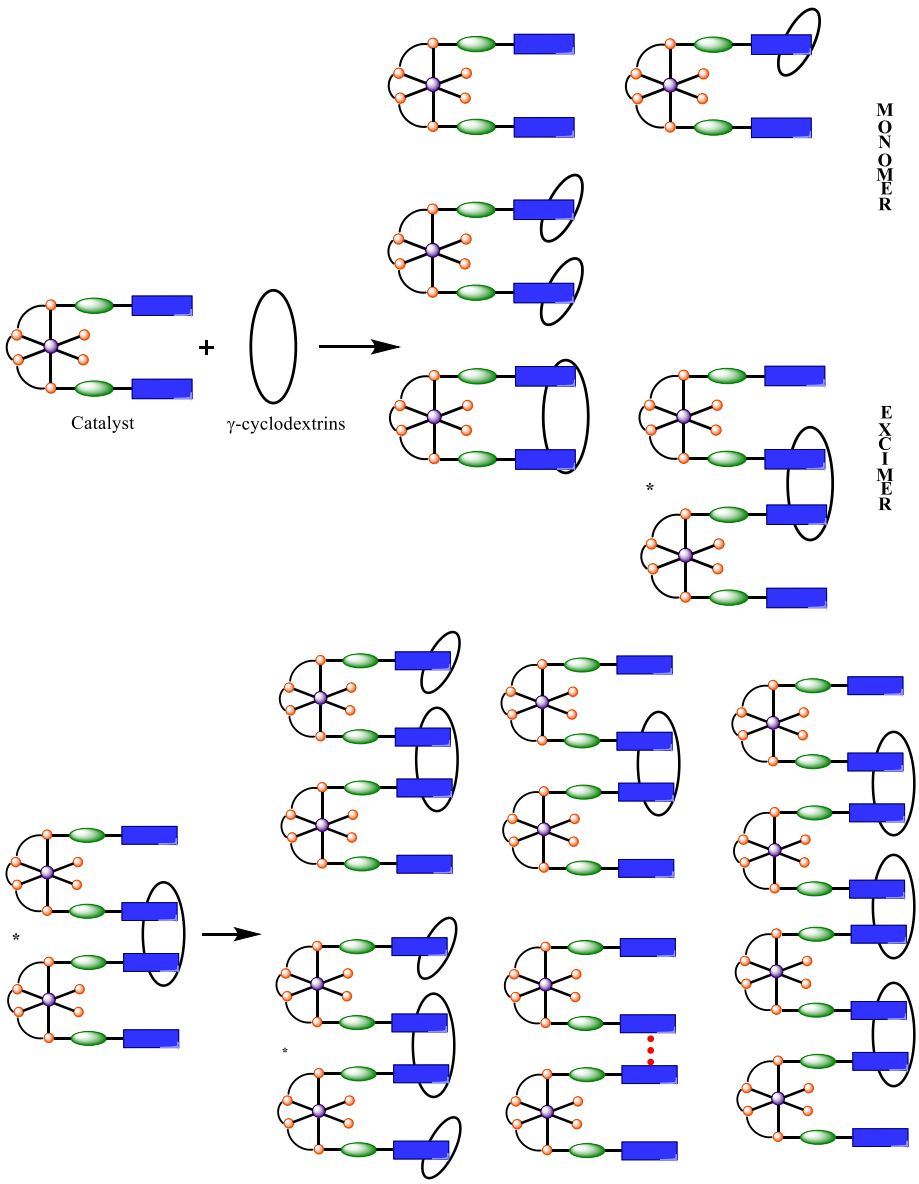

Scheme IV. 8 *Possible interactions between catalyst and γ-cyclodextrins.*

*IV.2.3.3 Encapsulation of **1c** protected precursor.*

To get better understanding of the formation of host-guest molecules between γ-cyclodextrines and synthetized Ni^{II} and Co^{II} complexes, experiments with the ligand precursor pyren-1-ylmethyl 3-(6-(((tert-butyldimethylsilyl)oxy)methyl)pyridin-3-yl)benzoate (**1c**) were carried out. In previous studies, **1c** (Figure IV.1) revealed only monomer species in

acetonitrile. Encapsulation studies were performed in more polar solvents like water/acetonitrile mixture or water itself to disclose the conduct of one arm of ligand in the solution and possibility of forming inclusion complex with certain ratio of host-guest molecules.

20 μM solution of **1c** in water/acetonitrile (6:4 ratio, 2 mL) mixture under nitrogen atmosphere was prepared and titrated by adding aliquots of the host molecules to the solution of a guest. Aliquots of γ-CD were added with 2 μM increments of the host (Figure IV.36). The absorption spectrum slightly decreased, while the emission was dominated by the pyrene excimer (420 -590 nm) and increased with the γ-CD due to the insertion of two pyrene units of **1c** into one γ-CD molecule.

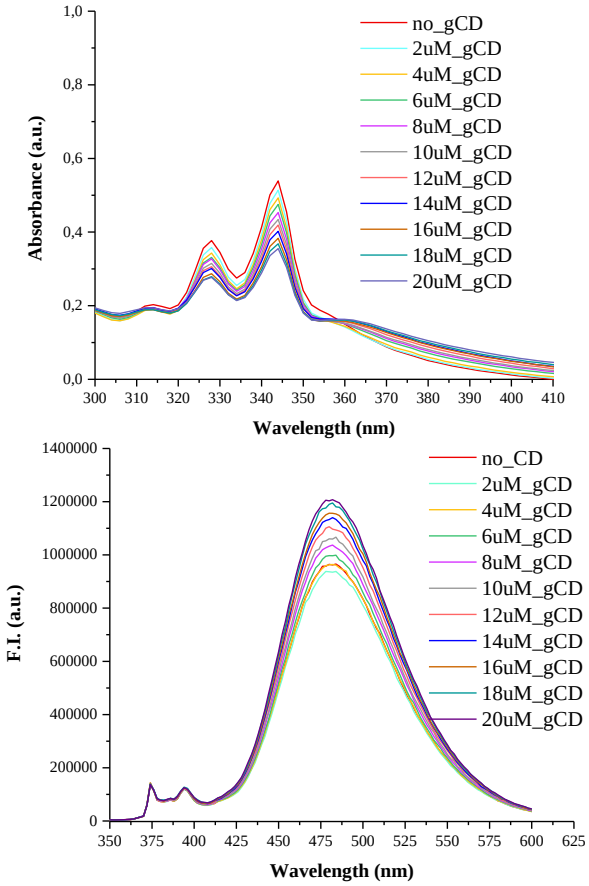

Figure IV. 36 *Titration of γ-cyclodextrin into 20 μM solution of* ***1c*** *measured by absorption (top) and emission (bottom) spectroscopy in water/acetonitrile (3:2) mixture.*

Next, the inverse titration, a cuvette with γ–cyclodextrin (20 μM) in water/acetonitrile (6:4 ratio, 2 mL) mixture titrated with aliquots of **1c** (Figure IV.37) showed a growing intensity in absorbance spectra peaks reveal increasing concentration of pyrene moiety. The fluorescence spectra showed also an increasing intensity by the **1c** addition. But this time the monomeric emission was the dominant.

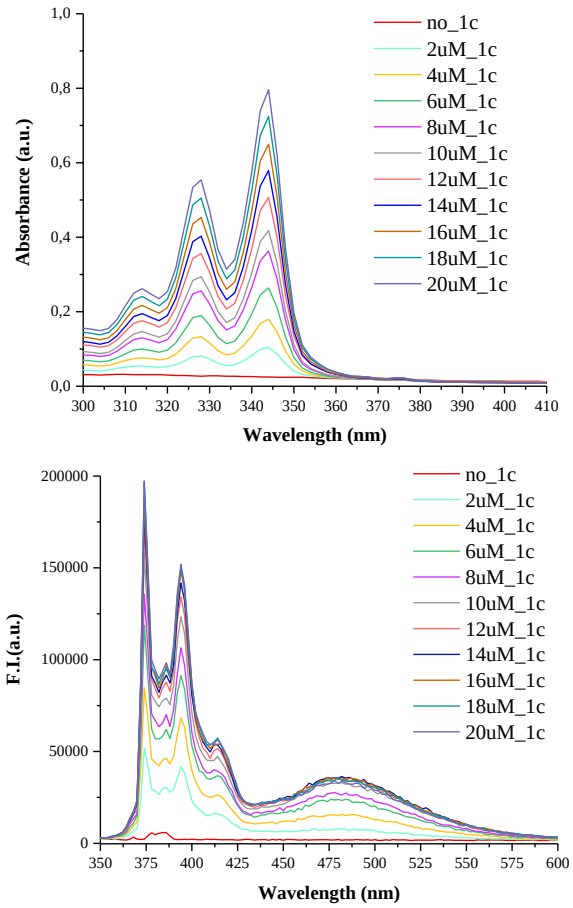

Figure IV. 37 *Titration of* ***1c*** *into 20 μM solution of γ-cyclodextrin measured by absorption (top) and emission (bottom) spectroscopy in water/acetonitrile (3:2) mixture.*

Solvent for photophysical experiment was changed from water/acetonitrile (3:2) mixture to water to enhance the hydrophobic π–π interactions between pyrene units and to ease solubilizing of γ-CD. To the cuvette containing 20 μM solution of **1c** in water prepared under nitrogen atmosphere and titrated with

aliquots of **1c** into the solution of a host and monitored by recording absorption and emission spectras (Figure IV.38).

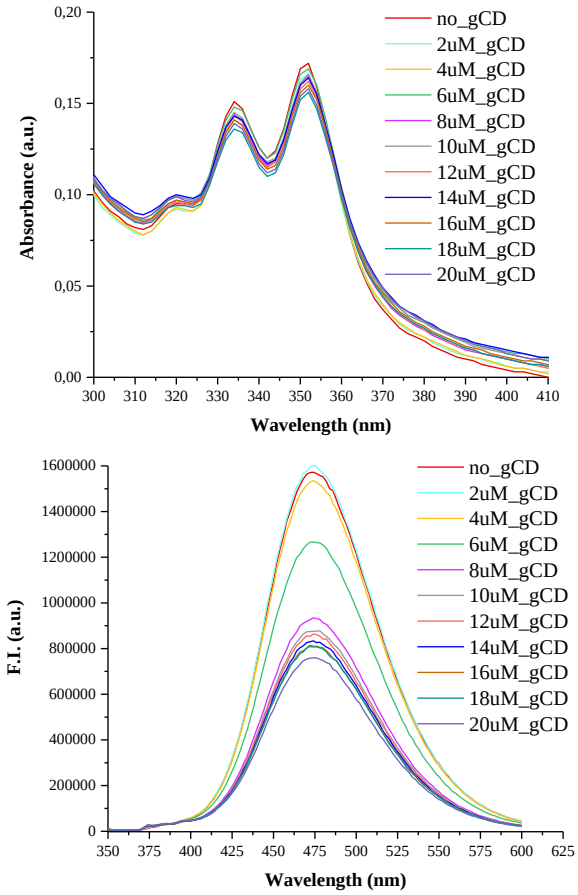

Figure IV. 38 *Titration of γ-cyclodextrin into 20 μM solution* ***1c*** *measured by absorption (top) and emission (bottom) spectroscopy in water.*

Absorption spectra reveled small drop in the intensity after addition of the host. Emission spectra exhibit a huge band (390 – 290 nm) of pyrene excimer, while the PAH monomer peaks are absent. We hypothesize the drop in the intensity of pyrene excimer occurs due to the shallow or very loose inclusion[314] of **1c** into γ-CD, followed by disintegration of excimers (lower intensity). However, single pyrene units seem to not form inclusion complexes with host molecule.

Reverse titration of **1c** into the cuvette filled with 20 μM solution of γ-CD in water prepared under nitrogen atmosphere was conducted (Figure IV.39). Absorption intensity was growing while addition of **1c** due to increasing

concentration. Fluorescence spectra showed interesting behaviour, intensity of peaks grew until concentration of **1c** reached 6 μM, then the intensity decreased with addition of next 4 μM of **1c,** to drastically increase with following additions.

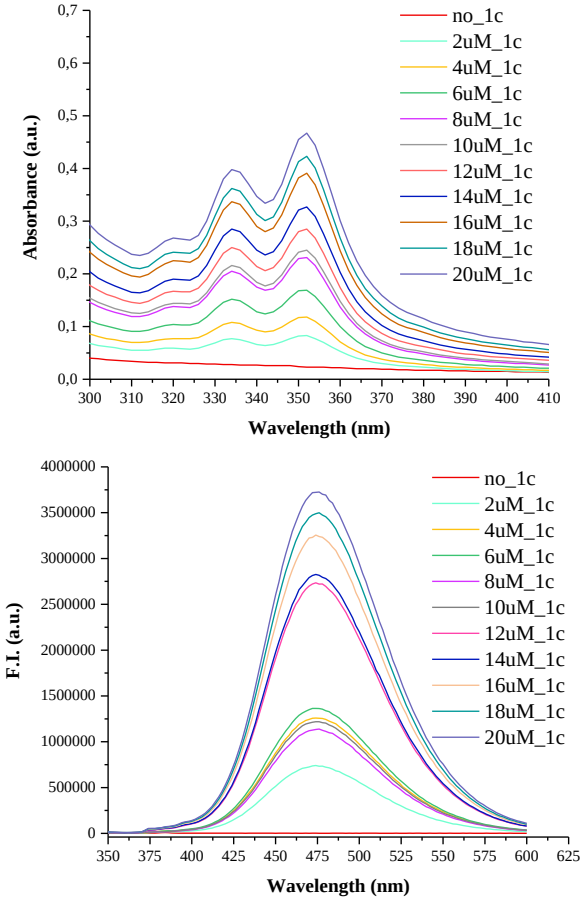

Figure IV. 39 *Titration of* ***1c*** *into 20 μM solution γ-cyclodextrin measured by absorption (top) and emission (bottom) spectroscopy in water.*

In water the hydrophobic π–π interactions between pyrene units are enhanced, leading to a large emission band of the pyrene excimer (390 – 290 nm), while the PAH monomer peaks were absent. These experiments disclose the affinity of pyrene units to form dimer over staying in monomer phase.

IV.2.3.4 Encapsulation of low concentrated Ni^{II} and Co^{II} catalysts

To further understanding of the system we carried out experiments at lower concentrations to possibly facilitate extracting information from obtained data. To a 2 μM solution of $Co(^{PyB}mcp)(OTf)_2$ γ-CD aliquots were added as showed in (Figure IV.40).

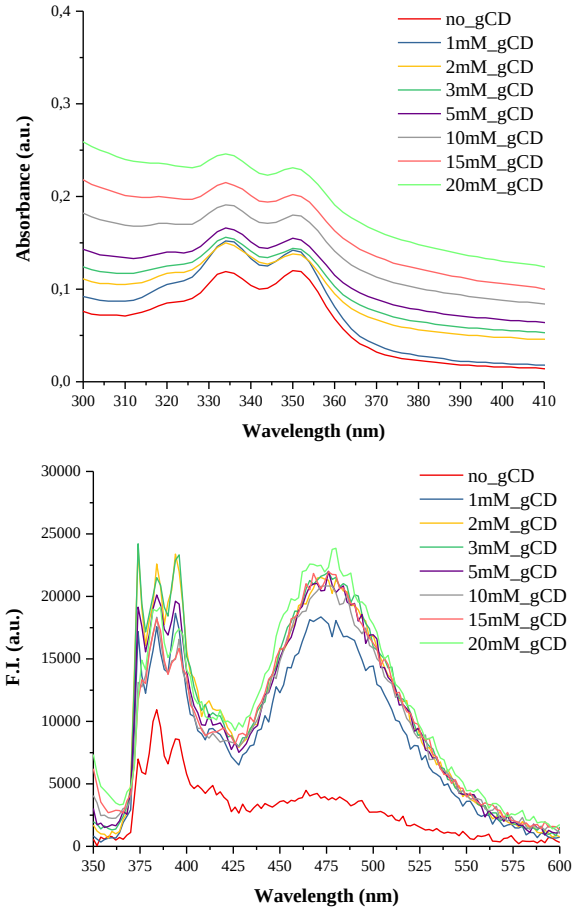

Figure IV. 40 *Titration of γ-cyclodextrin into 2 μM solution $Co(^{PyB}mcp)(OTf)_2$ measured by absorption (top) and emission (bottom) spectroscopy in water.*

Absorption spectra revealed interesting result. Growing peak in a region 330 – 340 nm, indicated changing polarity of the environment to more polar.[410] This indicated the interaction between host and guest molecules. Emission intensity grew under addition of host molecules enhancing formation of excimer phase.

However, the emission spectra confirmed the hypothesis that the excimer was internalized in the γ-CD, and is not modify by the presence of γ-CD.

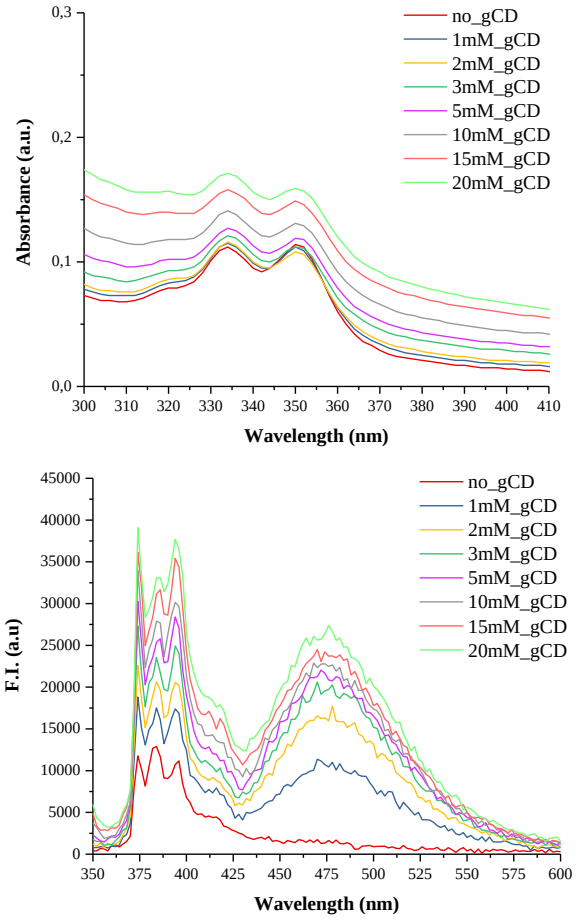

Figure IV. 41 *Titration of γ-cyclodextrin into 2 μM solution Co(^{PyB}pdp)(OTf)$_2$ measured by absorption (top) and emission (bottom) spectroscopy in water.*

Titration of Co(^{PyB}pdp)(OTf)$_2$ was perform in same manner by addition of γ-CD and spectroscopy measurements (Figure IV.41). In absorbance spectra the first peak (330 -340 nm) grows in intensity, thus inclusion is present. Formation of pyrene excimer is enhanced after addition of host molecules together with increase in monomer.

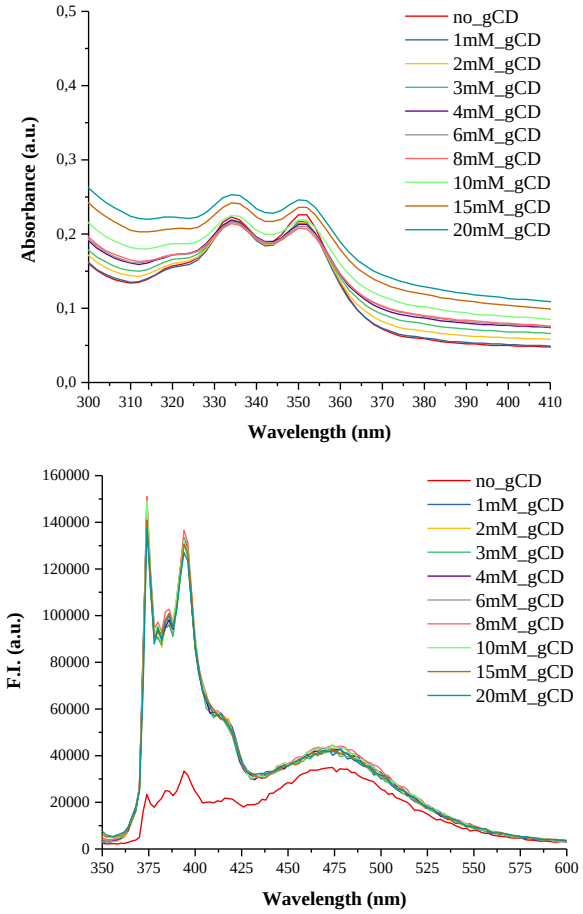

Figure IV. 42 *Titration of γ-cyclodextrin into 2 μM solution Ni(^{PyB}mcp)(OTf)$_2$ measured by absorption (top) and emission (bottom) spectroscopy in water*

Titration of γ-CD into Ni(^{PyB}mcp)(OTf)$_2$ displayed smaller rise in absorption spectra. Together with the fluorescence spectra, divulging presence of mostly monomer specie with small contribution of inclusion excimer complex (Figure IV.42).

Last titration with γ-CD was performed for Ni(^{PyB}pdp)(OTf)$_2$ and as for another samples each step was monitored by spectroscopy techniques (Figure IV.43). As in case of Co(^{PyB}mcp)(OTf)$_2$ and Co(^{PyB}pdp)(OTf)$_2$, increase of intensity in absorbance of the first peak was observed due to the interactions between catalyst and γ-CD, together with higher polarity of the environment. Fluorescence of Ni(^{PyB}pdp)(OTf)$_2$ revealed peculiar behavior, 1 mM and 2 mM of g-CD in the solution enhanced formation of excimer, however after

concentration of host molecule was higher, excimer was decomposing on behalf of monomer species.

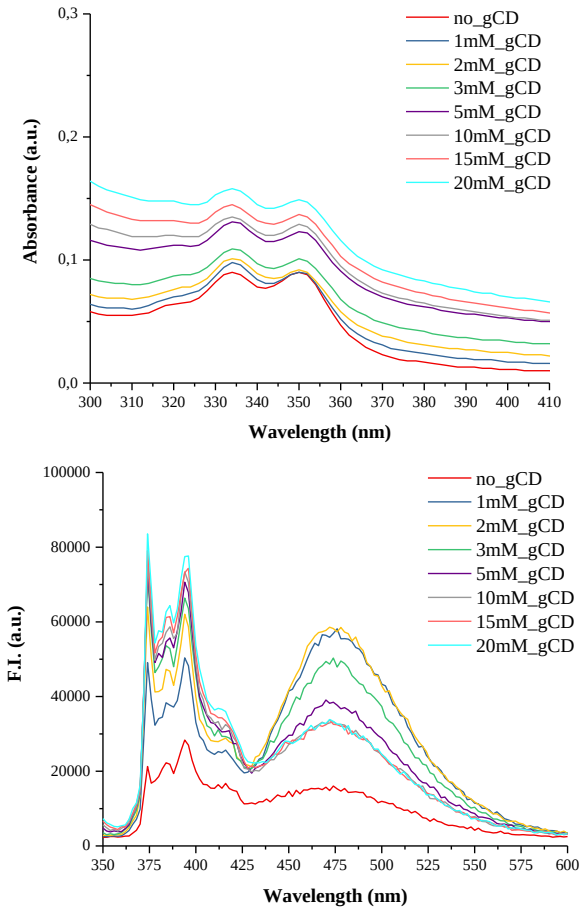

Figure IV. 43 *Titration of γ-cyclodextrin into 2 μM solution Ni(^{PyB}pdp)(OTf)$_2$ measured by absorption (top) and emission (bottom) spectroscopy in water.*

Reducing concentration of complexes to 2 μM exhibit different ways of interaction between Co^{II} and Ni^{II} catalysts. Cobalt based catalysts prone to form excimers under addition of γ-cyclodextrins, while nickel catalysts rather stay in monomer phase. At this point it was clear that the ratio and distribution of monomers and excimers with γ-cyclodextrins is not straightforward, it can lead to several combinations that were mentioned in previous section.

IV.2.3.5 Anchoring the catalysts on carbon nanomaterials

One of the goals of the project was to control the reactivity and induce the enantioselectivity in light-driven catalytic reactions. The control of enantioselectivity could be achieved by the interactions of the pyrenes with π-conjugated materials. The interactions of the pyrenes with the π-conjugated materials could form chiral pockets and then influence in the reactivity. As a model, we investigated the interactions with the buckyball (C_{60}) to progress on the interactions graphene surface and its analogues.

IV.2.3.5.1 Interactions with low concentrations of fullerene C_{60}

To better understand the interactions of fullerene with PAH of our complexes, we first characterized the complexes in the acetonitrile/1,2-dichlorobenzene mixture (1:1) ($Co(^{PyB}mcp)(OTf)_2$ - Figure IV.44 and $Co(^{PyB}pdp)(OTf)_2$, $Ni(^{PyB}mcp)(OTf)_2$, $Ni(^{PyB}pdp)(OTf)_2$, $Co(^{PerB}mcp)(OTf)_2$ - Figures in appendix of the chapter - Figure IVa.16 – IVa.19). Cobalt and nickel complexes showed only traces of the excimer formation under applied conditions.

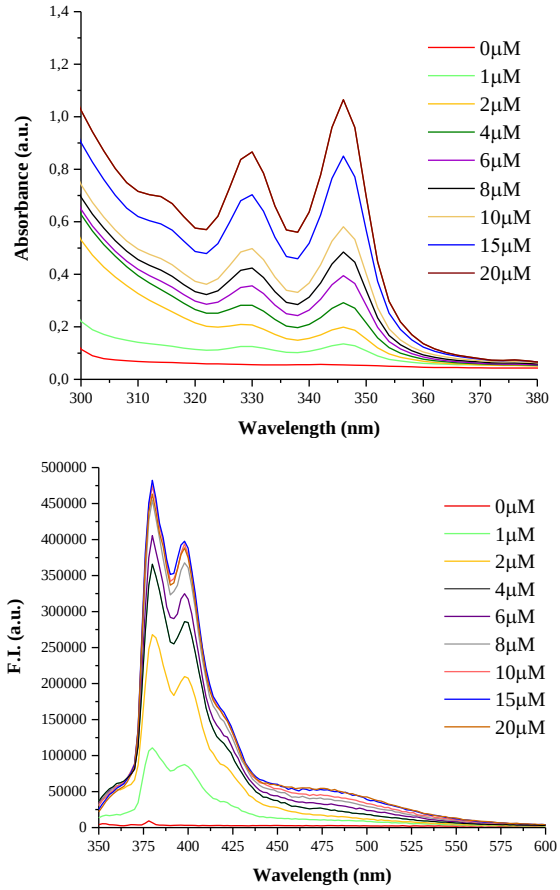

Figure IV. 44 *Co(^{PyB}mcp)(OTf)$_2$ in acetonitrile/1,2-dichlorobenzene mixture (1:1) at different concentrations.*

Then, we studied the interaction of of Co(^{PyB}mcp)(OTf)$_2$, Co(^{PyB}pdp)(OTf)$_2$, Co(^{PerB}mcp)(OTf)$_2$, Ni(^{PyB}mcp)(OTf)$_2$ and Ni(^{PyB}pdp)(OTf)$_2$ with fullerene C_{60}. Here the changes in the emission spectra were attributed to the quenching process between the C60 and the PAH.[416]

Co(^{PyB}mcp)(OTf)$_2$ (20 µM) treated with with aliquots of C_{60} (2 mM), showed the peaks of C_{60} and pyrene moiety in the absorption spectra. (Figure IV.45). The excited state emission decreased upon addition of the C_{60}, which was interpreted as a quenching process. The same behaviour was observed for the other complexes (Appendix of Chapter IV, Figure IVa.20 – IVa-23).

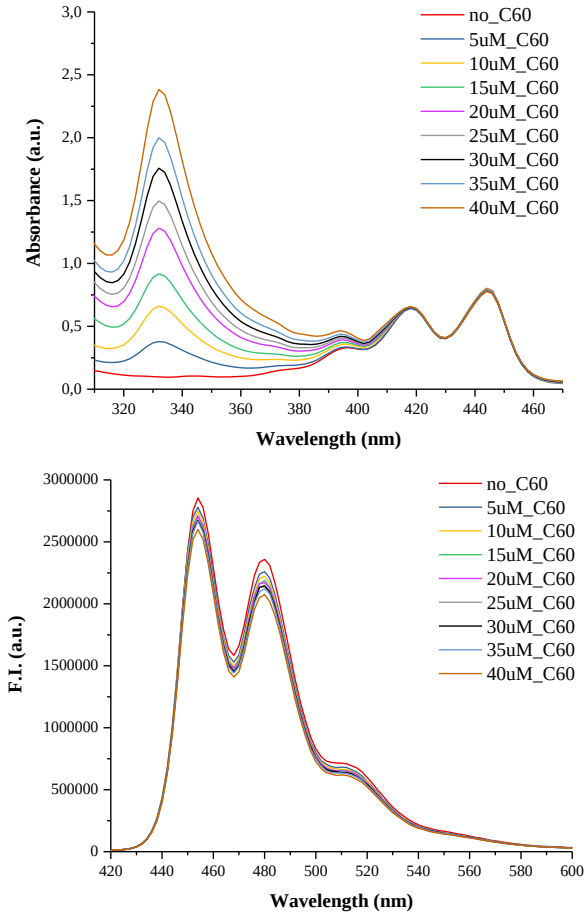

Figure IV. 45 *Titration of C_{60} into solution of Co(^{PerB}mcp)$(OTf)_2$ measured by absorption (top) and emission (bottom) spectroscopy in acetonitrile/1,2-dichlorobenzene mixture (1:1).*

Complex containing perylene as a polyaromatic moiety Co(^{PerB}mcp)$(OTf)_2$ was also studied to understand influence of different PAH units. 20 μM solution of Co^{II} complex was titrated with 5 μM aliquots of C_{60} (Figure IV.45). The absorption intensity of C_{60} is increasing while reaching higher concentration in a region 320-350 nm and perylene moiety was not affected but it's tale in region 380-405 nm due to weak interaction between C_{60} and Co(^{PerB}mcp)$(OTf)_2$. Under the addition of C_{60}, there was found only slight decrease in fluorescence intensity. This confirms our hypothesis of weak interactions between two species.

Results obtained from the titration resembling job plot disclosed interaction between two species, to be precise: nickel or cobalt complex with pyrene or

perylene units and fullerene – C_{60}. Quenching studies disclosed electron transfer from donor (pyrene moiety) to acceptor (C_{60}). However, from our results, it is not clear which is the geometry of complexes in the interaction between C_{60} and catalysts with polyaromatic tails.

IV.2.3.5.3 Interaction with higher concentrations of fullerene C_{60}

In previous section, we obtained fundamental knowledge about the interaction between our complexes and fullerene C_{60}. However, we wanted to understand it better, how the interactions occurs and if the chiral cavity is created by attaching the catalyst to the carbon-based nanomaterial. Studies with higher concentrations of buckyball were performed to understand the mechanism of anchoring the catalyst.

Quenching experiments of $Co(^{PerB}mcp_)(OTf)_2$ showed peak 320-350 nm due to increasing concentration of the fullerene and increase of intensity with change of the profile of the monomeric absorption bands in region between absorbance of C_{60} and perylene 380-420 nm indicating weak interaction of these two species, since only little effect is observed.

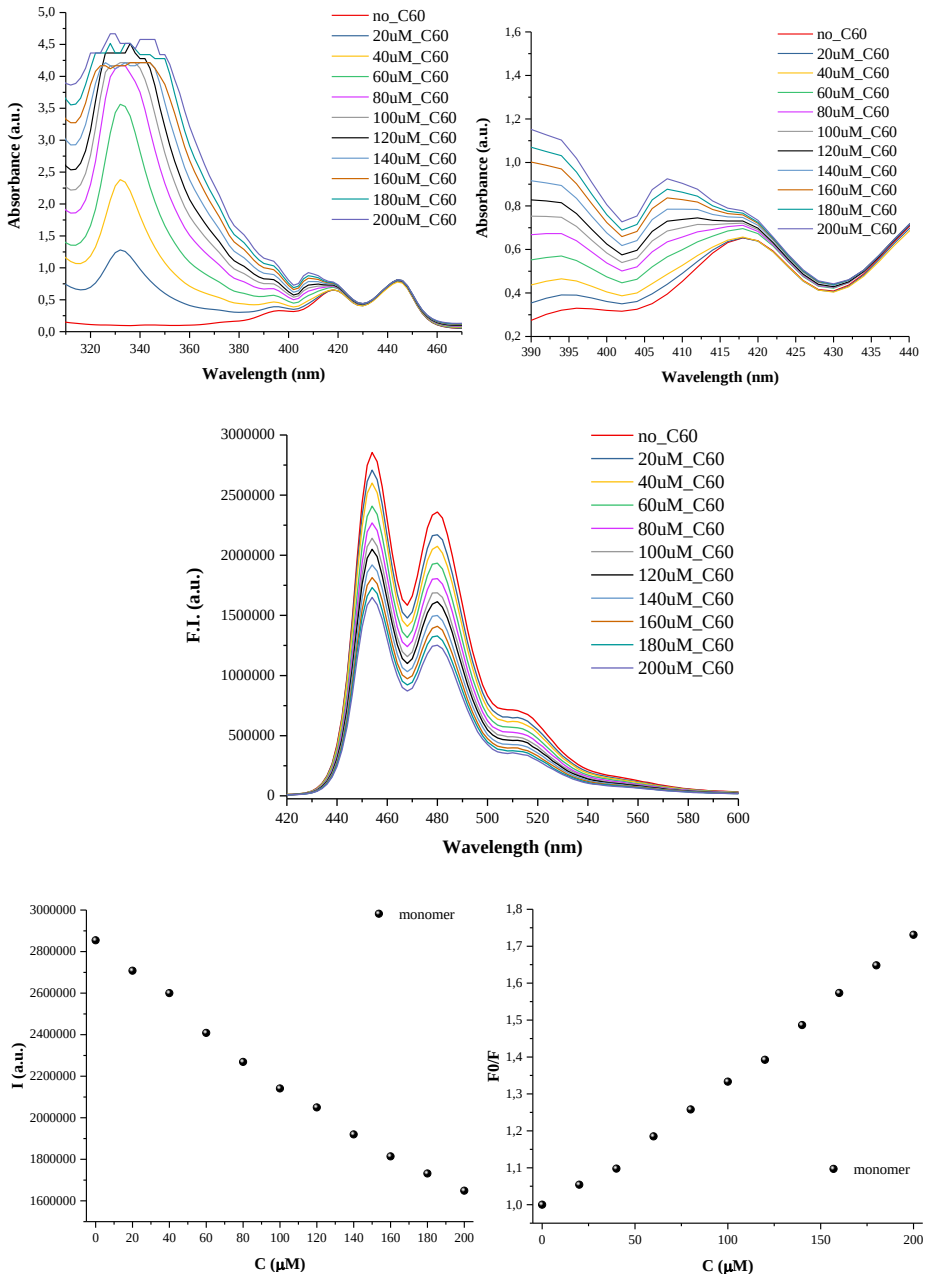

Figure IV. 46 *Titration of higher concentrations of C_{60} into solution of Co(^{PerB}mcp)$(OTf)_2$ measured by absorption (left) and emission (right) spectroscopy in acetonitrile/1,2-dichlorobenzene mixture (1:1).*

Fluorescence spectra was also recorded to get more insight into the electronic communication between the host and guest molecules. [417] Under titration of C_{60} into solution of Co(^{PerB}mcp)$(OTf)_2$ the intensity of perylene monomer was

decreasing due an energy transfer from excited perylene to fullerene. Anyhow, these results show only limited effect upon the electronic nature of the host and the guest.

IV.2.3.5.3 Immobilization of the catalyst on carbon nanotubes and GO

Inspired by work of Mata and co-workers we wanted to stack our anchoring catalysts on carbon based nanomaterials by the method described by authors.[321] First, we wanted to attach the cobalt complex Co(^{PyB}pdp)$(OTf)_2$ to carbon nanotubes with the mass ratio 1:1 (10 mg : 10 mg). We wanted to immobilized the complex on the surface of the nanotube at room temperature by impregnation of a nanotube suspension with a solution of Co(^{PyB}pdp)$(OTf)_2$ in dichloromethane and stirring for 24h. The resulting solution was centrifuged, solid was removed washed with MeCN four times (after every washing the mixture was centrifuged) and the remaining solvent was analyzed by spectroscopy techniques to check the remaining amount of complex in the solvent (Figure IV.47). Intensity of absorbance after first centrifugation was very high, which means that not all used in reaction complex was anchored to the surface of nanomaterial. Next centrifugations delivered remaining solvents which showed decreasing tendency with the number of washing cycles due to lower concentrations of present dissolved catalyst in the analyzed sample.

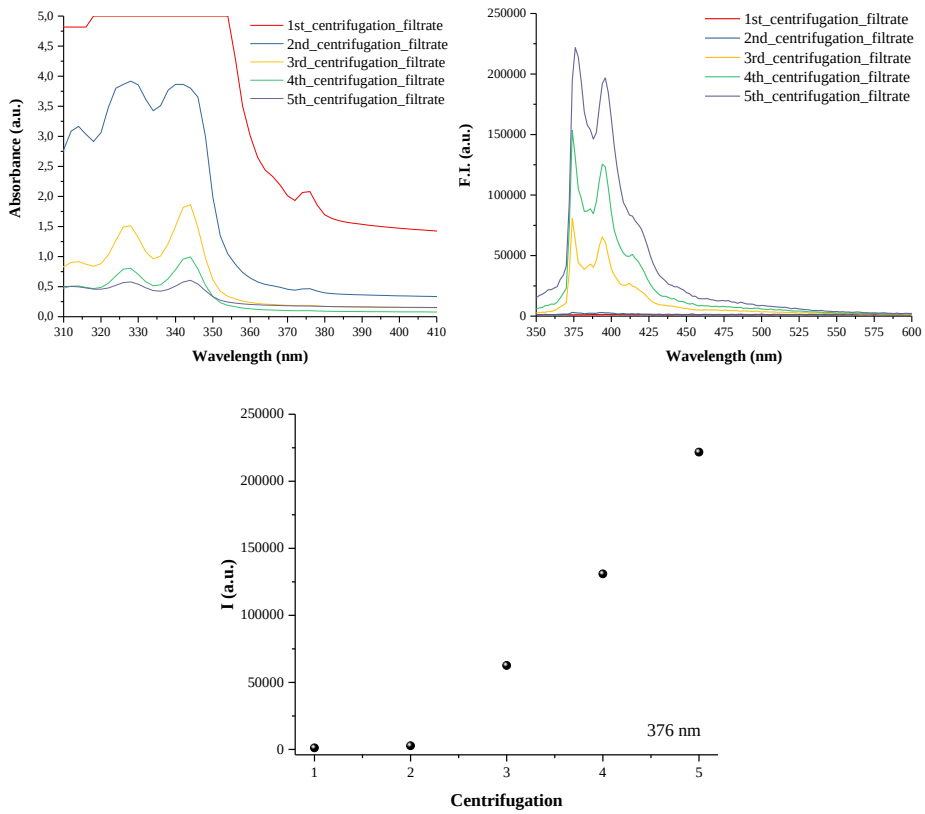

Figure IV. 47 *Absorption and emission spectra of remaining solvent after washing immobilized Co(^{PyB}pdp)(OTf)$_2$ on nanotubes with MeCN.*

Fluorescence studies were performed to get more insight into obtained results in the absorbance. However, after first and second centrifugation no intensity was observed in the emission spectra, which we hypothesized as the effect of quenching the emission of pyrene by nanotubes. Next solutions measured after third, fourth and fifth centrifugations showed to have increasing intensity, which we reason as an effect of lower amount of the nanotubes in the solution thus less energy of catalyst is transferred to the nanotubes. The analysis of solid was also performed by ICP cobalt analysis revealing the metal loading 4.31 mg/g of cobalt.

Next, the Co(^{PyB}pdp)(OTf)$_2$ was immobilized on the surface of graphene oxide (GO) with the mass ratio 1:5 (5 mg : 25 mg) by stirring solution of catalyst with suspension of GO during 24h. The mixture was centrifuged, solid was separated, washed four times with acetonitrile (the mixture was centrifuged

after every washing with MeCN) and the solutions were examined by absorption and emission spectroscopy (See Figure IV.48).

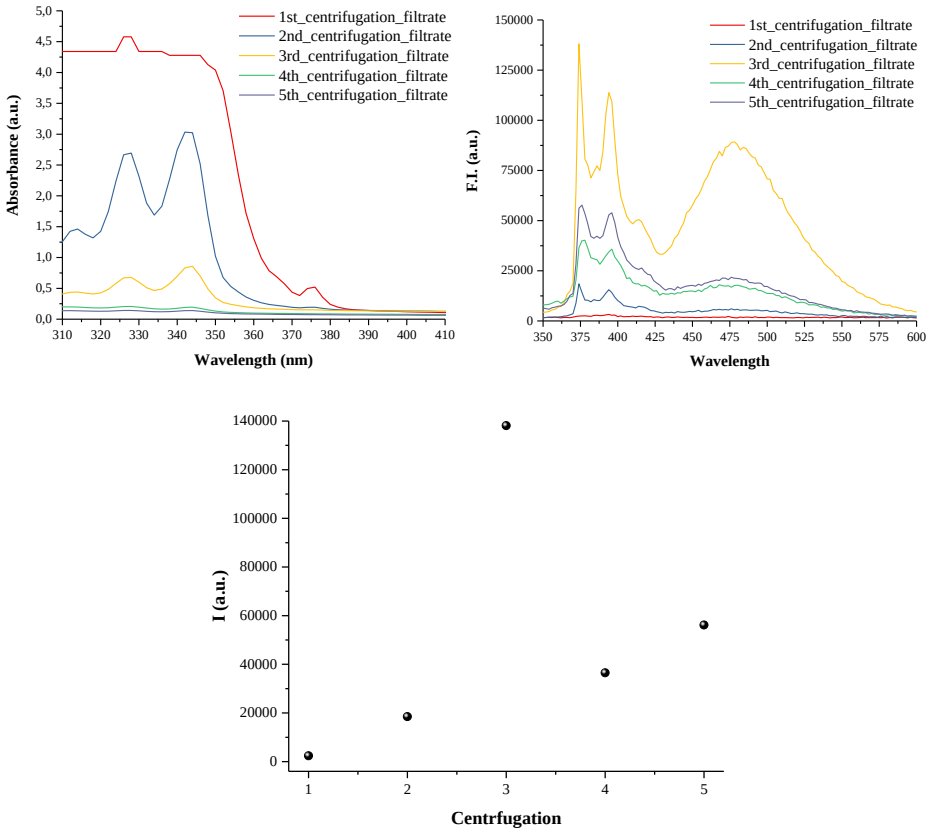

Figure IV. 48 *Absorption and emission spectra of remaining solvent after washing immobilized Co(^{PyB}pdp)(OTf)$_2$ on graphene oxide with MeCN.*

After the first centrifugation the absorbance intensity was very high indicating on remaining complex in the solution after anchoring reaction. Nonetheless, after every washing and centrifuging, the absorbance intensity was lower caused by lower concentration of the complex in the filtrate. To complete the analysis, these samples were checked also in fluorescence. Filtrate from first centrifugation didn't show any peaks from pyrene monomer as the emission is effected by graphene oxide quenching. The emission intensity of second and third filtrate after centrifugations disclosed growing tendency caused by removal of quencher while separating solid phase from the mixture. The fourth and fifth filtrate coming after centrifugation showed to have lower intensities

as a result of washing the remaining “unreacted” complex from the reaction mixture. The analysis of solid (immobilized catalyst on the surface of GO) performed by ICP cobalt analysis revealing the metal loading 5.06 mg/g of cobalt.

A cobalt catalyst Co(^{PyB}pdp)$(OTf)_2$ was immobilized on the carbon nanotubes and graphene oxide providing two new host-guest complexes. The stability and geometry of obtained catalysts cannot be defined by our results due to the complexity of the interaction between the nanomaterial and catalyst containing two anchoring groups.

IV.3 Conclusion

Cobalt and nickel complexes containing pyrene or perylene anchoring moieties ($Co(^{PyB}mcp)(OTf)_2$, $Co(^{PyB}pdp)(OTf)_2$, $Ni(^{PyB}mcp)(OTf)_2$ and $Ni(^{PyB}pdp)(OTf)_2$) were characterized in different solvent mixtures by optical methods of analysis revealing a complex behaviour in solution. The pyrene complexes aggregate more in polar solvents, and interact with γ-CD in a host-guest fashion.

Anyhow upon addition of water into the solvent mixture (acetonitrile/water 4:6) to induce the π-stacking interaction between two pyrene units did not reveal excimer bands. While characterization experiments were performed in water, the interaction between the polyaromatic parts became very strong due to the hydrophobic nature of π–π stacking interactions and excimer bands were observed.

Prepared materials have shown in earlier experiments very promising possibilities in catalysis that can be further extended.

Future research will focus on the preparation of new host-guest structures, expanding the scope of the catalytic reactions, understanding and improving the control over the interactions between guest, host and surface will allow for this immobilization strategy to be used in many different applications.

IV.4 Experimental section

IV.4.1 Material and reagents

Reagents and solvents were used as received from the commercial supplier unless otherwise stated. γ-cyclodextrins were purchased from FluoroChem (96%). For the analysis of ligands and complexes, the solvents as anhydrous acetonitrile and 1,2-dichlorobenzene were purchased from Sigma-Aldrich® and water was purified with a Milli-Q Millipore Gradient AIS system. Water used for photophysical experiments was degassed by freeze-pump-thaw method (repeated 3 cycles) and stored under argon.

The preparation of experiments was conducted inside a nitrogen-filled glove box (mBraun Unilab) with concentrations of O_2 and H_2O lower than 0.5 ppm and using Schlenk techniques under argon atmosphere.

IV.4.2 Instrumentation

UV-Vis measurements were carried out on a Shimadzu UV-2401PC spectrophotometer equipped with a photomultiplier detector, double beam optics and D2 and W light sources

Fluorescence measurements were carried out on a Fluorolog Horiba Jobin Yvon spectrofluorimeter equipped with photomultiplier [or InGaAs if using the nitrogen cooled detector] detector, double monochromator and Xenon light source.

IV.4.3 Experimental procedure

Absorption and fluorescence characterization of the ligands and their corresponding Co^{II} and Ni^{II} complexes in different solvent systems. All samples for the analysis were conducted in a 2.5 mL air-tight quartz cuvette with optical length of 10mm and surface flatness 1 μm. Each analysis was performed at RT and under N_2 atmosphere. To a 2 mL solution of either catalyst ($Co(^{PyB}mcp)(OTf)_2$, $Co(^{PyB}pdp)(OTf)_2$, $Ni(^{PyB}mcp)(OTf)_2$, $Ni(^{PyB}mcp)(OTf)_2$) or nanomaterial (γ-CD, C_{60}) (20 μM or 20 mM) in the solvent mixture (acetonitrile, acetonitrile/water (1:1), water or acetonitrile/1,2-dichlorobenzene

(1:1)) under N_2 atmosphere in a quartz cuvette, subsequent additions of either catalyst or nanomaterial in aliquots of 10 μL were added and led to the formation of host-guest complexes. After each addition of aliquot, the UV-Vis and emission spectrum was measured before further titration.

IV.5 Appendix of chapter V.

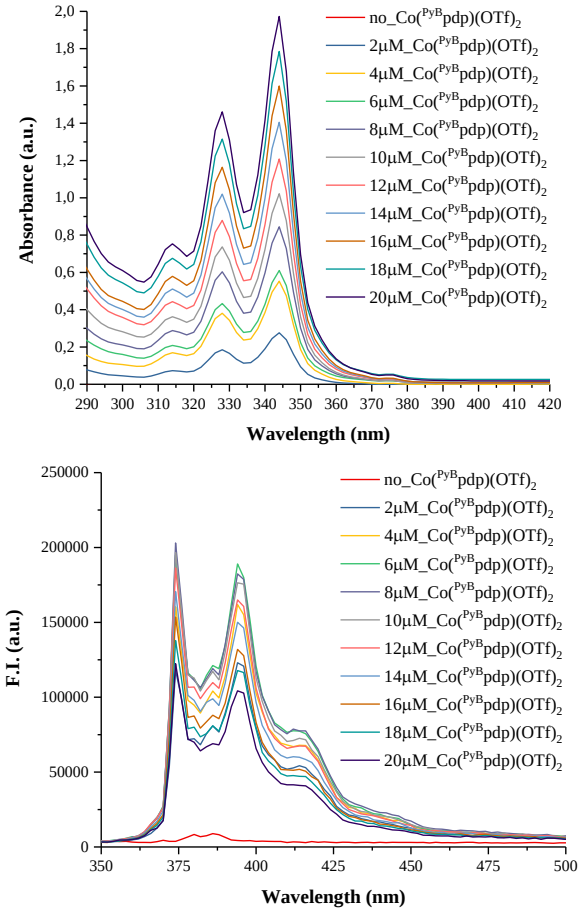

Figure IVa. 1 *Titration of Co(^{PyB}pdp)(OTf)$_2$ into solution of γ-cyclodextrin measured by absorption (top) and emission (bottom) spectroscopy in water/acetonitrile (6:4 mL) mixture.*

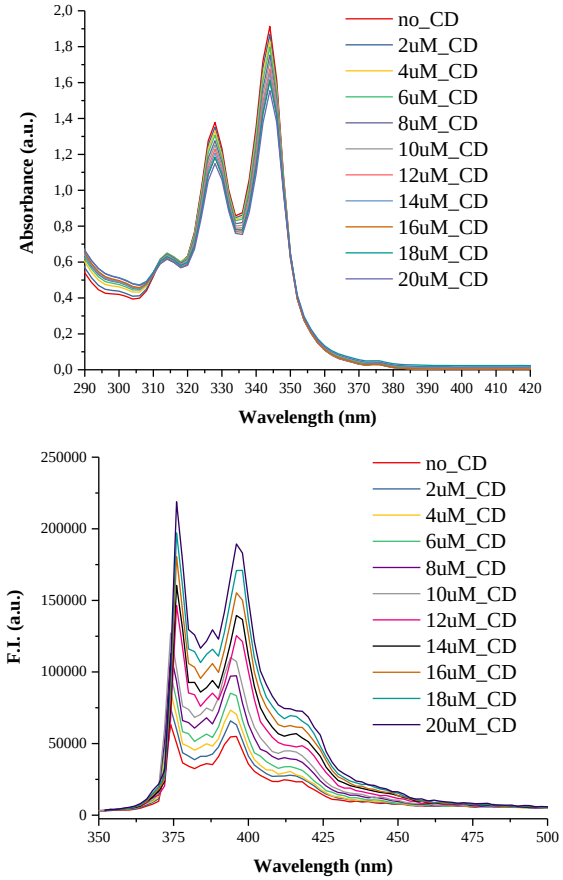

Figure IVa. 2 *Titration of γ-cyclodextrin into solution of Co(^{PyB}pdp)(OTf)$_2$ measured by absorption (top) and emission (bottom) spectroscopy in water/acetonitrile (6:4 mL) mixture.*

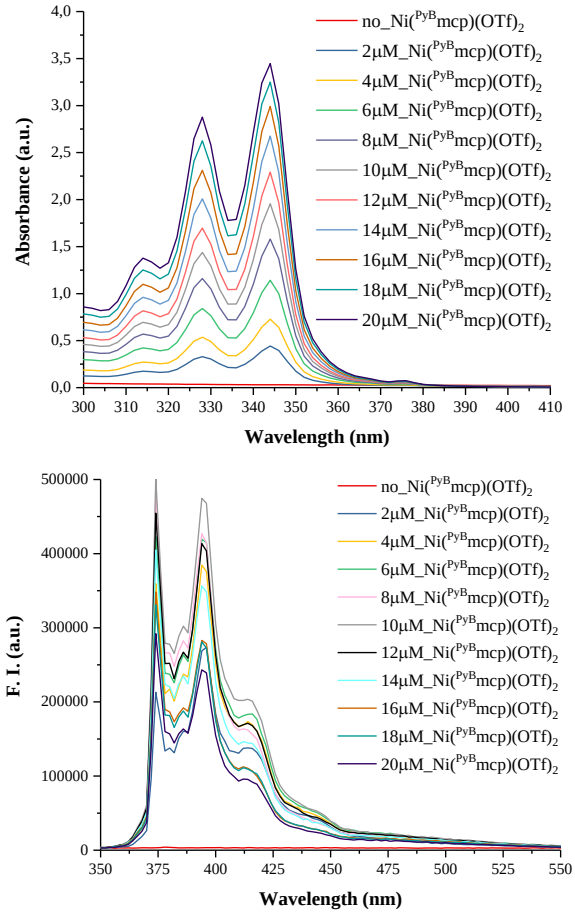

Figure IVa. 3 *Titration of Ni(^{PyB}mcp)(OTf)$_2$ into solution of γ-cyclodextrin measured by absorption (top) and emission (bottom) spectroscopy in water/acetonitrile (6:4 mL) mixture.*

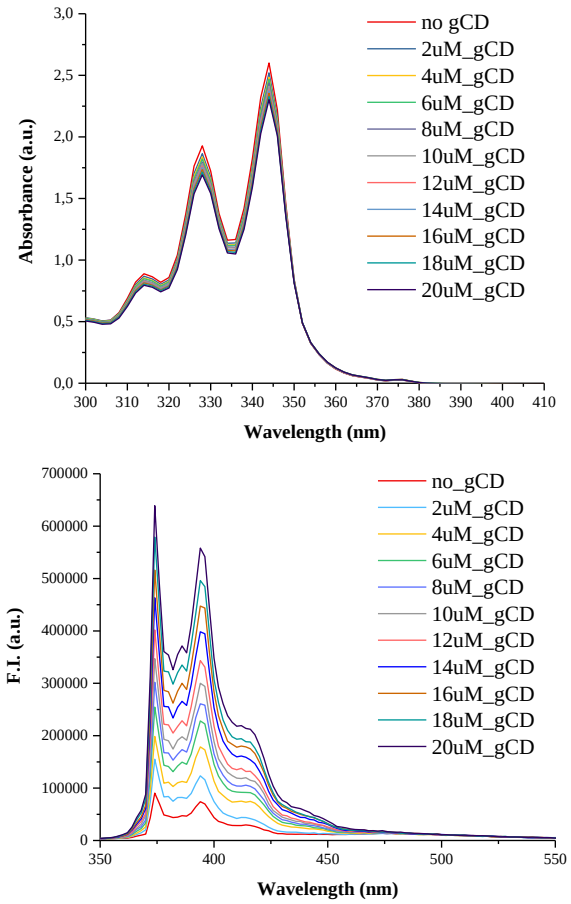

Figure IVa. 4 *Titration of γ-cyclodextrin into solution of Ni(^{PyB}mcp)(OTf)$_2$ measured by absorption (top) and emission (bottom) spectroscopy in water/acetonitrile (6:4 mL) mixture.*

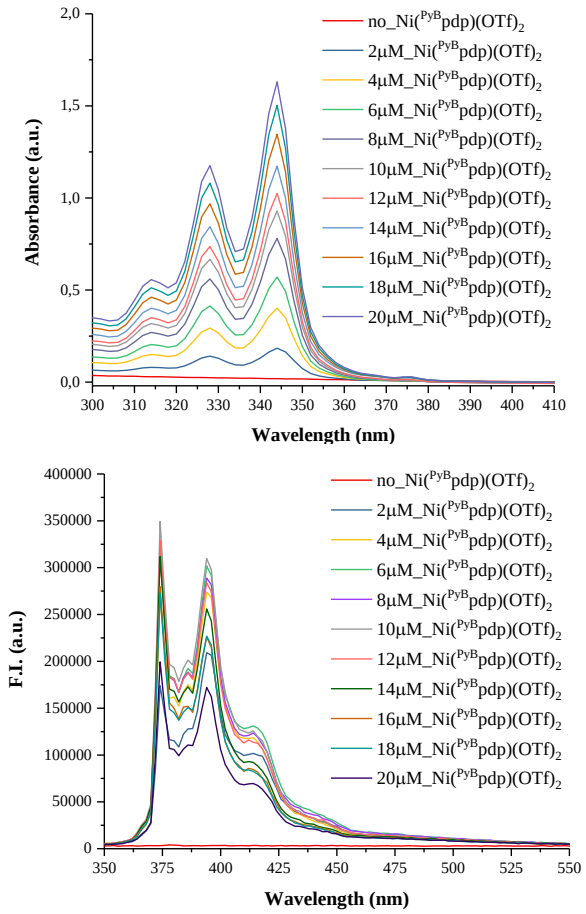

Figure IVa. 5 *Titration of Ni(^{PyB}pdp)(OTf)$_2$ into solution of γ-cyclodextrin measured by absorption (top) and emission (bottom) spectroscopy in water/acetonitrile (6:4 mL) mixture.*

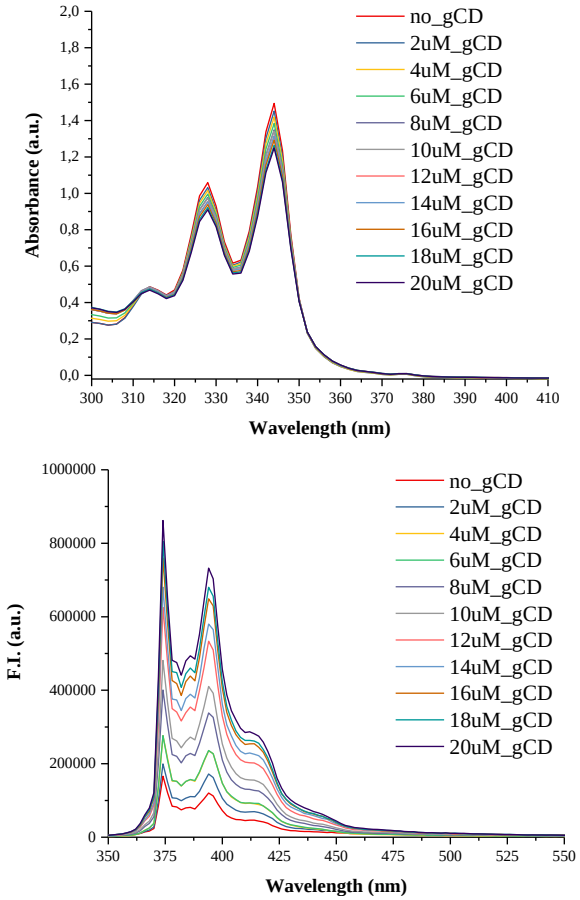

Figure IVa. 6 *Titration of γ-cyclodextrin into solution of Ni(^{pyB}pdp)(OTf)$_2$ measured by absorption (top) and emission (bottom) spectroscopy in water/acetonitrile (6:4 mL) mixture.*

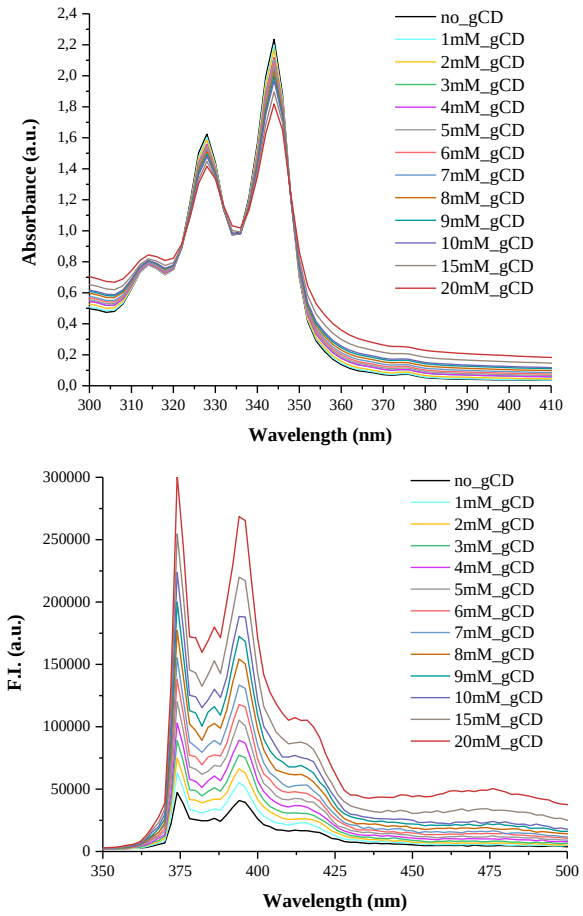

Figure IVa. 7 *Titration of concentrated solution of γ-cyclodextrin into solution Ni(^{PyB}pdp)(OTf)$_2$ measured by absorption (top) and emission (bottom) spectroscopy in water/acetonitrile (6:4 mL) mixture.*

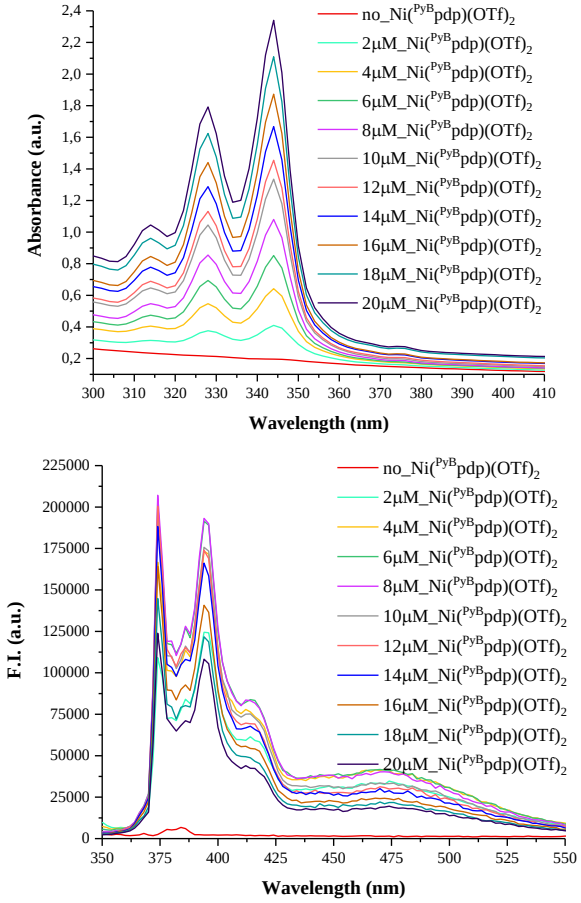

Figure IVa. 8 *Titration of Ni(*^{PyB}*pdp)(OTf)*$_2$ *solution into concentrated solution of γ-cyclodextrin measured by absorption (top) and emission (bottom) spectroscopy in water/acetonitrile (6:4 mL) mixture.*

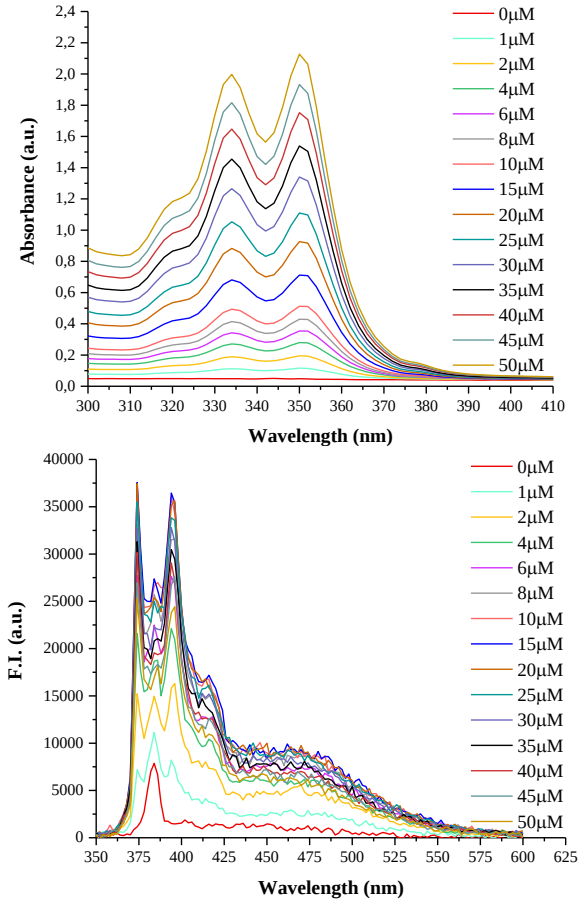

Figure IVa. 9 *Absorption (top) and emission (bottom) spectra of Co(^{PyB}pdp)(OTf)$_2$ at different concentrations in water.*

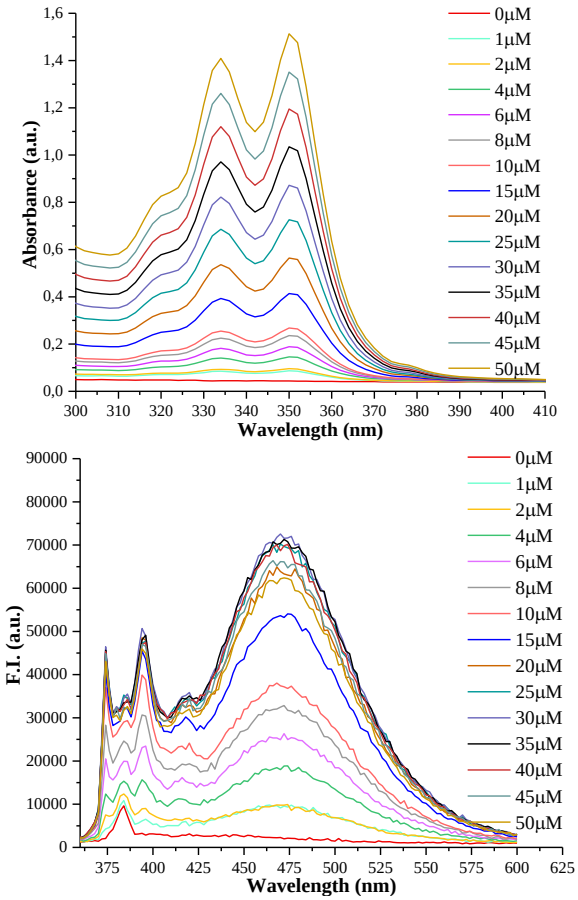

Figure IVa. 10 *Absorption (top) and emission (bottom) spectra of* $Ni(^{PyB}mcp)(OTf)_2$ *at different concentrations in water.*

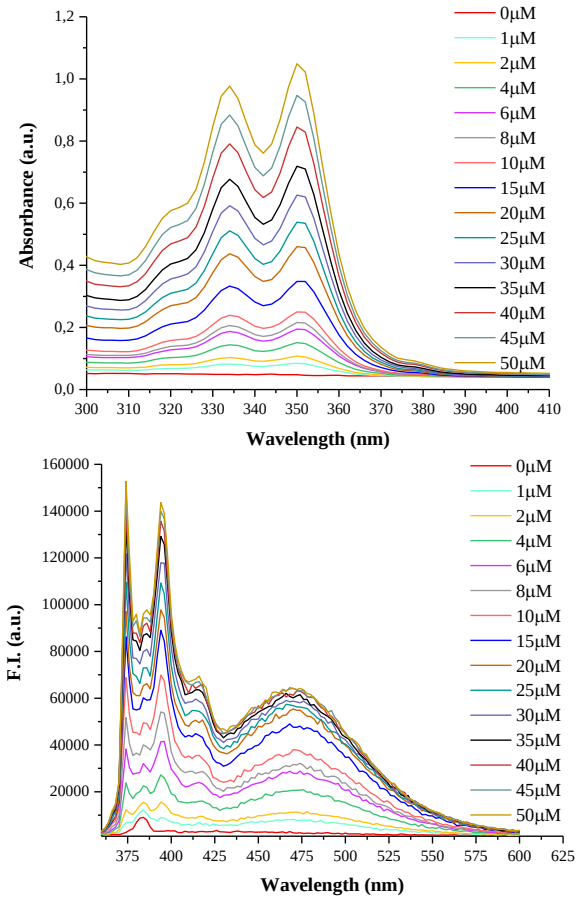

Figure IVa. 11 *Absorption (top) and emission (bottom) spectra of* $Ni(^{PyB}pdp)(OTf)_2$ *at different concentrations in water.*

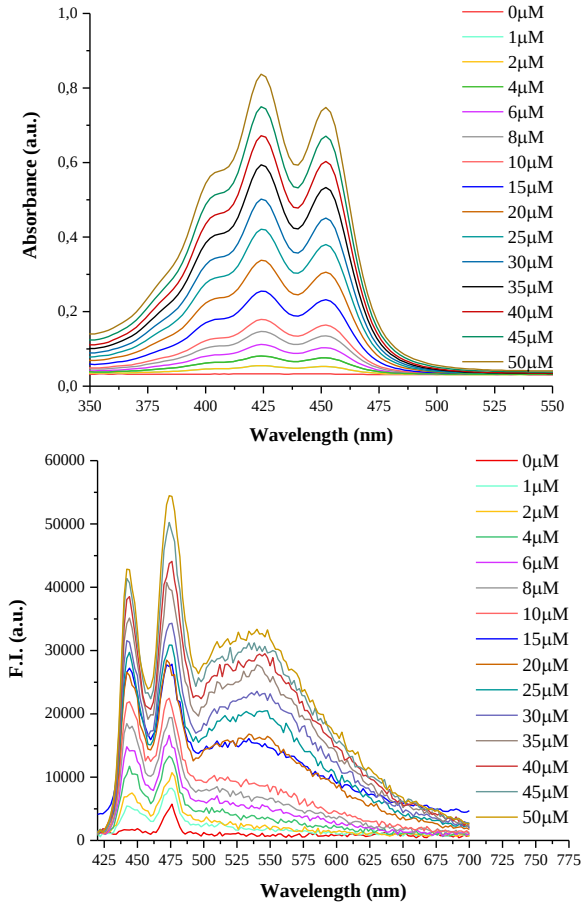

Figure IVa. 12 *Absorption (top) and emission (bottom) spectra of Co(^{PerB}mcp)(OTf)$_2$ at different concentrations in water.*

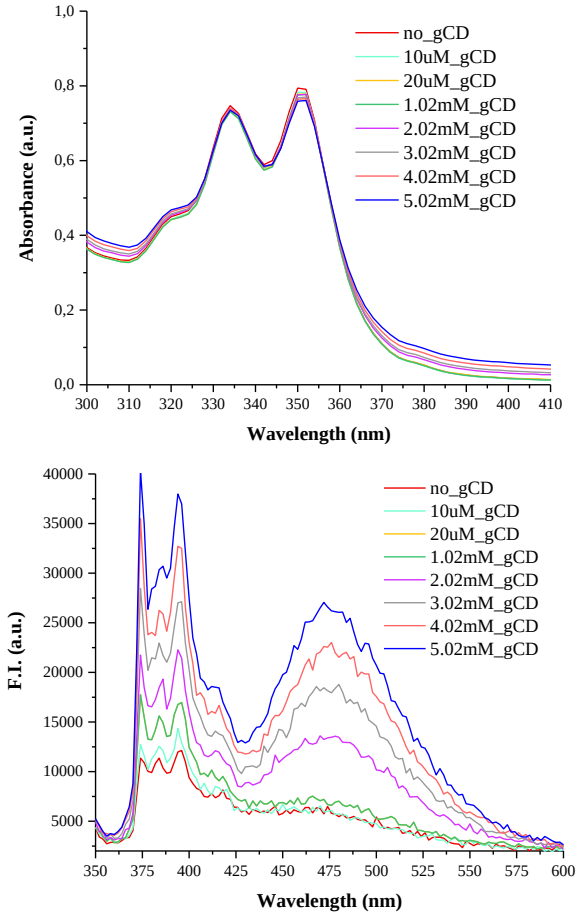

Figure IVa. 13 *Absorption (top) and emission (buttom) spectra after addition of aliquots of γ-CD into 20 μM solution of* $Co(^{PyB}pdp)(OTf)_2$.

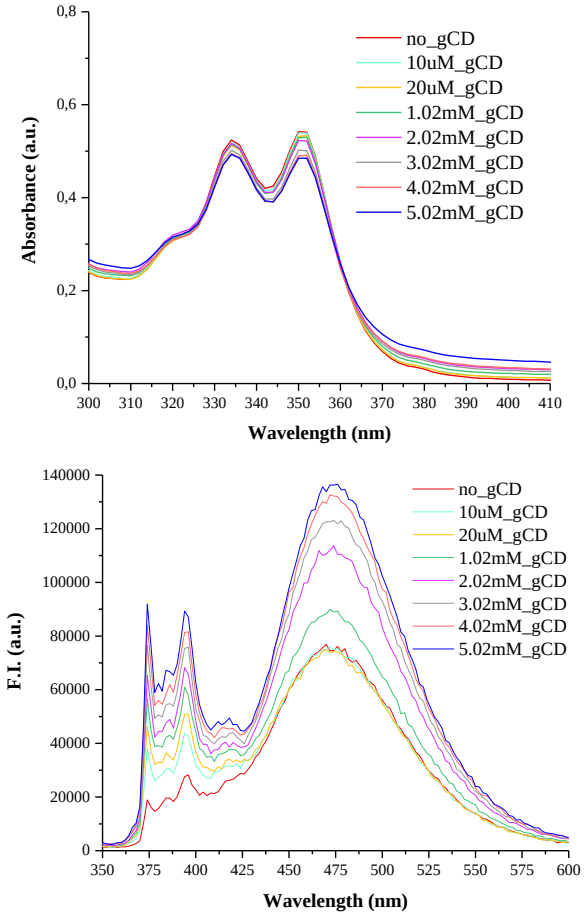

Figure IVa. 14 *Absorption (top) and emission (bottom) spectra after addition of aliquots of γ-CD into 20 μM solution of Ni(^{PyB}mcp)(OTf)$_2$.*

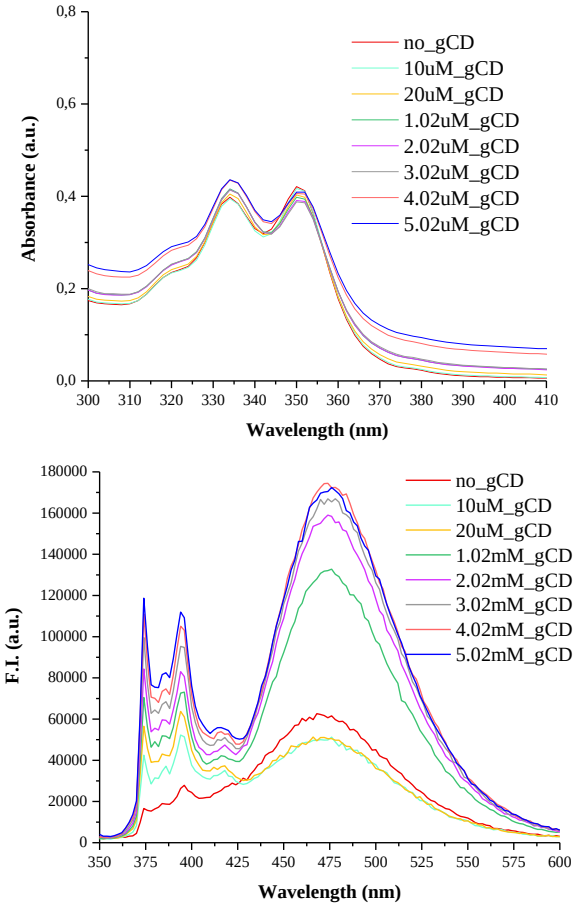

Figure IVa. 15 *Absorption (top) and emission (bottom) spectra after addition of aliquots of γ-CD into 20 μM solution of* $Ni(^{PyB}pdp)(OTf)_2$.

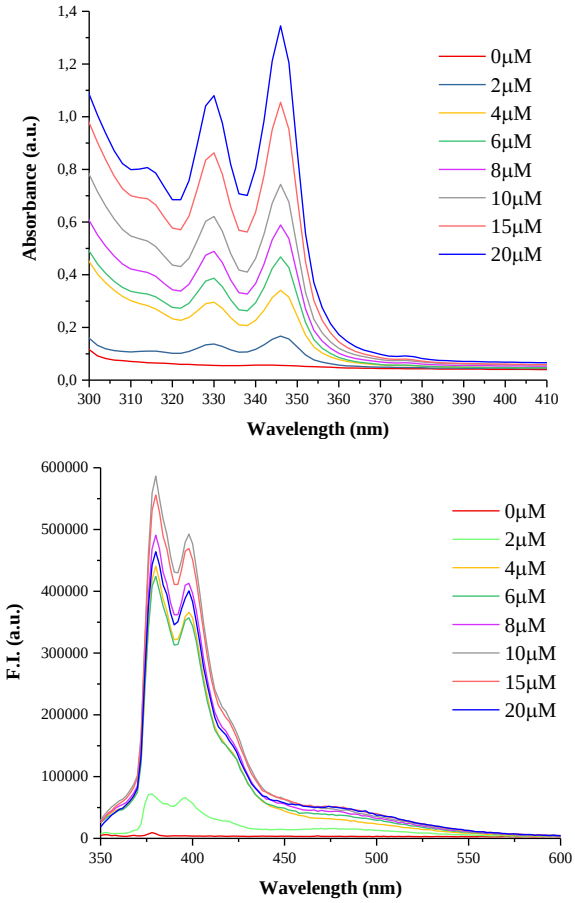

Figure IVa. 16 *Co(^{PyB}pdp)(OTf)$_2$ in acetonitrile/1,2-dichlorobenzene mixture (1:1) at different concentrations.*

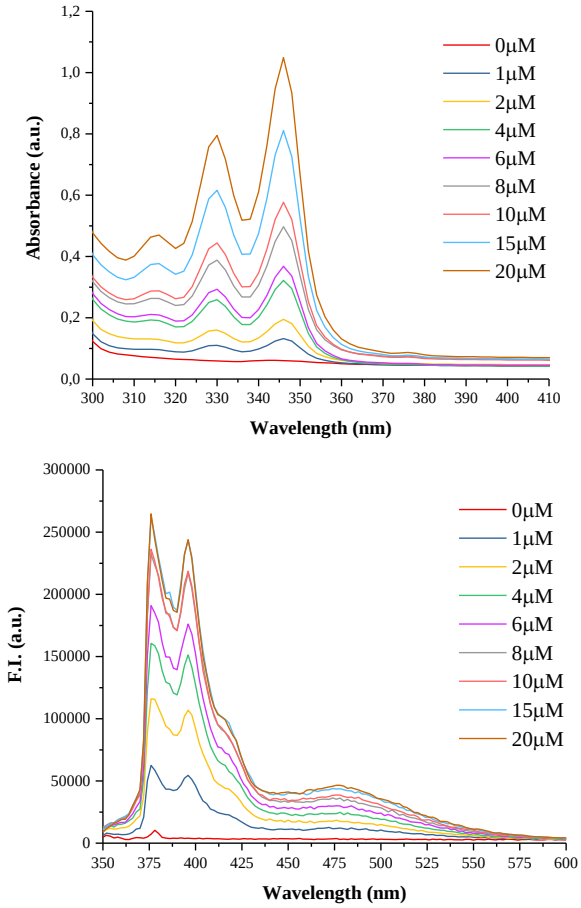

Figure IVa. 17 *Ni(^{PyB}mcp)(OTf)$_2$ in acetonitrile/1,2-dichlorobenzene mixture (1:1) at different concentrations.*

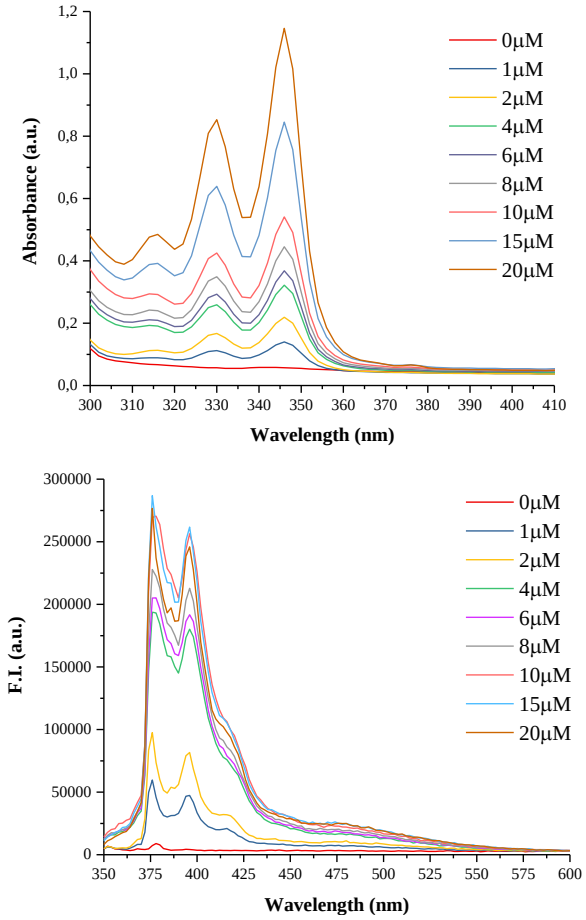

Figure IVa. 18 *Ni(^{PyB}pdp)$(OTf)_2$ in acetonitrile/1,2-dichlorobenzene mixture (1:1) at different concentrations.*

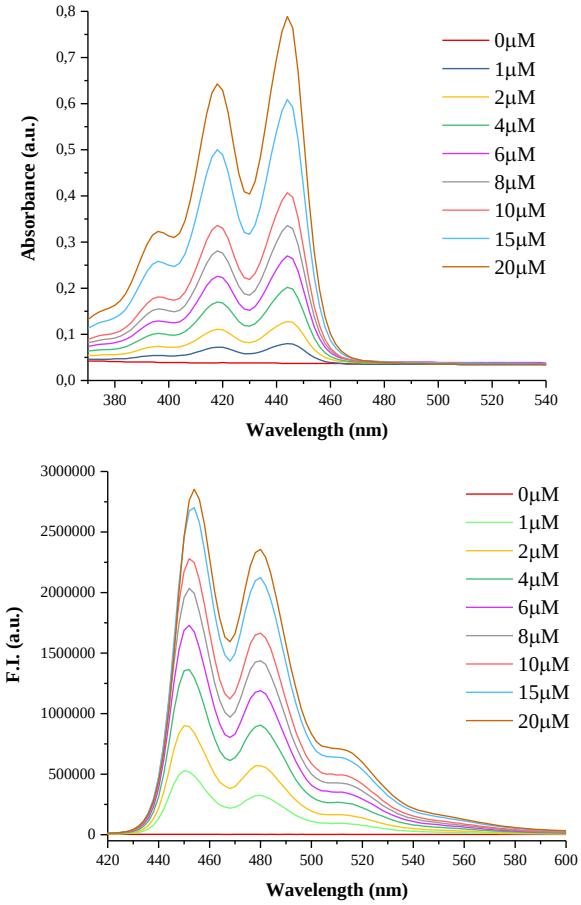

Figure IVa. 19 *$Co(^{PerB}mcp)(OTf)_2$ in acetonitrile/1,2-dichlorobenzene mixture (1:1) at different concentrations.*

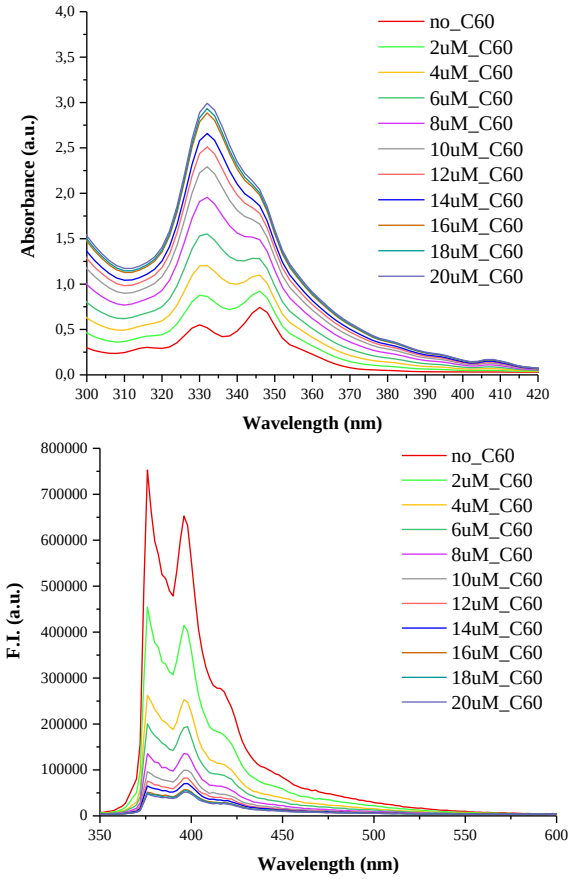

Figure IVa. 20 *Titration of C_{60} into solution of $Co(^{PyB}mcp)(OTf)_2$ measured by absorption (top) and emission (bottom) spectroscopy in acetonitrile/1,2-dichlorobenzene mixture (1:1).*

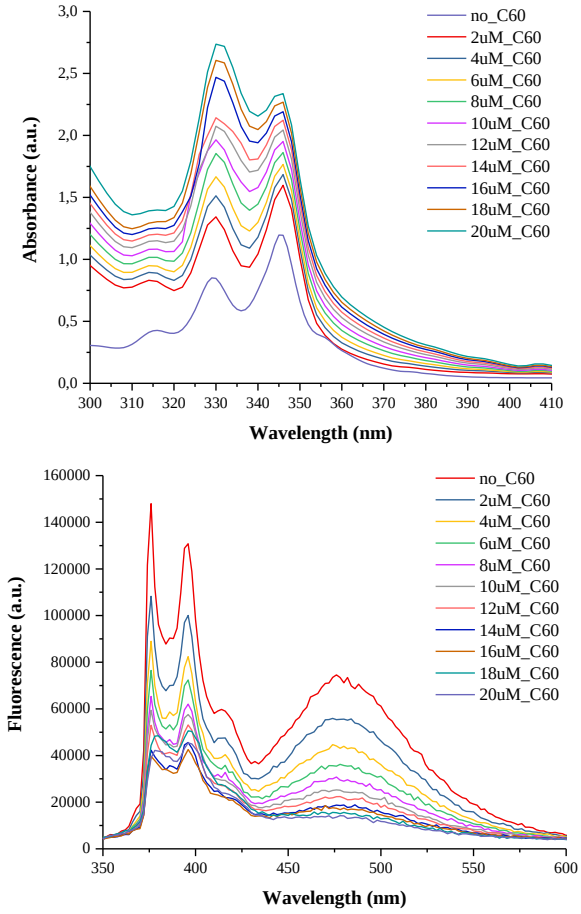

Figure IVa. 21 *Titration of C_{60} into solution of $Co(^{PyB}pdp)(OTf)_2$ measured by absorption (top) and emission (bottom) spectroscopy in acetonitrile/1,2-dichlorobenzene mixture (1:1).*

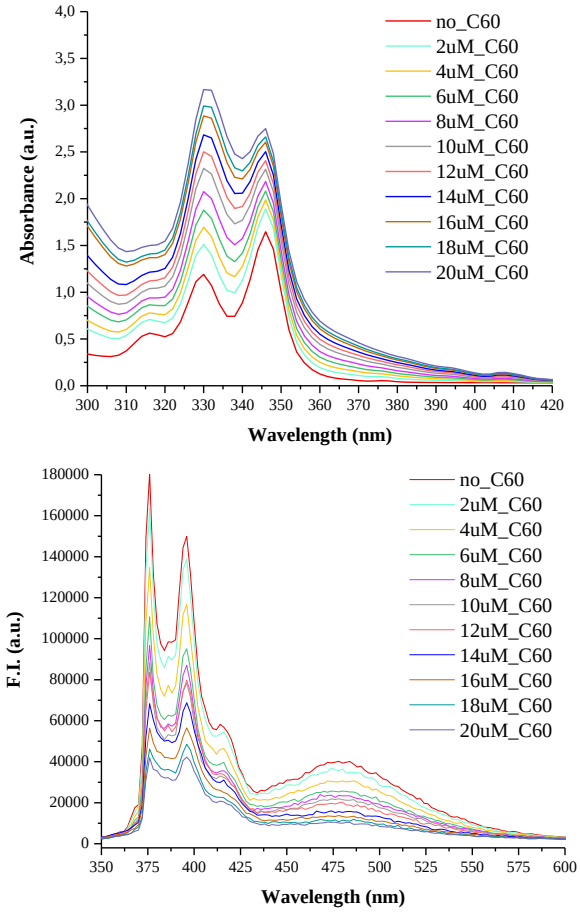

Figure IVa. 22 *Titration of C_{60} into solution of $Ni(^{PyB}mcp)(OTf)_2$ measured by absorption (top) and emission (bottom) spectroscopy in acetonitrile/1,2-dichlorobenzene mixture (1:1).*

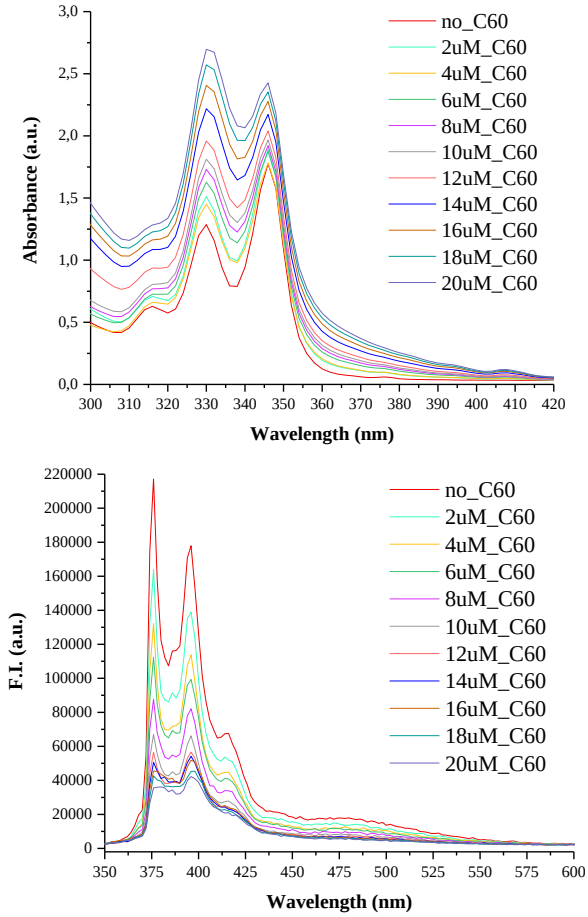

Figure IVa. 23 *Titration of C_{60} into solution of $Ni(^{PyB}pdp)(OTf)_2$ measured by absorption (top) and emission (bottom) spectroscopy in acetonitrile/1,2-dichlorobenzene mixture (1:1).*

IV.6 References of the Chapter

356. Lehn, J.-M., *Supramolecular Chemistry: Receptors, Catalysts, and Carriers.* Science, 1985. **227**(4689): p. 849-856.

357. Lehn, J.-M., *Supramolecular chemistry.* Science, 1993. **260**(5115): p. 1762+.

358. *Front Matter.* 2009: p. i-xxxi.

359. Jayawickramarajah, J. and A.J. Wilson, *Volume 5: Supramolecular Medicinal Chemistry and Chemical Biology.* 2017: p. 1.

360. Mohanty, J., et al., *Mechanistic Aspects of Host–Guest Binding in Cucurbiturils: Physicochemical Properties.* 2017: p. 435-457.

361. Villalonga, R., R. Cao, and A. Fragoso, *Supramolecular Chemistry of Cyclodextrins in Enzyme Technology.* Chemical Reviews, 2007. **107**(7): p. 3088-3116.

362. 1978. **6**.

363. Okamoto, Y. and T.R. Ward, *Supramolecular Enzyme Mimics.* 2017: p. 459-510.

364. Bender, M.L. and M. Komiyama, *Properties.* 1978. **6**: p. 2-9.

365. Wimmer, T., *Cyclodextrins.* 2003.

366. Dodziuk, H., *Molecules with Holes - Cyclodextrins.* 2006: p. 1-30.

367. Hashidzume, A., Y. Zheng, and A. Harada, *Interaction of cyclodextrins with pyrene-modified polyacrylamide in a mixed solvent of water and dimethyl sulfoxide as studied by steady-state fluorescence.* Beilstein Journal of Organic Chemistry, 2012. **8**: p. 1312-1317.

368. Absolom, D.R., *A review of: "Membrane Mimetic Chemistry J. H. Fendler John Wiley and Sons, New York, 1982 Hardcover, 522 pages, $59.95".* Preparative Biochemistry, 2006. **13**(1): p. 75-76.

369. Du, X.-Z., et al., *Phosphorescence-probed study on the association of surfactants with β-cyclodextrin.* Chemical Physics Letters, 1997. **268**(1-2): p. 31-35.

370. Hashimoto, S. and J.K. Thomas, *Fluorescence study of pyrene and naphthalene in cyclodextrin-amphiphile complex systems.* Journal of the American Chemical Society, 2002. **107**(16): p. 4655-4662.

371. VanEtten, R.L., et al., *The mechanism of the cycloamylose-accelerated cleavage of phenyl esters.* Journal of the American Chemical Society, 2002. **89**(13): p. 3253-3262.

372. Macaev, F. and V. Boldescu, *Cyclodextrins in Asymmetric and Stereospecific Synthesis.* Symmetry, 2015. **7**(4): p. 1699-1720.

373. Bai, C., et al., *Cyclodextrin-Catalyzed Organic Synthesis: Reactions, Mechanisms, and Applications.* Molecules, 2017. **22**(9): p. 1475.

374. Srivastava, M., et al., *Role of β-CD in Water as Supramolecular Catalysis.* Current Organocatalysis, 2015. **3**(1): p. 32-38.

375. Breslow, R. and S.D. Dong, *Biomimetic Reactions Catalyzed by Cyclodextrins and Their Derivatives.* Chemical Reviews, 1998. **98**(5): p. 1997-2012.

376. Takahashi, K., *Organic Reactions Mediated by Cyclodextrins.* Chemical Reviews, 1998. **98**(5): p. 2013-2034.

377. Zhang, Q.-W., et al., *A manganese porphyrin–α-cyclodextrin conjugate as an artificial enzyme for the catalytic epoxidation of polybutadiene.* Chemical Communications, 2018. **54**(44): p. 5586-5589.

378. Hapiot, F., et al., *Recent breakthroughs in aqueous cyclodextrin-assisted supramolecular catalysis.* Catalysis Science & Technology, 2014. **4**(7): p. 1899.

379. Hapiot, F., et al., *Catalysis in Cyclodextrin-Based Unconventional Reaction Media: Recent Developments and Future Opportunities.* ACS Sustainable Chemistry & Engineering, 2017. **5**(5): p. 3598-3606.

380. Nan, M.I., et al., *Mono- and di-substituted pyrene-based donor-π-acceptor systems with phenyl and thienyl π-conjugating bridges.* Dyes and Pigments, 2020. **181**: p. 108527.

381. Bains, G.K., et al., *The Extent of Pyrene Excimer Fluorescence Emission Is a Reflector of Distance and Flexibility: Analysis of the*

Segment Linking the LDL Receptor-Binding and Tetramerization Domains of Apolipoprotein E3. Biochemistry, 2012. **51**(31): p. 6207-6219.

382. Lakowicz, J.R., 2006.

383. Förster, T. and K. Kasper, *Ein Konzentrationsumschlag der Fluoreszenz des Pyrens.* Zeitschrift für Elektrochemie, Berichte der Bunsengesellschaft für physikalische Chemie, 1955. **59**(10): p. 976-980.

384. Forster, T., *Molecular Electronic Spectroscopy.* Annual Review of Physical Chemistry, 1957. **8**(1): p. 331-352.

385. v. Bünau, G., *J. B. Birks: Photophysics of Aromatic Molecules. Wiley-Interscience, London 1970. 704 Seiten. Preis: 210s.* Berichte der Bunsengesellschaft für physikalische Chemie, 1970. **74**(12): p. 1294-1295.

386. Winnik, M.A. and F.M. Winnik, *Fluorescence Studies of Polymer Association in Water*. 1993. **236**: p. 485-505.

387. Goedeweeck, M., M. Van der Auweraer, and F.C. De Schryver, *Molecular dynamics of a peptide chain, studied by intramolecular excimer formation.* Journal of the American Chemical Society, 2002. **107**(8): p. 2334-2341.

388. Hammarström, P., et al., *Pyrene excimer fluorescence as a proximity probe for investigation of residual structure in the unfolded state of human carbonic anhydrase II.* FEBS Letters, 1997. **420**(1): p. 63-68.

389. Sahoo, D., et al., *Lipid-triggered Conformational Switch of Apolipophorin III Helix Bundle to an Extended Helix Organization.* Journal of Molecular Biology, 2002. **321**(2): p. 201-214.

390. Lewis, F.D., Y. Zhang, and R.L. Letsinger, *Bispyrenyl Excimer Fluorescence: A Sensitive Oligonucleotide Probe.* Journal of the American Chemical Society, 1997. **119**(23): p. 5451-5452.

391. Yamana, K., et al., *Bis-Pyrene-Labeled Oligonucleotides: Sequence Specificity of Excimer and Monomer Fluorescence Changes upon*

Hybridization with DNA. Bioconjugate Chemistry, 2002. **13**(6): p. 1266-1273.

392. Yamana, K., M. Takei, and H. Nakano, *Synthesis of oligonucleotide derivatives containing pyrene labeled glycerol linkers: Enhhanced excimer fluorescence on binding to a complementary DNA sequence.* Tetrahedron Letters, 1997. **38**(34): p. 6051-6054.
393. Tong, G., et al., *Oligonucleotide-Polyamide Hybrid Molecules Containing Multiple Pyrene Residues Exhibit Significant Excimer Fluorescence.* Journal of the American Chemical Society, 2002. **117**(49): p. 12151-12158.
394. Lee, E.D., T.C. Werner, and W.R. Seitz, *Luminescence ratio indicators for oxygen.* Analytical Chemistry, 2002. **59**(2): p. 279-283.
395. Aoyagi, T., H. Ikeda, and A. Ueno, *Fluorescence Properties, Induced-Fit Guest Binding and Molecular Recognition Abilities of Modifiedγ-Cyclodextrins Bearing Two Pyrene Moieties.* Bulletin of the Chemical Society of Japan, 2001. **74**(1): p. 157-164.
396. Yang, R.-H., et al., *A Ratiometric Fluorescent Sensor for AgI with High Selectivity and Sensitivity.* Journal of the American Chemical Society, 2003. **125**(10): p. 2884-2885.
397. Strauss, J. and J. Daub, *Optically Active Cyclic Hexapeptides with Covalently Attached Pyrene Probes: Selective Alkaline Earth Metal Ion Recognition Using Excimer Emission.* Organic Letters, 2002. **4**(5): p. 683-686.
398. Ludwig, R. and N. Dzung, *Calixarene-Based Molecules for Cation Recognition.* Sensors, 2002. **2**(10): p. 397-416.
399. Farcas, A. and M. Grigoras, *Semiconducting polymers with rotaxane architecture.* Journal of Optoelectronics and Advanced Materials, 2000.
400. Hamai, S., *Pyrene excimer formation in .gamma.-cyclodextrin solutions: association of 1:1 pyrene-.gamma.-cyclodextrin inclusion*

compounds. The Journal of Physical Chemistry, 2002. **93**(17): p. 6527-6529.

401. Ueno, A., *Review: fluorescent cyclodextrins for molecule sensing.* Supramolecular Science, 1996. **3**(1-3): p. 31-36.
402. Yorozu, T., et al., *Photoexcited inclusion complexes of .beta.-naphthol with .alpha.-, .beta.-, and .gamma.-cyclodextrins in aqueous solutions.* The Journal of Physical Chemistry, 2002. **86**(22): p. 4422-4426.
403. Udachin, K.A. and J.A. Ripmeester, *A Novel Mode of Inclusion for Pyrene in β- Cyclodextrin Compounds: The Crystal Structures of β-Cyclodextrin with Cyclohexanol and Pyrene, and with n-Octanol and Pyrene.* Journal of the American Chemical Society, 1998. **120**(5): p. 1080-1081.
404. Shown, I., M. Ujihara, and T. Imae, *Sensitizing of pyrene fluorescence by β-cyclodextrin-modified TiO2 nanoparticles.* Journal of Colloid and Interface Science, 2010. **352**(2): p. 232-237.
405. Sun, L., et al., *Electrocatalytic reduction of carbon dioxide: opportunities with heterogeneous molecular catalysts.* Energy & Environmental Science, 2020. **13**(2): p. 374-403.
406. Sévery, L., et al., *Immobilization of molecular catalysts on electrode surfaces using host–guest interactions.* Nature Chemistry, 2021. **13**(6): p. 523-529.
407. Wang, J., Z. Chen, and B. Chen, *Adsorption of Polycyclic Aromatic Hydrocarbons by Graphene and Graphene Oxide Nanosheets.* Environmental Science & Technology, 2014. **48**(9): p. 4817-4825.
408. Georgakilas, V., et al., *Noncovalent Functionalization of Graphene and Graphene Oxide for Energy Materials, Biosensing, Catalytic, and Biomedical Applications.* Chemical Reviews, 2016. **116**(9): p. 5464-5519.
409. Ehli, C., et al., *Interactions in Single Wall Carbon Nanotubes/Pyrene/Porphyrin Nanohybrids.* Journal of the American Chemical Society, 2006. **128**(34): p. 11222-11231.

410. Barry, N.P.E. and B. Therrien, *Pyrene: The Guest of Honor.* 2016: p. 421-461.

411. Ulatowski, F., et al., *Recognizing the Limited Applicability of Job Plots in Studying Host–Guest Interactions in Supramolecular Chemistry.* The Journal of Organic Chemistry, 2016. **81**(5): p. 1746-1756.

412. Zhou, R., 2015.

413. Pistolis, G. and A. Malliaris, *Evidence for Highly Selective Supramolecular Formation between Perylene/γ-CD and Pyrene/γ-CD Complexes in Water.* The Journal of Physical Chemistry B, 2004. **108**(9): p. 2846-2850.

414. Hayashi, K., et al., *Observation of Circularly Polarized Luminescence of the Excimer from Two Perylene Cores in the Form of [4]Rotaxane.* Chemistry – A European Journal, 2018. **24**(55): p. 14613-14616.

415. Takahashi, N., et al., *Luminescences of Pyrene Single Crystal and Pyrene Molecules Inserted in a Molecular Vessel of Cyclodextrin.* Journal of the Physical Society of Japan, 2007. **76**(3): p. 034703.

416. Sluch, M.I., I.D.W. Samuel, and M.C. Petty, *Quenching of pyrene fluorescence by fullerene C60 in Langmuir–Blodgett films.* Chemical Physics Letters, 1997. **280**(3-4): p. 315-320.

417. Martin, R.B., et al., *Interesting fluorescence properties of C60-centered dendritic adduct with twelve symmetrically attached pyrenes.* Chemical Communications, 2003(18): p. 2368.

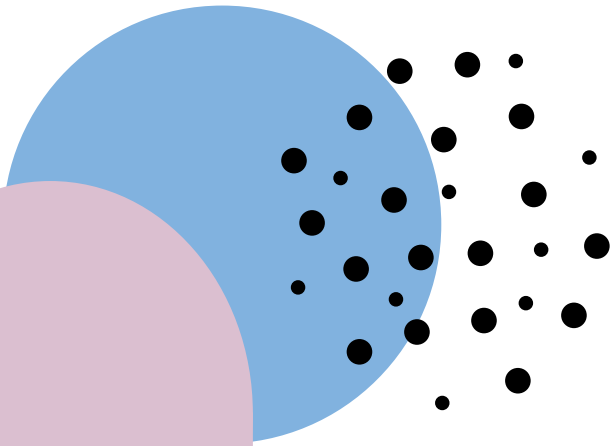

Chapter V

Well-defined tripodal Ni Complexes as Selective Catalysts for Hydrogenation of *N*-Heteroarenes Under Mild Conditions.

UNIVERSITAT ROVIRA I VIRGILI
ORGANIC TRANSFORMATIONS USING TRANSITION METALS AND PHOTOREDOX CATALYSTS
Klaudia Michaliszyn

UNIVERSITAT ROVIRA I VIRGILI
ORGANIC TRANSFORMATIONS USING TRANSITION METALS AND PHOTOREDOX CATALYSTS
Klaudia Michaliszyn

V.1 State-of-the-art

Hydrogen (H_2) as the simplest diatomic molecule is also very important promising fossil-fuel alternative. H_2, despite its simplicity is desired product as energy vector in homogeneous water splitting (hydrogen evolution reaction - HER) for possible practical applications. One of these is hydrogenation – the most fundamental chemical process in industry of addition of H_2 as a reducing agent to unsaturated bonds in molecules.[418, 419]

Nevertheless, hydrogen needs to be activated to react with another molecules, the H-H covalent bond must be split under mild conditions mediated by transition-metal-based catalyst[420] (homogeneous or heterogenous), either in homolytic or heterolytic way. Noble and non-noble metals were found to be crucial to lower the activation barrier of hydrogenation reaction.

Longstanding interest in studying the hydrogenation reactions, despite the fact of many established technologies, research continues to uncover new ways to effect this fundamental transformation.[420] A class of tetradentate C_3-symmetric phosphine ligands are the rather unique **P3CH** ligands, where the apical central carbon atom can be metallated. Nevertheless, the derivate metalated organometallic complexes have only rarely explored, most probably due to the challenging synthetic access.[421] The tripodal complexes of first-row-transition metals have shown to activate small molecules[422-426], however to our knowledge any practical application were found as far.

N-heteroarenes reduction is a challenging but appealing methodology to obtain bioactive products of difficult access[427-429] and organic hydrogen storage material.[281, 430, 431] To this end, the *N*-heteroarene hydrogenation is a direct and convenient route to obtain *N*-tetrahydro-heteroarenes due to the availability of starting materials and the use of molecular hydrogen as clean reducing agent. Until recently, the reduction of *N*-heteroarenes have required hard reaction conditions, limiting the selectivity and incompatible with other reducible functional groups installed in the same molecule and therefore limiting the scope tolerance to particular examples.[432-435]

Despite the progress, only limited examples of selective homogenous first-row-transition based catalytic systems are reported, with limited tolerance of functional groups. Nevertheless, catalysts based on well-defined metal complexes have the potential to yield high levels of selectivity and reactivity.[436] A remarkable activity obtained by Beller's group, using simple manganese carbonyl complex **[Mn(CO)$_5$Br]**[437] (Scheme V.1) under mild conditions, and (tris(2-(di-phenyl-phosphino)-phenyl)-phosphine-cobalt-fluoride for hydrogenation of *N*-heteroerenes. An outstanding example was reported for the [**Co(F)P$_4$**][438] complex, with the tetrahedral **P4** ligand that forms highly stable bipyramid trigonal metal complexes.[439, 440]

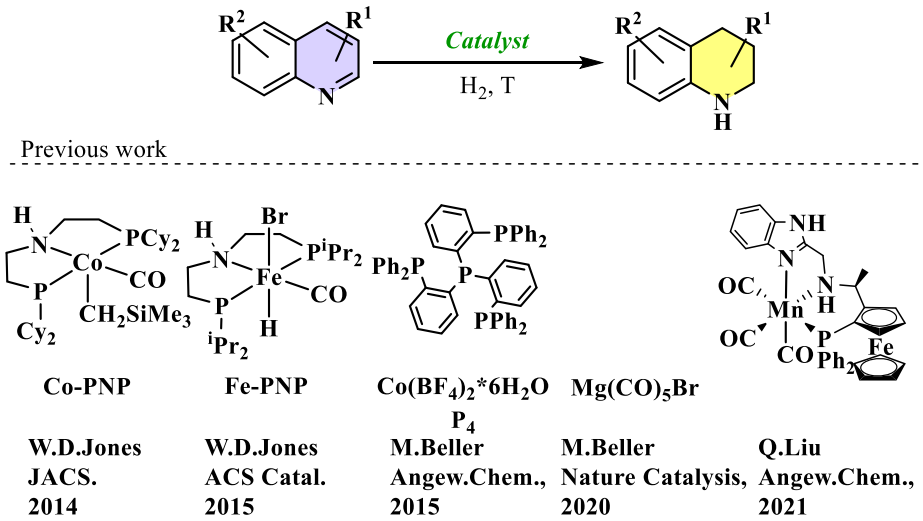

Scheme V. 1 *Hydrogenation of quinolines with homogeneous catalysts.*

The tetradentate C_3-symmetric phosphorus phosphine ligands present some similarities to **P$_4$**. The coordination of P_3C type ligand have been have only rarely explored, most probably due to the challenging synthetic access. To note is the apical P atom and its potential strong trans influence or effect in the exchangeable coordination site where catalysis may occur. We were intrigued by the catalytic capacity of [**Co(F)P$_4$**] and hypothesized if the potential strong trans influence and effect of the apical phosphorous atom could be a key motive of the catalytic hydrogenation activity against N-heteroarenes. However, until now, there is not information about how this catalyst operate. Certainly, in

general, the mechanistic information about catalytic hydrogenation of *N*-heteroarenes with metal complexes is still scarce. Only the picer complexes promoting hydrogenation of *N*-heteroarenes **Fe-PNP**[441] and **Co-PNP**[442] have been studied by Jones and co-workers with some detail. However, their structure is radically different and cannot explain the merit of [**Co(F)P$_4$**].

We investigated the nickel complexes with a metalated tripodal ligand tris[1-(diphenylphosphanyl)-3-methyl-1H-indol-2-yl]methane (**HTIM(PR$_2$)$_3$**) ligand) (Scheme V.2), with a carbon atom in apical position, and the study of their electronic structure by DFT. The complexes are bench stable and catalyse the hydrogenation of *N*-heteroarenes. To our knowledge, this is the first example of a well-defined homogeneous nickel complex for the hydrogenation of *N*-heteroarenes. Despite the capacity of nickel as heterogeneous hydrogenation catalyst[443][432, 444, 445], homogeneous hydrogenation catalysts are not known. In our case, we propose the hydrogenation proceeding under mild conditions, with excellent tolerance to other reducible functional groups and with insignificant catalyst decomposition. Based on labelling and computational studies we proposed a heterolytic hydrogenation mechanism initiated by a dual activation of the hydrogen molecule by the nickel complex and the quinoline operating alike a frustrated Lewis pair.

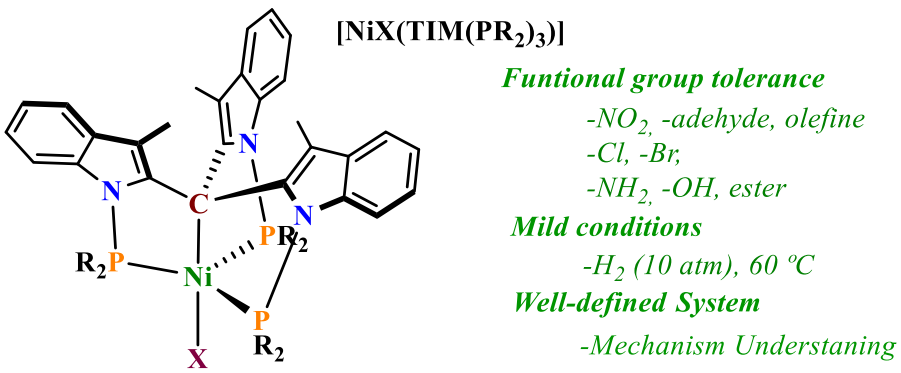

Scheme V. 2 *Homogeneous tripodal nickel based catalyst.*

Objectives:

- To develop and characterize new class of well-defined nickel and cobalt complexes based on P_3^C ligands;

- To explore the effect of ligand's electron donating and electron withdrawing groups in quinoline hydrogenation;
- To study catalytic activity towards N-heteroarenes;
- To explore the mechanistic aspects of the hydrogen activation by designed catalysts.

V.2 Results and Discussion

V.2.1 Synthesis of HTIM(PR$_2$)$_3$ ligands and their complexes

We synthetized ligands tris(1-(diphenylphosphaneyl)-3-methyl-1H-indol-2-yl)methane (**HTIM[P(Ph$_2$)]$_3$**) by a modified protocol for the synthesis of tris(*N*-diisopropylphosphino-3-methyl-2-indolyl)methane (HTIM(P*i*Pr$_2$)$_3$)[446] that was optimized previously in our group. 3-Methylindole (V.1) was coupled with triethyl orthoformate (V.2) to yield HTIM (67%), which was then deprotonated with washed NaH (4 eq.) and treated with *P*-Chlorodiphenylphosphine (3.5 eq.) to obtain desired ligand HTIM(PPh$_2$)$_3$ (74%).

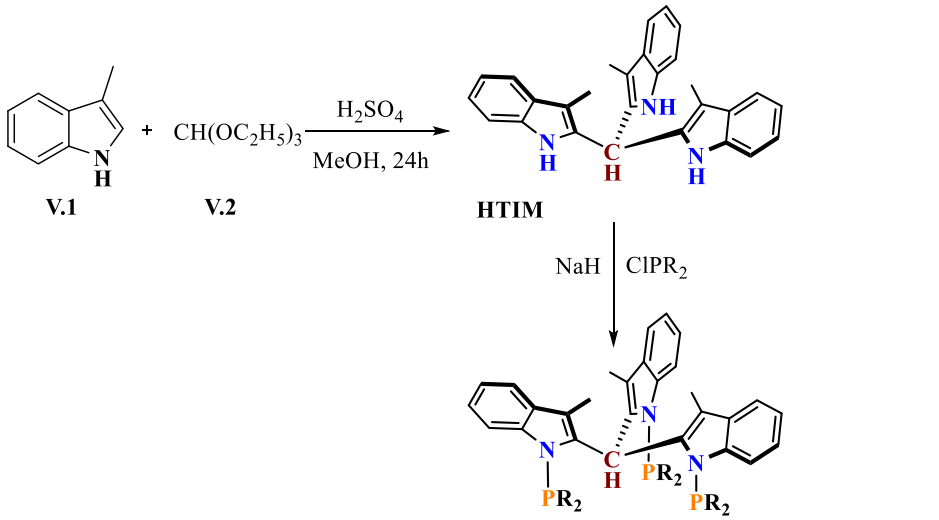

***Scheme V. 3** Synthesis of tripodal ligands.*

The modular synthetic procedure of the ligand allowed us to modify its electronic property by modifying the aryl groups over the phosphine with electron donating and electron withdrawing groups. This way we synthetized ligands tris(*N*-di(paratolyl)phosphino-3-methyl-2-indolyl)methane (**HTIM[P($^{p\text{-Me}}$C$_6$H$_4$)$_2$]$_3$**) and tris(*N*-di(parafluorophenyl)phosphino-3-methyl-2-indolyl)methane (**HTIM[P($^{p\text{-F}}$C$_6$H$_4$)$_2$]$_3$**) (Scheme V.3).

We wanted to focus on first row transition metals since the complexes with this class of ligand are not well known, due to the difficulties with metalation. NiX_2 salts (X = Cl, Br, I, OTf), Ni(glyme)X_2 (X = Cl, Br) or bis(1,5-cyclooctadiene)nickel(0) and CoX_2 (X=Cl, I, OTf) salts do not directly react with the **HTIM(PPh$_2$)$_3$** ligand even at high temperatures (~150 ºC).[446] However, the ligand can be metallated in good yield (93%) by addition of NEt_3 to the reaction mixture (Scheme V.4). Reactions performed under the same conditions did not proceed in the absence of the base. The full conversion of ligand to nickel complex occurs after 15h, yielding dark green diamagnetic complex **NiTIM(PPh$_2$)$_3$Br** (93%) and to dark brown paramagnetic complex **CoTIM(PPh$_2$)$_3$I** (84%). Then treatment of **NiTIM(PPh$_2$)$_3$Br** with the $AgNTf_2$ salt yields **NiTIM(PPh$_2$)$_3$NTf$_2$** with good yield (85%). Metallation reactions of **HTIM[P($^{p\text{-Me}}$C$_6$H$_4$)$_2$]$_3$** and **HTIM[P($^{p\text{-F}}$C$_6$H$_4$)$_2$]$_3$** were performed following the same procedure, leading to Ni^{II} and Co^{II} complexes **NiTIM[P($^{p\text{-Me}}$C$_6$H$_4$)$_2$]$_3$Br (**85%**), CoTIM[P($^{p\text{-Me}}$C$_6$H$_4$)$_2$]$_3$I** (62%), **NiTIM[P($^{p\text{-F}}$C$_6$H$_4$)$_2$]$_3$Br** (87%) and **CoTIM[P($^{p\text{-F}}$C$_6$H$_4$)$_2$]$_3$I** (71%), nevertheless these ligands required higher temperatures (140 ºC instead of 105 ºC) than their simpler analogues.

Interesting feature of the synthesis of these complexes was the reactivity. Binding the cobalt salt to the ligand was challenging, therefore we performed the oxidation reaction of Co^{II} to Co^{III} to check if this action may facilitate CH bond activation by pressurizing the reaction tube with high pressure of O_2. These conditions let us obtain the conversion to the complex in shorter time. To understand how the reaction proceeds, we wanted to understand if the reaction goes through Co^{III} by creating some active species with oxygen and to know the role of the oxygen since it speeds up the reaction. Then, we tried the

reaction in the presence of nitrosyl hexafluorophosphate, which has enough redox potential to oxidize the Co(II) to Co(III) but it was unsuccessful. Next, magic blue was also used in the reaction as an oxidant that is known to abstract proton. In ^{31}P NMR spectra two diamagnetic peaks (singlets) were observed that were not present before the reaction and in addition the ^{1}H NMR showed formation of new paramagnetic species. Then reaction was left stirring over the weekend to let the reaction finish but unexpected in ^{31}P NMR multiplicity of peaks changed and paramagnetic species disappeared in ^{1}H NMR. To understand how the reaction occurs more experiments are needed but for the moment we can propose that the use of magic blue we can either oxidize the ligand or create another species while leaving the reaction to perform over the weekend. These reactions showed better reactivity in the absence of O_2, but only in the ligand substituted with methyl groups, we observed complete conversion to paramagnetic product.

The ligands their and cobalt and nickel complexes were characterized by NMR, ESI-MS, X-Ray analysis and elemental analysis (See section V.4.6). All the complexes structure could be stablished by X-Ray diffraction analysis. The recrystallization of compounds to grow the crystals was carried out by slow diffusion and small crystals were obtained in all cases. These single-crystals were analyzed and the analysis confirms the formation of bipyramid trigonal geometry complexes formed by a tridentate ligand bonded to the cobalt or nickel by three phosphines and central carbon atom.

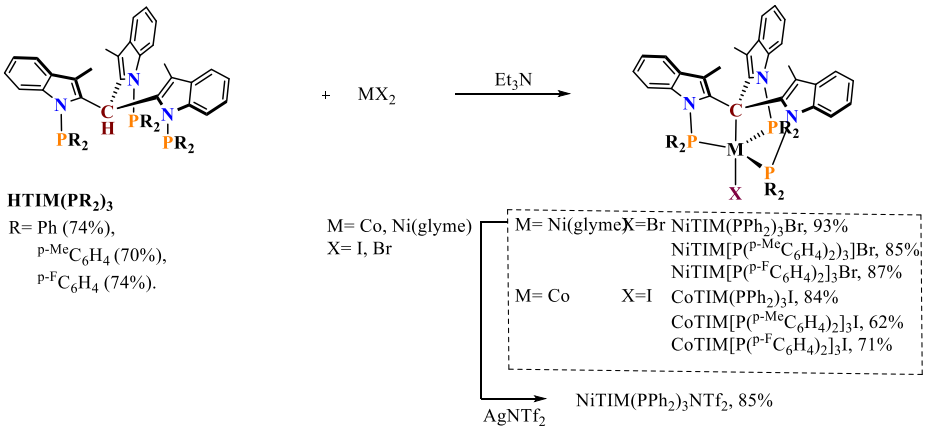

Scheme V. 4 *Synthesis of nickel and cobalt based tripodal complexes.*

^{1}H-NMR spectroscopy at room temperature of nickel complexes, collected in Figure V.1 exhibit in diamagnetic region, which is consistent with d^8 Ni^{II} diamagnetic complexes with bipyramid trigonal geometry are collected in Figure V.2 spectrum of cobalt complexes, revealed paramagnetic spectra expanding from -9 to 14 ppm. The most deshielded peaks belong to the protons from the substituents on phosphines groups, since these are the hydrogens closest to the paramagnetic Co^{II} center[345], because of Fermi contact interactions with the metal center. Peaks found in more shielded region are assigned to indole moieties, indicating that these parts are placed far away from the metal center, hence the influence of the metal affect them in slight manner. All complexes exhibit features, which are united with the configuration of trigonal bipyramidal Co^{II} paramagnetic family.

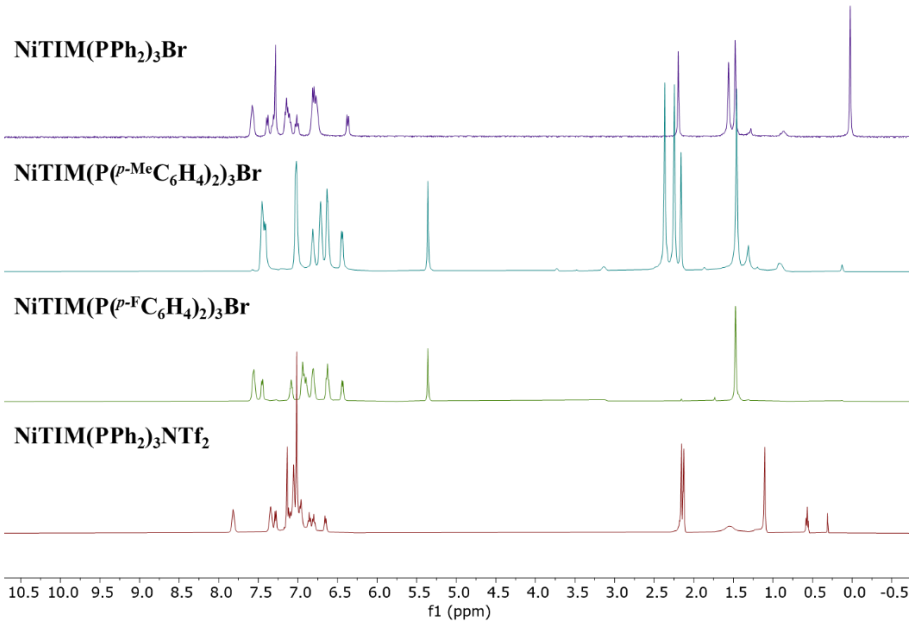

Figure V. 1 *^{1}H NMR spectra of* ***NiTIM(PPh$_2$)$_3$Br, NiTIM[P(p-MeC$_6$H$_4$)$_2$]$_3$Br, NiTIM[P(p-FC$_6$H$_4$)$_2$]$_3$Br*** *and* ***NiTIM(PPh$_2$)$_3$NTf$_2$****.*

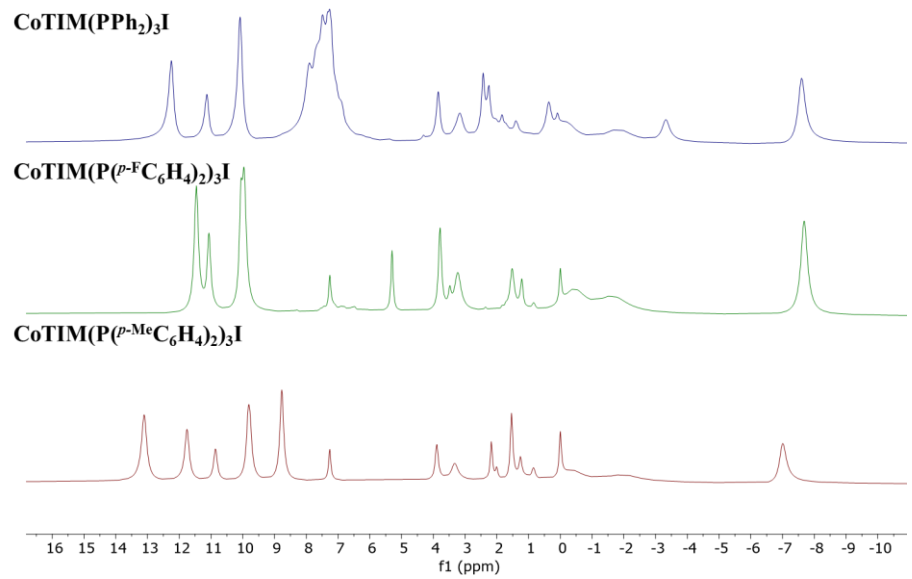

Figure V. 2 *^{1}H NMR spectra of* ***CoTIM(PPh$_2$)$_3$I, CoTIM[P(p-FC$_6$H$_4$)$_2$]$_3$I*** *and* ***CoTIM[P(p-MeC$_6$H$_4$)$_2$]$_3$I****.*

High resolution mass spectrometry using electrospray ionization (ESI) and matrix-assisted laser desorption/ionization (MALDI) agree with the

characterization. Mono charged molecular peaks were observed for complexes NiTIM(PPh_2)$_3$Br ([M-Br-H]$^+$; 1013.0056 m/z), NiTIM(PPh_2)$_3$$NTf_2$ ([M-NTf_2]$^+$; 1012.2658 m/z), NiTIM[P($^{p\text{-Me}}C_6H_4$)$_2$]$_3$Br ([M]$^+$; 1175.2746 m/z), NiTIM[P($^{p\text{-F}}C_6H_4$)$_2$]$_3$Br ([M]$^+$; 1199.1239 m/z), CoTIM(PPh_2)$_3$I ([M]$^+$; 1140.1670 m/z), CoTIM[P($^{p\text{-Me}}C_6H_4$)$_2$]$_3$I ([M-H]$^+$; 1224.2605 m/z) and CoTIM[P($^{p\text{-F}}C_6H_4$)$_2$]$_3$I ([M]$^+$; 1248.1136 m/z).

All of the desired solid state structures of NiTIM(PPh_2)$_3$Br, NiTIM[P($^{p\text{-Me}}C_6H_4$)$_2$]$_3$Br, NiTIM[P($^{p\text{-F}}C_6H_4$)$_2$]$_3$Br, NiTIM(PPh_2)$_3$$NTf_2$, CoTIM($PPh_2$)$_3$I, CoTIM[P($^{p\text{-F}}C_6H_4$)$_2$]$_3$I and CoTIM[P($^{p\text{-Me}}C_6H_4$)$_2$]$_3$I could be stablished by X-Ray diffraction analysis. Crystals of complexes were grown by performed slow diffusion of dichloromethane with hexane. The analysis of monocrystals (Figure V.3 and V.4) confirmed the formation of complexes with bipyramid trigonal geometry formed by tetradentate ligand bonded to metal by three phosphines and one carbon (connecting three 3-methylindoles); last coordination site occupied by a labile bromide (nickel complexes) or iodide (cobalt complexes) ion.

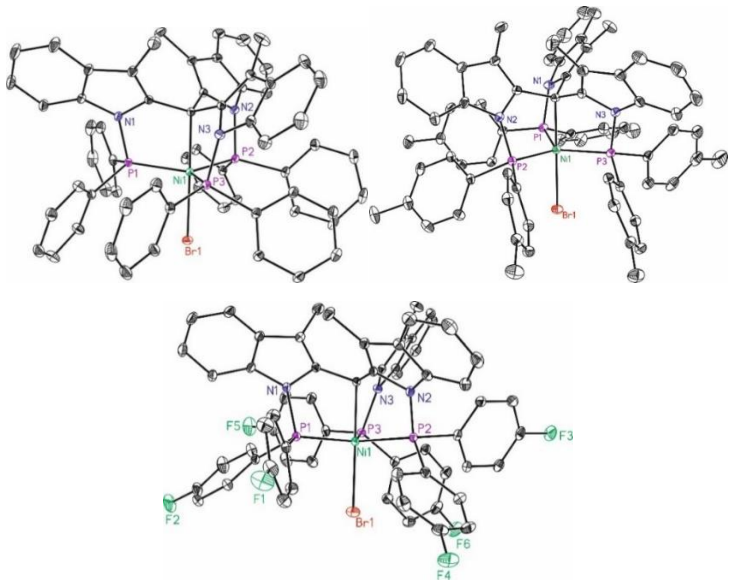

Figure V. 3 *Structures of NiTIM(PPh_2)$_3$Br, NiTIM[P($^{p\text{-Me}}C_6H_4$)$_2$]$_3$Br and NiTIM[P($^{p\text{-F}}C_6H_4$)$_2$]$_3$Br from the X-Ray diffraction analysis. Hydrogen atoms have been omitted for clarity.*

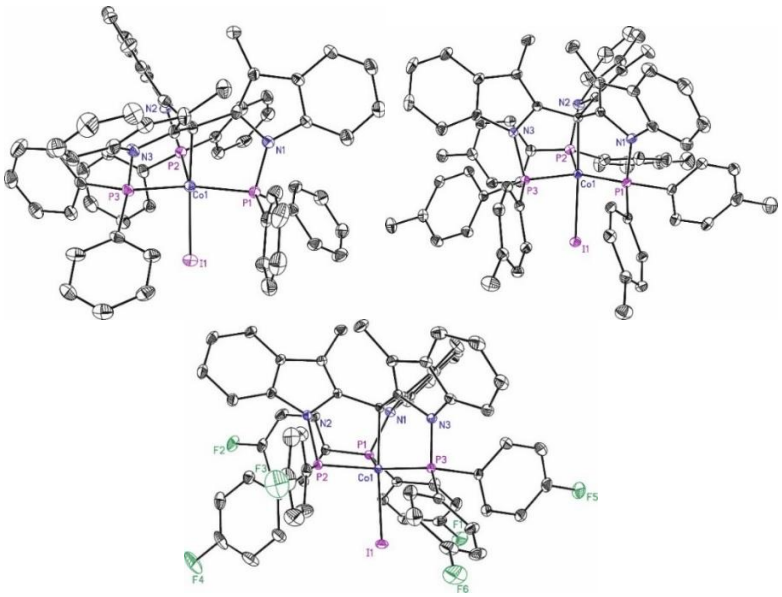

Figure V. 4 *Structures of CoTIM(PPh$_2$)$_3$I, CoTIM[P($^{p\text{-}Me}$C$_6$H$_4$)$_2$]$_3$I and CoTIM[P($^{p\text{-}F}$C$_6$H$_4$)$_2$]$_3$I from the X-Ray diffraction analysis. Hydrogen atoms have been omitted for clarity.*

Selected bond distances (Å) and angles (°) are collected in Table V.1-6. The average Ni-P and Co-P bond lengths are between 2.1 and 2.3 Å, which are in the range of expected values for the three phosphines.[424, 446] The average Ni-C bond lengths were found to be between 2.06 and 2.07 Å and Co-C bond lengths are around 2.0 and 2.1 Å being considerably shorter for the metal with apical carbon.[447]

Table V.1 Selected bond lengths (Å) and angles (°) of NiTIM(PPh$_2$)$_3$Br.

NiTIM(PPh$_2$)$_3$Br			
Ni1-P1	2.1917(3)	P1-Ni1-P2	120.717(10)
Ni1-P2	2.1935(3)	P2-Ni1-P3	118.874(10)
Ni1-P3	2.1932(3)	P1-Ni1-P3	119.8261(10)
Ni1-Br1	2.42734(17)	C1-Ni1-P1	86.33(3)
Ni1-C1	2.0623(10)	C1-Ni1-P2	86.51(2)
		C1-Ni1-P3	86.47(2)
		P1-Ni1-Br1	92.873(9)

Table V.2 Selected bond lengths (Å) and angles (°) of NiTIM[P(p-MeC$_6$H$_4$)$_2$]$_3$Br.

NiTIM[P(p-MeC$_6$H$_4$)$_2$]$_3$Br			
Ni1-P1	2.2129(5)	P1-Ni1-P2	118.833(19)
Ni1-P2	2.2116(5)	P2-Ni1-P3	114.185(19)
Ni1-P3	2.1998(5)	P1-Ni1-P3	125.689(19)
Ni1-Br1	2.4402(3)	C1-Ni1-P1	85.72(5)
Ni1-C1	2.0651(16)	C1-Ni1-P2	86.60(5)
		C1-Ni1-P3	86.42(5)
		P1-Ni1-Br1	94.690(15)

Table V.3 Selected bond lengths (Å) and angles (°) of NiTIM[P(p-FC$_6$H$_4$)$_2$]$_3$Br.

NiTIM[P(p-FC$_6$H$_4$)$_2$]$_3$Br			
Ni1-P1	2.1933(4)	P1-Ni1-P2	127.182(17)
Ni1-P2	2.2158(4)	P2-Ni1-P3	110.647(17)
Ni1-P3	2.2596(3)	P1-Ni1-P3	119.725(17)
Ni1-Br1	2.4270(3)	C1-Ni1-P1	84.98(4)
Ni1-C1	2.0613(15)	C1-Ni1-P2	83.39(4)
		C1-Ni1-P3	86.21(4)
		P1-Ni1-Br1	91.742(13)

Table V.4 Selected bond lengths (Å) and angles (°) of CoTIM(PPh$_2$)$_3$I.

CoTIM(PPh$_2$)$_3$I			
Co1-P1	2.1899(16)	P1-Co1-P2	112.80(6)
Co1-P2	2.2660(16)	P2-Co1-P3	107.97(6)
Co1-P3	2.2564(16)	P1-Co1-P3	136.63(6)
Co1-I1	2.6153(8)	C1-Co1-P1	86.49(16
Co1-C1	2.092(5)	C1-Co1-P2	84.31(15)
		C1-Co1-P3	83.35(15)
		P1-Co1-I1	89.00(4)

Table V.5 Selected bond lengths (Å) and angles (°) of CoTIM[P($^{p\text{-Me}}$C$_6$H$_4$)$_2$]$_3$I.

CoTIM[P($^{p\text{-Me}}$C$_6$H$_4$)$_2$]$_3$I			
Co1-P1	2.1959(5)	P1-Co1-P2	136.494(19)
Co1-P2	2.2611(5)	P2-Co1-P3	114.56(18)
Co1-P3	2.2054(5)	P1-Co1-P3	106.928(17)
Co1-I1	2.6191(3)	C1-Co1-P1	86.43(5)
Co1-C1	2.084(16)	C1-Co1-P2	84.18(4)
		C1-Co1-P3	85.75(4)
		P1-Co1-I1	95.502(14)

Table V.6 Selected bond lengths (Å) and angles (°) of CoTIM[P($^{p\text{-F}}$C$_6$H$_4$)$_2$]$_3$I.

CoTIM[P($^{p\text{-F}}$C$_6$H$_4$)$_2$]$_3$I			
Co1-P1	2.2458(5)	P1-Co1-P2	106.943(18)
Co1-P2	2.2285(5)	P2-Co1-P3	114.477(18)
Co1-P3	2.2217(5)	P1-Co1-P3	135.442(18)
Co1-I1	2.6009(3)	C1-Co1-P1	82.93(4)
Co1-C1	2.0787(16)	C1-Co1-P2	85.11(4)
		C1-Co1-P3	84.86(4)
		P1-Co1-I1	95.158(13)

Table V.7 Compared bond lengths (Å) of $P_3{}^C$ metal complexes.

	M1-P1	**M1-P2**	**M1-P3**	**M1-X1**	**M1-C**
NiTIM(PPh$_2$)$_3$Br	2.1917	2.1935	2.1932	2.42734	2.0623
NiTIM[P($^{p\text{-Me}}$C$_6$H$_4$)$_2$]$_3$Br	2.2129	2.2116	2.1998	2.4402	2.0651
NiTIM[P($^{p\text{-F}}$C$_6$H$_4$)$_2$]$_3$Br	2.1933	2.2158	2.2596	2.4270	2.0613
CoTIM(PPh$_2$)$_3$I	2.1899	2.2660	2.2564	2.6153	2.092
CoTIM[P($^{p\text{-Me}}$C$_6$H$_4$)$_2$]$_3$I	2.1959	2.2611	2.2054	2.6191	2.084
CoTIM[P($^{p\text{-F}}$C$_6$H$_4$)$_2$]$_3$I	2.2458	2.2285	2.2217	2.6009	2.0787

V.2.2 Hydrogenation of N-Heteroarenes

The catalytic reactions employing Ni^{II} and Co^{II} complexes were examined towards their activity. Catalysis was performed in autoclave HEL reactor (The HEL CAT24 multireactor consists in a cylindrical vessel in 316 SS; it has capacity for 24 vials (10 x75 mm)). The HEL reactor was purged three times with 30 bar of hydrogen, then pressurized to the working H_2 atmosphere (10 - 15 bars) and placed into an aluminium block, which was preheated at the corresponding temperature. After catalysis, the multireactor was cooled in an ice bath, and the remaining gas was carefully released. To determine the isolated yield of the hydrogenated products, the reaction mixture was purified by silica gel column chromatography (n-hexane/AcOEt mixtures) to give the corresponding desired heteroarene. The catalytic reactions were performed in a 3.5 mL glass tube in dry toluene (1.4 mL) as solvent.

The catalytic activity of nickel and cobalt tripodal complexes towards photocatalytic redaction of N-heteroarenes was carried out by preparing the reaction mixture containing 0.25 mmol of N-heterocycle, 2.5-5 mol% of $MTIM(PPR_2)_3X$ complex and 2.5-5 mol% of $AgNTf_2$ in dry solvent (1.4 mL) at corresponding temperature under hydrogen atmosphere which was run during 15h.

First, we have studied the bromide complex **NiTIM(PPh$_2$)$_3$Br** and its triflimide salt **NiTIM(PPh$_2$)$_3$NTf$_2$** (2.5 mol%) in the reduction of quinoline under standard reaction conditions: quinoline V.1a (0.25 mmol), nickel complex (2.5 mol%), SPS grade solvent (1.4 mL) and H_2 (10 bar) at T°C during 15 h (entries 1 and 2, Table V.8). Complex **NiTIM(PPh$_2$)$_3$Br** was inactive for the hydrogenation of quinoline. In contrast, **NiTIM(PPh$_2$)$_3$NTf$_2$** resulted very good activity. Product V.2a was isolated by preparative TLC chromatography. Nevertheless, the addition of a halogen abstracting salt ($AgNTf_2$) to the reaction mixture containing **NiTIM(PPh$_2$)$_3$Br** resulted in a similar catalytic activity to **1^{NTf2}** in both polar and non-polar solvents (10 atm of H_2 at 30 ºC, entries 3 - 6).

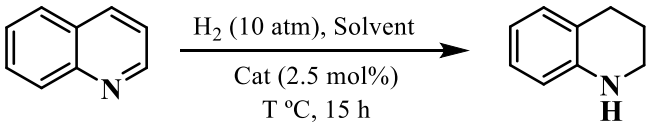

V.1a **V.2a**

Table V.8 Optimization of the reaction conditions for NiTIM(PPh$_2$)$_3$Br, NiTIM[P(*p*-^{Me}C$_6$H$_4$)$_2$]$_3$Br, NiTIM[P(*p*-^{F}C$_6$H$_4$)$_2$]$_3$Br and NiTIM(PPh$_2$)$_3$NTf$_2$.

Entry	T (ºC)	Solvent	Catalyst	Yield, %
1	60	toluene	**NiTIM(PPh$_2$)$_3$Br**	0
2	30	toluene	**NiTIM(PPh$_2$)$_3$NTf$_2$**	92
3	30	toluene	**NiTIM(PPh$_2$)$_3$Br** + AgNTf$_2$	90
4	30	THF	**NiTIM(PPh$_2$)$_3$Br** + AgNTf$_2$	84
5	30	acetone	**NiTIM(PPh$_2$)$_3$Br** + AgNTf$_2$	72
6	30	DMF	**NiTIM(PPh$_2$)$_3$Br** + AgNTf$_2$	70
7	60	toluene	**NiTIM(PPh$_2$)$_3$Br** + AgNTf$_2$ + Hg	90
8	60	toluene	AgNTf$_2$ (2.5 mol%)	0
9	60	toluene	**HTIM(PPh$_2$)$_3$** (2.5 mol%)	0
10	60	toluene	none	0
11	60	toluene	**NiTIM(PPh$_2$)$_3$Br** + AgNTf$_2$	95
12	60	THF	**NiTIM(PPh$_2$)$_3$Br** + AgNTf$_2$	90
13	30	toluene	**NiTIM[P(*p*-^{F}C$_6$H$_4$)$_2$]$_3$Br +** AgNTf$_2$	21
14	30	THF	**NiTIM[P(*p*-^{F}C$_6$H$_4$)$_2$]$_3$Br +** AgNTf$_2$	37
15	30	toluene	**NiTIM[P(*p*-^{Me}C$_6$H$_4$)$_2$]$_3$Br +** AgNTf$_2$	99
16	30	THF	**NiTIM[P(*p*-^{Me}C$_6$H$_4$)$_2$]$_3$Br +** AgNTf$_2$	95

Standard reaction conditions: quinoline V.1a (0.25 mmol), nickel complex (2.5 mol%), AgNTf$_2$ (2.5 mol%), SPS grade solvent (1.4 mL) and H$_2$ (10 bar) at T°C during 15 h. Isolated yields of product V.2a by preparative TLC chromatography reported.

The reduction of quinoline still occurs after mercury poisoning experiment, suggesting that the catalytic activity derives from the coordination complex (entry 7). The mercury drop test is a rapid commonly used method to distinguish the homogenous molecular catalysis from nanoparticle metal catalysis. This method is based on the assumption that the Hg will poison the nanoparticles acting as a catalytically active centers and will be inert towards molecular metal complexes. Blank experiments showed no reactivity in the

absence of nickel catalyst (entries 8 – 10). The temperature increase, insignificantly higher the yields of product (entries 11-12). When complex **NiTIM[P($^{p\text{-F}}$C$_6$H$_4$)$_2$]$_3$Br** was used instead of **NiTIM(PPh$_2$)$_3$Br**, 1,2,3,4-tetrahydroquinoline was obtained in low yields (entries 13 - 14)**,** while complex **NiTIM[P($^{p\text{-Me}}$C$_6$H$_4$)$_2$]$_3$Br** in combination with silver salt $AgNTf_2$ gave excellent yields in toluene as well in THF (entries 15 -16). Notably, the catalytic reaction can tolerate O_2 and small quantity of water. We obtained moderate yields (67% yield) when the reaction was set up in the air without taking any special measures and in the presence of 5 equiv. of H_2O respect to the catalyst. Screening the effect of pressure and temperature revealed that efficient hydrogenation of quinolines occurs already under mild conditions (10 bar of H_2, 30 ºC), with a low catalyst loading of 2.5 mol% to give full conversion of substrate **V.1a**.

This extensive studies revealed that complex **NiTIM(PPh$_2$)$_3$Br** and its analog containing electron donating group **NiTIM[P($^{p\text{-Me}}$C$_6$H$_4$)$_2$]$_3$Br** demonstrated high activity in hydrogenation of quinoline to 1,2,3,4-tetrahydroquinoline. In the presence of withdrawing group in the complex **NiTIM[P($^{p\text{-F}}$C$_6$H$_4$)$_2$]$_3$Br**, the efficiency reduced significantly.

Then, we studied the catalytic activity towards reduction of N-heteroarenes by cobalt tripodal complexes under standard reaction conditions: quinoline V.1a (0.25 mmol), cobalt complex (2.5 mol%), SPS grade solvent (1.4 mL) and H_2 (10 bar) at corresponding temperature during 15 h (entries 17, 18 and 19, Table V.9). **CoTIM(PPh$_2$)$_3$I**, **CoTIM[P($^{p\text{-F}}$C$_6$H$_4$)$_2$]$_3$I** and **CoTIM[P($^{p\text{-Me}}$C$_6$H$_4$)$_2$]$_3$I** were found inactive for the hydrogenation of quinoline. The addition of 2.5 mol% of $AgNTf_2$ to the reaction mixture containing **CoTIM(PPh$_2$)$_3$I**, **CoTIM[P($^{p\text{-F}}$C$_6$H$_4$)$_2$]$_3$I** or **CoTIM[P($^{p\text{-Me}}$C$_6$H$_4$)$_2$]$_3$I** also resulted in inactive system (enties 20, 21 and 22).

Table V.9 Optimization of the reaction conditions for CoTIM(PPh_2)$_3$I, CoTIM[P(p-FC_6H_4)$_2$]$_3$I and CoTIM[P(p-MeC_6H_4)$_2$]$_3$I.

Entry	T (ºC)	Solvent	Catalyst	Conversion, %
17	65	chloroform	**CoTIM(PPh_2)$_3$I**	0
18	65	chloroform	**CoTIM[P(p-MeC_6H_4)$_2$]$_3$I**	0
19	65	chloroform	**CoTIM[P(p-FC_6H_4)$_2$]$_3$I**	0
20	60	toluene	**CoTIM(PPh_2)$_3$I** +AgNTf	0
21	60	toluene	**CoTIM[P(p-MeC_6H_4)$_2$]$_3$I** + AgNTf	0
22	60	toluene	**CoTIM[P(p-FC_6H_4)$_2$]$_3$I** + AgNTf	0
23	60	toluene	**CoTIM(PPh_2)$_3$I** + $AgNTf_2$	11[a]
24	60	THF	**CoTIM(PPh_2)$_3$I** + $AgNTf_2$	13[a]
25	60	toluene	**CoTIM(PPh_2)$_3$I** + AgOTf	7[a]
26	60	THF	**CoTIM(PPh_2)$_3$I** + AgOTf	12[a]
27	100	toluene	**CoTIM(PPh_2)$_3$I** +AgNTf	0
28	100	toluene	**CoTIM[P(p-MeC_6H_4)$_2$]$_3$I** + AgNTf	0
29	100	toluene	**CoTIM[P(p-FC_6H_4)$_2$]$_3$I** + AgNTf	0
30	110	toluene	**CoTIM(PPh_2)$_3$I** + $AgBF_4$	0[b]
31	110	toluene	**CoTIM[P(p-MeC_6H_4)$_2$]$_3$I** + AgBF	0[b]
32	110	toluene	**CoTIM[P(p-FC_6H_4)$_2$]$_3$I** + AgBF	0[b]
33	110	THF	**CoTIM(PPh_2)$_3$I** + $AgBF_4$	0[a]
34	110	methanol	**CoTIM(PPh_2)$_3$I** + $AgNTf_2$	0[a]
35	110	toluene	**CoTIM(PPh_2)$_3$I** + $AgBF_4$	0[c]
36	110	toluene	**CoTIM[P(p-MeC_6H_4)$_2$]$_3$I** + AgOTf	0[c]

Standard reaction conditions: quinoline V.1a (0.25 mmol), cobalt complex (2.5 mol%), silver salt (2.5 mol%), SPS grade solvent (1.4 mL) and H_2 (10 bar) at T°C during 15 h. Conversion of product V.2a is reported by NMR. [a] Silver salt (5.0 mol%). [b] Silver salt (5.0 mol%) at 15 bar of H_2.[c] Silver salt (5.0 mol%), 48h.

Higher loadings of $AgNTf_2$ and AgOTf (5 mol%) revealed low activity towards hydrogenation of quinoline (entries 23-26). The temperature increase was not effective in improving activity of the system (entries 27-29), nor longer reaction time (33 and 34). When hydrogen pressure was increased to 15 bar, system still stayed inactive (entries 30-32). Examination of cobalt complexes **CoTIM(PPh_2)$_3$I**, **CoTIM[P(p-FC_6H_4)$_2$]$_3$I** and **CoTIM[P(p-MeC_6H_4)$_2$]$_3$I** in quinoline hydrogenation by screening the effect of halogen abstracting salt,

pressure, temperature and time of the reaction showed very low to none activity. At this point it was difficult to speculate the reduced activity compared to nickel complexes. However, this result encouraged us to try these cobalt complexes in different kind of reaction such as reduction of ketone (4-methoxybenzaldehyde) also without success.

With the aim of studying the reaction scope and functional group tolerance, we have studied the hydrogenation of representative examples of substituted quinolines with the most reactive nickel complexes, **NiTIM(PPh$_2$)$_3$Br** and **NiTIM[P($^{p\text{-Me}}$C$_6$H$_4$)$_2$]$_3$Br** (Table V.10). The nickel complexes **NiTIM(PPh$_2$)$_3$Br** and **NiTIM[P($^{p\text{-Me}}$C$_6$H$_4$)$_2$]$_3$Br** revealed to be very active in the hydrogenation of a large scope of quinoline derivatives. A part quinoline **V.2a**, several monosubstituted quinolines (**V.2b**, **V.2d, V.2e** and **V.2h**) can be reduced in high yield at 60°C using only 2.5% of catalyst loading and 10 bar H_2. Remarkably, also more complex disubstituted quinoline **V.2i**, quinoxaline **V.2p** and conjugated quinoline **V.2m** were found to easily react under those mild conditions. However, in the case of monosubstituted substrate **V.2c**, disubstituted **V.2j- V.2l**, and challenging 8-substituted quinoline **V.2t**, the temperature needed to be increased up to 100°C to observe high yields. Catalysts **1** and **2** demonstrated outstanding activity even with substrate with increased complexity. Challenging electron-withdrawing substituents **V.2g**, para monosubstituted **V.2f**, conjugated quinoline **V.2n**, trisubstituted quinoline **V.2o**, quinoxaline **V.2q** and 8-substituted quinolines **V.2r**, **V.2s**, **V.2u** and **V.2v** were hydrogenated in good yields although catalyst loadings, temperature and pressure need to be increased to 5%, 100°C and 15 bar, respectively.

To remark is the high selectivity achieved with this catalytic system in the presence of reducible groups such as ester (**V.2o**), hydroxyl (**V.2v**), amine (**V.2t**), bromide (**V.2d, V.2r**), but also to highly sensitive functional groups such as nitro (**V.2g, V.2u**), aldehyde (**V.2e**) and olefin (**V.2h**). These results show that **[Ni(TIM(P(R)$_2$)$_3$](NTf$_2$)** complexes are competitive catalysts for the reduction of quinolines to 1,2,3,4-tetrahydroquinolines.

Table V.9 Substrate scope for the hydrogenation of N-heteroarenes.

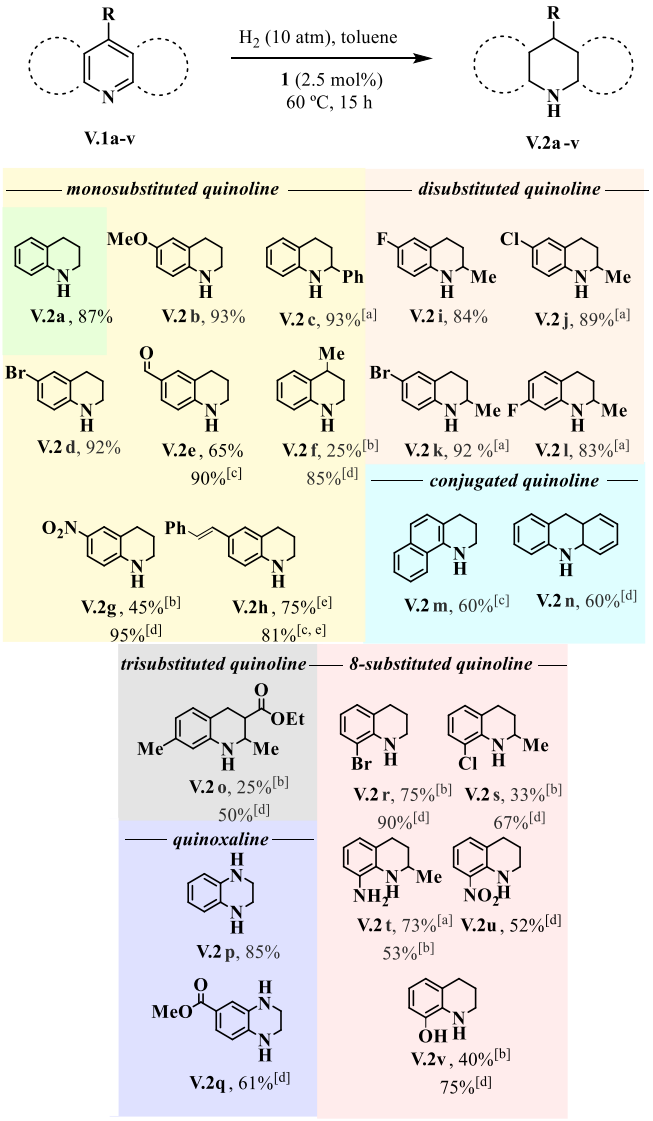

Initial reaction conditions: substrate (0.25 mmol), complex NiTIM(PPh_2)$_3$Br (2.5 mol%), $AgNTf_2$ (2.5 mol%) in toluene at 60 ºC and 10 bar of H_2 for 15 h. [a] Initial reaction conditions at 100 ºC. [b] Complex NiTIM(PPh_2)$_3$Br (5.0 mol%) at 15 bar of H_2, 100 ºC and 24 h. [c] Complex NiTIM[P($^{p\text{-Me}}C_6H_4$)$_2$]$_3$Br was used instead of NiTIM(PPh_2)$_3$Br. [d] Complex NiTIM[P($^{p\text{-Me}}C_6H_4$)$_2$]$_3$Br (5.0 mol%) instead of NiTIM(PPh_2)$_3$Br at 15 bar of H_2, 100 ºC, 24 h. [e] Just traces of 6-phenethyl-1,2,3,4-tetrahydroquinoline observed. Isolated yields are given after TLC preparative chromatography.

To summarize the discoveries of this part, new nickel and cobalt complexes containing ligands HTIM(PR_2)$_3$ with the C_3 symmetry were synthesized, where first row transition metal activates H-C_{sp3} resulting in well-defined coordination

geometry species. The new efficient, non-air-sensitive method of reducing N-heteroarenes catalyzed by nickel complexes was developed. We envision that this method may be also active for reduction of other organic functionalization.

V.2.3 Mechanistic studies of N-heterocycles hydrogenation

To give some light on the hydrogenation mechanism we have performed an NMR study in combination of deuterium labelling using quinoline as a model substrate and catalyst **NiTIM(PPh$_2$)$_3$Br**. We have also modelled using DFT the full catalytic cycle to reinforce the NMR evidence.

The reaction between quinoline and hydrogen under dry conditions was found to be very fast, as the product was mostly formed after only 15 minutes (Figure V.6). Instead, upon the addition of 5 eq. D_2O the reaction required more time.

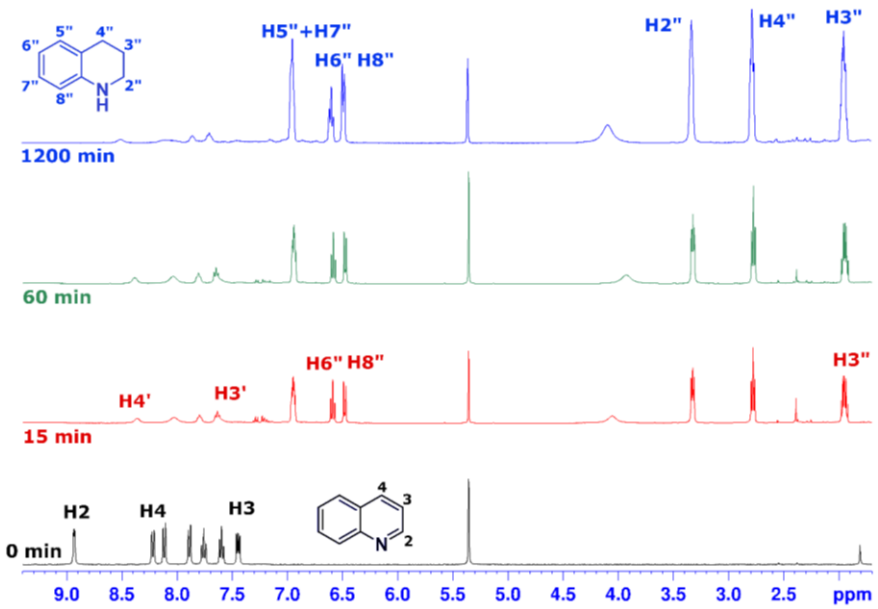

Figure V. 5 *Reaction progress of quinoline with molecular hydrogen catalyzed* ***NiTIM(PPh$_2$)$_3$Br****. In blue (bottom) the initial quinoline before reaction started, in red the reaction after 15 min, in green after 60 min, in blue after 1200 min.*

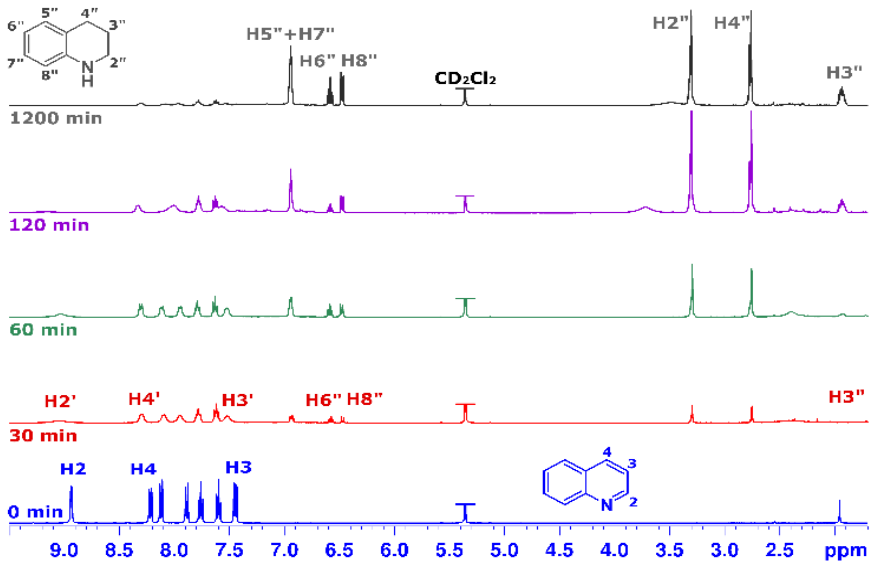

Figure V. 6 *Reaction progress of quinoline with molecular hydrogen catalyzed by* ***NiTIM(PPh$_2$)$_3$Br*** *in the presence of D_2O. In blue (bottom) the initial quinoline before reaction started, in red the reaction after 30 min, in green after 60 min, in purple after 120 min and after 1200 min (gray).*

The reaction progress was followed during time by means of ^{1}H and ^{2}H-NMR spectroscopy. After 30 min the original signals from the quinoline disappeared, with concomitant formation of only a small fraction of the reduced product. A novel set of broad resonances appear in the aromatic region (denoted by H' in the spectra of Figure V.7), suggesting the formation of an intermediated species with dynamic nature. Analogous species can be observed for the reaction without added water (Figure V.6).

1H-1H-COSY NMR spectrum confirms that those new signals belong to the same molecular framework, whose resonances all lie in the aromatic region, pointing that this intermediated species is not reduced (Figure V.8).

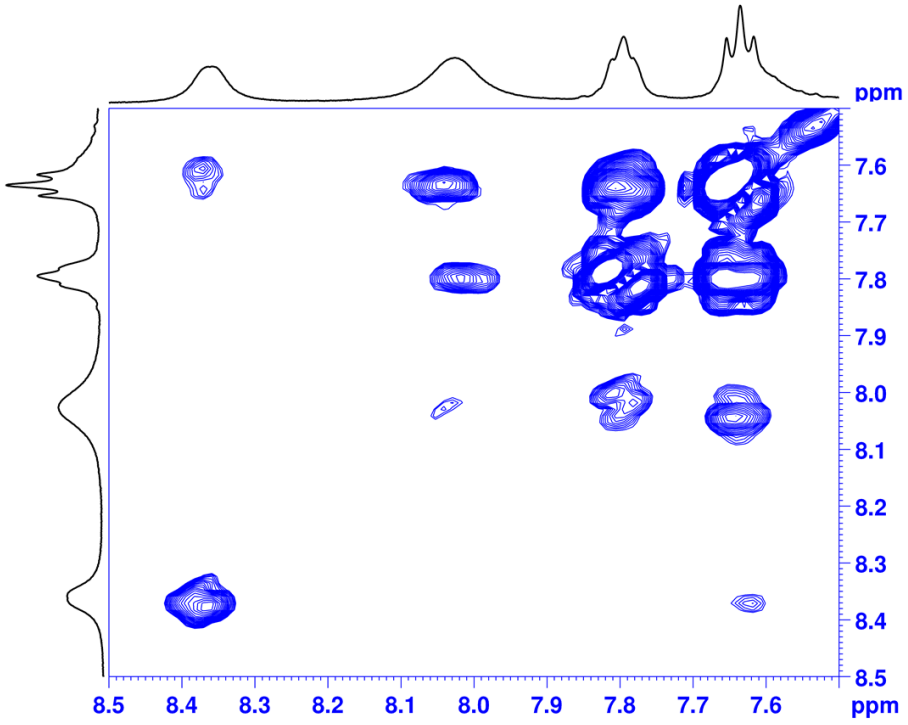

Figure V. 7 *^{1}H-^{1}H-COSY NMR spectrum of the intermediate species formed in the aromatic region.*

Taken together, those pieces of evidence indicate that the quinoline undergoes to fast protonation of the pyridine nitrogen (signal at 9.24 ppm, Figure V.9). Interestingly, the establishment of the equilibrium between the quinoline and its protonated form, along with the absence of any species arising from the progressive hydrogenation of the quinoline allow us to depict two major corollaries: i) the mechanism proceeds through a heterolytic pathway and ii) the rate determining step of the reaction consists in the first hydride transfer step. However, we were not able to detect any Ni-H species (Figure V.10), probably due to the low amount of catalyst adopted under the reaction conditions.

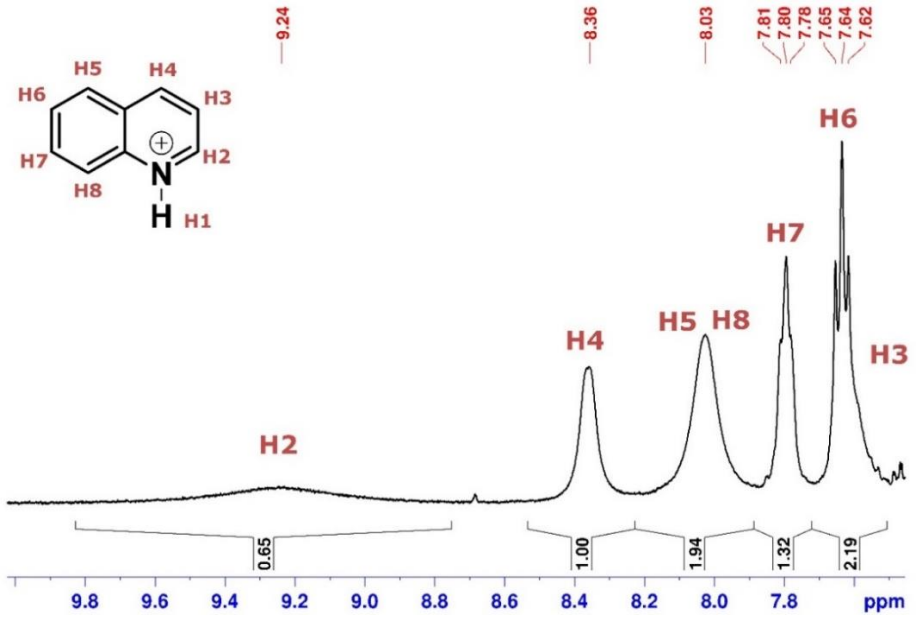

Figure V. 8 *Enlargement of the ^{1}H-NMR spectrum in the aromatic region, collected after 15 minutes of the reaction between the quinoline and molecular hydrogen in the presence of* ***NiTIM(PPh$_2$)$_3$Br****. The spectrum shows the intermediate protonated quinoline.*

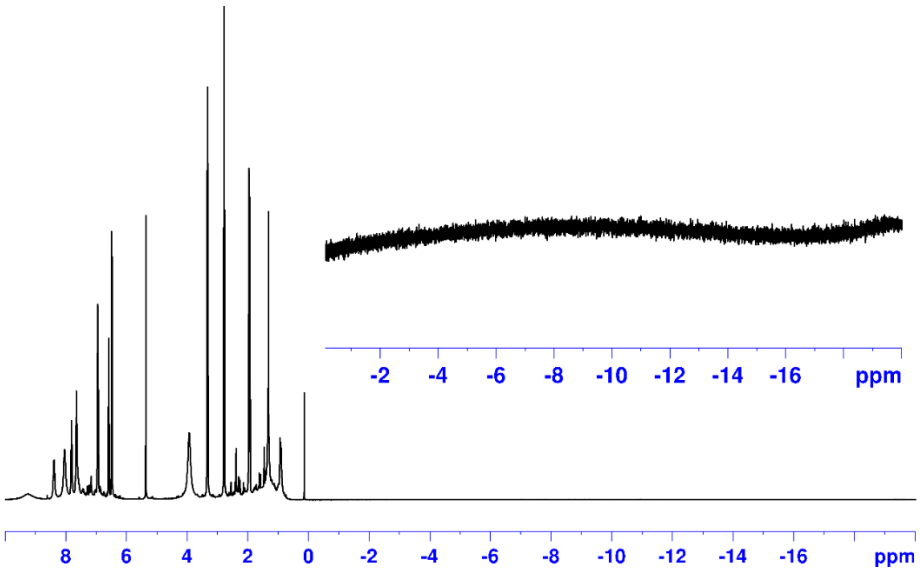

Figure V. 9 *^{1}H-NMR spectrum of the reaction between the quinoline and molecular hydrogen catalysed by* ***NiTIM(PPh$_2$)$_3$Br****, with a magnification in the negative ppm region (top right) to detect eventual Ni-H species.*

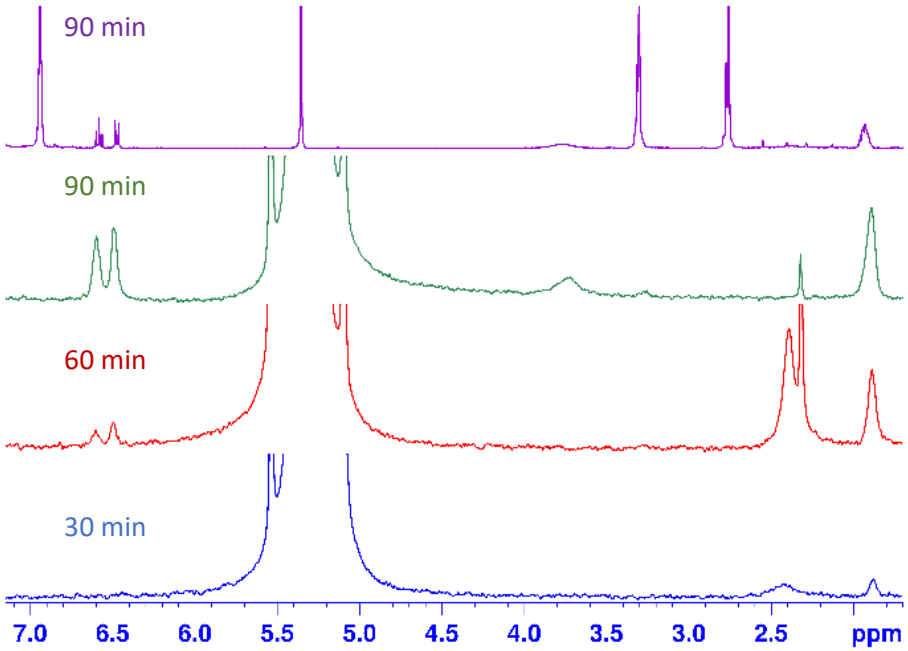

Figure V. 10 *Reaction progress followed by ^{2}H-NMR spectroscopy of quinoline with molecular hydrogen catalysed by* ***NiTIM(PPh$_2$)$_3$Br*** *in the presence of 5 eq. of D_2O. From bottom to the reaction after 30 min (blue), 60 min (red), 90 min (green) and on top ^{1}H-NMR (purple) of the reaction after 90 min.*

More interestingly, the evolution of ^{2}H-NMR spectra during time clearly shows selectivity in the deuteration positions (Figure V.11). In the specific, deuterium inserts on the pyridinic nitrogen and on the position 3 of the pyridine. Notably, two more signals appear in the ^{2}H-NMR spectra after ca. one hour, corresponding to positions 6 and 8 of the benzyl moiety of the product. The same finding was also corroborated by the specular experiment using deuterated quinoline and H_2. In this case ^{1}H-NMR shows proton signals arising from the positions 2,3,4,6 and 8 of the tetrahydroquinoline (Figure V.12).

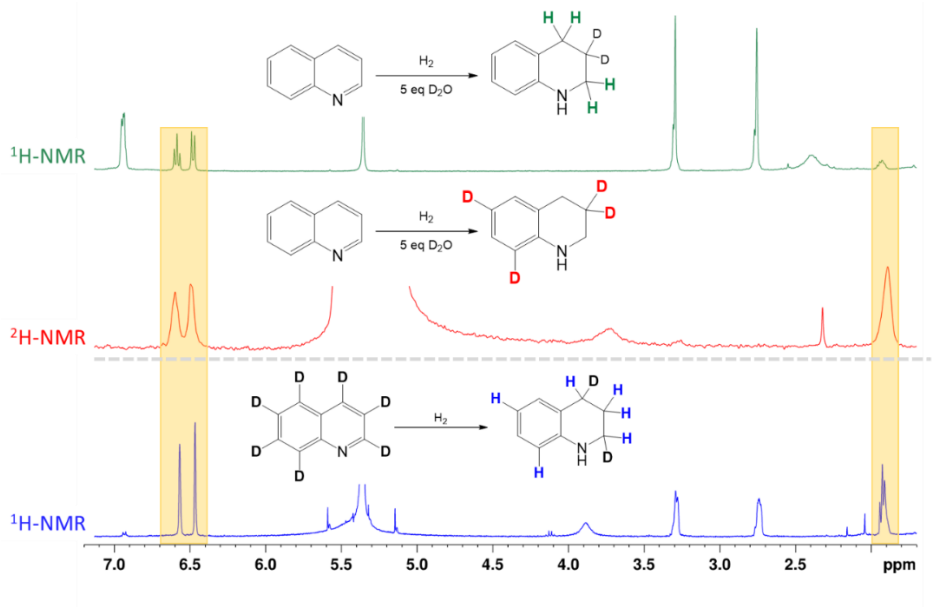

Figure V. 11 *Selectivity of the hydrogen/deuterium exchanges. The spectrum in green represents the ^{1}H-NMR recorded at the end of the reaction between* ***V.1a*** *and H_2 in the presence of 5 equivalents of D_2O. In red the corresponding ^{2}H-NMR experiment is represented. In blue the specular case of deuterated* ***V.1a*** *after reacting with H_2. Yellow shadows highlight the positions of protons 3, 6 and 8.*

In order to rationalize all the results and explain the deuterium distribution in the product, a mechanistic pathway based on NMR and DFT calculations is proposed in the **Scheme V.5**.

The first step consists in the H_2 activation, whose transition state resembles that of a frustrated Lewis pairs in which the pyridine acts as the base and the nickel complex is the acid. The as-generated protonated quinoline **V.1a$_{(NH)}$** undergoes to nucleophilic attack by the intermediate Ni(II)-H species in the position 4 *via* a low energy transition state ($\Delta G^{\ddagger}$ = 19.6 kcal·mol^{-1}, **Scheme V.5**).

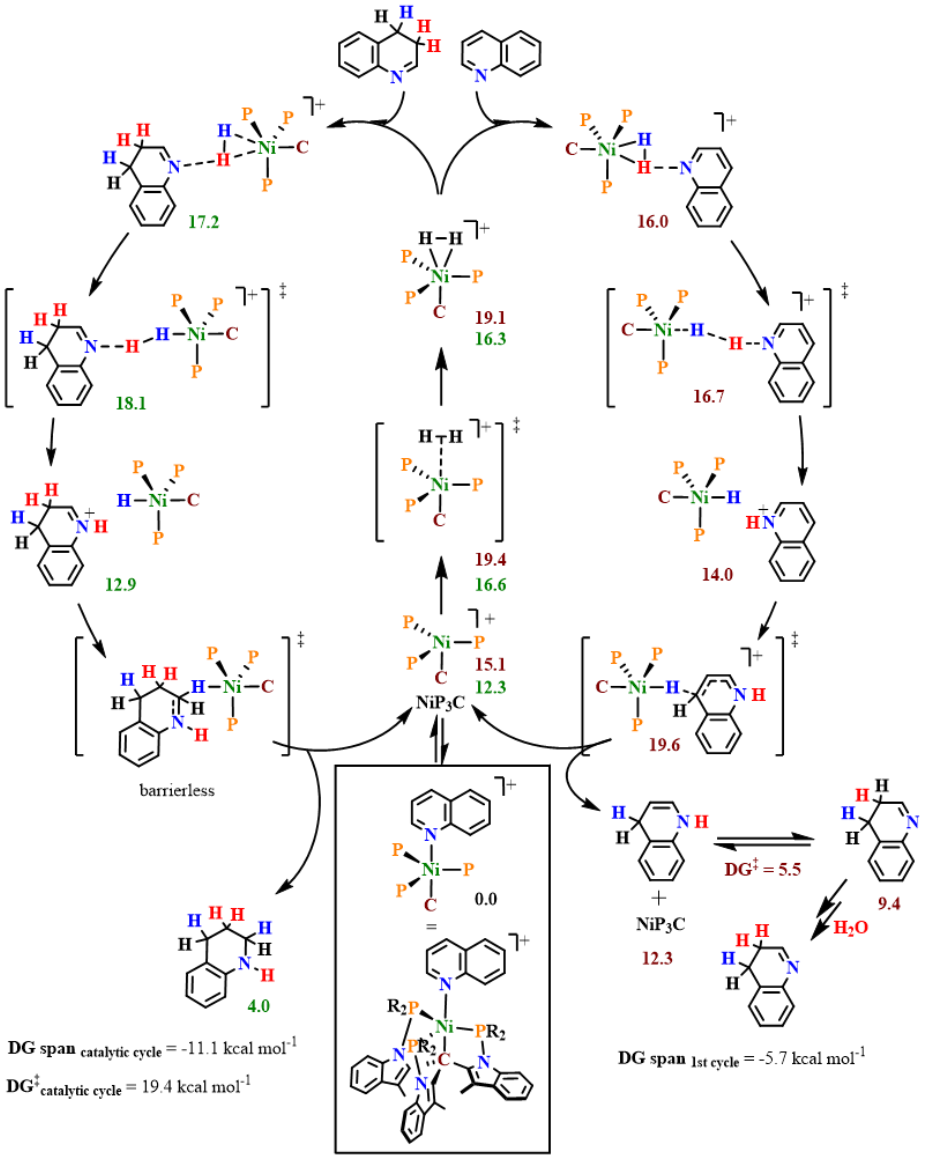

Scheme V. 5 *Proposed mechanistic cycle.*

The reduced product **V.1a$_{(NH,4H)}$** can establish an isomerization equilibrium to yield **V.1a$_{(3H,4H)}$** ($\Delta G = 9.4$ kcal·mol^{-1}). This is confirmed by the deuteration experiments, since the proton exchange equilibrium takes place between **V.1a$_{(NH,4H)}$** – **V.1a$_{(3H,4H)}$**. Finally, further heterolytic H_2 activation can yield **V.1a$_{(NH,3H,4H)}$**, which can suffer a barrier less Ni(II)-H attack to the position **2** forming the final product **V.2a**.

V.3 Conclusions

In conclusion, we synthetized new nickel and cobalt complexes containing ligands HTIM(PR_2)$_3$ with the C_3 symmetry. The first row transition metal (Co, Ni) activates H-C_{sp3} bond of the tripod ligand, resulting in well-defined coordination geometry species. Tripodal P-based complexes with electron-donating and electron withdrawing groups were examined for the reduction of N-heteroarenes obtaining very good yields for the use of Ni-based catalysts (NiTIM(PPh_2)$_3$Br, NiTIM[P($^{p\text{-Me}}C_6H_4$)$_2$]$_3$Br), while Co-based catalysts remained inactive.

All the components in the reaction (catalyst, silver salt, and hydrogen) of this new efficient, non-air sensitive method of reducing N-heteroarenes catalyzed by nickel complexes were demonstrated to be needed for the reaction to occur.

We envision that this method may be also active for reduction of other organic functionalization.

V.4 Experimental section

V.4.1 Material and Reagents

Reagents and solvents were used as received from the commercial supplier unless otherwise stated. Triethylamine was distilled over potassium hydroxide and stored under argon. For the synthesis of ligands and complexes, the solvents (Et_2O, MeCN, THF, methanol, hexane and toluene) were used from a SPS-400, Innovative Technology solvent purification system and stored under argon.

Anhydrous m-Xylene was purchased from Sigma-Aldrich®. Deuterated solvents were purchased from Sigma-Aldrich. Reagents for catalysis were purchased from commercial sources and used as received unless otherwise stated. (E)-6-styrylquinoline was synthesized following reported reaction procedure.

All reactions were performed under a N_2 atmosphere using standard Schlenk techniques or conducted after preparation inside a nitrogen-filled glove box (mBraun Unilab) with concentrations of O_2 and H_2O lower than 0.5 ppm.

V.4.2 Instrumentation

Nuclear magnetic resonance (NMR) spectra were recorded on a Bruker 300 MHz, 400 MHz or 500 MHz spectrometers at room temperature. All ^{1}H and ^{13}C NMR chemical shifts are reported in parts per million (ppm), relative to the residual solvent peak as the internal reference. Multiplicities are reported as follows: singlet (s), doublet (d), doublet of doublet (dd), triplet of doublets (td), triplet (t) and multiplet (m). Coupling constants (J) are reported in hertz (Hz). Deuterated solvents ($CDCl_3$, CD_3CN) were stored with activated 4 Å molecular sieves, and they were degassed by freeze-pump-thaw method when it was required for catalytic reactions.

High resolution Mass Spectrometry (HRMS) data was collected on an HPLC-QqTOF (Maxis Impact, Bruker Daltonics), HPLC-TOF (MicroTOF Focus, Bruker Daltonics) or MALDI-TOF-MS (Autoflex, bruker Daltonics) mass spectrometer using 1 mM solution of the analyzed compound.

X-Ray crystallography. Crystal structure determinations were carried out using a MM-007HF diffractometer equipped with a Pilatus 200K hybrid pixel detector, a rotating anode for Mo *Kα* radiation and Oxfrod Cryostream 700 plus low temperature device (T = – 183º C). Full-sphere data collection was used with ω scans. Programs used: Data collection and data reduction, CrysAlisPro 1.171.39.12b and absorption correction SADABS-2014/5. Structure Solution and Refinement: Crystal structure solution was achieved using the VLD procedure implemented in SIR2014. Spherical model refinement was done using the program ShelXle. All non-hydrogen atoms were refined including anisotropic displacement parameters.

Elemental analyses were performed using a LECO CHNS 932 elemental microanalyzer.

V.4.3 Experimental procedures

Synthesis of tris(1-(diphenylphosphaneyl)-3-methyl-1H-indol-2-yl)methane HTIM[P(Ph$_2$)]$_3$, tris(*N*-di(paratolyl)phosphino-3-methyl-2-

indolyl)methane HTIM[P($^{p\text{-Me}}C_6H_4)_2]_3$ or tris(*N*-di(parafluorophenyl)phosphino-3-methyl-2-indolyl)methane HTIM[P($^{p\text{-F}}C_6H_4)_2]_3$. The ligand was synthesized by a modified protocol for the synthesis of tris(*N*-diisopropylphosphino-3-methyl-2-indolyl)methane (HTIM(P*i*Pr$_2)_3$). The tris(3-methyl-2-indolyl)methane (2.0 g, 4.95 mmol) in 70 ml of THF was added to a stirred solution of washed NaH (475.2 mg, 19.8 mmol, 4.0 equiv) in THF (60 ml) at 23 ºC during 15 min. After vigorous stirring at 50 ºC for 1 h, the solution was cooled down to 23 ºC. A solution of ClPPh$_2$ (99% purity) (3.0 ml, 17.33mmol, 3.5 equiv.), ClP(*p*-Me-C$_6$H$_4)_2$ (95% purity) (3.7 mL, 17.33 mmol, 3.5 equiv) or ClP(*p*-F-C$_6$H$_4)_2$ (98% purity) (4.5 g, 17.33 mmol, 3.5 equiv) respectively in THF (50 mL) was added dropwise and the reaction mixture was stirred overnight at 23 ºC or – 78 ºC in the latter case. The resulting reaction mixture (bright orange) was filtrated under argon flow and the resulting orange filtrate was concentrated in vacuum to 20 mL. Addition of dry methanol (100 mL) or dry hexane (for R = $^{p\text{-Me}}C_6H_4$) resulted in the immediate formation of the crystalline pale-yellow precipitate which could be separated by filtration under air. The obtained phosphines were found to be soluble in chlorinated alkane solvents, toluene, acetone and ether. Yields: **HTIM[P(Ph$_2)]_3$** 3.52 g, 3.68 mmol (74%), **HTIM[P($^{p\text{-Me}}C_6H_4)_2]_3$** 3.61 g, 3.47 mmol (70%), **HTIM[P($^{p\text{-F}}C_6H_4)_2]_3$** 3.90 g, 3.66 mmol (74%). Once precipitated from the reaction mixture, the ligand can be bench stored during months in the presence of moisture and air without any traces of degradation.

General procedure for the synthesis of Ni complexes: To a mixture of HTIM(PR$_2)_3$ (R = Ph, 2 mmol, 2.0 g; R = $^{p\text{-F}}C_6H_4$, 2 mmol 2.23 g; R = $^{p\text{-Me}}C_6H_4$, 2 mmol, 2.08 g) and Ni(glyme)Br$_2$ (2.2 mmol, 678 mg) in toluene (50 mL) or *m*-Xylene (for R = $^{p\text{-Me}}C_6H_4$), Et$_3$N (anhydrous, 5 equiv, 0.0100 mol, 4.2 mL) was added. Reaction was stirred vigorously at 105 ºC (140 ºC for R = $^{p\text{-Me}}C_6H_4$) for 10 h leading to an intense dark-green coloured solution in the final reaction mixture. After being cooled down to 23 ºC the solvent was removed under reduced pressure. The obtained solid was suspended in MeCN (HPLC grade,

25 mL) for NiTIM(PPh_2)$_3$Br, and Et_2O in the case of NiTIM(PR_2)$_3$ (R = $^{p\text{-F}}C_6H_4$ or $^{p\text{-Me}}C_6H_4$). After filtration, filtrate was concentrated and dried in vacuum obtaining dark-green-brown solid (R = Ph, 2.03 g, 1.8 mol, 93%, R = $^{p\text{-F}}C_6H_4$, 2.09 g, 1.7 mol, 87%, R = $^{p\text{-Me}}C_6H_4$, 2.0 g, 1.7 mol, 85%).

General procedure for the hydrogenation of N-heterocycles: A 3.5 mL glass tube containing a stirring bar was sequentially charged with NiTIM(PR_2)$_3$Br complex (2.5–5 mol%), $AgNTf_2$ (2.5 – 5 mol%), N-heterocycle (0.25 mmol), and dry toluene (2 mL, SPS) as solvent. Afterwards, the reaction tube was placed into a HEL reactor (The HEL CAT24 multireactor consists in a cylindrical vessel in 316 SS; it has capacity for 24 vials (10 x75 mm)). The HEL reactor was purged three times with 30 bar of hydrogen, then pressurized to the working H_2 atmosphere (10 - 15 bars) and placed into an aluminium block, which was preheated at the corresponding temperature. After catalysis, the multireactor was cooled in an ice bath, and the remaining gas was carefully released. To determine the isolated yield of the hydrogenated products, the reaction mixture was purified by silica gel column chromatography (n-hexane/AcOEt mixtures) to give the corresponding desired heteroarene.

Procedure for the hydrogenation of quinoline in the presence of D_2O: A 3.5 mL glass tube containing a stirring bar was sequentially charged with NiTIM(PPh_2)$_3$Br complex (5.0 mol%), $AgNTf_2$ (5.0 mol%), quinoline (0.25 mmol, 32.25 mg), and dry toluene (2 mL, SPS) as solvent. Afterwards, 5.0 equiv. (22.6 µL) of D_2O (purchased from Merck, 99.9 atom % D) were added and the reaction tube was placed into a HEL reactor. The multireactor was purged three times with 20 bar of hydrogen, then pressurized to 10 bar and placed into an aluminium block, which was preheated at the 60 ºC. In order to monitor the reaction, the reaction was run during different time: 30 min, 60 min, 120 min and 1200 min, at the end of which an NMR spectrum was recorded. To stop the reaction, the multireactor was cooled in an ice bath and the remaining gas was carefully released. After 15 hours reaction, the yield of D-

1,2,3,4-tetrahydroquinoline was 55% by silica gel column chromatography purification (n-hexane/AcOEt mixtures).

V.4.4 Characterization of ligands and complexes

HTIM[P(Ph$_2$)]$_3$. Pale yellow crystalline solid obtained in 74% by precipitation and filtration from THF/methanol. **^{1}H NMR** (400 MHz, $CDCl_3$) δ = 8.69 (d, *J* = 9.2 Hz, 1H), 7.36 (d, *J* = 7.8 Hz, 3H), 7.25 – 7.08 (m, 30H), 7.02 (ddd, *J* = 7.9, 5.6, 2.4 Hz, 3H), 6.85 – 6.78 (m, 6H), 1.78 (s, 9H) ppm. **^{31}P NMR** (162 MHz, $CDCl_3$) δ = 35.55 (s) ppm. **^{13}C NMR** (101 Hz, $CDCl_3$) *δ* = 139.1 (s, C), 138.8 (s, C), 138.7-138.6 (m, C), 135.9-135.7 (m, C), 138.3-135.0 (m, C), 132.9 (s, C), 132.1-131.6 (m, CH), 128.9 (s, CH), 128.5 (s, CH), 128.3-127.9 (m, CH), 121.7 (s, CH), 120.0 (s, CH), 118.5 (s, CH), 116.1-115.9 (m, C), 114.7 (s, CH), 39.9 (q, $^3J_{C\text{-}P}$ = 26.4 Hz, H–C_{sp3}), 8.4 (s, CH_3) ppm.

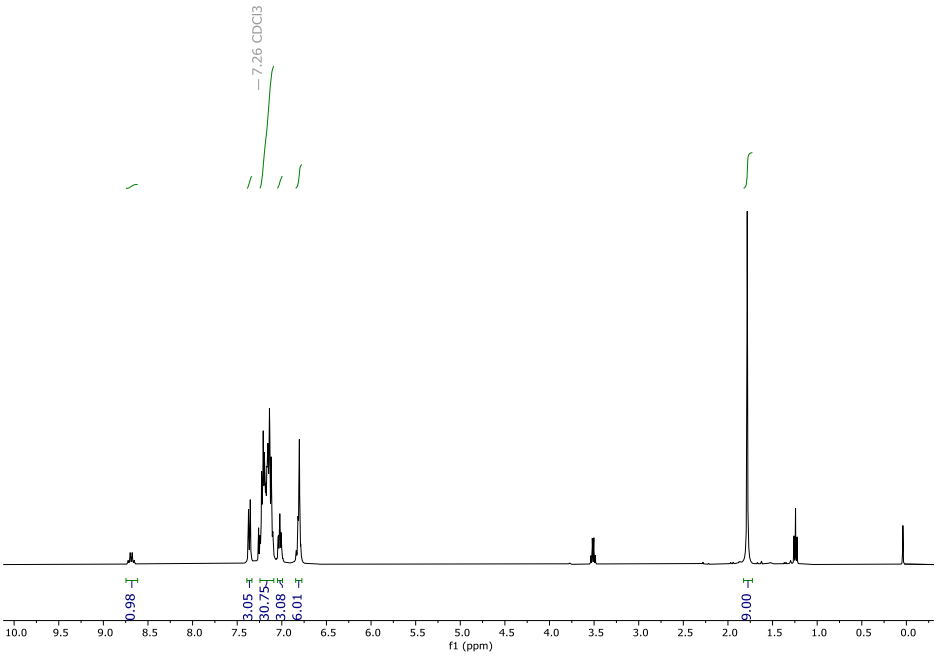

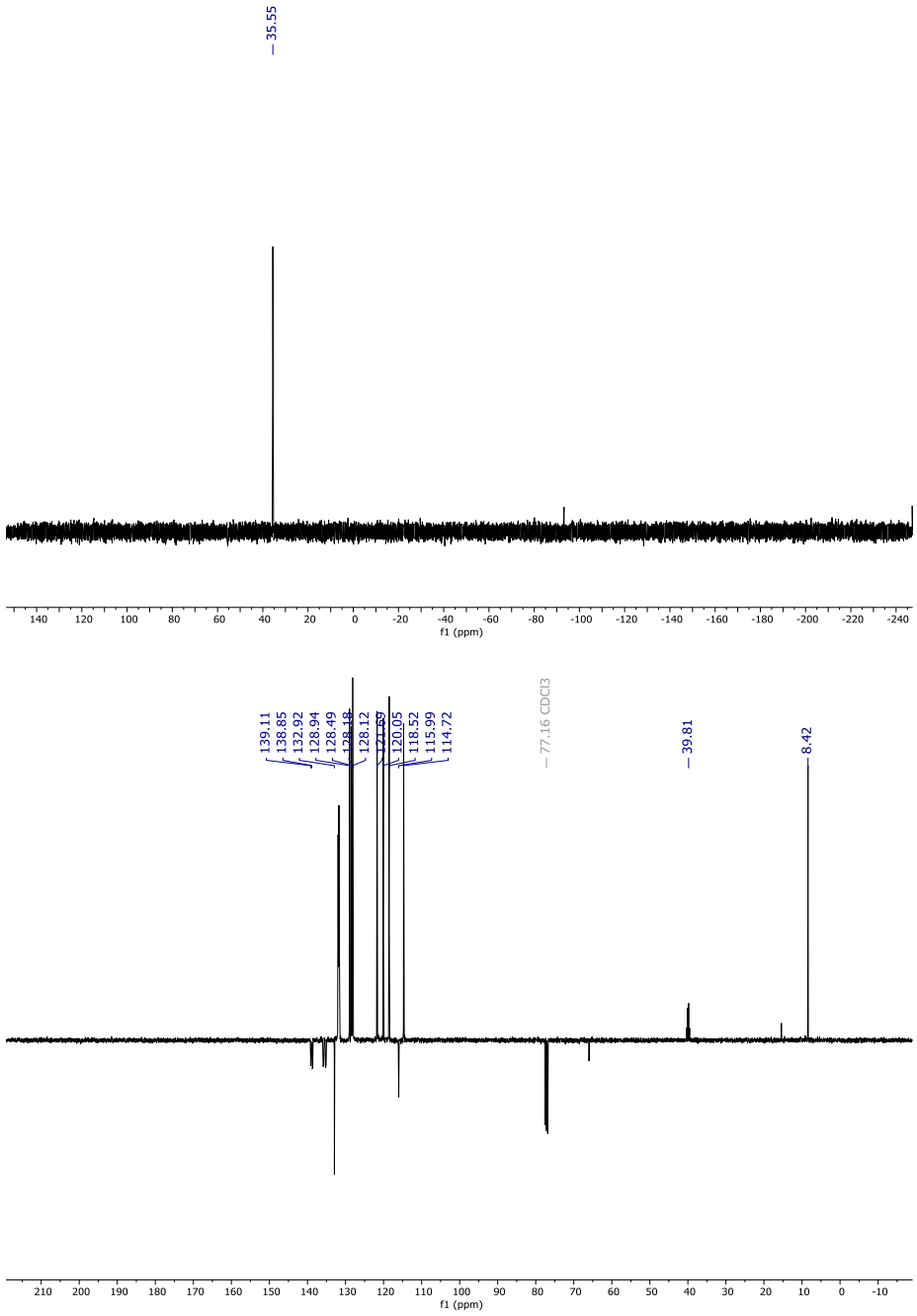

HTIM[P(*p*-$^{Me}C_6H_4)_2]_3$. White crystalline solid obtained in 70 % by precipitation and filtration from THF/methanol. **^{1}H NMR** (400 Hz, $CDCl_3$) δ = 8.5 (q, 1H, $^4J_{H\text{-}P}$ = 11.4Hz), 7.36−7.34 (m, 3H), 7.22−7.18 (m, 6H), 7.10−7.07 (m, 9H), 7.06−6.97 (m, 6H), 6.93−6.82 (m, 12H), 2.25 (d, *J* = 10.0 Hz, 18H),

1.73 (s, 9H) ppm; **^{31}P NMR** (162 Hz, $CDCl_3$) δ = 36.24 (s) ppm; **^{13}C NMR** (101 Hz, $CDCl_3$) δ = 139.3−139.1 (m, C), 138.8 (s, CH), 138.8−138.6 (m, C), 138.2 (s, CH), 132.9 (s, CH), 132.7−132.6 (m, C), 132.3−131.8 (m, C, CH), 128.8−128.7 (m, CH), 121.4 (s, CH), 119.7 (s, CH), 118.4 (s, C), 115.7 (s, C), 114.8 (s, CH), 40.0 (q, $^3J_{C\text{-}P}$ = 21.0 Hz, H–$\underline{C}_{sp3}$), 21.4 (s, CH_3), 8.4 (s, CH_3) ppm; **HRMS** (ESI) *m/z* calculated for $[C_{70}H_{65}N_3P_3]^+$, $[M+H]^+$: 1040.4386, found 1040.4370.[446]

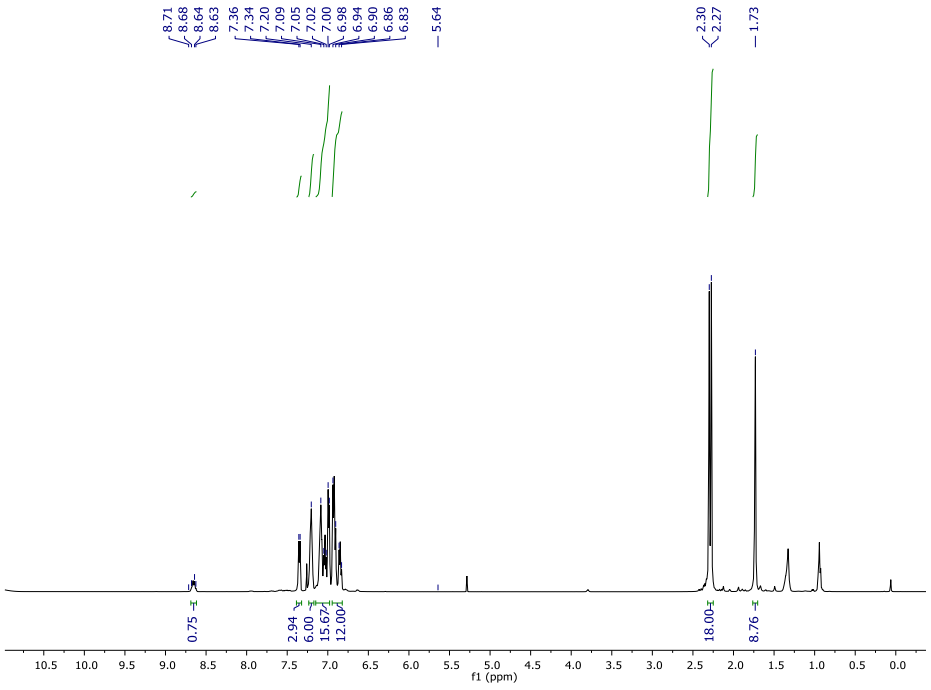

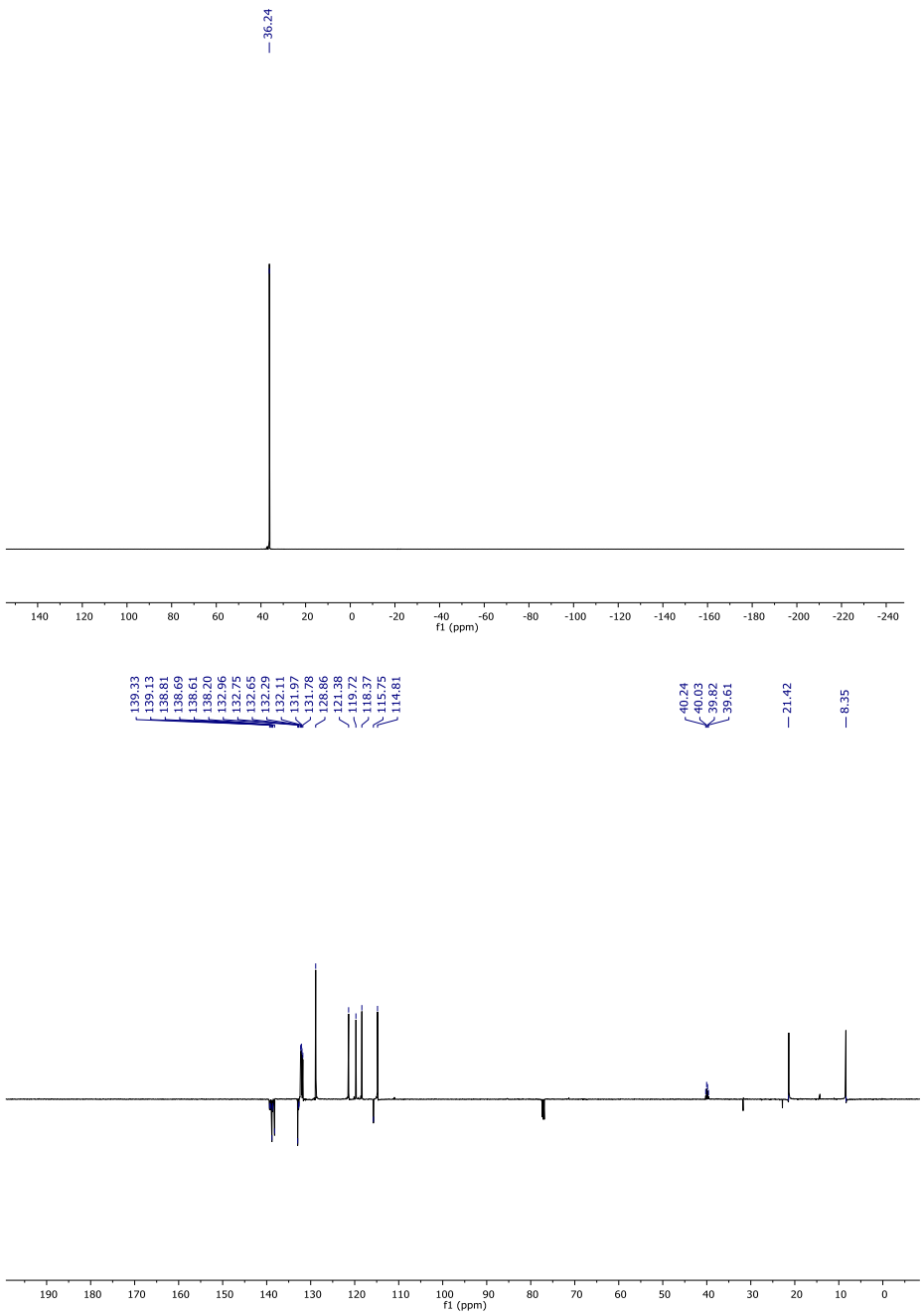

HTIM[P($^{p\text{-F}}$C$_6$H$_4$)$_2$]$_3$. White crystalline solid obtained in 74 % by precipitation and filtration from THF/methanol. **^{1}H NMR** (400 Hz, $CDCl_3$) δ = 8.48 (q, 1H, $^4J_{H\text{-}P}$ = 9.3), 7.34−7.33 (m, 3H), 7.21−7.18 (m, 6H), 7.07−7.04 (m, 10H), 6.89−6.86 (m, 9H), 6.83−6.76 (m, 9H), 1.68 (s, 9H) ppm; **^{31}P NMR** (162 Hz,

$CDCl_3$) δ = 35.29 (s) ppm; **^{13}C NMR** (101 Hz, $CDCl_3$) δ = 164.5 (d, C, J = 20.1Hz), 162.5 (d, C, J = 18.4Hz), 138.6−138.2 (m, C), 134.1−133.6 (m, CH), 132.9 (s, C), 131.3−130.4 (m, C), 122.3 (s, CH), 120.6 (s, CH), 118.9 (s, CH), 116.4 (s, C), 115.8−115.7 (m, CH), 114.3 (s, CH), 39.9 (q, $^3J_{C\text{-}P}$ = 21.2 Hz, H–$\underline{C}_{sp3}$), 8.9 (s, CH_3) ppm; **^{19}F NMR** (376 MHz, $CDCl_3$) δ = -111.1 (d, J = 313.6 Hz, 6F) ppm. **HRMS** (ESI) *m/z* calculated for $[C_{64}H_{47}F_6N_3P_3]^+$, $[M+H]^+$: 1064.2882, found 1064.2874.

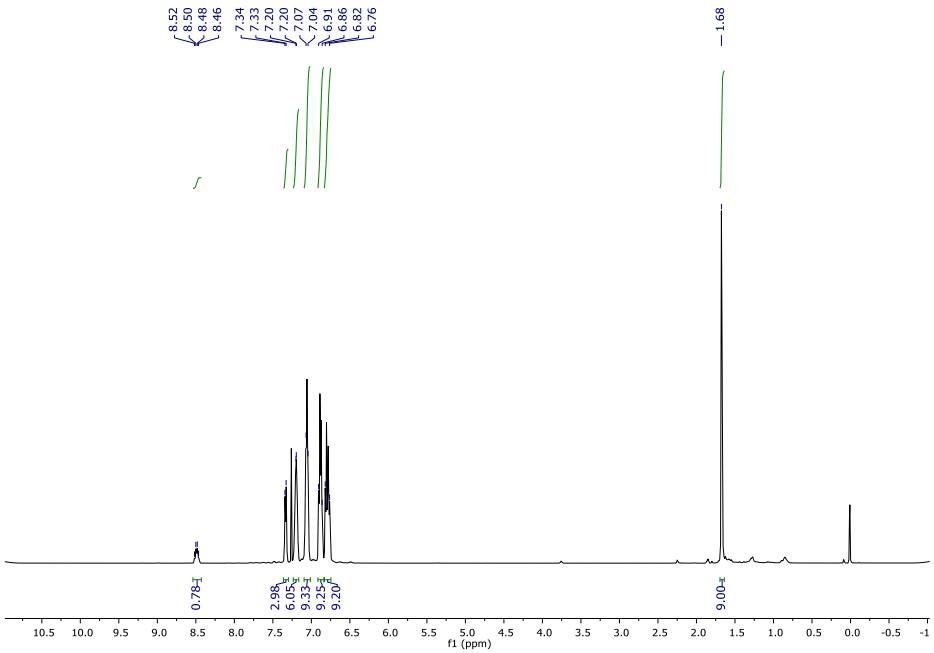

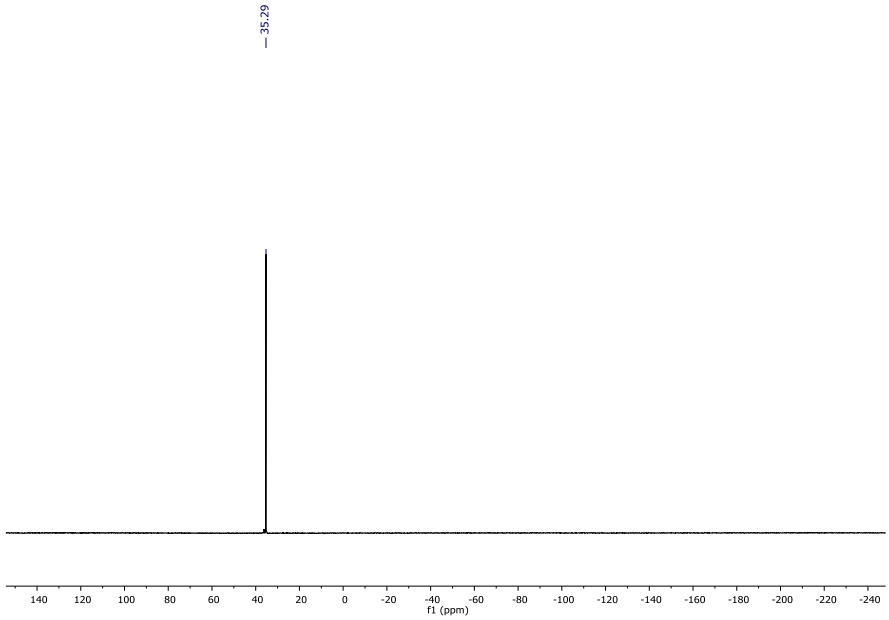
35.29
140 120 100 80 60 40 20 0 -20 -40 -60 -80 -100 -120 -140 -160 -180 -200 -220 -240
f1 (ppm)

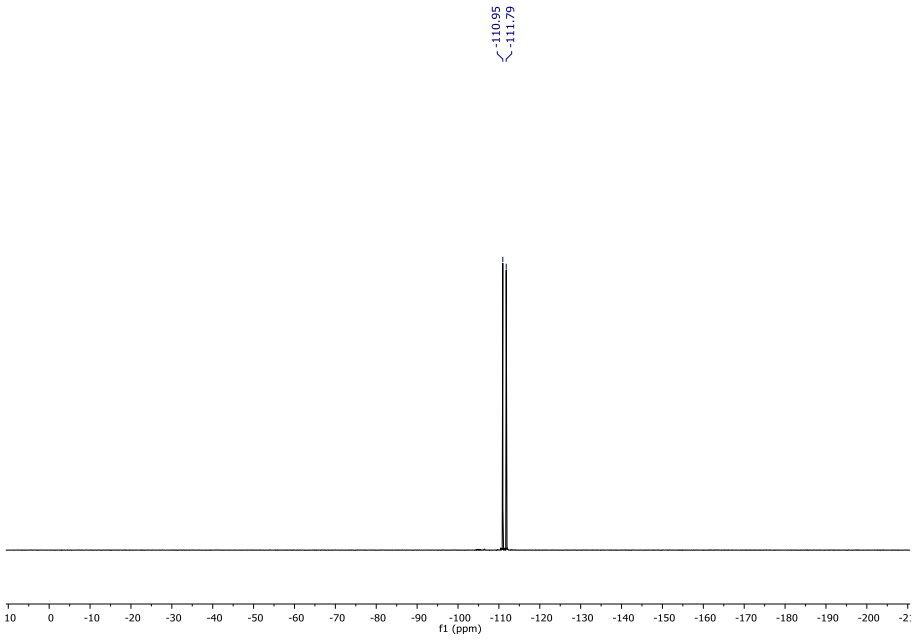
-110.95
-111.79
10 0 -10 -20 -30 -40 -50 -60 -70 -80 -90 -100 -110 -120 -130 -140 -150 -160 -170 -180 -190 -200
f1 (ppm)

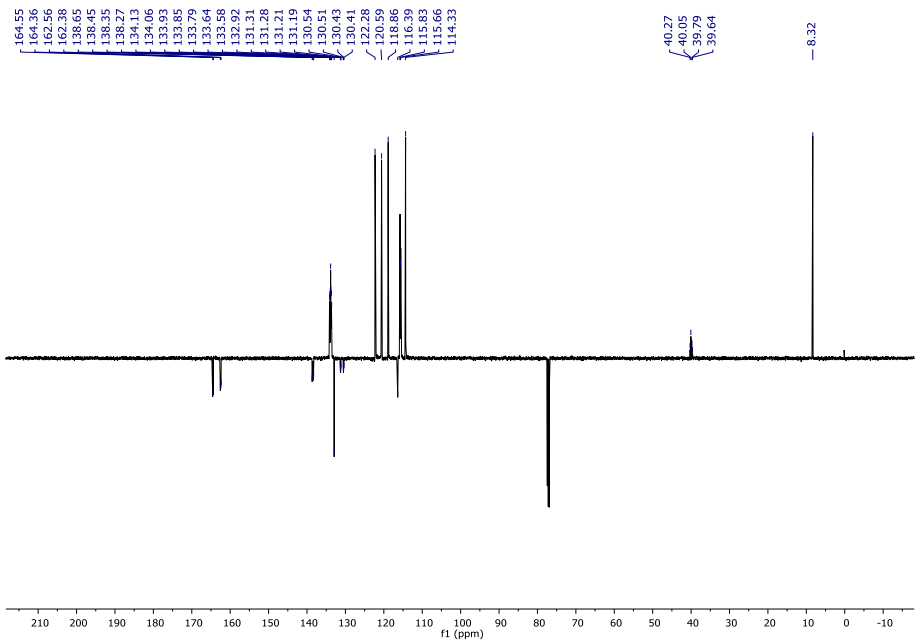

NiTIM(PPh$_2$)$_3$Br. Dark green crystalline solid obtained in 93% by precipitation and filtration from MeCN. **^{1}H NMR** (400 Hz, CD_2Cl_2) δ = 7.55−7.50 (m, 6H), 7.40−7.32 (m, 6H), 7.26−7.12 (m, 12H), 7.01−6.96 (m, 3H), 6.85−6.74 (m, 12H), 6.35−6.32 (m, 3H), 1.45 (s, 9H) ppm; **^{31}P NMR** (162 Hz, CD_2Cl_2) δ = 51.55 (s) ppm; **^{13}C NMR** (101 Hz, CD_2Cl_2) δ = 152.9−152.8 (m, C), 136.9−136.4 (m, C), 134.1 (s, C), 132.9 (s, CH), 131.1 (s, CH), 129.9−129.4 (m, CH), 128.0 (s, CH), 122.7 (s, CH), 121.8 (s, CH), 119.5 (s, CH), 114.7 (s, CH), 113.8 (s, C), 46.7 (m, Ni–C_{sp3}), 8.2 (s, CH_3) ppm; **HRMS** (ESI) *m/z* calculated for $[C_{71}H_{68}N_3P_3Ni]^+$, $[M\text{-}Br]^+$: 1013.9948, found 1013.0056. **Elemental analysis** (%) calc. for $C_{64}H_{51}BrN_3NiP_3$: C% 70.29 H% 4.70 N% 3.84, found C% 69.76 H% 4.93 N% 3.89; **X-Ray** quality crystals were obtained by slow diffusion of hexane into the solution of the **NiTIM(PPh$_2$)$_3$Br** in CH_2Cl_2 at 23 ºC.

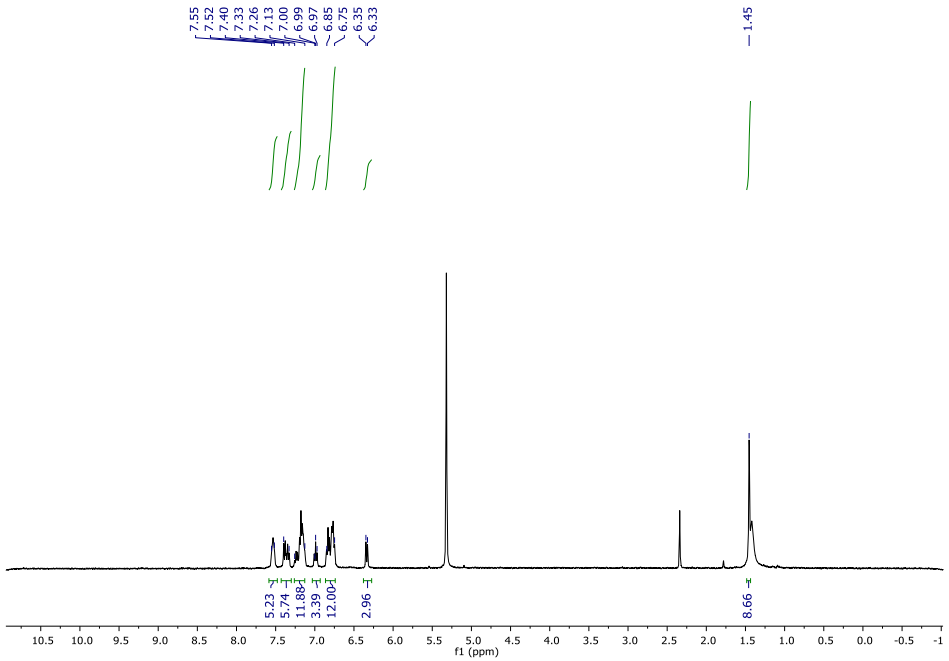
7.55
7.52
7.40
7.33
7.26
7.13
7.00
6.99
6.97
6.85
6.75
6.35
6.33
1.45
5.23
5.74
11.88
3.39
12.00
2.96
8.66
f1 (ppm)

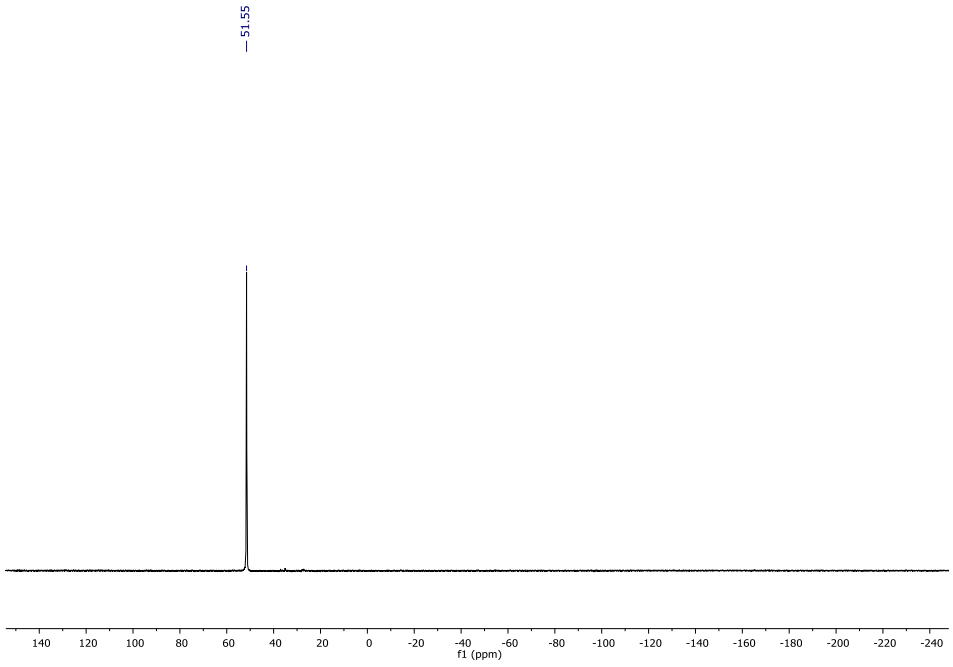
51.55
f1 (ppm)

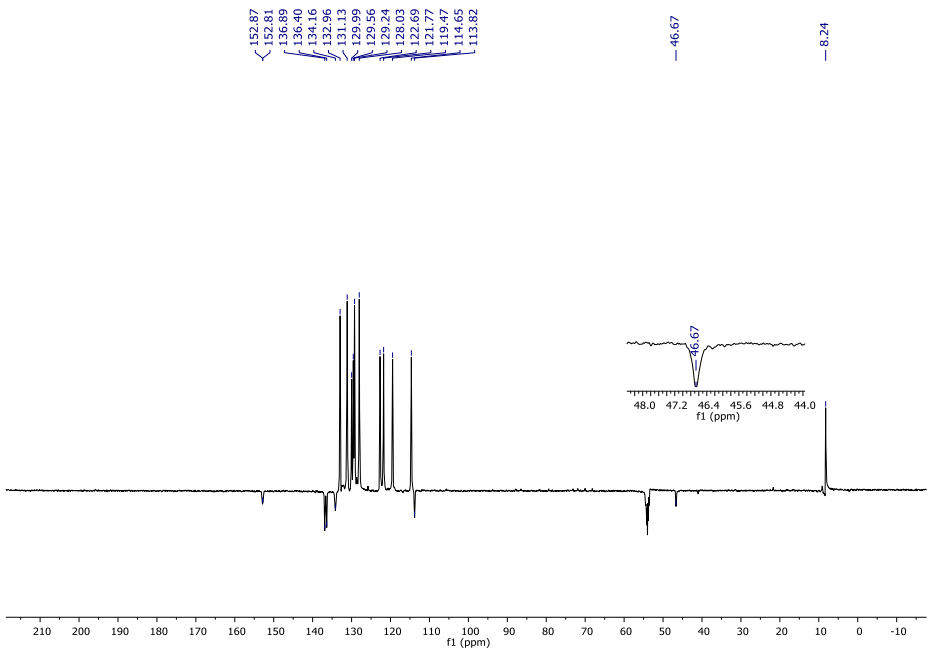

NiTIM(PPh$_2$)$_3$NTf$_2$. Dark violet crystalline solid obtained in 85% by recrystallization from toluene. **^{1}H NMR** (400 Hz, toluene-d_8) δ = 7.80−7.76 (m, 4H), 7.33−7.28 (m, 5H), 7.25 (d, J = 9.0 Hz, 2H), 7.08−6.96 (m, 19H), 6.94−6.90 (m, 5H), 6.84−6.73 (m, 5H), 6.62−6.59 (m, 2H), 2.12 (s, 9H) ppm; **^{31}P NMR** (162 Hz, toluene-d_8) δ = 56.38 (s) ppm; **^{13}C NMR** (101 Hz, toluene-d_8) δ = 151.8 (s, C), 137.1 (s, C), 135.7 (s, CH), 133.6 (m, CH), 131.9 (s, CH), 130.8 (s, CH), 130.8 (s, CH), 130.4 (s, CH), 123.7 (s, CH), 122.8 (s, CH), 119.4 (s, CH), 115.1 (s, CH), 113.8 (s, C), 46.5 (s, Ni–C_{sp3}), 8.8 (s, CH_3) ppm; **^{19}F NMR** (282 MHz, toluene-d_8) δ = -77.90 (s) ppm; **HRMS** (ESI) *m/z* calculated for $[C_{64}H_{51}N_3NiP_3]^+$, $[M\text{-}NTf_2]^+$: 1012.2644, found 1012.2658.

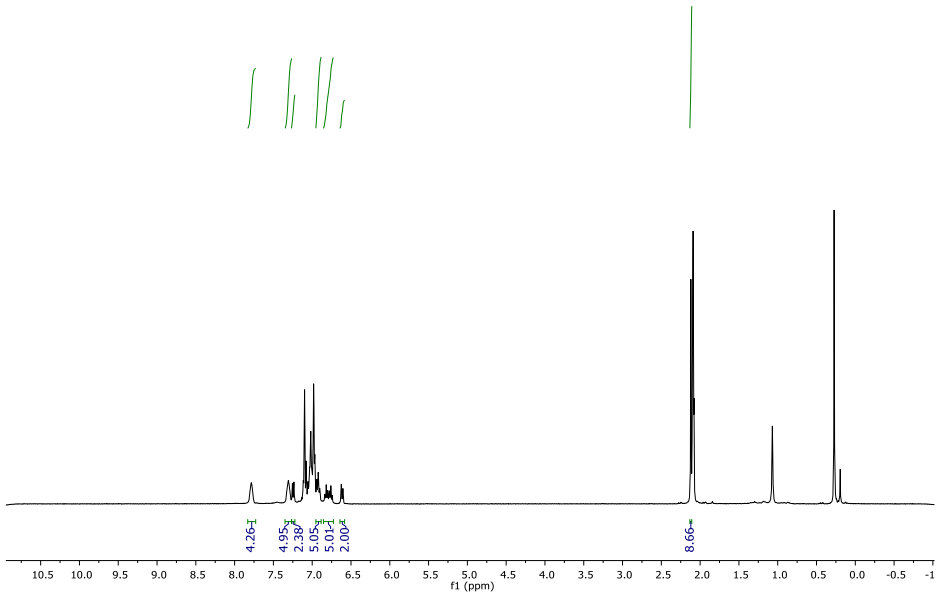
4.26
4.95
2.38
5.05
5.01
2.00
8.66
f1 (ppm)

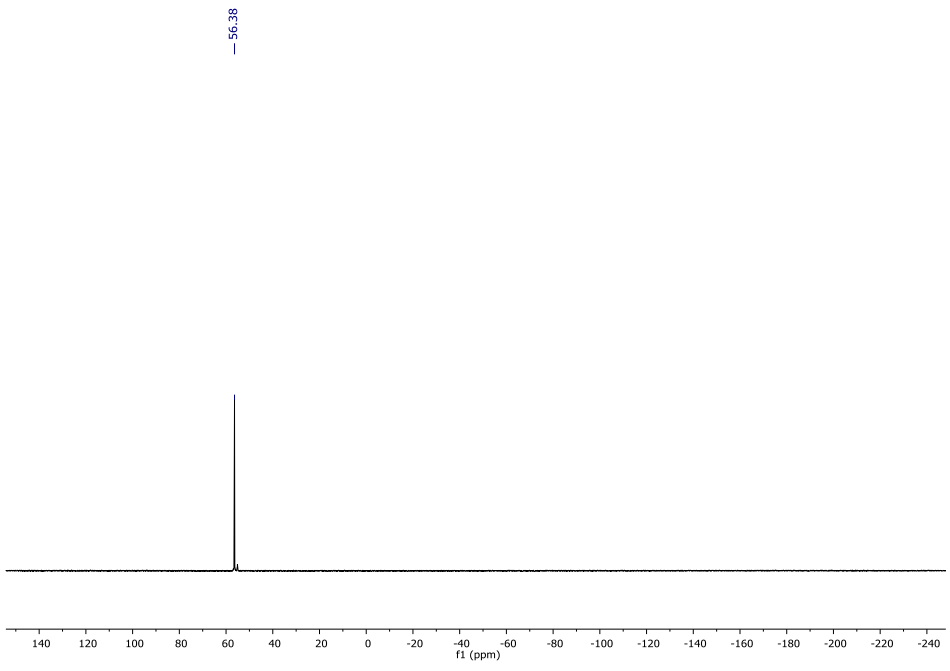
56.38
f1 (ppm)

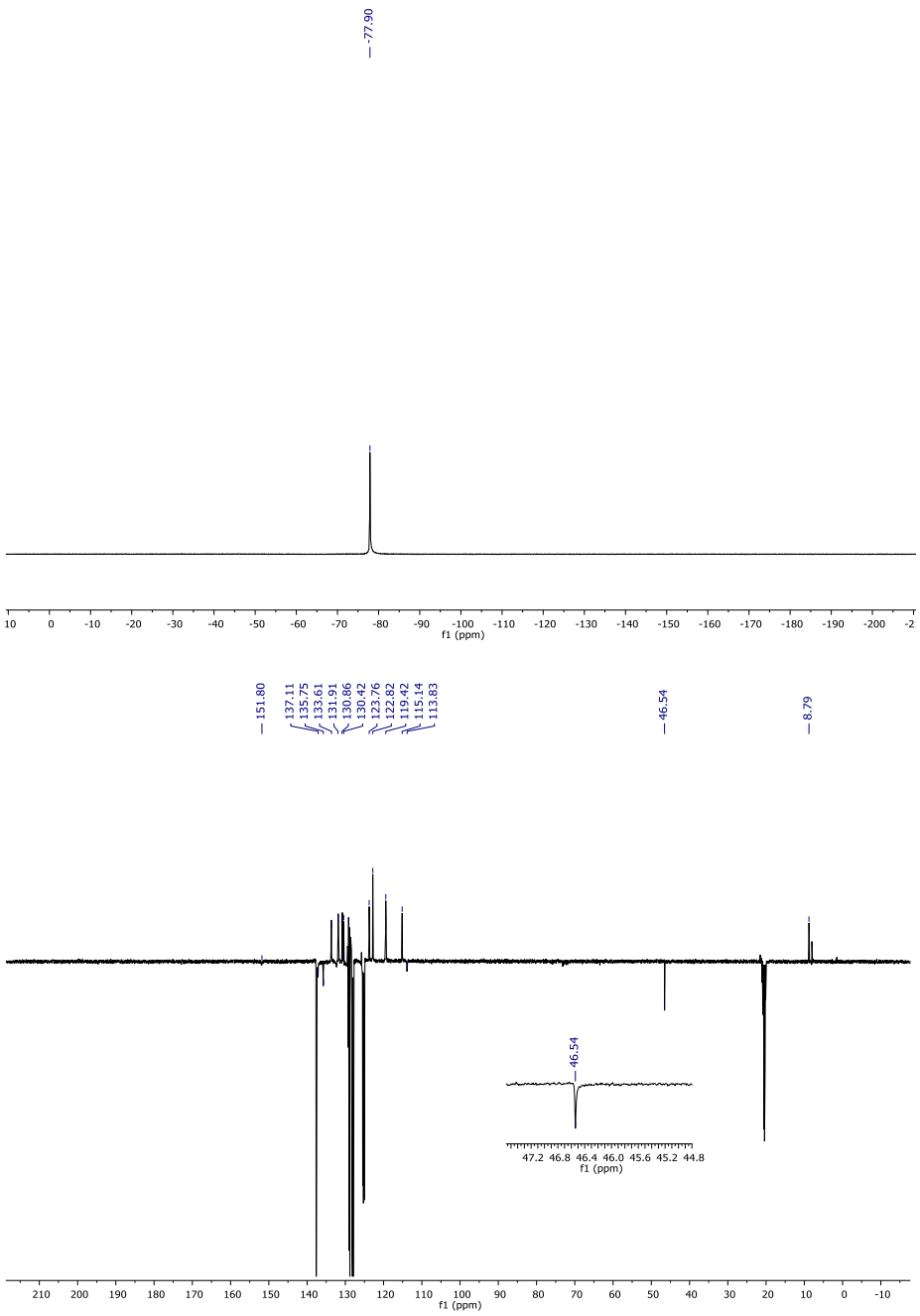

NiTIM[P($^{p\text{-Me}}$C$_6$H$_4$)$_2$]$_3$Br. Dark green crystalline solid obtained in 85% by precipitation and filtration from MeCN. **^{1}H NMR** (400 Hz, $CDCl_3$) δ = 7.44−7.40 (m, 6H), 7.37−7.34 (m, 3H), 6.98 (t, J = 9.52 Hz, 4H), 6.91−6.88 (m, 6H), 6.77 (t, J = 10.32 Hz, 3H), 6.65−6.61 (m, 6H), 6.54−6.51 (m, 6H),

6.44−6.41 (m, 3H), 2.29 (s, 9H), 2.16 (s, 9H),1.42 (s, 9H) ppm; **^{31}P NMR** (162 Hz, CD_2Cl_2) δ = 51.64 (s) ppm; **^{13}C NMR** (101 Hz, CD_2Cl_2) δ = 153.3−153.1 (m, C), 139.9 (s, C), 139.6 (s, C), 137.1 (s, C), 136.5 (s, C), 132.9 (s, CH), 131.0 (s, CH), 129.7 (s, CH), 128.6 (s, CH), 122.5 (s, CH), 121.6 (s, CH), 119.4 (s, CH), 114.75 (s, CH), 113.4 (s, C), 46.7 (m, Ni–$\underline{C}_{sp3}$), 21.7 (s, CH_3), 21.6 (s, CH_3), 8.1 (s, CH_3) ppm; **HRMS** (ESI) *m/z* calculated for $[C_{70}H_{63}BrN_3NiP_3]^{+\cdot}$, $[M]^+$: 1175.2766, found 1175.2746; **X-Ray** quality crystals were obtained by slow diffusion of hexane into the solution of the **NiTIM[P((p-MeC_6H_4)$_2$]$_3$Br** in CH_2Cl_2 at 23 ºC.

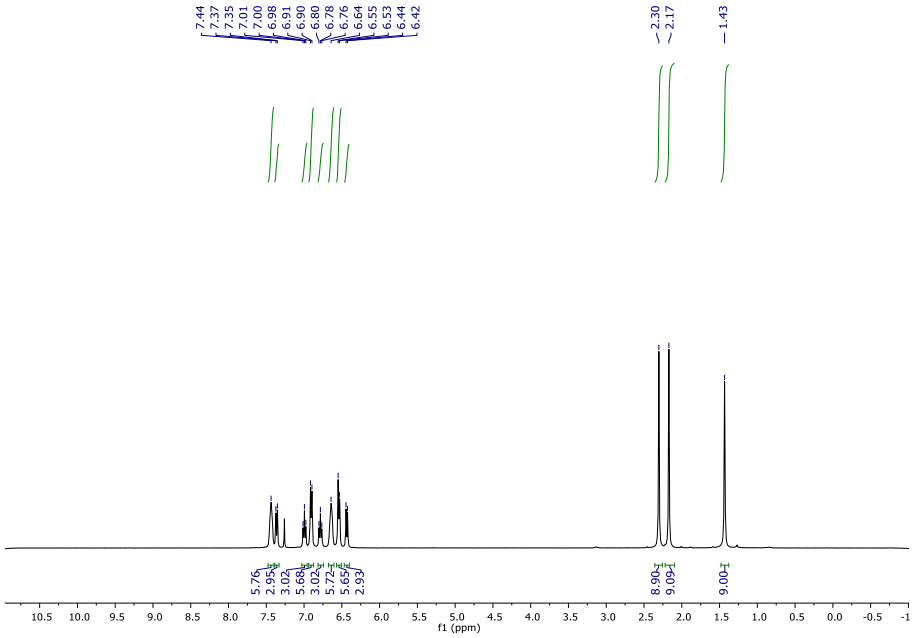

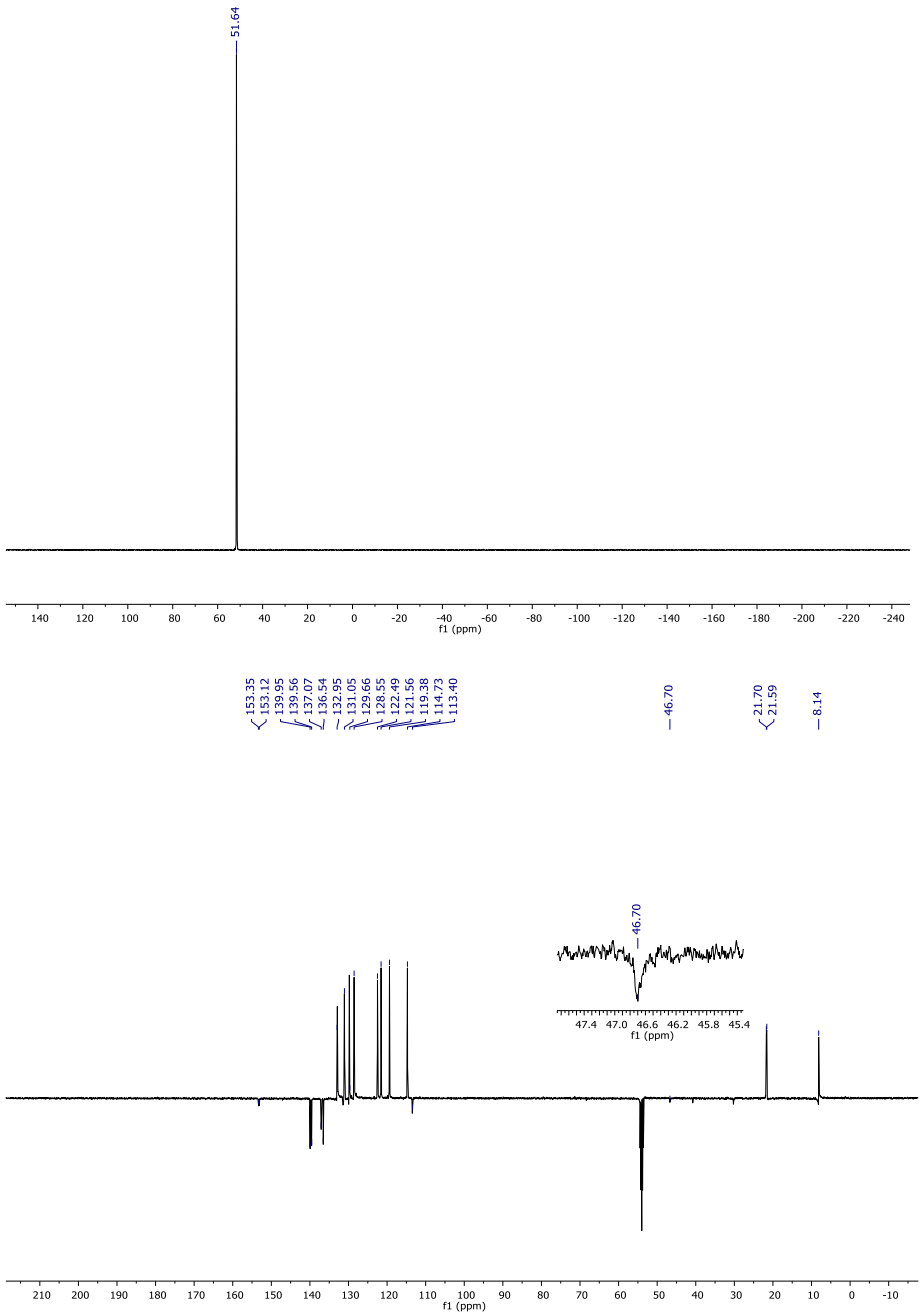

NiTIM[P(*p*-FC$_6$H$_4$)$_2$]$_3$Br. Dark green crystalline solid obtained in 87% by precipitation and filtration from MeCN. **^{1}H NMR** (400 Hz, $CDCl_3$) δ = 7.52−7.49 (m, 6H), 7.40−7.37 (m, 3H), 7.08−7.03 (m, 3H), 6.88−6.84 (m, 8H), 6.75−6.70 (m, 6H), 6.57−6.53 (m, 6H), 6.39−6.36 (m, 3H), 1.43 (s, 9H) ppm,

^{31}P NMR (162 Hz, CD_2Cl_2) δ = 51.27 (s) ppm; **^{13}C NMR** (101 Hz, CD_2Cl_2) δ = 165.0 (d, J = 39.9 Hz, C), 163.0 (d, J = 40.2 Hz, C),152.6−152.5 (m, C), 136.7 (s, C), 136.4 (s, C), 135.2−135.0 (m, CH), 133.3−133.1 (m, CH), 130.2−130.0 (m, C), 128.2−127.9 (m, C), 123.4 (s, CH), 122.2 (s, CH), 120.0 (s, CH), 116.7−116.4 (m, CH), 115.3−115.0 (m, CH), 114.5 (s, CH), 114.4 (s, C), 46.6 (m, Ni–$\underline{C}_{sp3}$), 8.2 (s, CH_3) pm; **^{19}F NMR** (282 MHz, CD_2Cl_2) δ = -109.65 (d, J = 127.6 Hz, 6F) ppm. **HRMS** (ESI) *m/z* calculated for $[C_{64}H_{45}BrF_6N_3NiP_3]^{+\cdot}$, $[M]^{+\cdot}$: 1199.1262, found: 1199.1239. **X-Ray** quality crystals were obtained by slow diffusion of hexane into the solution of the **NiTIM[P(*p*-FC_6H_4)$_2$]$_3$Br** in CH_2Cl_2 at 23 ºC.

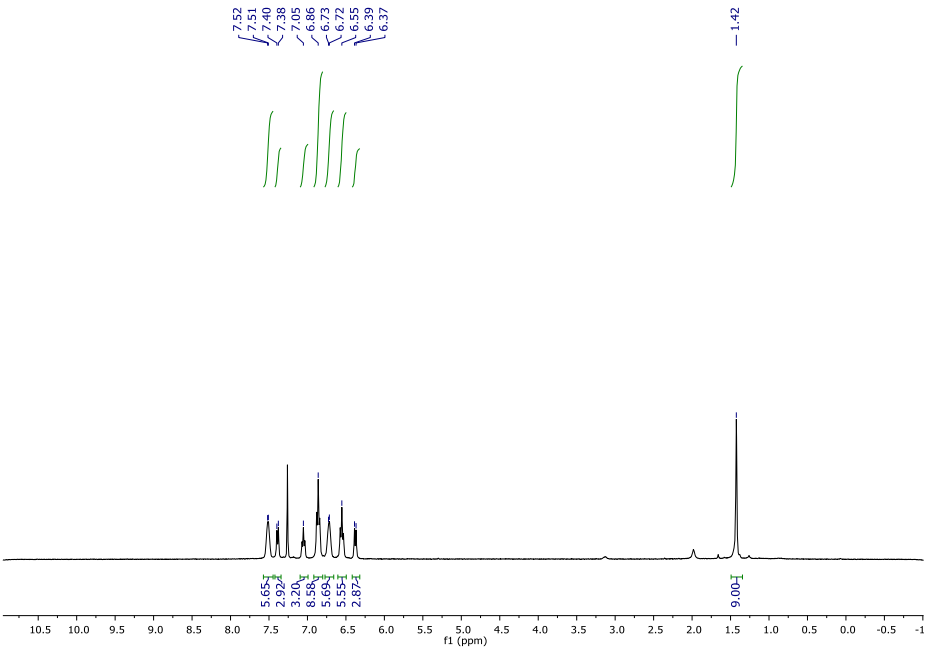

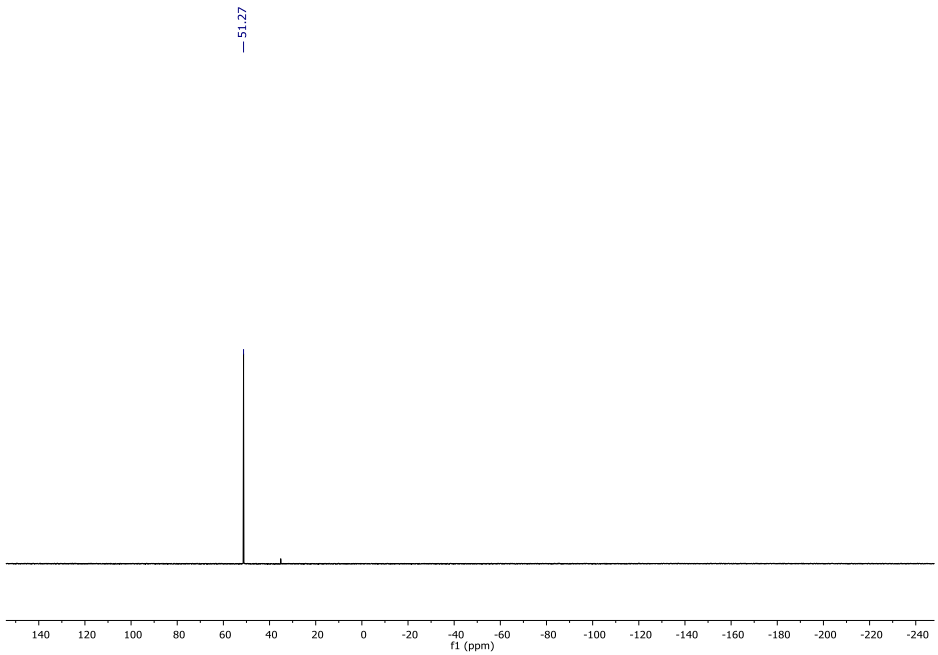
51.27
140 120 100 80 60 40 20 0 -20 -40 -60 -80 -100 -120 -140 -160 -180 -200 -220 -240
f1 (ppm)

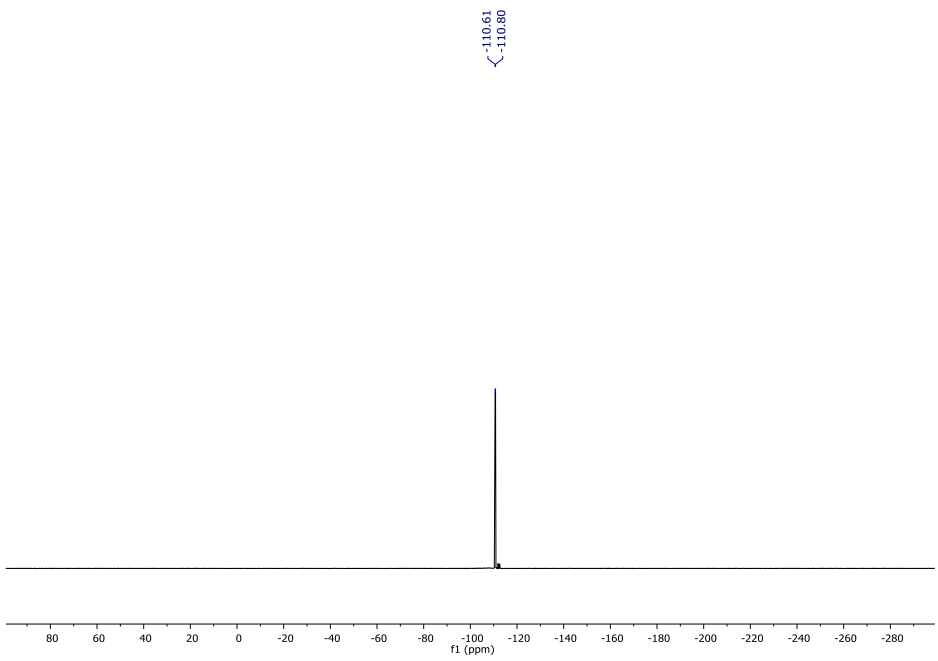
-110.61
-110.80
80 60 40 20 0 -20 -40 -60 -80 -100 -120 -140 -160 -180 -200 -220 -240 -260 -280
f1 (ppm)

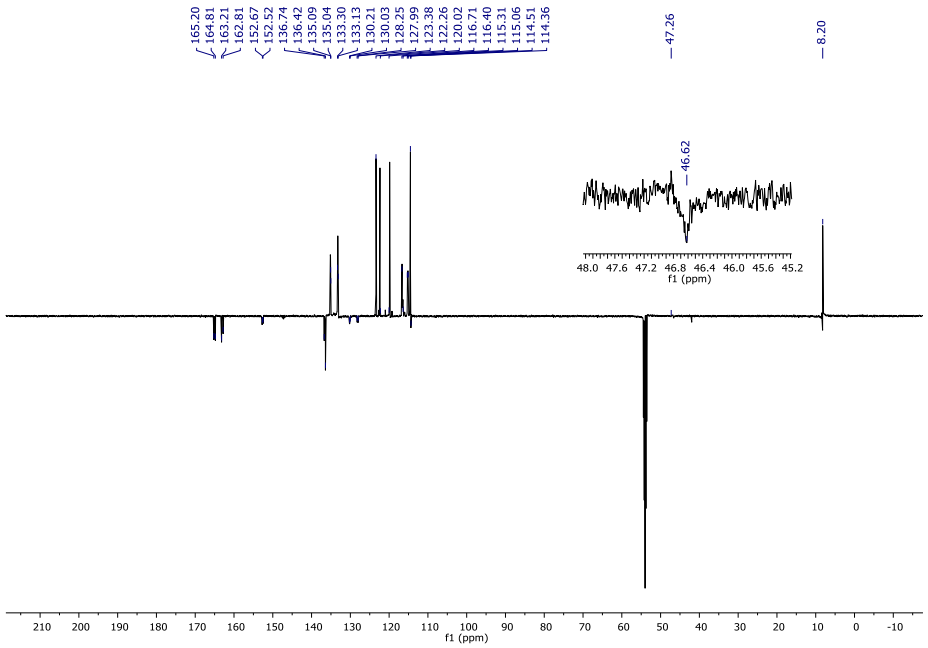

V.4 Characterization of isolated products

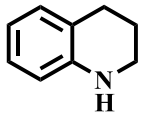

1,2,3,4-tetrahydroquinoline (**V.2a**).[448] Isolated yield: 87%. (The NMR spectrum is consistent with the reported data). ^{1}H NMR (400 MHz, $CDCl_3$) δ = 6.99-6.95 (m, 2H), 6.62 (td, J = 7.4, 1.2, 1H), 6.48 (d, J = 8.0, 1H), 3.40 (bs, NH), 3.31 (t, J = 5.6, 2H), 2.78 (t, J = 6.0, 2H), 1.97-1.92 (m, 2H). ^{13}C NMR (100 MHz, $CDCl_3$) δ: 145.0 (C), 129.6 (CH), 126.8 (CH), 121.4 (C), 116.5 (CH), 114.3 (CH), 41.5 (N-CH_2), 27.3 (CH_2), 21.8 (CH_2) ppm.

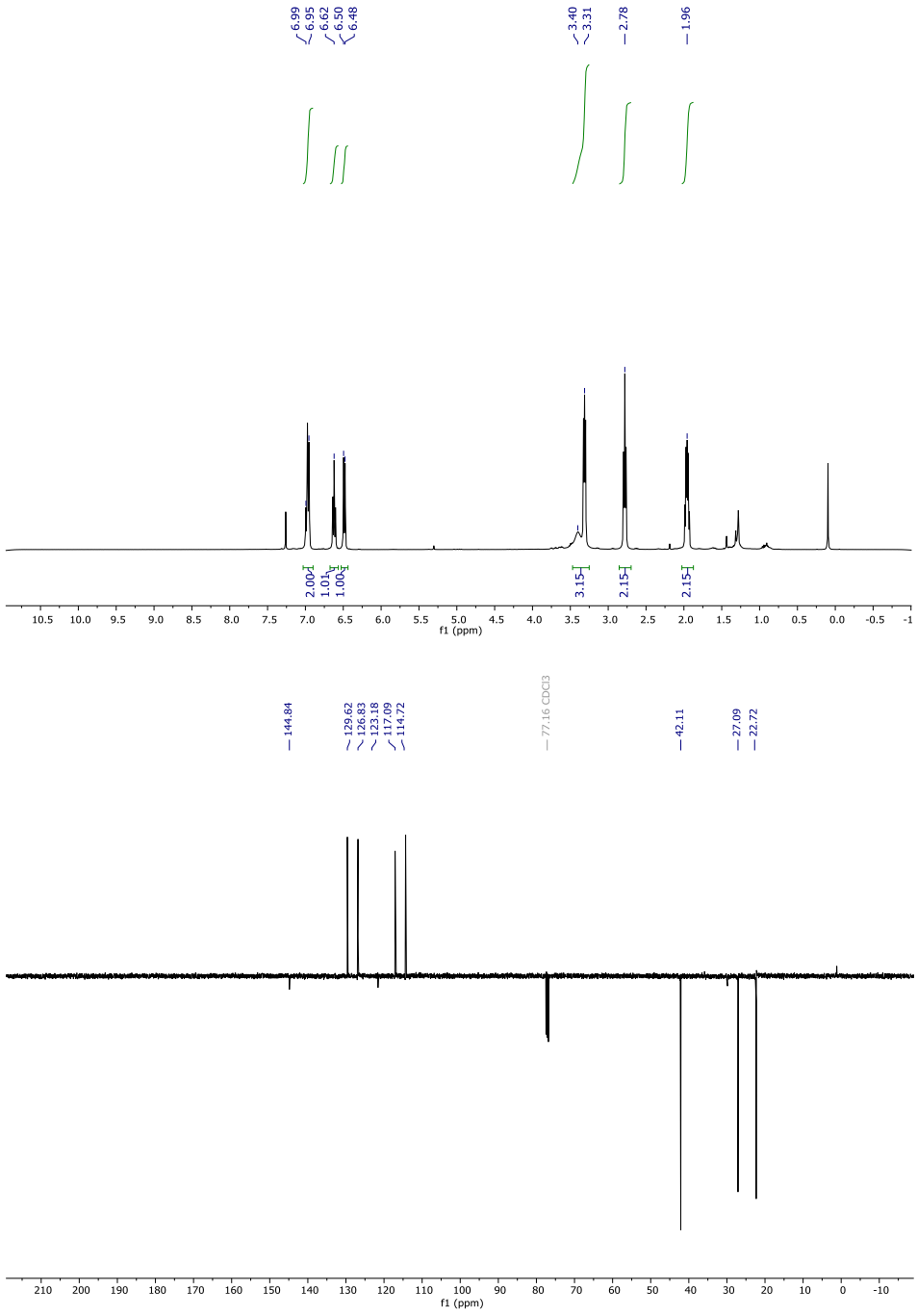
6.99
6.95
6.62
6.50
6.48
3.40
3.31
2.78
1.96
2.00
1.01
1.00
3.15
2.15
2.15
f1 (ppm)
144.84
129.62
126.83
123.18
117.09
114.72
77.16 CDCl3
42.11
27.09
22.72
f1 (ppm)

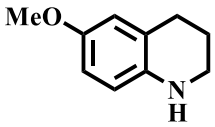

6-methoxy-1,2,3,4-tetrahydroquinoline (**V.2b**).[449] Isolated yield: 93%. (The NMR spectrum is consistent with the reported data). ^{1}H NMR (400 MHz, $CDCl_3$) δ = 6.62-6.57 (m, 2H), 6.46 (d, J = 8.2, 1H), 3.74 (s, 3H), 3.34 (bs, NH), 3.27-3.25 (m, 2H), 2.76 (t, J = 7.6, 2H), 1.96-1.90 (m, 2H). 13C NMR (100 MHz, $CDCl_3$) δ: 151.9 (C), 138.6 (C), 122.9 (C), 115.6 (CH), 114.9 (CH), 112.9 (CH), 55.8 (O-CH_3), 42.3 (N-CH_2), 27.2 (CH_2), 22.9 (CH_2) ppm.

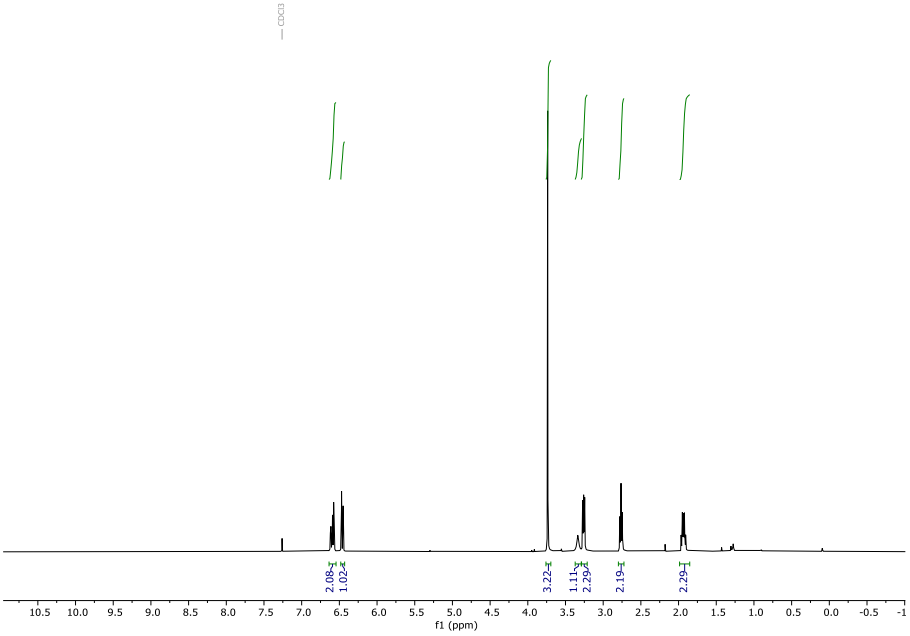

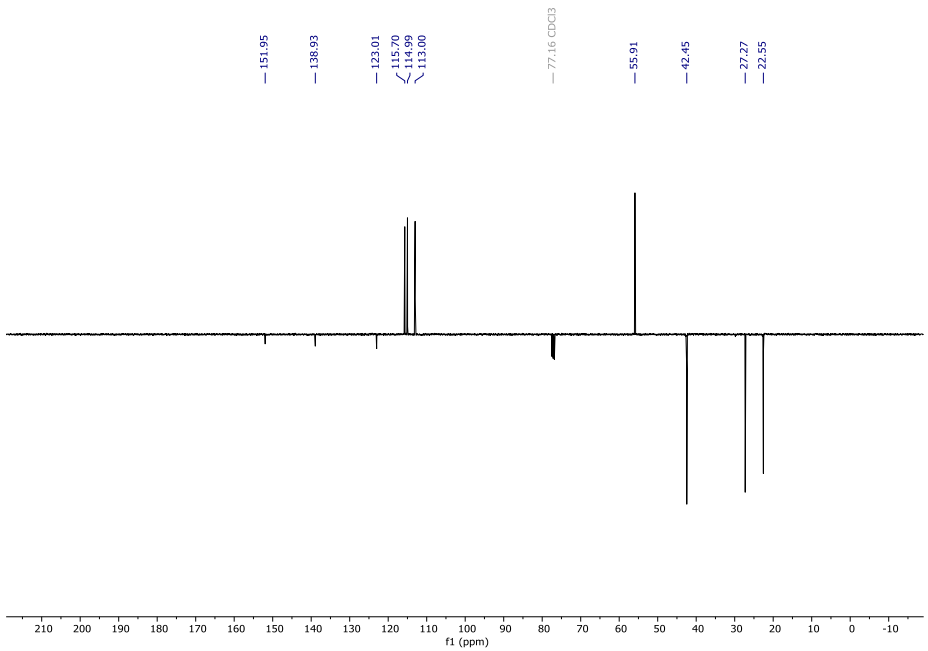

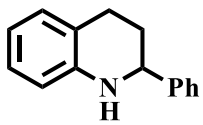

2-phenyl-1,2,3,4-tetrahydroquinoline (**V.2c**).[450] Isolated yield: 93%. (The NMR spectrum is consistent with the reported data). ^{1}H NMR (400 MHz, $CDCl_3$) δ = 7.44-7.30 (m, 5H), 7.07-7.02 (m, 2H), 6.69 (t, J = 7.0, 1H), 6.58-6.56 (m, 1H), 4.47 (dd, J = 9.4, 3.3, 1H), 4.05 (bs, NH), 2.99-2.92 (m, 1H), 2.77 (dt, J = 16.3, 5.9, 1H), 2.19-2.12 (m, 1H), 2.07-1.98 (m, 1H) ppm. ^{13}C NMR (100 MHz, $CDCl_3$) δ = 144.9 (C), 129.4 (CH), 128.7 (CH), 127.5 (CH), 127.0 (CH), 126.7 (CH), 121.0 (C), 117.3 (CH), 114.1 (CH), 56.4 (N-CH), 31.1 (CH_2), 26.5 (CH_2) ppm.

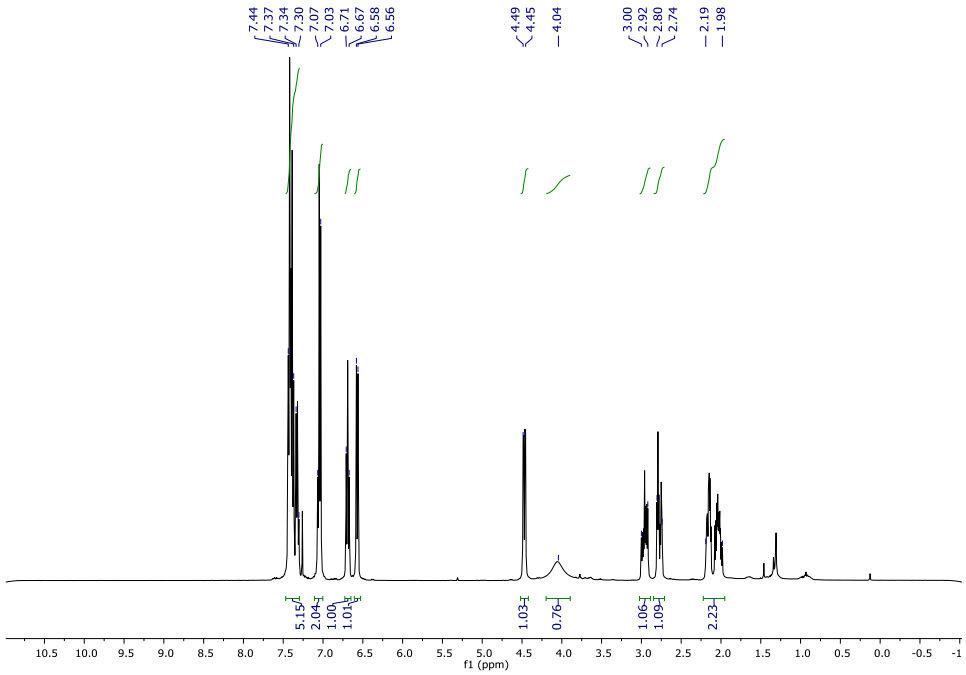
7.44
7.37
7.34
7.30
7.07
7.03
6.71
6.67
6.58
6.56
4.49
4.45
4.04
3.00
2.92
2.80
2.74
2.19
1.98
5.15
2.04
1.00
1.01
1.03
0.76
1.06
1.09
2.23
f1 (ppm)

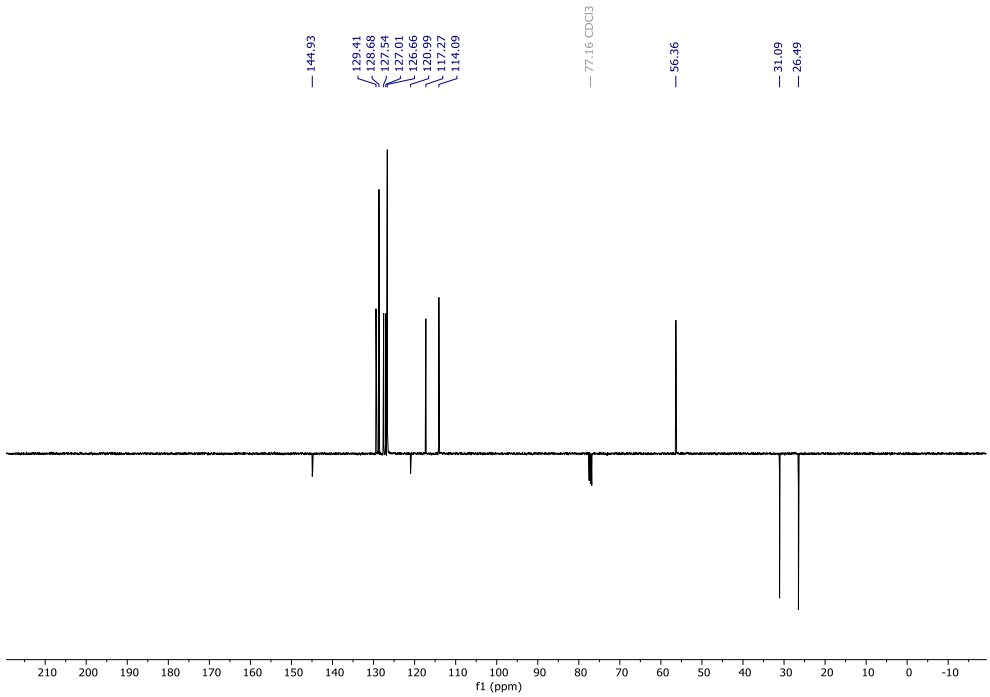
144.93
129.41
128.68
127.54
127.01
126.66
120.99
117.27
114.09
77.16 CDCl3
56.36
31.09
26.49
f1 (ppm)

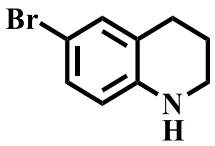

6-bromo-1,2,3,4-tetrahydroquinoline (**V.2d**).[451] Isolated yield: 92%. (The NMR spectrum is consistent with the reported data). ^{1}H NMR (400 MHz, $CDCl_3$) δ = 7.05-7.01 (m, 2H), 6.33 (d, J = 8.1, 1H), 3.50 (bs, NH), 3.28 (t, J = 5.8, 2H), 2.72 (t, J = 7.1, 2H), 1.94-1.88 (m, 2H) ppm. ^{13}C NMR (100 MHz, $CDCl_3$) δ = 143.8 (C), 131.9 (CH), 129.5 (CH), 123.5 (C), 115.6 (CH), 108.3 (C), 42.3 (N-CH_2), 26.9 (CH_2), 21.8 (CH_2) ppm.

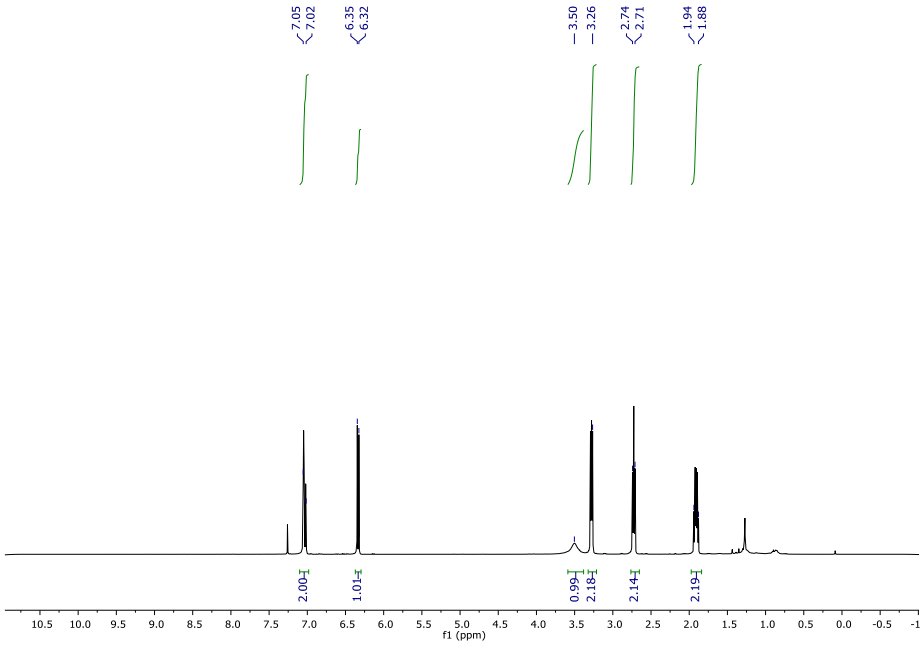

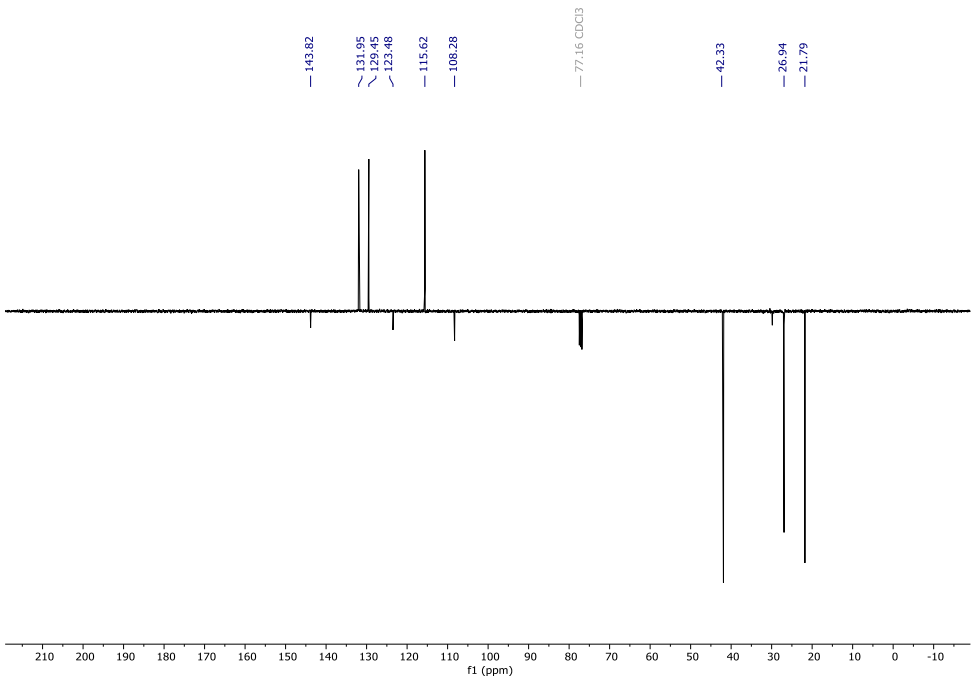

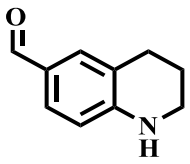

1,2,3,4-tetrahydroquinoline-6-carbaldehyde (V.2e).[438] Isolated yield: 90%. (The NMR spectrum is consistent with the reported data). ^{1}H NMR (400 MHz, $CDCl_3$) δ = 9.66 (s, 1H), 7.49-7.46 (m, 2H), 6.45 (d, J = 8.6, 1H), 4.56 (bs, NH), 3.39 (t, J = 5.7, 2H), 2.79 (t, J = 6.3, 2H), 2.02-1.82 (m, 2H) ppm. ^{13}C NMR (100 MHz, $CDCl_3$) δ = 190.4 (C=O), 150.5 (C), 131.8 (CH), 130.4 (CH), 126.1 (C), 120.5 (C), 113.1 (CH), 41.9 (N-CH_2), 27.0 (CH_2), 21.3 (CH_2) ppm.

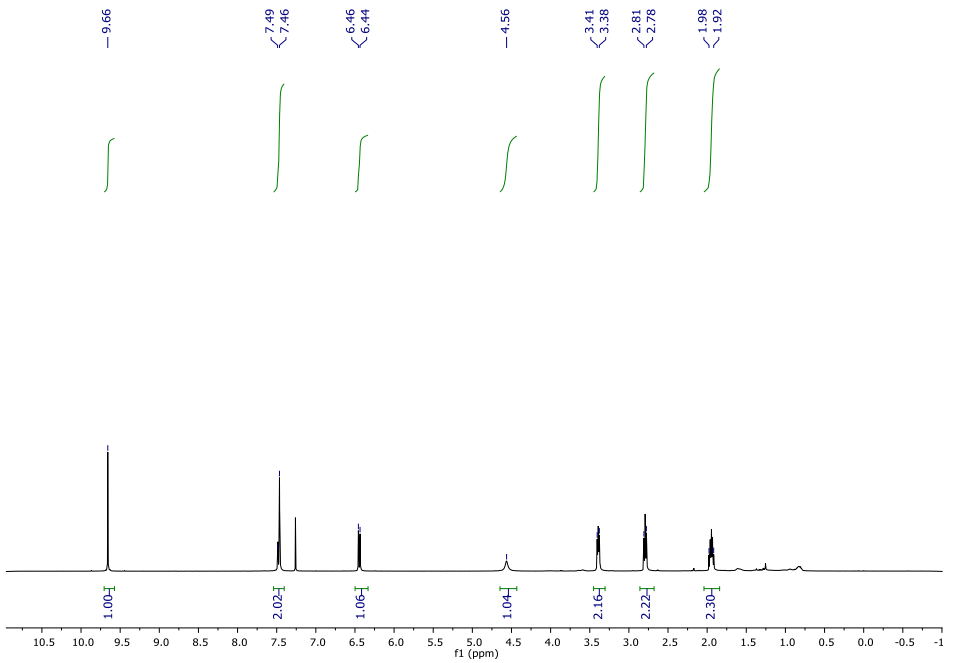
9.66
7.49
7.46
6.46
6.44
4.56
3.41
3.38
2.81
2.78
1.98
1.92
1.00
2.02
1.06
1.04
2.16
2.22
2.30
f1 (ppm)

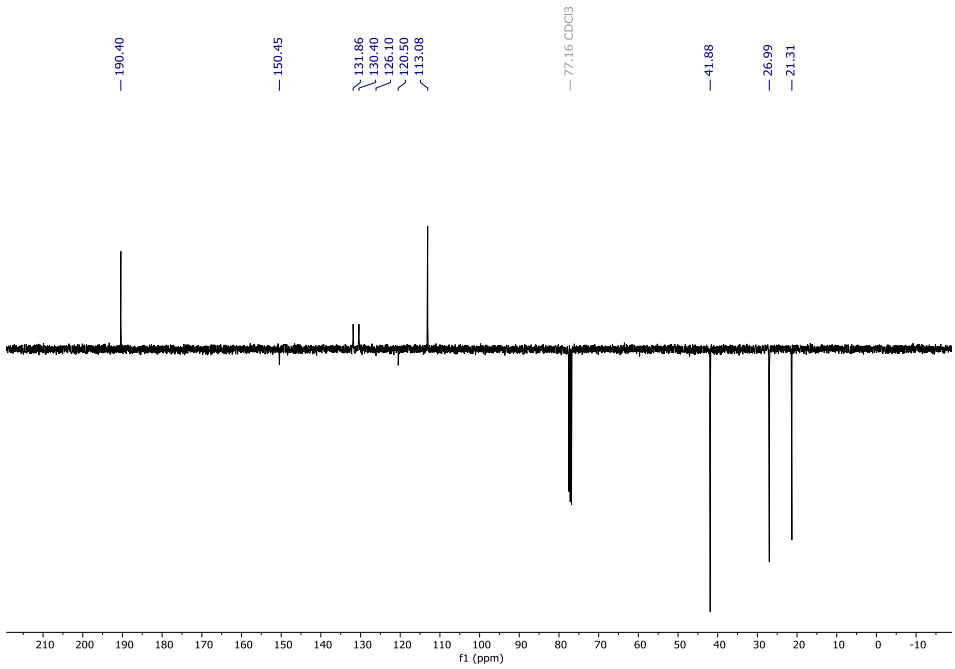
190.40
150.45
131.86
130.40
126.10
120.50
113.08
77.16 CDCl3
41.88
26.99
21.31
f1 (ppm)

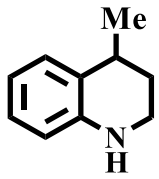

4-methyl-1,2,3,4-tetrahydroquinoline (**V.2f**).[452] Isolated yield: 85%. (The NMR spectrum is consistent with the reported data). ^{1}H NMR (400 MHz, $CDCl_3$) δ = 7.06 (d, J = 7.5, 1H), 6.99-6.94 (m, 1H), 6.64 (td, J = 7.3, 1.3, 1H), 6.48 (dd, J = 8.1, 1.2, 1H), 3.88 (bs, NH), 3.37-3.24 (m, 2H), 2.93 (h, J = 6.6, 1H), 2.03-1.95 (m, 1H), 1.68 (dtd, J = 12.8, 6.3, 3.7, 1H), 1.30 (d, J = 7.0, 3H) ppm. ^{13}C NMR (100 MHz, $CDCl_3$) δ = 144.4 (C), 128.6 (CH), 126.9 (CH), 126.7 (C), 117.1 (CH), 114.3 (CH), 39.1 ($N\text{-}CH_2$), 30.4 (CH), 29.9 (CH_2), 22.8 (CH_3) ppm.

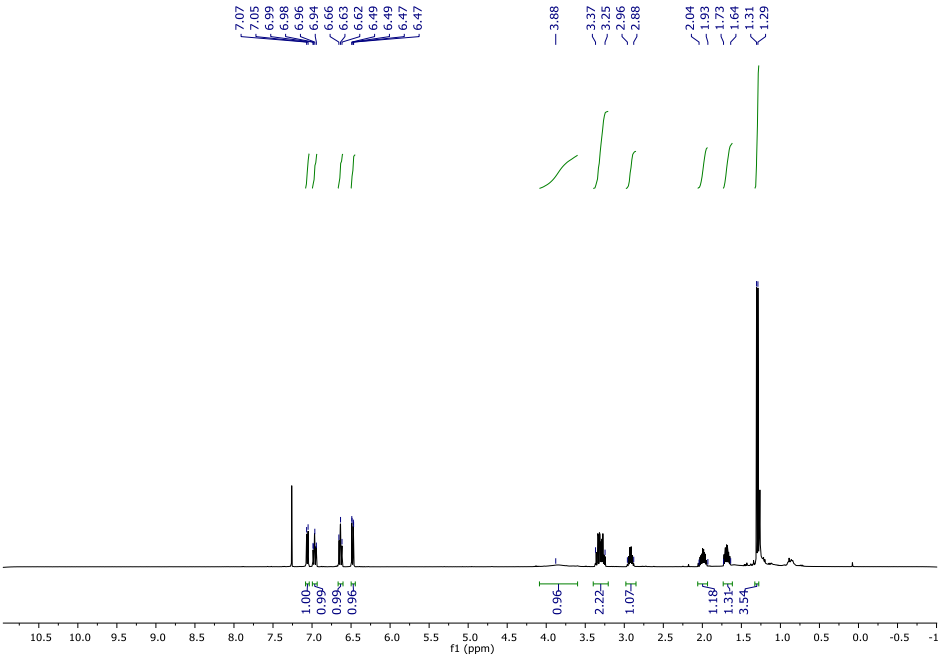

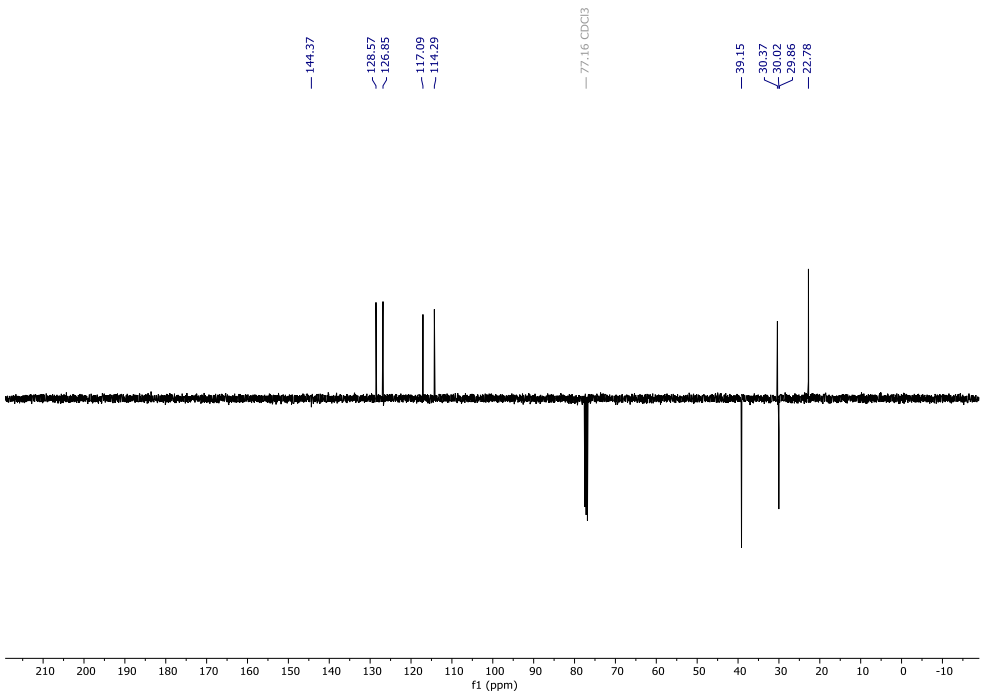

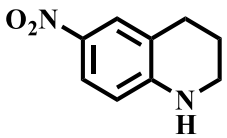

6-nitro-1,2,3,4-tetrahydroquinoline (V.2g).[453] Isolated yield: 95%. (The NMR spectrum is consistent with the reported data). ^{1}H NMR (400 MHz, $CDCl_3$) δ = 7.90-7.87 (m, 2H), 6.37-6.35 (m, 1H), 4.71 (bs, NH), 3.41 (td, J = 4.9, 1.5, 2H), 2.79 (t, J = 4.6, 2H), 1.98-1.92 (m, 2H) ppm. ^{13}C NMR (100 MHz, $CDCl_3$) δ = 179.3 (C), 150.5 (C), 126.0 (CH), 124.4 (CH), 119.9 (C), 112.3 (CH), 41.9 (N-CH_2), 27.0 (CH_2), 20.9 (CH_2) ppm.

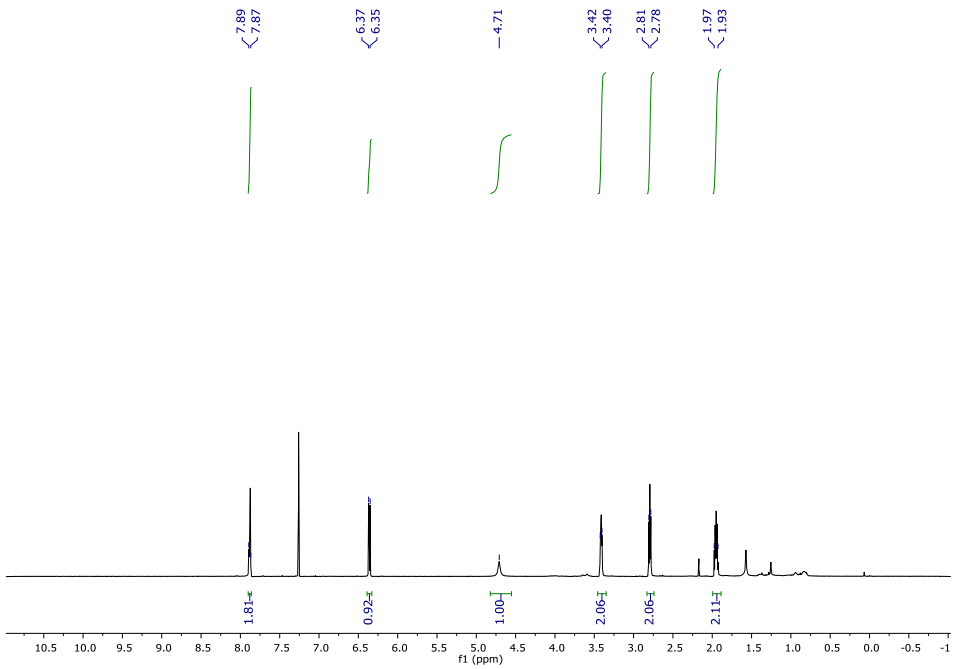
7.89
7.87
6.37
6.35
4.71
3.42
3.40
2.81
2.78
1.97
1.93
1.81
0.92
1.00
2.06
2.06
2.11
f1 (ppm)

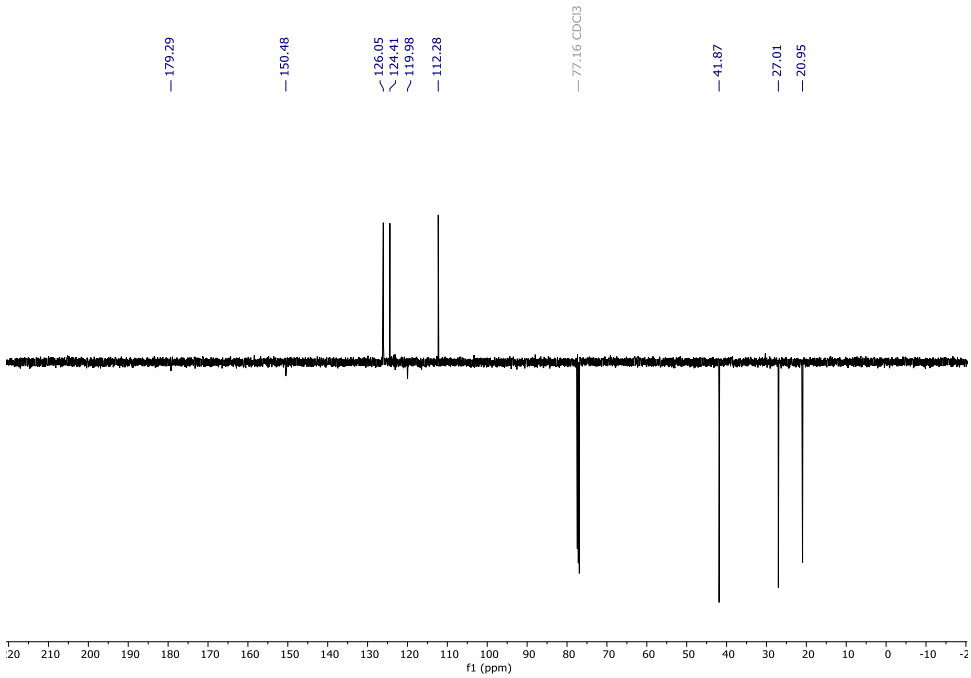
179.29
150.48
126.05
124.41
119.98
112.28
77.16 CDCl3
41.87
27.01
20.95
f1 (ppm)

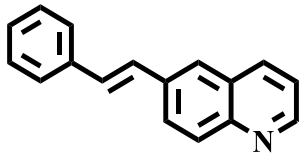

***(E)*-6-styrylquinoline** (**V.1h**). Isolated yield: 65%. (The NMR spectrum is consistent with the reported data).[438] ^{1}H NMR (400 MHz, $CDCl_3$) δ = 8.87 (dd, *J* = 4.1, 1.6, 1H), 8.14 (dd, *J* = 8.3, 1.4, 1H), 8.09 (d, *J* = 8.9, 1H), 7.98 (dd, *J* = 8.7, 2.0, 1H), 7.83 (d, *J* = 1.7, 1H), 7.59-7.56 (m, 2H), 7.41-7.39 (m, 3H), 7.31 (dt, *J* = 4.5, 1.8, 1H), 7.27 (s, 2H) ppm. ^{13}C NMR (100 MHz, $CDCl_3$) δ = 150.3 (CH), 148.2 (C), 136.0 (C), 135.9 (CH), 135.7 (C), 130.4 (CH), 129.9 (CH), 128.9 (CH), 128.7 (C), 128.2 (CH), 128.0 (CH), 127.4 (CH), 126.8 (CH), 126.1 (CH), 121.7 (CH) ppm.

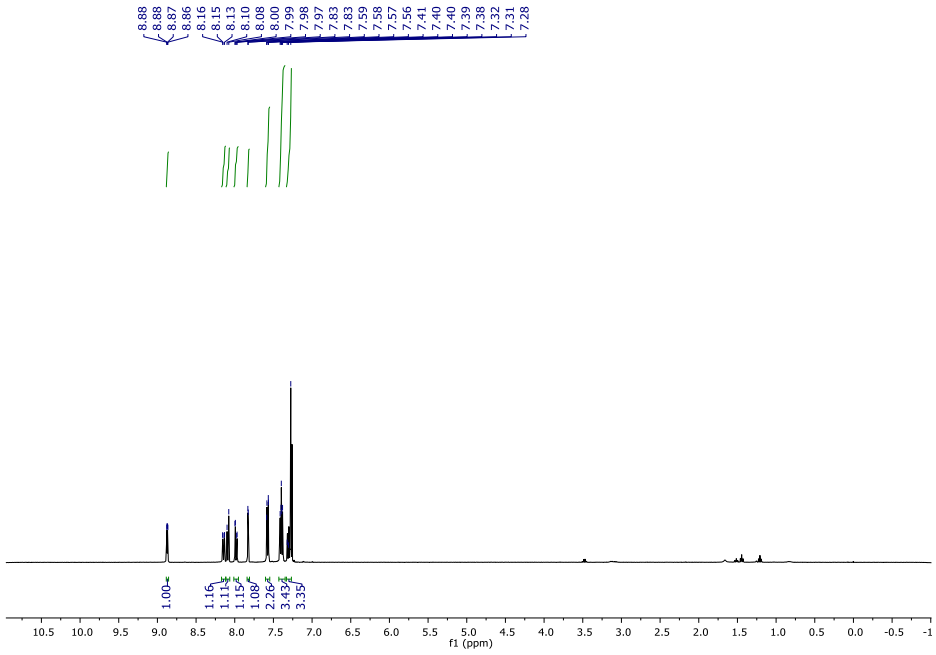

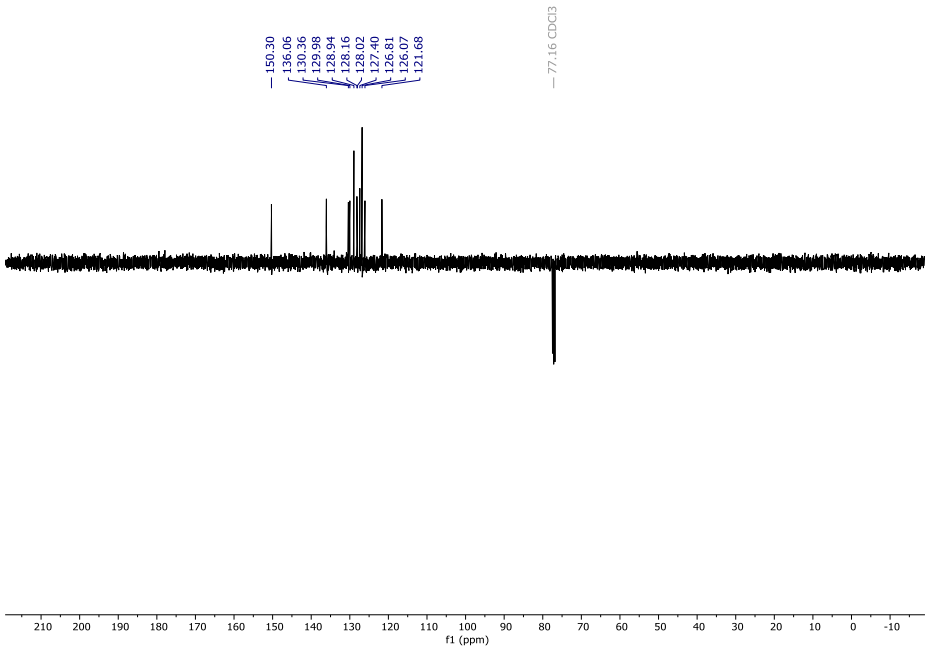

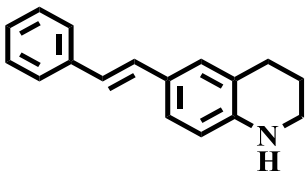

***(E)*-6-styryl-1,2,3,4-tetrahydroquinoline** (**V.2h**).[438] Isolated yield: 81%. (The NMR spectrum is consistent with the reported data). ^{1}H NMR (400 MHz, $CDCl_3$) δ = 7.47 (dd, *J* = 8.1, 0.9, 2H), 7.33 (t, *J* = 7.6, 2H), 7.23-7.14 (m, 3H), 7.01 (d, *J* = 16.2, 1H), 6.89 (d, *J* = 16.2, 1H), 6.48 (d, J = 8.0, 1H), 3.65 (bs, NH), 3.33 (t, *J* = 6.2, 2H), 2.80 (t, *J* = 6.4, 2H), 1.99-1.93 (m, 2H) ppm. ^{13}C NMR (100 MHz, $CDCl_3$) δ = 144.6 (C), 138.3 (C), 129.2 (CH), 128.7 (CH), 127.9 (CH), 126.7 (CH), 126.4 (C), 126.1 (CH), 125.6 (CH), 124.1 (CH), 121.4 (C), 114.3 (CH), 42.1 (N-CH_2), 27.1 (CH_2), 22.2 (CH_2) ppm.

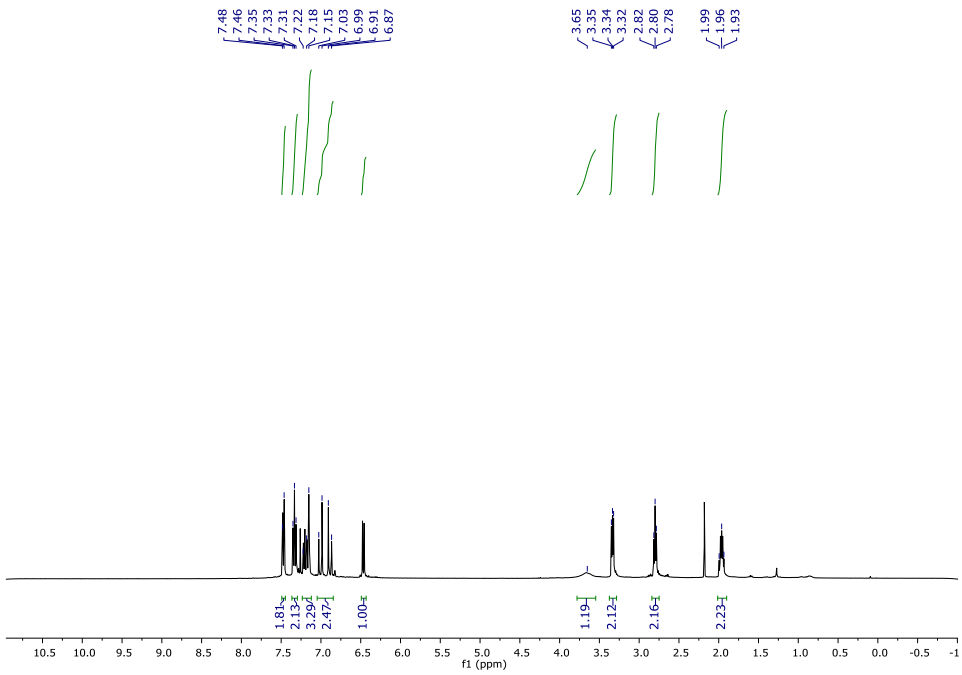
7.48
7.46
7.35
7.33
7.31
7.22
7.18
7.15
7.03
6.99
6.91
6.87
3.65
3.35
3.34
3.32
2.82
2.80
2.78
1.99
1.96
1.93
1.81
2.13
3.29
2.47
1.00
1.19
2.12
2.16
2.23
f1 (ppm)

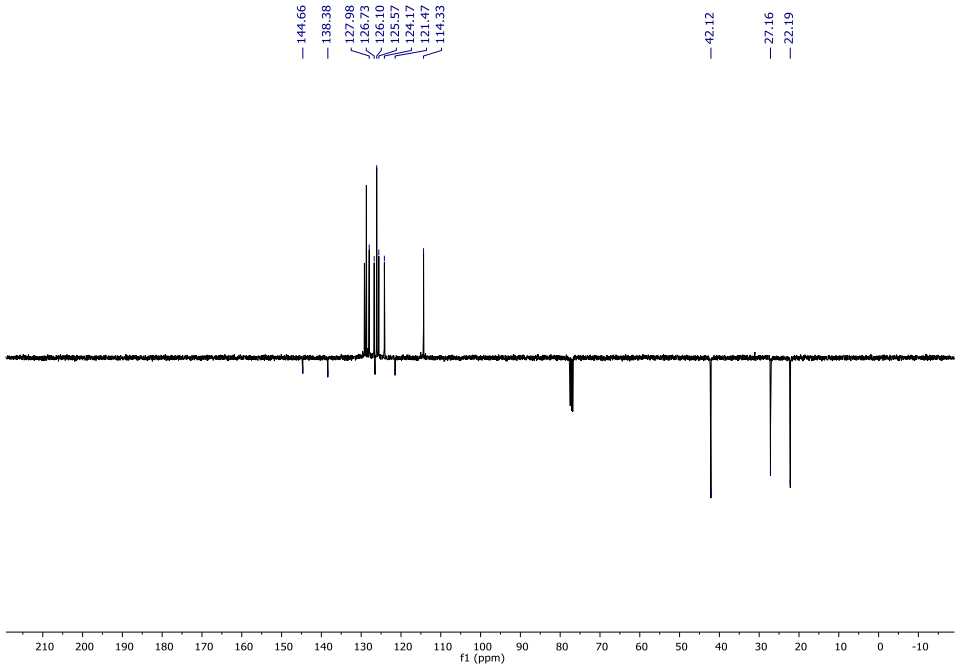
144.66
138.38
127.98
126.73
126.10
125.57
124.17
121.47
114.33
42.12
27.16
22.19
f1 (ppm)

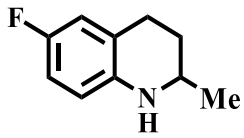

6-fluoro-2-methyl-1,2,3,4-tetrahydroquinoline (**V.2i**).[454] Isolated yield: 84%. (The NMR spectrum is consistent with the reported data). ^{1}H NMR (400 MHz, $CDCl_3$) δ = 6.71-6.65 (m, 2H), 6.42-6.38 (m, 1H), 3.35 (dqd, *J* =10.0, 6.1, 2.5, 1H), 3.22 (bs, NH), 2.88-2.78 (m, 1H), 2.70 (ddd, *J* = 16.5, 5.3, 3.6, 1H), 1.92 (ddt, *J* = 12.2, 6.2, 3.0, 1H), 1.57 (dddd, *J* = 12.8, 11.3, 10.1, 5.4, 1H), 1.21 (d, *J* = 6.3, 3H) ppm. ^{13}C NMR (100 MHz, $CDCl_3$) δ = 156.7 (C), 140.93 (C), 122.5 (C), 115.4 (d, J^2C-F = 22.0, CH), 114.77 (d, J^3C-F = 7.9, CH), 113.2 (d, J^2C-F = 22.1, CH), 47.3 (N-CH), 29.9 (CH_2), 26.7 (CH_2), 22.5 (CH_3) ppm. ^{19}F NMR (378 MHz, $CDCl_3$) δ = -128.42 (s, 1F) ppm.

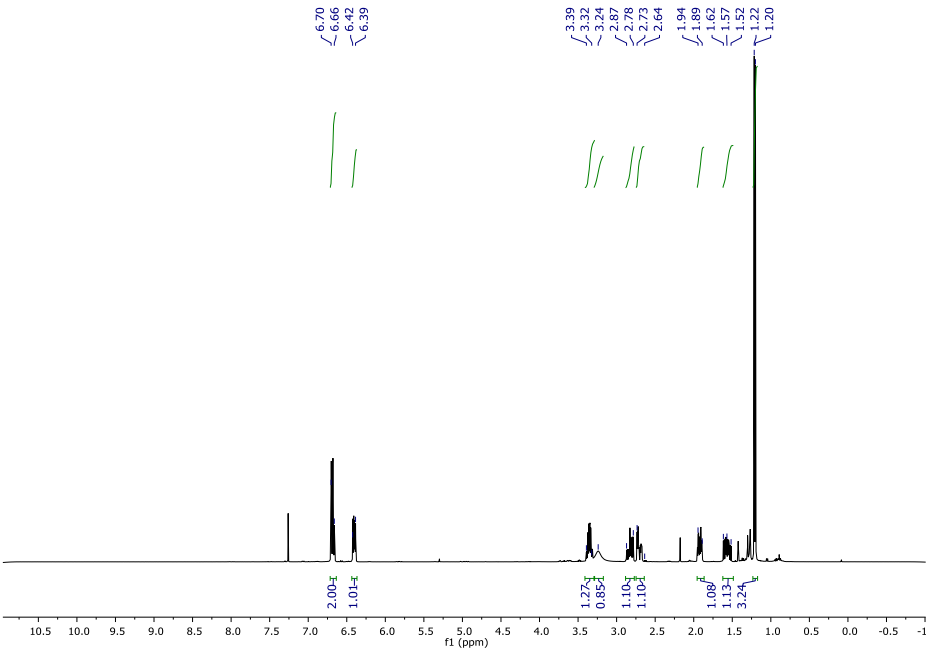

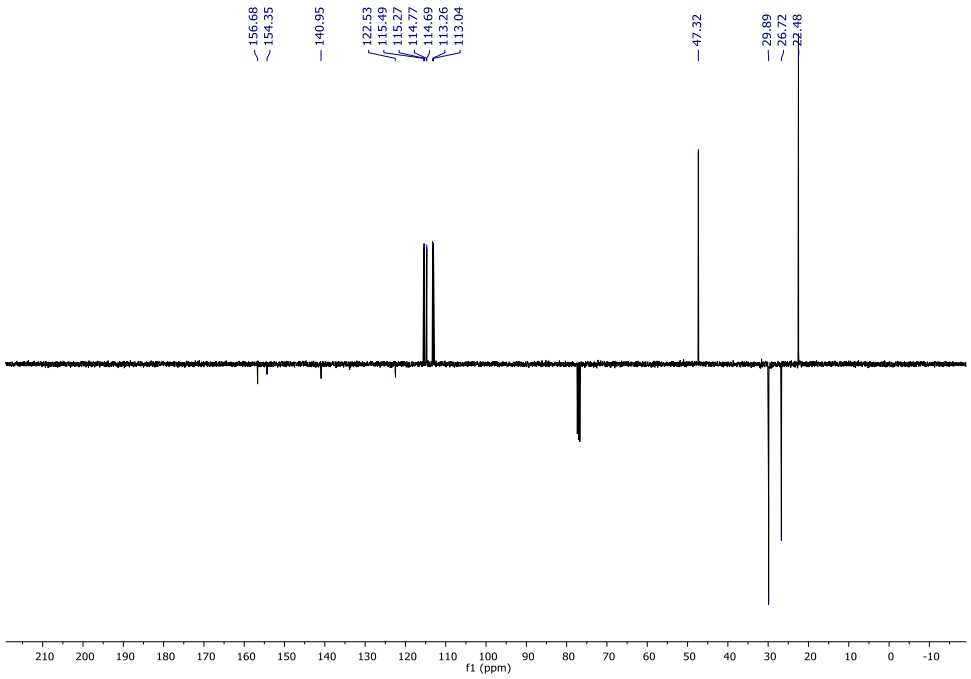
156.68
154.35
140.95
122.53
115.49
115.27
114.77
114.69
113.26
113.04
47.32
29.89
26.72
22.48
f1 (ppm)

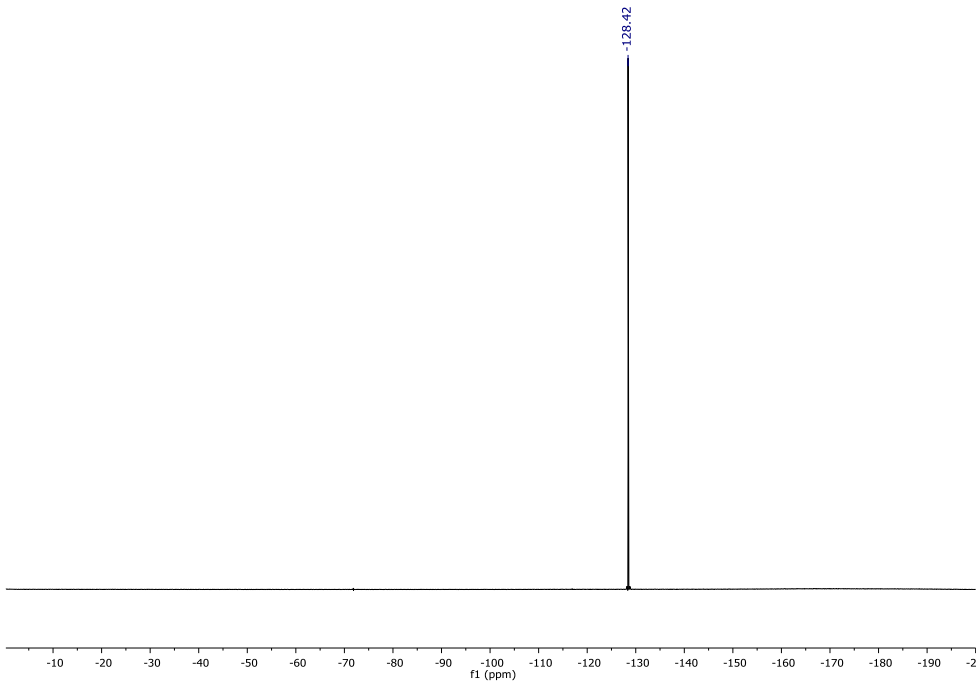
-128.42
f1 (ppm)

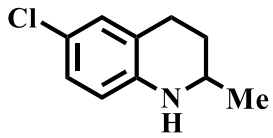

6-chloro-2-methyl-1,2,3,4-tetrahydroquinoline (**V.2j**).[451] Isolated yield: 89%. (The NMR spectrum is consistent with the reported data). ^{1}H NMR (400 MHz, $CDCl_3$) δ = 6.92-6.88 (m, 2H), 6.38 (d, J = 8.1, 1H), 3.58 (bs, NH), 3.34 (dqd, J =10.0, 6.0, 2.5, 1H), 2.84-2.65 (m, 2H), 1.92 (ddt, J = 12.2, 6.0, 3.1, 1H), 1.55 (dddd, J = 12.7, 11.3, 10.0, 5.4, 1H), 1.20 (d, J = 6.2, 3H) ppm. ^{13}C NMR (100 MHz, $CDCl_3$) δ = 143.5 (C), 128.9 (CH), 126.6 (CH), 122.7 (C), 121.5 (C), 115.1 (CH), 47.3 (N-CH), 29.8 (CH_2), 26.2 (CH_2), 22.6 (CH_3) ppm.

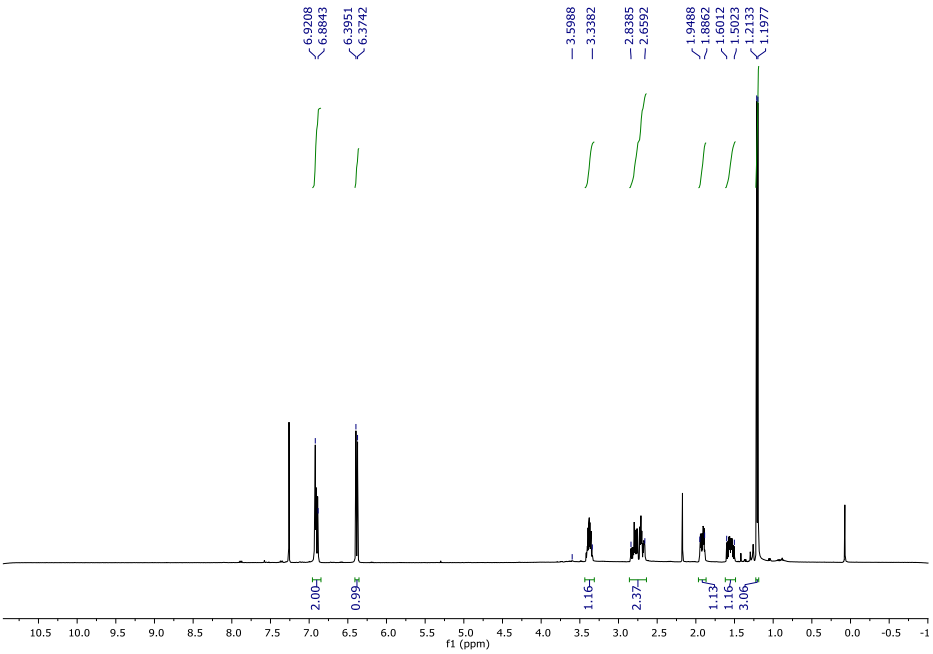

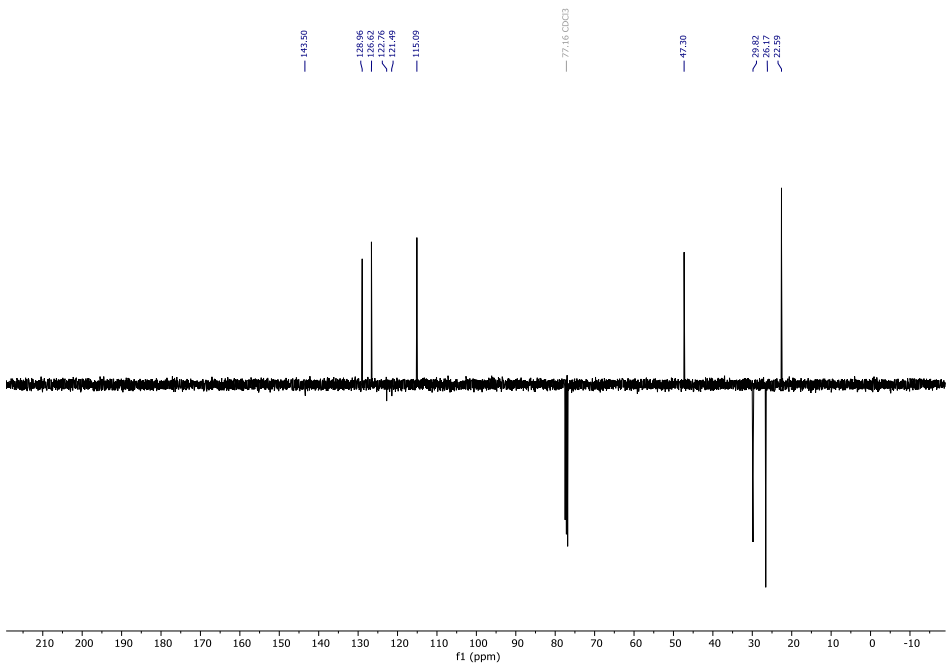

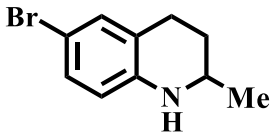

6-bromo-2-methyl-1,2,3,4-tetrahydroquinoline (**V.2k**).[451] Isolated yield: 92%. (The NMR spectrum is consistent with the reported data). ^{1}H NMR (400 MHz, $CDCl_3$) δ = 6.71-6.65 (m, 2H), 6.42-6.38 (m, 1H), 3.35 (dqd, *J* =10.0, 6.1, 2.5, 1H), 3.22 (bs, NH), 2.88-2.78 (m, 1H), 2.70 (ddd, *J* = 16.5, 5.3, 3.6, 1H), 1.92 (ddt, *J* = 12.2, 6.2, 3.0, 1H), 1.57 (dddd, *J* = 12.8, 11.3, 10.1, 5.4, 1H), 1.21 (d, *J* = 6.3, 3H) ppm. ^{13}C NMR (100 MHz, $CDCl_3$) δ = 143.8 (C), 131.8 (CH), 129.5 (CH), 115.5 (CH), 108.5 (C), 47.2 (N-CH), 29.8 (CH_2), 26.5 (CH_2), 22.3 (CH_3) ppm.

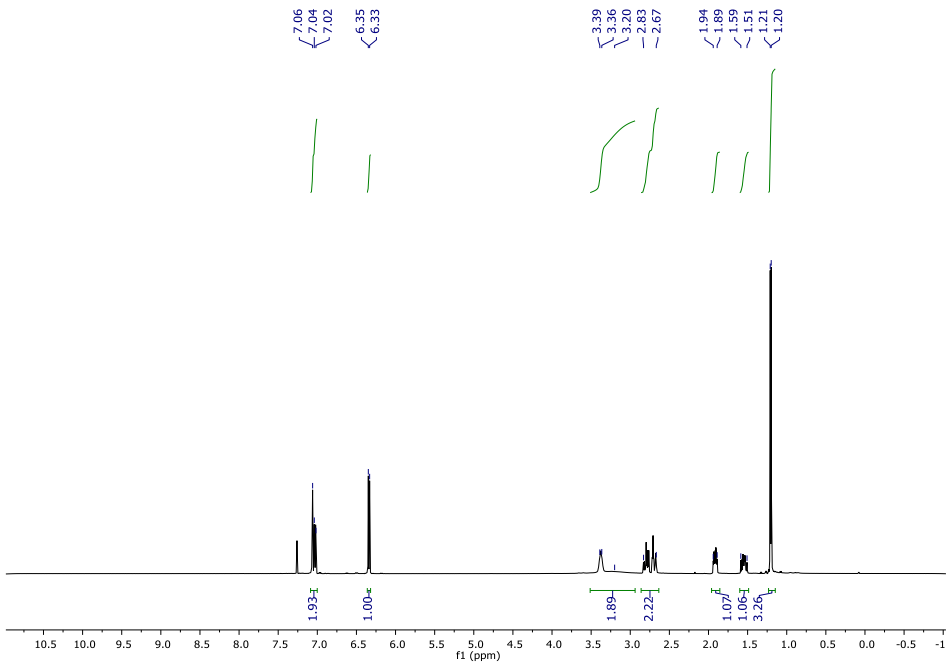
7.06
7.04
7.02
6.35
6.33
3.39
3.36
3.20
2.83
2.67
1.94
1.89
1.59
1.51
1.21
1.20
1.93
1.00
1.89
2.22
1.07
1.06
3.26
f1 (ppm)

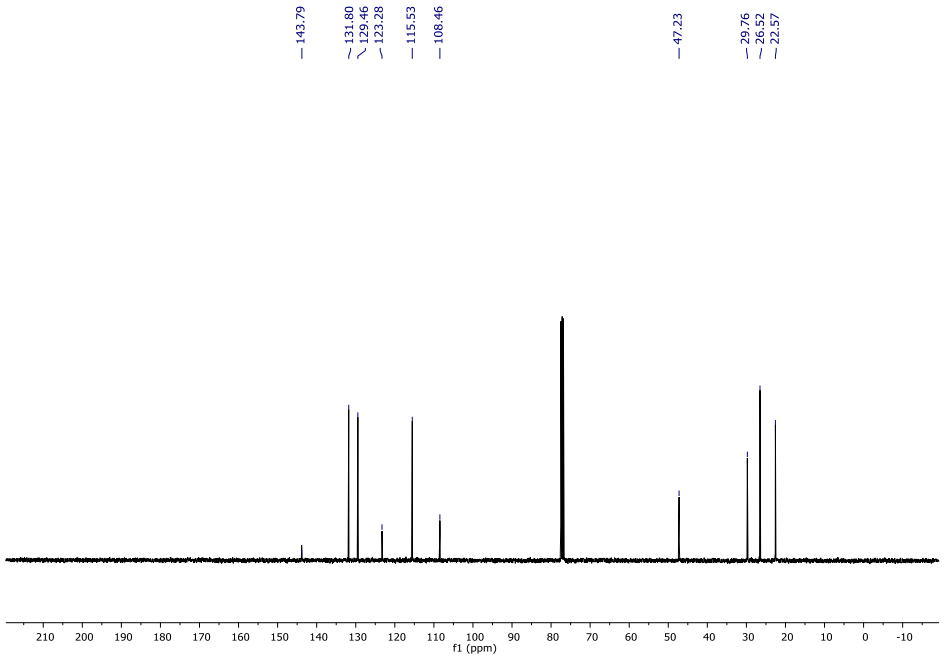
143.79
131.80
129.46
123.28
115.53
108.46
47.23
29.76
26.52
22.57
f1 (ppm)

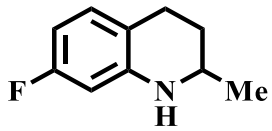

7-fluoro-2-methyl-1,2,3,4-tetrahydroquinoline (**V.2l**).[454] Isolated yield: 83%.(The NMR spectrum is consistent with the reported data). ^{1}H NMR (400 MHz, $CDCl_3$) δ = 6.86 (t, *J* = 11.5, 1H), 6.28 (td, *J* = 6.9, 2.0, 1H), 6.16 (dd, *J* = 8.6, 2.6, 1H), 3.64 (bs, NH), 3.39 (dqd, *J* = 9.1, 6.0, 3.2, 1H), 2.79-2.66 (m, 2H), 1.92 (dddd, *J* = 12.7, 5.2, 3.6, 3.0, 1H), 1.56 (dddd, *J* = 13.0, 11.2, 9.7, 5.8, 1H), 1.21 (d, *J* = 5.0, 3H) ppm. ^{13}C NMR (100 MHz, $CDCl_3$) δ = 163.8 (d, J^3C-F = 10.7, C), 145.9 (d, *J*C-F = 10.6, C),130.2 (d, J^3C-F = 9.7, CH), 116.6 (C), 103.4 (d, J^2C-F = 21.4, CH), 100.29 (d, J^2C-F = 24.3, CH), 47.14 (N-CH), 30.1 (CH_2), 26.1 (CH_2), 22.6 (CH_3) ppm. ^{19}F NMR (378 MHz, $CDCl_3$) δ = -117.26 (s, 1F) ppm.

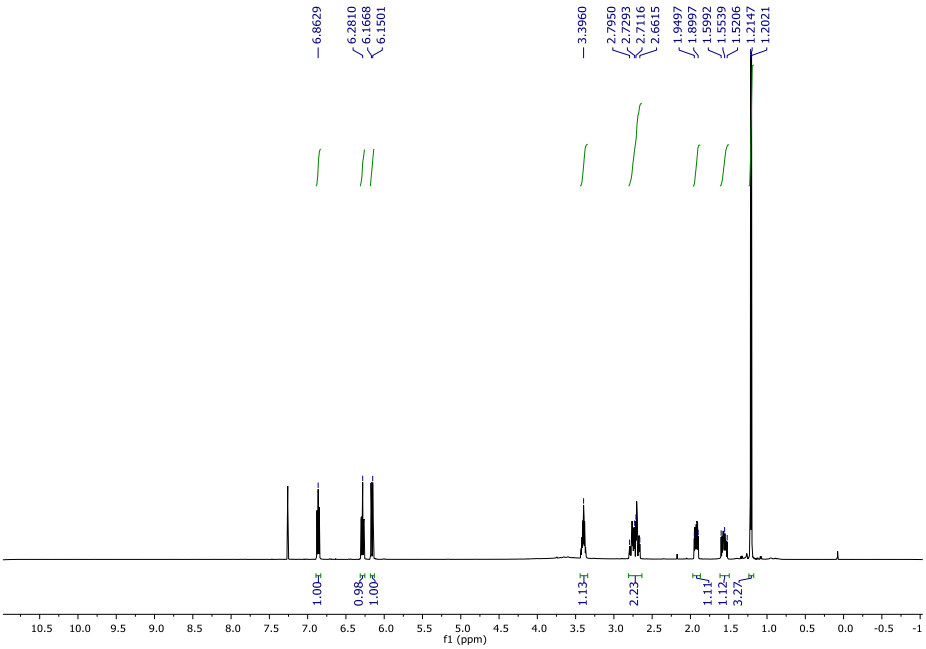

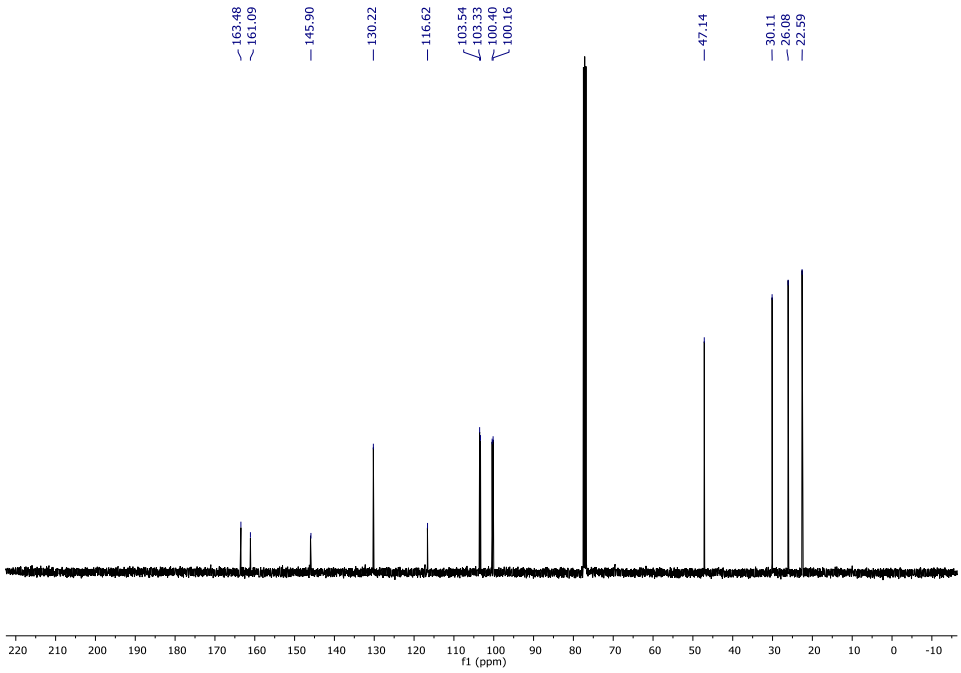
163.48
161.09
145.90
130.22
116.62
103.54
103.33
100.40
100.16
47.14
30.11
26.08
22.59
f1 (ppm)

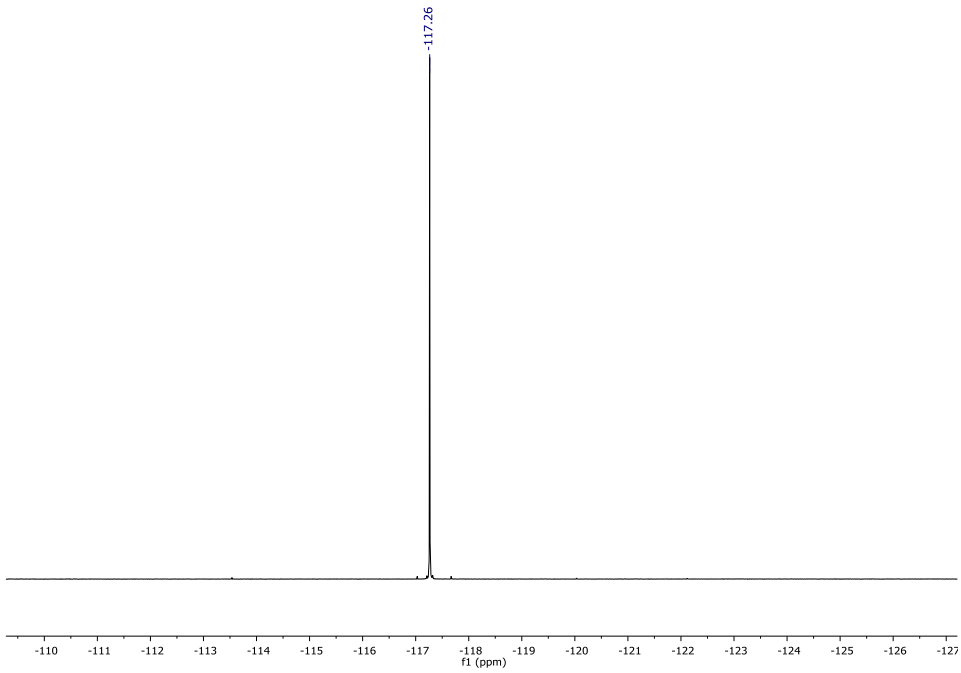
-117.26
f1 (ppm)

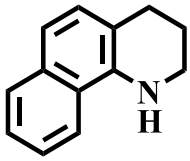

1,2,3,4-tetrahydrobenzo[h]quinoline (**V.2m**).[455] Isolated yield: 60%. (The NMR spectrum is consistent with the reported data). ^{1}H NMR (400 MHz, $CDCl_3$) δ = 7.77-7.71 (m, 2H), 7.45-7.38 (m, 2H), 7.19 (d, *J* = 8.3, 1H), 7.14 (d, *J* = 8.3, 1H), 4.41 (bs, NH), 3.52 (t, *J* = 5.4, 2H), 2.95 (t, J = 6.4, 2H), 2.07 (tdd, *J* = 6.4, 5.2, 3.2, 2H) ppm. ^{13}C NMR (101 MHz, $CDCl_3$) δ = 139.1 (C), 133.2 (C), 128.7 (CH), 125.1 (CH), 124.9 (CH), 123.4 (C), 119.5 (CH), 117.1 (CH), 116.1 (C), 42.6 (N-CH_2), 27.6 (CH_2), 22.3 (CH_2) ppm.

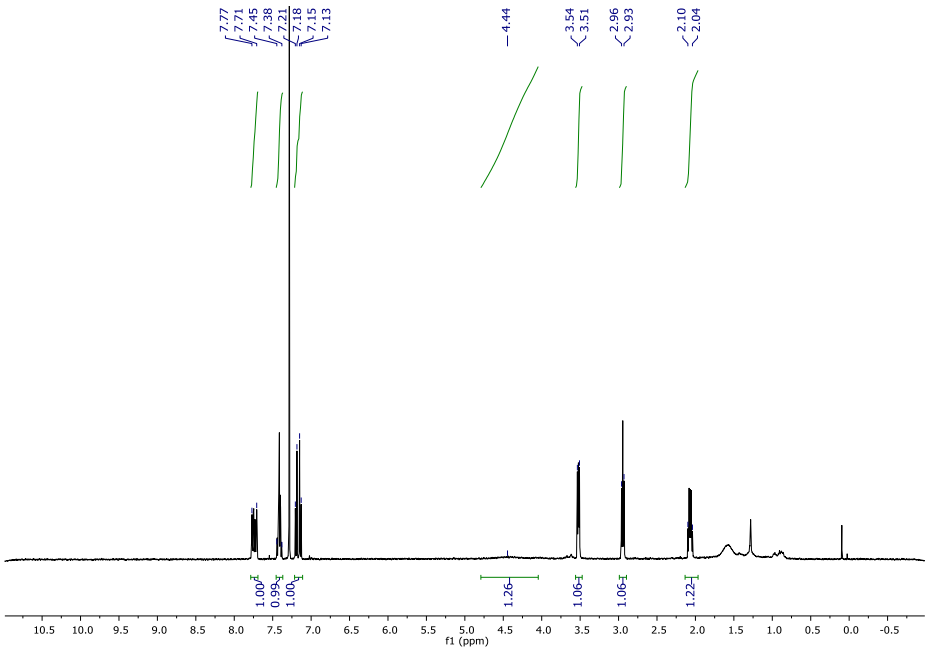

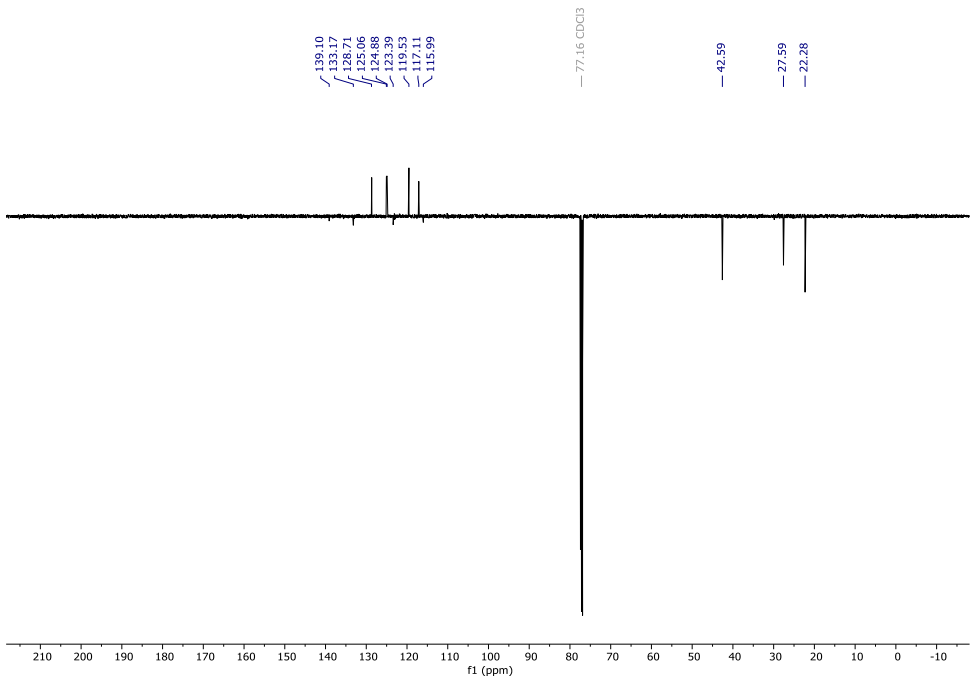

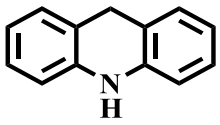

9,10-dihydroacridine (**V.2n**).[456] Isolated yield: 60%. (The NMR spectrum is consistent with the reported data). ^{1}H NMR (400 MHz, $CDCl_3$) δ = 7.11-7.07 (m, 4H), 6.86 (td, J = 7.3, 1.1, 2H), 6.67 (d, J = 7.7, 2H), 5.95 (bs, NH), 4.06 (s, 2H) ppm. ^{13}C NMR (101 MHz, $CDCl_3$) δ = 140.3 (C), 128.8 (CH), 127.1 (CH), 120.7 (CH), 120.2 (C), 113.5 (CH), 31.5 (CH_2) ppm.

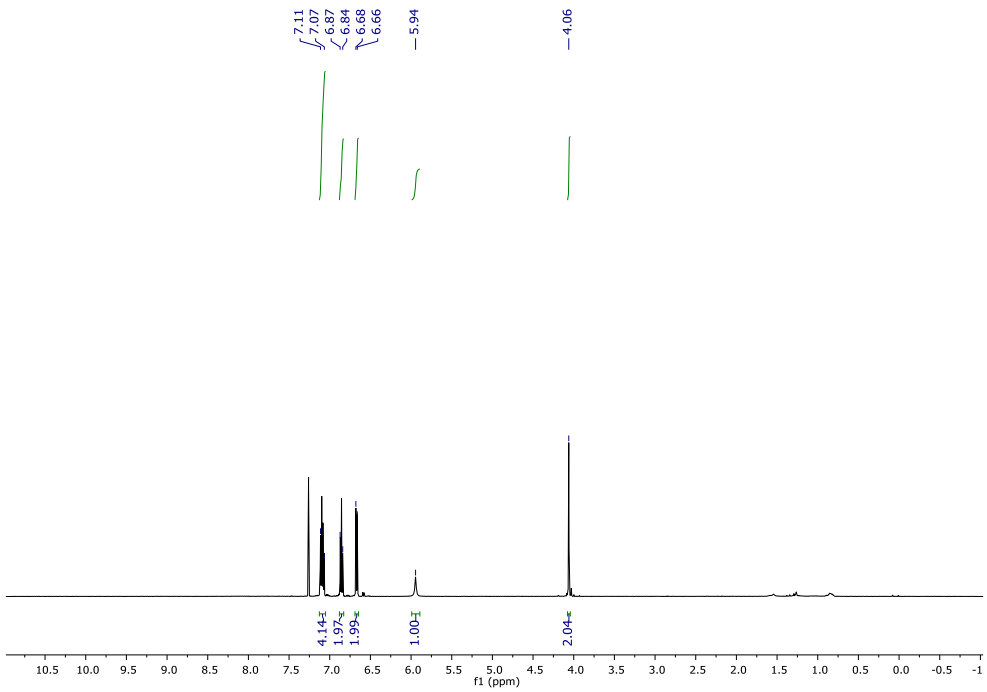
7.11
7.07
6.87
6.84
6.68
6.66
5.94
4.06
4.14
1.97
1.99
1.00
2.04
f1 (ppm)

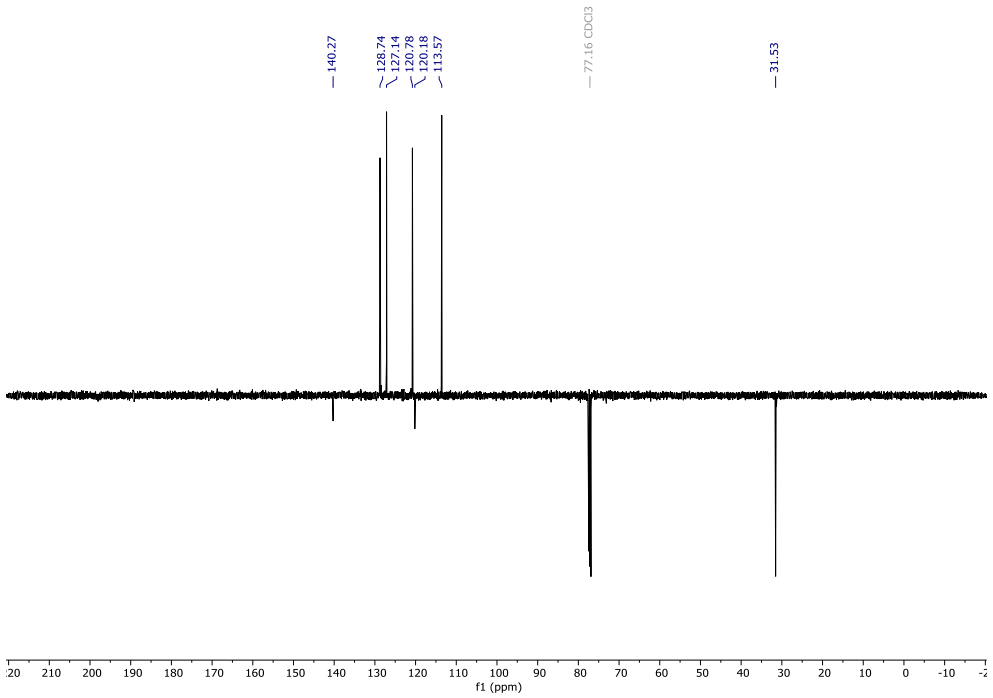
140.27
128.74
127.14
120.78
120.18
113.57
77.16 CDCl3
31.53
f1 (ppm)

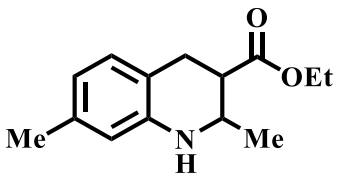

Ethyl-2,7-dimethyl-1,2,3,4-tetrahydroquinoline-3-carboxylate (**V.2o**). Isolated yield: 50%. ^{1}H NMR (400 MHz, $CDCl_3$) δ = 6.87 (d, J = 5.4, 1H), 6.46 (d, J = 5.4, 1H), 6.33 (s, 1H), 4.24-4.15 (m, 2H), 3.60 (bs, NH), 3.53-3.49 (m, 1H), 3.00 (dd, J = 13.3, 3.2, 1H), 2.88 (dd, J = 13.0, 4.3, 1H), 2.45 (dddd, J = 13.0, 11.1, 9.6, 5.7 1H), 2.22 (s, 3H), 1.28 (t, J = 6.0, 3H), 1.23 (d, J = 4.9, 3H) ppm. ^{13}C NMR (101 MHz, $CDCl_3$) δ = 174.2 (COOEt), 142.31 (C), 136.0 (C), 129.1 (CH), 118.5 (CH), 116.7 (C), 114.5 (CH), 60.7 (CH_2), 49.2 (CH), 46.0 (N-CH_2), 30.4 (CH_2), 21.3 (CH_3), 20.7 (CH_3), 14.4 (CH_3) ppm. HRMS calcul. for $C_{14}H_{20}NO_2$, $[M+H]^+$ 234.1489, found 234.1495.

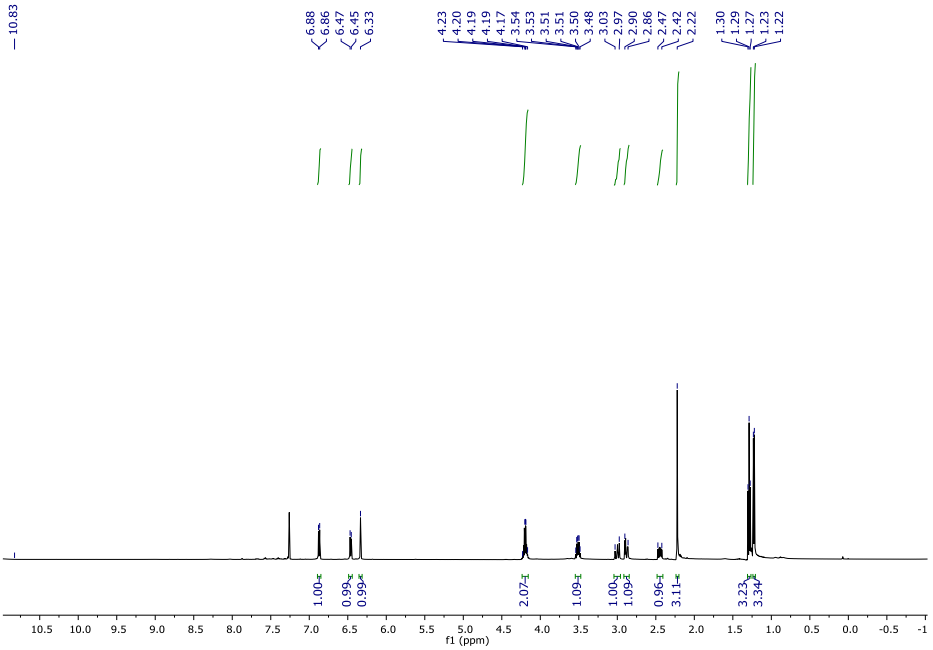

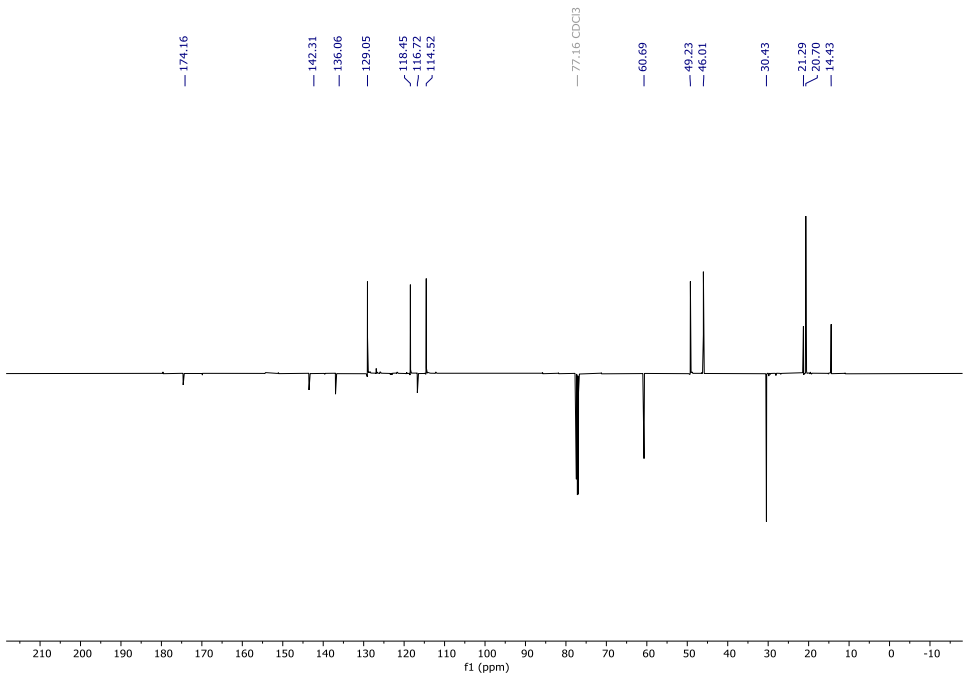

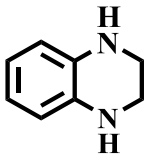

1,2,3,4-tetrahydroquinoxaline (**V.2p**).[450] Isolated yield: 85%. (The NMR spectrum is consistent with the reported data). ^{1}H NMR (400 MHz, $CDCl_3$) δ = 6.61-6.57 (m, 2H), 6.52-6.48 (m, 2H), 3.42 (bs, 4H), 3.30 (bs, 2NH) ppm. ^{13}C NMR (101 MHz, $CDCl_3$) δ = 133.7 (2xC), 118.9 (2xCH), 114.9 (2xCH), 41.5 ($2xCH_2$) ppm.

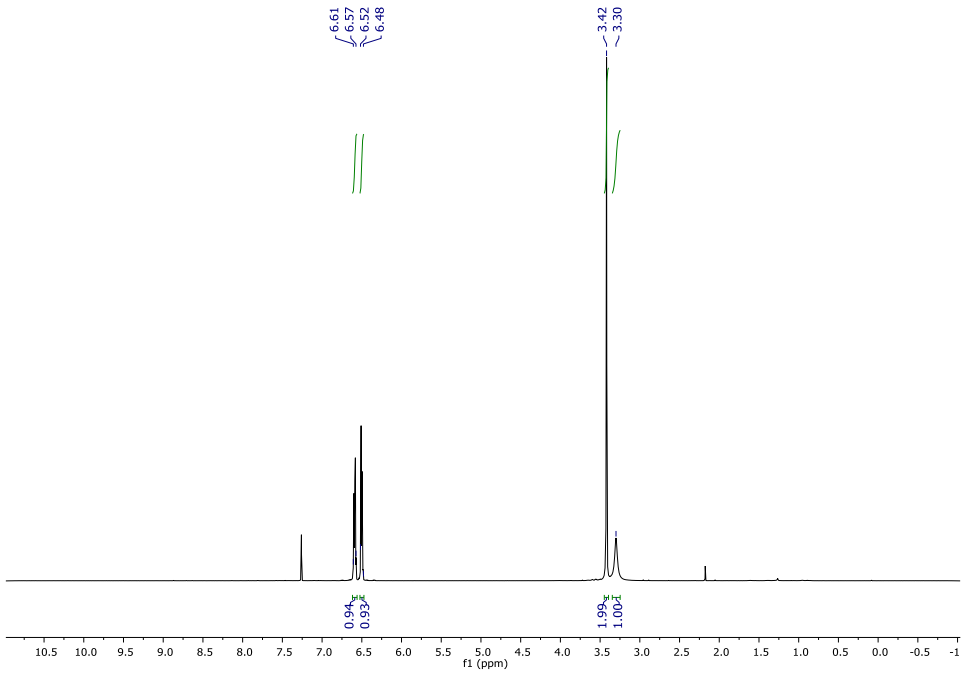
6.61
6.57
6.52
6.48
3.42
3.30
0.94
0.93
1.99
1.00
f1 (ppm)

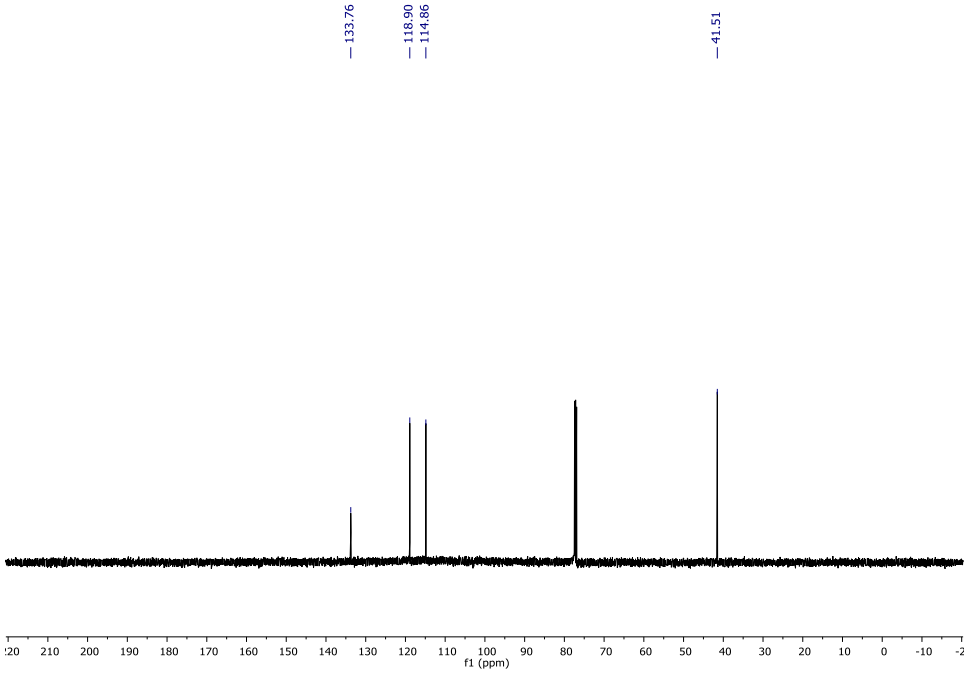
133.76
118.90
114.86
41.51
f1 (ppm)

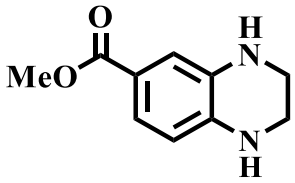

Methyl 1,2,3,4-tetrahydroquinoxaline-6-carboxylate (**V.2q**).[457] Isolated yield: 61%. (The NMR spectrum is consistent with the reported data). ^{1}H NMR (400 MHz, $CDCl_3$) δ = 7.32 (dd, *J* = 8.2, 1.9 Hz, 1H), 7.17 (d, *J* = 1.9 Hz, 1H), 6.42 (d, *J* = 8.2 Hz, 1H), 3.82 (s, 3H), 3.52 – 3.45 (m, 2H), 3.43 – 3.36 (m, 2H) ppm.^{13}C NMR (101 MHz, $CDCl_3$) δ = 121.9 (CH), 116.9 (CH), 113.45 (CH), 52.1 (CH_3), 42.1 (CH_2), 39.8 (CH_2) ppm.

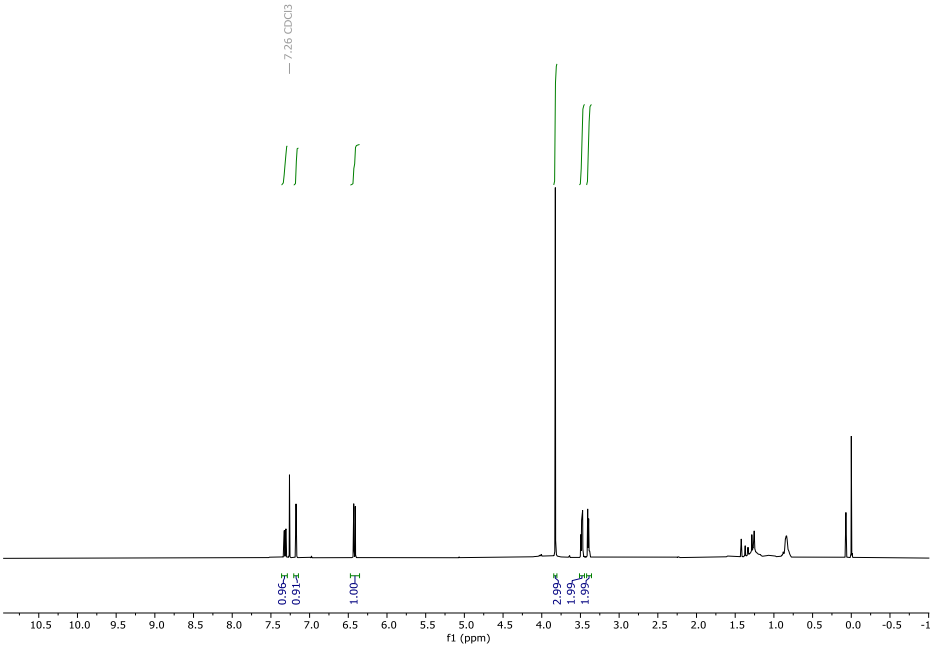

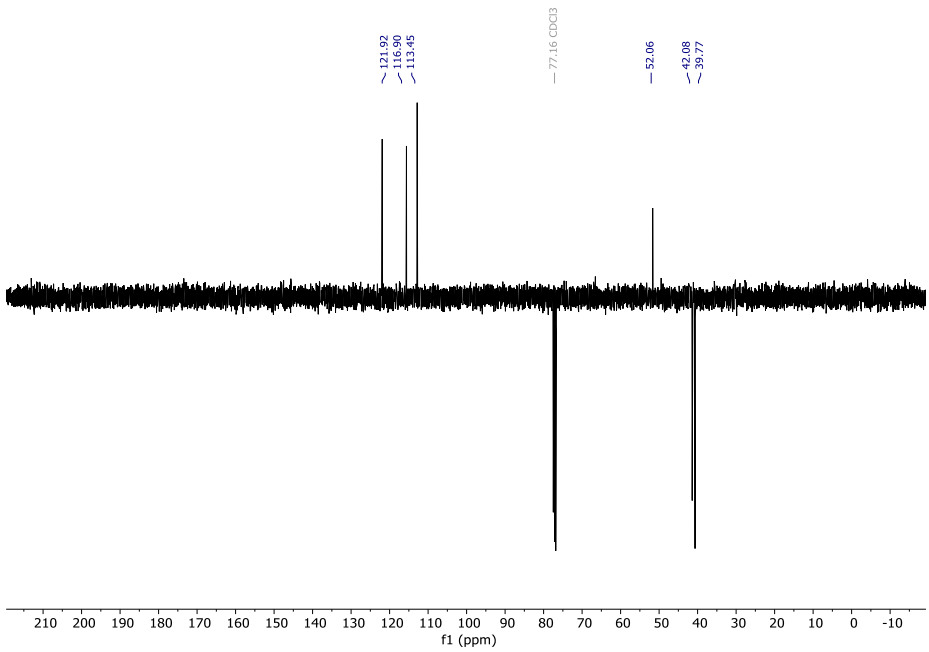

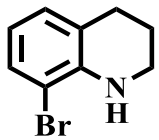

8-bromo-2-methyl-1,2,3,4-tetrahydroquinoline (**V.2r**).[453] Isolated yield: 90%. (The NMR spectrum is consistent with the reported data). ^{1}H NMR (400 MHz, $CDCl_3$) δ = 7.22 (dt, J = 7.9, 0.7, 1H), 6.89-6.87 (m, 1H), 6.45 (t, J = 6.9, 1H), 4.42 (bs, NH), 3.41-3.37 (m, 2H), 2.79-2.75 (m, 2H), 1.96-1.89 (m, 2H) ppm. ^{13}C NMR (100 MHz, $CDCl_3$) δ = 142.1 (C), 130.1 (CH), 128.5 (CH), 123.0 (C), 117.0 (CH), 108.8 (C), 42.2 (N-CH), 27.6 (CH_2), 21.8 (CH_2) ppm.

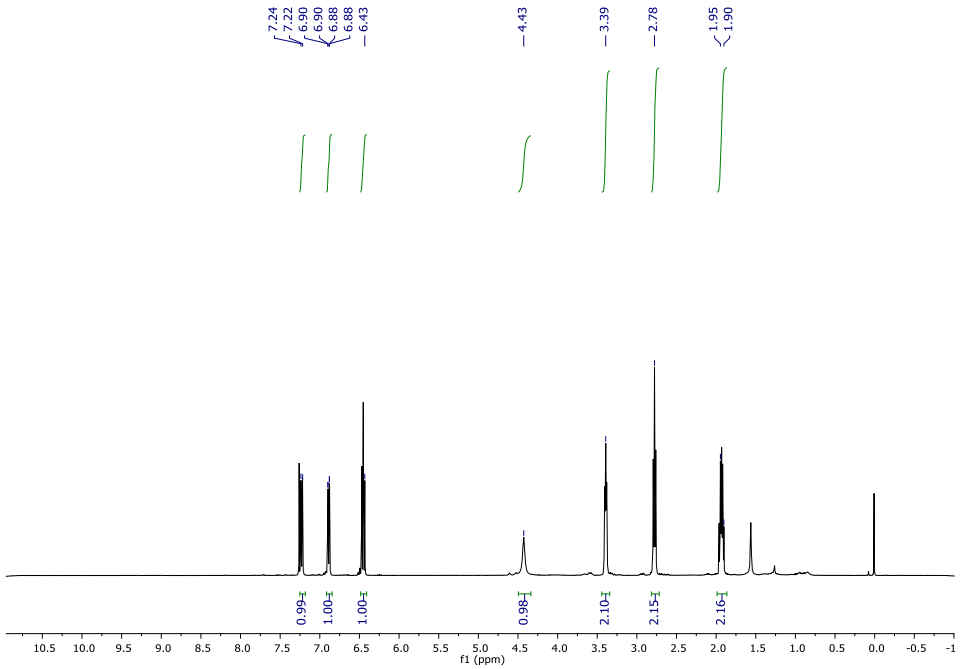
7.24
7.22
6.90
6.90
6.88
6.88
6.43
4.43
3.39
2.78
1.95
1.90
0.99
1.00
1.00
0.98
2.10
2.15
2.16
f1 (ppm)

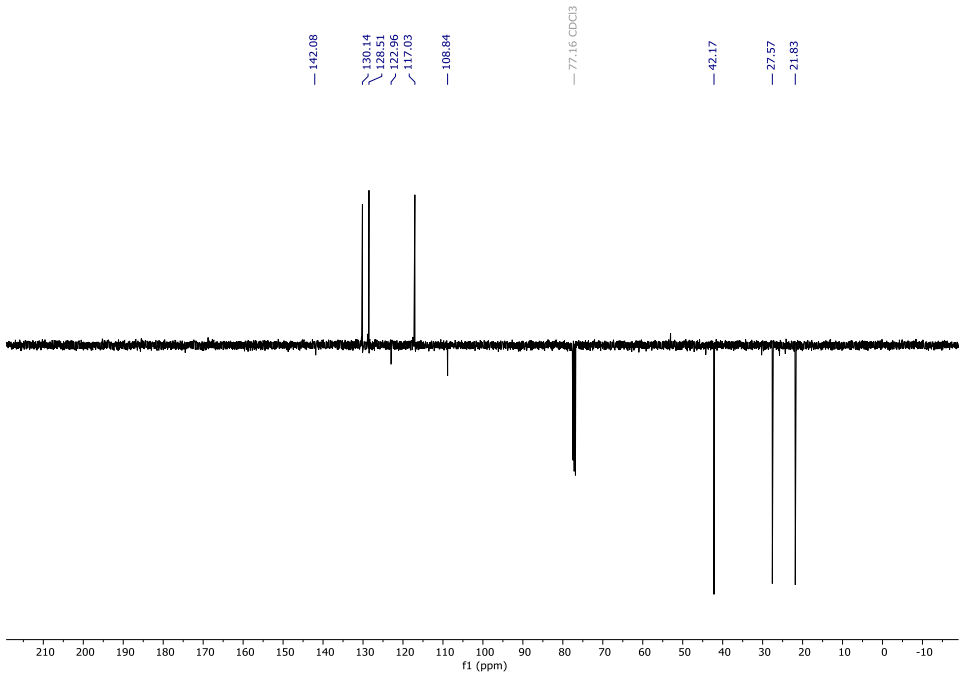
142.08
130.14
128.51
122.96
117.03
108.84
77.16 CDCl3
42.17
27.57
21.83
f1 (ppm)

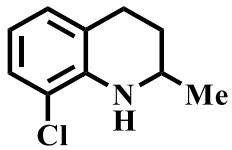

8-chloro-2-methyl-1,2,3,4-tetrahydroquinoline (**V.2s**).[454] Isolated yield: 67%. (The NMR spectrum is consistent with the reported data). ^{1}H NMR (400 MHz, $CDCl_3$) δ = 7.06 (d, *J* = 7.9, 1H), 6.87 (d, *J* = 7.5, 1H), 6.51 (t, *J* = 7.7, 1H), 4.27 (bs, NH), 3.47 (dqd, *J* = 9.2, 6.1, 2.9, 1H), 2.88-2.72 (m, 2H), 1.98-1.92 (m, 1H), 1.58 (dddd, *J* = 12.8, 11.0, 9.7, 5.5, 1H), 1.28 (d, *J* = 6.3, 3H) ppm. ^{13}C NMR (100 MHz, $CDCl_3$) δ = 140.8 (C), 127.6 (CH), 126.8 (CH), 122.5 (C), 117.9 (C), 116.8 (CH), 47.4 (N-CH), 29.9 (CH_2), 26.9 (CH_2), 22.9 (CH_3) ppm.

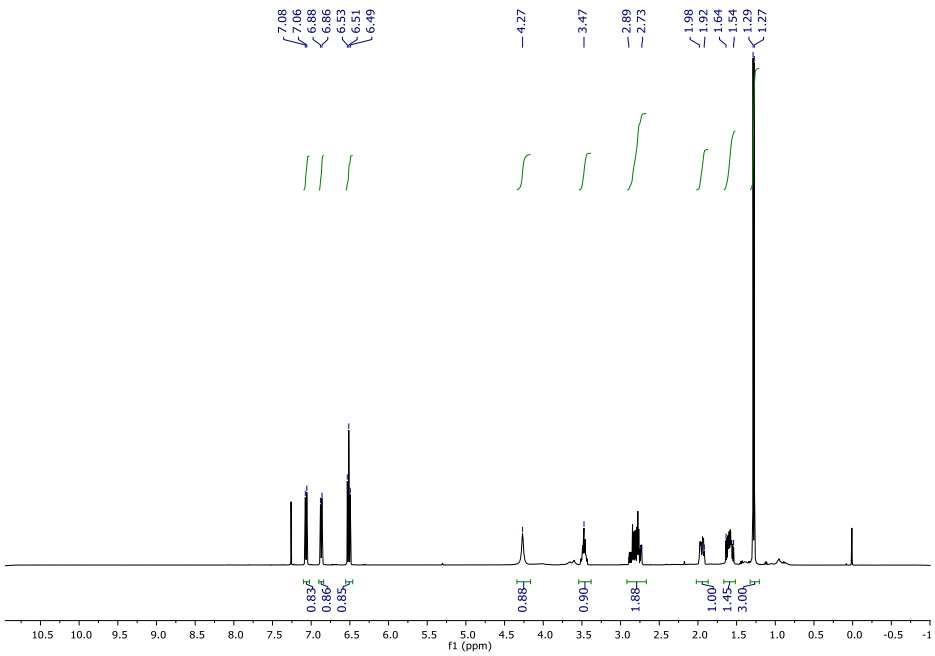

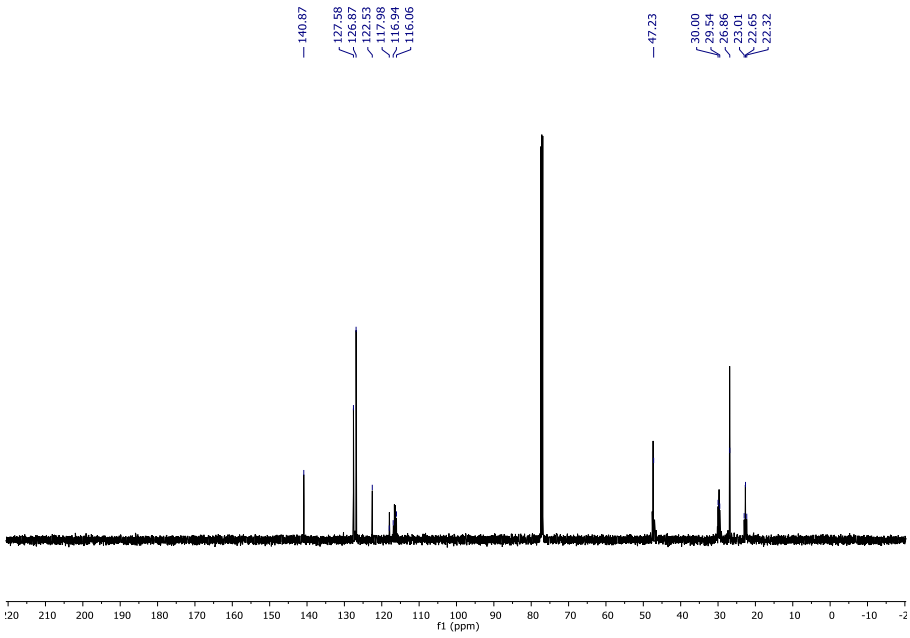

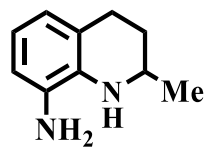

8-amino-2-methyl-1,2,3,4-tetrahydroquinoline (**V.2t**).[458] Isolated yield: 73%. (The NMR spectrum is consistent with the reported data). ^{1}H NMR (400 MHz, $CDCl_3$) δ = 6.59-6.54 (m, 3H), 3.39-3.34 (m, 1H), 3.06 (bs, N$\underline{H}_2$+N$\underline{H}$), 2.89-2.82 (m, 1H), 2.76-2.71 (m, 1H), 1.94 (ddt, J =12.1, 6.3, 2.1, 1H), 1.56 (dddd, J = 12.6, 11.2, 10.0, 5.3, 1H), 1.27 (d, J = 4.9, 3H) ppm. ^{1} ^{13}C NMR (101 MHz, $CDCl_3$) δ = 134.2 (C), 133.5 (CH), 122.8 (C), 121.1 (CH), 117.9 (CH), 114.3 (CH), 47.8 (N-CH_2), 30.3 (CH), 26.9 (CH_2), 22.8 (CH_3) ppm.

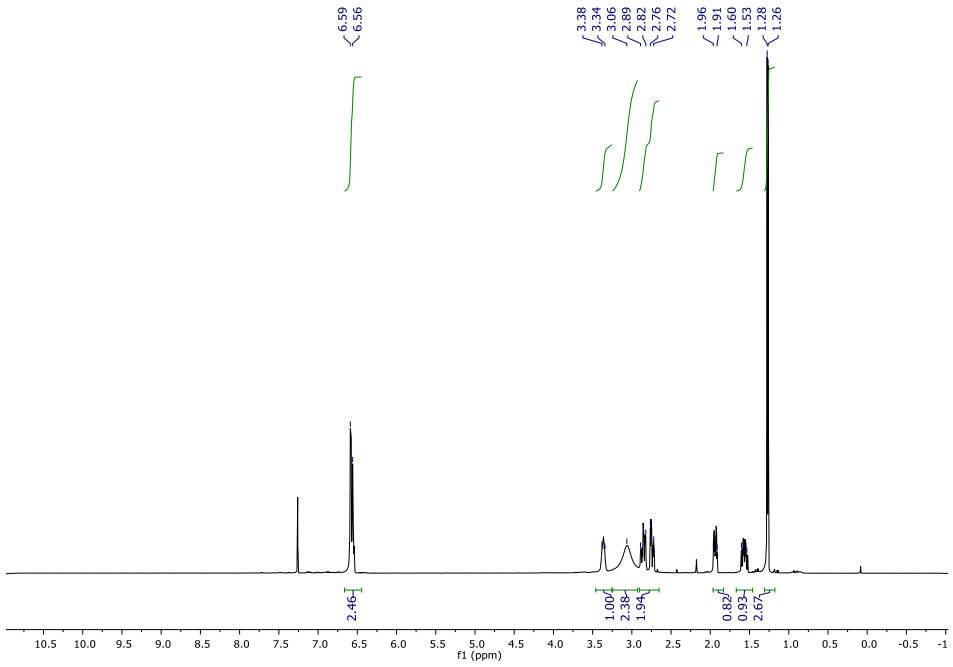
6.59
6.56
3.38
3.34
3.06
2.89
2.82
2.76
2.72
1.96
1.91
1.60
1.53
1.28
1.26
2.46
1.00
2.38
1.94
0.82
0.93
2.67
f1 (ppm)

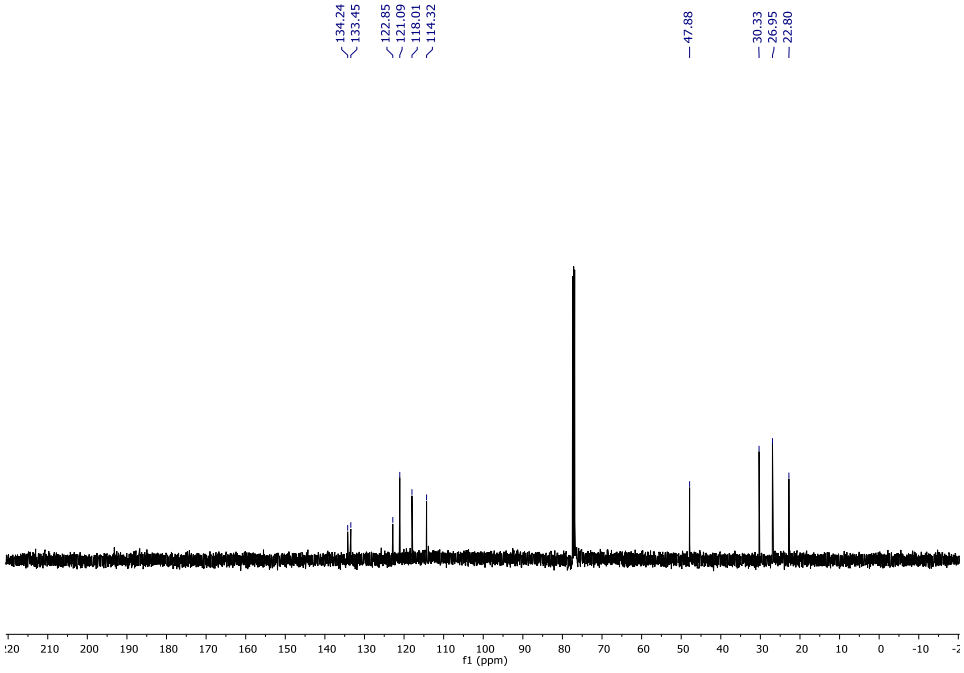
134.24
133.45
122.85
121.09
118.01
114.32
47.88
30.33
26.95
22.80
f1 (ppm)

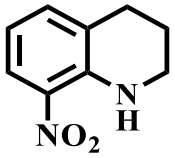

8-nitro-1,2,3,4-tetrahydroquinoline (**V.2u**).[459] Isolated yield: 52%. (The NMR spectrum is consistent with the reported data). ^{1}H NMR (400 MHz, $CDCl_3$) δ = 8.33 (s, 1H), 7.97 (ddt, *J* = 8.7, 1.5, 0.7 Hz, 1H), 7.11 (ddt, *J* = 7.0, 2.0, 1.0 Hz, 1H), 6.49 (dd, *J* = 8.7, 7.0 Hz, 1H), 3.53 (ddd, *J* = 6.6, 5.7, 3.0 Hz, 2H), 2.83 (t, *J* = 6.4 Hz, 2H), 2.01 – 1.91 (m, 2H) ppm. ^{13}C NMR (100 MHz, $CDCl_3$) *δ* = 153.7 (C), 136.0 (C), 135.1 (CH), 125.9 (C), 124.2 (CH), 113.3 (CH), 41.6 (CH_2), 28.0 (CH_2), 20.3 (CH_2) ppm.

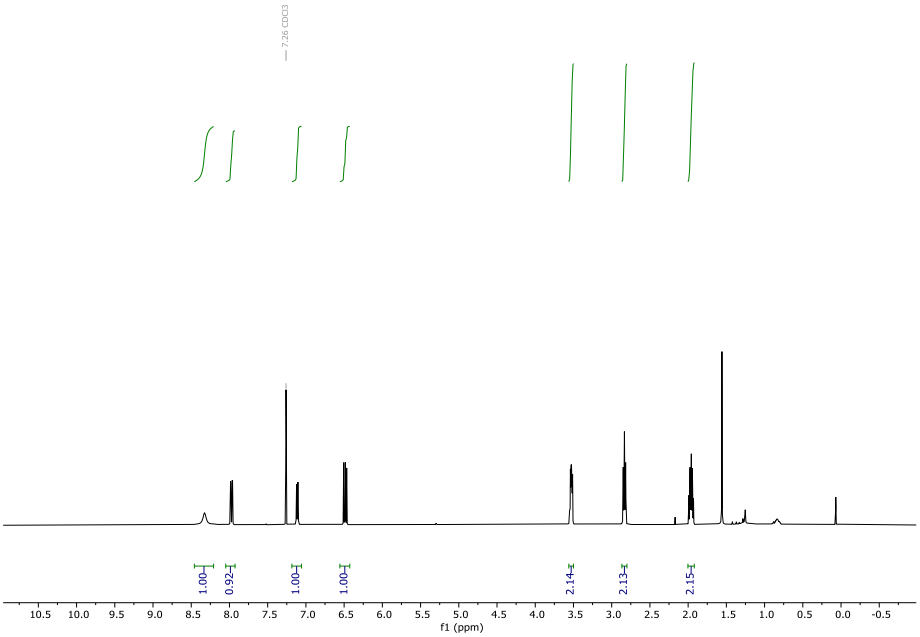

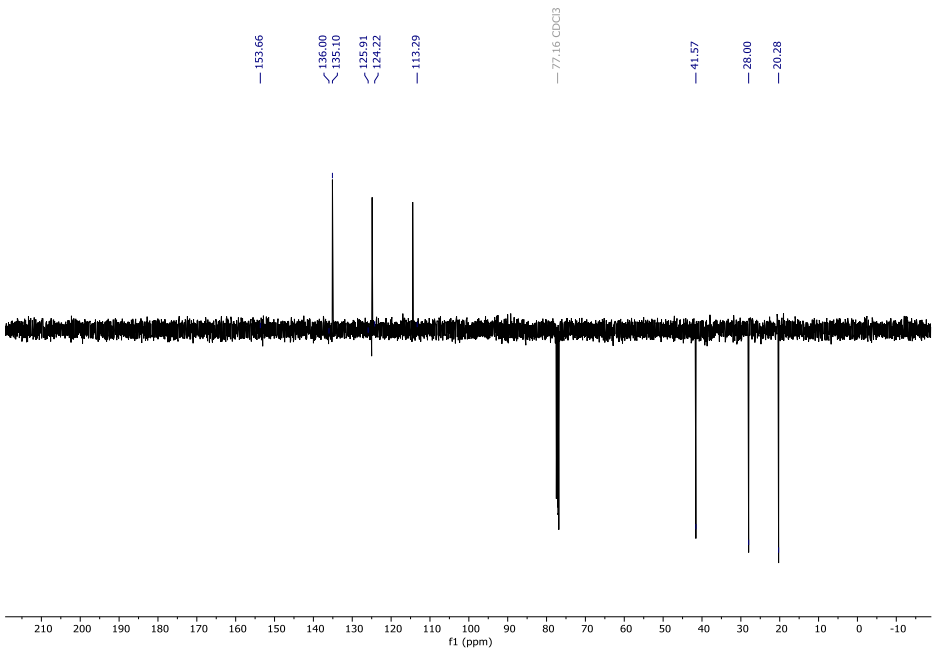

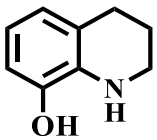

1,2,3,4-tetrahydroquinolin-8-ol (**V.2v**).[460] Isolated yield: 75%. (The NMR spectrum is consistent with the reported data). ^{1}H NMR (400 MHz, $CDCl_3$) δ = 6.62-6.48 (m, 3H), 6.43-6.41 (m, 1H), 4.00 (bs, N<u>H</u>+O<u>H</u>), 3.33 (t, J = 6.3, 2H), 2.77 (t, J = 4.8, 2H), 1.97-1.92 (m, 2H) ppm. ^{13}C NMR (100 MHz, $CDCl_3$) δ = 142.7 (C), 133.2 (C), 123.1 (C), 121.7 (CH), 116.7 (CH), 111.9 (CH), 41.6 (N-CH_2), 26.7 (CH_2), 22.4 (CH_2) ppm.

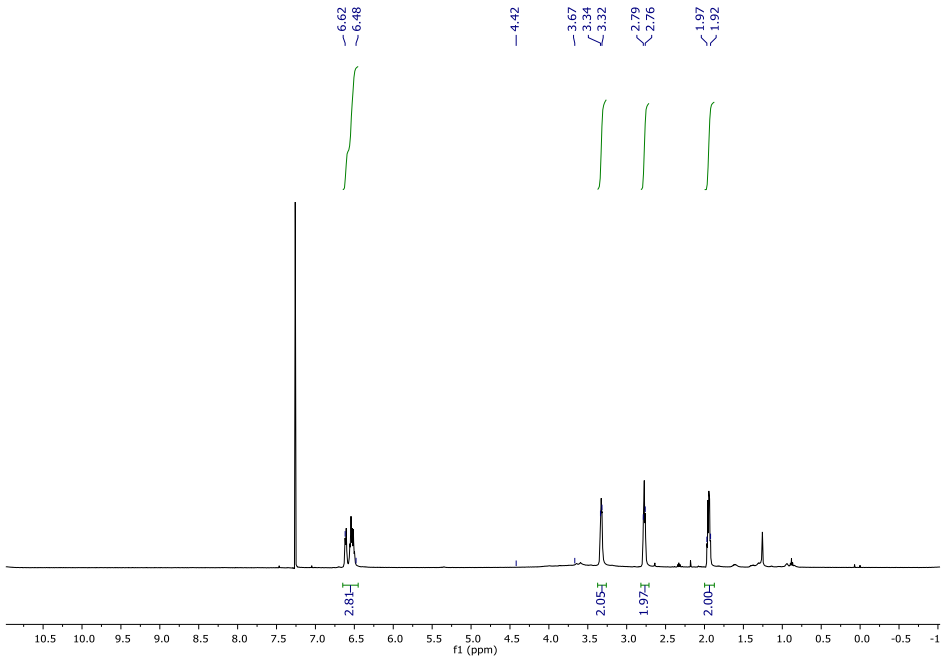
6.62
6.48
4.42
3.67
3.34
3.32
2.79
2.76
1.97
1.92
2.81
2.05
1.97
2.00
f1 (ppm)

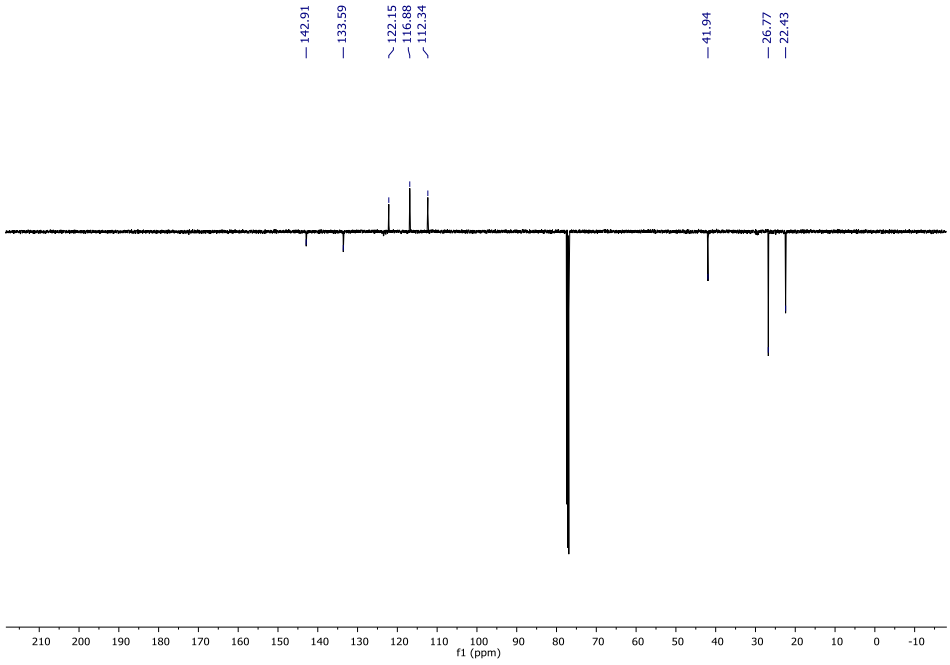
142.91
133.59
122.15
116.88
112.34
41.94
26.77
22.43
f1 (ppm)

V.5 References of the Chapter

418. Vries, J.G.d. and C.J. Elsevier, *The handbook of homogeneous hydrogenation*2007, Weinheim: Wiley-VCH.

419. Ishida, N., et al., *Sustainable System for Hydrogenation Exploiting Energy Derived from Solar Light.* Journal of the American Chemical Society, 2021. **143**(5): p. 2217-2220.

420. Farrell, J.M., J.A. Hatnean, and D.W. Stephan, *Activation of Hydrogen and Hydrogenation Catalysis by a Borenium Cation.* Journal of the American Chemical Society, 2012. **134**(38): p. 15728-15731.

421. Chalkley, M.J., et al., *Fe-Mediated Nitrogen Fixation with a Metallocene Mediator: Exploring pKa Effects and Demonstrating Electrocatalysis.* Journal of the American Chemical Society, 2018. **140**(19): p. 6122-6129.

422. Gu, N.X., P.H. Oyala, and J.C. Peters, *Hydrazine Formation via Coupling of a Nickel(III)–NH 2 Radical.* Angewandte Chemie International Edition, 2020. **60**(8): p. 4009-4013.

423. Deegan, M.M., K.I. Hannoun, and J.C. Peters, *Dihydrogen Adduct (Co–H 2) Complexes Displaying H-Atom and Hydride Transfer.* Angewandte Chemie International Edition, 2020. **59**(50): p. 22631-22637.

424. Fajardo, J. and J.C. Peters, *Tripodal P3XFe–N2 Complexes (X = B, Al, Ga): Effect of the Apical Atom on Bonding, Electronic Structure, and Catalytic N2-to-NH3 Conversion.* Inorganic Chemistry, 2021. **60**(2): p. 1220-1227.

425. Gu, N.X., P.H. Oyala, and J.C. Peters, *H2 Evolution from a Thiolate-Bound Ni(III) Hydride.* Journal of the American Chemical Society, 2020. **142**(17): p. 7827-7835.

426. Matson, B.D. and J.C. Peters, *Fe-Mediated HER vs N2RR: Exploring Factors That Contribute to Selectivity in P3EFe(N2) (E = B, Si, C) Catalyst Model Systems.* ACS Catalysis, 2018. **8**(2): p. 1448-1455.

427. Brahmachari, G., 2013.

428. Sridharan, V., P.A. Suryavanshi, and J.C. Menéndez, *Advances in the Chemistry of Tetrahydroquinolines.* Chemical Reviews, 2011. **111**(11): p. 7157-7259.

429. Scott, J.D. and R.M. Williams, *Chemistry and Biology of the Tetrahydroisoquinoline Antitumor Antibiotics.* Chemical Reviews, 2002. **102**(5): p. 1669-1730.

430. Eberle, U., M. Felderhoff, and F. Schüth, *Chemical and Physical Solutions for Hydrogen Storage.* Angewandte Chemie International Edition, 2009. **48**(36): p. 6608-6630.

431. Crabtree, R.H., *Hydrogen storage in liquid organic heterocycles.* Energy & Environmental Science, 2008. **1**(1): p. 134.

432. Ryabchuk, P., et al., *Intermetallic nickel silicide nanocatalyst—A non-noble metal–based general hydrogenation catalyst.* Science Advances, 2018. **4**(6).

433. Baralt, E., et al., *Homogeneous catalytic hydrogenation. 6. Synthetic and mechanistic aspects of the regioselective reductions of model coal nitrogen, sulfur, and oxygen heteroaromatic compounds using the (.eta.5-pentamethylcyclopentadienyl)rhodium tris(acetonitrile) dication complex as the catalyst precursor.* Journal of the American Chemical Society, 2002. **114**(13): p. 5187-5196.

434. Mahdi, T. and D.W. Stephan, *Facile Protocol for Catalytic Frustrated Lewis Pair Hydrogenation and Reductive Deoxygenation of Ketones and Aldehydes.* Angewandte Chemie International Edition, 2015. **54**(29): p. 8511-8514.

435. Wiesenfeldt, M.P., et al., *Selective Arene Hydrogenation for Direct Access to Saturated Carbo- and Heterocycles.* Angewandte Chemie International Edition, 2019. **58**(31): p. 10460-10476.

436. Wang, T., et al., *Highly Enantioselective Hydrogenation of Quinolines Using Phosphine-Free Chiral Cationic Ruthenium Catalysts: Scope,*

Mechanism, and Origin of Enantioselectivity. Journal of the American Chemical Society, 2011. **133**(25): p. 9878-9891.

437. Papa, V., et al., *Development of a practical non-noble metal catalyst for hydrogenation of N-heteroarenes.* Nature Catalysis, 2020. **3**(2): p. 135-142.
438. Adam, R., et al., *A General and Highly Selective Cobalt-Catalyzed Hydrogenation of N-Heteroarenes under Mild Reaction Conditions.* Angewandte Chemie International Edition, 2017. **56**(12): p. 3216-3220.
439. Ginsberg, A.P. and W.E. Lindsell, *Rhodium complexes with the molecular unit P4 as a ligand.* Journal of the American Chemical Society, 2002. **93**(8): p. 2082-2084.
440. Scheer, M., C. Troitzsch, and P.G. Jones, *The Formation ofcyclo-P4 Ligands with Maximum Electron Donor Ability.* Angewandte Chemie International Edition in English, 1992. **31**(10): p. 1377-1379.
441. Chakraborty, S., W.W. Brennessel, and W.D. Jones, *A Molecular Iron Catalyst for the Acceptorless Dehydrogenation and Hydrogenation of N-Heterocycles.* Journal of the American Chemical Society, 2014. **136**(24): p. 8564-8567.
442. Xu, R., et al., *Acceptorless, Reversible Dehydrogenation and Hydrogenation of N-Heterocycles with a Cobalt Pincer Catalyst.* ACS Catalysis, 2015. **5**(11): p. 6350-6354.
443. Yun, R., et al., *Ni@PC as a stabilized catalyst toward the efficient hydrogenation of quinoline at ambient temperature.* Catalysis Science & Technology, 2019. **9**(23): p. 6669-6672.
444. Wei, Z., F. Shao, and J. Wang, *Recent advances in heterogeneous catalytic hydrogenation and dehydrogenation of N-heterocycles.* Chinese Journal of Catalysis, 2019. **40**(7): p. 980-1002.
445. Shaw, J.E. and P.R. Stapp, *Regiospecific hydrogenation of quinolines and indoles in the heterocyclic ring.* Journal of Heterocyclic Chemistry, 1987. **24**(5): p. 1477-1483.

446. Smirnova, E.S., et al., *Synthesis and Reactivity of Copper(I) Complexes Based on C 3 -Symmetric Tripodal HTIM(PR$_2$)$_3$ Ligands.* European Journal of Inorganic Chemistry, 2018. **2018**(23): p. 2612-2620.

447. Creutz, S.E. and J.C. Peters, *Catalytic Reduction of N2 to NH3 by an Fe–N2 Complex Featuring a C-Atom Anchor.* Journal of the American Chemical Society, 2014. **136**(3): p. 1105-1115.

448. Abarca, B., R. Adam, and R. Ballesteros, *An efficient one pot transfer hydrogenation and N-alkylation of quinolines with alcohols mediated by Pd/C/Zn.* Organic & Biomolecular Chemistry, 2012. **10**(9): p. 1826.

449. Chaudhaery, S.S., et al., *Novel Carbamates as Orally Active Acetylcholinesterase Inhibitors Found to Improve Scopolamine-Induced Cognition Impairment: Pharmacophore-Based Virtual Screening, Synthesis, and Pharmacology.* Journal of Medicinal Chemistry, 2010. **53**(17): p. 6490-6505.

450. Wu, J., et al., *The Remarkable Effect of a Simple Ion: Iodide-Promoted Transfer Hydrogenation of Heteroaromatics.* Chemistry - A European Journal, 2012. **18**(31): p. 9525-9529.

451. Wu, J., et al., *Robust cyclometallated Ir(iii) catalysts for the homogeneous hydrogenation of N-heterocycles under mild conditions.* Chemical Communications, 2013. **49**(63): p. 7052.

452. Higuchi, R.I., et al., *4-Alkyl- and 3,4-dialkyl-1,2,3,4,-tetrahydro-8-pyridono[5,6-g]quinolines: Potent, nonsteroidal androgen receptor agonists.* Bioorganic & Medicinal Chemistry Letters, 1999. **9**(9): p. 1335-1340.

453. Yang, C.-H., et al., *Iodine catalyzed reduction of quinolines under mild reaction conditions.* Chemical Communications, 2018. **54**(62): p. 8622-8625.

454. Talwar, D., et al., *A Simple Iridicycle Catalyst for Efficient Transfer Hydrogenation of N-Heterocycles in Water.* Chemistry - A European Journal, 2015. **21**(14): p. 5370-5379.

455. Chen, F., et al., *Selective Catalytic Hydrogenation of Heteroarenes with N-Graphene-Modified Cobalt Nanoparticles (Co3O4–Co/NGr@α-Al2O3).* Journal of the American Chemical Society, 2015. **137**(36): p. 11718-11724.

456. Nandi, P., J.L. Dye, and J.E. Jackson, *Birch Reductions at Room Temperature with Alkali Metals in Silica Gel (Na2K-SG(I)).* The Journal of Organic Chemistry, 2009. **74**(16): p. 5790-5792.

457. Clarke, P. and A. Moorhouse, *911. The synthesis of some 6-substituted 1,2,3,4-tetrahydroquinoxalines.* Journal of the Chemical Society (Resumed), 1963: p. 4763.

458. Sorribes, I., et al., *Nanolayered Cobalt–Molybdenum Sulfides as Highly Chemo- and Regioselective Catalysts for the Hydrogenation of Quinoline Derivatives.* ACS Catalysis, 2018. **8**(5): p. 4545-4557.

459. Cordeiro, A., et al., *Synthesis of 6-Nitro-1,2,3,4-tetrahydroquinoline: An Experimental and Theoretical Study of Regioselective Nitration.* European Journal of Organic Chemistry, 2011. **2011**(8): p. 1504-1513.

460. Chen, C., et al., *Ruthenium(II)-Catalyzed Regioselective C-8 Hydroxylation of 1,2,3,4-Tetrahydroquinolines.* Organic Letters, 2018. **20**(21): p. 6799-6803.

UNIVERSITAT ROVIRA I VIRGILI
ORGANIC TRANSFORMATIONS USING TRANSITION METALS AND PHOTOREDOX CATALYSTS
Klaudia Michaliszyn

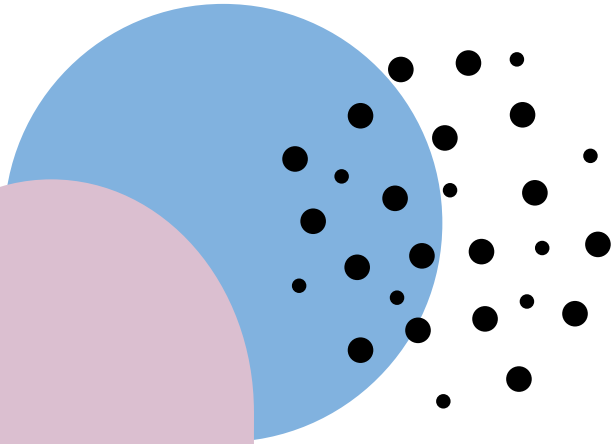

Chapter VI

General Conclusions

UNIVERSITAT ROVIRA I VIRGILI
ORGANIC TRANSFORMATIONS USING TRANSITION METALS AND PHOTOREDOX CATALYSTS
Klaudia Michaliszyn

VI.1 General Conclusions

In **Chapter III**, family of new ligands with *N*,*N*′-dimethyl-1,2-cyclohexanediamine and 2,2′-bipyrrolidine backbones and their corresponding complexes based on first-row transitions metals have been developed for light-driven H_2 evolution. The systems formed by photoredox catalysts and Co^{II} complexes in presence of trimethylamine as an electron donor were found to be powerful towards water reduction to hydrogen, while Ni^{II} complexes revealed to reduce water with low activity.

Addition of γ-cyclodextrin into the catalytic solution for hydrogen evolution enhance solubility of catalyst in water due to the non-covalent interactions with PAH moiety, showing a catalytic enhancement not only in pure water, but also in solvent mixtures. While the same strategy was applied for the photoredox catalyst (containing PAH moiety), its solubility was enhanced in aqueous solutions, but the catalytic activity was very low.

Anchoring Co^{II} based catalysts have been tested in the reduction of acetophenone in combination with ^{NMe2}**PC$_{Ir}$** as a photosensitizer and Et_3N as a source of electrons, yielding the desired product with high yields. Although more studies are needed to increase the enenatioselectivity and to explore different anchoring strategies, these systems are very promising.

Ni^{II} catalysts were tested towards the cleavage of C_{sp3}-Cl bonds and were found active in the cross-coupling reaction, with ^{NMe2}**PC$_{Ir}$** photosensitizer obtaining the product with good yield, while Co^{II} based catalysts were found inactive.

In **Chapter IV**, cobalt and nickel complexes containing pyrene or perylene anchoring moieties ($Co(^{PyB}mcp)(OTf)_2$, $Co(^{PyB}pdp)(OTf)_2$, $Ni(^{PyB}mcp)(OTf)_2$ and $Ni(^{PyB}pdp)(OTf)_2$) developed in Chapter III, were characterized in different solvent mixtures by optical methods of analysis revealing a complex behaviour in solution. The pyrene complexes aggregate more in polar solvents, and interact with γ-CD in a host-guess fashion. Anyhow upon addition of water into the solvent mixture (acetonitrile/water 4:6) to induce the π-stacking interaction

between two pyrene units did not reveal excimer bands. While characterization experiments were performed in water, the interaction between the polyaromatic parts became very strong due to the hydrophobic nature of π–π stacking interactions and excimer bands were observed. Prepared materials have shown in earlier experiments very promising possibilities in catalysis that can be further extended.

In **Chapter V**, new nickel and cobalt complexes containing ligands $HTIM(PR_2)_3$ with the C_3 symmetry were synthetized. The first row transition metal (Co, Ni) activates $H\text{-}C_{sp3}$ bond of the tripod ligand, resulting in well-defined coordination geometry species. Tripodal P-based complexes with electron-donating and electron withdrawing groups were examined for the reduction of N-heteroarenes obtaining very good yields for the use of Ni-based catalysts ($NiTIM(PPh_2)_3Br$, $NiTIM[P(^{p\text{-}Me}C_6H_4)_2]_3Br$), while Co-based catalysts remained inactive.

All the components in the reaction (catalyst, silver salt, and hydrogen) of this new efficient, non-air sensitive method of reducing N-heteroarenes catalyzed by nickel complexes were demonstrated to be needed for the reaction to occur.

We envision that this method may be also active for reduction of other organic functionalization.

UNIVERSITAT ROVIRA I VIRGILI
ORGANIC TRANSFORMATIONS USING TRANSITION METALS AND PHOTOREDOX CATALYSTS
Klaudia Michaliszyn

UNIVERSITAT ROVIRA I VIRGILI
ORGANIC TRANSFORMATIONS USING TRANSITION METALS AND PHOTOREDOX CATALYSTS
Klaudia Michaliszyn

UNIVERSITAT
ROVIRA i VIRGILI